Enantioselective synthesis of carbon-oxygen and carbon-nitrogen bonds using bisamidine Brønsted acid/base catalysis, investigations of intermediates, applications, and mechanistic insights of catalyst symmetry effects unveiled by DFT

By

Thomas James Struble

Dissertation

Submitted to the Faculty of the

Graduate School of Vanderbilt University

in partial fulfillment of the requirements

for the degree of

DOCTOR OF PHILOSOPHY

in

Chemistry

January 31, 2018

Nashville, Tennessee

Approved: Date:

_____   _____

Jeffrey N. Johnston, Ph.D. (Advisor)

_____   _____

Lawrence J. Marnett, Ph.D.

_____   _____

Ned A. Porter, Ph.D.

_____   _____

Steven D. Townsend, Ph.D.

To all my family and friends who have never stopped believing and supporting me

To my lifeline Katie Chong who I cannot imagine a life without

Andrew Stubenrauch for going through similar experiences in medical school and understanding my graduate school frustrations, as well as visiting Nashville often to remind me how important friends are.

My family was instrumental in encouraging me in my pursuits of science and have been there for all of the success and failures. I would never have applied to graduate school without the influences from my parents and grandparents. My parents have always been there, pushed me, and believed in me, even when I was at my worst. My brother Michael moved to Nashville with me, making the transition to a new city not only easier, but the making my time here the best experience of my life. Ed and Darcy have always taken me in when I need an escape and every time I visit they let me spoil Molly and Neil! Finally, I have been fortunate to gain new family during graduate school and have to thank the whole Chong family for accepting me and treating me like one of their own.

I owe anything and everything I have accomplished to my incredibly supportive, patient, and loving partner Katie Chong. We have been together for the duration of our time at Vanderbilt, through the graduate experiences that consisted of extraordinary highs and impossible lows. She has been a rock for me to lean on, and the most perfect confidant during every moment. Katie has constantly challenged me to be a better scientist by having a passionate and unwavering belief in me, even when I gave up on myself. Because of her, I continue to grow into a better scientist and a better person even in our life we are making in a new city. Katie, you deserve more of this Ph.D than I do, and for that, I will never be able to thank you enough.

Table of Contents

List of Tables

List of Figures

List of Schemes

Chapter 1   Enantioselective small molecule synthesis using carbon dioxide as a feedstock

1.1   Introduction

1.1.1   Introduction: Bifunctional catalysis

Organocatalytic transformations have many features in common with enzyme mediated reactions, as the latter do not always rely on metals for activation and stereocontrol. Recent research in the field of organocatalysis has demonstrated the utility of organic Brønsted acid and Brønsted base catalysts that use hydrogen bonding for activation and stereocontrol.[1] Among the plethora of ligands that have been used for enantioselective transformations are the chiral Bis(Amidine) (BAM)-based catalysts that use a protonated amidine as the hydrogen bond donor. More specifically named a "chiral proton" (H^+) catalyst, it employs polar ionic hydrogen bonding to achieve high enantioselection. The Johnston group has established that the combination of a strong Brønsted acid (most often $HNTf_2$ or HOTf) and a chiral non-racemic BAM catalyst provides a bifunctional "chiral proton" catalyst salt (Figure 1).[2] Once monoprotonated, these catalysts have a Brønsted acidic and a Brønsted basic site, which allows for the possibility of coordination of the nucleophile *and* electrophile (Figure 1, complex **1**).

These are key features of the BAM catalysts that make them desirable as ligands

---

[1] For reviews on H-bonding catalysis see: Taylor, M. S.; Jacobsen, E. N. *Angew. Chem. Int. Ed.* **2006**, *45*, 1520–1543; Doyle, A. G.; Jacobsen, E. N. *Chem. Rev.* **2007**, *107*, 5713–5743; Terada, M. *Synthesis* **2010**, *2010*, 1929–1982; Rueping, M.; Koenigs, R.; Atodiresei, I. *Chem. Eur. J.* **2010**, *16*, 9350–9365; Rueping, M.; Nachtsheim, B. J.; Ieawsuwan, W.; Atodiresei, I. *Angew. Chem. Int. Ed.* **2011**, *50*, 6706–6720; Pihko, E. P., *Hydrogen Bonding In Organic Synthesis*; Wiley-Interscience, Weinheim: 2009.

[2] Nugent, B. M.; Yoder, R. A.; Johnston, J. N. *J. Am. Chem. Soc.* **2004**, *126*, 3418–3419.
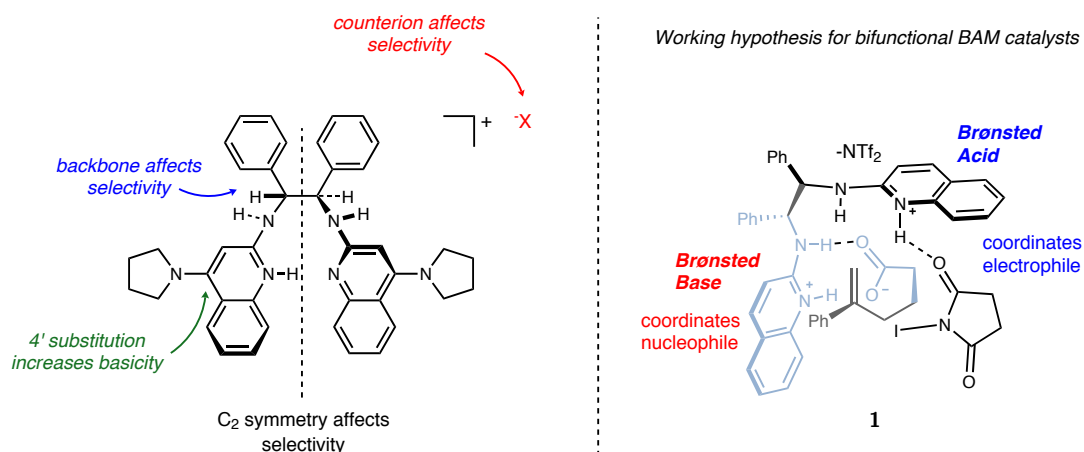
Figure 1: BisAmidine (BAM) catalyst structure: substitution trends on selectivity and reactivity and mechanistic hypothesis for bifunctional catalyst

in organocatalysis. First they are C_2-symmetric which greatly facilitates the synthesis with only a two or three step sequence[3] and allows rapid access to electronic and steric variants. An important finding for BAM catalysis was that the electronics can be "tuned" for higher reactivity without impacting the enantioselectivity. Placing electron donating groups on the quinoline (with the premier catalysts having pyrrolidine in the 4-position) can greatly modulate the basiciity of the catalysts allowing for substrate-catalyst pK_a matching.[4] The backbone can be easily modified to optimize for higher selectivity, and the most successful backbones are (R,R)-1,2-diaminocyclohexane (in the aza-Henry reactions) and (R,R)-1,2-phenylenediamine (in the halocyclization reactions). Symmetry of the catalyst can be changed to make a C_1 catalyst, and although it complicates the synthesis, diastereoselectivity can be improved[5] or reversed.[6] Finally, the achiral counterion ($^-$NTf$_2$

[3]Davis, T. A.; Dobish, M. C.; Schwieter, K. E.; Chun, A. C.; Johnston, J. N. *Org. Synth.* **2012**, *89*, 380–393.

[4]Davis, T. A.; Wilt, J. C.; Johnston, J. N. *J. Am. Chem. Soc.* **2010**, *132*, 2880–2882; Dobish, M. C.; Johnston, J. N. *Org. Lett.* **2010**, *12*, 5744–5747.

[5]Vara, B. A.; Mayasundari, A.; Tellis, J. C.; Danneman, M. W.; Arredondo, V.; Davis, T. A.; Min, J.; Finch, K.; Guy, R. K.; Johnston, J. N. *J. Org. Chem.* **2014**, *79*, 6913–6938.

[6]Singh, A.; Yoder, R. A.; Shen, B.; Johnston, J. N. *J. Am. Chem. Soc.* **2007**, *129*, 3466–3467; Singh, A.; Johnston, J. N. *J. Am. Chem. Soc.* **2008**, *130*, 5866–5867.

in Scheme 1B) can easily be changed to modify reactivity of the catalyst.[7] These features allow for many catalyst variables to be investigated without long synthetic sequences or laborious purifications, thereby creating more rapid reaction discovery and optimization.[8]

Prior work completed by Dr. Mark Dobish demonstrates that one can use a bifunctional BAM catalyst to form enantioenriched δ-lactones from achiral carboxylic acids (Scheme 1A). The optimized reaction can produce 6-membered δ-lactones in up to 98% ee and 97% yield using a variety of aryl substituted alkenes (R = Ar in Scheme 1). Several aspects of this reaction were identified in this study: A) non-coordinated counterions perform better and achieve higher % ee; B) the backbone of the catalyst plays a defining role in the selectivity. The role of the backbone remains unclear, but the dihedral angle of the diamine could have a large impact on the size of the catalytic pocket.[9] The ability of the diphenylethylene diamine backbone to have free rotation could also allow for a more dynamic pocket which could "open and close" when substrates bind and products are released. Finally, the study by Dobish indicates that catalyst iodinates at the 3' position when using N-iodosuccinimide as the iodine source.[10]

BAM catalyst methodology has been expanded to new iodocyclization reactions over the recent years. The two most interesting of these are shown in Scheme 2. A phosphoramidic acid cyclization which is the first and only of our halocyclization reactions to be enantioselective *AND* diastereoselective was developed by Dr. Yasunori Toda.[11] The catalyst must desymmetrize the phosphoramidic acid to set both the P and C chiral

[7]Dobish, M.; Johnston, J. *J. Am. Chem. Soc.* **2012**, *134*, 6068–6071.

[8]For in depth mechanistic discussion about the aza-Henry reaction see Chapter 3: Mechanistic investigation of the influence of catalyst structure on the stereodivergence of nitroester additions to *N*-boc aldimines unveiled by DFT calculations.

[9]Kim, H.; Yen, C.; Preston, P.; Chin, J. *Org. Let.* **2006**, *8*, 5239–5242.

[10]It is important to note that the conditions under which iodination of the catalyst are observed differ greatly from those of the reaction conditions. In addition, a hydrogen bonding interaction could account for the same observation of the disappearance of the 3' peak of StilbPBAM·HNTf$_2$.

[11]Toda, Y.; Pink, M.; Johnston, J. N. *J. Am. Chem. Soc.* **2014**, *136*, 14734–14737.
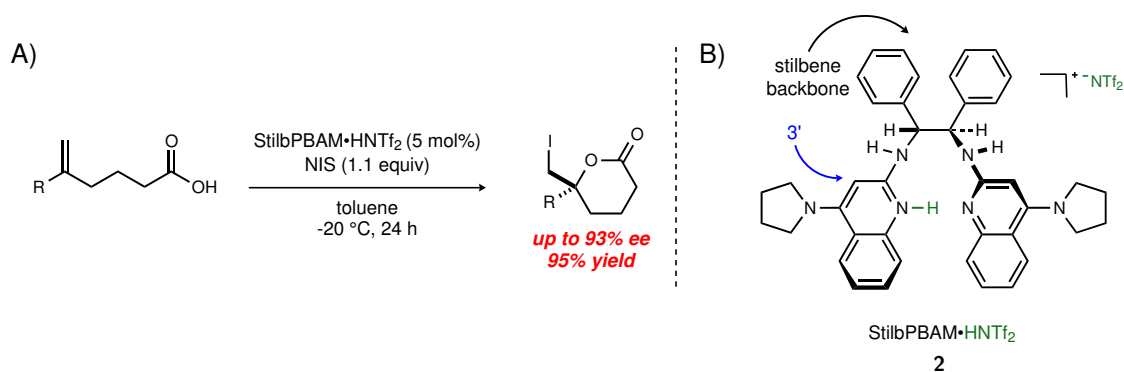
Scheme 1: A) Enantioselective iodolactonization B) Triflimidic acid salt of StilbPBAM

centers to furnish **4**. Unpublished work using the the same conditions, but employing 1,2-disubstituted alkenes, hints that the cyclization selectivity is driven by the formation of a chiral nucleophile (Nu·**2**).[12] This was the first example of a BAM catalyst demonstrating the ability to take symmetric non-chiral materials and set two stereocenters using a halocyclization reaction (i.e. using a catalyst to desymmetrize the phosphoramidic acid). The catalyst-nucleophile control paradigm has been extended by Matthew Knowe to desymmetrize carboxylic acids furnishing an interesting bicyclic product **5** with high enantioselectivity.[13] This study yielded the first co-crystal structure of a BAM catalyst (specifically catalyst **3**) with a substrate, finally providing structural insight to the interactions between substrate and catalyst. It is important to note that many aspects of this reaction differ from the typical conditions that use a protonated catalyst such as StilbPBAM·HNTf$_2$ **2**. The desymmetrization of a carboxylic acid uses free base catalyst, with the triflimide salt performing significantly worse.[14] The 4-position is substituted with an aniline and not the usual pyrrolidine creating a presumably less basic active site. This demonstrates that the catalyst easily deprotonates a carboxylic acid substrate but

---

[12]The 5-*endo* product obtained in this cyclization is low d.r but high % ee. Further functionalization revealed that the carbon is close to racemic while the phosphorous enrichment is high.

[13]Knowe, M.T.; Sun, S.; Danneman, M.W.; Pink. M.; Johnston, J.N. *Unpublished Results.*

[14]At room temperature StilbPBAM·HNTf$_2$ gives 16% ee and StilbPBAM free base gives 48% ee.

also hints that the bifunctional nature of the BAM catalysts are not absolutely necessary for high enantioselection.
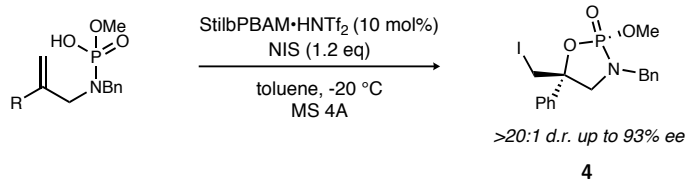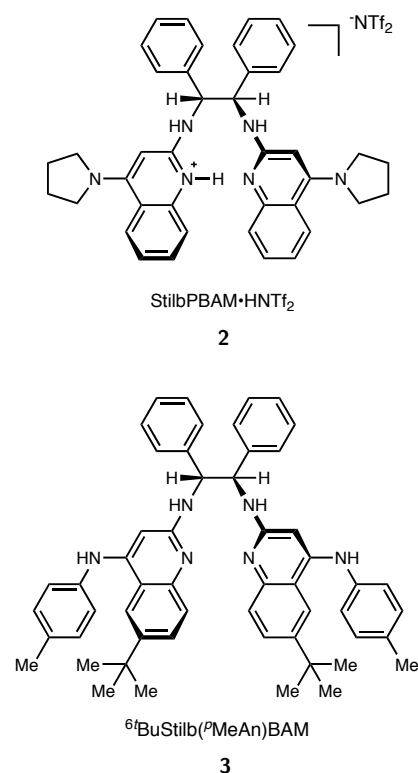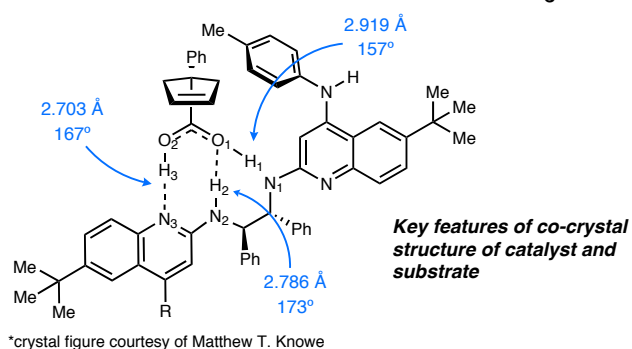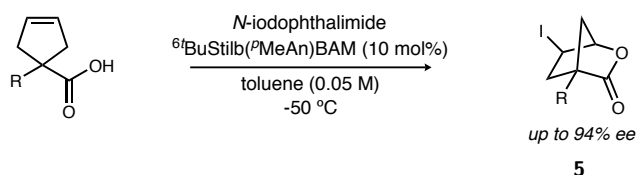
Scheme 2: Elaboration of BAM catalysts to new reactions and the features of a co-crystal structure of a catalyst-substrate pair

The crystal structure combined with mechanistic studies that will be discussed in the following sections leave the role of the halogen source (NIS, *N*-iodophthalimide, and *N*-iodopyrrolidinone) unclear. Although the role of the electrophilic halogen source is still not completely understood, the optimization of the following sections are based on the hypothesis that the bifunctional catalyst coordinates both the nucleophile *AND* the electrophile. Some important attributes of electrophilic halogen sources are preserved in all cases when high enantioselectivity is obtained. First is that an amide/imide is necessary for high enantioselectivity and reactivity (Figure 1, complex **1**). Second is that the halogen source needs to be iodine. Using bromine or chlorine sources lead to

suppressed reactivity and lower enantioselectivity. Finally, the basicity of the catalyst must be matched to the substrate for optimal reactivity as demonstrated previously with 4'-substituted catalysts (Figure 1). Finally, additional substitution of the quinoline can help achieve substrate/catalyst pK_a matching.[15]

The ease in synthesis and rapid access to derivatives of BAM catalysts allow for their continued use as ligands for new methodologies. Discussion throughout the following chapters will hopefully shed some insight into the interactions and controlling factors that play key roles in the halocyclization reactions and the aza-Henry reactions. Mechanistic studies will include discussion of results ranging from pK_a measurements and state of the art NMR methods such as ^{19}F-DOSY, and extend to more theoretical approaches in the aza-Henry reaction using computational DFT calculations (Chapter 3).

1.1.2 Introduction: Catalytic asymmetric halofunctionalizations

Catalytic asymmetric halofunctionalization of alkenes is a field that has gained much momentum in the past decade.[16] Halocyclizations have been useful in the realm of target synthesis and total synthesis although they often rely on substrate (i.e. diastereoselective[17]) control of the cyclization. The following section will detail the evolution of enantioselective methods for halofunctionalization reactions all the way from stoichiometric reagent control to catalytic enantioselective methods.

Enantioselective halofunctionalization reactions have been approached in a few direc-

[15]Davis, T. A.; Danneman, M. W.; Johnston, J. N. *Chem. Commun.* **2012**, *48*, 5578–5580; Vara, B. A.; Johnston, J. N. *J. Am. Chem. Soc.* **2016**, *138*, 13794–13797.

[16]For reviews see: Cardillo, G.; Orena, M. *Tetrahedron* **1990**, *46*, 3321–3408; Denmark, S. E.; Kuester, W. E.; Burk, M. T. *Angew. Chem. Int. Ed.* **2012**, *51*, 10938–53; Castellanos, A.; Fletcher, S. P. *Chem. Eur. J.* **2011**, *17*, 5766–5776; Cheng, Y. A.; Yu, W. Z.; Yeung, Y.-Y. *Org. Biomol. Chem.* **2014**, *12*, 2333–2343.

[17]Some early examples using substrate control: Corey, E. J.; Keck, G. E.; Szekely, I. *J. Am. Chem. Soc.* **1977**, *99*, 2006–2008; Still, W. C.; Schneider, M. J. *J. Am. Chem. Soc.* **1977**, *99*, 948–950; Tamaru, Y.; Hojo, M.; Kawamura, S.; Sawada, S.; Yoshida, Z. *J. Org. Chem.* **1987**, *52*, 4062–4072.

tions, including activation by Brønsted acids, Lewis acids, Lewis bases, and phase transfer catalysis (Figure 2, red boxes = halide source). A method that has found much success in controlling the halide delivery is with a Brønsted acid. In this mechanism the acid can either perform a metathesis reaction with the halide source in order to form a more reactive halide species, or hydrogen bond to the halide source to "activate" it as in complex **6**.[18] The second method is Lewis acid activation of the halide source, most commonly using Co^{II}/salen, $Cr^{III}Cl$/salen complex, and $Ti(OiPr)_4$. The coordination of the Lewis acid to the halide source provides a complex in which the halide is slightly more electrophilic **7**. The third strategy is using a Lewis base to form a complex that is in equilibrium with a cationic halonium **8** which applies of the general principle of Lewis base activation of Lewis acids.[19] These methods all require the use of an acid or base to activate a halide source that, on its own, would not be reactive toward the alkenes of interest. In contrast to the these methods, is the last activation strategy, using a phase transfer catalyst. This process involves a halide source that is either in the aqueous or solid layer, which upon interaction with the catalyst, will come in contact with the substrate in the organic layer. Each of these modes of catalysis require the use of an otherwise unreactive halide source which only is active upon interaction with the catalyst, causing subsequent reaction with the alkene.

Pioneering studies into enantioselective halocyclizations were reported using stoichiometric Lewis base complexes (Figure 2, complex **8**) that, in most cases deliver the halide from a chiral amine. Initial reports by Grossman used cinchona alkaloid derivatives to

---

[18]Olah, G. A.; Prakash, G. K. S.; Mathew, T.; Hoole, D.; Esteves, P. M.; Wang, Q.; Rasul, G. *J. Am. Chem. Soc.* **2004**, *126*, 15770–6.

[19]Denmark, S. E.; Beutner, G. L. *Angew. Chem. Int. Ed.* **2008**, *47*, 1560–638; Gutmann, V. *Coord. Chem. Rev.* **1975**, *15*, 207–237.
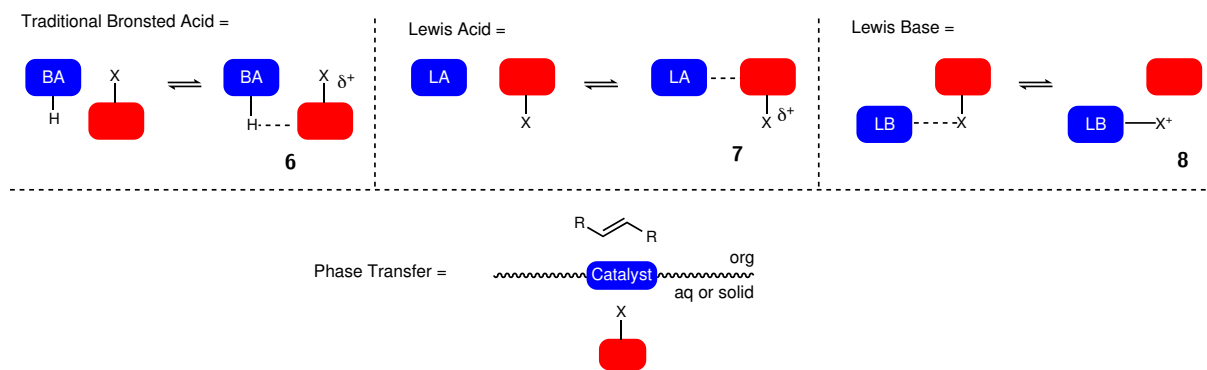
Figure 2: Methods for activation in halofunctionalization of alkenes

generate a chiral iodinating source, achieving up to 15% ee.[20] Following shortly after, reports from Brown using chiral pyridine bromonium triflates,[21] and Wirth using chiral secondary amines[22] were published. Although these methods all use a stoichiometric amount of chiral ligand for stereoinduction, much was learned about the use of Lewis bases and the stability of the resulting halonium complexes.[23] The most elegant use of a stoichiometric chiral Lewis base for enantioselective cyclizations was reported by Ishihara shown in Scheme 3, where a chiral phosphoramidite **9** is used to effect the polyene cyclization.[24] This is the only example that achieves high enantioselection and is a great example of the potential of enantioselective halocyclizations. The reaction suffers from using a stoichiometric amount of phosphoramidite but much insight was gained from the study of this system resulting in the proposition of selectivity models. These systems paved the way for new methods that would ultimately gain more traction by evolving into catalytic enantioselective methods.

[20]Grossman, R. B.; Trupp, R. J. *Can. J. Chem.* **1998**, *76*, 1233–1237.

[21]Cui, X.-L.; Brown, R. S. *J. Org. Chem.* **2000**, *65*, 5653–5658.

[22]Haas, J.; Piguel, S.; Wirth, T. *Org. Lett.* **2002**, *4*, 297–300; Haas, J.; Bissmire, S.; Wirth, T. *Chem. Eur. J.* **2005**, *11*, 5777–5785.

[23]Neverov, A. A.; Brown, R. S. *J. Org. Chem.* **1998**, *63*, 5977–5982; Neverov, A. A.; Feng, H. X.; Hamilton, K.; Brown, R. S. *J. Org. Chem.* **2003**, *68*, 3802–3810; Yousefi, R.; Whitehead, D. C.; Mueller, J. M.; Staples, R. J.; Borhan, B. *Organic Letters* **2011**, *13*, 608–611.

[24]Sakakura, A.; Ukai, A.; Ishihara, K. *Nature* **2007**, *445*, 900–903.
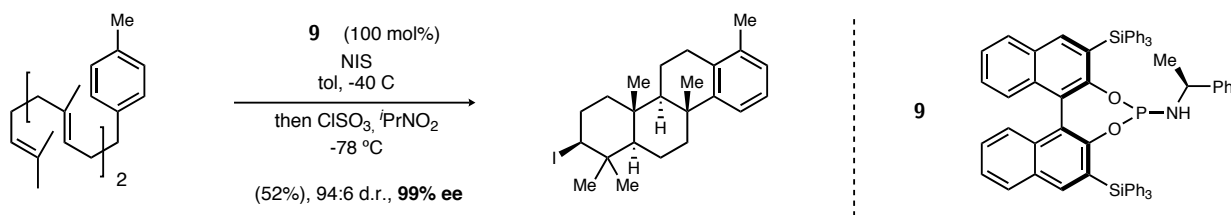
Scheme 3: Ishihara's stoichiometric method for an enantioselective polyene cyclization

In organocatalytic approaches there is some ambiguity in the mechanism and stereo-controlling factors with similar catalysts. Mechanistic proposals will be presented but as the reader will notice, they differ greatly from one another. It is apparent that not all of the mechanisms proposed can be operating, but it is clear that further mechanistic studies have not been reported by the groups disseminating the reactions. The following section will briefly touch on the proposals and will highlight the key studies that support them.

The first approach that will be discussed is the use of Brønsted acids, and more specifically, chiral phosphoric acids (or their salts). An initial report by Hennecke employs the sodium salt of a phosphoric acid to achieve up to 68% ee in the iodoetherification of symmetric alkenes (Figure 3).[25] They find that the iodocyclization proceeds with a higher selectivity than the bromocyclization possibly due to the greater stability of an iodonium than a bromonium, leading to less nonselective background reactivity. The group proposes that the *meso*-iodonium **12** is an ion pair with the chiral phosphate anion **11**. This type of ion pair has been proposed many times before in the employ of chiral phosphoric acids.[26] The chiral anion desymmertizes the iodonium forcing the approach of only one of the prochiral alcohols. A possibility that the authors note is that the

[25] Hennecke, U.; Müller, C. H.; Fröhlich, R. *Org. Lett.* **2011**, *13*, 860–863.

[26] For reviews see: Rueping, M.; Koenigs, R.; Atodiresei, I. *Chem. Eur. J.* **2010**, *16*, 9350–9365; Terada, M. *Synthesis* **2010**, *2010*, 1929–1982; Rueping, M.; Nachtsheim, B. J.; Ieawsuwan, W.; Atodiresei, I. *Angew. Chem. Int. Ed.* **2011**, *50*, 6706–6720.

catalyst could act as a Lewis base to form a phosphate hypoiodide and deliver the I$^+$ with concerted cyclization.
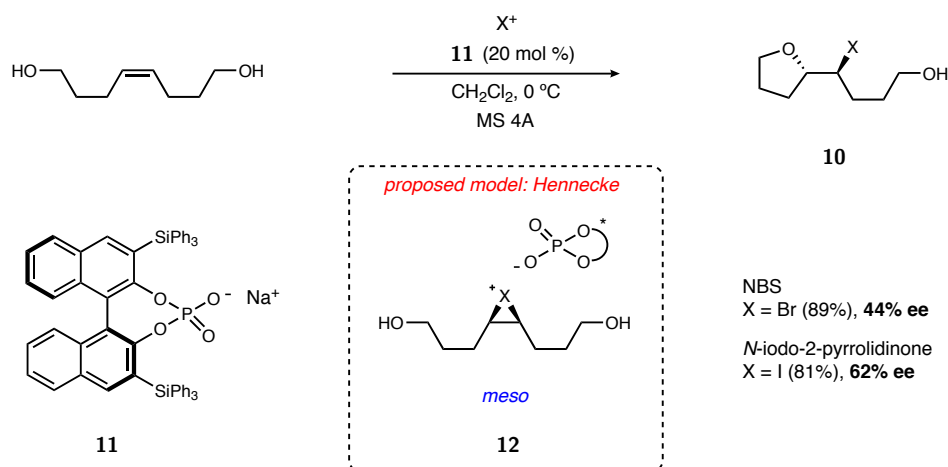
Figure 3: Hennecke's method to desymmetrize a 1,2-disubstituted alkene using a chiral phosphoric acid catalyst and the proposed model for the stereodetermining step

Two groups within a year both published results of an enantioselective organocatalytic bromoetherification using TRIP as a catalyst (Figure 4). With many of the substrates, both groups obtain a mixture of the 5-*exo* **13a** and the 6-*endo* **13b** product. This is often the case when 1,2-disubstituted alkenes are used in halocyclization reactions and more will be discussed on this topic in the next chapter. The two systems by Shi and Denmark are similar to the one reported by Hennecke (*vida supra*) but both propose different mechanisms. The authors of the review by Denmark acknowledge the difference in mechanisms and state: "Given the similarities between the Denmark and Shi systems it is unlikely that they have two different mechanisms of enantioselection; ergo, one (or both) of these proposals is probably incorrect."[27]

The most simple of the phosphoric acid catalyst system was developed by Shi's in the cyclization of γ-hydroxy-alkenes and γ-amino-alkenes.[28] Their conditions can achieve

[27]Denmark, S. E.; Kuester, W. E.; Burk, M. T. *Angew. Chem. Int. Ed.* **2012**, *51*, 10938–53.

[28]Huang, D.; Wang, H.; Xue, F.; Guan, H.; Li, L.; Peng, X.; Shi, Y. *Org. Lett.* **2011**, *13*, 6350–6353.

moderate to high enantioselection and the alkene can tolerate substitution (% ee ranging from 21-81). Additionally they report that in the same system, trisyl amides (2,4,6-triisopropylbenzenesulfonyl) can be used as competent cyclization substrates with TRIP, achieving moderate to high enantioselection (% ee ranging from 53-90). This remains one of the few successes (when compared to carboxylic acids and alcohols) in achieving an organocatalytic cyclization with a nitrogen nucleophile, demonstrating the generalizability of chiral phosphoric acid catalysis. The mechanism proposed by the authors involves phosphoric acid coordination of the *N*-bromosuccinimide and substrate (Figure 4, complex **14**), invoking the bifunctional nature that has been proposed with other chiral phosphoric acid systems.
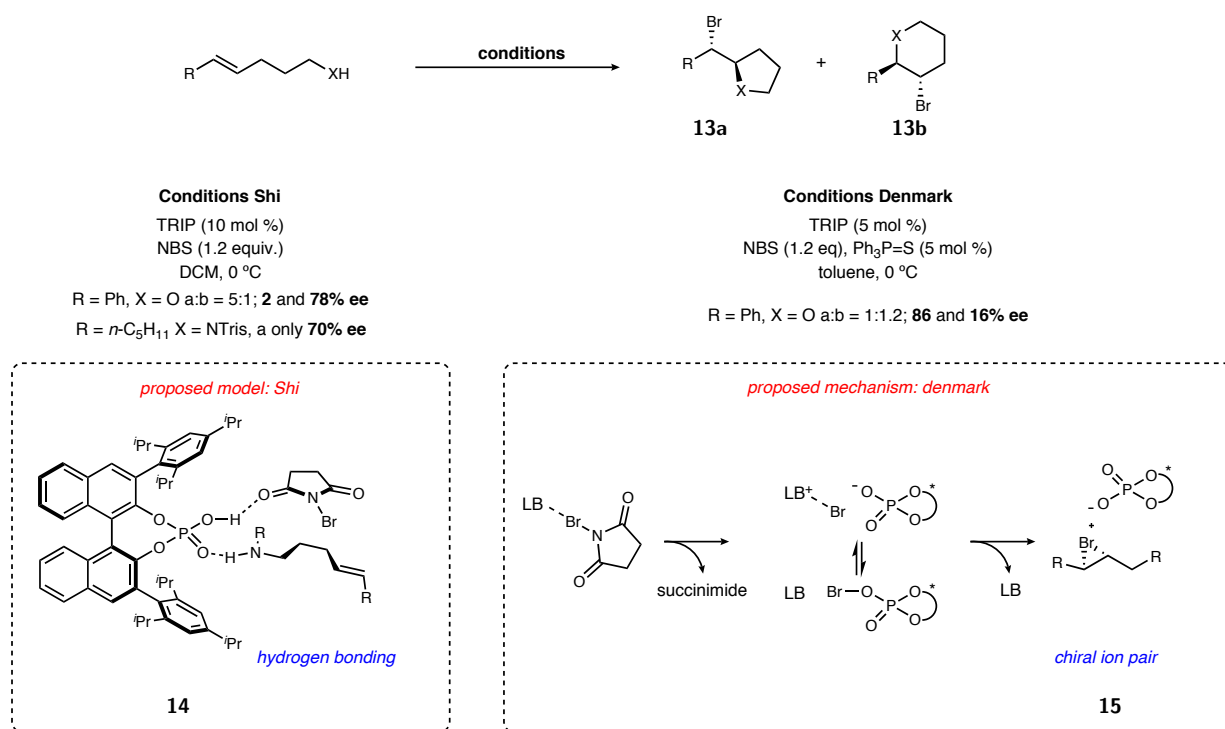
Figure 4: Chiral phosphoric acid catalyzed haloetherification and models proposed by Shi and Denmark

In contrast to the work by Shi, a report by the Denmark group uses the same catalyst

but adds a catalytic amount of Lewis base (Ph$_3$P=S).[29] The authors term the use of the additive as a "cooperative Lewis base/chiral Brønsted acid system". They report a range of 1,2-disubstituted alkenes and in some cases get a mixture of both 5-*exo* and 6-*endo* products. The *exo* products cyclize with high selectivity (up to 94% ee) but the *endo* products are produced with low selectivity (30% ee). The authors note that the *endo/exo* selectivity, nor the enantioselectivity, is affected by the removal of the Lewis base (although the reactivity is greatly impacted). The model they propose in Figure 4 invokes the Lewis base as the active iodinating species which forms an ion pair **15** with the chiral catalyst. The chiral ion pair model does seem to be a more popular proposal and is even further vindicated by the employ of chiral phosphoric acids in phase transfer systems.

The Toste group in 2011 reported the use of an organocatalytic phase transfer system for a highly enantioselective fluorocyclization[30] and is later extended to bromocyclizations.[31] The substrates are tailored for the use in a fluorination by using an activated alkene. However, overcoming the difficulty in an enantioselective fluorocyclization eclipses the narrow substrate scope and low substrate tolerability. They can achieve excellent d.r. and up to 94% ee with a 24 h reaction time. The authors propose a model in which the catalyst is acting as a phase transfer reagent to the insoluble Selectfluor (Scheme 4). This report is the first using an anionic phase-transfer system compared to the often reported cationic phase-transfer systems. An impressive substrate that was used in the cyclization is an unactivated alkene that can be transformed in up to 70% ee. Finally, a non-linear effect study was conducted that suggests there are two chiral phosphate anions in the

[29]Denmark, S. E.; Burk, M. T. *Org. Lett.* **2012**, *14*, 256–259.

[30]Toste, F. D.; Rauniyar, V.; Lackner, A. D.; Hamilton, G. L. *Science* **2011**, *334*, 1681–1684.

[31]Wang, Y.-M.; Wu, J.; Hoong, C.; Rauniyar, V.; Toste, F. D. *J. Am. Chem. Soc.* **2012**, *134*, 12928–12931.

stereodetermining step, supporting the hypothesis that the dicationic Selectfluor is an ion pair with two catalysts. The ion pair in this proposal differs from **12** and **15** but the authors do not speculate on the stereodetermining step and the possibility remains that once the fluorine is transfered, the phosphate anion is present as a chiral counterion.
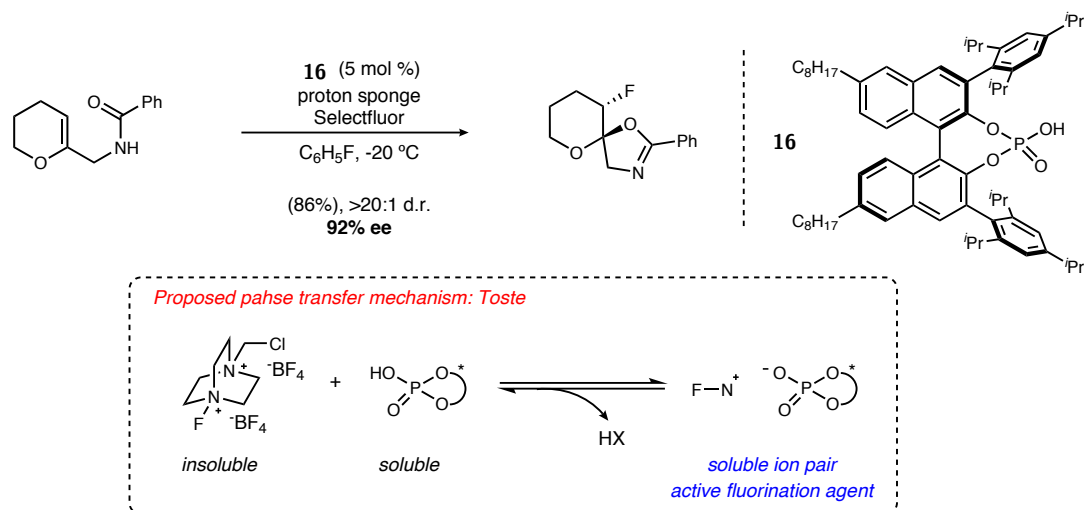
Scheme 4: Enantioselective fluorocyclization of activated alkenes and a phase transfer mechanism proposed by Toste

The second approach which has found much success in organocatalytic enantioselective approaches to halocyclization reactions is the use of Brønsted basic catalysts such as quinine derivatives such as $(DHQD)_2PHAL$, bisamidines, and urea tethered amines. With some of these catalysts it is still unclear whether the basic nitrogen is acting as a Brønsted or Lewis base and these hypotheses will be discussed.

The first of the reports in this category was by the Borhan group using $(DHQD)_2PHAL$ in an enantioselective chlorolactonization.[32] It is important to note that chlorolactonizations can be difficult to achieve in a highly selective manner due to the lower propensity of chlorine to make the chloronium ion, which suggests that the cyclization does not open the

---

[32]Whitehead, D. C.; Yousefi, R.; Jaganathan, A.; Borhan, B. *J. Am. Chem. Soc.* **2010**, *132*, 3298–3300.

chloronium from a backside attack. However there could be a discreet carbocation which would be harder to control in terms of selectivity and reactivity. The chlorolactonization can achieve excellent enantioselection (up to 89% ee) using a Cinchona derivative (DHQD)$_2$PHAL (Figure 5). Soon after the initial report, an enantioselective cyclization of amides by the same group,[33] and a dichlorination by Nicolaou[34] were reported using the same catalyst designs.

Mechanistic studies were conducted by the Borhan group using the catalyst and dichlorohydantoin shown in Figure 5. The analysis by NMR at $-50\,°C$ revealed a shift and splitting of the hydantoin protons indicating some interaction between the catalyst and the hydantoin. The authors speculate about the two possible interactions, indicating that there could be a hydrogen bonding interaction such as **18** or a transfer of the chlorine to the Lewis basic nitrogen as depicted in **19**. Since the reaction conditions use an equivalent of benzoic acid, the former (**18** in Figure 5) appears to be more likely. It is important to note that the reaction selectivity is not impacted greatly when no benzoic acid is present (86 vs 89% ee). The group furthers their hypothesis of the hydantoin associating with the catalyst by employing chiral chlorinated hydantoins.[35] They find a matched/mismatched case when employing a chiral hydantoin with (DHQD)$_2$PHAL indicating some interaction of the chlorine source with the catalyst. They further verify by using the pseudoenantiomer (DHQ)$_2$PHAL and the enantiomer of the chlorohydantoin.

Soon after, Jacobsen demonstrated the use of a urea-derived catalyst with a chiral

[33]Jaganathan, A.; Garzan, A.; Whitehead, D. C.; Staples, R. J.; Borhan, B. *Angew. Chem. Int. Ed.* **2011**, *50*, 2593–2596.

[34]Nicolaou, K. C.; Simmons, N. L.; Ying, Y.; Heretsch, P. M.; Chen, J. S. *J. Am. Chem. Soc.* **2011**, *133*, 8134–8137.

[35]Yousefi, R.; Whitehead, D. C.; Mueller, J. M.; Staples, R. J.; Borhan, B. *Organic Letters* **2011**, *13*, 608–611.

tertiary amine (Figure 5, compound **20**).[36] This is one of the few studies that finds success with an enantioselective cyclization that can achieve both δ-lactones and γ-lactones both with excellent enantioselectivity. The authors speculate about the mechanism based on low temperature NMR analysis and mixing their active iodnating species (4-fluoro-*N*-iodophthalimide and I_2) with catalyst **20**, although they do not state at what temperature (this is important because Borhan and co-workers see the collapse of the coordination when the temperature is raised). The authors observe shifts consistent with iodination or protonation of the amine. From this they conclude that the iodine is transferred to the catalyst which is then the active iodinating reagent in the cyclization. Interestingly the optimized reaction conditions use a catalytic amount of I_2 which the authors propose will make the triiodo phthalimide.[37]

Finally, the Yeung group developed an approach to γ-lactones using a thiocarbamate tethered to a cinchona alkaloid.[38] They can achieve high enantioselection finding that an additive of nosylamine ($NsNH_2$) aided in yield and % ee although the results without the additive are only marginally worse (no additive 96% yield, 87% ee vs. additive 99% yield, 90% ee). High enantioselectivity is achieved on a variety of 1,2-disubstituted alkenes with both aryl and alkyl groups. Mechanistically they propose that the sulfur of the thiocarbamate is acting as a Lewis base to transfer the bromine to the substrate, while the alkaloid is deprotonating the carboxylic acid as depicted in complex **21**. The authors hypothesize that the additive aids bromine transfer from *N*-bromosuccinimide to the Lewis basic sulfur on the catalyst. Finally, they report the use of the γ-lactone in

---

[36]Veitch, G. E.; Jacobsen, E. N. *Angew. Chem. Int. Ed.* **2010**, *49*, 7332–7335.

[37]Chaikovskii, V. K.; Funk, A. A.; Filimonov, V. D.; Petrenko, T. V.; Kets, T. S. *Russ. J. Org. Chem.* **2008**, *44*, 935–936.

[38]Zhou, L.; Tan, C. K.; Jiang, X.; Chen, F.; Yeung, Y.-Y. *J. Am. Chem. Soc.* **2010**, *132*, 15474–15476.
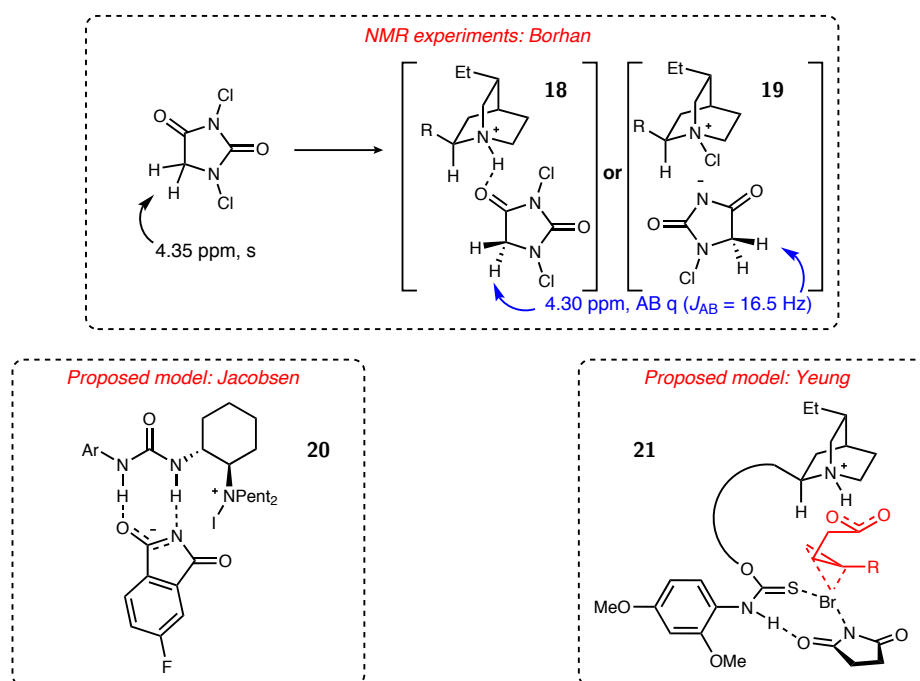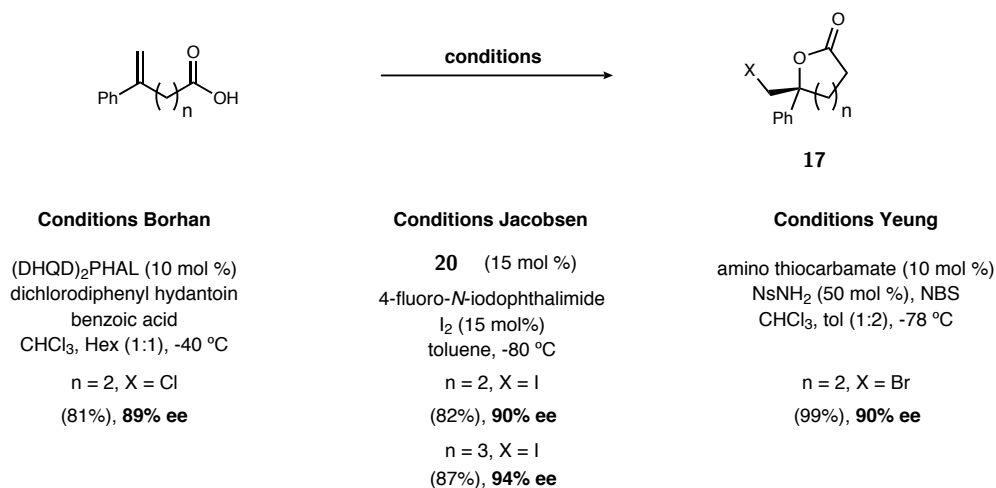
Figure 5: Brønsted base/Lewis base methods for halocyclization of carboxylic acids and mechanistic studies

the enantioselective synthesis of a precursor to some VLA-4 antagonists which represents the first application of an enantioselective organocatalyzed halocyclization to a small molecule target.

These studies are the seminal works associated with organocatalytic enantioselective cyclizations. They initiated the discovery of various mechanistic details, and paved the way for more methods in this field using many different cyclization precursors. A plethora

of elegant methods using metal catalysts exist but are not within the scope of this introduction but will be discussed briefly in Chapter 2. Indeed there is room for improvement in the scope of many of these reactions with the limitation to styrene-derived substrates and a clearer understanding of the function of the catalysts. Additional mechanistic work to elucidate catalyst-substrate complexes will be helpful in further detailing the mechanism of halocyclization reactions.

1.1.3 Introduction: CO_2 as an one carbon (C1) or oxygen source in organic synthesis

In the past two decades CO_2 capture and activation has become a popular research topic for chemists due to the abundance, availability, and low cost of this fairly inert gas. A quick SciFinder search provides over 26,000 publications pertaining to CO_2 in 2014 alone. The growing demand for strategies to fix this relatively unreactive gas has supplied profuse amounts of research on reactivity, fixation methods, and possible uses. The increasing interest in the use of carbon dioxide in organic synthesis is a result of its relatively inert nature, which provides a reagent that is non-toxic and easy to handle. Despite these clear benefits, the safe properties of CO_2 reflect its poor reactivity. The consequence is that carbon dioxide requires additional means to activate and incorporate (fix) it within organic molecules. CO_2 can be useful in organic synthesis as a one-carbon (C1) building block[39,40] but new and innovative techniques are required to catalytically

---

[39] For reviews see: Liu, Q.; Wu, L.; Jackstell, R.; Beller, M. *Nat. Commun.* **2015**, *6*, 5933 EP; Aresta, M.; Dibenedetto, A. *Dalton Trans.* **2007**, 2975–2992; Sakakura, T.; Choi, J.-C.; Yasuda, H. *Chem. Rev.* **2007**, *107*, 2365–2387; Alper, E.; Orhan, O. Y. *Petroleum* **2017**, *3*, 109–126; Ola, O.; Maroto-Valer, M. M.; Mackintosh, S. *Energy Procedia* **2013**, *37*, 6704–6709.

[40] For prospectives see: Fullerton, D.; Stavins, R. *Nature* **1998**, *395*, 433–434; Arrow, K. J.; Cropper, M. L.; Eads, G. C.; Hahn, R. W.; Lave, L. B.; Noll, R. G.; Portney, P. R.; Russell, M.; Schmalensee, R.; Smith, V. K.; Stavins, R. N. *Science* **1996**, *272*, 221–222.

activate carbon dioxide for fixation.[41]
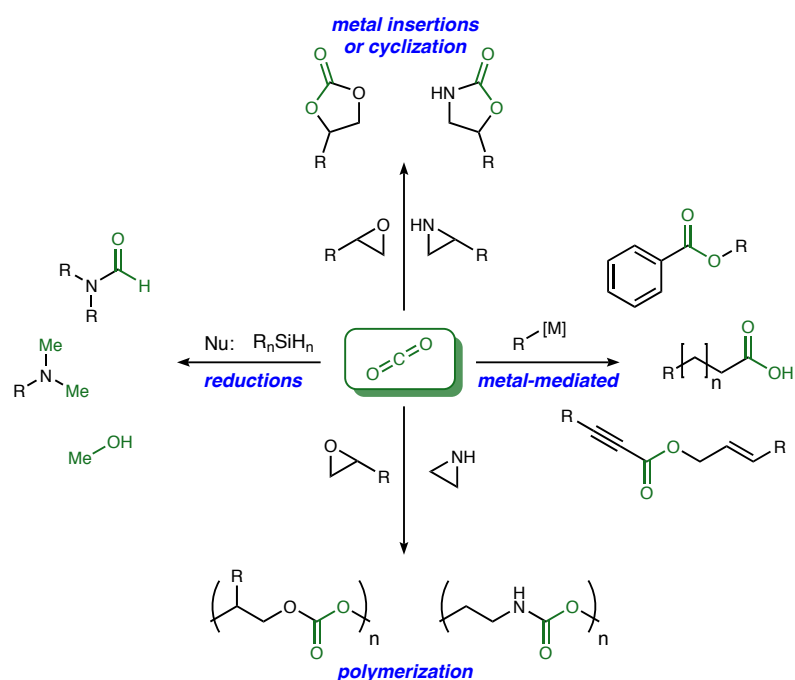
Figure 6: The most common transformations of CO_2 in organic synthesis

Polyoxygenated scaffolds are very common among natural products and clinically approved drugs. The introduction of oxygen atoms into small molecules is an important aspect for the construction of these scaffolds en route to complex natural products. Many motifs such as polyurethanes, polycarbonates, carboxylic acids, alcohols, carbamates, and carbonates can all be sourced from CO_2. Arguably these are the largest areas of research pertaining to carbon dioxide incorporation in organic synthesis and are outlined in Figure 6. Creative approaches have been explored for utilizing CO_2 as a chemical reagent but are only recently finding success in enantioselective approaches.[42] The rate limiting step to providing drugs and natural products can be either a) introduction of oxygen in an enantioselective manner or b) time consuming separation of enantiomers

[41]Maeda, C.; Miyazaki, Y.; Ema, T. *Catal. Sci. Technol.* **2014**, *4*, 1482–1497.
[42]Vaitla, J.; Guttormsen, Y.; Mannisto, J. K.; Nova, A.; Repo, T.; Bayer, A.; Hopmann, K. H. *ACS Catal.* **2017**, *7*, 7231–7244.

or diastereomers. To date, the most useful of these methods create enantioenriched alcohols and epoxides through well developed and robust techniques of functional group manipulation most often by alkene functionalization.

Traditionally to achieve incorporation of CO_2, a metal, surrogate, or forcing reaction conditions such as strong acids, strong bases, and high pressures are used.[43] Recently there has been an interest in finding carbon dioxide fixation methods using mild conditions.[44] Although many examples provide a method for CO_2 capture, they rely on metals such as Cu^I, Ag^I, and Al^{III}-salen complexes to activate the CO_2. The metals are typically used to activate a C_{Sp^2} or C_{Sp^3}-halogen or hydrogen bond.[45] To improve on the current methodology, the use of mild reagents in combination with a non-toxic catalyst would be ideal for new CO_2 fixation reactions.

In recent years there has been an abundance of research on the synthesis of cyclic carbonates and carbamates with CO_2 that highlight both mild methods,[46] and enantios-election.[47] However, many common methods for synthesizing carbonates use phosgene or phosgene equivalents, and can be expensive, pose great hazards to health, and are not always amenable to process scale. One can imagine that there may be easier ways to introduce this carbonate functionality using less toxic reagents, fewer steps, and milder conditions. The use of CO_2 instead of phosgene offers many great advantages such as the availability, low cost, and non-toxic properties. CO_2 is also already in the carbonate (4^+)

---

[43]Chu, F.; Dueno, E. E.; Jung, K. W. *Tetrahedron Lett.* **1999**, *40*, 1847–1850; Bhanage, B. M.; Fujita, S.-i.; Ikushima, Y.; Arai, M. *Applied Catalysis A: General* **2001**, *219*, 259–266; Clegg, W.; Harrington, R.; North, M.; Pasquale, R. *Chemistry (Weinheim an der Bergstrasse, Germany)* **2010**, *16*, 6828–6843.

[44]Martín, R.; Kleij, A. W. *Chem. Sus. Chem.* **2011**, *4*, 1259–1263.

[45]Cai, X.; Xie, B. *Synthesis* **2013**, *45*, 3305–3324.

[46]Sakakura, T.; Kohno, K. *Chem. Commun.* **2009**, 1312–1330.

[47]For reviews on stereoselective synthesis of organic carbonates see: Gómez, J. E.; Kleij, A. W. *Curr. Opin. Green Sus. Chem.* **2017**, *3*, 55–60; Kielland, N.; Whiteoak, C. J.; Kleij, A. W. *Adv. Synth. Catal.* **2013**, *355*, 2115–2138; and for Poylmerization see: Childers, M. I.; Longo, J. M.; Van Zee, N. J.; LaPointe, A. M.; Coates, G. W. *Chem. Rev.* **2014**, *114*, 8129–8152.

oxidation state making it a suitable reagent for fixing. Despite the benefits, CO_2 is a poor electrophile which requires additional means to activate and subsequently incorporate in an organic molecule.

Work on catalytic stereoselective synthesis of carbonates using CO_2 starts with the use of epoxides for a ring expansion to a cyclic carbamate. An early report uses an epoxide and a Cr(III) salen catalyst **22** to afford cyclic carbamates **23**.[48] The reaction is stereospecific which allows cyclic carbonates to be synthesized from enantioenriched precursors. Unfortunately the reaction has to be run neat in the reactant (propylene oxide in Scheme 5), under elevated pressure, and heat is necessary for complete conversion. Other groups have expanded on this methodology such that racemates can be used in kinetic resolutions,[49] and in more mild conditions.[50] Unfortunately the kinetic resolutions can only achieve up to 50% yield and recovery of the undesired enantiomer of the starting material. These studies improve the methodology and the understanding of CO_2 capture reactions but could be improved by the use of achiral starting materials.

Yamada and co-workers improved the field of stereoselective carbonate synthesis by desymmetrizing bispropargylic alcohols shown in Scheme 5 to afford cyclic carbamates such as **25**.[51] The use of achiral starting materials does not limit the reaction yields to 50% or less and allows for a more broad exploration of competent cyclization precursors. Although this system uses a very specific substrate, it demonstrates the potential for the use of CO_2 in enantioselective reactions. The expansion from the use of alkynes is necessary and the functionalization of alkenes holds great potential for the use with CO_2.

---

[48]Paddock, R. L.; Nguyen, S. T. *J. Am. Chem. Soc.* **2001**, *123*, 11498–11499.

[49]Lu, X.-B.; Liang, B.; Zhang, Y.-J.; Tian, Y.-Z.; Wang, Y.-M.; Bai, C.-X.; Wang, H.; Zhang, R. *J. Am. Chem. Soc.* **2004**, *126*, 3732–3733.

[50]Berkessel, A.; Brandenburg, M. *Org. Let.* **2006**, *8*, 4401–4404.

[51]Yoshida, S.; Fukui, K.; Kikuchi, S.; Yamada, T. *J. Am. Chem. Soc.* **2010**, *132*, 4072–4073.
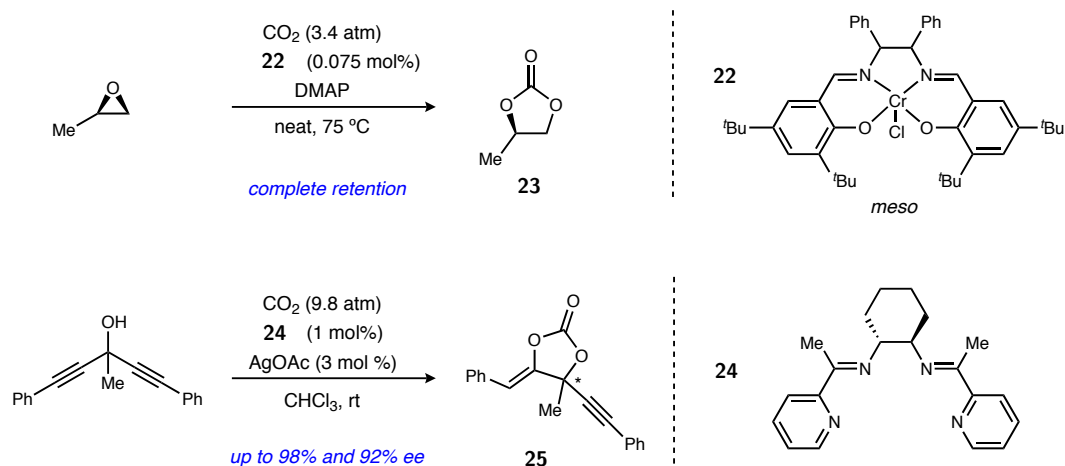
Scheme 5: Common methods for synthesizing enantioenriched cyclic carbonates

Previous studies have demonstrated the possibility of regioselective CO_2 cyclization with an allylic or homoallylic alcohol.[52] Seminal work by Cardillo and co-workers demonstrated that it is possible to achieve regioselectivity of the 5-*exo* versus the 6-*endo* cyclization product as shown in Scheme 6. Unfortunately these reaction conditions require the use of *n*-butyl lithium which makes this procedure less safe compared to recent alternatives.[53] Recent work by Minakata and co-workers demonstrate the ability to capture CO_2 using milder conditions. Using an allylic or homoallylic alcohol, *tert*-butyl hypochlorite (*t*BuOCl), and sodium iodide (NaI) at $-20\,°C$ they were able to capture CO_2 and subsequently cyclize to form iodocarbonates[54] and iodocarbamates.[55] The iodocyclization reactions, once again, typically favor the 5 or 6-*exo* products and illustrate that regioselectivity can be obtained under mild conditions. The authors propose that the reason this system can operate under such mild conditions is through the formation of **27** which helps pull the equilibrium of the starting material to **26**. Additionally, the carbonate

[52]Cai, X.; Xie, B. *Synthesis* **2013**, *45*, 3305–3324.
[53]Cardillo, G.; Orena, M.; Porzi, G.; Sandri, S. *J. Chem. Soc., Chem. Commun.* **1981**, *197*, 465–466.
[54]Minakata, S.; Takeda, Y.; Okumura, S.; Tone, S.; Sasaki, I. *Org. Lett.* **2012**, *14*, 4874–4877.
[55]Minakata, S.; Sasaki, I.; Ide, T. *Angew. Chem. Int. Ed.* **2010**, *49*, 1309–1311.

hypoiodite **27** would be a much more electrophilic source of I^+. These nice investigations demonstrate the ability to capture CO_2 in mild conditions, however they lack the ability to form enantioenriched products.
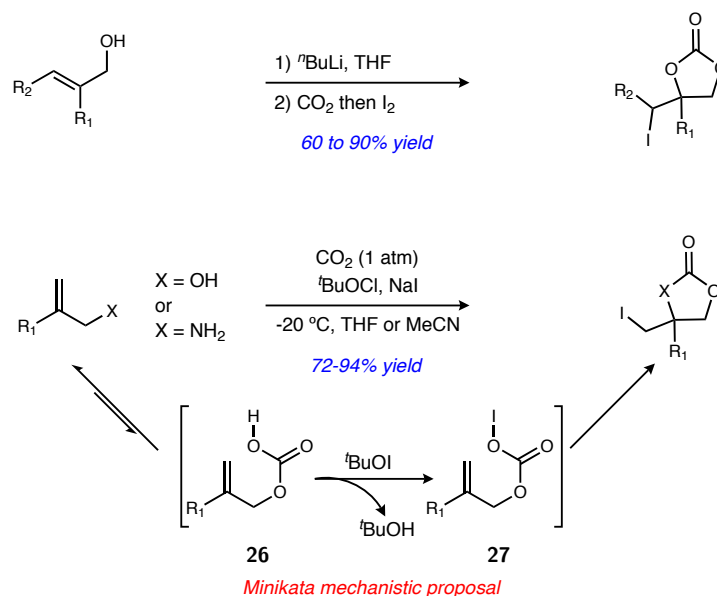
Scheme 6: Early methods for alkene functionalization with CO_2

Demonstrated throughout this section is the evolution of approaches for catalytic stereoselective synthesis of cyclic carbamates. Most of the methodology is fraught with high pressures, toxic metals, and high temperatures which are unraisable in to scale-up and industry. An approach that embodies the values of mild reaction conditions and non toxic reagents such as organocatalysts, while maintaining high regio- and enantio-selectivity would be of value to the synthetic community.

1.2 Development of an enantioselective iodocarbonation reaction and mechanistic insights

1.2.1 Proposal for an enantioselective CO_2 capture halocyclization reaction

Extending the methodology from carboxylic acids, using StilbPBAM·HNTf$_2$ (**2**) was envisioned to achieve activation and stereocontrol in a three component CO_2 capture/cyclization strategy. Multicomponent reactions can be difficult to catalyze in an asymmetric fashion due to the number of possible fleeting intermediates whose rates of formation and consumption must be controlled. Multicomponent reactions often employ a metal catalyst and an organic ligand to achieve stereoselection.[56] However, examples of multi component organocatalyzed reactions are not abundant, and even fewer form an enantioenriched product. The difficulties lie in the ability to control the enantioselective step in an organized manner. In a simple proposed reaction (Scheme 7) one can envision that there are three distinct steps (in no particular order) that would need to be controlled in an enantioselective halocarboxylation reaction. One is capture of CO_2, to make an alkyl carbonic acid **28**, followed by halonium formation **29**, and finally the cyclization and moreover if the carbonic acid formation and reaction are not facilitated by the catalyst then the background reaction will dominate, forming racemic product.

A bifunctional BAM-based organocatalytic method is now applied to an unprecedented enantioselective CO_2 capture reaction. Carbon dioxide is a key reagent and its innovative use as an oxygen donor is highlighted. The focus is as follows:

1. *To develop and optimize new CO_2 capture reactions using bifunctional catalysts,*

---

[56]Perreault, S.; Rovis, T. *Chem. Soc. Rev.* **2009**, *38*, 3149–3159.

while achieving high enantioselection and yields.

2. *Use analytical tools and experimental design to gather mechanistic insight into the*
   iodocarbonation reaction.
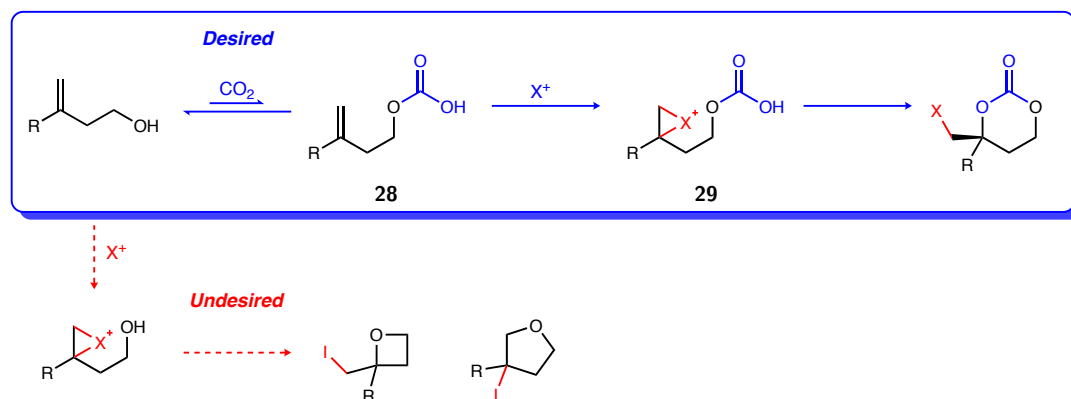
Scheme 7: Three component reaction

1.2.2 Initial investigation and Reaction Optimization

An innovative approach to asymmetric cyclic carbonate formation using a bifunctional BAM catalyst has recently been realized.[57] Preliminary work centered on development of ideal reaction conditions and catalyst. Using an alkyl 1,1-disubstituted homoallylic alcohol **30** as a model substrate and PBAM·HNTf$_2$ (**32**), a summer REU student Wei-wei Wang, found reaction conditions that would achieve up to 68% ee and 54% yield (Scheme 8). These results were extremely promising but lacked the good yields and enantioselection that would make this reaction useful. The goals regarding optimization of this reaction were to *a) increase the yield, b) increase the enantioselection, and c) to lower catalyst loading and time of reaction.*

---

[57]Vara, B. A.; Struble, T. J.; Wang, W.; Dobish, M. C.; Johnston, J. N. *J. Am. Chem. Soc.* **2015**, *137*, 7302–7305.
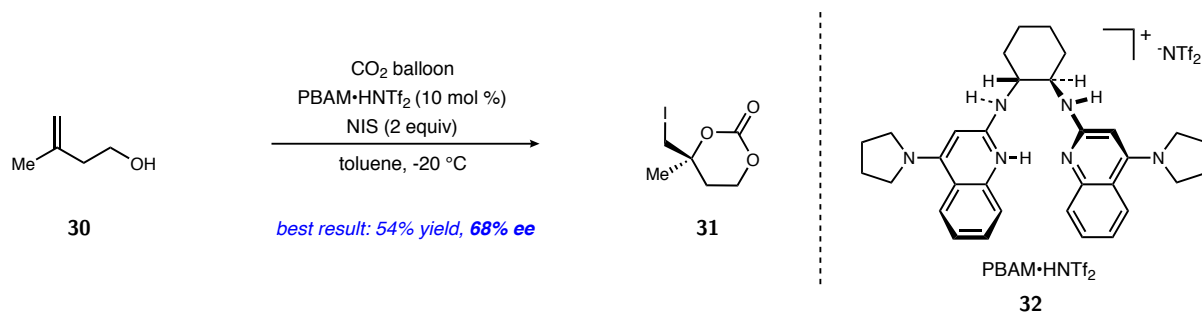
Scheme 8: Initial results and conditions for the BAM catalyzed iodocarbonation reaction

The initial experiments were directed at probing the effects of each reagent systematically to obtain the elusive high yield and enantioselection. Previous experiments demonstrated the necessity of using super-stoichiometric amounts of N-iodosuccinimide (NIS) due to possible iodination of the catalyst (see Scheme 1, 3' position of **2**). Addition of NIS to catalyst **2** in CDCl$_3$ shows a disappearance the 3' quinoline peak suggesting iodination of the catalyst. However, besides NMR experiments that do not replicate reaction conditions, no evidence is put forward to characterize **2** + I or **2** + 2I as the active catalyst. A short screen of loading amounts of NIS provided the same conclusion as the iodolactonization: the optimal amount was 1.2 equivalents. Upon further investigation, using the specific reaction conditions of toluene at $-20\,°C$, followed by a typical workup (see appendix 4.1) and LC-MS analysis, evidence suggested that the catalyst is not iodinated at the 3-position. Without an understanding of the benefit of excess loading of NIS, we continued with the optimal loading of 1.2 equivalents of NIS for the rest of the investigation. Examination of other sources of iodine or bromine did not provide the methyl substituted carbonate in higher % ee. Moving forward, NIS was chosen as the optimal source of electrophilic halogen, and catalyst modification were investigated.

Previous studies in the Johnston lab indicate that enantioselection may be affected

Table 1: *N*-Iodosuccinimide Screen
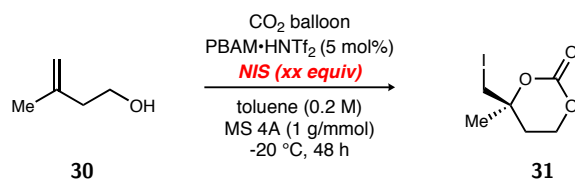
entry	NIS (equiv)	yield[a]	ee (%)[b]
1	0.5	12	**69**
2	1.0	49	**73**
3	2.0	54	**64**

[a]Isolated yields are listed. [b]Enantiomeric excess (% ee) determined by HPLC chiral stationary phase.

by the catalyst backbone, basicity, and the counterion of the catalyst salt.[58] A small library of catalysts were evaluated in the iodo-carbonation reaction. Laid out in Table 2A are triflic acid salts of various catalysts and their results in the iodocarbonation reaction (**33**-**38**). Additional groups to increase sterics of the catalyst showed no improvement shown by **34** and **35**. Changes to the backbone in **37** and **38** do not increase enantioselection as well. The next focus was the use of a slightly more dissociated counterion that proved optimal for the aforementioned iodolactonization reactions, the triflimide counterion (Table 2B). The triflimide salts did, as expected, achieve a slightly higher % ee than their triflic acid counterparts. In this sequence of catalyst salts, quinoline electronics were altered in **41** and **42** with no large effect on enantioselection. At this point the highest enantioselection obtained was around 70%. From these results it is clear that the addition of CO_2 and subsequent cyclization can be catalyzed in an asymmetric fashion albeit with lower enantioselection than desired.

A plaguing problem was the reaction time that extended beyond 2 days. A test of additives to the reaction, in an effort to increase the reproducibility and yield, was con-

---

[58]Dobish, M.; Johnston, J. *J. Am. Chem. Soc.* **2012**, *134*, 6068–6071; Johnston, J. N.; Davis, T. A.; Wilt, J. C. *J. Am. Chem. Soc.* **2010**, *132*, 2880–2.

Table 2: Catalyst Screen: A) Triflic Acid Counterion, B) Triflimidic Acid Counterion

A) Triflic Acid BAM Catalysts

33 PBAM (**41% ee**)

Triflic Acid
pK$_a$ = -12[a]

34 ^{7,8}Me$_2$PBAM (**-5% ee**)

35 ^{8}MePBAM (**7% ee**)

36 ^{4}Me$_2$NStilbBAM (**0% ee**)

37 StilbPBAM (**35% ee**)

38 ^{4}MeOStilbBAM (**25% ee**)

[a] Raamat, E. et al. *J. Phys. Org. Chem.* **2013**, *26*, 162

B) Triflimidic Acid BAM Catalysts

39 PBAM (**70% ee**)

40 ^{6}MeOPBAM (**50% ee**)

Bistriflimide

2 StilbPBAM (**64% ee**)

41 ^{6}MeOStilbPBAM (**65% ee**)

42 ^{7}MeOStilbPBAM (**67% ee**)
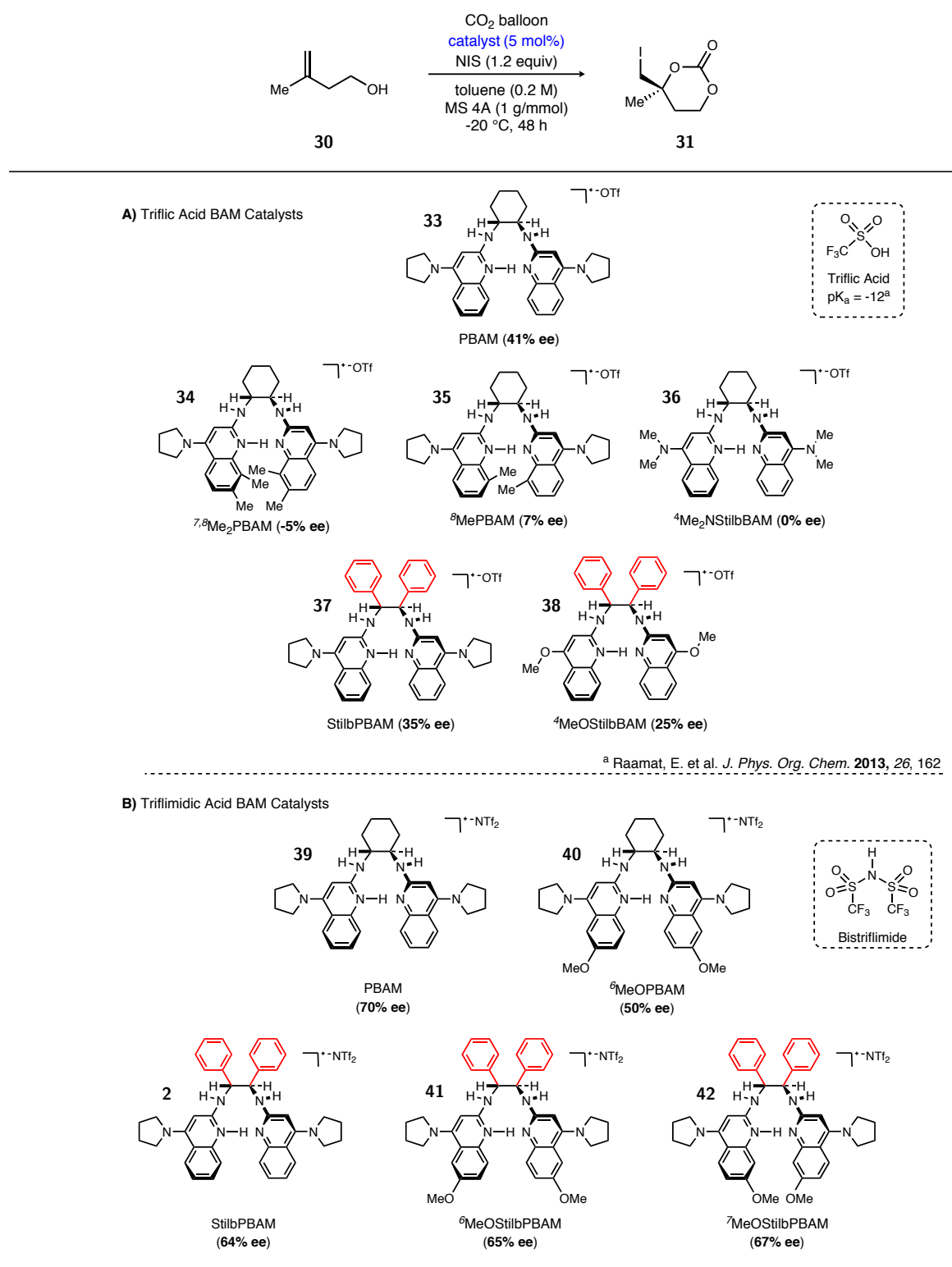
ducted. Previous studies have demonstrated that CO_2 can be absorbed by 4 Å molecular sieves (MS 4A) and this was the first additive that was used in the iodocarbonation

reaction.[59] Indeed the conversion and yield were increased after 48 h at $-20\,°C$. The increase in reproducibility and yield with the addition of MS 4A was welcome but not fully understood at this point. Although the initial reasoning for using molecular sieves was for increased CO_2 availability, upon further investigation trace amounts of water in the reaction was hypothesized to affect the catalyst.
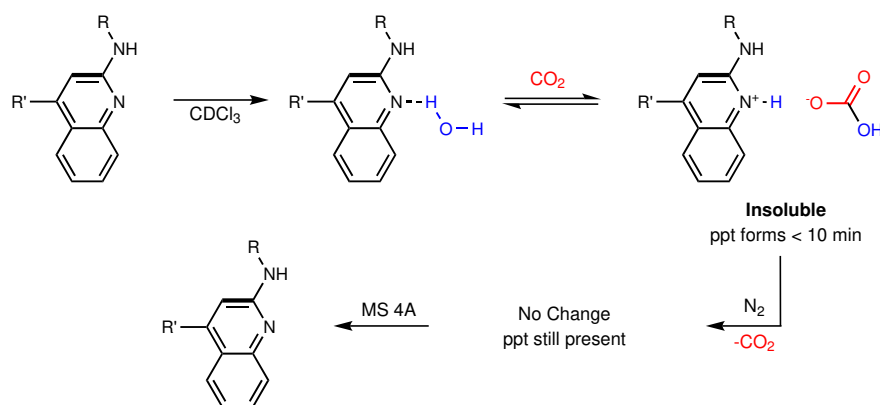
Figure 7: Catalyst bicarbonate salt formation

The inconsistency between initial experiments when using MS 4A were absent can be explained by a deleterious catalyst pathway involving a bicarbonate salt (Figure 7). Trace water in the solvent or reagents can, once CO_2 is added, form bicarbonate which can subsequently be deprotonated by the catalyst providing the *insoluble* catalyst bicarbonate salt. This amount of catalyst removed from the reaction would vary depending on the trace amounts of water in the solvent and therefore would provide much different levels of conversion from reaction to reaction. Using MS 4A was the solution to the reproducibility problems that pervaded the early optimization stages but results using **30** remained poor.

At this point the yields were not optimal and conversion measurements by NMR of crude reaction mixtures were necessary for ongoing studies. 3-Methyl-3-butene-1-ol **30** used as the starting material was not optimal due to its volatility. Although this is

---

[59]Siriwardane, R. V.; Shen, M.; Fisher, E. P.; Poston, J. A. *Energy & Fuels* **2001**, *15*, 279–284.

convenient for purification, no accurate conversions measured by ^{1}H NMR, or by recovery after flash chromatography could be obtained. The next step was to investigate alternate substrates that would be less volatile and perhaps give the high enantioselection desired.

Table 3: Additives and reaction concentration for optimization of the iodocarbonation reaction

entry	additive	concentration	yield^a	ee (%)^b
1	-	0.1 M	33	**36**
2	MS 4A	0.1 M	35	**60**
3	MS 4A	0.2 M	51	**89**
4^c	MS 4A	0.4 M	83	**91**

^{a}Isolated yields are listed. ^{b}Enantiomeric excess (% ee) determined by HPLC chiral stationary phase. ^{c}Run with 1 g of starting material.

An aryl substituted alkene **43** was the next logical step as it it most similar to the earlier iodolactonization reactions. Submitting this to the newly optimized reaction conditions and using PBAM·HNTf$_2$ **32** as the catalyst, 70% ee was obtained, minimally better than the methyl substituted alkene. However, using StilbPBAM·HNTf$_2$ **2** (a stilbene diamine backbone as opposed to cyclohexane diamine) 60% ee was achieved reproducibly, with a lower than optimal yield (Table 3, entries 1 and 2). Full conversion was a problem and we supposed that low measured % ee was due to background reactivity with unreacted alkene during the quench. The final goal was to limit the reaction time to 48 hours and increase conversion. By simply increasing the concentration to 0.4 M (Table 3, entry 4) from 0.2 M (Table 3, entry 2) the reaction could achieve > 90% conversion in 48 h with 91% ee.

Upon verification of this result, the subsequent course of action was to broaden the aryl substituted substrate scope, in order see if other substitutions were amenable to the

Table 4: Substrate scope of iodocarbonation reaction using 1,1-disubstituted alkenes
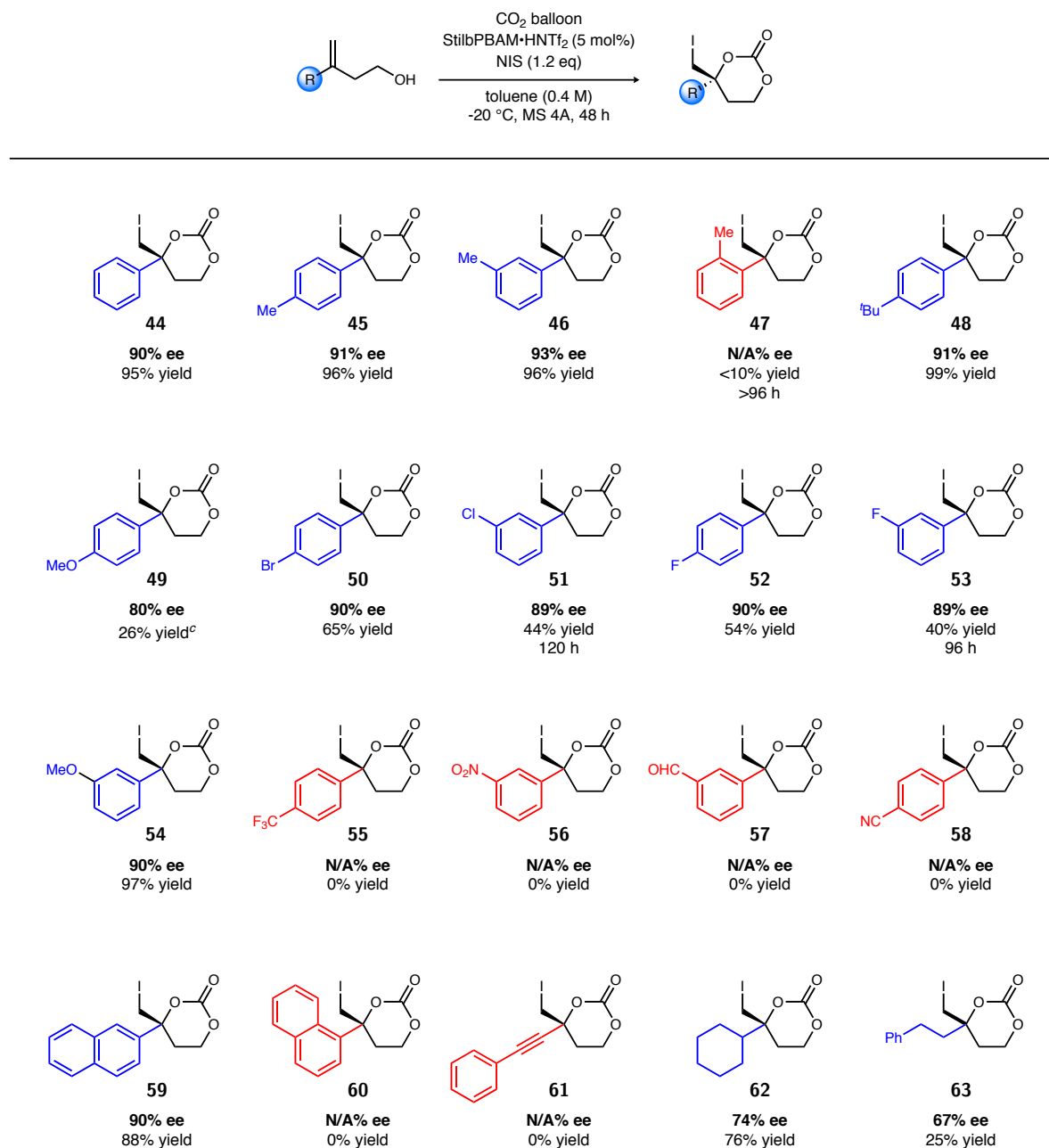
Reaction scheme: R–(alkene)–OH with CO$_2$ balloon, StilbPBAM·HNTf$_2$ (5 mol%), NIS (1.2 eq), toluene (0.4 M), -20 °C, MS 4A, 48 h → iodocarbonate product

44	**45**	**46**	**47**	**48**
90% ee	91% ee	93% ee	N/A% ee	91% ee
95% yield	96% yield	96% yield	<10% yield >96 h	99% yield
49	**50**	**51**	**52**	**53**
80% ee	90% ee	89% ee	90% ee	89% ee
26% yield^c	65% yield	44% yield 120 h	54% yield	40% yield 96 h
54	**55**	**56**	**57**	**58**
90% ee	N/A% ee	N/A% ee	N/A% ee	N/A% ee
97% yield	0% yield	0% yield	0% yield	0% yield
59	**60**	**61**	**62**	**63**
90% ee	N/A% ee	N/A% ee	74% ee	67% ee
88% yield	0% yield	0% yield	76% yield	25% yield

^{a}Isolated yields are listed. ^{b}Enantiomeric excess (% ee) determined by HPLC chiral stationary phase. Absolute stereochemistry for **44** determined by X-ray analysis and remaining examples were assigned by analogy. Reactions were run on 0.1 mmol scale and 0.4 M in toluene. ^{c} Reaction temperature -50 °C, this substrate is prone to decomposition at room temperature.

iodocarbonation reaction. The reaction is fairly robust and many aryl-substituted alkenes were reactive however there were a few alkenes that did not react. The substituted-phenyl alkenes was tolerable to many electron neutral and donating groups. A small decrease in enantioselection was observed with strong electron donating groups shown by the *para*-methoxy phenyl **49**. On a side note, these *para*-methoxy substituted alkenes have proved problematic in electrophilic halogen functionalization.[60] As a general trend, the electron withdrawing groups -CF_3 **55**, -NO_2 **56**, -CHO **57**, and -CN **58** substituted on the aryl ring showed no reactivity. This is not unexpected as the alkene needs to be sufficiently nucleophilic to capture the electrophilic iodine. Since the alkene is in conjugation with the aryl substituent, the reasoning was that lower reactivity should be expected when making the halonium intermediate. The puzzling result was the *ortho*-methyl substituted arene **47**. This is a slightly election donating group and would be expected to show conversion, however no reactivity was observed. This may be due to overriding steric factors when the substrate binds to the catalyst, also demonstrated by the even more sterically congested 1-naphthyl substrate **60**. With many aryl groups investigated in the iodocarbonation reaction, other aliphatic and more highly substituted alkenes were sought fore examination.

Some aliphatic substrates were investigated in order to probe the enantioselection of alkenes lacking the aryl substituent which often achieve the highest selectivity in BAM catalyzed cyclizations. The optimized iodocarbonation reaction is amenable to trisubstituted alkenes such as **64** affording a 6-6 spirocycle **65** although with lower ee (70% ee). This particular substrate is interesting because the trisubstituted alkene provides a more hindered π-face, which would be expected to exhibit much lower reactivity than observed.

[60]Denmark, S. E.; Kuester, W. E.; Burk, M. T. *Angew. Chem. Int. Ed.* **2012**, *51*, 10938–53.

Table 5: Alkyl Substrates

$$\text{Starting Material} \xrightarrow[\substack{\text{toluene (0.4M)} \\ \text{-20 °C, MS 4A, 48 h}}]{\substack{\text{CO}_2 \text{ balloon} \\ \text{StilbPBAM·HNTf}_2 \text{ (5 mol\%)} \\ \text{NIS (1.2 eq)}}} \text{Product}$$

Starting Material	Product		Starting Material	Product

64
- hindered π-face
- cyclic *E*-alkene
- tri-substituted

65
62% yield, **70% ee**

66

67
30% yield, **0% ee**
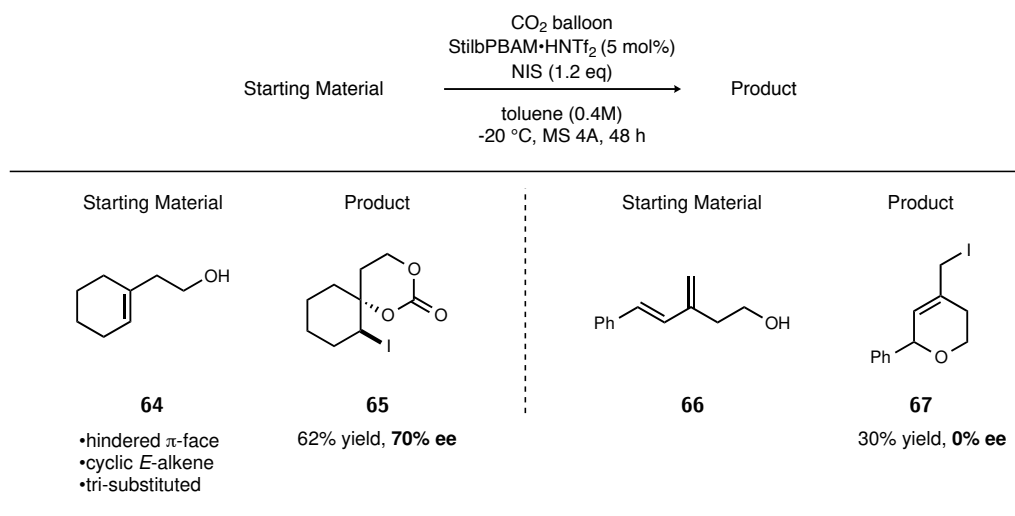
[a]Isolated yield. [b]Enantiomeric excess (% ee) determined by HPLC chiral stationary phase.

This substrate was also submitted to the reaction conditions on a gram-scale using 3 mol% catalyst with no decrease in yield or enantioselection demonstrating the robustness of the catalyst and the optimized conditions. Finally the spirocycle can be fractionally recrystallized up to 85% ee. Using conjugated alkene **66** we found that etherification proceeded faster than the carbonation reaction, affording 6-membered pyran **67**. This result is not surprising as the the etherification product is a result of an intramolecular reaction compared to the slow capture of CO_2 and subsequent cyclization.

With the reaction conditions optimized and a substrate scope finished, the utility of the products was briefly explored. During the exploration of derivatives it was found that the iodocarbonates are unstable and often will undergo a retro reaction to the starting material **43**. Alternative methods for creating a chiral oxygen-carbon bond on a fully substituted carbon are often difficult so these routes to reduced and hydrolyzed products have the potential to be incredibly useful. Note that in these reactions shown in Figure 29 the enantioenrichment is not eroded. The iodide can be functionalized with a tributyltin hydride reduction to furnish **68**. Lithium aluminium hydride reduction of the carbonate

proceeds well to give the diol **69**. Also notice that in the LiAlH$_4$ reduction, CO$_2$ is formally reduced to methanol through the carbonate intermediate. Finally hydrolysis of the carbonate will provide the enantioenriched homoallylic epoxide **70**.
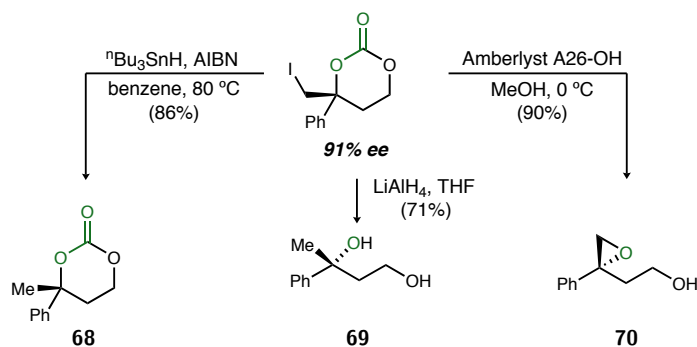
Scheme 9: Derivatives of iodocarbonates

Key findings en route to final optimized reaction conditions for the iodocarbonation reaction are: a) MS 4A increase reproducibility, b) more concentrated reactions performed better, and c) the scope is limited to aryl 1,1-disubstituted alkenes (for above 88% ee). Mechanistic understanding of the iodocarbonation reaction was limited to the hypothesis of our catalyst as a bifunctional catalyst (Figure 1, complex **1**). More studies were needed to probe this hypothesis and elucidate the catalyst role in complexing and stabilizing CO$_2$ adducts such as **28**.

1.2.3 Mechanistic studies of the iodocarbonation reaction

To further investigate the mechanism of the iodocarbonation *in situ* attenuated total reflectance (ATR) FTIR spectroscopy was employed. As previously described (see Figure 1) the iodocarbonation reaction has three distinct steps that need to be realized in order to obtain enantioenriched carbonate product: iodination of the alkene either through a cyclic iodonium or a carbocation; capture of CO$_2$ by the alcohol; and enantioselective cyclization. At the outset of this study there were a few hypotheses for CO$_2$ coordination.

33

In situ IR provided evidence for carbonic acid (**71**) or carbonic acid catalyst complex (**72**) formation.

Scheme 10: Carbonic acid stabilization by amidine of catalyst and associated absorption (ReactIR) peaks

When the alcohol is added to toluene without catalyst, the disappearance of the alcohol peak occurs when a) only 4 Å molecular sieves are added or b) when stoichiometric NIS is added. The latter supports the previous hypothesis by Minikata and co-workers that the hypoiodate is formed from the substrate alcohol and iodonium, which can then act as an intramolecular source of electrophilic iodine.[61] However no appreciable background reactivity is detected when the reactions are run without a catalyst at $-20\,°C$. The reaction conditions for the iodocarbonation reaction using StilbPBAM·HNTf$_2$ **2** are slightly different than that of Minikata which uses acetonitrile, because our reaction uses toluene, a solvent in which NIS has low solubility. This slow background reaction could point to coordination or activation of the *N*-iodosuccinimide by the catalyst.

One step that is vital for the reaction is the capture of CO_2 and formation of the carbonic acid. Using the in situ IR, the slow formation of the alkyl carbonic acid can be followed in the absence of any *N*-iodosuccinimide. The IR data shows a shift from a large broad $-OH$ stretch at $3400\,cm^{-1}$ to a sharper peak at $3290\,cm^{-1}$ (Figure 8).

In the absence of the catalyst this shift is not observed. The carbonate C-O bond

---

[61]Minakata, S.; Sasaki, I.; Ide, T. *Angew. Chem. Int. Ed.* **2010**, *49*, 1309–1311.

Figure 8: IR trace of carbonic acid formation

formation can also be followed by a large increase in the 1300-1400 region. In an attempt to elucidate if this is the rate determining step, the alcohol was allowed to be converted to the putative alkyl carbonic acid monitored by IR for 24 h (carbonic acid formation can be followed as seen in Figure 9). The hypothesis is that if carbonic acid formation is the rate determining step, then addition NIS would allow for rapid formation of iodonium and concurrent product formation. NIS was added after 24 h and after 6 h more, no product was observed by IR and only minimal product formation was observed after reaction workup and analysis by ^{1}H NMR.[62] This suggests that another facet of this reaction may be the limiting factor to the rate or the detrimental catalyst-bicarbonate complex is forming.[63]

The insolubility of NIS in toluene may play a role in limiting the rate of the iodocarbonation reaction. The experimental solubility of NIS in toluene is about 3 mg/mL at room temperature. In a typical reaction, 26 mg of NIS (1.2 eq) and 0.5 mL of toluene (0.4 M) are used. From this it can be calculated that there is only 1.5 mg of NIS (5.7%)

---

[62]Typical conditions are 48 h reaction times.

[63]These investigations were performed before the hypothesis that detrimental carbonic acid·catalyst complexes could form. MS 4A were left out of these experiments initially because solids could block the IR window.
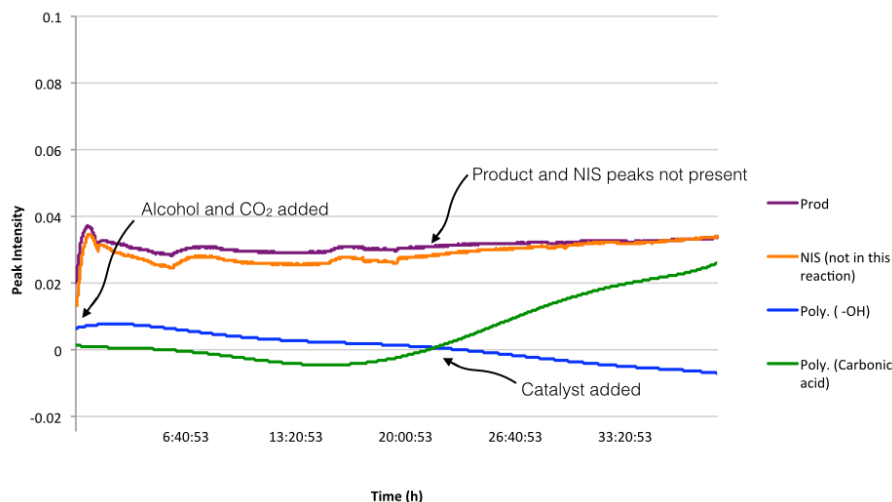
Figure 9: ReactIR Sspectra for carbonic acid formation

available at any time (ignoring any competing solubility of succinimide and the reaction temperature of $-20\,^\circ\text{C}$). This is beneficial to the CO_2 capture reaction because it slows the competing 4-*exo* or 5-*endo* etherification reactions. The solubility of NIS however could be one of limiting factors of this reaction. One hypothesis is that StilbPBAM·HNTf$_2$ may act as a phase transfer catalyst to draw the solid NIS into solution and presenting it to the substrate (Figure 10).[64] Another possibility is that the low solubility of NIS in toluene is suppressing background reactivity, allowing for the catalyst to associate with starting materials and catalyze the reaction. Other more soluble iodine sources such as molecular iodine (I_2) provide complex reaction mixtures and no desired product formation (most likely 4-*exo* etherification is faster than CO_2 capture and catalyzed cyclization when a strong and soluble halogen source is employed).
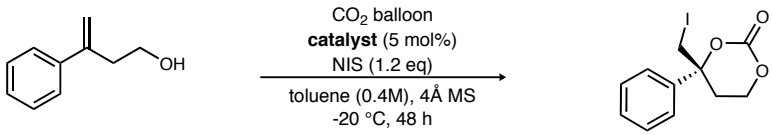
These studies demonstrate the necessity of the catalyst for the formation of the carbonic acid using a homoallylic alcohol. The unique characteristics of this bifunctional BAM catalyst may allow the coordination of a CO_2 adduct. Insight into the mechanism of this unique reaction is a key aspect to understanding the observed reactivity

---

[64] Jacobsen, E. N.; Brindle, C. S.; Yeung, C. S. *Chem. Sci.* **2013**, *4*.
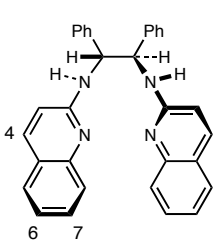
as well as development of new reactions using bifunctional catalysts. In order to better understand the balance between acidity of the substrate and coordination of the catalyst, some modifications to StilbPBAM·HNTf$_2$ were synthesized, and then evaluated in the iodocarbonation reaction.

Table 6: Electronic effects of StilbPBAM·HNTf$_2$ on the iodocarbonation reaction

entry	catalyst	yield (%)	ee (%)
1	[4]Cl-StilbBAM·HNTf$_2$	0	n/a
2	[4]HQuin-StilbBAM·HNTf$_2$	10	22
3	[4]MeO-StilbBAM·HNTf$_2$	12	29
4	StilbPBAM·HNTf$_2$	78	93
5	[7]F-StilbPBAM·HNTf$_2$	69	88
6	[7]MeO-StilbPBAM·HNTf$_2$	60	83
7	[6,7](MeO)$_2$StilbPBAM·HNTf$_2$	0	n/a

cutoff of solubility

[a]Isolated yield, [b]Enantiomeric excess (% ee) determined by HPLC chiral stationary phase.

Table 6 shows the electronic effects of the catalyst on the reaction. StilbPBAM·HNTf$_2$ is originally the optimized catalyst for this reaction and perturbing the electronics of the catalyst in the iodocarbonation reaction shows marked effects on conversion and enantioselection. However results for 7- and 6,7-dimethoxy substituted catalysts (Table 6, entries 6 and 7) presumably are poor due to insolubility noticed at the optimal concentration of 0.2 M. The matching of the substrate to the electronics of the catalyst are crucial for maintaining a hydrogen bond or tight ion pair between the catalyst and carbonate. This electronic effect can be elaborated to incorporate other substrates into a CO_2 capture reaction by careful modification of the catalyst to match the acidity of the substrate.

The subtle interplay of electronics of the catalyst and solubility are key facets to the iodocarbonation reaction. The fleeting nature of the carbonic acid intermediate promotes side reactions such as etherification or halohydrin formation. Critical findings were that
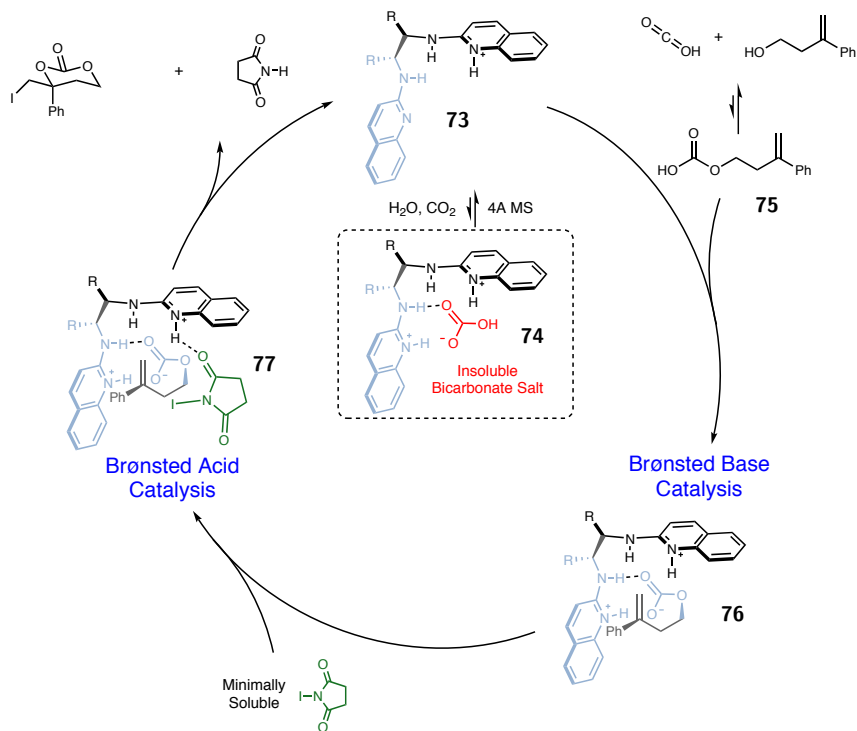
Figure 10: Proposed catalytic cycle of bifunctional BAM-catalyst

water can form a deleterious insoluble bicarbonate complex **74** in toluene, but reverts upon the addition of a desiccant MS 4A. Mechanistically, we can infer that if the catalyst can stabilize a bicarbonate adduct **74** that the carbonic acid intermediate **75** can coordinate to the Brønsted basic side of the catalyst (Figure 10, **76**) to stabilize the carbonate anion, effectively forcing the equilibrium to formation of **75**. No mechanistic data to date explains the rest of the mechanism,[65] but the hypothesis is that the bifunctional nature will allow complex **77** to form. Complex **77** coordinates both the nucleophile *and* electrophile which imparts high control of the cyclization.

---

[65]One observation that does support the proposed hypothesis is that only halogen sources with carbonyls will impart any enantioselection. However, if this bifunctional nature is at play, other halogens should be amenable to the cyclization but when NBC or NCS is used, low enantioselection is observed.

1.3 Development of the iodocarbamation reaction and mechanistic insights

1.3.1 Introduction to the iodocarbamation reaction

At the same time as success was found for the iodocarbonation reaction using homoallylic alcohols, an iodocarbamation reaction using a homoallylic secondary amine was in development. Dr. Roozbeh Yousefi found that using a similar catalyst ^{7}MeOStilbPBAM·HNTf$_2$ **42** in more dilute conditions can afford the corresponding carbamates in high yield and enantioselectivity (Figure 11).[66] The use of the more electron-rich 7-methoxy catalyst proves essential for the high conversion and enantioselection in the iodocarbamation reaction.
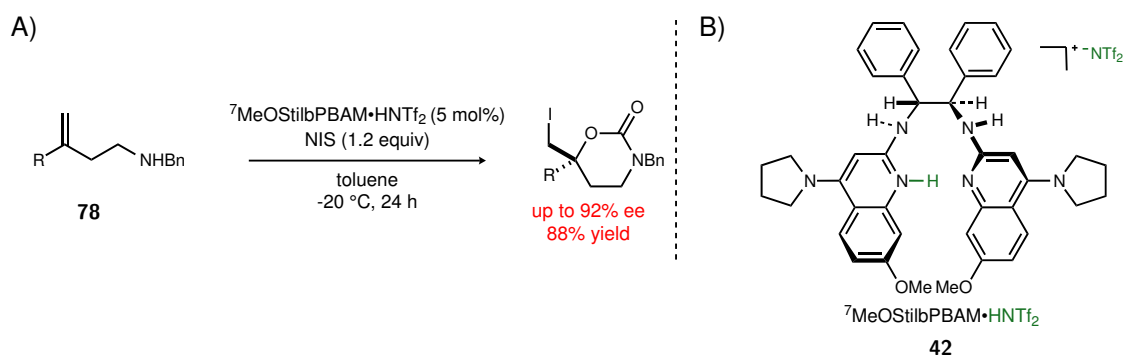
Figure 11: A) Enantioselective iodocarbamation B) Triflimidic acid salt of ^{7}MeOStilbPBAM

1.3.2 Mechanistic investigation of the iodocarbamation reaction

During optimization, Dr. Yousefi determined that a more Brønsted basic catalyst is crucial to high yield and enantioselectivity. These results demonstrate the necessity for pK$_a$

---

[66]Although high reactivity and enantioselectivity was observed, reproducibility plagues this reaction. For more complete details see Appendix 4.1.

matching between the hydrogen bond acceptors/donors in BAM catalyzed halofunctionalization reactions. The CO_2 adduct of an amine is longer lived than its homoallylic alcohol counterpart (*vida supra*) allowing for detailed investigation into the mechanism behind the CO_2 capture reactions. We undertook an investigation of two main factors in the iodocarbamation reaction: 1) titrations to determine the pK_a of catalysts StilbPBAM **2** and [7]MeOStilbPBAM **42**[67] and 2) ^{19}F NMR studies using diffusion-ordered spectroscopy (DOSY) to elucidate molecular weights of catalyst-substrate complexes in solution.

Previous findings indicate that the Brønsted basicity of the BAM catalyst is important for increased reactivity but does not greatly affect selectivity.[68] In the course of investigating the basicity of the BAM catalysts, the pK_a of H,Quin-BAM was measured by NMR titrations in DMSO to be 5.78.[69] The basicity of the catalyst clearly has an effect on the reactivity in the iodocarbamation reaction with the more basic [7]MeOStilbPBAM triflimidic acid salt being optimal when compared to StilbPBAM·HNTf$_2$ (Figure 12). The pK_a's of both catalysts were measured, to demonstrate that the 7-position substitution with an activating group such as methoxy, has an affect on basicity. Upon pK_a titrations in DMSO following the reported procedure,[70] we found that the 7-methoxy substituted catalyst has a pK_a is 8.04 and the unsubstituted StilbPBAM has a pK_a of 7.88. Figure 12 shows the clear trend in reactivity going from the most basic [7]MeOStilbPBAM·HNTf$_2$ with an 82% yield and decreasing to the less basic StilbPBAM·HNTf$_2$ achieving a 10% yield. The selectivity is presumably such a drastic difference (92 and 50% ee) with the two catalysts due to the low conversion of the less reactive catalysts. The small amount

[67]The pK_a measurements were all conducted on the free base catalysts and not the salts which are represented in many of the figures.

[68]Dobish, M. C.; Johnston, J. N. *Org. Lett.* **2010**, *12*, 5744–5747; Johnston, J. N.; Davis, T. A.; Wilt, J. C. *J. Am. Chem. Soc.* **2010**, *132*, 2880–2.

[69]Hess, A. S.; Yoder, R. A.; Johnston, J. N. *Synlett* **2006**, *2006*, 0147–0149.

[70]Perrin, C. L.; Fabian, M. A. *Anal. Chem.* **1996**, *68*, 2127–2134.

of racemic material produced in the low yielding reaction has much more of a dramatic impact on measured % ee than in the high yielding cases. Many efforts over the years have tried to address this problem with different methods of quenching but in all cases when we observe low conversion, the enantiomeric excess is impacted as well. Additionally, the use of 100 mol% catalyst in the reaction conditions are not successful because all the catalyst does not go into solution. As a final note on this topic, if we force low conversion by limiting the I^+ source to 10% (and ideally there is no reactive I^+ around while quenching) we measure the same high % ee as that in the optimized conditions. The pK_a titrations do support the hypothesis that the 7-position substitution can increase the basicity but more mechanistic insight is needed to truly understand this reaction.
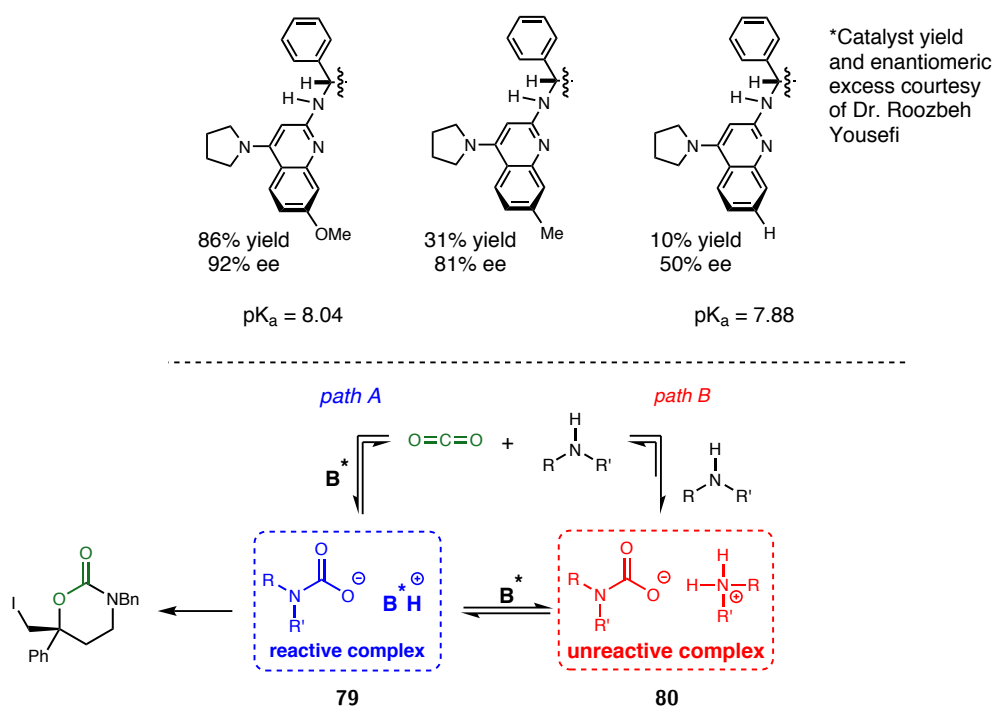
Figure 12: Effects of catalyst substitution on reactivity of the iodocarbamation reaction and mechanistic hypothesis of their affects

The supposition that the 7-position substitution of the catalyst can affect the basicity of the catalyst was finally supported experimentally by pK_a titrations. The hypothesis posited by Dr. Yousefi and I was that increased basicity in a catalyst could convert unre-

active aggregates of substrate$-CO_2^-\cdots{}^+$substrate complexes (unreactive complex **80** in Figure 12). There are two paths to arrive at the reactive complex **79** in Figure 12. Path A directly leads to the catalyst substrate complex that is necessary for product formation with high selectivity. Path B uses two molecules of substrate, one for capturing CO_2 and another as a base to deprotonate the carbamic acid intermediate. Since there is only 10 mol% catalyst, the hypothesis was that most of the substrate in the reaction conditions will be in the unproductive state as the unreactive complex. The equilibrium at $-20\,°C$ lies in favor of the CO_2 complex and was tested with low temperature NMR experiments. Upon addition of CO_2 to an NMR tube that contains substrate in d_8-toluene, we observe shifts by ^{1}H-NMR that indicate the CO_2 adduct is stable at low temperature (Figure 13). Unfortunately good spectral data is not obtained when 100 mol% of the catalyst is added to the amine/CO_2 adduct most likely due to the insolubility of the large amount needed for a 1:1 mixture with the substrate. With most of the substrate bound in complexes, the catalyst would need to convert the aggregates of substrate in order to make the reactive complex. This hypothesis needed further evaluation to determine the dominant complexes in solution.

Recently a method using ^{19}F DOSY NMR to characterize Brønsted acid-base complexes was reported.[71] Use of fluorine NMR greatly deconvolutes analysis of DOSY spectra due to the good separation of decoupled ^{19}F peaks. After diffusion rates are measured by NMR, internal standards of known formula weights are used to make a standard curve in which the formula weights of the unknowns can be calculated from their diffusion coefficients. Our catalyst salt ^{7}MeOStilbPBAM·HNTf$_2$ has two CF_3 groups for measurement of complexes in different environments.

---

[71]Subramanian, H.; Jasperse, C. P.; Sibi, M. P. *Org. Lett.* **2015**, *17*, 1429–1432.
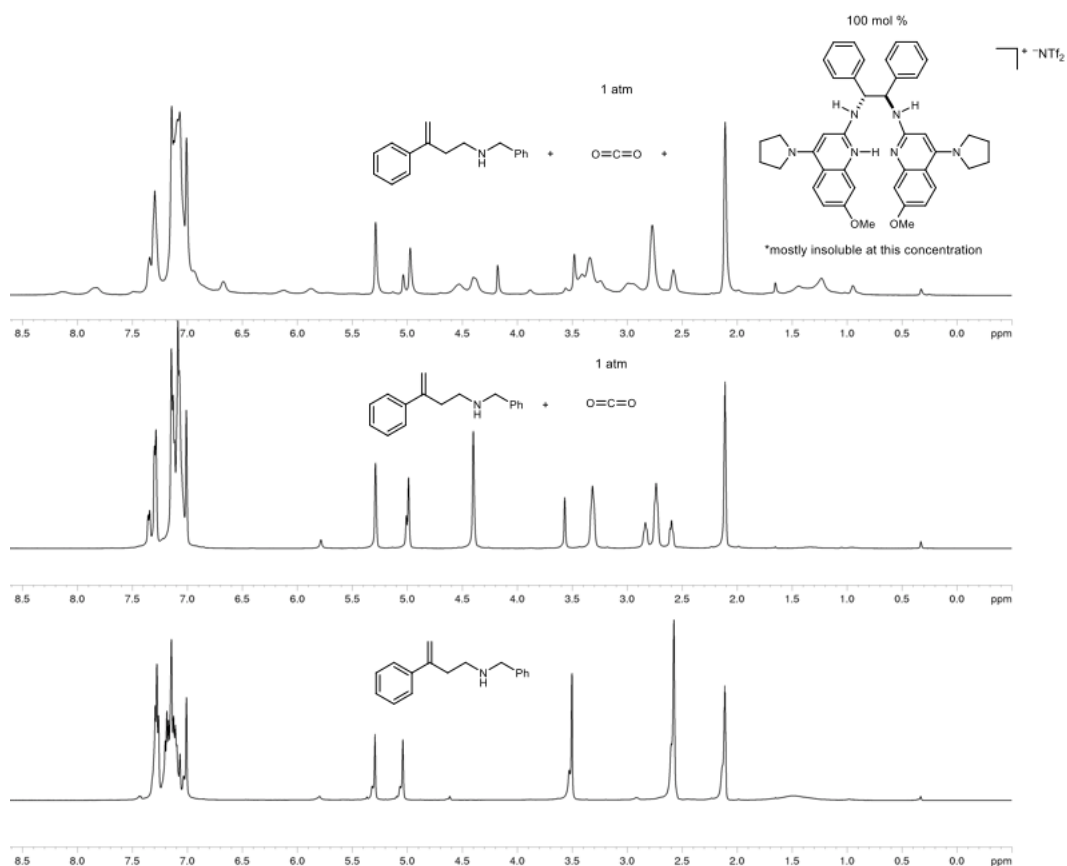
Figure 13: ^{1}H-NMR of substrate and resulting complexes at $-20\,^\circ$C

First CO_2 was added to a solution of only the substrate in d_8-toluene and the resulting formula weight calculated from the diffusion coefficients was 985, which correlates to 3 substrates and one CO_2 (Figure 14, complex-**81**) which has a formula weight of 960 (calculated error of 2.7%). This revises our hypothesis slightly so that now the unreactive complex in Figure 12 is not an aggregate of two substrates but most likely of three. This result still indicates that the resting state of the substrate, in the presence of CO_2, maybe in complexes such as **81**. These studies support the hypothesis that aggregates of substrate form in the presence of CO_2 but still leave us in the dark in regards to catalyst·substrate complexes.

To be productive, the catalyst must interrupt aggregates to form reactive complex **79** in Figure 12. The next logical step was to measure the dominant complex when

43
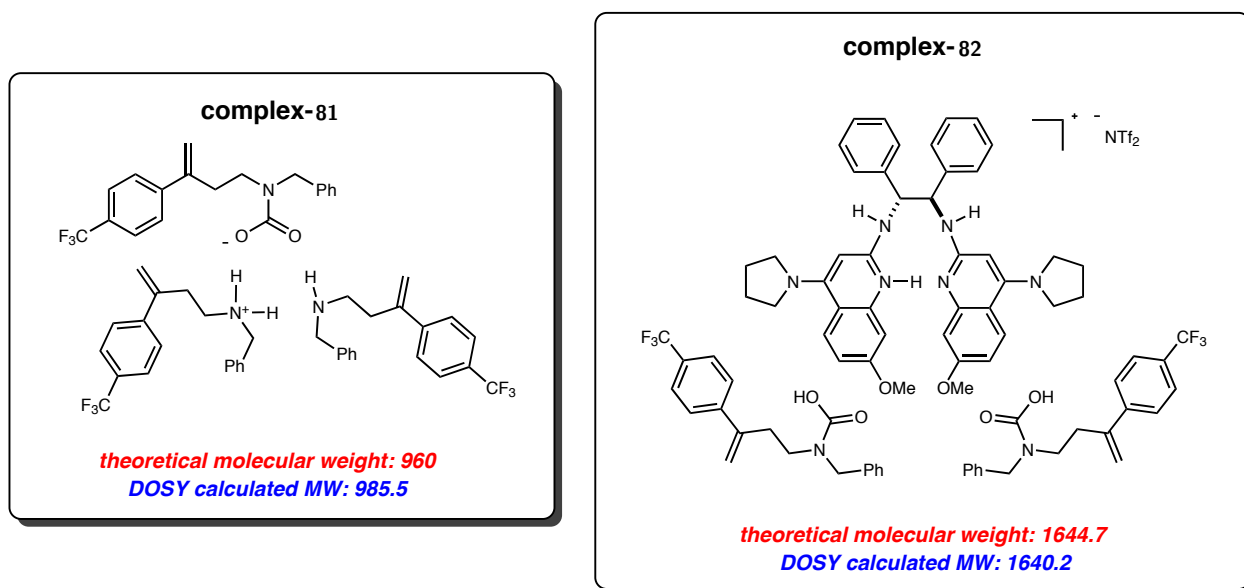
Figure 14: Theoretical and DOSY calculated weights of complexes observed without and with catalyst

there is a 1:1 mixture of ^{7}MeOStilbPBAM·HNTf$_2$ and substrate under an atmosphere of CO$_2$.[72] The formula weight can now be calculated from fluorine shifts on the substrate and on the catalyst giving two distinct measurements related ideally to the same complex. Gratifyingly, the substrate gives a formula weight of 1485, and the triflimide shift gives 1640. The latter weight of 1640 correlates well with two possible scenarios: first is shown in Figure 14 as complex-**82** with CO$_2$ incorporated into both amines and the second scenario could correlate with only one substrate as the CO$_2$ adduct (not shown but complex-**82** $-$CO$_2$). The hypothesized bifunctional nature of the catalyst (as in Figure 10) cannot be investigated using this method because the productive reaction (with NIS) would complicate the DOSY measurements. In addition, NIS solubility is low in toluene further complicating any studies that could be conducted by NMR in regards to catalyst·NIS complexes. It is clear from these experiments that when catalyst

---

[72]These studies were conducted in dilute conditions such that the whole mixture is soluble. Under normal reaction conditions, there is observed small amounts of precipitate that interfere with NMR experiments.

is in low quantity (i.e. 10 mol%), the substrates will form aggregates with 3 substrates, thus being the dominant form in solution. When catalyst is in present, the catalyst-substrate complex can be observed, indicating the ability of the catalyst to coordinate the substrate-CO_2 adduct. These experiments also address the equilibrium between the reactive $\rightleftharpoons$ unreactive complexes in Figure 12. The catalyst-substrate complex is clearly favored as indicated by the measurement of the diffusion coefficients and correlation with formula weight.[73]

The difficulty in controlling the equilibrium in formation of complexes of the amine starting material and CO_2 raise problems with high control and turnover in the iodocarbamation reaction. To complicate matters, low solubility of reactants in BAM-catalyzed CO_2 capture reactions result in difficultly in elucidation of full complexes (i.e. catalyst-substrate-NIS) in halocyclization reactions. The use of low temperature NMR in conjunction with ^{19}F DOSY have finally allowed a glimpse at probable complexes that form before electrophilic halogen is present. These studies suggest that the catalyst is capable of breaking substrate aggregates allowing for productive reactivity, the first picture we have captured of substrate·catalyst interaction in CO_2 capture reactions. Finally, continued studies for illumination of the halogen role are crucial for full understanding of BAM catalysis and sustainable new methodology development.

1.4 Conclusions and long term outlook

In conclusion, a mild method for CO_2 capture using a bifunctional organocatalyst has been developed. This reaction is unprecedented due to the fact there is no known enan-

---

[73]No measurements in the catalyst-substrate-CO_2 experiments would correlate to substrate aggregates being present. The only two diffusion coefficients observed were over 1400 MW.

tioselective organocatalyzed methods for CO_2 capture. In addition the low reactivity of alcohols towards CO_2 is overcome by balancing of substrate and catalyst acid/base properties. The iodocarbonation reaction is amenable to a wide array of aryl substrates except for electron withdrawing groups and steric introduction at the *ortho*-position. Using the information gained from the substrate scope, the mechanism of the iodocarbonation reaction was probed using *in-situ* ReactIR monitoring. This provided some valuable insight on the usefulness of BAM catalysis. The catalyst is necessary for the capture and possible coordination of CO_2 to form the carbonic acid intermediate. Due to the insolubility of NIS in toluene this may be a limiting factor of the observed rate, showing the necessity for the catalyst to coordinate to the *N*-iodosuccinimide in order to solubilize it. The understanding gained from the iodocarbonation and iodocarbamation reactions can now be extended to the development of new catalytic asymmetric methods.

An ordered network of hydrogen bonding (*vide infra*) between the protonated catalyst and NIS is possible, which in combination with the low solubility of NIS in toluene, aids the delivery of iodine to the substrate in the iodolactonization and iodocarbonation reaction. The bifunctional nature of the Brønsted acid BAM catalysts could allow for the coordination of both the nucleophile *and* the electrophile. A bifunctional catalyst would prove ideal for elaboration of the intramolecular halofunctionalization into intermolecular reactions. This can be envisioned by cutting the tether from the alkene and the acid (including the carboxylic, carbonic, and carbamic acid) providing a three component reaction Figure 15A.

Multi-component reactions theoretically are much harder to develop due to the decreased likelihood that three components can collide to make one product. In the case of the halofunctionalization the challenges to overcome are decreased reactivity, decreased
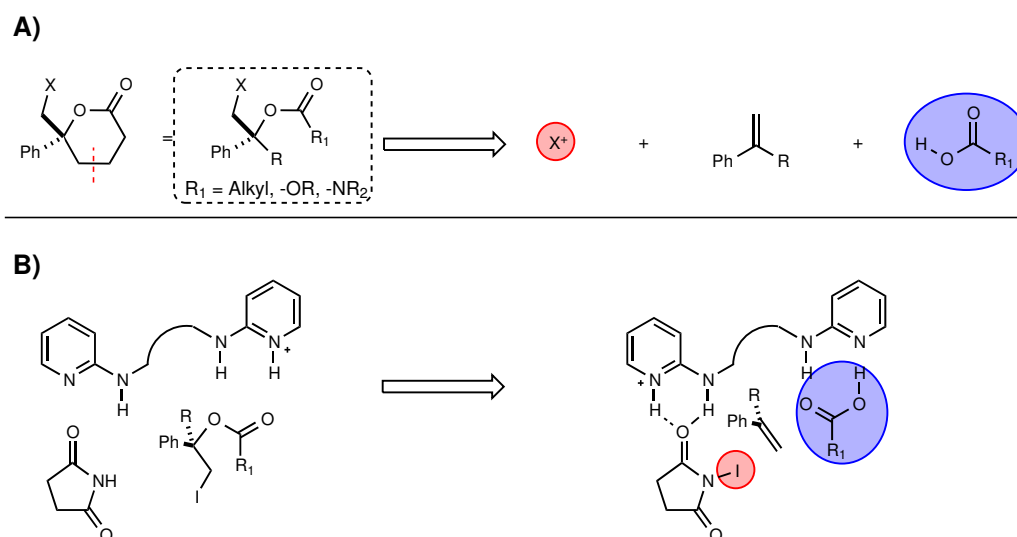
Figure 15: Intermolecular halofunctionalization

likelihood of a tight hydrogen bonding network with the catalyst, and background reactivity into undesired side products. Enantioselective intermolecular halofunctionalizations have been achieved in good yields and enantioselectivity by Snider and co-workers by using chiral sulfonium halides for chloro and iodohydroxylation reactions.[74,75,76] These examples demonstrate the ability to afford enantioenriched products from a three component halofunctionalization reaction however still use a stoichiometric chiral halide source to afford the product.

As in the preceding project with the iodocarbonation, a three component reaction proves difficult in controlling every step in an enantioselective fashion. The system developed in the Johnston lab appears to be ideal for elaboration to an intermolecular reaction. The ability to control both the nucleophile *and* the electrophile (see Figure 15B) provide a distinct advantage for expansion of the methodology using bifunctional catalysis such as StilbPBAM·HNTf$_2$.

[74]Cheng, Y. A.; Yu, W. Z.; Yeung, Y.-Y. *Org. Biomol. Chem.* **2014**, *12*, 2333–43.

[75]Brucks, A. P.; Treitler, D. S.; Liu, S.-A.; Snyder, S. A. *Synthesis* **2013**, *45*, 1886–1898.

[76]Snyder, S. A.; Tang, Z.-Y.; Gupta, R. *J. Am. Chem. Soc.* **2009**, *131*, 5744–5.

Any initial attempts at an intermolecular catalytic enantioselective halofunctional-ization reaction using BAM-based catalysts have not proven successful. Reactivity has been observed in various substrates, however no enantioselection has been obtained. The difficulty of controlling all three substrates with one catalyst will likely necessitate mod-ifications to the catalyst in order for a better reactive pocket. A variety of intra and intermolecular reactivity has been observed using some protecting groups, therefore it is crucial for future attempts to balance this reactivity.

The long term goals of a project that would focus on intermolecular reactivity are to develop one pot enantioselective reaction in route to di-functionalized alkenes such as diols, diamines, epoxides, and amino alcohols. The intermediate halohydrin that is currently attempting to be accessed in high enantioselection INT-**83** can lead to a variety of different di-functionalized products. One good example is starting with enantioenriched halohyrin intermediate **84**, using the Woodward and Prévost reactions would give access to enantioenriched *syn* and *anti*-diols shown in Figure 16.
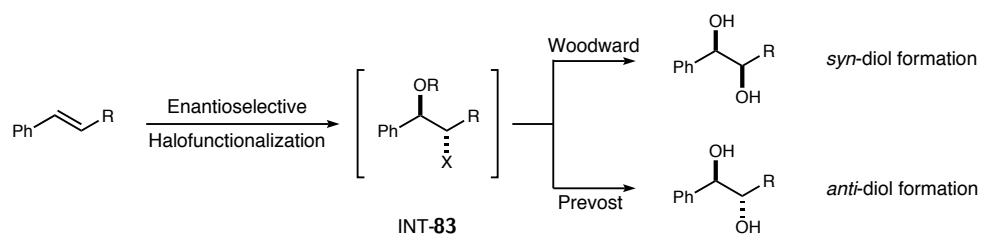
Figure 16: Long term goals of intermolecular halofunctionalization reaction creating *syn* and *anti*-diols

These organocatalytic reactions would allow for complimentary means to access enan-tioenriched diols without using toxic materials such as Osmium.

In conclusion, research into intermolecular catalytic enantioselective di-functionalization of alkenes is currently underway. The success may hinge on a better understanding of the catalytic system currently being used for other reactions such as the iodocarbonation and

iodolactonizaiton reaction. Ongoing studies probing catalyst structure and function are will likely lead to stronger hypotheses in moving forward. The continued development of new methodology using BAM catalysts will undoubtedly lead to new systems that will find success in the intramolecular halofunctionalization reaction.

The role and coordination of the nucleophile has been investigated and results suggest a complex of catalyst·substrates. Although many hypotheses in this chapter have presented the catalyst as bifunctional, and hyped the benefits of such a system, no evidence to date has supported this mechanism besides the necessity for a carbonyl on the halogen source. Additionally, the role of the counterion is not fully understood but provides an incredibly useful strategy for study of new reactions. Continued study of this system is vital for future reaction prediction, development, and optimization. Despite these unknowns, carboxylic, carbonic, carbamic, and phosphoramidic acids are all amenable to enantioselective BAM-based catalysis and new reactivity is currently being studied and applied.

Chapter 2   Enantioselective urea synthesis

2.1   Introduction

2.1.1   Introduction: Chiral cyclic ureas, their utility, and synthesis

Chiral ureas are an immensely useful class of building blocks in the fields of organic and inorganic chemistry as protected diamines. However, the limited methods for enantioselective preparation restricts the potential of these molecules to synthesis from symmetric or commercial diamines. Natural products, small molecule therapeutics,[77] ligands, organocatalysts,[78] and chiral auxiliaries[79] are but a few diverse areas of study that ureas, and urea derivatives such as diamines, find utility (Figure 17). Some examples of well-studied therapeutics such as cisplatin derivatives,[80] HIV protease inhibitors,[81] and NK1-antagonists[82] all contain 1,2-diamino functionality where the chirality is essential to activity.[83] In addition, there are many instances where 1,3-imidazolidinone and tetrahydro-2-pyrimidone ureas are useful precursors for synthesis of chiral imidazolines,

---

[77]Kotti, S. R. S.; Timmons, C. *Chem. Biol. Drug. Des.* **2006**, *62*, 101–104.

[78]Taylor, M. S.; Jacobsen, E. N. *Angew. Chem. Int. Ed.* **2006**, *45*, 1520–1543; Doyle, A. G.; Jacobsen, E. N. *Chem. Rev.* **2007**, *107*, 5713–5743.

[79]Lucet, D.; Gall, T.; Mioskowski, C. *Angew. Chem. Int. Ed.* **1998**, *37*, 2580–2627.

[80]Dufrasne, F.; Galanski, M. *Current pharmaceutical design* **2007**, *13*, 2781–2794; Apps, M. G.; Choi, E. H. Y.; Wheate, N. J. *Endocrine-related cancer* **2015**, *22*, R81–R97.

[81]Kazmierski, W. M.; Furfine, E.; Gray-Nunez, Y.; Spaltenstein, A.; Wright, L. *Bioorg. Med. Chem. Lett.* **2004**, *14*, 5685–5687.

[82]Shue, H.-J.; Chen, X.; Schwerdt, J. H.; Paliwal, S.; Blythin, D. J.; Lin, L.; Gu, D.; Wang, C.; Reichard, G. A.; Wang, H.; Piwinski, J. J.; Duffy, R. A.; Lachowicz, J. E.; Coffin, V. L.; Nomeir, A. A.; Morgan, C. A.; Varty, G. B.; Shih, N.-Y. *Bioorg. Med. Chem. Lett.* **2006**, *16*, 1065–1069; Ho-Jane, S.; Xiao, C.; John, H. S.; Sunil, P.; David, J. B.; Ling, L.; Danlin, G.; Cheng, W.; Gregory, A. R.; Hongwu, W.; John, J. P.; Ruth, A. D.; Jean, E. L.; Vicki, L. C.; Amin, A. N.; Cynthia, A. M.; Geoffrey, B. V.; Neng-Yang, S. *Bioorg. Med. Chem. Lett.* **2006**, *16*, 1065–1069.

[83]Ho-Jane, S.; Xiao, C.; John, H. S.; Sunil, P.; David, J. B.; Ling, L.; Danlin, G.; Cheng, W.; Gregory, A. R.; Hongwu, W.; John, J. P.; Ruth, A. D.; Jean, E. L.; Vicki, L. C.; Amin, A. N.; Cynthia, A. M.; Geoffrey, B. V.; Neng-Yang, S. *Bioorg. Med. Chem. Lett.* **2006**, *16*, 1065–1069; Reichard, G. A.; Stengone, C.; Paliwal, S.; Mergelsberg, I.; Majmundar, S.; Wang, C.; Tiberi, R.; McPhail, A. T.; Piwinski, J. J.; Shih, N.-Y. *Org. Lett.* **2003**, *5*, 4249–4251.

guanidines, hydantoins, and aminals.[84] Classically, enantiopure diamine precursors were resolved from racemates[85] leaving half of the material to waste, or synthesized through stereospecifc rearrangements from enantioenriched starting materials.[86]
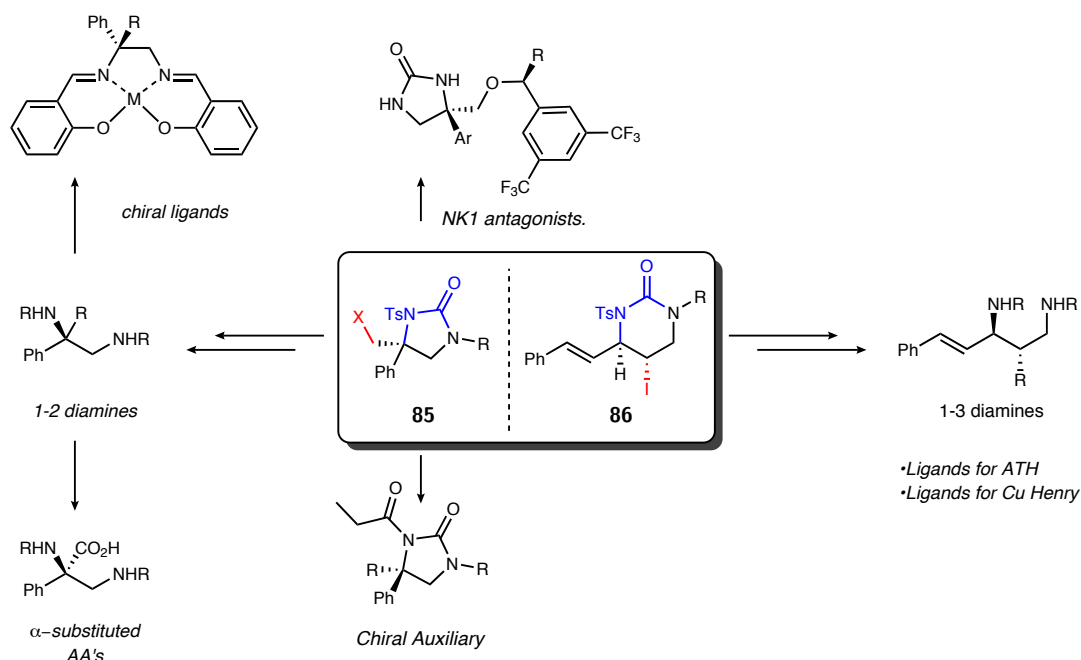
Figure 17: Utility of chiral urea derivatives as a building block in organic synthesis

The most common method for accessing chiral ureas is through the carbonylation of a diamine. Typical methods use strong electrophilic sources such as phosgene or carbonyldiimidazole which are reactive and toxic reagents. Of course this does not solve the problem of establishing the crucial stereocenters that are often required in the target compound. The stereoselective synthesis of vicinal diamines is rich in elegant methodology[87] but unfortunately will not be discussed in full detail. Although this route to

[84] Alexakis, A.; Mangeney, P.; Lensen, N.; Tranchier, J. P.; Gosmini, R.; Raussou, S. *Pure Appl. Chem.* **1996**, *68*, 531–534.

[85] Sakai, T.; Korenaga, T.; Washio, N.; Nishio, Y.; Minami, S.; Ema, T. *Bull. Chem. Soc.* **2004**, *77*, 1001–1008; Ryoda, A.; Yajima, N.; Haga, T.; Kumamoto, T.; Nakanishi, W.; Kawahata, M.; Yamaguchi, K.; Ishikawa, T. *J. Org. Chem.* **2008**, *73*, 133–141.

[86] Kim, H.; Nguyen, Y.; Yen, C.; Chagal, L.; Lough, A. J.; Kim, M. B.; Chin, J. *J. Am. Chem. Soc.* **2008**, *130*, 12184–12191; Kim, H.-J.; Kim, H.; Alhakimi, G.; Jeong, E.; Thavarajah, N.; Studnicki, L.; Koprianiuk, A.; Lough, A. J.; Suh, J.; Chin, J. *J. Am. Chem. Soc.* **2005**, *127*, 16370–16371.

[87] For Reviews: Lucet, D.; Gall, T.; Mioskowski, C. *Angew. Chem. Int. Ed.* **1998**, *37*, 2580–2627;

cyclic ureas has numerous avenues for stereoselective preparation, laborious protection and deprotection steps are often required that can complicate the sequence. Additionally, many stereoselective methods to access the vicinal diamine precursors require many steps to accomplish. More traditional routes to diamines could be employed by the resolution of racemic materials which is often less steps, and wastes half of the valuable materials that have to be carried through many steps (i.e. carrying through two times the material through 3-5 steps just to throw away half at the end). Clearly, improvements of diamination strategies are needed and direct access to chiral ureas would allow for more rapid access to important building blocks.
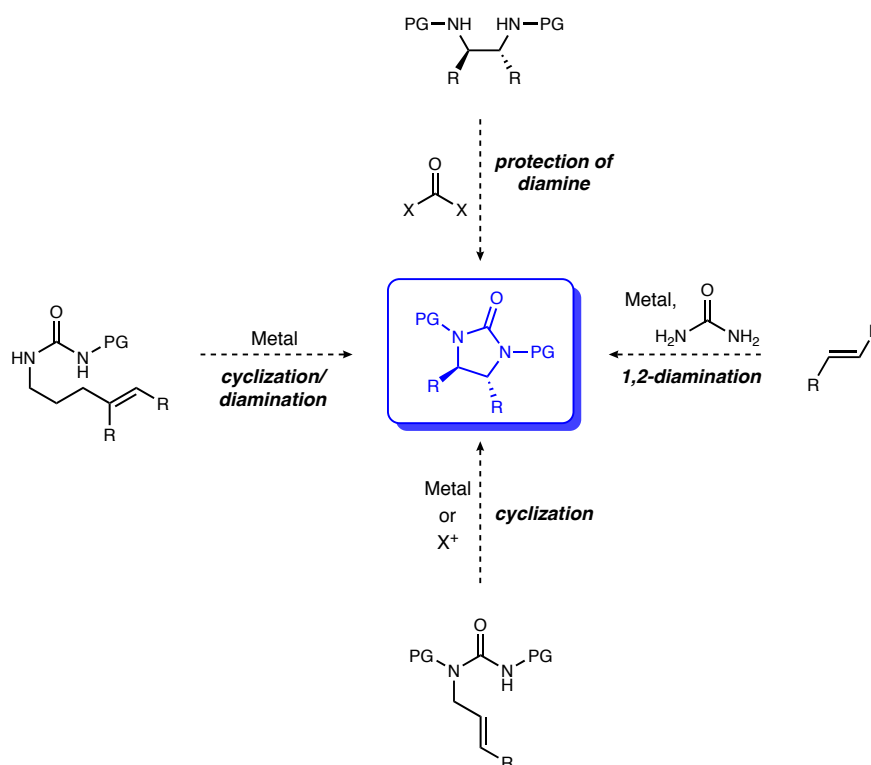
Figure 18: Common methods for synthesis of chiral cyclic ureas

More direct methods that use cyclization strategies include electrophilic halide sources[88]

Jong, S.; Nosal, D. G.; Wardrop, D. J. *Tetrahedron* **2012**, *68*, 4067–4105; Ji, X.; Huang, H. *Org. Biomol. Chem.* **2016**, *14*, 10557–10566.

[88]details on the use of halocyclizations will be covered in the next section.

or metal catalysis to achieve high selectivity. The Wolfe group found that the use of an an allylic amine can trap an isocyanate and subsequently undergo a palladium mediated carboamination of an olefin to furnish imidazolidin-2-ones.[89] Following this report was work by the White group using palladium and a Lewis acid catalyst to control the nitrogen versus oxygen allylic functionalization.[90] This is the only study, en route to chiral ureas using metal catalysis, that addresses the problem of nucleophile control in the cyclization and can achieve both oxygen and nitrogen cyclizations using Lewis acid control. They find that the simple change of ligand and Lewis acid can achieve high selectivity for oxygen (using AgOTf) or nitrogen (using $B(C_6F_5)_3$) cyclization. Finally the Hara group reported a palladium-mediated C-H amination to directly access cyclic ureas in a similar manner to the White group but without the need of a Lewis acid.[91] Additionally, this is the only report to achieve nitrogen cyclization for the formation of *both* 5- and 6-membered ureas in high diastereoselectivity. These methods are great examples of the utility and broad applicability of palladium catalysis for the synthesis of cyclic ureas. These conditions can achieve high diastereoselection in some cases, but still have not found success with enantioselective catalysis.
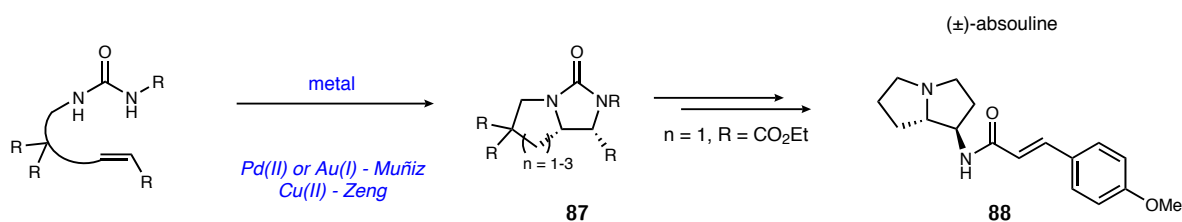
Scheme 11: Cyclization/diamination strategy for the synthesis of cyclic ureas

Amino cyclizations were improved upon by a new intramolecular diamination of

[89]Fritz, J. A.; Nakhla, J. S.; Wolfe, J. P. *Org. Lett.* **2006**, *8*, 2531–2534.
[90]Strambeanu, I. I.; White, M. C. *J. Am. Chem. Soc.* **2013**, *135*, 12032–12037.
[91]Nishikawa, Y.; Kimura, S.; Kato, Y.; Yamazaki, N.; Hara, O. *Org. Lett.* **2015**, *17*, 888–891.

alkenes to afford fused bicyclic ureas shown in Scheme 11. The first contribution in this class of reaction was developed by Muñiz[92] using palladium(II) catalysis with a superstoichiometric amount of phenyl iododiacetate (PIDA) to afford bicyclic products such as **87**.[93] The Pd/PIDA system was further refined to a palladium(II)/Cu(I) system which allowed access to improved reactivity and a new set of products including less reactive α, β-unsaturated esters (**87**, R = CO_2Et).[94] The authors applied their methodology to the synthesis of racemic absouline **88** which, similar to their product **87**, has a trisubstituted amine in the core of the molecule and a 1,2-diamino functionality. An improvement on the diastereoselective but racemic cyclizations developed by Muñiz was reported by Zeng and co-workers. Using a chiral bis(oxazoline) ligand in conjunction with a copper(II) catalyst, the authors achieve enantioselection ranging from 49 to 95%. In all cases of these cyclizations, the best reactivity and enantioselectivity is achieved using a geminal disubstituted substrate as shown in Scheme 11 and is a large limitation when the desire is to apply the methodology to pharmaceutically relevant targets or natural products. The intramolecular diamination strategy is a unique way to access bicyclic ureas but are limited to this class of fused bicycles. To address the limitations in diamination strategies by Muñiz and Zeng, new versions that could access a broader set of products would be useful.

Improvements on the diamination/cyclization strategies en route to cyclic ureas were realized by intermolecular diamination. The most prolific contributer to this field is the

---

[92]For a synopsis of this research see: Muñiz, K.; Martínez, C. *J. Org. Chem.* **2013**, *78*, 2168–2174.

[93]Streuff, J.; Hövelmann, C. H.; Nieger, M.; Muñiz, K. *J. Am. Chem. Soc.* **2005**, *127*, 14586–14587; Muñiz, K.; Hövelmann, C. H.; Streuff, J. *J. Am. Chem. Soc.* **2008**, *130*, 763–773.

[94]Muñiz, K.; Hövelmann, C.; Campos-Gómez, E.; Barluenga, J.; González, J.; Streuff, J.; Nieger, M. *Chem. Asian J.* **2008**, *3*, 776–788; Muñiz, K.; Streuff, J.; Chávez, P.; Hövelmann, C. *Chem. Asian J.* **2008**, *3*, 1248–1255.

Shi group who commonly employs a metal for nitrogen-nitrogen bond activation.[95] The seminal report uses di-*tert*-butyldiaziridinone **89** for the regioselective diamination of internal conjugated alkenes (top of Scheme 12).[96] Nitrogen-nitrogen bond activation was proposed to go through a metal intermediate such as **91** which could be tuned depending on the metal that was employed. The reaction using palladium was extended for use on C-H amination of terminal olefins[97] and an asymmetric diamination achieving 85-95% ee.[98] These versions of the diamination reaction are particularly elegant when compared to more traditional approaches using osmium complexes that are toxic and have to be pre-synthesized.[99] A complementary system to the palladium activation of nitrogen-nitrogen bonds was discovered and used copper(I) chloride and triphenyl phosphite to achieve selectivity for terminal alkenes[100] and was adapted to an enantioselective version using (*R*)-DTBM-SEGPHOS.[101] The methodology is applied to targets such as (+)-CP-99,994 and Sch-425078 (key step shown in bottom of Scheme 12 to furnish **93**) that both have the vicinal diamino functionality.[102] To date this is still one of the premier methods for direct diamination of alkenes and has been adapted to be diastereoselective and enantioselective.

Chiral ureas hold immense promise for utility in organic synthesis but are often accessed from the chiral pool. The methodology described above includes processes that are not only diastereoselective but enantioselective. All come with limitations on substrates

---

[95]Zhu, Y.; Cornwall, R. G.; Du, H.; Zhao, B.; Shi, Y. *Acc. Chem. Res.* **2014**, *47*, 3665–3678.

[96]Xu, L.; Du, H.; Shi, Y. *J. Org. Chem.* **2007**, *72*, 7038–7041; Zhao, B.; Du, H.; Cui, S.; Shi, Y. *J. Am. Chem. Soc.* **2010**, *132*, 3523–3532.

[97]Du, H.; Yuan, W.; Zhao, B.; Shi, Y. *J. Am. Chem. Soc.* **2007**, *129*, 7496–7497.

[98]Du, H.; Yuan, W.; Zhao, B.; Shi, Y. *J. Am. Chem. Soc.* **2007**, *129*, 11688–11689; Xu, L.; Shi, Y. *J. Org. Chem.* **2008**, *73*, 749–751.

[99]Chong, A. O.; Oshima, K.; Sharpless, K. B. *J. Am. Chem. Soc.* **1977**, *99*, 3420–3426.

[100]Yuan, W.; Du, H.; Zhao, B.; Shi, Y. *Org. Lett.* **2007**, *9*, 2589–2591; Zhao, B.; Peng, X.; Cui, S.; Shi, Y. *J. Am. Chem. Soc.* **2010**, *132*, 11009–11011.

[101]Du, H.; Zhao, B.; Yuan, W.; Shi, Y. *Org. Lett.* **2008**, *10*, 4231–4234.

[102]Fu, R.; Zhao, B.; Shi, Y. *J. Org. Chem.* **2009**, *74*, 7577–7580; Wen, Y.; Zhao, B.; Shi, Y. *Org. Lett.* **2009**, *11*, 2365–2368.
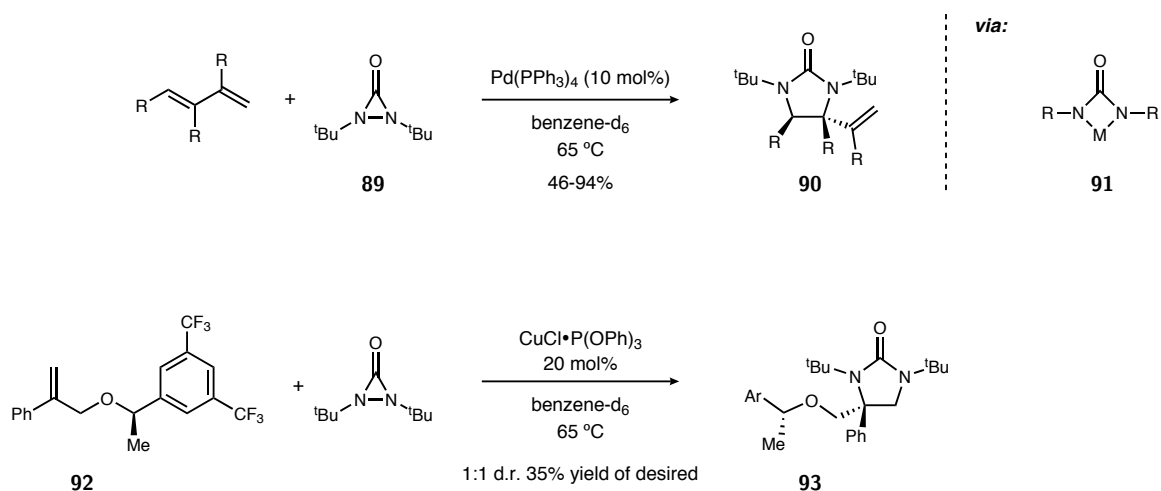
Scheme 12: Synthesis of cyclic ureas through metal activation of a nitrogen-nitrogen bond and direct alkene functionalization

which often do not include orthogonal protecting groups on the nitrogens, creating longer synthetic sequences in order to differentiate them. New methods that could set stereocenters with a more dense array of functional groups would give access to new classes of small molecule building blocks. The reactions appear to be mostly limited to formation of 5-membered ureas (also referred to as 1,3-imidazolidinones and imidazolidin-2-ones) but larger ring sizes are necessary for target and natural product synthesis. In diamination strategies there is not much concern for nucleophile control in regards to nitrogen/oxygen selectivity but this still remains a large problem in the cyclization strategy shown in Figure 18 using a metal or electrophilic halogen source. An amino cyclization embodying the principles of minimalism and mild reaction conditions would be of great use for accessing chiral 1,3-imidazolidinone and tetrahydro-2-pyrimidinone ureas.

2.1.2 Introduction: Amino halocyclizations and the control of ambient nucleophiles

The literature is inundated with studies on halocyclizations that use oxygen as a nucleophile, and also as the stereocontrolling handle[103] in enantioselective versions. Among these reports are a plethora of mechanistic insights and applications to small molecule targets.[104] Although much has been learned about halocyclization reactions, new nucleophiles such as nitrogen, phosphorous, or sulfur have not been abundant. More specifically, nitrogen cyclizations would be useful for their ability to make chiral amines, pyrrolidines, and 1,2/1,3-diamine precursors. Access to these products in a mild and enantioselective manner would be of great use in organic synthesis by giving facile access to chiral building blocks. Additionally, the control of a nitrogen cyclization using an organocatalyst and an ambident nucleophile would be the first of its kind.

Shown in Figure 19 is the problem associated with the control of an ambident nucleophile. Starting with an amide **94**, an electrophilic source of halogen or selenium can be used to effect the cyclization on the alkene. It is important to note that many other cyclization precursors can be used such as carbamates, ureas, and thioureas and the problem of nucleophile control is not limited to amides. Four different products shown in Figure 19 as **95**, **96**, **97** and **98** can be obtained from this reaction. Some guiding principles and discoveries will be discussed below in regards to controlling the cyclization and selecting for one of these pathways. Many different aspects of this reaction can be manipulated to achieve control such as changing alkene substitution or geometry, ma-

---

[103]More specifically oxygen is used for catalyst coordination which often dictates the outcome in the enantioselective cyclization.
[104]See Chapter 1.1.2 and references herein.

nipulating the electrophilicity of the halogen or selenium, addition of Lewis acids, and incorporation of a protecting group on the nitrogen of the amide, specifically to attenuate its nucleophilicity using electronic and steric effects.
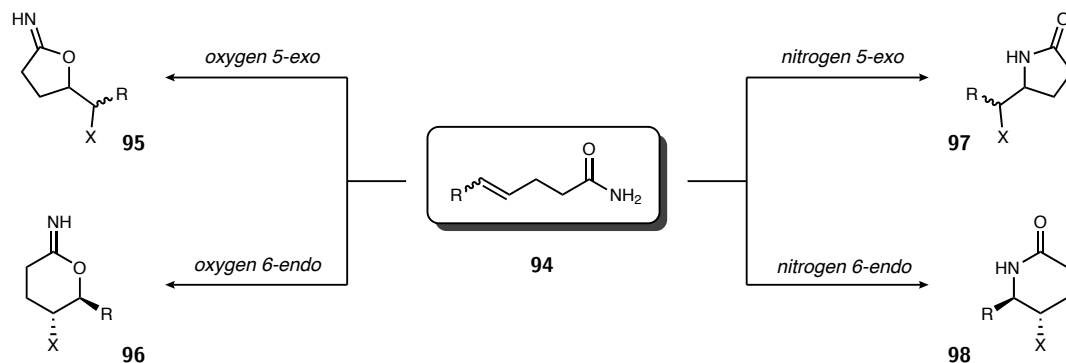
Figure 19: Difficulty in controlling amides in halocyclization reactions

Early reports of aminocyclization reactions[105] used an amide as the cyclization precursor analogous to Figure 19. Similar to the iodolactonization reaction, the iodolactamization reaction was a sought after target for the use in synthetic routes due to the abundance of cyclic amide motifs in drugs and natural products. A reason for the use of amides as a cyclization precursor is most likely due to the lower propensity of the amide nitrogen to halogenate compared to its more nucleophilic amine counterpart (although a common method that will be discussed is the use of sulfonyl amides which seem to balance electronics perfectly for aminocyclizations).[106] An added benefit for the use of an amide as a cyclization precursor is the ease of access from readily available, and inexpensive carboxylic acids. The characteristics that enable an amide as a good cyclization precursor can also bestow obstacles to control or its ambidenticity. Shown in Figure 19

---

[105]For a review on aminocyclizations see: Chemler, S. R.; Bovino, M. T. *ACS Catal.* **2013**, *3*, 1076–1091.

[106]Some systems have found success in using non-protected amines but are substrate specific: Beshore, D. C.; Smith, A. B. *J. Am. Chem. Soc.* **2008**, *130*, 13778–13789; Beshore, D. C.; Smith, A. B. *J. Am. Chem. Soc.* **2007**, *129*, 4148–4149; Verhelst, S. H. L.; Paez Martinez, B.; Timmer, M. S. M.; Lodder, G.; van der Marel, G. A.; Overkleeft, H. S.; van Boom, J. H. *J. Org. Chem.* **2003**, *68*, 9598–9603.

is the difficulty of controlling not only the regioselectivity (5-*exo* vs. 6-*endo*) of an amide cyclization but also the selectivity of the nucleophile (nitrogen vs. oxygen). In early reports where with no additional control elements were employed (protecting groups, Lewis acids, catalysts, etc.) the oxygen is typically more reactive toward cyclization furnishing either **95** or **96**.[107] Control of the seemingly more difficult nitrogen cyclization (Figure 19, **97** and **98**) prompted continued studies of these systems.

Initial approaches to the nitrogen oxygen chemoselectivity problem focused on "masked" amide cyclizations. One of the first reports was used in the synthesis of corrins by Eschenmoser.[108] The protection of an amide to form a diimidate **99** removes the possibility of oxygen cyclization. A problem with this approach is evident in that protection and deprotection sequences are needed to get to the final lactam **101**. A similar approach was popularized more than a decade later by the Knapp laboratory.[109] The use of TMSOTf forms an *N,O*-bis(trimethylsilyl) derivative **102** which, upon treatment with iodine in THF, gives the nitrogen-cyclized product **103**. The monosilylated amide (confirmed to be silylated at the nitrogen) undergoes an oxygen cyclization and upon workup the imidate hydrolyzes to furnish the iodolactone. Due to this monosilylated intermediate not forming desired product, rigorous exclusion of water is necessary or else the bis(silyl) intermediate **102** converts to monosilylated amide. The Knapp procedure was applied to the synthesis of (-)-slaframine[110] (see Scheme 13), *O*-methyl-β,D-ezoaminouric acid,[111]

[107]Corey, E.; Fleet, G.; Kato, M. *Tetrahedron Lett.* **1973**, *14*, 3963–3966; Hirama, M.; Uei, M. *Tetrahedron Lett.* **1982**, *23*, 5307–5310.

[108]Bertele, E.; Boos, H.; Dunitz, J. D.; Elsinger, F.; Eschenmoser, A.; Felner, I.; Gribi, H. P.; Gschwend, H.; Meyer, E. F.; Pesaro, M.; Scheffold, R. *Angew. Chem.* **1964**, *76*, 393–399.

[109]Knapp, S.; Rodriques, K. E.; Levorse, A. T.; Ornaf, R. M. *Tetrahedron Lett.* **1985**, *26*, 1803–1806; Knapp, S.; Levorse, A. T.; Potenza, J. A. *J. Org. Chem.* **1988**, *53*, 4773–4779; Knapp, S.; Levorse, A. T. *J. Org. Chem.* **1988**, *53*, 4006–4014; Knapp, S.; Gibson, F. S. *Org. Synth.* **1992**, *70*, 101.

[110]Knapp, S.; Gibson, F. S. *J. Org. Chem.* **1992**, *57*, 4802–4809.

[111]Knapp, S.; Levorse, A. T.; Potenza, J. A. *J. Org. Chem.* **1988**, *53*, 4773–4779.

and approaches to the synthesis of oseltamivir by the Corey group.[112] Nitrogen selective cyclization procedures clearly found utility in the realm of target and total synthesis but still lacked a facile procedure that avoided the protection or "masking" of the oxygen.
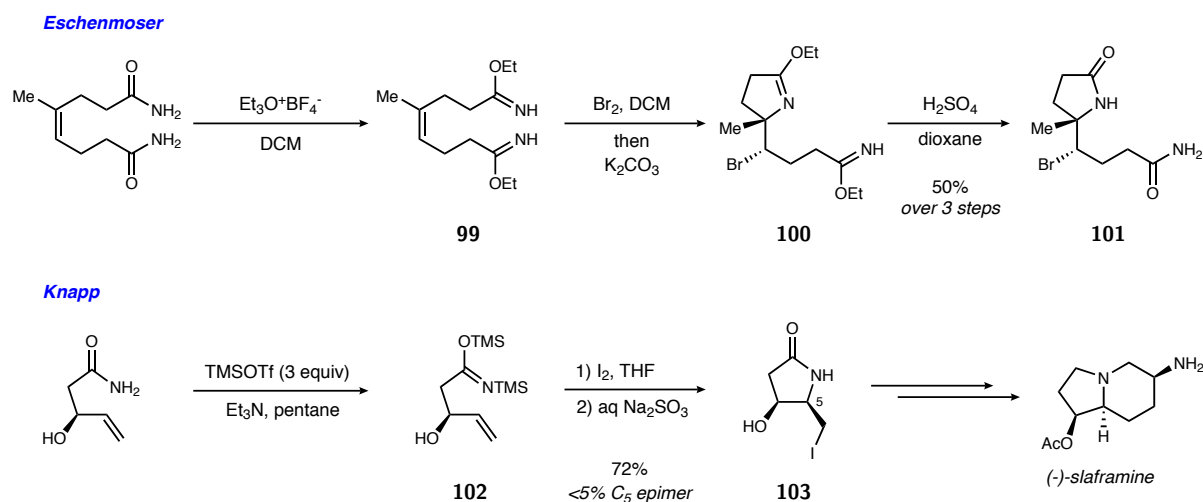
Scheme 13: Approach to controlling the nitrogen cyclization of amides using a "masked" amide nucleophile

The use of a controlling element such as a protecting group on the nitrogen has been explored, however it requires the need for deprotection later in a sequence. Early examples employing protecting group control for nitrogen cyclization of amides by the Corey group used an epoxide as the terminal electrophile.[113] In their approach to prostaglandins, an amide was protected with a *para*-biphenyl group and they obtained oxygen cyclization, and consequently, the lactone was isolated. In the footnotes, the authors remark that the use of a nitrosyl-protected amide in combination with *n*-BuLi can afford the lactam, albeit in lower yields. The first breakthrough in protecting group control came with a very specialized system to access β-lactams.[114] This report is the first to hypothesize that

---

[112]Yeung; Hong, S.; Corey, E. J. *J. Am. Chem. Soc.* **2006**, *128*, 6310–6311; Yeung, Y.-Y.; Corey, E. *Tetrahedron Lett.* **2007**, *48*, 7567–7570.

[113]Corey, E.; Fleet, G.; Kato, M. *Tetrahedron Lett.* **1973**, *14*, 3963–3966.

[114]Biloski, A. J.; Wood, R. D.; Ganem, B. *J. Am. Chem. Soc.* **1982**, *104*, 3233–3235.

the pK_a of the cyclization precursor could affect the cyclization. To lower the pK_a closer to known cyclization precursors such as carboxylic acids, sulfonyl groups were added, resulting in an imide precusor. Results of the bromocyclization in aqueous bicarbonate were much improved compared to the low yields observed by the Corey group. This work was further elaborated by the Itô group who investigated many different conditions including the dramatic affect the sulfonyl group, and more specifically the tosyl (Ts) group has on cyclization selectivity.[115] Finally, many other non-sulfonyl groups were studied with no clear trend using aromatic groups.[116] These studies demonstrated the applicability of substrate control in amide cyclizations and their utility in target synthesis of prostaglandins and β-lactams.

A breakthrough was reported by Taguchi that could give control of nitrogen cyclization, not based on substrate but instead through chelation control.[117] The conditions achieve high selectivity for nitrogen cyclization of a variety of substrates using either n-butyllithium or $\text{LiAl}(\text{O}t-\text{Bu})_4$ as the base and subsequent treatment with molecular iodine. Interestingly, other bases such as sodium bicarbonate, potassium *tert*-butoxide, and sodium hydride either gave mixtures of product or exclusive *O*-cyclization with ureas, carbamates, or amides (Scheme 14, X=O,NR, or CH_2). The authors hypothesize that the lithium ion can chelate the oxygens of the deprotonated imide **105** which presents the nitrogen for cyclization. A possible hard/hard interaction can explain the chelation of both oxygens, where a more unfavored hard/soft interaction would be necessary to coordinate one oxygen and one nitrogen. With a chiral center present in a urea cyclization precursor, diastereoselection can be controlled by changing the protecting group on

---

[115]Hirama, M.; Iwashita, M.; Yamazaki, Y.; Itô, S. *Tetrahedron Lett.* **1984**, *25*, 4963–4964.

[116]Balko, T.; Brinkmeyer, R.; Terando, N. *Tetrahedron Lett.* **1989**, *30*, 2045–2048.

[117]Kitagawa, O.; Fujita, M.; Li, H.; Taguchi, T. *Tetrahedron Lett.* **1997**, *38*, 615–618; Fujita, M.; Kitagawa, O.; Suzuki, T.; Taguchi, T. *J. Org. Chem.* **1997**, *62*, 7330–7335.

the non-reacting nitrogen to DPM (Scheme 14, X = NDPM). Palladium catalyst systems with copper halide additives reported by the Chemler[118], Liu[119], and White[120] groups finally demonstrate catalytic systems where the control of nitrogen cyclization can be achieved. All of these groups find the sulfonyl protecting group on the nitrogen to be optimal for high control. These reports represent some of the seminal work in stereoselective *and* ambident nucleophile control in amino cyclization reactions and reinforce that the protecting group on the nitrogen is crucial for success.
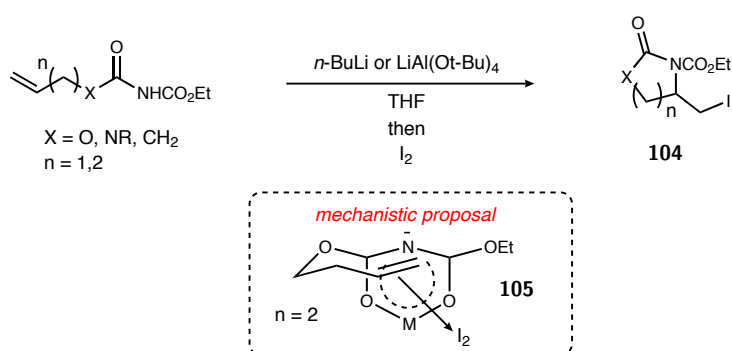
Scheme 14: Taguchi's chelation control for control of an ambident nucleophile

It is clear that control of the ambident nucleophile can be achieved in cyclization of amides, carbamates, and ureas but enantioselective versions are still few and far between. Some closely related systems use diamination strategies to achieve control over the cyclization process and achieve diastereoselection or enantioselection.[121,122] Strategies to induce enantioselection in aminocyclizations using catalysts have been studied by a few groups but substrates are all tailored to remove the competition between oxygen and ni-

[118]Manzoni, M. R.; Zabawa, T. P.; Kasi, D.; Chemler, S. R. *Organometallics* **2004**, *23*, 5618–5621.

[119]Lei, A.; Lu, X.; Liu, G. *Tetrahedron Lett.* **2004**, *45*, 1785–1788.

[120]Strambeanu, I. I.; White, M. C. *J. Am. Chem. Soc.* **2013**, *135*, 12032–12037.

[121]Some selected publications: Fritz, J. A.; Wolfe, J. P. *Tetrahedron* **2008**, *64*, 6838–6852; Muñiz, K.; Hövelmann, C.; Campos-Gómez, E.; Barluenga, J.; González, J.; Streuff, J.; Nieger, M. *Chem. Asian J.* **2008**, *3*, 776–788; Li, H.; Song, F.; Widenhoefer, R. A. *Adv. Synth. Catal.* **2011**, *353*, 955–962

[122]For Reviews: Lucet, D.; Gall, T.; Mioskowski, C. *Angew. Chem. Int. Ed.* **1998**, *37*, 2580–2627; Jong, S.; Nosal, D. G.; Wardrop, D. J. *Tetrahedron* **2012**, *68*, 4067–4105; Ji, X.; Huang, H. *Org. Biomol. Chem.* **2016**, *14*, 10557–10566.

trogen cyclization. Initial successes in the field of organocatalytic amino-cyclizations were found by the Shi group using a chiral phosphoric acid catalyst (see Chapter 1).[123] Following soon after, other catalysts were discovered to be useful in asymmetric induction of amino cyclization reactions. Among the successes were: a chiral amino thiocarbamate catalyst,[124] Schiff-base urea catalysts,[125] C_2 symmetric selenium catalyst,[126] and a thiourea catalyst.[127] These enantioselective amino-cyclizations using organocatalysts are all clear advances to the field of halocyclizations but the substrates are all tailored to not have an ambident nucleophile. Most use a sulfonyl amide as the cyclization precursor which furthers the hypothesis of the importance of lowering the pK_a of the amine for aminocyclization reactions. Although there are many examples of diastereoselective or enantioselective amino cyclizations, the use of an amide, due to its propensity for oxygen cyclization, remains a difficult challenge.

Insight into the control of ambident nucleophiles in a halocyclization reaction has been gained by the studies described above. The most crucial element in control not only in the ambident nucleophile, but also in enantioselectivity is the protecting group of the reactive nitrogen. Other controlling factors are the electrophilicity of the halide source and additives, such as Lewis acids. Hard-hard interactions can be taken advantage of by using lithium counterions which are hypothesized to coordinate oxygen better than the nitrogen. Catalytic and enantioselective versions to the aminocyclization reaction have been investigated but often tailor the substrate to remove the possibility of oxygen substitution. To date there has not been an organocatalytic, enantioselective version of the

[123]Huang, D.; Wang, H.; Xue, F.; Guan, H.; Li, L.; Peng, X.; Shi, Y. *Org. Lett.* **2011**, *13*, 6350–6353.
[124]**yeung:2011; yeung:2012; yeung:2013a**
[125]Brindle, C. S.; Yeung, C. S.; Jacobsen, E. N. *Chem. Sci.* **2013**, *4*, 2100–2104.
[126]Chen, F.; Tan, C. K.; Yeung, Y.-Y. *J. Am. Chem. Soc.* **2013**, *135*, 1232–1235.
[127]Tripathi, C. B.; Mukherjee, S. *Org. Lett.* **2014**, *16*, 3368–3371.

amino cyclization reaction that uses only substrate and catalyst control, and can achieve high selectivity for nitrogen cyclization. Finally, no catalytic enantioselective routes to chiral ureas have found success in achieving selectivity in both 5- and 6-membered ring formation.

2.2 Development of organocatalytic enantioselective urea cyclization

2.2.1 Proposal for an enantioselective urea cyclization reaction

Although accessing chiral 1,2- and 1,3-diamines is rich in elegant synthetic methodology, to date there are no examples of enantioselective organocatalyzed methods for preparation of ureas from achiral starting materials. Effecting the transformation from an allylic amine by the capture of an isocyanate to form a urea and subsequent alkene functionalization (Figure 20) holds promise for establishing a carbon-nitrogen bond and stereogenic center. Similar attempts in this field using halo-functionalization have been demonstrated by the enantioselective cyclization of sulfonyl amides and cyclizations of amides. An additional challenge presented when using ureas for enantioselective cyclizations, is the competition between nitrogen **106** and oxygen **107** as both are capable nucleophiles. Control of ambient nucleophiles has been an obstacle in organic synthesis which has prompted research to provide insight into observed selectivities.[128] Many examples demonstrate the ability of amides to be used as enantioselective cyclization precursors, however in many cases oxygen is a more capable nucleophile due to the larger size

[128]For some selected publications see: Kornblum, N.; Smiley, R. A.; Blackwood, R. K.; Iffland, D. C. *J. Am. Chem. Soc.* **1955**, *77*, 6269–6280; Hopkins, G.; Jonak, J.; Minnemeyer, H.; Tieckelmann, H. *J. Org. Chem.* **1967**, *32*, 4040–4044; Stirling, C. J. M. *J. Chem. Soc.* **1960**, *0*, 255–262; Breugst, M.; Tokuyasu, T.; Mayr, H. *J. Org. Chem.* **2010**, *75*, 5250–5258; Rao, W.-H.; Yin, X.-S.; Shi, B.-F. *Org. Lett.* **2015**, *17*, 3758–3761; Strambeanu, I. I.; White, C. M. *J. Am. Chem. Soc.* **2013**, *135*, 12032–12037.

of protected nitrogen nucleophiles.[129] Contrasted to these examples, selective cyclization of the seemingly more difficult nitrogen of a urea, using an organocatalyst, has not been studied in an enantioselective manner.
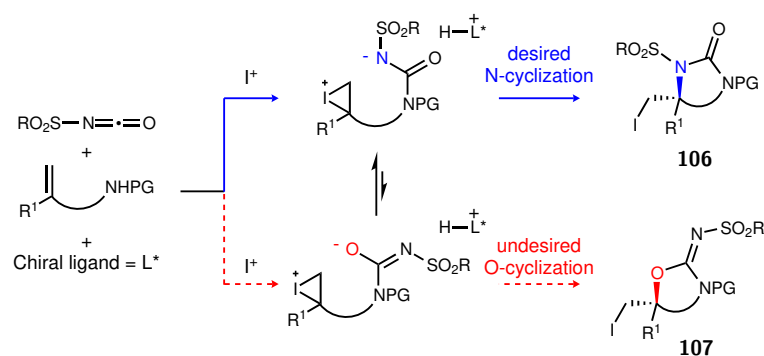
Figure 20: Catalyst control of an ambident nucleophile: Selectivity of the desired nitrogen cyclization vs oxygen cyclization

Using a BAM based catalyst, a new enantioselective reaction with high selectivity for nitrogen cyclization of an ambident nucleophile has been developed. In situ formation of a sulfonyl imide, followed by enantioselective nitrogen cyclization furnishes chiral ureas that can access 1,2- and 1,3-diamines, hydantoins, and is applied to the synthesis of an NK$_1$ antagonist. The goals of the project are as follows:

1. *To control an ambident nucleophile using BAM catalysis while achieving enantio- and regioselection in an alkene iodoamination cyclization.*

2. *Probe the effects of protecting groups and ring size to inform mechanistic hypotheses.*

3. *Apply the methodology to target synthesis, particularly an NK₁ antagonist, improving upon previously reported routes.*

[129]Rauniyar, V.; Lackner, A. D.; Hamilton, G. L.; Toste, F. D. *Science* **2011**, *334*, 1681–1684; Arai, T.; Watanabe, O.; Yabe, S.; Yamanaka, M. *Angew. Chem. Int. Ed.* **2015**, *54*, 12767–12771; Jaganathan, A.; Garzan, A.; Whitehead, D. C.; Staples, R. J.; Borhan, B. *Angew. Chem. Int. Ed.* **2011**, *123*, 2641–2644.

2.2.2 Optimization, scope, and derivatization of the iodourea cyclization reaction

Initial attempts at urea cyclization focused on homoallylic amines (Figure 21, compound **108**) similar to the CO_2 cyclization in the Chapter 1. Using p-toluenesulfonyl isocyanate and StilbPBAM free base **109** at $-20\,°C$, the reaction exhibited low selectivity and two cyclization products with the one that was slightly favored isolated at 31% yield and 31% ee.[130] One product could be favored by employing a more basic guanidine catalyts catalyst **110** achieving a 70% yield and but a low 5% ee.[131] Unfortunately, upon reduction of the major cyclization product, a 1,3 amino alcohol **111** was isolated and is identical to the the reduction product of the cyclic carbamates in Chapter 1. The oxygen cyclization product was clearly favored with a homoallylic amine and the product ratio could never be reversed to favor the product which would presumably be nitrogen cyclization (never derivatized or confirmed). The simple change from a homoallylic amine to an allylic amine was investigated, with the idea that the sulfonyl imide would have less conformational flexibility when coordinated with the catalyst. Indeed, this minor change to the precursor amine, in conjunction with employing StilbPBAM, achieved a major product that was a ratio of 92:8 major:minor and 57% ee of the major product (Figure 22, **112**). Encouragingly, upon $LiAlH_4$ reduction of the major product, the 1,2-diamine **113** was isolated. The subsequent optimization focused on three main areas 1) catalyst changes, 2) sulfonyl manipulations, and 3) nitrogen protecting groups on the substrate.

Shown in Figure 22 are the different catalysts that were employed in the initial cy-

---

[130]See Vara, B dissertation pg. 171 for preliminary results. The optimal catalyst AnthPBAM could achieve up to 70% ee but the product was not characterized correctly. The product in the shown reaction is actually the imidate not the urea as shown in Figure 21.

[131]Investigation of guanidine based catalysts were underway at the time and the hypothesis that a less basic imide cyclization precursor would necessitate a more basic catalyst.
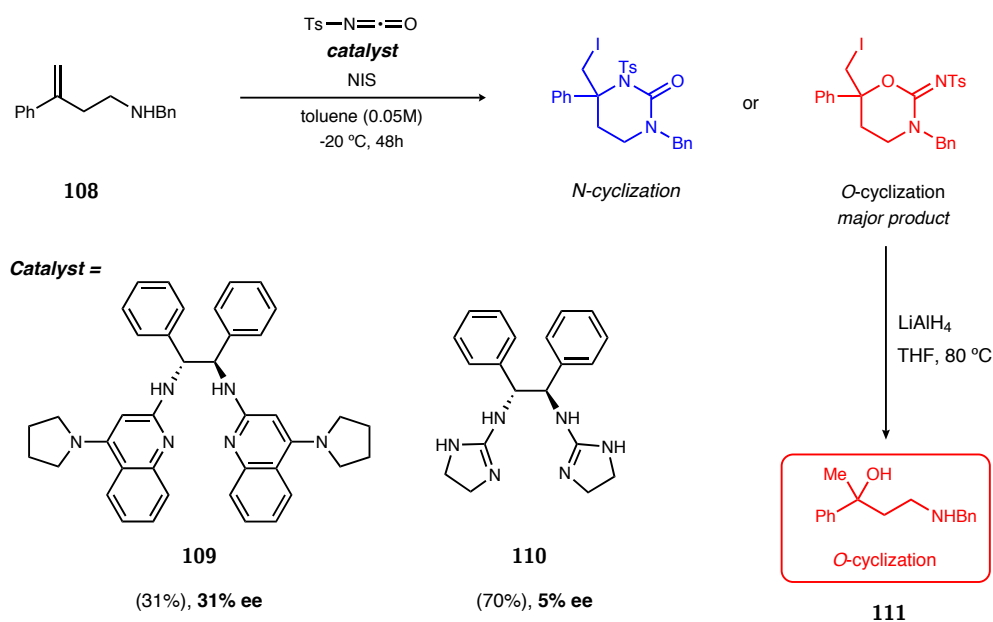
Figure 21: Initial investigations to finding a selective nitrogen cyclization to form chiral ureas

clization conditions. Based on previous studies in Chapter 1, we hypothesized that a more Brønsted basic catalyst would be necessary due to the lower acidity of the sulfonyl imide compared to the carboxylic acid in the iodolactonization reaction[132] or the carbonic acid in the iodocarbonation reaction.[133,134] Indeed when electron donating groups on the catalyst were included, enantioselection rose to a moderate 65% ee with the more basic [7]MeOStilbPBAM shown in Figure 22. Interestingly, the bis-triflimide salt of [7]MeOStilbPBAM required for the all of the previous halocyclizations, furnishes 58% ee when used in the urea cyclization. This is the first time that BAM catalyst salts have shown a negative impact on enantioselection of halocyclization reactions. This may be due to the nucleophile size as the imide is much larger in the amine cyclization compared to the smaller oxygen nucleophile. Preforming and isolating the urea intermediate was

[132]Dobish, M.; Johnston, J. *J. Am. Chem. Soc.* **2012**, *134*, 6068–6071.

[133]Vara, B. A.; Struble, T. J.; Wang, W.; Dobish, M. C.; Johnston, J. N. *J. Am. Chem. Soc.* **2015**, *137*, 7302–7305.

[134]Yousefi, R.; Struble, T.J.; Payne, J.L.; Johnston, J.N. Unpublished results - see chapter 1.

undertaken to rule out the possibility of residual water reacting with the *p*-toluenesulfonyl isocyanate forming an acid that could act as a counterion. The preformed imide performs identically to in situ formation. Finally, changes to the sterics of the backbone were not fruitful with the *meta*-methyl and 1-naphthyl backbones with enantioselection of 61% and 45% ee respectivly. Investigations into the catalyst structure demonstrated that the most important factor was the electronics of the amidine, once again demonstrating the need for matching the Brønsted basicity of the catalyst to the acidity of the substrates. However, the enantioselection remained moderate even with catalyst changes, necessitating further optimization.

p-Toluenesulfonyl isocyanate was initially employed for in-situ urea formation due to the low cost and availability, however, optimization required the synthesis of other urea derivatives. The derivatives were pre-synthesized and isolated for investigation of the impact of size and electronic nature of the imide. Figure 23 shows the effects of changing the imide character. No reaction is observed when a benzoyl imide (**114**) is used, demonstrating the necessity for a more acidic sulfonyl imide in the cyclization. The reaction is tolerant (in these unoptimized conditions) of sulfonyl changes to methyl (**115**) and a more electron withdrawing *o*-nitrobenzene sulfonyl imide (**116**). The moderate change in enantioselection between a smaller mesyl and larger tolyl or nosyl indicates that the imide substituent does not have significant catalyst interactions in the transition state to impact enantioselection. During this course of study, a post-doc in the our group, Mahesh Vishe, co-crystallized an aryl-triflyl amide with the catalyst StilbPBAM. The binding of the sulfonyl amide to the catalyst amidine was such that the -CF$_3$ group was oriented away from the backbone (see Figure 25 for representative hypothesis). The experimental results combined with crystal structure visualization bespoke the sulfonyl
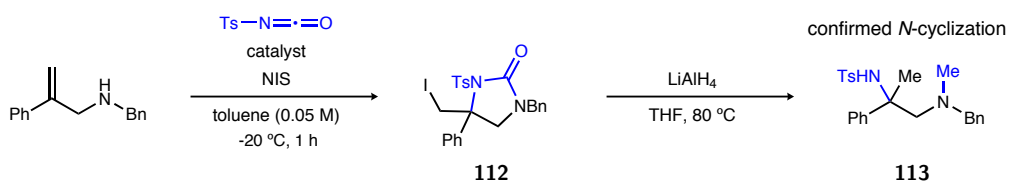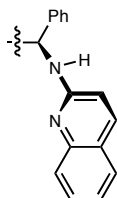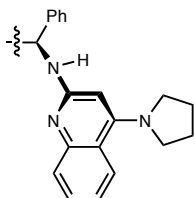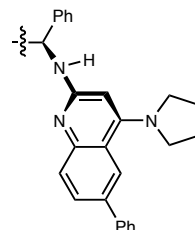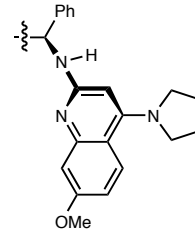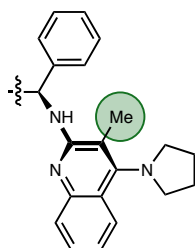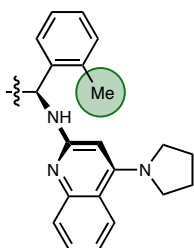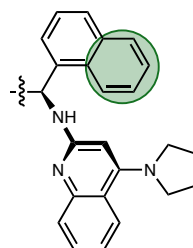
Figure 22: Catalyst modifications employed to probe the ideal electronics of the quinoline and the ideal sterics of the backbone

substituent orienting away from the backbone. The low effects observed in size and electronic changes to the sulfonyl imide indicated that focus on this substituent would not be fruitful for achieving the desired high enantioselection.
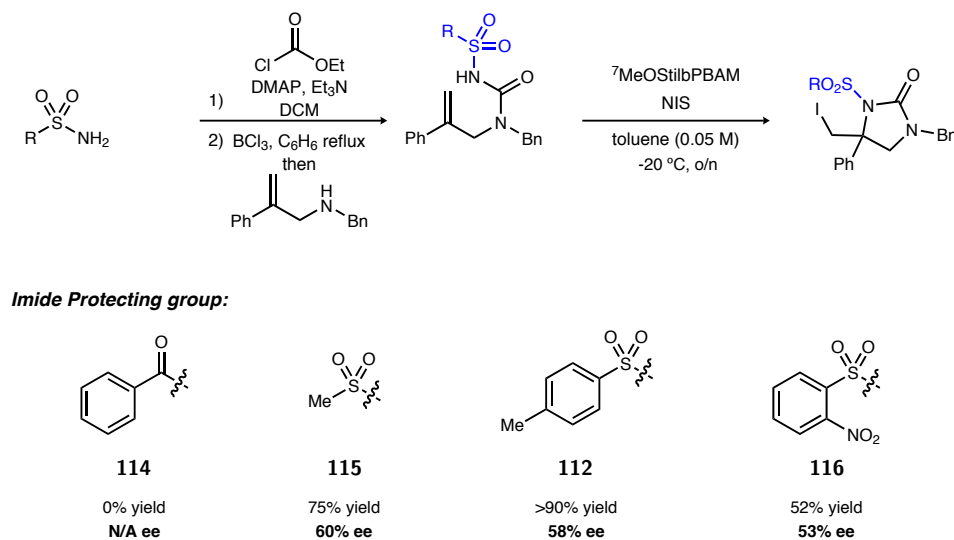
Figure 23: Effect of the size of the imide protecting group on the reactivity and selectivity of the urea cyclization reaction

The only factor not investigated at this point was the protecting group on the amine of the staring material. Previous investigations in the iodocarbamation reaction indicated that the benzyl group was necessary for high reactivity and high enantioselection. As indicated earlier, there are significant differences between the iodourea reaction achieving nitrogen cyclization with an allylic amine and the CO_2 capture reaction using the homoallylic amine. The previous investigations demonstrated no significant improvement in enantioselection when the sulfonyl imide was altered, hinting that the allylic nitrogen protecting group would be the key to achieving high selectivity. A representative screen of protecting groups demonstrate the importance of this group to enantioselection (Figure 26). When the protecting group is removed (**118a**), the monosubstituted amine is weakly reactive and delivers racemic product. On the opposite side of size, a large *tert*-butyl group (**118f**) achieves good reactivity but the reaction is not enantioselective.

70

Substrates that include an α-substition (methylene or methine) to the amine have similar outcomes in regard to enantioselection such as ethyl **118b**, benzyl **118c**, and the seemingly more bulky DPM **118e** all achieve 60-70% ee.
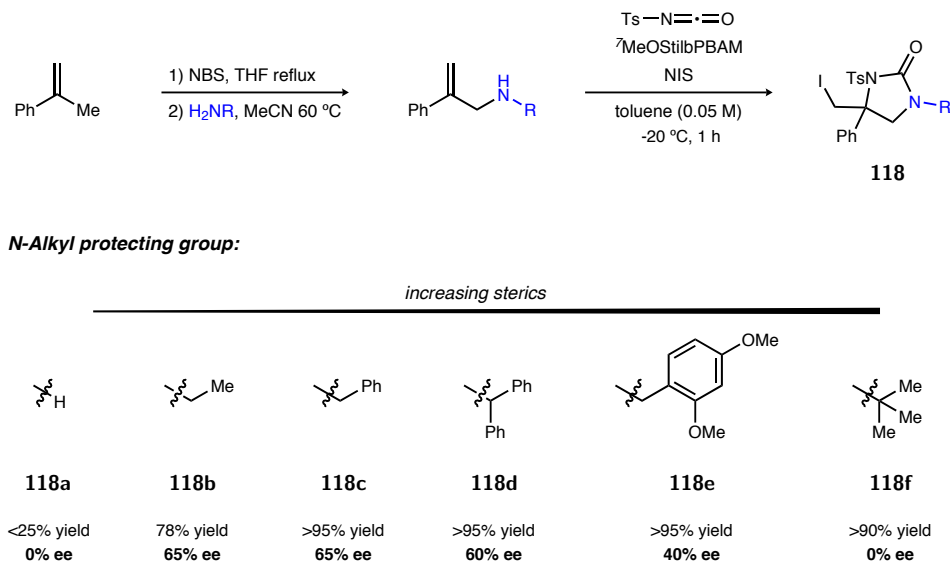
Figure 24: Affect of the *N*-alkyl protecting group on selectivity

The combined results from the catalyst and protecting group screens led to the generation of a proposed binding model for the catalyst substrate pair (Figure 25). Based on the empirical results along with visualization of a crystal structure of a catalyst salt complex, a hypothesis could be forwarded in regard to substrate binding. Important factors observed in this small screen include: 1) a more basic catalyst is necessary (most likely due to the decreased acidity of the imide compared to the carboxylic acid), 2) size of the sulfonyl protecting group does not impact enantioselectivity, and 3) the size of the protecting group of the allylic amine is an important factor for determining enantioselection. Although the exact influence of the allylic amine protecting group on enantioselection was not elucidated, the largest impact was seen in this series and was the focus of the continued optimization.

Alkyl amines reacted to give cyclic ureas in high yields with moderate enantioselection

larger alkyl group = lower selectivity

sulfonyl size and substitution pattern do not affect selectivity

larger backbone = lower selectivity
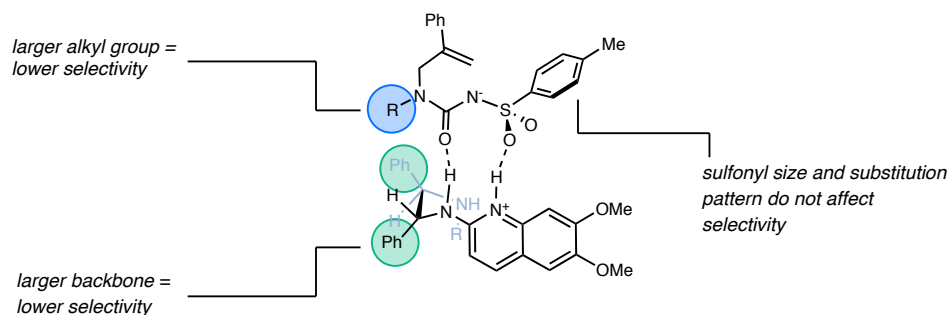
Figure 25: Binding model based on substituent effects of the substrate and catalyst

and for further optimization it was decided to focus on aryl amines. A series of aryl amines were synthesized and submitted to the reaction conditions. Surprisingly, a negative steric effect anticipated for **119d** did not materialize, and substituents at the 3- and 5-positions of the aniline provided results almost identical to the others (i.e. **119e** vs **119a** and **119d**). The optimal group in the series was the *p*-methoxy phenyl (PMP **119c**) achieving perfect selectivity for nitrogen cyclization, 71% yield, and 76% ee. Additionally, the PMP group is ideal because it is easily deprotected under oxidative conditions that are orthogonal to the sulfonyl group, allowing for differentiation of the nitrogens during derivatization of the products. The increased enantioselection with the PMP group and the added benefits of ease of deprotection served as the basis for moving this substrate forward in further optimization.

At this juncture a new catalyst ^{6,7}(MeO)$_2$StilbPBAM was employed due to the relative ease of synthesis compared to ^{7}MeOStilbPBAM.[135] The two catalysts perform nearly identically with the more basic ^{6,7}(MeO)$_2$StilbPBAM achieving slightly higher yields.[136] Changing the source of the iodine did not have a significant impact on enantioselectivity or nitrogen selectivity, however, the reaction time is fastest with the more soluble iodinat-

---

[135]Catalyst synthesis itself is similar for both catalysts, however the 6,7-disubsituted quinoline precursor is faster to synthesize because no regioisomeric mixtures have to be fractionally recrystallized.

[136]For complete optimization details see Appendix 4.1
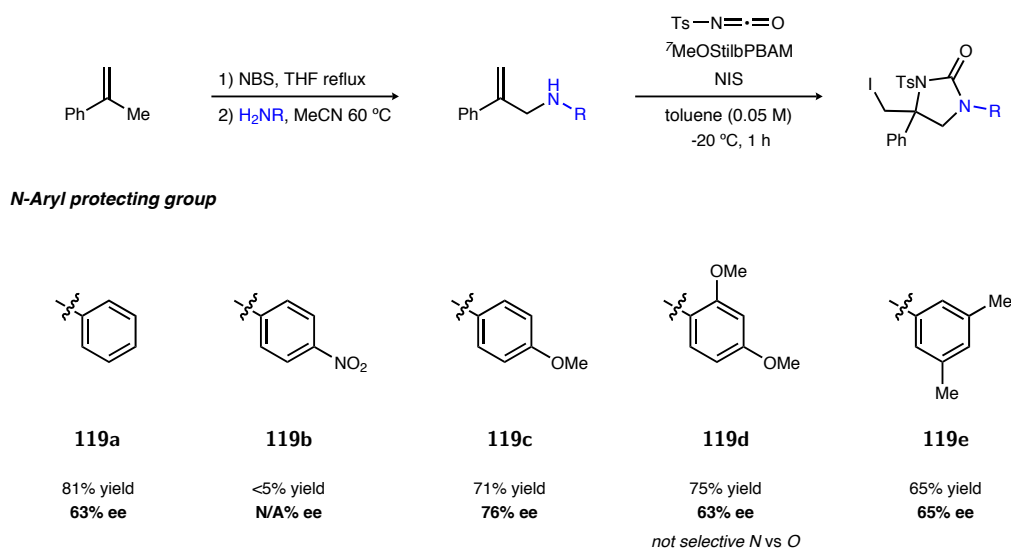
Figure 26: Affect of the *N*-aryl protecting group on selectivity

ing reagent *N*-iodo pyrrolidinone (NIP). This reaction is the first, using BAM catalysis, that is amenable to other iodinating sources of similar structure (i.e. high yields *and* high % ee). The new conditions using ^{6,7}(MeO)$_2$StilbPBAM and NIP resulted in greater than 90% yield and 81% ee. It is important to note that the reaction at room temperature (25 °C) is fully converted within 10 minutes of addition of NIP suggesting that signifi-cant background reactivity during quench could lower measured % ee. The quench used aqueous sodium thiosulfate (Na$_2$S$_2$O$_3$) which could warm up the reaction mixture and result in lower % ee material.[137] Various methods for reducing the oxidant (NIP) as a quench was studied which led to a more facile and higher throughput process. Pouring the reaction mixture directly from the -50 °C reaction onto a pad of 15% mixture of pow-dered sodium thiosulfate in silica (SiO$_2$) and eluting with 50% ethyl acetate in hexanes leads to almost quantitative yields and 91% ee (Figure 27). A great benefit of the new method of quenching is the allowance for higher throughput since there are no aqueous

---

[137]Cooling of the quench mixture is not sufficient since the lowest the aqueous solution can be cooled is 0 °C.

procedures. The silica removes catalyst starting material, and pyrrolidinone, and the thiosulfate quenches any remaining NIP. The NMR in Figure 27 shows that the purity of product is extremely high in the crude NMR and in fact the substrate for derivatizations (*vide infra*) are not further purified after the quench. With improved quenching methods, optimized protecting groups, and use of a more basic [6,7](MeO)$_2$StilbPBAM catalyst, the reaction could achieve excellent yield and enantioselectivity leaving the only unexplored territory of groups on the 1,1-disubstituted alkene.
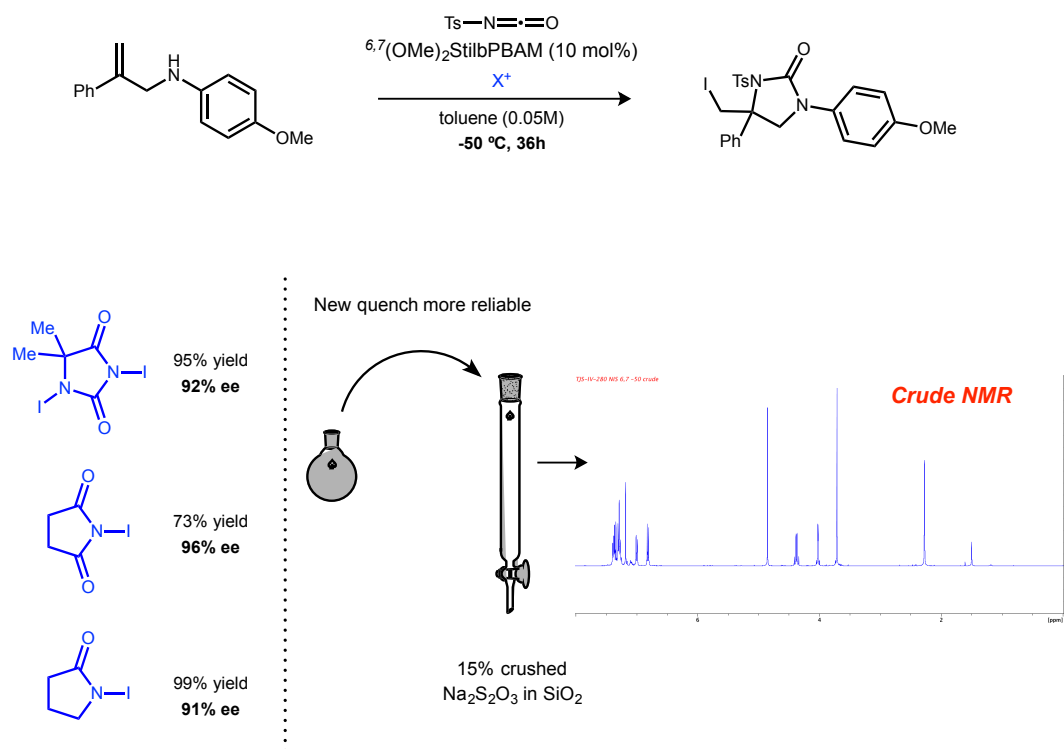
Figure 27: Halogen sources and new quench method for higher throughput

A brief substrate scope demonstrates the tolerability to differentially substituted aryl groups. The most interesting in this series is the notoriously difficult *para*-methoxy sub-

74

Table 7: Substrate tolerability of the enantioselective iodourea cyclization

entry	R_1	R_2	product	time(h)	yield(%)	ee (%)[a]
1[b]	C_6H_5	H	**121a**	36	82	**91**
2[c]	C_6H_5	H	**121b**	36	86	**55**
3	$^pMeC_6H_4$	H	**121c**	36	97	**92**
4	$^mMeC_6H_4$	H	**121d**	36	88	**91**
5	$^oMeC_6H_4$	H	**121e**	96	15	**49**
6	$^pBrC_6H_4$	H	**121f**	36	90	**88**
7	$^pFC_6H_4$	H	**121g**	36	90	**89**
8	$^pCF_3C_6H_4$	H	**121h**	48	75	**90**
9	$^pMeOC_6H_4$	H	**121i**	36	80	**90**
10	3-thiophenyl	H	**121j**	36	93	**88**
11	Bn	H	**121k**	36	75	**49**
12	Me	H	**121l**	36	93	**29**
13	H	H	**121m**	36	70	**38**
14[d]	H	C_6H_6	**122a**	36	93	**93**

[a]Enantiomeric excess (ee) determined by HPLC using a chiral stationary phase. Reactions are run on 0.1 mmol scale 0.05 M in toluene. Isolated yields are listed. See Appendix 4.1 for complete experimental details. Absolute configuration for **121f** assigned using X-ray analysis, remaining examples assigned by analogy. [b]1.0 mmol of starting material used. [c]NBS used as electrophilic halogen source. [d]Absolute configuration assigned by derivatization and comparison to L-Phe see appendix 4.1 for details.

strate[138] **121i** which cyclizes with 80% yield and 90% ee and is bench stable for weeks at the minimum. In addition, a heteroaromatic substrate **121j** prone to electrophilic aromatic substitution is tolerated with 93% yield and 88% ee. Significantly, substrates that have not been tolerated in previous chemistry (See Chapter 1 iodocarbonation and iodolactonization) such as the *para*-CF$_3$ phenyl **121h** achieve good yields and high enantioselectivity. Alkyl substrates, no matter the size were tolerated and retained selectivity for nitrogen cyclization, but low enantioselection (29-49% ee) was observed. Of particular

---

[138]Veitch, G. E.; Jacobsen, E. N. *Angew. Chem. Int. Ed.* **2010**, *49*, 7332–7335; Whitehead, D. C.; Yousefi, R.; Jaganathan, A.; Borhan, B. *J. Am. Chem. Soc.* **2010**, *132*, 3298–3300; Zhou, L.; Tan, C. K.; Jiang, X.; Chen, F.; Yeung, Y.-Y. *J. Am. Chem. Soc.* **2010**, *132*, 15474–15476; Murai, K.; Matsushita, T.; Nakamura, A.; Fukushima, S.; Shimura, M.; Fujioka, H. *Angew. Chem. Int. Ed.* **2010**, *49*, 9174–9177.

note is the product **122a** which employs a 1,2-disubstituted *cis*-alkene in the starting material and retains nitrogen selectivity and perfect preference for a 5-*exo* cyclization. The selectivity for the 5-*exo* product is curious due to a more stabilized carbocation in the benzylic position would lead to a 6-*endo* cyclization. The alteration of the alkene from a 1,1-disubstuted alkene to a 1,2-*cis*-disubstuted alkene with retention of nitrogen-, 5-*exo*-, *AND* enantioselectivity promoted the study of more differentially substituted alkenes.

Interestingly, when a 1,2-disubstituted *trans*-alkene (**125b**) is submitted to the urea cyclization reaction, 6-*endo* selectivity is observed with an isolated yield of 60% and 93% ee. It is also important to point out that the minor product of the *trans*-alkenes is 5-*exo* (**123**) which is the diastereomer of **122** and is isolated with 15% yield and 20% ee.[139,140] The simple manipulation of the geometry of the alkene has a drastic impact on regioselectivity of the amino cyclization. The observed regio-divergence must be catalyst controlled in the 6-*endo* cyclization because when an achiral base (1,1,3,3-tetramethylguanidine, TMG) is employed for synthesis of racemic product, the crude NMR shows a lower regioselectivity of about 60:40 of 6-*endo* to 5-*exo* and racemic catalyst has to be employed to achieve good reactivity and isolated yield. Interestingly, no erosion of regioselectivity is observed in the *cis*-alkene cyclization with TMG, producing one regioisomer and one diastereomer. Previous reports of halocyclizations that use 1,2-disubstituted alkenes by Shi and Denmark (Chapter 1, Figure 4) can use both *E*- and *Z*-alkenes to achieve high enantioselection for a 5-*exo* product (lower regioselection is observed with *Z*-alkenes). Contrasted to the previous work, our aminocyclization gives the opposite result when

---

[139]Absolute stereochemistry for **122** was determined by comparison to a derivative from L-Phe. Deiodination of **123** results in the same major enantiomer as the same product using **122**. See appendix 4.1 for complete details.

[140]Longer reaction times to ensure full reactivity at low temperature and not in the quench improve the observed *endo:exo* selectivity. Additionally, scaling of the reaction to 1 mmol yields similar results.

employing an *E*-alkene, producing the 6-*endo* product in higher yields and enantioselectivity. Compared to the cyclization of 1,1-disubstituted alkenes in the urea cyclization reaction (Table 7), where the product is a fully substituted carbon, the 1,2-disubstituted alkenes can produce an enantioenriched secondary amine which are not accessible using substrates similar to **121m**. With access to 1,3-imidazolidinone products already explored (Table 7), a small scope of 1,2-di and tri-substituted amines were tested to produce tetrahydro-2-pyrimidone products, and explore the less reported enantioselective 6-*endo* cyclization.
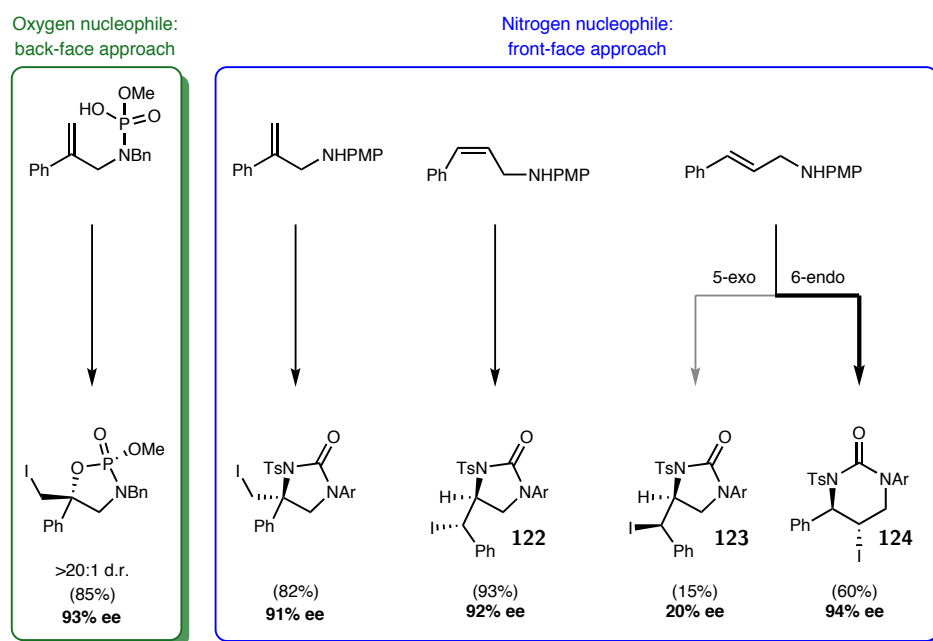
Figure 28: Regiodivergence of the iodourea cyclization reaction based on alkene geometry

The substate scope of the 6-*endo* cyclization was explored with substitution of the alkene distal to the allylic amine (Table 8, R_1). The requirement for high enantioselection in this brief scope was for a *trans*-alkene with an sp^2 carbon adjacent to the reactive alkene (i.e. alkyl groups at R_1 did not perform well) Higher substitution of the alkene can achieve good enantioselection (Table 8, entry 4) but have depressed reactivity most

likely due to the very crowded catalyst pocket. Interestingly, moderate enantioselection was retained when the dimethyl substituted alkene (Table 8, entry 5) is submitted to the reaction condition. This result reiterates that the the 6-*endo* cyclization is under catalyst control since the good enantioselection is observed (compare to 5-*exo*, Table 7, entry 12 which has very low selectivity when the methyl group is attached to the 1,1-disubstituted alkene). With the substrate scope of both 1,1- and 1,2-disubstituted alkenes, the only investigations remaining were examination of the utility of the products.

Table 8: Substrate tolerability of 1,2-disubstituted alkenes in the enantioselective iodourea cyclization
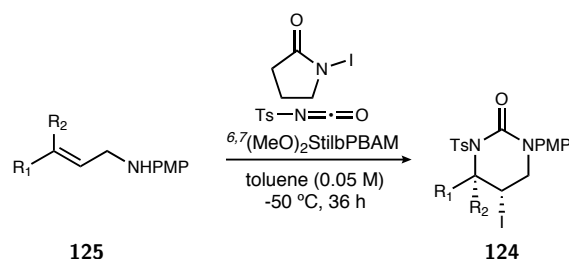
entry	R_1	R_2	product	time(h)	yield(%)	ee (%)[a]
1[b]	-CH=CHC$_6$H$_5$	H	**124a**	36	74	93
2	-C$_6$H$_5$	H	**124b**	84	60	94
3	-CH=CHCH$_3$	H	**124c**	36	40	94
4[c]	C$_6$H$_5$	CH$_3$	**124d**	72	31	86
5	CH$_3$	CH$_3$	**124e**	36	75	63

[a]Enantiomeric excess (ee) determined by HPLC using a chiral stationary phase. Reactions are run on 0.1 mmol scale 0.05 M in toluene. Isolated yields of 6-*endo* product are listed. See Appendix 4.1 for complete experimental details. Absolute configuration for **124a** assigned using X-ray analysis, remaining examples assigned by analogy. [b]1.0 mmol of starting material used. [c]Starting amine 19:1 Z:E.

Derivatization focused on the enantioenriched tetrahydro-2-pyrimidone products simply due to the access to material (Figure 29). Radical mediated substitution of the iodide proceed smoothly to give the alkylated urea **126**. Hydrolysis of the urea gives a di-amino alcohol **127** and reduction produces methyl diamine **128**. Surprisingly in the process of trying to find a substitution reaction of sodium methoxide on the alkyl iodide, an isomerization reaction was observed to the carbamate **129**. The conditions were altered to use a mild base in methanol in the microwave to give the same product with

a good yield (conditions shown in Figure 29). Double deprotection of the orthogonal protecting groups can be achieved using cerium(IV) ammonium nitrate for the oxidation of the *p*-methoxyphenyl group (PMP) and subsequent sodium naphthalene reduction of the *p*-toluenesulfonyl (Ts) to compound **130**. Finally the oxidation of **131** to the chiral hydantoin **132** is completed using DMP in fluorobenzene.[141] This derivatization is particularly useful because other methods for access to enantioenriched hydantoins are limited. Additionally, fully substituted hydantoins are an important class of compounds in therapeutic development because racemization (by enolization) is not possible in physiological conditions.
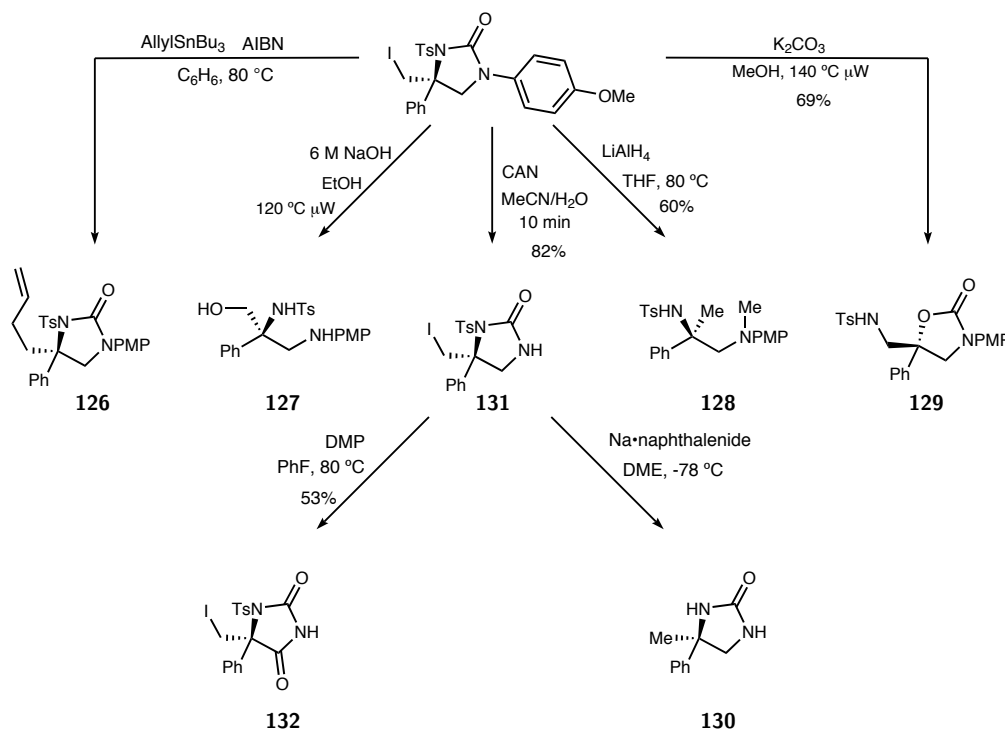
Figure 29: Derivatives of the chiral ureas produced by the enantioselective iodourea cyclization

---

[141]Nicolaou, K. C.; Mathison, C. J. N. *Angew. Chem. Int. Ed.* **2005**, *44*, 5992–5997.

2.3 Application of enantioselective alkene iodoamination to the cylic urea therapeutic Sch-425078

Neurokinin-1 (NK_1) is one of the three known mammalian tachykinin receptors (a subfamily of GPCRs) and is a target for therapeutics with antidepressant,[142] anxiolytic,[143] and antiemetic properties. Substance P,[144] an undecapeptide, acts as a neurotransmitter on the NK_1 receptor which are located in brain regions associated with regulating emotion (i.e. the hypothalamus and amygdala). NK_1 inhibitors block this interaction of substance P with the NK_1 receptor and are an important class of compounds that target this receptor for the therapeutic benefits stated earlier. One series of investigations initiated by Schering-Plough identified a series of inhibitors of NK_1 that are orally active and are CNS brain penetrant.[145] In addition the same studies identified the most potent diastereomer of this series of compounds and resulted in the optimized compound Sch-425078.

Sch-425078 **138** is a chiral cyclic urea with an appended chiral benzylic ether where both of the chiral centers were optimized for activity. The chiral bis(trifluoromethyl)benzylic ether resembles the commercially marketed therapeutic Emend and is a common motif

---

[142]Kramer, M. S.; Cutler, N.; Feighner, J.; Shrivastava, R.; Carman, J.; Sramek, J. J.; Reines, S. A.; Liu, G.; Snavely, D.; Wyatt-Knowles, E.; Hale, J. J.; Mills, S. G.; MacCoss, M.; Swain, C. J.; Harrison, T.; Hill, R. G.; Hefti, F.; Scolnick, E. M.; Cascieri, M. A.; Chicchi, G. G.; Sadowski, S.; Williams, A. R.; Hewson, L.; Smith, D.; Carlson, E. J.; Hargreaves, R. J.; Rupniak, N. M. J. *Science* **1998**, *281*, 1640–1645.

[143]Varty, G. B.; Cohen-Williams, M. E.; Morgan, C. A.; Pylak, U.; Duffy, R. A.; Lachowicz, J. E.; Carey, G. J.; Coffin, V. L. *Neuropsychopharmacology* **2002**, *27*, 371–379.

[144]Datar, P.; Srivastava, S.; Coutinho, E.; Govil, G. *Curr. Top. Med. Chem.* **2004**, *4*, 75–103; Harrison, S.; Geppetti, P. *Int. J. Biochem. Cell. Biol.* **2001**, *33*, 555–576.

[145]Shue, H.-J.; Chen, X.; Schwerdt, J. H.; Paliwal, S.; Blythin, D. J.; Lin, L.; Gu, D.; Wang, C.; Reichard, G. A.; Wang, H.; Piwinski, J. J.; Duffy, R. A.; Lachowicz, J. E.; Coffin, V. L.; Nomeir, A. A.; Morgan, C. A.; Varty, G. B.; Shih, N.-Y. *Bioorg. Med. Chem. Lett.* **2006**, *16*, 1065–1069; Ho-Jane, S.; Xiao, C.; John, H. S.; Sunil, P.; David, J. B.; Ling, L.; Danlin, G.; Cheng, W.; Gregory, A. R.; Hongwu, W.; John, J. P.; Ruth, A. D.; Jean, E. L.; Vicki, L. C.; Amin, A. N.; Cynthia, A. M.; Geoffrey, B. V.; Neng-Yang, S. *Bioorg. Med. Chem. Lett.* **2006**, *16*, 1065–1069.

in NK$_1$ antagonists. The need for enantiopure cyclic ureas for the continued investigation of activity necessitated a revised route which was accomplished from the chiral pool (phenylglycine) and the use of a diastereoselective alkylation.[146] The stereoselective route starts with the methyl ester of phenylglycine **133** and condenses pivaldehyde to furnish the aminal **134**. A diastereoselective alkylation termed "self reproduction of the center of chirality" was used to afford the alkylated aminal **136**. The alkyl halide **135** was synthesized from a CBS reduction of 3,5-bis(trifluoromethyl)acetophenone then condensation on formaldehyde in the presence of HBr. The chiral aminal was hydrolyzed to give the α-amino amide **137** and the synthesis was finished with formation of the hydantoin and selective reduction to the urea arriving at target compound Sch 425078 (**138**). The route is efficient and direct, however entry to other derivatives of the aryl ring attached to the chiral urea is difficult. More importantly is that access to exotic phenylglycine derivatives is expensive (i.e. unusual substitution on the aryl ring of phenylglycine)[147] and not amenable to scale.

Other methodology that provides access to this class of cyclic ureas is the Shi procedure using a copper catalyzed diamination of olefins that was described in the introduction. Unfortunately the reaction is not enantioselective and in their route to Sch-425078 separation of diastereomers results in a 35% yield (See introduction Scheme 12).[148] The route is more direct, and access to derivatives would be much faster, but suffers from no enantioselective version and relies on diastereoselection imparted by the chiral methyl of the appended ether. Although the synthesis is not enantioselective, a more recent version

[146]Reichard, G. A.; Stengone, C.; Paliwal, S.; Mergelsberg, I.; Majmundar, S.; Wang, C.; Tiberi, R.; McPhail, A. T.; Piwinski, J. J.; Shih, N.-Y. *Org. Lett.* **2003**, *5*, 4249–4251.

[147]On October 30, 2017 4-fluoro-D-α-phenylglycine was $647 for 1g and the methyl ester HCl salt $51 for 250 mg.

[148]Wen, Y.; Zhao, B.; Shi, Y. *Org. Lett.* **2009**, *11*, 2365–2368.
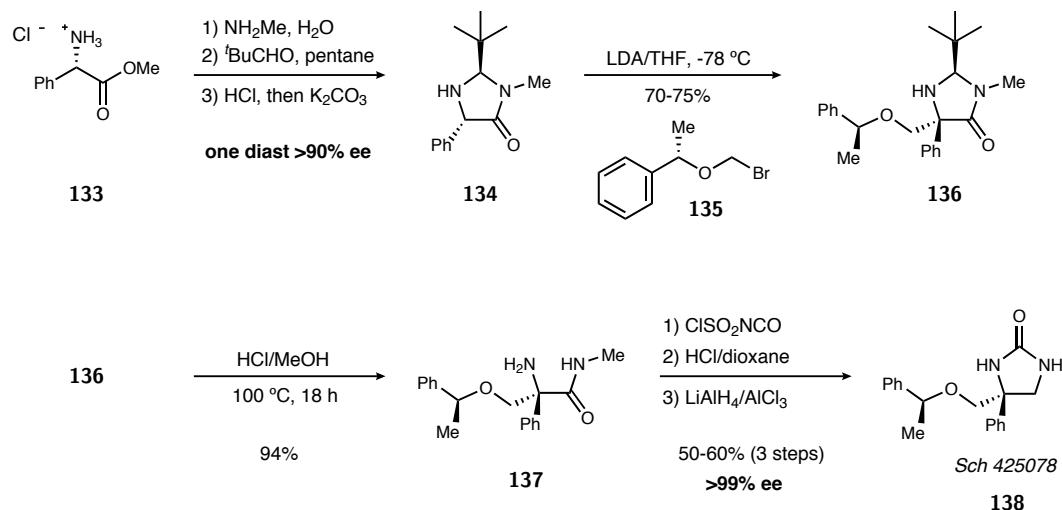
Scheme 15: Schering-Plough's asymmetric synthesis of NK$_1$ antagonist

of Shi's diamination chemistry[149] could possibly access Sch 425078 in an enantioselective

manner but has not yet been demonstrated.

A more efficient route was envisioned using a convergent process shown in Figure 30.

The disconnection of the ether bond in **139** would lead to the chiral alcohol **142** and

urea **140**. An enantioselective CBS reduction can set the chirality of the alcohol from

ketone **143**, and the enantioselective BAM catalyzed urea cyclization can be used to set

the nitrogen stereocenter in **141**.

The urea cyclization proceeds smoothly and can be scaled up with the highest at-

tempted scale using 1 gram of allylic amine to produce the cyclic urea **121g** with high

yields and 92% ee. The CBS reduction also achieves high yields and 89% ee of the ben-

zylic alcohol **142**. With both stereocenters set in the first steps, simple manipulation of

functional groups and a substitution were necessary. Unsurprisingly, attempts at substi-

tution of the *neo*-pentyl iodide **140** using NaH or AgOTf were unsuccessful with starting

material recovered in all cases. Reversal of the coupling partners necessitated the conver-

---

[149]See introduction and references 95-102
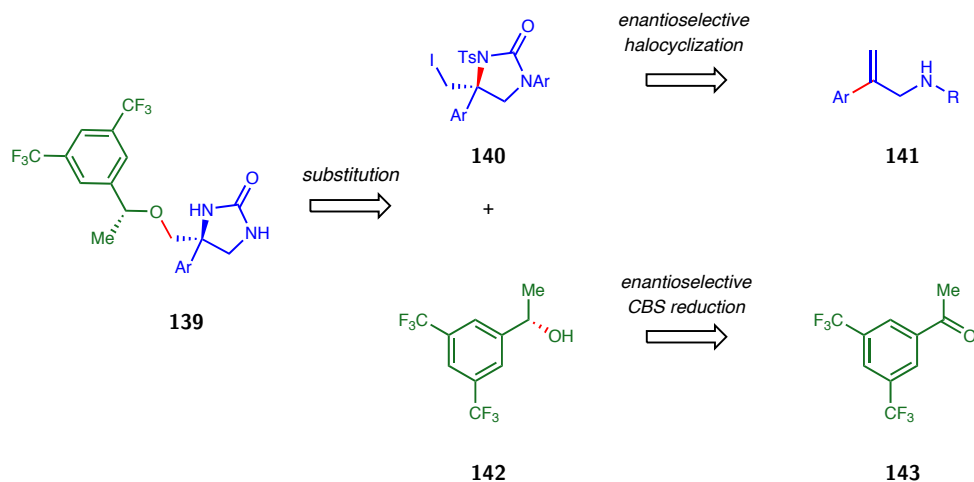
Figure 30: Retrosynthetic analysis of Sch-425078

sion of the iodide **140** to an alcohol. The chiral alcohol **142** would consequently need to be made electrophilic by conversion to a bromide or a mesylate. Synthesis of the alcohol from the iodide turned out to be the crux of this synthesis.

Initial attempts focused on the simple substitution of the neopentyl iodide of **121g** with either hydroxide or an alcohol. Using heat and sodium hydroxide, not surprisingly, hydrolysis of the the urea is observed (Figure 29, **127**). Some precedence in functionalization of the carbamates from the CO_2 work led us to try sodium methoxide substitution with heating. Indeed a product was isolated in 69% yield that retains the enantioexcess of the starting material (91% ee) and was initially thought to be the neo-pentyl alcohol **144**. Conditions were optimized and we found that methoxide was not necessary and simply microwaving the iodide with potassium carbonate in methanol would give us the product as well. The alcohol was thought to either come from the water in the wet methanol or by de-methylation of the methyl ether.

This material was moved forward in the synthetic sequence toward Sch-425078 by investigating the substitution reaction trying to synthesize the protected precursor to **139**. This is the first stage where we started to realize that the substitution reaction
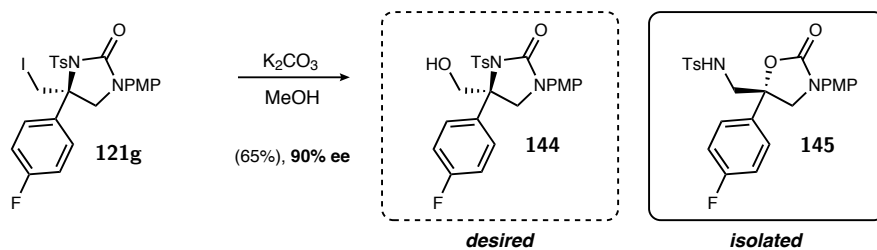
Scheme 16: Rearrangment of alkyl iodide to form carbamate

may not be giving the desired alkylated product. In addition to the mesylate of alcohol **142**, the bromide was synthesized by an Appel reaction. The isolated product from the substitution reaction (what we thought of as **144** but was **145**) would alkylate in many of the simple benzylic protection conditions for alcohols, including silver salts or sodium hydride in THF. More forcing conditions were necessary using NaH in DMF at elevated temperatures. The bromide was not the ideal substitution partner, giving a mixture of diastereomers, and the mesylate was employed which did not racemize in the substitution conditions.

The coupled product was characterized and it was at this point that we realized a rearrangement reaction was occurring in the step indicated in Scheme 16. A HMBC was obtained and we elucidated the structure to be rearranged product **145**. Interestingly, the rearrangement has to be completely stereospecific since we do not observe any erosion in enantioexcess during the reaction. This result, however disappointing in route to the target, brings a new interesting derivative which can access chiral oxazolidinones and their derivatives.
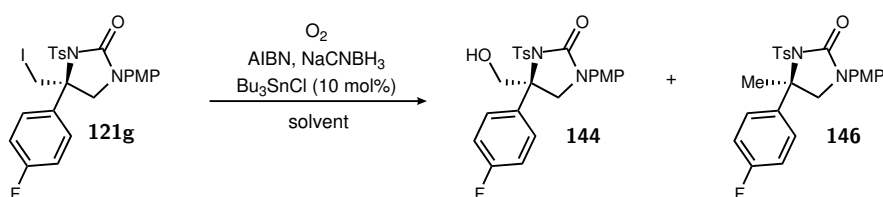
Scheme 17: Radical oxygenation of neo-pentyl iodide

A new scheme for substitution of the alkyl iodide was needed to complete the target synthesis of Sch-425078. The only substitution that had proceeded at this point was the radical mediated allylation using AllylSnBu$_3$. Trapping of oxygen and reduction of the resulting peroxide would be another method for accessing the desired neo-pentyl alcohol **144**. This route and subsequent optimization was investigated by an undergraduate researcher from Xavier University, Hannah Lankswert.
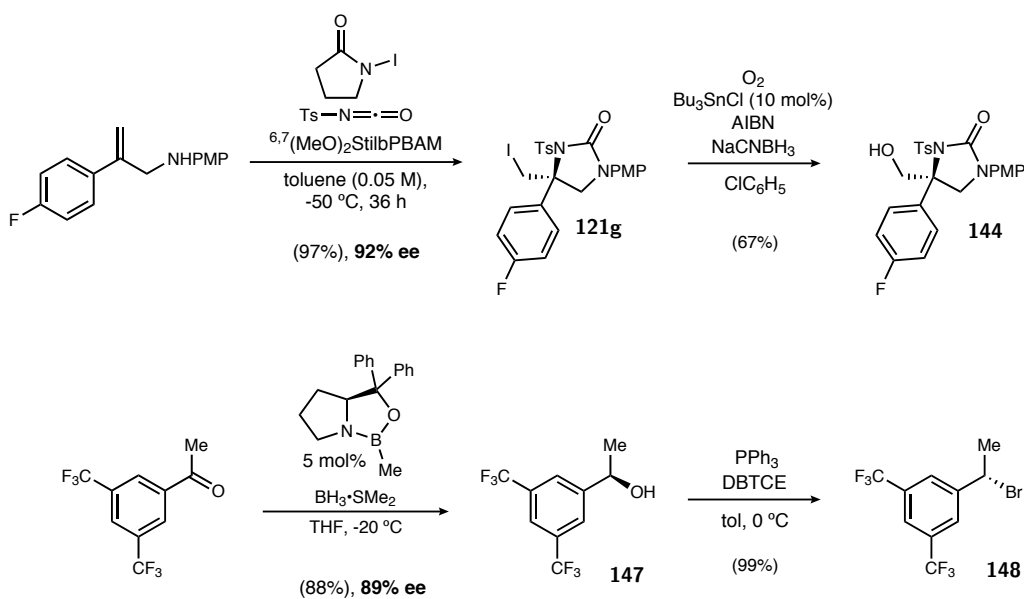
Scheme 18: Synthesis of precursors for Sch-42507

Initial results following literature procedure[150] using a catalytic amount of Bu$_3$SnCl, AIBN, and 2 equivalents of NaCNBH$_3$ in ^{t}BuOH were poor with less than 10% yield of the isolated product. The major product in these reactions was direct reduction of the iodide to the methyl group **146**. The addition of perfluorodecalin doubled the yield of the alcohol **144** to around 15-20% but changing to other tin halides did not prove fruitful. Finally, the addition of 1.2 equalivents of AIBN boosted the isolated yield up to 42%, a great ending to Hannah's summer rotation. In an effort to further improve the yield, we

---

[150]Sawamura, M.; Kawaguchi, Y.; Nakamura, E. *Synlett* **1997**, *1997*, 801–802.

decided to change to a solvent that would be less likely to donate a hydrogen atom to the primary radical formed by radical de-iodination of the urea. Chlorobenzene was chosen for its high boiling point and higher tolerability to heating under an oxygen atmosphere. This change produced full conversion and about a 70:30 ratio of desired alcohol **144** to reduced product **146**. Further optimization by bubbling oxygen for the duration of heating, suppressed the side reaction leading to reduced product **146**. Isolated yields of this step range from 55-68% with no erosion of enantiomeric excess.
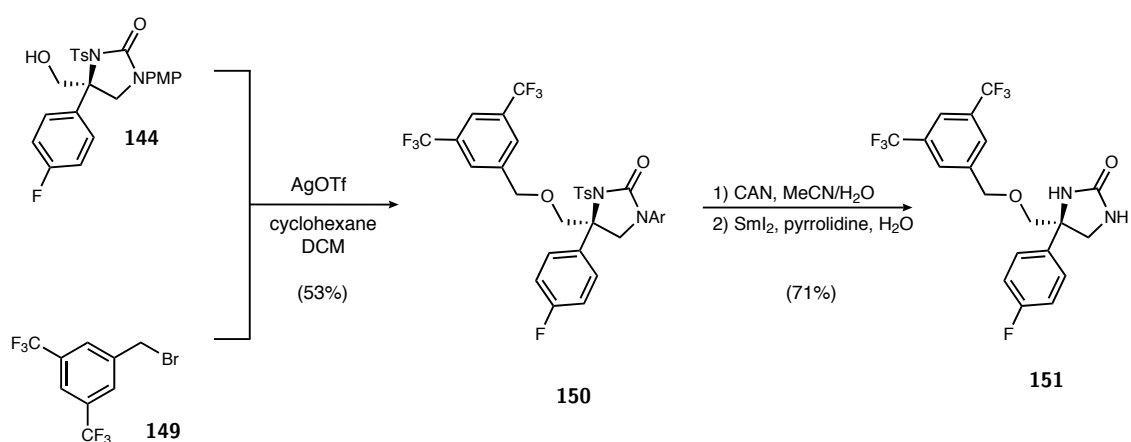
Scheme 19: Synthesis of NK$_1$ antagonist

With the alcohol **144** and bromide **148** in hand, investigations to couple the two were initiated. In this case substitution of the benzylic bromide proceeded using a superstoichiometric amount of AgOTf in cyclohexane/DCM. Unfortunately, the benzylic bromide racemizes[151] in the reaction conditions leading to a 1:1 diastereomeric ratio. One diastereomer was isolated and verified to be the ether by HMBC. Additional attemts using sodium hydride and the benzylic mesylate gave starting material and styrene. The activity of Sch-425078 and the desmethyl version are comparative in activity, CNS penetration, and suppression in the gerbil foot tapping model. Since the methyl group of

---

[151]Bromide precursor was verified to be high ee by optical rotation of pure sample.

the benzylic ether is not necessary for high activity, it was envisioned to use a non-chiral benzylic bromide **149** for the alkylation. The endgame synthesis was accomplished using AgOTf and **149** followed by double deprotection of the PMP and tosyl groups.

2.4 Conclusions and future outlook

In conclusion, a new organocatalytic enantioselective urea halocyclization reaction was developed that overcomes the difficulty of controlling an ambident nucleophile for forming nitrogen-carbon bonds. Interesting aspects of the reaction arise when using differentially substituted alkenes, and the catalyst can retain high regio- and enantio-control of both 5-*exo* and 6-*endo* iodocyclizations. The catalyst is not an acid salt which contrasts to former halocyclization reaction developed in the Johnston lab and the facial selectivity is reversed, possibly due to a larger nucleophile.

The changes to the catalyst system (i.e. catalyst salt performing poorly) hint that the bifunctional nature that has been proposed for the BAM catalysts may not be functioning. These results combined with the crystal structure by Matt Knowe described in Chapter 1 may necessitate further investigation into mechanism and binding of the electrophile to the catalyst. Another hypothesis is that the catalyst salts are acting as an additional steric parameter that can be easily modulated to increase enantioselection. It may be impossible to distinguish between the two and to date we have not found good experiments to elucidate the true nature of the counterion for these catalyst systems. Regardless of the true operating mechanism, counterions offer an extremely powerful tool for rapid optimization of new enantioselective reactions.

Additionally, derivitization of the products can furnish diamines, hydantoins, and deprotected ureas. The urea cyclization was successfully applied to the synthesis of

an NK$_1$ antagonist demonstrating the utility of this reaction for access to chiral small molecule therapeutics. This study offers the first enantioselective nitrogen-carbon bond-forming reaction to the repertoire of BAM-based catalysis and offers a new realm of reactions for these ligands.
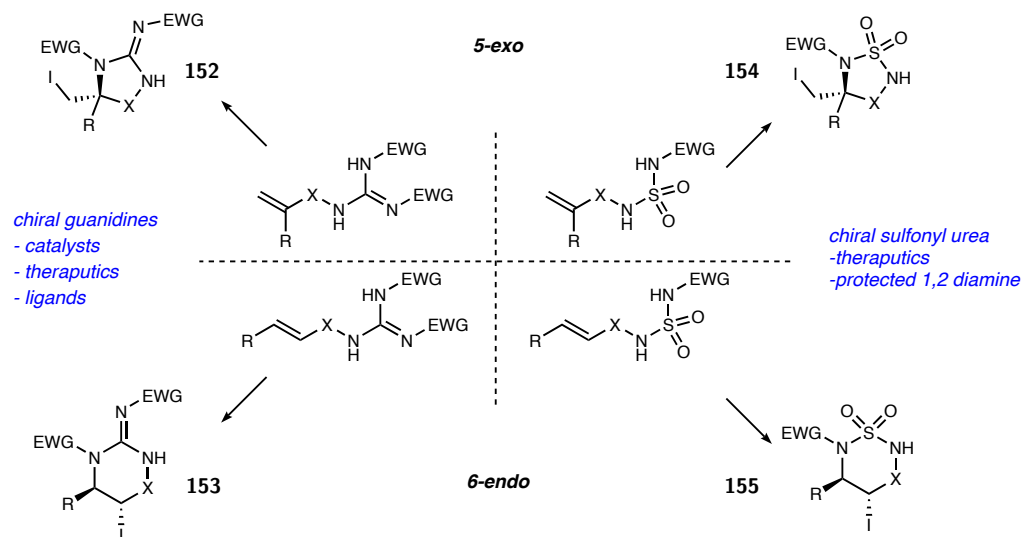
Figure 31: Future directions of nitrogen cyclizations using BAM-based catalysis

Future studies could achieve cyclizations of other types of amides or imides to build useful small molecule heterocycles. Figure 31 shows the possibilities of expanding the urea methodology into new classes of enantioselective cyclizations. The ability to use BAM-based catalysts to effect cyclizations such as guanidines would be teach us how to match pK$_a$ to more basic substrates while maintaining high enantioselectivity. Therapeutic candidates such as Verubecestat contain a sulfonyl guanidine (similar to **153**, X = SO$_2$) whose chirality is essential for activity. Additionally, sulfonyl ureas could be accessed through the cyclization strategy which would allow for synthesis of these important scaffolds. These motifs mentioned have not been investigated with BAM catalysis, however would give a unique opportunity to find design aspects that would be important to optimization using less acidic cyclization precursors. Finally, the use of alkene geom-

etry to access both 5- and 6-membered heterocycles allows for facile access to a diverse set of substrates. The continued study of new reactions will teach us about BAM catalyst control mechanisms in halocyclization reactions, and give us predictive power when applying the methodology to target synthesis.

Chapter 3 Mechanistic investigations of the influence of catalyst symmetry on the stereodivergence of nitroester additions into aldimines unveiled by DFT calculations

3.1 Introduction

3.1.1 Introduction of nitroester additions to aldimines

α, α-Disubstituted α-amino acids have many unique properties that make them attractive in biomedical research and drug discovery.[152,153] These non-proteinogenic amino acids can induce conformational helix changes that display broad-spectrum antibiotic activity[154] due to the modification at the α-position can diminish proteolytic[155] and chemical degradation[156] pathways. Due to their increased stability, α, α-disubstituted α-amino acids have been used as peptidomimetic enzyme inhibitors without the worry of degradation in biological systems.[157]

---

[152]Goodman, M.; Ro, S. In *Burger's Medicinal Chemistry and Drug Discovery*; 5th ed.; Wolff, M. E., Ed.; Wiley: 1995; Vol. 1, p 803.

[153]Saari, W. S.; Freedman, M. B.; Hartman, R. D.; King, S. W.; Raab, A. W.; Randall, W. C.; Engelhardt, E. L.; Hirschmann, R.; Rosegay, A. *J. Med. Chem.* **1978**, *21*, 746–753; Walsh, J. J.; Metzler, D. E.; Powell, D.; Jacobson, R. A. *J. Am. Chem. Soc.* **1980**, *102*, 7136–7138; Saari, W. S.; Halczenko, W.; Cochran, D. W.; Dobrinska, M. R.; Vincek, W. C.; Titus, D. C.; Gaul, S. L.; Sweet, C. S. *J. Med. Chem.* **1984**, *27*, 713–717.

[154]Degenkolb, T.; Berg, A.; Gams, W.; Schlegel, B.; Gräfe, U. *J. Pept. Sci.* **2003**, *9*, 666–678.

[155]Almond, H. R.; Manning, D. T.; Niemann, C. *Biochemistry* **1962**, *1*, 243–249; Khosla, M. C.; Stachowiak, K.; Smeby, R. R.; Bumpus, F. M.; Piriou, F.; Lintner, K.; Fermandjian, S. *Proc. Natl. Acad. Sci. USA* **1981**, *78*, 757–760.

[156]Irie, K.; Koizumi, F.; Iwata, Y.; Ishii, T.; Yanai, Y.; Nakamura, Y.; Ohigashi, H.; Wender, P. A. *Bioorg. Med. Chem. Lett.* **1995**, *5*, 453–458; O'Connor, S. J.; Liu, Z. *Synlett* **2003**, *2003*, 2135–2138.

[157]Fasella, P.; Giartosio, A.; Hammes, G. G. *Biochemistry* **1966**, *5*, 197–202; Schirlin, D.; Gerhart, F.; Hornsperger, J. M.; Hamon, M.; Wagner, J.; Jung, M. J. *J. Med. Chem.* **1988**, *31*, 30–36.

In addition to the α-substitution of amino acids, incorporation of a β-amino group imbues new biological activity.[158] In fact, naturally occurring α,β-diamino acids have been identified and include: Dap, D-DPR, α,β-DAP (Figure 32). Many isolated secondary metabolites such as β-substituted alanines, L-quisqualic acid, and mimosine also include this interesting moiety. An incredible discovery was that α,β-diamino acids were identified in meteorites,leading to the hypothesis that these motifs were crucial for prebiotic evolution to nucleic materials such as DNA and RNA.[159]
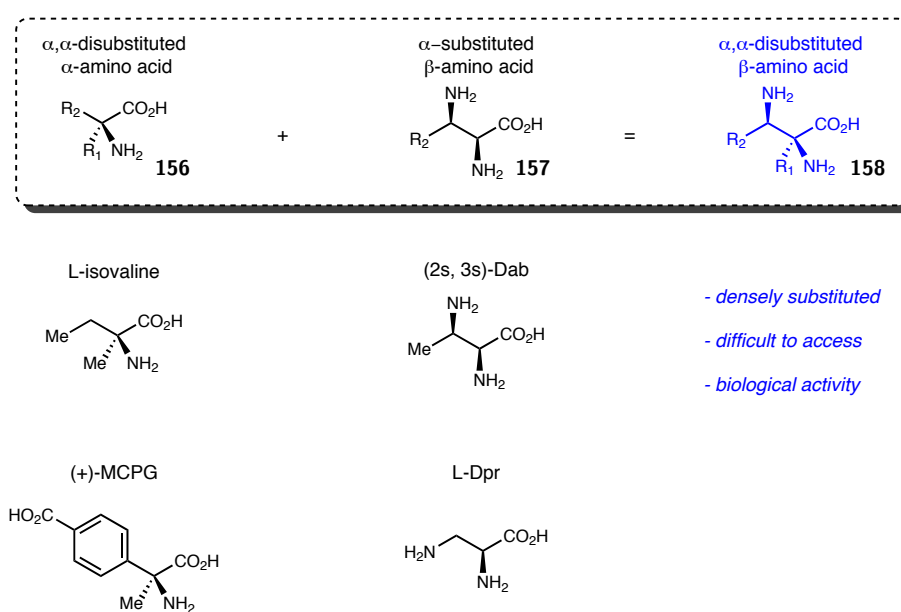
Figure 32: Structures of substituted amino acids and thier naturally occurring derivatives

The combination of these two structural motifs would furnish α-substituted α,β-diamino acids, a challenging target in synthetic chemistry, which could lead to substances that benefit from multiple features of each constituent. The densely functionalized quaternary center adjacent to a chiral amine is difficult to synthesize in an enantioselective

[158]For review see: Viso, A.; Fernández de la Pradilla, R.; García, A.; Flores, A. *Chem. Rev.* **2005**, *105*, 3167–3196.

[159]Meierhenrich, U. J.; Muñoz Caro, G. M.; Bredehöft, J. H.; Jessberger, E. K.; Thiemann, W. H.-P. *Proc. Natl. Acad. Sci. USA* **2004**, *101*, 9182–9186.

and diastereoselective manner. Even more challenging is developing a catalytic asymmetric method for synthesis of these potentially useful targets. The synthesis of α-substituted α,β-diamino acids are most commonly accomplished by a carbon-carbon bond forming step between an aldimine and a nitroester (commonly referred to as an aza-Henry or nitro-Mannich reaction)[160] However with two *pro*chiral reactants, control of diasteroselection and enantioselection are not been predictable *a priori.*

Shibasaki was the first to develop a catalytic asymmetric approach to the aza-Henry reaction using a heterobimetallic complex.[161] They were able to achieve a d.r. of 6:1 *anti:syn* and 76% ee for the major diastereomer. They later evolved the catalyst to a chiral Ni_2-Schiff base complex for the synthesis of *anti-α,β*-diamino acid surrogates.[162] The improved reaction could achieve up to >97:3 d.r *anti:syn* with 95% ee for the major diastereomer. The catalyst loading of this reaction can be lowered to 1 mol% without significant impact on selectivity.[163]

Using the combination of a chiral Lewis acid and a chiral organocatalyst, Jørgensen accomplished the first diastereoselective and enantioselective addition of nitroesters **159** to α-aminoesters **160**.[164] The use of quinine in conjunction with (S)-Ph-BOX could achieve a 14:1 d.r. *anti:syn* and 98% ee for the major diastereomer (**161**). They propose a simple model for achieving high selectivity using this cooperative catalyst system where the Brønsted basic quinine deprotonates the nitroester and the Lewis acid coordinates the α-

---

[160]For reviews see: Noble, A.; Anderson, J. C. *Chem. Rev.* **2013**, *113*, 2887–2939; Marqués-López, E.; Merino, P.; Tejero, T.; Herrera, R. P. *Eur. J. Org. Chem.* **2009**, *2009*, 2401–2420; Ting, A.; Schaus, S. E. *Eur. J. Org. Chem.* **2007**, *2007*, 5797–5815; Cozzi, P. G.; Hilgraf, R.; Zimmermann, N. *Eur. J. Org. Chem.* **2007**, *2007*, 5969–5994; Friestad, G. K.; Mathies, A. K. *Tetrahedron* **2007**, *63*, 2541–2569; Kobayashi, S.; Mori, Y.; Fossey, J. S.; Salter, M. M. *Chem. Rev.* **2011**, *111*, 2626–2704.

[161]Yamada, K.-i.; Moll, G.; Shibasaki, M. *Synlett* **2001**, *2001*, 0980–0982.

[162]Chen, Z.; Morimoto, H.; Matsunaga, S.; Shibasaki, M. *J. Am. Chem. Soc.* **2008**, *130*, 2170–2171.

[163]1 mol% catalyst achieves 88:12 d.r. and 98% ee while 5 mol% achieves 91:9 d.r and 98% ee with the same substrate.

[164]Knudsen, K. R.; Jørgensen, K. A. *Org. Biomol. Chem.* **2005**, *3*, 1362–1364.
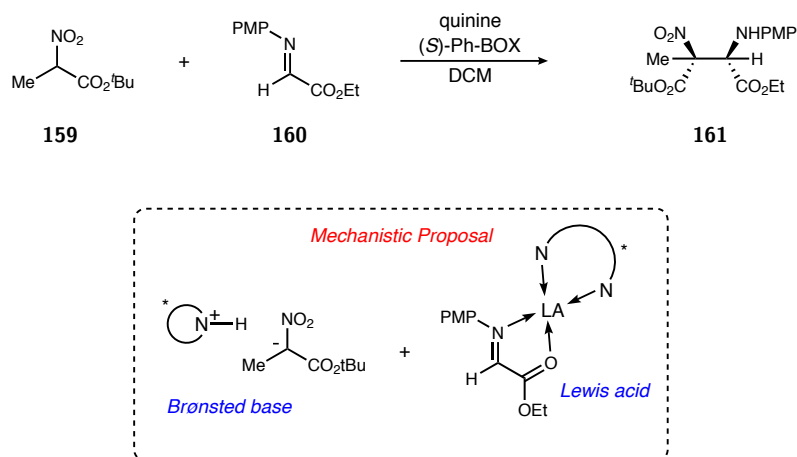
Scheme 20: Jørgensen's cooperative catalytic system for diastereoselective and enantioselective additions of nitroesters to α-aminoesters

aminoester as shown in Scheme 20. The authors propose that there is a "chiral molecular recognition" between the chiral Brønsted base and the chiral Lewis acid, and they employ a variety of different ligands for both base and acid to support their claims. Finally, due to the chiral recognition between the base and acid, they cannot reverse the enantioselectivity without a significant impact on the diastereoselectivity. Additional *anti*-selective reactions have been reported[165] but an interesting and particularly useful contribution to the *anti*-selective methodology was reported by Liu (useful due to the ease of access to the catalyst and simple reaction system).[166] The use of a toluene-brine solvent system in conjunction with a cinchona derived quaternary ammonium salt achieves over 22:1 d.r. *anti:syn* and over 99% ee.

Contrasted to the *anti* selective additions described above, Ooi developed a catalyst system that could achieve high diastereoselectivity and enantioselectivity for the *syn*

[165]Han, B.; Liu, Q.-P.; Li, R.; Tian, X.; Xiong, X.-F.; Deng, J.-G.; Chen, Y.-C. *Chem. Eur. J.* **2008**, *14*, 8094–8097; Puglisi, A.; Raimondi, L.; Benaglia, M.; Bonsignore, M.; Rossi, S. *Tetrahedron Lett.* **2009**, *50*, 4340–4342; Han, B.; Huang, W.; Xu, Z. R.; Dong, X. P. *Chin. Chem. Lett.* **2011**, *22*, 923–926.

[166]Li, M.; Ji, N.; Lan, T.; He, W.; Liu, R. *RSC Adv.* **2014**, *4*, 20346–20350.

product.[167] The catalyst is an interesting chiral ammonium betaine that the authors propose is bifunctional using the phenolic alkoxide as both base and hydrogen bond acceptor, while the quaternary ammonium salt acts as an ionic counterion that aids in coordination. In their substrate scope they can achieve up to 5.2:1 d.r of *syn:anti* with 98/93% ee respectively.
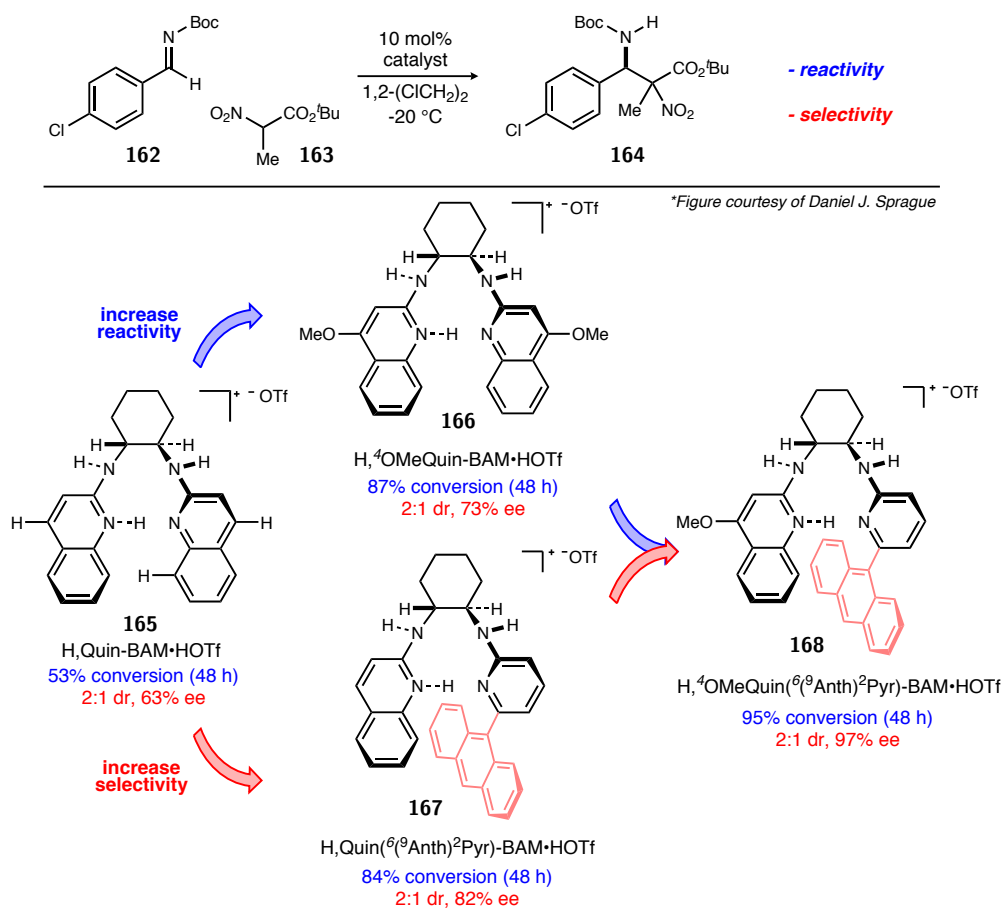
Figure 33: Optimization of catalyst for achieving higher conversion and enantioselection

Although incredibly high selectivity is achieved in all of these catalyst systems, there is no unifying theme to what catalyst systems or attributes will give rise to either *anti-* or *syn*-selectivity. The closest system so far was discovered by the Johnston group using

[167]Uraguchi, D.; Koshimoto, K.; Ooi, T. *J. Am. Chem. Soc.* **2008**, *130*, 10878–10879.

BisAmidine (BAM) catalysts.[168,169] Initial discovery of the BAM-catalyzed addition of nitroesters to aldimines were moderately successful using the first generation BAM catalyst **165**. A broad outline of the optimization of the catalyst (by Anand Singh) is shown in Figure 33. The discovery that a methoxy group could make the amidine more basic and increase reactivity (**166**, Figure 33), complimented the finding that catalyst symmetry could be leveraged to increase the enantioselectivity (**167**, Figure 33). The diasterometic ratio of *syn* to *anti* was still low at 2:1, but the simple change from a *tert*-butyl ester **163** to a diisopropyl aryl ester $(2,6\text{-}^{i}\text{Pr}_2\text{-}\text{C}_6\text{H}_3)$ increased the ratio of *syn:anti* to 12:1 with the same electrophile shown in Figure 33, while maintaining high % ee of the major diastereomer. This is one of the few examples of a *syn*-selective nitroester addition to aldimines.

It was discovered by Daniel Sprague and Anand Singh that a surprising stereodivergence could be observed when manipulating catalyst symmetry (Scheme 21). Using a more Brønsted basic catalyst (PBAM, **32**), a complete reversal in diastereoselectivity was observed with a greater than 20:1 ratio of *anti:syn* products and 96% ee.[170] The most interesting aspect of this stereodivergent reaction is that the imine retains its absolute facial selectivity and both catalysts lead to the benzyl amine configuration shown in Scheme 21.. It appears the catalyst symmetry has some effect on the nucleophile (nitroester) which forces altered binding leading to the epimeric center at the nitro carbon. Unlike any of the previous systems, this is the first approach that can give access to all four diastereomers in high selectivity by using catalyst enantiomers or symmetry

---

[168]Singh, A.; Yoder, R. A.; Shen, B.; Johnston, J. N. *J. Am. Chem. Soc.* **2007**, *129*, 3466–3467; Singh, A.; Johnston, J. N. *J. Am. Chem. Soc.* **2008**, *130*, 5866–5867.

[169]For an overview of the important functionalities of the BAM catalysts see Chapter 1 Introduction.

[170]Scheme 21 shows the triflimide catalyst salt with PBAM but the triflic acid salt performs similarly. Triflimide was chosen due to the ease of using a solid acid for salt formation.

elements.
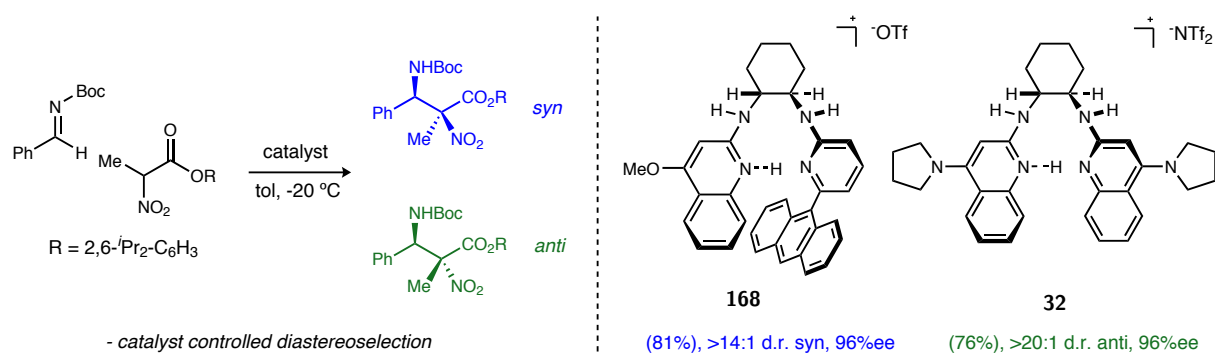
Scheme 21: Catalyst symmetry influences the outcome of the major diastereomer

3.1.2 Indroduction: Previous mechanistic studies of BAM catalysts in the aza-Henry reaction

Recent theoretical studies conducted by Dudding produced a detailed depiction of catalyst-substrate interactions of BAM catalysts using computational analysis.[171] They first elucidated what gives rise to enantioselectivity in the simple system of nitromethane addition to an *N*-Boc imine. The original BAM catalyzed aza-Henry developed in the Johnston lab used HQuin-BAM·HOTf (**165**) and can achieve on around 80% ee as shown in Figure 34.[172] The hypothesis prior to the computational work by Dudding was that the catalyst acts in a bifunctional manner binding both the electrophile (imine) and the nucleophile (nitronate). This was the starting point for the computational study in which they sought to uncover the manner in which the electrophile or the nucleophile bind to the catalyst leading to high enantioselectivity.

The first step in these studies was to elucidate the binding mode of the imine, since the

---

[171]Belding, L.; Taimoory, S. M.; Dudding, T. *ACS Catal.* **2015**, *5*, 343–349; Taimoory, S. M.; Dudding, T. *J. Org. Chem.* **2016**, *81*, 3286–3295.

[172]Nugent, B. M.; Yoder, R. A.; Johnston, J. N. *J. Am. Chem. Soc.* **2004**, *126*, 3418–3419.

N-Boc imine has two key hydrogen bond acceptors. Additionally the imine has two main conformations: s-*cis* and s-*trans*. Palomo addressed the latter concern of conformation in the computational analysis of an aza-Henry reaction using a phase transfer catalyst.[173] They found that the s-*cis* and s-*trans* conformations have similar energies without the presence of a catalyst, but the s-*trans* is favored by 3.6 kcal/mol when coordinated to a catalyst because two hydrogen bond acceptors are presented and coordinated to the catalyst. Dudding confirmed the hypothesis that the s-*trans* conformation is favored but also showed that the polar ionic hydrogen preferred homonuclear charge assisted hydrogen bonding to imine nitrogen and not the Boc oxygen. The imine in the s-*trans* conformation binds in a bidentate manner with the BAM catalyst, and the nitrogen of the imine coordinates to the polar ionic hydrogen bond of the quinoline (Figure 34, complex **169**).

The binding modes were uncovered but other secondary effects were elucidated by natural bond orbital (NBO) analysis. The reactive orientation of the pro-(R) transition state shows that the angle of attack between the nitro and the *N*-Boc imine as $\theta_{\text{pro-}(R)}$ = 39.1° indicating a synclinal arrangement of the reactants. The synclinal alignment also shows subtle secondary orbital interaction between the Boc group and the nitronate (Figure 34, **170**). On the other hand, the pro-(S) transition state has a $\theta_{\text{pro-}(S)} = -51.1°$ arrangement which does not allow for the secondary orbital overlap. The hydrogen bonding system, angle of attack, and secondary orbital overlap all contribute to the pro-(R) being favored in the transition state by 2.4 kcal/mol.

These findings were elaborated to explain the diastereoselection observed in the BAM

[173]Gomez-Bengoa, E.; Linden, A.; López, R.; Múgica-Mendiola, I.; Oiarbide, M.; Palomo, C. *J. Am. Chem. Soc.* **2008**, *130*, 7955–7966.
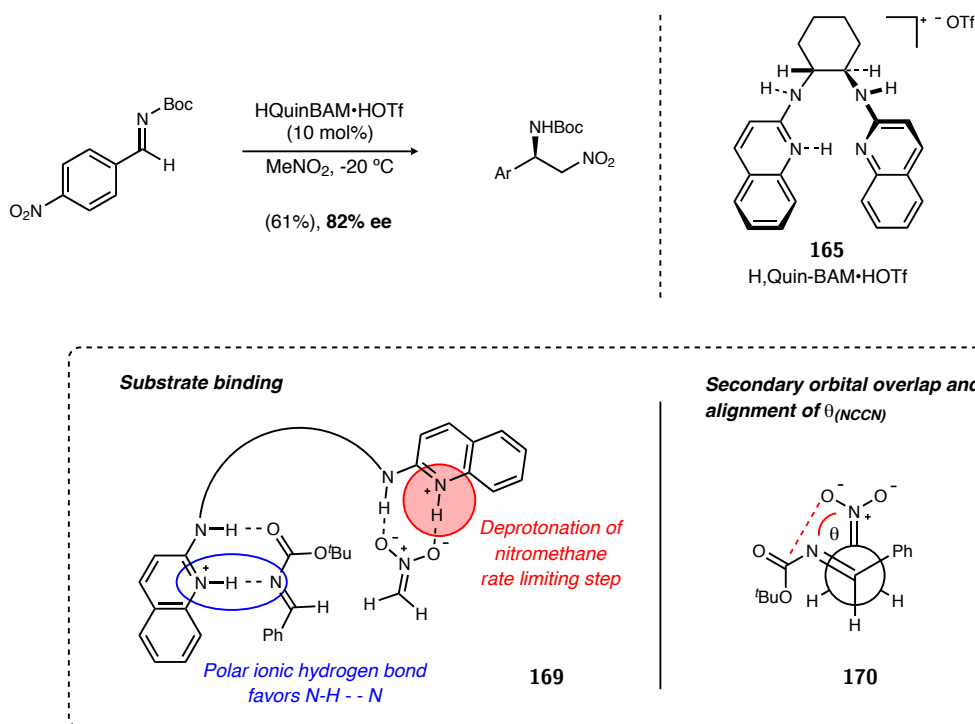
Figure 34: Key findings in the computational analysis of the BAM catalyzed aza-Henry

catalyzed aza-Henry reaction when employing nitroethane (Figure 35). Similar conclusions were reported about the secondary orbital overlap and angle of approach which help dictate the selectivity at the imine (Figure 35, θ_{NCCN}). However, the approach of the nitronate now can have two orientations depending on the face that is attacking the imine. The main interactions dictating facial selectivity are shown in Figure 35. The *anti*-diastereomer is favored by approximately 4 kcal/mol. Further analysis of the transition states indicates that the approach of the nitronate leading to the *syn*-diastereomer has significant intermolecular interactions that distorts the Boc group, resulting in some loss of conjugation with the imine (measured by θ_{CCNC} angle of 169° and 166°). The distortion and minor loss of conjugation is due to interactions between the large *tert*-butyl carbamate interacting with the methyl of the nitronate as shown in the bottom of Figure 35. These substrate interactions in the transition state contribute highly to the
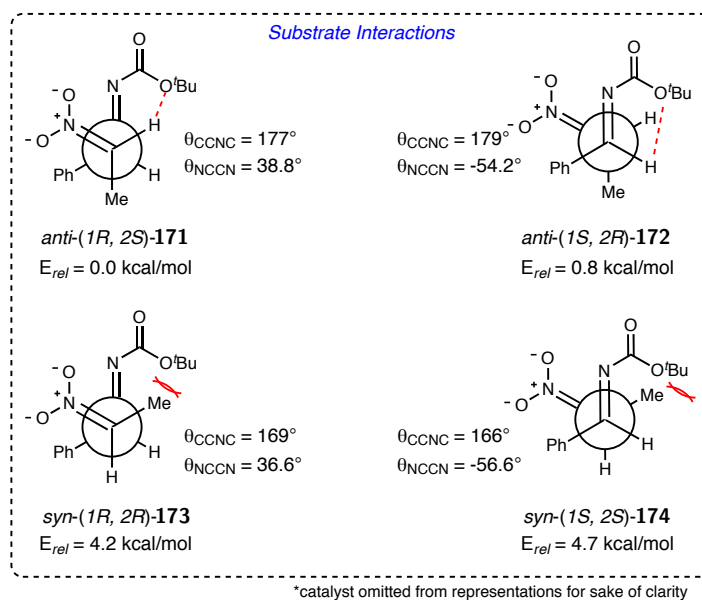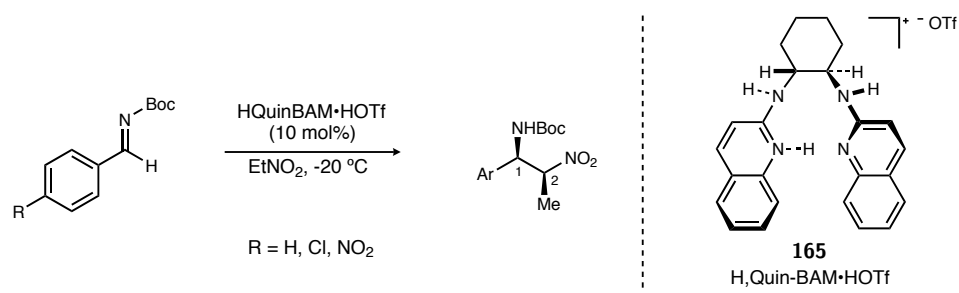
Figure 35: Key findings in the computational analysis of the diastereoselective BAM catalyzed aza-Henry

observed diastereoselection but do not describe the subtle catalyst interactions that lead to high selectivity.

Diastereoselection partly relies on the substrate interactions but enantioselection is imparted by the catalyst. Two main conformations of the catalyst are observed in the calculated transition states: closed and open which either reinforce or weaken inramolecular (intrahost) and intermolecular (host-guest) interactions. Initial analysis of the transition states indicate that the distance between the two quinoline rings of the catalyst differ and the open/closed state of the catalyst lead to catalyst distortions which disfavor the *syn* products. Noncovalent interaction calculations (NCI) were conducted to identify the subtle attractive and repulsive contributions to the catalyst distortions. Intra

host $\pi_{Ar} \cdots \pi_{Ar}$ interactions were found to be present between the quinolines in the most favored transition state. Other contributing weak interactions were: a) intermolecular host-guest interactions $N^+ - H \cdots \pi_{Ar}$ between the polar ionic $N^+ - H$ and a hydrogen on the aromatic ring of the aldimine, b) intermolecular host-guest interactions $\pi_{Ar} \cdots \pi_{Ar}$ or $C - H_{Ar} \cdots \pi_{Ar}$ stacking interactions between the catalyst quinoline rings and the aromatic ring of the aldimine, and c) intrahost interactions between the quinoline rings and the cylcohexane backbone.

The combined effects of substrate-substrate, substrate-catalyst (host-guest), and catalyst-catalyst (intrahost) interactions all contribute to the observed selectivity in the *anti*-selective aza-Henry. The combination of a synclinal alignment, no imine distortion, a closed catalyst binding pocket, and subtle attractive interactions lead to the the lowest energy transition state. The disfavored enantiomer and diastereomers lacked some of these key attributes in the transition state. Furthermore, calculations using electron poor aldimines such as the *para*-chloro or *para*-nitro (R = Cl or NO_2 in Figure 35) reinforce the findings that host-guest interactions are crucial because the electron poor groups lower the transition state of the favored enantiomer (i.e. comparing the TS energies of *para*-nitro $\Delta G = 4.8$ kcal/mol to an unsubstituted aldimine $\Delta G = 7.2$ kcal/mol, the electron poor transition states are lower, thereby accelerating the reaction). These calculated results correlate well with the measured diastereoselection and enantioselection obtained experimentally using HQuinBAM·HOTf.

The studies by Dudding provide a key step for understanding the BAM catalyzed aza-Henry reaction and will facilitate the development of new reactions by providing a quantitative mechanistic picture. Future elucidation of the role of the counterion will be necessary but will be challenging due to the low understanding of counterion effects in

BAM-catalysis. Other C_1-symmetric catalysts have been employed with high success in the Johnston group that find high selectivity in various diastereoselective and enantioselective aza-Henry reactions. A crucial facet for developing new reactions hinges on the testing the hypotheses and understanding of the design elements that are crucial for BAM catalysts. Further amalgamation of experimental data and theoretical calculations will facilitate reaction development using BAM-catalysis using mechanism based prediction.

3.2 The influence of catalyst symmetry on the sterodivergent addition of nitroesters to aldimines unveiled by DFT calculations

3.2.1 Current hypotheses and proposal for studies of the stereodivergent α-nitroester addition to aldimines

The regiodivergent aza-Henry reaction shown in Scheme 21 leverages symmetry elements of the catalyst to effect a complete reversal of diastereoselection. Using this simple change from C_2-symmetric to C_1-symmetric, all four stereoisomers can be synthesized selectively (the enantiomers of the compounds in Scheme 21 are easily accessed using the enantiomers of the catalyst, something many of the other "cooperative" systems based on the chiral pool cannot achieve). Although the utility of this system is demonstrated, an understanding of the guiding principles of catalyst function leading to an inversion in diastereoselection is missing.

Initial hypotheses centered around the ability of the ester to compete for hydrogen bonding of the catalyst (Figure 36). Two main proposals arose from this line of thinking for how the two different catalysts can differentiate the *pro*chiral nitroester: 1) a smaller
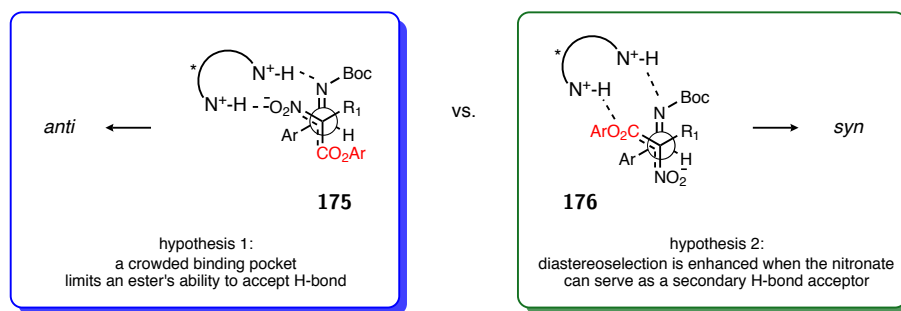
Figure 36: Initial hypotheses for regiodivergence in BAM catalyzed α-nitroester addition to aldimines

binding pocket would not be able to accommodate the bulky aryl ester $(2,6\text{-}^i\mathrm{Pr}_2\text{-}C_6H_3)$ and as a result the nitro group would preferentially bind to the catalyst as shown in complex **175** and 2) a more open binding pocket could accommodate the bulky aryl ester and would preferentially coordinate the ester (or compete with nitro coordination). It is clear from the studies by Dudding that hypothesis 1 (Figure 36) is active in the *anti*-additions but the binding of substrates and what factors give rise to *syn*-addition still have not been investigated.

Using conformation searches and subsequent refinement of the models with DFT calculations, possible binding modes of the substrates in the *syn*-selective addition of α-nitroester addition to aldimines has been uncovered. New coordination modes of the imine and the nitroester have been illuminated for the first time. The goals of the project are as follows:

1. *Use conformation searches of truncated catalysts to propose binding modes of the imine and nitronate.*

2. *Use DFT transition state calculations to validate the proposed binding modes from the truncated catalyst.*

3.2.2 DFT studies of the *syn*-selective α-nitroester addition to aldimines catalyzed by a C_1-symmetric catalyst

Computational Methods: Initial conformation searches were performed using Barista/ Conflex software using MMFF94S.[174] DFT calculations were performed using Gaussian 09.[175] Geometry optimization was performed on the truncated systems using the B3LYP[176]/6-31G(d) and the IEF-PCM solvation model (toluene default parameters).[177] Geometry optimizations in full catalyst systems were performed using the hybrid ωB97X-D[178] functional and the IEF-PCM solvation model (toluene default parameters). All optimized structures were verified by frequency computations as minima (zero imaginary frequencies) or transitions state structures (single imaginary frequency). Additional single point calculations were obtained using ωB97X-D/6-311+g(d,p), and M06-2X/6-311+g(d,p)[179] levels on the previously optimized ωB97X-D/6-31G(d) structures. The thermal corrections from ωB97X-D/6-31G(d) were added to the single point calculations to obtain the free energies.

To better understand the catalyst-nitroester interactions that might exist in competing transition states, investigations were initiated with the α-nitro ester deprotonation by modeling the structure of the salt formed from the nitroester with 2-amino quinoline **177**, forming complexes shown in Figure 37. It has been shown in the aza-Henry reaction that the 4-methoxy or 4-pyrrolidinyl substituents affect reactivity, with little or no impact on selectivity so a simple quinoline unsubstituted at the 4-position was used in these initial

---

[174]Halgren, T. A. *J. Comp. Chem.* **1999**, *20*, 720–729.

[175]Frisch, M. J. et al. *Gaussian 09* **2009**.

[176]Vosko, S. H.; Wilk, L.; Nusair, M. *Can. J. Phys.* **1980**, *58*, 1200–1211; Lee, C.; Yang, W.; Parr, R. G. *Phys. Rev. B* **1988**, *37*, 785–789; Becke, A. D. *J. Chem. Phys.* **1993**, *98*, 5648–5652.

[177]Tomasi, J.; Mennucci, B.; Cancès, E. *Comput. Theor. Chem.* **1999**, *464*, 211–226.

[178]Chai, J.-D. D.; Head-Gordon, M. *Phys. Chem. Chem. Phys.* **2008**, *10*, 6615–6620.

[179]Zhao, Y.; Truhlar, D. G. *Theor. Chem. Acc.* **2008**, *120*, 215–241.

conformational analyses. The hindered ester shown in Figure 37 (Ar = 2,6-^{i}Pr$_2$-C$_6$H$_3$) was chosen to represent hindered α-nitro esters, and its conjugate base was modeled in complexation with the quinolinium. The delocalized nitroalkane conjugate base has the ability for one or both anion stabilizing groups (nitro *or* ester) to engage in a hydrogen bonding interaction with the catalyst representing the hypotheses posited earlier in Figure 36. The lowest energy orientations between α-nitro ester and amidinium are those involving nitronate binding shown in complexes **179** and **180**. Amidinium binding to the enolate oxygen, which shows a two-point binding complex to the ester oxygen **178**, was disfavored by over 10 kcal/mol compared to dual binding to the nitro oxygens. The difference in energy between nitronate **179** and **180** was much lower at 0.6 kcal/mol, with the large ester favored in a syn relationship to the quinoline fused ring. Isomer **179** would be expected to be higher in energy when considering the chiral catalyst (*vide infra*), where the large cyclohexane diamine backbone replaces the small methyl of the truncated catalyst **177**. These interactions were found to be the same in a truncated version of anthracenyl catalyst 2, in which 6-(1-anthracenyl)-2-methylamino quinoline was modeled demonstrating the preferred binding of the nitro group in both enviroments of the unsymmetric catalyst **168**.

We revisited the initial assumption that imine binding to the catalyst is conserved, leading to high selectivity for product diastereomers homochiral at the amine carbon. This proposal could be explored by modeling the individual diastereomers both without and with the catalyst. Analysis of the relative energy of *syn-* and *anti*-addition products (without the catalyst) led to the finding that the *syn* diastereomer is lower in energy than *anti* by 1.64 kcal/mol. This energetic preference for the *syn*-diastereomer is consistent with all of the past work, where thermodynamic conditions that establish reversible aza-
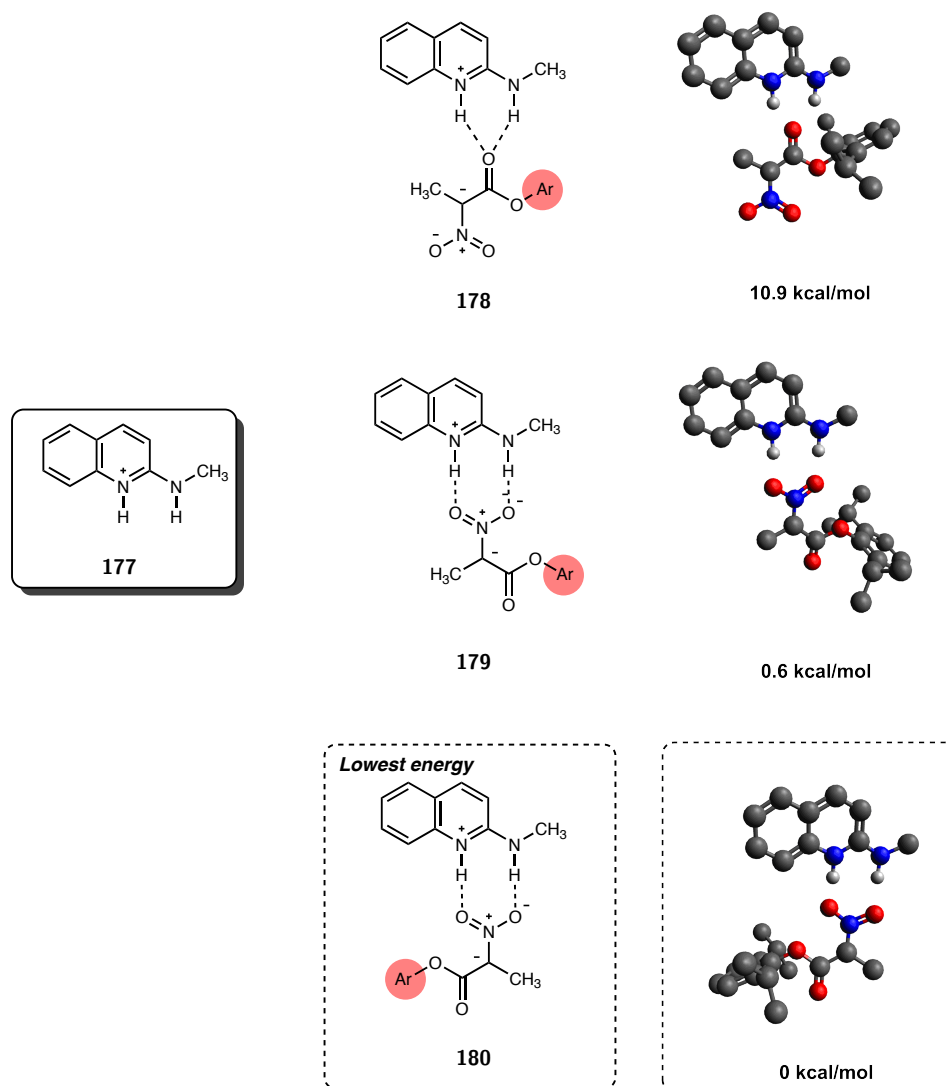
Figure 37: Coordination modes for the truncated catalyst with a deprotonated α-nitroester calculated with B3LYP/6-31G(d)

Henry, or reversible deprotonation at the α-position of the nitroalkane, led to maximal syn:anti ratios of 2-3:1. It is clear that *anti*-selectivity is both kinetically favored in most of the previous aza-Henry work, and torsional strain alone is insufficient to provide a high degree of diastereoselectivity for either *syn-* or *anti*-diastereomers. The path forward necessitated a careful analysis of imine binding to the unsymmetric catalyst.

The continued assumption was that two point binding of the aldimine, proposed by Dudding with the symmetric catalyst, was conserved with the C_1-symmetric catalyst. In Dudding's model, both nitrogen and carbamate oxygen of the N-Boc imine serve as

hydrogen bond acceptors to the N–H bonds of the quinoline and backbone N–H. There are two possible orientations for the *N*-Boc imine, that lie co-planar to the quinoline such as in Dudding's model (see Figure 34, compound **169** for representative co-planar orientation). A conformation search of the analogous complex using the truncated anthracenyl pyridine **181** was performed, but a completely different arrangement was observed (Figure 38). Unlike the coplanar orientation of the C_2-symmetric catalyst **165**, a single-point binding of the polar ionic hydrogen of the amidinium to the Boc-oxygen was favored (N$^+$–H$\cdots$O, 1.7 Å vs. N$^+$–H$\cdots$N 2.9 Å), allowing the large planar surface of the imine to situate coplanar with the anthracenyl ring (Figure 38, complexes **182** and **183**). Since the anthracene ring is perpendicular to the pyridine ring, the overall orientation of the imine represented in Figure 38 is unique and an intriguing finding. This change of imine binding, however, does not result in a change of facial presentation of the aldimine (i.e. same configuration at the amine carbon in products). Finally, Palomo found that the s-*trans* conformation of the imine is preferred when bound to catalyst due to the stabilization by two hydrogen bonds. However, in the new model, only one hydrogen bond is present and the conformation of the imine had to be reassessed. Similar to prior findings, the imine prefers the s-*trans* conformation **182** when bound to catalyst by 4.5 kcal/mol, ruling out the possibility that the s-*cis* **183** is the reactive conformation.

The denticity of Boc-imine binding to the catalyst in combination with the low energy conformation of nitronate binding were combined and complexed to the full catalyst **168**. The anthracenyl-pyridine catalyst **168** exists in a trans-diaxial conformation when the imine and nitronate are bound simultaneously (conformation represented in Figure 39). This is contrasted to the preferred *trans*-diequatorial conformation of the C$_2$-symmetric catalyst **165**. This effect is attributed to the congestion of the pocket in the unsymmet-
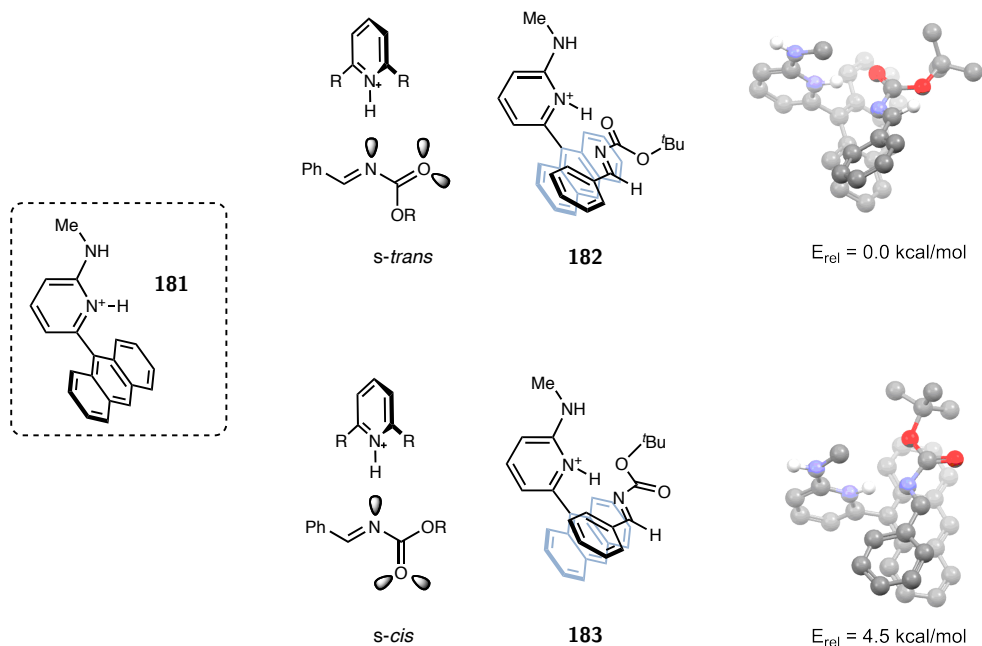
Figure 38: Coordination modes for the truncated catalyst with the Boc-aldimine

ric catalyst **168**, which is magnified upon imine and nitronate binding. Accordingly, the strain also appears to favor a single-point hydrogen bond between the aminopyridinium and oxygen of the Boc group as discussed before. A benefit of the *trans*-diaxial conformation is the enlargement of the binding pocket, which can accommodate the protonated aminoquinoline-nitronate ion pair in the new proposed binding modes. Despite induced change to single-point hydrogen bonding and enlarged pocket, the anthracene rescues control of the azomethine's facial differentiation by aligning parallel to it. This conformation maintains the azomethine *Si*-face selectivity as observed in both symmetric and unsymmetric catalysts.

While the *Si*-face selectivity of the azomethine is preserved, facial control of the nitronate is reversed upon changing catalyst **32** (symmetric, *anti*-selectivity) to **168** (unsymmetric, *syn*-selectivity). Minimizations of the complexed aldimine and nitronate starting materials were performed to elucidate the key interactions for diasteromeric binding of the nitronate. The coordinated nitroester's orientation is dictated by interactions

syn-approach*   vs.   **anti-approach***

184   **185**

*distances between aldimine and nitroester exaggerated for sake of clarity
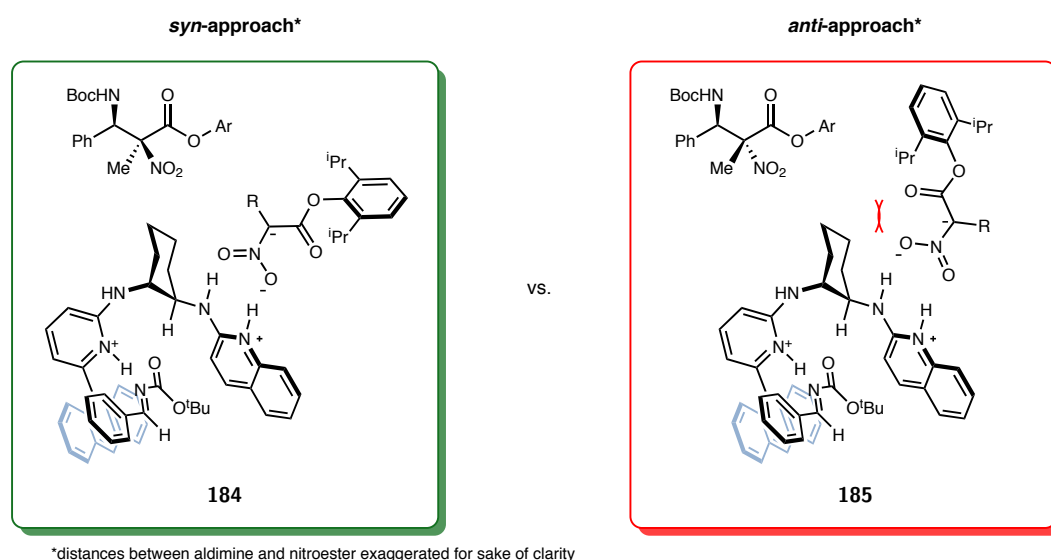
Figure 39: Full catalyst complexation hypothesis of both aldimine and nitroester

between the backbone of the catalyst and any large group which in this case is the bulky

phenolic ester. In the orientation that would lead to *syn*-selectivity (complex **184**) there

are no interactions between the backbone and the bulky ester. However, the complex

leading to *anti*-selectivity (complex **185**) shows an interaction between the bulky ester

and the backbone. The steric interactions close to the backbone arise from the *trans*-

diaxial conformation of the cyclohexane backbone, further demonstrating the importance

of the backbone conformation for selectivity in BAM catalyzed reaction.

favored   **186**

positioned in area of binding pocket between anthracene and quinoline

positioned in open area of binding pocket
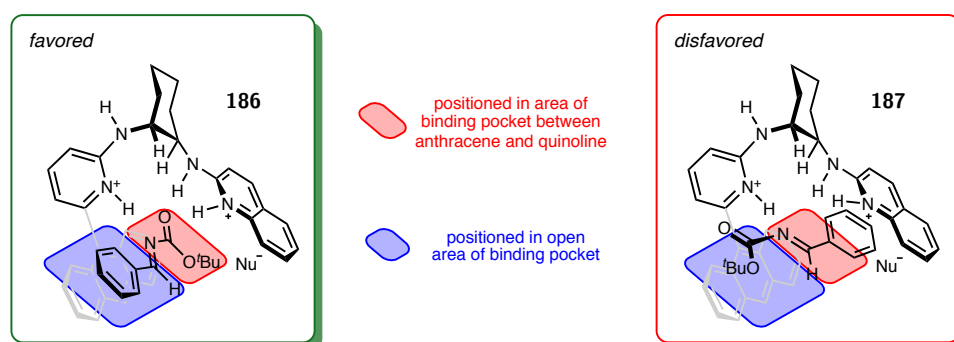
disfavored   **187**

Figure 40: Comparison of *Si*-favored and *Re*-disfavored facial presentation of the imine complexed to the full catalyst

The *syn*-selectivity observed when employing the unsymmetric catalyst results from

backbone interactions with the bulky ester. The *trans*-diaxial conformation of the an-

thracenyl catalyst creates steric interactions near the backbone close to the quinoline which forces the bulky ester in the nitronate in an orientation away from the backbone. Interestingly, the imine binding appears to only have one productive pathway when using the unsymmetric catalyst. A conformation search of the imine and a truncated 2-(5-anthracenyl)-6-methylamino pyridine **181** favors a relationship where the imine is parallel to the anthracenyl ring system. In the full catalyst system, this binding mode allows for two orientations leading to *Si* and *Re* face selectivity. The *Si* face of the electrophile is presented when oriented in the open area of the binding pocket (Figure 40, complex **186**) and the large *tert*-butyl group of the Boc-carbamate is sandwiched between the anthracene and the quinoline ring. The *Re* facial presentation of the electrophile is unproductive because, in this orientation, the azomethine is sandwiched between the anthracene and the quinoline, disallowing the approach of a nucleophile (Figure 40, complex **187**). This finding suggests that the bulky aryl ester on the nucleophile does not significantly influence orientation in electrophile binding (i.e. torsional interactions between approaching nucleophile and electrophile do not dictate binding). Furthermore, the azomethine *Si* face selectivity is under catalyst-control and not likely due to an interaction with the bulky nitro ester and is evidenced by the use of a smaller nucleophile; bromonitromethane which exhibits high enantioselection at the imine but uniformly low diastereoselection.[180]

Unfortunately the findings presented above, using the minimizations of the complexed starting materials, were not reflected in the transition state calculations. Initial results indicated that the hypothesis advanced in Figure 39 was correct but were reversed when diffuse basis sets and functionals were used (moving from M06/6-31(d) to ωB97X-D/6-

---

[180]Shen, B.; Makley, D. M.; Johnston, J. N. *Nature* **2010**, *465*, 1027–1032.

Table 9: Relative energies of *syn* and *trans* transision states in different levels of theory and basis sets

	MO62x/ 6-31g(d)	ωB97X-D/ 6-31g(d)	ωB97X-D/ 6-311+g(d,p)[a]	M062x/ 6-311+g(d,p)[a]
syn-TS	0	+.038	+2.09	+2.26
trans-TS	+0.42	0	0	+0

[a] Single point energies were calculated and corrected using the thermochemistry corrections from the frequency calculations of M062x/6-31g(d)

311+g(d,p) and M062x/6-311+g(d,p)). It was found that in the disfavored transition state complex **185**, the interactions of the sterically large ester with the backbone forced the nitronate into a monodentate binding where only one of the nitro oxygens was coordinated with both of the N–H bonds. Sadly this led to lower energies in the transition state, since key steric interactions were relieved by the altered binding. Shown in Table 9 are the relative energies of the two transition states and clearly the *tran*-TS was favored when higher level calculations were performed. At this stage, revision of the full catalyst system models were necessary.
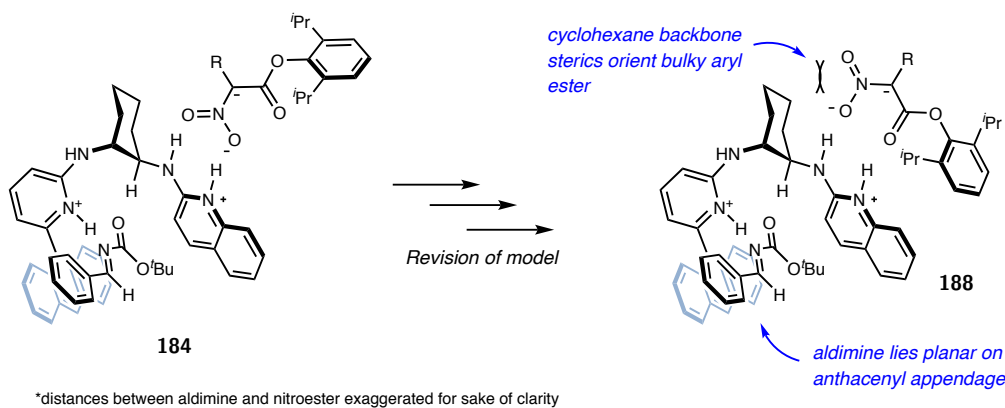
Figure 41: Revision of the models to from a bidentate nitro coordination to bidentate mixed coordination

It was clear that the proposed models were not reflecting energy differences that correlated to experimental results. Another possibility for the coordination of the nitronate would be bidentate binding to one nitro oxygen and the ester carbonyl (See hypotheses in proposal section, complex **176**). The new models hinged on the previous hypothesis

that the ester carbonyl could account for some of the coordination in the *syn*-TS. In the truncated models this binding mode was unfavored and no minimum was found. Translation of the new model (Figure 41, complex **188**) into the full catalyst system allowed for revision of the previous model **184** and found success in locating a transition state. The next step was to compare transition states of the *syn*- and *anti*-transition states.

Table 10: Relative energies of *syn* and *trans* transision states in different levels of theory and basis sets for the revised model

	ωB97X-D/ 6-31g(d)	ωB97X-D/ 6-311+g(d,p)[a]	M062x/ 6-311+g(d,p)[a]
syn-TS	0	0	0
trans-TS	+0.9	+3.9	+2.9

[a] Single point energies were calculated and corrected using the thermochemistry corrections from the frequency calculations of ωB97X-D/6-31g(d)

Calculations were run initially using ωB97X-D/6-31g(d) and refined by single point calculations using diffuse basis sets and functionals. The relative energies, in the revised binding model, between the two transition states finally reflected experimental results. Shown in Table 10 are the energies using different basis sets and functionals. This time all the relative energies agree that the *syn*-TS is favored over the *anti*-TS. Accordingly, when moving to the higher level calculations, the relative energies reflect the high selectivity observed in the *syn*-selective α-nitroester addition to aldimines using **168**. The ωB97X-D functional by Grimme was used in Dudding's work and in this case slightly overestimates the energy differences but is still in good agreement. Finally, calculation of the starting materials (SM) and products (prod) complexed to the catalyst were performed to visualize the full transition state diagram. The calculations in Figure 42 were performed using ωB97X-D/6-311+g(d,p) and show that in SM, TS, and prod, the relative energies of the *syn*-complexes are lower than the *trans*-complexes.

The revised model is a hybrid of hypotheses stemming from Dudding's two-point nitro
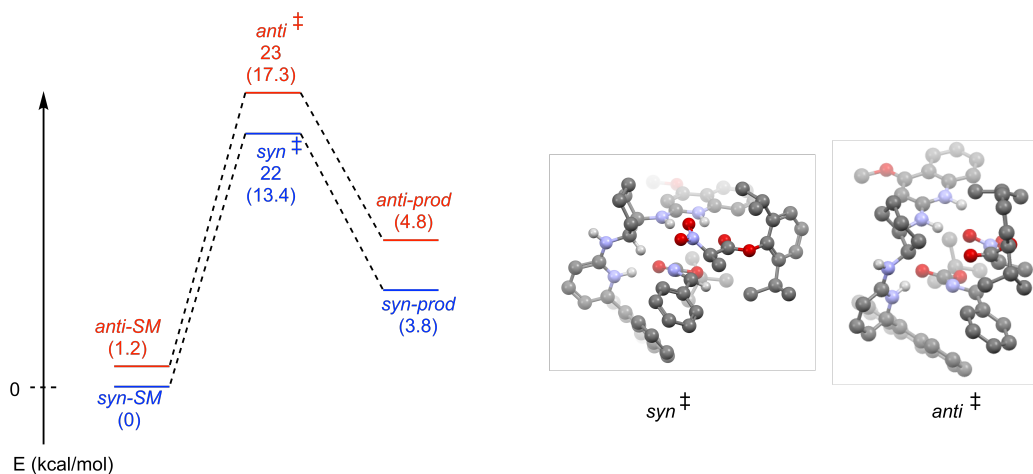
Figure 42: Transition state diagram and visualization comparing *syn-* and *trans*-models

binding and the idea that the ester carbonyl could compete for coordination. New findings in regard to aldimine binding were elucidated and the catalyst contains two pockets where the aldimine coordination can or cannot react. The switch from a C_2-symmetric catalyst to a C_1-symmetric catalyst leads to an interesting diastereodivergence and it is clear that new coordination modes may be operating to exact this change in selectivity.

3.3 Conclusions

In conclusion, proposals for the overarching influences leading to diastereodivergence in additions to α-nitroester addition of aryl aldimines have been advanced and investigated by DFT calculations for the first time. New binding modes of both nitroester and aldimine have been uncovered, which lead to reversed selectivity at the nitroester while retaining facial selectivity of the aldimine. Contrasted to C_2-symmetric catalysts, the C_1 symmetric catalyst demonstrates a preferred *trans*-diequatorial conformation leading to changes in steric interactions within the catalytic pocket. Induced change to the pocket increases steric interactions near the backbone, forcing the nitroester to bind with both the nitro oxygen and the ester oxygen in the *syn*-transition state.

The combination of Dudding's work with the findings presented above proffer detailed pictures of catalyst·substrate interactions. Hopefully these models may be used by future investigations to make hypotheses in regards to the development of new BAM catalyzed reactions. The conformational change of the unsymmetric catalysts leading to a change in binding pocket could lead to new reactants to be fit in this pocket. Continued investigations in catalyst design have since uncovered new reactivity (See Chapter 1 introduction) and binding modes, which coupled with computational investigations, provide a powerful program for further development of methodology centering around BisAmidine catalysis.

The continued study of BAM catalysts using DFT is necessary for a greater understanding of the possible mechanisms. Hopefully the hypotheses garnered in this chapter will allow for further study of other BAM catalyzed reactions such as the halocyclizations. There is much still to be learned about BAM catalysis, and DFT provides a powerful tool for testing hypotheses related to mechanism that are not easy to probe experimentally.

Appendix 4.1 Characterization of organic molecules

Experimental Section

All reagents and solvents were commercial grade and purified prior to use when necessary. Acetonitrile (MeCN), tetrahydrofuran (THF), dichloromethane (CH_2Cl_2), and toluene were dried by passage through a column of activated alumina as described by Grubbs[1] for microscale reactions. Flame-dried (under vacuum) glassware was used for all reactions. Stainless steel syringes or cannulae were used to transfer air- and moisture-sensitive liquids. Anhydrous sodium sulfate (Na_2SO_4) was used as a drying agent after extractions unless otherwise indicated.

Thin layer chromatography (TLC) was performed using glass-backed silica gel (250 μm) plates and flash chromatography utilized 230–400 mesh silica gel from Sorbent Technologies. Automated flash chromatography was performed using a Teledyne ISCO Combiflash R_f and Biotage SNAP KP-Sil columns. UV light, I_2 chamber, and/or the use of *p*-anisaldehyde, potassium permanganate or phosphomolybdic acid solutions were used to visualize products.

IR spectra were recorded on a Nicolet Avatar 360 spectrophotometer and are reported in wavenumbers (cm^{-1}) analyzed as neat films on NaCl plates (transmission). Nuclear magnetic resonance spectra (NMR) were obtained on a Bruker DRX-500 (500 MHz), Bruker AV-400 (400 MHz), or Bruker AV II-600 (600 MHz). Chemical shifts are measured relative to residual solvent peaks as an internal standard. Mass spectra were recorded on a high resolution Thermo Electron Corporation MAT 95XP-Trap by use of chemical ionization (CI), electron impact ionization (EI), or electro-spray ionization (ESI) by the Indiana University Mass Spectrometry Facility. Optical rotations were measured on a Perkin Elmer-341 polarimeter. Chiral HPLC analysis was conducted on an Agilent 1260 series instrument using the designated ChiralPak column at 30 °C unless otherwise indicated. Absolute configuration determined by X-ray by the Indiana University Molecular Structure Center.

The purification of StilbPBAM (**2**), which was prepared according to the previously published procedure,[2] was carried out as follows: The resulting crude solid from the reaction was dissolved in dichloromethane and transferred to a 125 mL separatory funnel, washed with 6 M NaOH (50 mL) and water (3 x 50 mL). The organic layers were combined, dried ($MgSO_4$), filtered, and concentrated to provide a light brown solid (1.1 g, >95%). This solid was dissolved in benzene (70 mL) and precipitated by the slow addition of hexanes (80 mL) over 5 min to the stirring slurry at rt. The solid was filtered with hexanes to provide a light tan solid (700 mg, 62%). Analytical data matches that previously reported in the literature.[2]

---

[1] Pangborn, A.; Giardello, M.; Grubbs, R.; Rosen, R.; Timmers, F. *Organometallics* **1996**, 15, 1518-1520
[2] Dobish, M. C.; Johnston, J. N. *J. Am. Chem. Soc.* **2012**, 134, 6068–6071

General Procedure for the Preparation of Alcohol Substrates
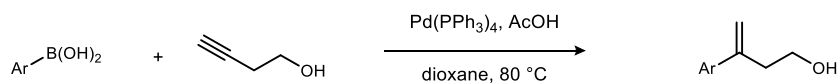
Alcohols were prepared according to the procedure by Oh and coworkers[3] as follows. A flame–dried round–bottomed flask was charged with a stir bar, degassed 1,4-dioxane (0.4 M), tetrakis(triphenylphosphine)palladium(0) (5 mol%), 3-butyn-1-ol (1 equiv), and boronic acid (1.5 equiv). This mixture was stirred at room temperature for 10 min, acetic acid (20 mol%) was added, and the reaction mixture was heated to 80 °C for 13 h. The reaction mixture was cooled to room temperature, diluted with methanol to dissolve the solids, and then concentrated.[4] The resulting dark brown oil was filtered through a plug of silica using 50% ethyl acetate in hexanes. The resulting yellow oil was purified by flash column chromatography (SiO$_2$) to afford the desired alcohol.

General Procedure for Enantioselective Carbonations
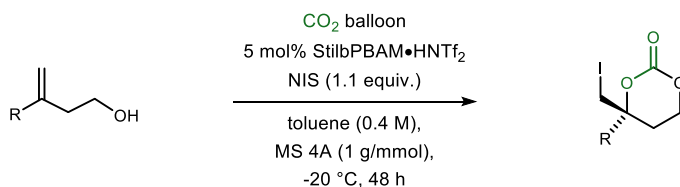
A flame-dried vial equipped with a stir bar and molecular sieves 4A (1g/mmol) was backfilled with CO$_2$, and charged with the alcohol (1 equiv) and StilbPBAM·HNTf$_2$ (5 mol%). The vial was evacuated and refilled with CO$_2$ prior to the addition of dry toluene (0.4 M). The reaction mixture was cooled to -20 °C for 30 min under a balloon of CO$_2$, and then *N*-iodosuccinimide (1.2 equiv) was added. The reaction mixture immediately became bright pink in color and was stirred for 48 h. The resulting dark red mixture was treated with 0.5 M aq Na$_2$S$_2$O$_3$ at -20 °C and extracted with diethyl ether. The organic layers were combined, dried, and concentrated to a yellow residue that was purified by flash column chromatography (SiO$_2$, ethyl acetate in hexanes) to give the title compound.
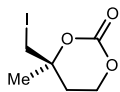
 (*S*)-4-(Iodomethyl)-4-methyl-1,3-dioxan-2-one (31). Prepared according to the general procedure using 10 mol % catalyst **8** and 3-methyl-3-buten-1-ol (1.00 g, 11.6 mmol), and purified by flash column chromatography (SiO$_2$, 40% ethyl acetate in hexanes) to afford a viscous yellow oil (2.10 g, 72%) and 68% ee by chiral HPLC (Chiralpak IA: 6% EtOH/hexanes, 1 mL/min: t_r(major) = 40.6 min, t_r(minor) = 45.3 min). OR analysis was taken after recrystallization[5] on 80% ee material. $[\alpha]_D^{20}$ -31.9 (*c* 0.74, CHCl$_3$); ^{1}H NMR (400 MHz, CDCl$_3$) δ 4.41 (ddd, *J* = 5.2, 4.6, 1.5 Hz, 2H), 3.40 (dd, *J* = 11.7, 11.7 Hz, 2H), 3.68 (ddd, *J* = 14.2, 6.5, 5.8 Hz, 1H), 2.09 (ddd, *J* = 14.5, 5.1, 4.7 Hz, 1H), 1.66 (s, 3H). Analytical data matches that previously reported in literature. [6]
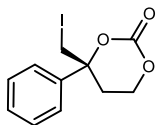
 (*R*)-4-(Iodomethyl)-4-phenyl-1,3-dioxan-2-one (44). Prepared according to the general procedure using 3-phenylbut-3-en-1-ol (14.8 mg, 100 μmol), and purified by flash column chromatography (SiO$_2$, 30-45% ethyl acetate in hexanes) to give the title compound as a yellow solid (31.1 mg, 98%). The product was determined to be 91% ee by chiral HPLC analysis (Chiralpak IA, 10%

[3] Oh, C. H.; Jung, H. H.; Kim, K.S.; Kim, N. *Angew. Chem. Int. Ed.* **2003**, 42, 805–808.
[4] If not dissolved in this manner, solids will form and block the plug of silica when filtering.
[5] Recrystallized in 0.1 M diethyl ether at -20 °C.
[6] Minakata, S.; Sasaki, I.; Ide, T. *Angew. Chem. Int. Ed.* **2010**, 49, 1309–1311

^{i}PrOH/hexanes, 1.0 mL/min, t_r(major) = 21.0 min, t_r(minor) = 22.9 min; mp 59-64 °C; $[\alpha]_D^{20}$ -19 (*c* 0.95, CHCl$_3$); R$_f$ = 0.5 (50% EtOAc/hexanes) visualized with *p*-anisaldehyde; IR (film) 3050, 3023, 2923, 2926, 1755, 1138 cm^{-1}; ^{1}H NMR (400 MHz, CDCl$_3$) δ 7.46-7.36 (m, 5H), 4.37 (ddd, *J* = 11.0, 5.0, 2.4 Hz, 1H), 4.06 (ddd, *J* = 12.0, 12.0, 3.2 Hz, 1H), 3.61 (s, 2H), 2.77 (ddd, *J* = 14.4, 12.2, 5.0 Hz, 1H) 2.47 (ddd, *J* = 14.4, 2.9, 2.9 Hz, 1H); ^{13}C NMR (100 MHz, CDCl$_3$) 147.9, 138.3, 129.3, 129.1, 124.8, 83.7, 65.0, 31.4, 15.2 ppm; HRMS (ESI): Exact mass calcd for C$_{11}$H$_{11}$IO$_3$ [M]$^+$ 317.9747, found 317.9745
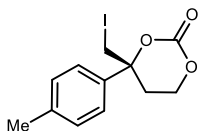
(*R*)-4-(Iodomethyl)-4-(*p*-tolyl)-1,3-dioxan-2-one (45). Prepared according to the general procedure using 3-(*p*-tolyl)but-3-en-1-ol (16.7 mg, 103 μmol), and purified by silica gel chromatography (SiO$_2$, 20-30% ethyl acetate in hexanes) to afford a yellow oil (33 mg, 96%) and was determined to be 91% ee by chiral HPLC (Chiralpak IA: 15% EtOH /hexanes, 1.0 mL/min: t_r(minor) = 15.8 min, t_r(major) = 20.9 min). $[\alpha]_D^{20}$ -12.2 (*c* 0.28, CHCl$_3$); R$_f$ = 0.6 (33% EtOAc/hexanes); IR (film) 3033, 2957, 2922, 2852, 1754 cm^{-1}; ^{1}H NMR (400 MHz, CDCl$_3$) δ 7.27-7.22 (m, 4H), 4.35 (ddd, *J* = 10.8, 4.8, 2.4 Hz, 1H), 4.04 (ddd, *J* = 12.0, 12.0, 3.2 Hz, 1H), 3.59 (d, *J* = 7.2 Hz, 1H), 3.56 (d, *J* = 7.2 Hz, 1H), 2.73 (ddd, *J* = 14.4, 12.0, 4.8 Hz, 1H), 2.44 (ddd, *J* = 14.4, 2.8, 0.8 Hz, 1H), 2.37 (s, 3H); ^{13}C NMR (100 MHz, CDCl$_3$) ppm 148.0, 139.1, 135.5, 130.0 (2C), 124.7 (2C), 83.7, 65.1, 31.4, 21.0, 15.4; HRMS (ESI): Exact mass calcd for C$_{12}$H$_{13}$INaO$_3$ [M+Na]$^+$ 354.9807, found 354.9820.
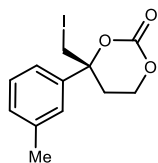
(*R*)-4-(Iodomethyl)-4-(*m*-tolyl)-1,3-dioxan-2-one (46). Prepared according to the general procedure with a 48 h reaction time using 3-(*m*-tolyl)but-3-en-1-ol (21.9 mg, 135 μmol). The organic extracts were washed with 2 M aq NaOH, dried and concentrated to a yellow oil (42 mg, 96%) that was determined to be 93% ee by chiral HPLC (Chiralpak IA: 10% iPrOH /hexanes, 1.0 mL/min: t_r (major) = 13.6 min, t_r(minor) = 15.0 min). $[\alpha]_D^{20}$ -6.9 (*c* 0.16, CHCl$_3$); R$_f$ = 0.4 (66% EtOAc/hexanes); IR (film) 3070, 2961, 2920, 2852, 1759 cm^{-1}; ^{1}H NMR (400 MHz, CDCl$_3$) δ 7.31 (t, *J* = 7.6 Hz, 1H), 7.19 (m, 2H), 7.13 (d, *J* = 7.6 Hz, 1H), 4.35 (ddd, *J* = 10.8, 4.8, 2.4 Hz, 1H), 4.04 (ddd, *J* = 12.0, 3.2, 0.8 Hz, 1H), 3.59 (br s, 2H) 2.73 (ddd, *J* = 14.4, 12.0, 4.8 Hz, 1H), 2.44 (ddd, *J* = 14.4, 2.8, 0.8 Hz, 1H), 2.38 (s, 3H); ^{13}C NMR (100 MHz, CDCl$_3$) ppm 148.0, 139.3, 138.2, 129.9, 129.2, 125.5, 121.8, 83.7, 65.0, 31.5, 21.6, 15.3; HRMS (ESI): Exact mass calcd for C$_{12}$H$_{13}$INaO$_3$ [M+Na]$^+$, 354.9807, found 354.9798.

(*R*)-4-(4-(*tert*-Butyl)phenyl)-4-(iodomethyl)-1,3-dioxan-2-one (48). Prepared according to the general procedure using 3-(4-(*tert*-butyl)phenyl)but-3-en-1-ol (19.8 mg, 97 μmol) with 96 h reaction time, and purified by washing the organic layers with 2 M aq NaOH, which were dried and concentrated to a yellow oil (36 mg, 99%) that was determined to be 91% ee by chiral HPLC (Chiralpak IA: 10% iPrOH/hexanes, 1.0 mL/min: t_r(minor) = 14.1 min, t_r(major) = 16.1 min). $[\alpha]_D^{20}$ -19.5 (*c* 0.19, CHCl$_3$); R$_f$ = 0.8 (50% EtOAc/hexanes); IR (film) 3035, 2966, 2904, 1746, 1406 cm^{-1}; ^{1}H NMR (400 MHz, CDCl$_3$) δ 7.42 (dd, *J* = 4.4, 2.4 Hz, 2H), 7.29 (dd, *J* = 4.4, 2.4 Hz, 2H), 4.34 (ddd, *J* = 10.8, 4.8, 2.4 Hz, 1H), 4.00 (ddd, *J* = 12.0, 3.2, 0.8 Hz, 1H), 3.59 (dd, *J* = 10.8, 11.2 Hz, 2H), 2.75 (ddd, *J* = 14.4, 12.0, 4.8 Hz, 1H), 2.44 (ddd, *J* = 14.4, 2.8, 0.8 Hz, 1H), 1.32 (s, 9H); ^{13}C NMR (100 MHz, CDCl$_3$) ppm 152.3, 148.0, 135.1, 126.2, 124.6, 83.6, 65.0, 34.6, 31.4, 31.3, 31.2; HRMS (ESI): Exact mass calcd for C$_{15}$H$_{19}$INaO$_3$ [M+Na]$^+$, 397.0277, found 397.0288.
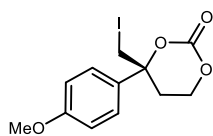
(*R*)-4-(Iodomethyl)-4-(4-methoxyphenyl)-1,3-dioxan-2-one (49). Prepared according to the general procedure using 3-(4-methoxyphenyl)but-3-en-1-ol (17.8 mg, 100 μmol) at -50 °C, and purified by flash column chromatography (SiO$_2$, 30-45% ethyl acetate in hexanes) to give the title compound as a yellow oil (14.5 mg, 41%). The product was determined to be 71% ee by chiral HPLC analysis (Chiralpak IA, 10% EtOH/hexanes, 1 mL/min, t_r(minor) = 35.3 min, t_r(major) = 40.7 min; $[\alpha]_D^{20}$ -84 (*c* 0.63, CHCl$_3$); R$_f$ = 0.4 (50% EtOAc/hexanes) visualized with *p*-anisaldehyde; IR (film) 2957, 2924, 2852, 1753, 1609, 1511, 1463, 1404, 1256 cm^{-1}; ^{1}H NMR (400 MHz, CDCl$_3$) δ 7.29 (d, *J* = 8.3 Hz, 2H), 6.94 (d, *J* = 8.3 Hz, 2H), 4.35 (d, *J* = 6.4 Hz, 1H), 4.11 (m, 1H), 3.82 (s, 3H), 3.56 (d, *J* = 6.5 Hz, 2H), 2.73

(ddd, J = 13.5, 4.7 Hz, 1H), 2.43 (ddd, J = 14.4, 3.2, 3.2 Hz, 1H); ^{13}C NMR (125 MHz, CDCl$_3$) ppm 160.0, 147.9, 130.0, 126.2, 114.6, 83.5, 65.0, 55.3, 31.2, 15.6; HRMS cannot be obtained due to instability of product during shipping.

(*R*)-4-(4-Bromophenyl)-4-(iodomethyl)-1,3-dioxan-2-one (50). Prepared according to the general procedure using 3-(4-bromophenyl)but-3-en-1-ol (22.7 mg, 100 µmol), and purified by flash column chromatography (SiO$_2$, 30-40% ethyl acetate in hexanes) to give the title compound as a yellow oil (26.1 mg, 65%). The product was determined to be 90% ee by chiral HPLC analysis (Chiralpak IA, 15% EtOH/hexanes, 1 mL/min, t_r(minor) = 19.5 min, t_r(major) = 27.7 min; $[\alpha]_D^{20}$ -7.0 (*c* 0.23, CHCl$_3$); R$_f$ = 0.4 (50% EtOAc/hexanes); IR (film) 2922, 2852, 1755, 1485 cm^{-1}; ^{1}H NMR (400 MHz, CDCl$_3$) δ 7.57 (d, J = 8.6 Hz, 2H), 7.27 (d, J = 8.2 Hz, 2H), 4.36 (dddd, J = 14.0, 11.2, 5.0, 2.3 Hz, 1H), 4.06 (ddd, J = 11.5, 11.5, 3.3 Hz, 1H), 3.56 (d, J = 2.4 Hz, 2H), 2.72 (ddd, J = 16.9, 14.5, 6.8 Hz, 1H) 2.45 (ddd, J = 14.5, 3.1, 3.1 Hz, 1H); ^{13}C NMR (125 MHz, CDCl$_3$) ppm 147.5, 137.5, 132.1, 126.6, 125.4, 83.3, 64.8, 31.3, 14.5; HRMS (ESI): Exact mass calcd for C$_{11}$H$_{11}$BrIO$_3$ [M+H]$^+$ 396.8931, found 396.8921.
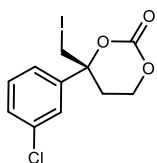
(*R*)-4-(3-Chlorophenyl)-4-(iodomethyl)-1,3-dioxan-2-one (51). Prepared according to the general procedure using 10 mol % catalyst **8** and 3-(3-chlorophenyl)but-3-en-1-ol (24.0 mg, 135 µmol) with a 5 d reaction time, and purified by silica gel chromatography (SiO$_2$, 30-40% ethyl acetate in hexanes) to afford a yellow oil (21 mg, 44%) and was determined to be 87% ee by chiral HPLC (Chiralpak IA: 12% EtOH /hexanes, 1.0 mL/min: t_r(minor) = 18.2 min, t_r(major) = 20.5 min). $[\alpha]_D^{20}$ -3.4 (*c* 0.65, CHCl$_3$); R$_f$ = 0.28 (30% EtOAc/hexanes); IR (film) 3067, 2957, 2922, 2846, 1754 cm^{-1}; ^{1}H NMR (400 MHz, CDCl$_3$) δ 7.40-7.39 (m, 3H), 7.30 (m, 1H), 4.39 (ddd, J = 10.9, 4.8, 2.3 Hz, 1H), 4.06 (ddd, J = 12.0, 12.0, 3.2 Hz, 1H), 3.60 (d, J = 7.2 Hz, 1H), 3.56 (d, J = 7.2 Hz, 1H), 2.78-2.70 (m, 1H), 2.44 (ddd, 14.4, 14.4, 2.8 Hz, 1H); ^{13}C NMR (100 MHz, CDCl$_3$) ppm 147.5, 140.5, 135.6, 130.6, 129.4, 125.5, 123.2, 83.2, 64.9, 31.4, 14.5; HRMS (ESI): Exact mass calcd for C$_{11}$H$_{10}$ClINaO$_3$ [M+Na]$^+$ 374.9261, found 374.9259.
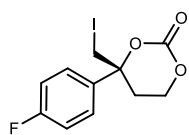
(*R*)-4-(4-Fluorophenyl)-4-(iodomethyl)-1,3-dioxan-2-one (52). Prepared according to the general procedure using 3-(4-fluorophenyl)but-3-en-1-ol (16.6 mg, 100 µmol), and purified by flash column chromatography (SiO$_2$, 30-40% ethyl acetate in hexanes) to give the title compound as a yellow oil (18.1 mg, 54%). The product was determined to be 90% ee by chiral HPLC analysis (Chiralpak IA, 15% EtOH/hexanes, 1 mL/min, t_r(minor) = 16.4 min, t_r(major) = 19.6 min; $[\alpha]_D^{20}$ -5.4 (*c* 0.11, CHCl$_3$); R$_f$ = 0.4 (50% EtOAc/hexanes) visualized with *p*-anisaldehyde; IR (film) 2960, 2917, 2847, 1745, 1600, 1507, 1403, 1257, 1126, 1088 cm^{-1}; ^{1}H NMR (400 MHz, CDCl$_3$) δ 7.37 (ddd, J = 9.7, 8.9, 5.0 Hz, 2H), 7.13 (dd, J = 6.5 Hz, 2H), 4.38 (ddd, J = 11.2, 7.8, 2.2 Hz, 1H), 4.06 (dd, J = 11.6, 11.6, 3.3 Hz, 1H), 3.57 (d, J = 2.2 Hz, 2H), 2.74 (ddd, J = 14.5, 11.8, 5.0 Hz, 1H), 2.47 (ddd J = 14.5, 3.0, 3.0 Hz, 1H); ^{13}C NMR (125 MHz, CDCl$_3$) ppm 162.8 (d, $^1J_{CF}$ = 249.7 Hz), 147.6, 134.2 (d, $^4J_{CF}$ = 3.3 Hz), 127.9 (d, $^3J_{CF}$ = 8.3 Hz), 116.3 (d, $^2J_{CF}$ = 21.9 Hz), 83.4, 64.9, 31.4, 15.0; HRMS (ESI): Exact mass calcd for C$_{11}$H$_{10}$FINaO$_3$[M+Na]$^+$ 358.9556, found 358.9542.
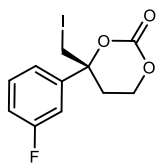
(*R*)-4-(3-Fluorophenyl)-4-(iodomethyl)-1,3-dioxan-2-one (53). Prepared according to the general procedure using 10 mol % catalyst **8** and 3-(3-fluorophenyl)but-3-en-1-ol (13.8 mg, 83.0 µmol) with 96 h reaction time, and purified by silica gel chromatography (SiO$_2$, 30-40% ethyl acetate in hexanes) to afford a yellow oil (12 mg, 40%) that was determined to be 89% ee by chiral HPLC (Chiralpak IA: 15% EtOH /hexanes, 1.0 mL/min: t_r(minor) = 14.3min, t_r(major) = 16.7 min). $[\alpha]_D^{20}$ -2.3 (*c* 0.22, CHCl$_3$); R$_f$ = 0.30 (30% EtOAc/hexanes); IR (film) 3064, 2919, 2857, 1762, 1103 cm^{-1}; ^{1}H NMR (600 MHz, CDCl$_3$) δ 7.44-7.31 (m, 1H), 7.18-7.16 (m, 1H), 7.13-7.10 (m, 2H), 4.40-4.37 (ddd, J = 13.2, 4.8, 3.0 Hz, 1H), 4.10-4.05 (ddd, J = 12.0, 3.0, 0.6 Hz, 1H), 3.59 (d, J = 11.4 Hz, 1H), 3.57 (d, J = 11.4 Hz, 1H), 2.76-2.72 (ddd, J = 9.6, 7.2, 3.0 Hz, 1H), 2.48-2.45 (ddd, 14.4, 6.0, 3.0 Hz, 1H); ^{13}C NMR (150 MHz, CDCl$_3$) ppm 163.0

($^1J_{CF}$ = 250 Hz), 147.5, 141.1, 131.1 ($^3J_{CF}$ = 7.5 Hz), 120.6 ($^4J_{CF}$ = 3 Hz), 116.2 ($^2J_{CF}$ = 21 Hz), 112.5 ($^2J_{CF}$ = 24 Hz), 83.3, 64.9, 31.5, 14.4 ppm; HRMS (ESI): Exact mass calcd for $C_{11}H_{10}FINaO_3$ [M+Na]$^+$ 358.3556, found 358.0557.
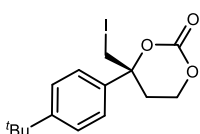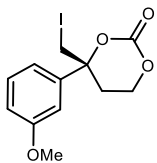
(*R*)-4-(Iodomethyl)-4-(3-methoxyphenyl)-1,3-dioxan-2-one (54). Prepared according to the general procedure using 3-(3-methoxyphenyl)but-3-en-1-ol (18.8 mg, 103 μmol), and purified by silica gel chromatography (SiO$_2$, 40-45% ethyl acetate in hexanes) to afford a yellow oil (27 mg, 75%) that was determined to be 90% ee by chiral HPLC (Chiralpak IA: 15% EtOH/hexanes, 1.0 mL/min: t_r(major) = 20.2 min, t_r(minor) = 23.6 min. [α]$_D^{20}$ -66.7 (*c* 0.24, CHCl$_3$); R$_f$ = 0.5 (50% EtOAc/hexanes); IR (film) 3060, 2962, 2921, 2839, 1753 cm^{-1}; ^{1}H NMR (400 MHz, CDCl$_3$) δ 7.34 (m, 1H), 6.94 (m, 3H), 4.35 (ddd, *J* = 10.8, 4.8, 2.4 Hz, 1H), 4.06 (ddd, *J* = 12.0, 3.2, 0.8 Hz, 1H), 3.83 (s, 3H), 3.59 (dd, *J* = 12.0, 11.2 Hz, 2H), 2.73 (ddd, *J* = 14.4, 12.0, 4.8 Hz, 1H), 2.44 (ddd, *J* = 14.4, 2.8, 0.8 Hz, 1H); ^{13}C NMR (100 MHz, CDCl$_3$) ppm 160.2, 147.8, 139.9, 130.4, 116.9, 114.1, 111.1, 83.6, 65.1, 55.4, 31.5, 15.1; HRMS (ESI): Exact mass calcd for $C_{12}H_{13}INaO_4$ [M+Na]$^+$, 370.9756, found 370.9766.
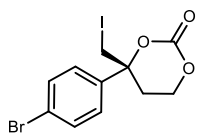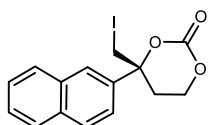
(*R*)-4-(Iodomethyl)-4-(naphthalen-2-yl)-1,3-dioxan-2-one (59). Prepared according to the general procedure using 3-(naphthalen-2-yl)but-3-en-1-ol (19.8 mg, 100 μmol), and purified by flash column chromatography (SiO$_2$, 30-45% ethyl acetate in hexanes) to give the title compound as a yellow oil (32.5 mg, 88%). The product was determined to be 90% ee by chiral HPLC analysis (Chiralpak IB, 20% ^{i}PrOH/hexanes, 0.8 mL/min, t_r(major) = 24.2 min, t_r(minor) = 26.1 min; [α]$_D^{20}$ -3.1 (*c* 0.10, CHCl$_3$); R$_f$ = 0.5 (50% EtOAc/hexanes) visualized with *p*-anisaldehyde; IR (film) 3020, 2921, 1752, 1447, 1403, 1259, 1128 cm^{-1}; ^{1}H NMR (400 MHz, CDCl$_3$) δ 7.91 (m, 2H), 7.87 (dd *J* = 13.6, 3.3 Hz, 2H), 7.55 (ddd, *J* = 16.8, 9.4, 3.0 Hz, 2H), 7.38 (dd, *J* = 8.7, 1.9 Hz, 1H), 4.36 (dddd, *J* = 13.6, 11.1, 5.0, 2.6 Hz, 1H), 4.05 (ddd, *J* = 12.1, 11.2, 3.2 Hz, 1H), 3.69 (d, *J* = 2.5 Hz, 2H), 2.81 (ddd, *J* = 12.2, 7.1, 5.0 Hz, 1H), 2.60 (ddd *J* = 5.7, 2.8 Hz, 1H); ^{13}C NMR (125 MHz, CDCl$_3$) ppm 147.9, 135.4, 133.1, 133.0, 129.4, 128.3, 127.6, 127.2, 127.1, 124.8, 121.5, 83.8, 65.0, 31.4, 15.0; HRMS (ESI): Exact mass calcd for $C_{15}H_{13}INaO_3$ [M+Na]$^+$ 390.9807, found 390.9825.
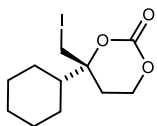
(*R*)-4-Cyclohexyl-4-(iodomethyl)-1,3-dioxan-2-one (62). Prepared according to the general procedure using 10 mol % catalyst **8** and 3-cyclohexylbut-3-en-1-ol (18.8 mg, 103 μmol) with a 52 h reaction time, and purified by silica gel chromatography (SiO$_2$, 35-40% ethyl acetate in hexanes) to afford a tan oil (31 mg, 76%) and was determined to be 74% ee by chiral HPLC (Chiralpak IA: 20% ^{i}PrOH/hexanes, 1.0 mL/min: t_r(major) = 14.5 min, t_r(minor) = 15.4 min). [α]$_D^{20}$ -2.9 (*c* 0.18, CHCl$_3$); R$_f$ = 0.20 (25% EtOAc/hexanes); IR (film) 2926, 2850, 1749, 1405, 1274, 1108 cm^{-1}; ^{1}H NMR (400 MHz, CDCl$_3$) δ 4.41-4.19 (m, 2H), 3.49 (d, *J* = 11.2 Hz, 2H), 2.30-2.16 (m, 2H), 1.91-1.68 (m, 6H), 1.28-1.07 (m, 5H); ^{13}C NMR (100 MHz, CDCl$_3$) ppm 149.2, 84.6, 64.3, 45.2, 27.3, 26.4, 26.3, 26.1 (2C), 25.9, 10.8; HRMS (ESI): Exact mass calcd for $C_{11}H_{17}INaO_3$ [M+Na]$^+$ 347.0120, found 347.0120.
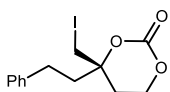
(*S*)-4-(Iodomethyl)-4-phenethyl-1,3-dioxan-2-one (63). Prepared according to the general procedure using 10 mol % catalyst **8** and 3-methylene-5-phenylpentan-1-ol (16.2 mg, 92 μmol) with 72 h reaction time, and purified by silica gel chromatography (SiO$_2$, 35-45% ethyl acetate in hexanes) to afford a yellow oil (22 mg, 71%) that was determined to be 67% ee by chiral HPLC (Chiralpak IA: 15% EtOH/hexanes, 1.0 mL/min: t_r(minor) = 16.7 min, t_r(major) = 21.9 min). [α]$_D^{20}$ -9.1 (*c* 0.27, CHCl$_3$); R$_f$ = 0.4 (30% EtOAc/hexanes); IR (film) 3023, 2948, 2920, 2858, 1750, 1120 cm^{-1}; ^{1}H NMR (500 MHz, CDCl$_3$) δ 7.31 (m, 2H), 7.24-7.21 (m, 3H), 4.40 (dd, *J* = 7.2, 6.0 Hz, 2H), 3.51 (d, *J* = 10.8 Hz, 1H), 3.43 (d, *J* = 10.8 Hz, 1H) 2.85-2.80 (ddd, *J* = 13.2, 4.8, 4.8 Hz, 1H), 2.74-2.69 (ddd, *J* = 13.2, 7.2, 4.8 Hz, 1H), 2.39-2.34 (m, 1H), 2.92-2.16 (m, 3H); ^{13}C NMR (150 MHz, CDCl$_3$) ppm 148.3, 140.1, 128.7 (2C), 128.3 (2C), 126.5, 82.8, 64.3, 40.3, 30.3, 28.7, 9.1; HRMS (ESI): Exact mass calcd for $C_{13}H_{15}INaO_3$ [M+Na]$^+$ 368.9964, found 368.9949.
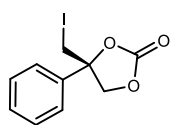
(*S*)-4-(Iodomethyl)-4-phenyl-1,3-dioxolan-2-one. Prepared according to the general procedure using 2-phenylprop-2-en-1-ol (13.4 mg, 100 μmol), with a 92 h reaction time and purified by flash column chromatography (SiO$_2$, 30-45% ethyl acetate in hexanes) to give the title compound as a yellow oil (25.0 mg, 83%). The product was determined to be 28% ee by chiral HPLC analysis (Chiralpak IA, 10% EtOH/hexanes, 1 mL/min, t_r(major) = 13.7 min, t_r(minor) = 25.5 min; $[\alpha]_D^{20}$ +11.0 (*c* 0.10, CHCl$_3$); R$_f$ = 0.7 (50% EtOAc/hexanes) visualized with PMA; IR (film) 3028, 2919, 1804, 1449, 1151, 1068 cm^{-1}; ^{1}H NMR (400 MHz, CDCl$_3$) δ 7.45-7.40 (m, 3H), 7.34 (dd, *J* = 8.2, 1.8 Hz, 2H), 4.77 (d, *J* = 8.5 Hz, 1H), 4.66 (d, *J* = 8.5 Hz, 1H), 3.68 (d, *J* = 11.5 Hz, 1H), 3.60 (d, *J* = 11.5 Hz, 1H); ^{13}C NMR (125 MHz, CDCl$_3$) ppm 153.2, 138.0, 129.3, 129.2, 124.3, 83.2, 74.4, 12.6; HRMS (ESI) Exact mass calcd for C$_{10}$H$_{10}$IO$_3$ [M+H]$^+$ 304.9669, found 304.9672
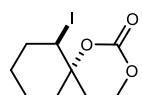
(6*S*,7*R*)-7-Iodo-1,3-dioxaspiro[5.5]undecan-2-one (65). Prepared according to the general procedure using 2-(cyclohex-1-en-1-yl)ethan-1-ol (1.00 g, 8.00 mmol), and purified by flash column chromatography (SiO$_2$, 30-45% ethyl acetate in hexanes) to give the title compound as a yellow solid (1.93 g, 82%). The product was determined to be 67% ee by chiral HPLC analysis (Chiralpak IA, 10% EtOH/hexanes, 1 mL/min, t_r(major) = 18.4 min, t_r(minor) = 23.1 min; $[\alpha]_D^{20}$ -67 (*c* 0.70, CHCl$_3$)[7]; Mp 38-40 °C (dec); R$_f$ = 0.55 (50% EtOAc/hexanes) visualized with *p*-anisaldehyde; IR (film) 2939, 2863, 1747, 1450, 1400 cm^{-1}; ^{1}H NMR (600 MHz, CDCl$_3$) δ 4.45 (dd *J* = 7.0, 3.5 Hz, 1H), 4.38 (m, 2H), 2.38 (ddd, *J* = 14.4, 9.1, 5.1 Hz, 1H), 2.34 (ddd, *J* = 15.9, 8.2, 3.8 Hz, 1H), 2.19 (m, 2H), 1.93 (m, 1H), 1.85 (m, 2H), 1.68 (m, 1H), 1.54 (m, 2H); ^{13}C NMR (150 MHz, CDCl$_3$) ppm 148.5, 83.3, 63.9, 38.0, 33.5, 32.8, 31.6, 23.9, 21.0; HRMS could not obtained due to product instability during shipping.

Derivatizations of Iodocarbonates and Iodocarbamates
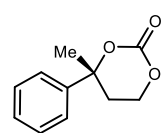
(*R*)-4-Methyl-4-phenyl-1,3-dioxan-2-one (68). A flame–dried microwave vial backfilled with N$_2$ was charged with a stir bar, degassed benzene (530 μL), (*R*)-4-(iodomethyl)-4-phenyl-1,3-dioxan-2-one (**44**, 25.4 mg, 80.0 μmol, 89% ee), and tributyltin hydride (93.1 mg, 320 μmol). The reaction mixture was warmed in an oil bath to 80 °C for 5 min and then AIBN (2.0 mg, 12.0 μmol) was added, and the mixture was stirred for 1 h. The reaction mixture was concentrated to a colorless residue that was purified by flash column chromatography as described by Harrowven (10% powdered K$_2$CO$_3$ in SiO$_2$, 30-60% ethyl acetate in hexanes)[8] to give the title compound as a colorless oil (16.9 mg, 88%). The product was determined to be 88% ee by chiral HPLC analysis (Chiralpak IA, 12% EtOH/hexanes, 1.0 mL/min: t_r(major) = 17.4 min, t_r(minor) = 13.3 min. $[\alpha]_D^{20}$ -54.4 (*c* 0.85, CHCl$_3$) Analytical data matches that previously reported in literature.[9]
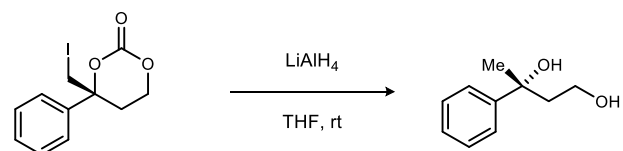
(*R*)-3-Phenylbutane-1,3-diol (69). A flame–dried vial was charged with LiAlH$_4$ (18.0 mg, 472 μmol) and dry THF (750 μL) under Ar. The carbonate (30 mg, 94 μmol, 91% ee) was added to the mixture as a solution in THF (200 μL) at rt and stirred for 1 h. The resulting mixture was quenched with satd aq NH$_4$Cl and extracted with ethyl acetate. The organic layers were combined, dried (MgSO$_4$), filtered, and concentrated to a residue that was purified by flash column chromatography (SiO$_2$, 50% ethyl acetate in hexanes) to

---

[7] Optical rotation measured using carbonate recrystallized from **2q**: 82% ee

[8] Harrowven, D. C. *et al. Chem. Comm.* **2010**, 46, 6335–6337

[9] Kartika, R. *et al. Org. Lett.* **2012**, 14, 3676-3679

give the title compound as a colorless oil (11 mg, 71%). The product was determined to be 91% ee by chiral HPLC analysis (Chiralpak IB, 6% EtOH/hexanes, 1.0 mL/min: t_r(major) = 13.1 min, t_r(minor) = 12.4 min. $[\alpha]_D^{20}$ +39 (c 0.36, CHCl$_3$); R$_f$ = 0.3 (50% EtOAc/hexanes); IR (film) 3364 (br), 3060, 2970, 2922, 2853, 1450 cm^{-1}; ^{1}H NMR (400 MHz, CDCl$_3$) δ 7.44 (d, J = 7.2, Hz, 2H), 7.35 (m, 2H), 7.23 (d, J = 7.2 Hz, 1H), 3.78 (m, 1H), 3.57 (ddd, J = 12.0, 8.8, 3.2 Hz, 1H), 3.47 (br s, 1H), 2.42 (br s, 1H), 2.15-2.01 (m, 2H), 1.59 (s, 3H); ^{13}C NMR (150 MHz, CDCl$_3$) ppm 147.5, 128.2, 126.6, 124.7, 75.9, 60.4, 44.0, 31.0.
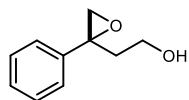
(R)-2-(2-Phenyloxiran-2-yl)ethan-1-ol (70). A vial backfilled with N$_2$ after drying was charged with a stir bar, (R)-4-(iodomethyl)-4-phenyl-1,3-dioxan-2-one (**44**, 31.8 mg, 100 μmol, 91% ee) and methanol (250 μL). The reaction mixture was cooled to 0 °C for 30 min and then Amberlyst A-26 hydroxide form (120 mg, 1.20 g/mmol) was added and stirred for 3 h. The resulting mixture was filtered through a glass frit and washed with ethyl acetate. The solution was dried and concentrated to a colorless residue that was purified by flash column chromatography (SiO$_2$, 20-40% ethyl acetate in hexanes) to give the title compound as a colorless oil (14.9 mg, 90%). The product was determined to be 91% ee by chiral HPLC analysis (Chiralpak AD-H, 5% ^{i}PrOH/hexanes, 1.0 mL/min: t_r(major) = 14.8 min, t_r(minor) = 16.5 min. $[\alpha]_D^{20}$ -4.7 (c 0.17, CHCl$_3$). Analytical data matches that previously reported in literature.[10]

A small sampling of the investigation into reproducibility problems that was necessary for the iodocarbamate chemistry is listed below. Reproducibility was not never achieved which was the goal of the initial investigations. Many of the entries will not make perfect sense (copied directly from subgroups) but the year that was invested on this project was held back by the restrictions that were inherent to publication with the original conditions. The freedom to investigate other avenues (besides the original reaction conditions that were reported) was never given, which resulted in slow progress and circling hypotheses. As you can see from the tables below, every single aspect was investigated that did not require the reoptimization of the reaction (i.e. new catalyst, protecting groups, or substrate substitution). Unfortunately, no success was found within the restrictions placed upon this project. The reaction suffers from the use of a basic substrate that can, and has been proven by DOSY to deprotonate the catalyst (not shown in this document). This means that if the bifunctional nature is crucial for high enantioselectivity, we can never fully predict or control the amount of catalyst salt that is present during the reaction which leads to low reproducibility. New optimization focusing on a catalyst that does not necessitate the use of a salt will be crucial for the reproducibility, high yields, and high enantioselectivities that are desired.
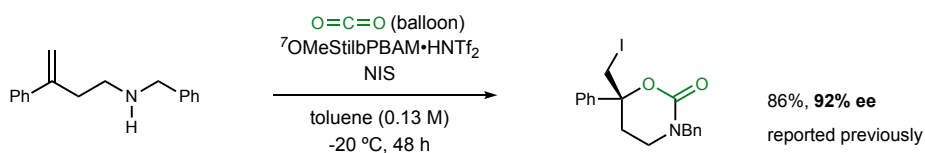
entry	reaction vessel	substrate	catalyst	NMR yield
1	300 mg / RB	TJS	TJS	20%
2	μW	TJS	TJS	18%
3	μW	TJS	RY	6%
4	μW / wet tol	TJS	TJS	7%
5	vial	TJS	TJS	<5%
6	vial	RY	TJS	70% / **83% ee**

---

[10] Yamamoto *et al. J. Am. Chem. Soc.* **2010**, 132, 7878–7880

entry	reaction vessel	substrate	catalyst	NMR yield	
1	vial base wash sub	TJS	TJS	<5%	
2	vial w/ its own balloon	TJS	TJS	<5%	
3	vial	TJS	TJS	<5%	new substrate
4	vial and 6,7omestilb	TJS	TJS	<5%	
5	vial + 1 μL pyrrolidine	TJS	TJS	20% / **85% ee**	new catalyst
6	vial + 1 μL BnNH$_2$	TJS	TJS	<5%	
7	vial + MS 4A	TJS	TJS	6%	
8	vial + 2mg RY sub	TJS	TJS	10%	

entry	notes	substrate	catalyst	NMR yield
1	3 μL pyrrolidine	TJS	TJS	49%
2	1 μL DMF	TJS	TJS	34%
3	2x dilute	TJS	TJS	<5%
4	40 mol% cat	TJS	TJS	57%/ **83% ee**
5	--	RY	TJS	20%
6	--	RY	RY	20%

entry	notes	Catalyst	HNTf$_2$	NMR yield
1	-	Old	Old	<5%
2	-	New	New	49%/ **70%ee**
3	-	New	Old	49%
4	-	Old	New	28%
5	RY substrate	New	New	58%/ **83% ee**
6	--	RY	RY	20%
7	mF substrate	New	New	<10%
8	mF substrate	New	Old	<10%
9	Free base cat	New	-	<10%
10	order of addition	New	New	20%

entry	notes	Catalyst:HNTf$_2$	SM	NMR yield
1	0.18 M	1:1	50%	55%, **81% ee**
2	0.18 M	1:1.2	40%	76%, **84% ee**
3	0.18 M, 2x scale	1:1.25	50%	25%
4	.25M	1:1.25	17%	53%, **81% ee**
5	0.18 M	1:0.77	25%	41%, **79% ee**

entry	notes	Catalyst:HNTf$_2$	additive	NMR yield
1	0.18 M	1:0.5	-	78%, **83% ee**
2	0.18 M	1:1	-	25%
3	0.18M	1:1.25	-	30%
4	0.18M	1:1.5	-	35%, **85% ee**
5	0.18 M	1:1	MS4A	74%, **87% ee**
6	0.18 M	1:1.25	MS4A	25%
7	0.18 M, 2x scale	1:1	MS4A	23%
8	0.18M	1:1 TJS cat	MS4A	31%
9	0.18M, ^{m}F sub	1:1	MS4A	23%
10	0.18 M	1:1	sigma HNTf$_2$	31%

Appendix 4.1-121

Catalyst Synthesis
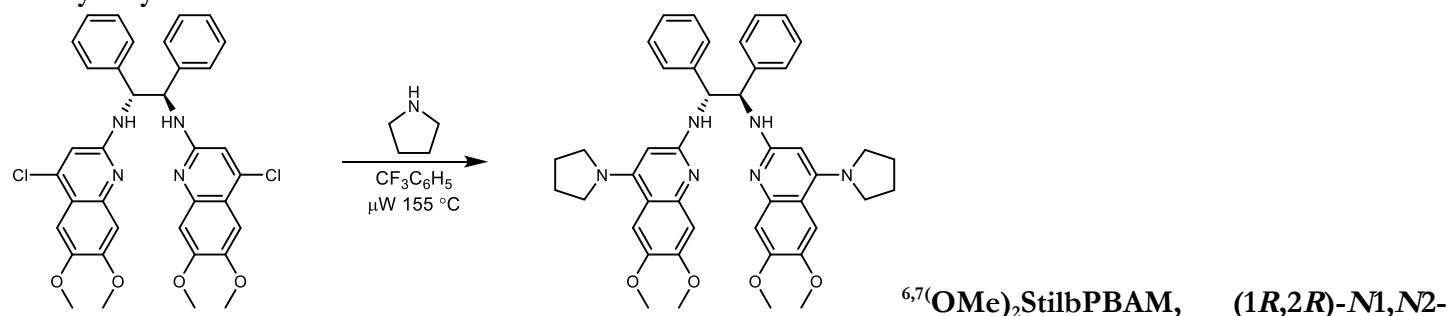
6,7(OMe)₂StilbPBAM, (1R,2R)-N1,N2-bis(6,7-Dimethoxy-4-(pyrrolidin-1-yl)quinolin-2-yl)-1,2-diphenylethane-1,2-diamine. To a 2-5 mL microwave vial was added $(1R,2R)$-N^1,N^2-bis(4-chloro-6,7-dimethoxyquinolin-2-yl)-1,2-diphenylethane-1,2-diamine (2.38 g, 3.63 mmol), pyrrolidine (1.5 mL, 18.1 mmol), and α,α,α,-trifluorotoluene (3.6 mL). The thick slurry was homogenized by sonication, and the resulting mixture was heated at 155 °C under microwave irradiation for 1 h. The reaction mixture was concentrated, diluted with dichloromethane, and washed with 6 M aq NaOH. The organic layer was dried and concentrated, and the crude brown solid was recrystallized[11] by slow evaporation from dichloromethane/hexanes to afford the title compound as a white solid (1.73 g, 66% yield). $[\alpha]_D^{20}$ +88.3 (*c* 1.02 CHCl₃); IR (film) 3236, 2957, 1584, 1511, 1429, 1273 cm⁻¹; ¹H NMR (400 MHz, CDCl₃) δ 7.39 (d, *J* = 7.4 Hz, 4H), 7.22, (s, 2H), 7.19 (dd, *J* = 7.4, 7.4 Hz, 4H), 7.11-7.06 (m, 4H), 6.81 (s, 2H), 5.79 (s, 2H), 5.52 (br s, 2H), 3.81 (s, 6H), 3.75 (s, 6H), 3.42 (m, 4H), 3.33 (m, 4H), 1.88 (s, 8H); ¹³C NMR (100 MHz, CDCl₃) ppm 157.1, 152.8, 151.0, 146.1, 143.8, 143.3, 128.0, 127.9, 126.6, 111.6, 107.1, 105.8, 91.6, 60.3, 55.9, 55.5, 51.5, 25.6; HRMS (ESI): Exact mass calcd for $C_{44}H_{49}N_6O_4$ [M+H]⁺ 725.3815, found 725.3824.

Starting Materials Synthesis
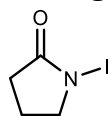
1-iodopyrrolidin-2-one. Procedure was followed as previously reported.[12] To a round bottom flask was added dioxane (44 mL), dry Pyrrolidin-2-one (1.35 mL, 17.6 mmol) and iodine (4.91 g, 19.3 mmol). Prepared *tert*-butyl hypochlorite[13,14] (2.50 mL, 21.1 mmol) was added dropwise over 10 min in the dark and stirred for 3 h. The precipitate was filtered, washed with dioxane, then excess solvent and iodine was removed by pumping on the off-white powder for 12 h to afford a white powder (1.61 g, 42%) with spectra match previously reported data.
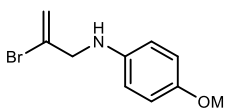
N-(2-Bromoallyl)-4-methoxyaniline. To a round-bottomed flask charged with a stir bar was added 2,3-dibromoprop-1-ene (5.00 g, 25.0 mmol), acetonitrile (192 mL), and aniline (12.2 g, 100 mmol) and heated at 65 °C for 16 h. After cooling to room temperature, the solvent was removed and the black residue was dissolved in 1M aq. HCl, and extracted with hexanes. The organic layers were combined, washed with 6M NaOH, dried, and concentrated to afford a yellow oil. The crude residue was purified filtering through a silica pad in a sintered glass filter by flushing with hexanes, and then eluting the product with 20% ethyl acetate in hexanes to afford the product as a yellow oil (4.03 g, 66%). R_f = 0.3 (20% EtOAc/hexanes) visualized with UV light or I₂; IR (film) 3409, 2997, 2937, 2833, 1631, 1515, 1449, 1242 cm⁻¹; ¹H NMR (400 MHz, CDCl₃) δ 6.78 (d, *J* = 8.9 Hz, 2H), 6.58 (d, *J* = 8.9

---

[11] Poorly recrystallized or precipitated catalyst leads to lower observed enantioselection in the reactions it catalyzes.

[12] Hennecke, U., Müller, C., Fröhlich, R. *Org. Lett.* 2011, *13*, 860.

[13] Mintz, M. J., Walling, C. *Org. Synth.* 1969, *49*, 9.

[14] *Tert*-butyl hypochlorite either freshly prepared or stored over calcium chloride at -20 °C work in similar yields. Commercial sources of *tert*-butyl hypochlorite did not give product.

Hz, 2H), 5.84 (d, *J* = 1.8 Hz, 1H), 5.55 (d, *J* = 1.8 Hz, 1H), 3.95 (s, 2H), 3.95 (s, 1H) 3.74 (s, 3H); ^{13}C NMR (100 MHz, CDCl$_3$) ppm 152.5, 140.6, 131.5, 116.7, 114.8, 114.3, 52.9, 52.6; HRMS (CI): Exact mass calcd for C$_{10}$H$_{12}$BrNO [M]$^+$ 241.0097, found 241.0097.
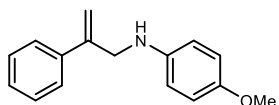
4-Methoxy-*N*-(2-phenylallyl)aniline (120a). To a round-bottomed flask charged with a stir bar was added (3-bromoprop-1-en-2-yl)benzene (2.50 g, 12.6 mmol), acetonitrile (100 mL), and aniline (6.19 g, 50.7 mmol) and heated at 60 °C for 16 h. After cooling to room temperature, the solvent was removed and the black residue was dissolved in 1 M aq. HCl, and extracted with hexanes. The organic layers were combined, washed with 6 M NaOH, dried, and concentrated to afford a yellow oil. The crude residue was purified filtering through a silica pad in a sintered glass filter by flushing with hexanes, and then eluting the product with 20% ethyl acetate in hexanes to afford the product as a yellow solid (2.01 g, 65%). Mp = 32-35 °C; R$_f$ = 0.3 (20% EtOAc/hexanes) visualized with UV light or I$_2$; IR (film) 3408, 3029, 2929, 2833, 1512, 1458, 1239 cm^{-1}; ^{1}H NMR (400 MHz, CDCl$_3$) δ 7.48 (dd, *J* = 6.8, 1.5 Hz, 2H), 7.36 (m, 3H), 6.80 (d, *J* = 8.9 Hz, 2H), 6.61 (d, *J* = 8.9 Hz, 2H), 5.49 (s, 1H), 5.35 (s, 1H), 4.13 (s, 2H), 3.76 (s, 3H), 3.66 (br s, 1H); ^{13}C NMR (100 MHz, CDCl$_3$) ppm 152.1, 145.0, 142.2, 139.3, 128.4, 127.8, 126.0, 114.8, 114.1, 113.5, 55.7, 48.9; HRMS (CI): Exact mass calcd for C$_{16}$H$_{18}$ON [M+H]$^+$ 240.1383, found 240.1375.
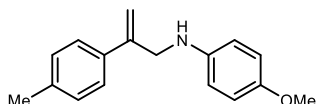
4-Methoxy-*N*-(2-(p-tolyl)allyl)aniline (120c). Prepared according to the general procedure using the allylic alcohol (265 mg, 1.79 mmol), and purified by flash column chromatography (SiO$_2$, 5-10% ethyl acetate in hexanes) to afford a yellow solid (250 mg, 55%). Mp = 46-48 °C; R$_f$ = 0.22 (10% EtOAc/hexanes) visualized with UV light or I$_2$; IR (film) 3408, 2995, 2923, 2834, 1622, 1514, 1459, 1240 cm^{-1}; ^{1}H NMR (400 MHz, CDCl$_3$) δ 7.36 (d, *J* = 8.1 Hz, 2H), 7.17 (d, *J* = 7.9 Hz, 2H), 6.79 (d, *J* = 8.9 Hz, 2H), 6.60 (d, *J* = 8.9 Hz, 2H), 5.44 (s, 1H), 5.29 (s, 1H), 4.10 (s, 2H), 3.75 (s, 3H), 3.63 (br s, 1H), 2.36 (s, 3H); ^{13}C NMR (100 MHz, CDCl$_3$) ppm 152.1, 144.8, 142.2, 137.6, 136.3, 129.1, 125.9, 114.8, 114.1, 112.8, 55.7, 49.1, 21.1; HRMS (ESI): Exact mass calcd for C$_{17}$H$_{20}$NO [M+H]$^+$ 254.1545, found 254.1554.
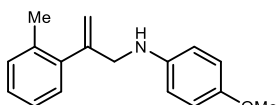
4-Methoxy-*N*-(2-(*o*-tolyl)allyl)aniline (120e). To a flask charged with a stir bar was added the bromide (360 mg, 1.05 mmol), *o*-tolylboronic acid (164 mg, 1.20 mmol), palladium(II) acetate (5.00 mg, 2.62 μmol), K$_2$CO$_2$ (434 mg, 3.15 mmol), SPhos (20.5 mg, 50 μmol), dioxane (8.75 mL), and water (870 μL) and then degassed by four vacuum (house: ~50 Torr)/nitrogen refill cycles. The reaction mixture was heated to 90 °C for 18 h, allowed to cool to room temperature, and then quenched with satd aq NH$_4$Cl. The aqueous layer was extracted with ether, and then the organic layers were combined, dried, and concentrated. The crude brown oil was dissolved in dichlormethane (1 mL) and trifluoroacetic acid (0.5 mL), stirred for 1 h and quenched by pouring into 6 M aq NaOH. The aqueous layer was extracted with ether, then the organic layers were combined, dried, and concentrated to afford a crude brown oil which was purified by flash column chromatography (SiO$_2$, 0-5-15% ethyl acetate in hexanes) to afford the product as a yellow oil (158 mg, 62%). R$_f$ = 0.35 (10% EtOAc/hexanes) visualized with UV light or I$_2$; IR (film) 3409, 2938, 1513, 1239, 1037 cm^{-1}; ^{1}H NMR (400 MHz, CDCl$_3$) δ 7.25-7.13 (m, 4H), 6.82 (d, *J* = 8.9 Hz, 2H), 6.63 (d, *J* = 8.9 Hz, 2H), 5.47 (s, 1H), 5.07 (s, 1H), 3.96 (s, 2H), 3.78 (s, 3H), 3.71 (s, 1H), 2.34 (s, 3H); ^{13}C NMR (100 MHz, CDCl$_3$) ppm 152.0, 146.7, 142.1, 140.6, 135.2, 130.2, 128.4, 127.2, 125.5, 114.7, 114.5,

115.2, 55.7, 50.3, 19.7; HRMS (ESI): Exact mass calcd for $C_{17}H_{20}NO$ [M+H]$^+$ 254.1545, found 254.1536.
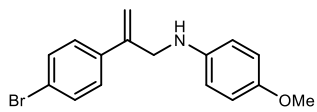
N-(2-(4-Bromophenyl)allyl)-4-methoxyaniline (120f). Prepared according to the general procedure using the allylic alcohol (314 mg, 1.47 mmol), and purified by flash column chromatography (SiO$_2$, 5-10-20% ethyl acetate in hexanes) to afford a yellow solid (150 mg, 32%). Mp = 44-47 °C; R$_f$ = 0.25 (10% EtOAc/hexanes) visualized with UV light or I$_2$; IR (film) 3406, 2994, 2936, 2832, 1513, 1239 cm^{-1}; ^{1}H NMR (400 MHz, CDCl$_3$) δ 7.47 (d, J = 8.6 Hz, 2H), 7.32 (d, J = 8.6 Hz, 2H), 6.78 (d, J = 8.9 Hz, 2H), 6.58 (d, J = 8.9 Hz, 2H), 5.46 (s, 1H), 5.35 (s, 1H), 4.08 (s, 2H), 3.75 (s, 3H), 3.60 (br s, 1H); ^{13}C NMR (100 MHz, CDCl$_3$) ppm 152.2, 144.1, 142.0, 138.2, 131.5, 127.7, 121.8, 114.8, 114.2, 114.1, 55.7, 48.9; HRMS (ESI): Exact mass calcd for $C_{16}H_{17}BrNO$ [M+H]$^+$ 318.0494, found 318.0501.
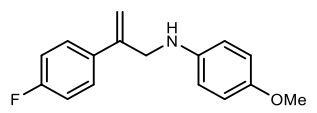
N-(2-(4-Fluorophenyl)allyl)-4-methoxyaniline (120g). To a 100 mL round-bottomed flask charged with a stir bar was added 1,2-dibromotetrachloroethane (6.25 g, 19.2 mmol), toluene (10.1 mL), and cooled to 0 °C. Triphenylphosphine (5.03 g, 19.2 mmol) was added and the reaction solidified. An additional amount of toluene (8 mL) was used to suspend the mixture which was then stirred for 30 min. The allylic alcohol (2.45 g, 16.1 mmol) was dissolved in toluene (10.1 mL) and added to the white suspension over 15 min, and then stirred at 0 °C for 2 h or until TLC showed full conversion. Hexanes (30 mL) was added and the suspension was filtered through a plug of Celite. The filtrate was concentrated, dissolved in acetonitrile (125 mL), and then *p*-anisidine (7.87 g, 64.5 mmol) was added. The black suspension was stirred for 4 h, cooled to 0 °C, filtered to remove excess *p*-anisidine, and concentrated. To the resulting black residue, triethyl amine (3 mL) was added, and the black oil was purified by filtration through a silica gel pad in a sintered glass funnel (5% ethyl acetate in hexanes), and then elution of the product (20% ethyl acetate in hexanes) as a yellow oil (3.28 g, 78%). R$_f$ = 0.3 (10% EtOAc/hexanes) visualized with UV light or I$_2$; IR (film) 3406, 2996, 2938, 2834, 1602, 1512, 1465, 1235 cm^{-1}; ^{1}H NMR (400 MHz, CDCl$_3$) δ 7.42 (dd, J = 8.8 Hz, $^4J_{HF}$ = 5.3 Hz, 2H), 7.03 (dd, J = 8.7 Hz, $^3J_{HF}$ = 8.7 Hz, 2H), 6.79 (d, J = 8.8 Hz, 2H), 6.59 (d, J = 8.8 Hz, 2H), 5.41 (s, 1H), 5.32 (s, 1H), 4.08 (s, 2H), 3.75 (s, 3H), 3.60 (br s, 1H); ^{13}C NMR (100 MHz, CDCl$_3$) ppm 162.5 (d, $^1J_{CF}$ = 247.0 Hz), 152.2, 144.1, 142.1, 135.4 (d, $^4J_{CF}$ = 3.0 Hz), 127.7 (d, $^3J_{CF}$ = 7.7 Hz), 115.3 (d, $^2J_{CF}$ = 21.3 Hz), 114.8, 114.1, 113.6, 55.7, 49.1; ^{19}F NMR (376 MHz, CDCl$_3$) ppm -114.4 (s); HRMS (ESI): Exact mass calcd for $C_{16}H_{17}FNO$ [M+H]$^+$ 258.1294, found 258.1282.
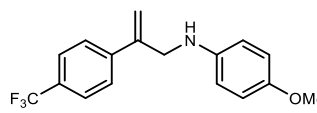
4-Methoxy-N-(2-(4-(trifluoromethyl)phenyl)allyl)aniline (120h). To a flask charged with a stir bar was added the alcohol (1.00 g, 4.94 mmol), diethyl ether (15 mL) and cooled to 0 °C. Phosphorous tribromide (187 μL, 1.97 mmol) was added in one portion and allowed to stir in the dark for 2 h. The reaction mixture was poured into satd aq sodium bicarbonate and extracted with ether. The organic layers were combined, dried with magnesium sulfate, and concentrated. The crude oil was dissolved in acetonitrile (38.0 mL), *p*-anisidine (2.43 g, 19.8 mmol) was added, and the mixture was stirred for 16 h. The mixture was concentrated to a black oil and immediately purified by flash column chromatography (SiO$_2$, 0-10-20% ethyl acetate in hexanes) to afford the product as a yellow solid (252 mg, 17%). mp = 34-36 °C; R$_f$ = 0.2 (20% EtOAc/hexanes) visualized with UV light or I$_2$; IR (film) 3406, 2936, 1617, 1513, 1324, 1240, 1119 cm^{-1}; ^{1}H NMR (400 MHz, CDCl$_3$) δ 7.60 (d, J = 8.4 Hz, 2H), 7.55 (d, J = 8.4 Hz, 2H), 6.79 (d, J = 8.8 Hz, 2H), 6.59 (d, J = 8.8 Hz, 2H), 5.54 (s, 1H), 5.44 (s, 1H), 4.12 (s, 2H), 3.75 (s, 3H), 3.61 (br s, 1H) ; ^{13}C NMR (100 MHz, CDCl$_3$) ppm 152.3, 144.1, 142.9, 141.9, 129.8 ($^2J_{CF}$ = 32 Hz), 126.4, 125.3 ($^3J_{CF}$ = 3.8 Hz), 124.1 ($^1J_{CF}$ = 270 Hz), 115.6, 114.8, 114.2, 55.7, 48.8; HRMS (ESI): Exact mass calcd for $C_{17}H_{17}F_3NO$ [M+H]$^+$ 308.1262, found 308.1254.
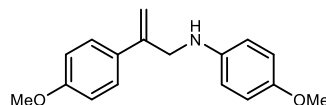
4-Methoxy-*N*-(2-(4-methoxyphenyl)allyl)aniline (120i). To a flask charged with a stir bar was added the alcohol (375 mg, 2.28 mmol), dichloromethane (5.1 mL), and triphenylphosphine (710 mg, 2.71 mmol), and the solution was then cooled to 0 °C. Carbon tetrabromide (829 mg, 2.50 mmol) was added in portions over 20 min and allowed to stir in the dark for 4 h. The reaction mixture was concentrated to a dark brown oil which was dissolved in acetonitrile (38.0 mL) and treated with *p*-anisidine (2.43 g, 19.8 mmol). The mixture was stirred for 5 h, and then concentrated to a black oil and immediately purified by flash column chromatography (SiO$_2$, 0-5-10% ethyl acetate in hexanes) to afford the product as a yellow solid (195 mg, 31%). Mp = 75-77 °C; R$_f$ = 0.2 (10% EtOAc/hexanes) visualized with UV light or I$_2$; IR (film) 3383, 2947, 2835 2357, 1609, 1513, 1459, 1244 cm^{-1}; ^{1}H NMR (400 MHz, CDCl$_3$) δ 7.40 (d, *J* = 8.7 Hz, 2H), 6.88 (d, *J* = 8.8 Hz, 2H), 6.78 (d, *J* = 8.8 Hz, 2H), 6.59 (d, *J* = 8.3 Hz, 2H), 5.39 (s, 1H), 5.24 (s, 1H), 4.09 (s, 2H), 3.82 (s, 3H), 3.75 (s, 3H) 3.62 (br s, 1H); ^{13}C NMR (100 MHz, CDCl$_3$) ppm 159.3, 152.1, 144.2, 142.2, 131.6, 127.2, 114.8, 114.2, 113.8, 112.1, 55.7, 55.2, 49.1; HRMS (ESI): Exact mass calcd for C$_{17}$H$_{20}$NO$_2$ [M+H]$^+$ 270.1494, found 270.1492.
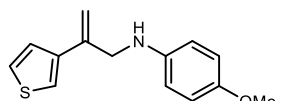
4-Methoxy-*N*-(2-(thiophen-3-yl)allyl)aniline (120j). To a round-bottomed flask charged with a stir bar was added the amine (200 mg, 584 μmol), 3-thienylboronic acid (89.0 mg, 701 μmol), potassium carbonate (241 mg, 1.75 mmol), palladium(II) acetate (3.0 mg, 1.4 μmol), SPhos (12.0 mg, 29.2 μmol), 1,4-dioxane (4.8 mL), and water (480 μL). The reaction mixture was roughly degassed by applying house vacuum (55 mmHg) for 1 min and refilling with argon (3x), then heated to 85 °C and stirred overnight. The reaction was cooled to room temperature, quenched with satd aq NH$_4$Cl and extracted with ether. The organic layers were combined, dried, and concentrated. The crude material was dissolved in dichloromethane (1 mL), trifluoroacetic acid (0.5 mL) was added, and the mixture was stirred for 1 h. The solvent was removed, the residue was dissolved in dichloromethane and poured into 6 M NaOH. The solution was extracted with dichloromethane, the organic layers were combined, dried, and concentrated, and the resulting brown oil was purified by flash column chromatography (SiO$_2$, 5-8-10% ethyl acetate in hexanes) to afford a pale yellow solid (65.0 mg, 45%). Mp = 93-95 °C; R$_f$ = 0.3 (10% EtOAc/hexanes) visualized with UV light or I$_2$; IR (film) 3407, 2931, 1513, 1239, 1034 cm^{-1}; ^{1}H NMR (400 MHz, CDCl$_3$) δ 7.30 (m, 3H), 6.79 (d, *J* = 8.9 Hz, 2H), 6.61 (d, *J* = 8.8 Hz, 2H), 5.51 (s, 1H), 5.29 (s, 1H), 4.08 (s, 2H), 3.75 (s, 3H), 3.71 (br s, 1H); ^{13}C NMR (100 MHz, CDCl$_3$) ppm 152.1, 142.2, 140.5, 139.6, 125.7, 125.6, 120.6, 114.8, 114.0, 112.2, 55.7, 49.0; HRMS (ESI): Exact mass calcd for C$_{14}$H$_{16}$NOS [M+H]$^+$ 246.0953 found 246.0941.
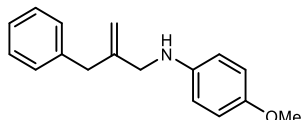
N-(2-Benzylallyl)-4-methoxyaniline (120k). To a flask charged with a stir bar was added the alcohol (1.00 g, 6.74 mmol), dichloromethane (15.3 mL), and triphenylphosphine (2.10 g, 8.02 mmol). The solution was then cooled to 0 °C and carbon tetrabromide (2.45 g, 7.41 mmol) was added in portions over 20 min, followed by a period of stirring in the dark for 4 h. The reaction mixture was concentrated to a dark brown oil which was dissolved in acetonitrile (51.0 mL) and treated with *p*-anisidine (3.32 g, 26.9 mmol). The mixture was stirred for 5 h, concentrated to a black oil, and immediately purified by flash column chromatography (SiO$_2$, 0-5-10% ethyl acetate in hexanes) to afford the product as a yellow oil (610 mg, 35%). R$_f$ = 0.4 (10% EtOAc/hexanes) visualized with UV light or I$_2$; IR (film) 3411, 2906, 2832, 1513, 1452, 1239 cm^{-1}; ^{1}H NMR (400 MHz, CDCl$_3$) δ 7.33 (dd, *J* = 6.9, 6.9 Hz, 2H), 7.27-7.23 (m, 3H), 6.78 (d, *J* = 8.8 Hz, 2H), 6.53 (d, *J* = 8.8 Hz, 2H), 5.14 (s, 1H), 4.97 (s, 1H), 3.76 (s, 3H), 3.64 (s, 2H), 3.58 (br s, 1H), 3.44 (s, 2H); ^{13}C NMR (100 MHz, CDCl$_3$) ppm 151.9, 146.3, 142.3, 139.1, 128.8, 128.3, 126.2, 114.7, 114.0, 112.2, 55.7, 48.9, 41.0; HRMS (ESI): Exact mass calcd for C$_{17}$H$_{20}$NO [M+H]$^+$ 254.1545, found 254.1550.
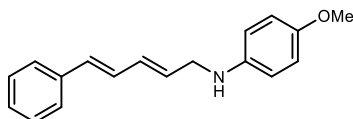
4-Methoxy-*N*-((2*E*,4*E*)-5-phenylpenta-2,4-dien-1-yl)aniline (125a). Bromide synthesized according to literature procedure.[15] To a round-bottomed flask charged with a stir bar was added the unpurified bromide (1.91 g, 8.70 mmol), acetonitrile (66.9 mL), and aniline (4.20 g, 34.8 mmol), and the solution was stirred for 13 h. The reaction mixture was concentrated to a black oil and purified by filtration (silica pad in a sintered funnel) by flushing with hexanes and then eluting the product with 10- 20% ethyl acetate in hexanes to afford a yellow oil (801 mg, 34%). mp = 76-80 °C; R_f = 0.25 (20% EtOAc/hexanes) visualized with UV light or I_2; IR (film) 3387, 3021, 2947, 2832, 1853, 1618, 1512, 1453, 1241 cm^{-1}; ^{1}H NMR (400 MHz, CDCl$_3$) δ 7.38 (d, J = 7.2 Hz, 2H), 7.31 (d, J = 7.3 Hz, 2H), 7.22 (dd, J = 7.3, 7.3 Hz, 1H), 6.79 (d, J = 8.9 Hz, 2H), 6.76 (d, J = 10.5 Hz, 1H), 6.62 (d, 8.9 Hz, 2H), 6.52 (d, 15.6 Hz, 1H), 6.44 (dd, 14.8, 10.1 Hz, 1H), 5.95 (ddd, J = 15.2, 5.9, 5.9 Hz, 1H), 3.83 (d, J = 5.8 Hz, 2H), 3.75 (s, 3H), 3.57 (br s, 1H); ^{13}C NMR (100 MHz, CDCl$_3$) ppm 152.2, 142.2, 137.2, 132.0, 131.9, 131.5, 128.5, 128.3, 127.4, 126.2, 114.8, 114.3, 55.7, 46.9; HRMS (CI): Exact mass calcd for C$_{18}$H$_{19}$ON [M]$^+$ 265.1461, found 265.1456.
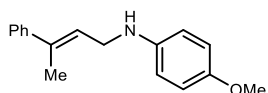
(*E*)-4-Methoxy-*N*-(3-phenylbut-2-en-1-yl)aniline (125d). To a 100 mL round-bottomed flask charged with a stir bar was added 1,2-dibromotetrachloroethane (2.08 g, 6.40 mmol), toluene (4.0 mL), and the solution was cooled to 0 °C. Triphenylphosphine (1.67 g, 6.40 mmol) was added, and the reaction mixture solidified. An additional amount of toluene (2 mL) was used to suspend the mixture which was then stirred for 30 min. The allylic alcohol (790 mg, 5.38 mmol) was dissolved in toluene (4 mL) and added to the white suspension over 15 min, which was then stirred at 0 °C for 2 h or until TLC showed full conversion. Hexanes (20 mL) was added and the suspension was filtered through a plug of Celite. The filtrate was concentrated, dissolved in acetonitrile (41.0 mL), and then *p*-anisidine (2.64 g, 21.5 mmol) was added. The black suspension was stirred for 4 h, cooled to 0 °C, filtered to remove excess *para*-anisidine, and concentrated. To the resulting black residue, triethyl amine (1 mL) was added, and the black oil was purified by automated flash chromatography (SiO$_2$, 0-40% ethyl acetate in hexanes) as an off white solid (588 mg, 43%, 95:5 *E:Z*). Mp = 67-71 °C; R_f = 0.3 (10% EtOAc/hexanes) visualized with UV light or I_2; IR (film) 3384, 2943, 1511, 1451, 1234, 1036 cm^{-1}; ^{1}H NMR (400 MHz, CDCl$_3$) δ 7.36 (d, J = 7.9 Hz, 2H), 7.28 (dd, J = 7.5, 7.5 Hz, 2H), 7.22 (d, J = 6.8 Hz, 1H), 6.77 (d, J = 8.7 Hz, 2H), 6.60 (d, J = 8.8 Hz, 2H), 5.89 (dd, J = 6.9, 6.9 Hz, 1H), 3.85 (d, J = 6.3 Hz, 2H), 3.71 (s, 3H), 3.46 (br s, 1H), 2.09 (s, 3H); ^{13}C NMR (100 MHz, CDCl$_3$) ppm 152.2, 142.9, 142.4, 137.3, 128.2, 127.0, 125.6, 125.4, 114.8, 114.3, 55.7, 43.5, 16.0; HRMS (ESI): Exact mass calcd for C$_{17}$H$_{20}$NO [M+H]$^+$ 254.1545, found 254.1540.
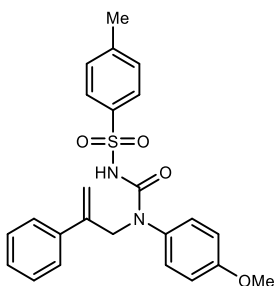
***N*-((4-Methoxyphenyl)(2-phenylallyl)carbamoyl)-4-methylbenzenesulfonamide.** To a round-bottomed flask charged with a stir bar was added the amine (200 mg, 835 μmol), dichloromethane (8.3 mL), and *p*-toluenesulfonyl isocyanate (127 μL, 835 μmol), and the solution was stirred for 30 min. The solvent was removed and the resulting

---

[15] *J. Am. Chem. Soc*. 2014, *136,* 4476–4479

pale yellow solid was purified by flash column chromatography (SiO$_2$, 30-50% EtOAc/hexanes) to afford a pale yellow solid (345 mg, 94%). Mp = 154-157 °C; R$_f$ = 0.1 (30% EtOAc/hexanes) visualized with UV light or I$_2$; IR (film) 3378, 3257, 3051, 3023, 2929, 1689, 1509, 1435, 1350, 1251, 1165 cm^{-1}; ^{1}H NMR (400 MHz, CDCl$_3$) δ 7.86 (d, J = 8.3 Hz, 2H), 7.32 (d, J = 8.0 Hz, 2H), 7.29-7.20 (m, 5H), 6.88 (br s, 1H), 6.83 (d, J = 9.0 Hz, 2H), 6.77 (d, J = 9.0 Hz, 2H), 5.29 (s, 1H), 4.93 (s, 1H), 4.65 (s, 2H), 3.81 (s, 3H), 2.47 (s, 3H); ^{13}C NMR (100 MHz, CDCl$_3$) ppm 159.7, 150.5, 144.4, 143.1, 137.9, 136.1, 130.7, 129.5, 129.4, 128.3, 128.2, 127.8, 126.2, 116.4, 115.4, 55.5, 52.5, 21.6; HRMS (ESI): Exact mass calcd for C$_{24}$H$_{24}$NaN$_2$O$_4$S [M+Na]$^+$ 459.1354 found 459.1360.

Optimization
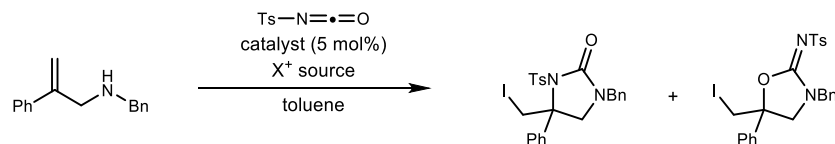
entry	Catalyst	Iodine source	Concentration (M)	time (h)	Temp (ºC)	NMR yield N:O (%)[a]	ee (N) (%)[b]
1	HQuinBAM	NIS	0.04	16	-20	85:15	24
2	StilbPBAM	NIS	0.04	16	-20	86:13	57
3	[7]OMeStilbPBAM	NIS	0.04	16	-20	95:5	71
4	[7]OMeStilbPBAM•HNTf	NIS	0.04	16	-20	92:10	58

[a]Relative to CH_2Br_2 as internal standard. [b]Enantiomeric excess (ee) determined by HPLC using a chiral stationary phase. Reactions are run on 0.05 mmol scale
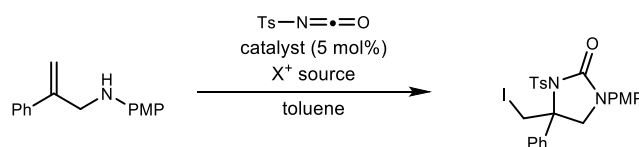
entry	Catalyst	Iodine source	Concentration (M)	time (h)	Temp (ºC)	NMR yield (%)[a]	ee (%)[b]
1	StilbPBAM	DIDMH	0.05	2	-20	>95	53
2	[7]OMeStilbPBAM	DIDMH	0.05	2	-20	>95	85
	[7]OMeStilbPBAM	NIS	0.05	2	-20	71	76
	[7]OMeStilbPBAM	NIPy	0.05	2	-20	80	79
	[7]OMeStilbPBAM•HNTf	NIS	0.05	16	-20	75	60
3	[6,7](OMe)₂StilbPBAM	DIDMH	0.05	2	-20	>95	82
4	[6,7](OMe)₂StilbPBAM	NIS	0.05	2	-20	>95	83
5	[6,7](OMe)₂StilbPBAM	NIPy	0.05	2	-20	>95	82
6	[6,7](OMe)₂StilbPBAM	NIPy	0.05	16	-20	95	85
7	[6,7](OMe)₂StilbPBAM	NIPy	0.05	16	-50	99	91
8	[6,7](OMe)₂StilbPBAM	NIPy	0.05	36	-50	99	91
9	[6,7](OMe)₂StilbPBAM	DIDMH	0.05	36	-50	>95	90
10	[6,7](OMe)₂StilbPBAM	NIS	0.05	36	-50	>95	91
11	[6,7](OMe)₂StilbPBAM	NBS	0.05	36	-50	86	55
12	[6,7](OMe)₂StilbPBAM•HNTf₂	NIPy	0.05	36	-50	94	81

[a]Relative to CH_2Br_2 as internal standard. [b]Enantiomeric excess (ee) determined by HPLC using a chiral stationary phase. Reactions are run on 0.05 mmol scale

NIPy   NIS   DIDMH

$R_1=R_2=H$ StilbPBAM
$R_1=H$ $R_2 = OMe$ [7]OMeStilbPBAM
$R_1=R_2= OMe$ [6,7](OMe)₂StilbPBAM

Appendix 4.1-128
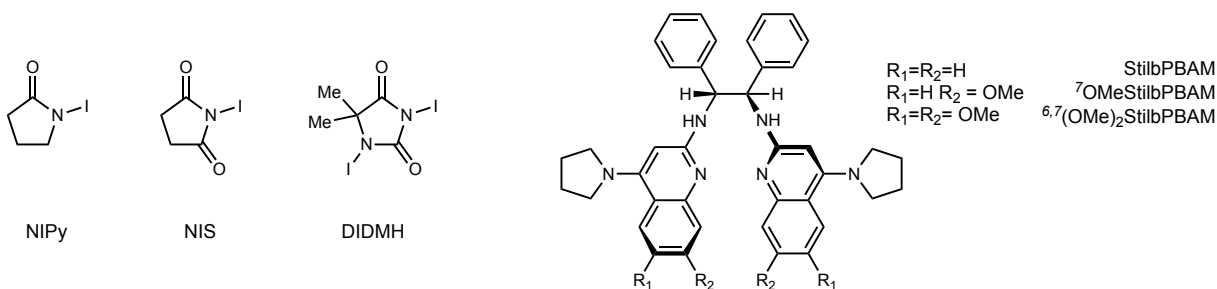
Enantioselective Urea Reactions
Representative Procedure:
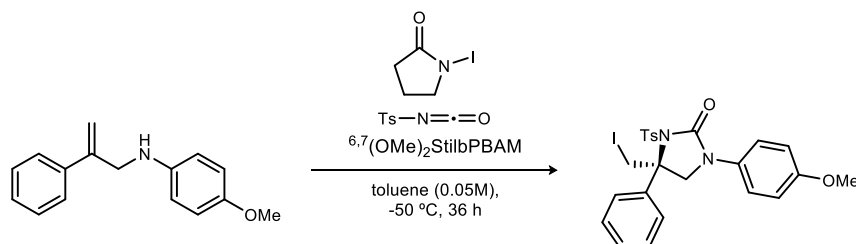
(*R*)-4-(Iodomethyl)-1-(4-methoxyphenyl)-4-phenyl-3-tosylimidazolidin-2-one (121a). To a 2-5 mL microwave vial equipped with a stir bar was added amine (22.9 mg, 100 μmol), toluene (2 mL), and isocyanate (15.2 μL, 100 μmol). After 5 min ^{6,7}(OMe)$_2$StilbPBAM (3.6 mg, 5.0 μmol)[16] was added, the reaction mixture was then cooled to -50 °C and stirred for 30 min. *N*-Iodopyrrolidine (25.3 mg, 120 μmol) was added and the resulting suspension was stirred for 36 h. Then was quenched by passing the suspension through a 15% w/w powdered Na$_2$S$_2$O$_3$/SiO$_2$ plug[17] then eluted with 50% ethyl acetate in hexanes and concentrated to a white solid. The crude material was purified by flash column chromatography (SiO$_2$, 20-35% ethyl acetate in hexanes) to afford the title compound as a white solid (23.0 mg, 82%). The product was determined to be 91% ee by chiral HPLC analysis (Chiralpak IB, 25% EtOH/hexanes, 1.0 mL/min, 30 °C, t_r(major) = 9.2 min, t_r(minor) = 12.6 min); mp = 140 °C (dec); [α]$_D^{20}$ +22[18] (*c* 0.81 CHCl$_3$); R$_f$ = 0.3 (35% EtOAc/hexanes) visualized with UV light or I$_2$; IR (film) 3056, 2978, 2839, 1730, 1596, 1509, 1408, 1362, 1251 cm^{-1}; ^{1}H NMR (400 MHz, CDCl$_3$) δ 7.46 (d, *J* = 7.3 Hz, 2H), 7.42 (d, *J* = 9.1 Hz, 2H), 7.37 (d, *J* = 8.1 Hz, 2H), 7.35 (d, *J* = 7.4 Hz, 2H), 7.33 (dd, *J* = 6.2, 6.2 Hz, 1H), 7.07 (d, *J* = 8.1 Hz, 2H), 6.88 (d, *J* = 8.9 Hz, 2H), 4.47 (d, *J* = 10.6 Hz, 1H), 4.42 (d, *J* = 10.6 Hz, 1H), 4.11 (d, *J* = 9.8 Hz, 1H), 4.08 (d, *J* = 9.8 Hz, 1H), 3.78 (s, 3H), 2.34 (s, 3H); ^{13}C NMR (100 MHz, CDCl$_3$) ppm 156.9, 151.5, 144.4, 139.1, 135.7, 130.7, 129.0, 128.8, 128.7 (2C), 126.9, 121.3, 114.3, 63.6, 61.1, 55.5, 21.5, 14.2; HRMS (ESI): Exact mass calcd for C$_{24}$H$_{24}$IN$_2$NaO$_4$S [M+Na]$^+$ 585.0321, found 585.0305.
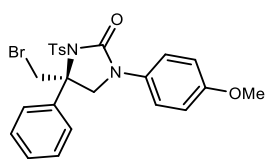
(*R*)-4-(Bromomethyl)-1-(4-methoxyphenyl)-4-phenyl-3-tosylimidazolidin-2-one (121b). Prepared according to the general procedure using 4-methoxy-*N*-(2-phenylallyl)aniline (11.9 mg, 50.0 μmol) and *N*-bromosuccinimide (16.7 mg, 60.0 μmol), purified by flash column chromatography (SiO$_2$, 20-35% EtOAc/hexanes) to afford a white foam (21.9 mg, 86%). The product was determined to be 55% ee by chiral HPLC analysis (Chiralpak IB, 25% EtOH/hexanes, 1.0 mL/min, 30 °C, t_r(major) = 9.0 min, t_r(minor) = 12.4 min); [α]$_D^{20}$ +8.3 (*c* 1.4 CHCl$_3$); R$_f$ = 0.3 (35% EtOAc/hexanes) visualized with UV light or I$_2$; IR (film) 2926, 1728, 1512, 1408, 1359, 1252, 1170 cm^{-1}; ^{1}H NMR (400 MHz, CDCl$_3$) δ 7.46-7.36 (m, 9H), 7.09 (d, *J* = 8.1 Hz, 2H), 6.88 (d, *J* = 9.1 Hz, 2H), 4.59 (s, 2H), 4.23 (d, *J* = 9.6 Hz, 1H), 4.05 (d, *J* = 9.6 Hz, 1H), 3.78 (s, 3H), 2.35 (s, 3H); ^{13}C NMR (100 MHz, CDCl$_3$) ppm 156.8, 151.5, 144.5, 139.6, 135.7, 130.8, 129.0, 128.9, 128.8, 126.5, 121.2, 114.3, 64.3, 58.6, 55.5, 38.3, 21.5; HRMS (ESI): Exact mass calcd for C$_{24}$H$_{23}$BrN$_2$O$_4$NaS [M+Na]$^+$ 537.0460, found 537.0476.

---

[16] Catalyst purity is essential for high %ee. Lower purity catalyst has been used without recrystallization and good reactivity is still obtained however the %ee is 85% or lower.

[17] Catalyst can be recovered from the thiosulfate/silica plug by stirring the mixture in 15% MeOH/DCM, filtering, and concentrating. For optimal reactivity and enantioselectivity with recovered catalyst, reverse phase HPLC and subsequent recrystallization in DCM/hexanes is necessary. With catalyst from this procedure, 90% yield and 91% ee material of the urea cyclization is observed.

[18] [α]$_D^{20}$ taken on 96% ee material

(*R*)-4-(Iodomethyl)-1-(4-methoxyphenyl)-4-(p-tolyl)-3-tosylimidazolidin-2-one (121c). Prepared according to the general procedure using the amine (25.3 mg, 100 μmol), and purified by flash column chromatography (SiO$_2$, 20-35% ethyl acetate in hexanes) to afford a white solid (55.9 mg, 97%). The product was determined to be 92% ee by chiral HPLC analysis (Chiralpak IB, 25% EtOH/hexanes, 1.0 mL/min, 30 °C, t_r(major) = 8.5 min, t_r(minor) = 9.8 min); mp = 71-75 °C; [α]$_D^{20}$ +34.5 (*c* 1.02 CHCl$_3$); R$_f$ = 0.3 (35% EtOAc/hexanes) visualized with UV light or I$_2$; IR (film) 2926, 1728, 1512, 1406, 1359, 1251, 1170 cm^{-1}; ^{1}H NMR (400 MHz, CDCl$_3$) δ 7.42 (d, *J* = 9.0 Hz, 2H), 7.41 (d, *J* = 8.1 Hz, 2H), 7.34 (d, *J* = 8.2 Hz, 2H), 7.14 (d, *J* = 8.2 Hz, 2H), 7.07 (d, *J* = 8.2 Hz, 2H), 6.88 (d, *J* = 9.0 Hz, 2H), 4.42 (dd, *J* = 10.8, 10.8 Hz, 2H), 4.08 (dd, *J* =10.3, 10.3 Hz, 2H), 3.78 (s, 3H), 2.39 (s, 3H), 2.35 (s, 3H); ^{13}C NMR (100 MHz, CDCl$_3$) ppm 156.8, 151.5, 144.3, 138.7, 136.1, 135.8, 130.7, 129.3, 129.0, 128.7, 126.8, 121.3, 114.3, 63.5, 61.1, 55.5, 21.5, 21.0, 14.3; HRMS (ESI): Exact mass calcd for C$_{25}$H$_{25}$IN$_2$NaO$_4$S [M+Na]$^+$ 599.0478 found 599.0463.
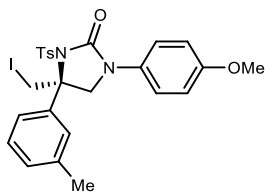
(*R*)-4-(Iodomethyl)-1-(4-methoxyphenyl)-4-(m-tolyl)-3-tosylimidazolidin-2-one (121d). Prepared according to the general procedure using the amine (25.3 mg, 100 μmol), and purified by flash column chromatography (SiO2, 20-30% ethyl acetate in hexanes) to afford a white solid (50.8 mg, 88%). The product was determined to be 91% ee by chiral HPLC analysis (Chiralpak IB, 25% EtOH/hexanes, 1.0 mL/min, 30 °C, t_r (major) = 7.7 min, t_r (minor) = 8.5 min); mp = 96-100 °C (dec); [α]$_D^{20}$ +1.4 (c 1.04 CHCl$_3$); R$_f$ = 0.3 (30% EtOAc/hexanes) visualized with UV light or I$_2$; IR (film) 2924, 1727, 1512, 1360, 1252 1169 cm^{-1}; ^{1}H NMR (400 MHz, CDCl$_3$) δ 7.43 (d, *J* = 9.1 Hz, 2H), 7.39 (d, *J* = 8.0 Hz, 2H), 7.28-7.22 (m, 2H), 7.17 (d, *J* = 7.0 Hz, 1H), 7.14 (s, 1H), 7.08 (d, *J* = 8.0 Hz, 2H), 6.89 (d, *J* = 9.1 Hz, 2H), 4.50 (d, *J* = 10.6 Hz, 1H), 4.36 (d, *J* = 10.6 Hz, 1H), 4.08 (d, *J* = 9.6 Hz, 1H), 4.04 (d, *J* = 9.5 Hz, 1H), 3.78 (s, 3H), 2.35 (s, 3H), 2.24 (s, 3H); ^{13}C NMR (100 MHz, CDCl$_3$) ppm 156.8, 151.5, 144.3, 139.0, 138.5, 135.8, 130.7, 129.3, 128.9, 128.7, 128.5, 127.5, 123.8, 121.3, 114.3, 63.6, 61.1, 55.4, 21.5, 21.4, 14.7; HRMS (ESI): Exact mass calcd for C$_{25}$H$_{26}$IN$_2$O$_4$S [M+H]$^+$ 577.0658, found 577.0649.

(*R*)-4-(4-Bromophenyl)-4-(iodomethyl)-1-(4-methoxyphenyl)-3-tosylimidazolidin-2-one (121f). Prepared according to the general procedure using the amine (31.8 mg, 100 μmol), and purified by flash column chromatography (SiO$_2$, 20-35% ethyl acetate in hexanes) to afford a white solid (59.1 mg, 90%). The product was determined to be 88% ee by chiral HPLC analysis (Chiralpak IB, 25% ^{i}PrOH/hexanes, 1.0 mL/min, 30 °C, t_r(major) = 15.9 min, t_r(minor) = 18.9 min); mp = 106-108 °C; [α]$_D^{20}$ +45.7 (*c* 0.99 CHCl$_3$); R$_f$ = 0.45 (30% EtOAc/hexanes) visualized with UV light or I$_2$; IR (film) 3055, 2931, 2840, 1729, 1511, 1405, 1359, 1252, 1170, 1142 cm^{-1}; ^{1}H NMR (400 MHz, CDCl$_3$) δ 7.47-7.43 (m, 4H), 7.41 (d, *J* = 9.1 Hz, 2H), 7.33 (d, *J* = 8.8 Hz, 2H), 7.12 (d, *J* = 8.1 Hz, 2H), 6.89 (d, *J* = 9.1 Hz, 2H), 4.42 (d, *J* = 10.7 Hz, 1H), 4.35 (d, *J* = 10.7 Hz, 1H), 4.08 (d, *J* = 9.7 Hz, 1H), 4.03 (d, *J* = 9.7 Hz, 1H), 3.78 (s, 3H), 2.37 (s, 3H); ^{13}C NMR (100 MHz, CDCl$_3$) ppm 156.9, 151.3, 144.7,

138.1, 135.7, 131.8, 130.5, 128.9, 128.8, 128.6, 122.9, 121.3, 114.3, 63.1, 60.8, 55.5, 21.6, 13.4 ; HRMS (ESI): Exact mass calcd for $C_{24}H_{23}BrIN_2O_4S$ [M+H]$^+$ 640.9607, found 640.9623.
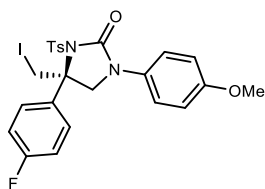
(*R*)-4-(4-Fluorophenyl)-4-(iodomethyl)-1-(4-methoxyphenyl)-3-tosylimidazolidin-2-one (121g). Prepared according to the general procedure using the amine (25.7 mg, 100 μmol), and purified by flash column chromatography (SiO$_2$, 20-30% ethyl acetate in hexanes) to afford a white solid (52.5 mg, 90%). The product was determined to be 89% ee by chiral HPLC analysis (Chiralpak IB, 25% EtOH/hexanes, 1.0 mL/min, 30 °C, t_r (major) = 8.4 min, t_r (minor) = 9.3 min); mp = 148-150 °C; [α]$_D^{20}$ +15.0 (*c* 0.73 CHCl$_3$); R$_f$ = 0.25 (30% EtOAc/hexanes) visualized with UV light or I$_2$; IR (film) 3108, 2931, 1727, 1600, 1511, 1406, 1358, 1249, 1170 cm^{-1}; ^{1}H NMR (400 MHz, CDCl$_3$) δ 7.47-7.39 (m, 6H), 7.12 (d, J = 8.1 Hz, 2H), 7.03 (dd, J = 9.1, $^3J_{HF}$ = 9.1 Hz, 2H), 6.89 (d; 9.1 Hz, 2H), 4.43 (d, J = 10.6 Hz, 1H), 4.39 (d, J = 10.6 Hz, 1H), 4.09 (d, J = 9.8 Hz, 1H), 4.05 (d, J = 9.7 Hz, 1H), 3.78 (s, 3H), 2.36 (s, 3H); ^{13}C NMR (100 MHz, CDCl$_3$) ppm 162.4 (d, $^1J_{CF}$ = 162.4 Hz), 156.9, 151.4, 144.6, 135.7, 134.9, 130.6, 129.0 (d, $^3J_{CF}$ = 8.4 Hz), 128.8, 121.3, 115.7, 155.5, 114.3, 63.1, 61.1, 55.5, 21.5, 13.8; ^{19}F NMR (376 MHz, CDCl$_3$) ppm -112.2 (s); HRMS (ESI): Exact mass calcd for $C_{24}H_{23}IN_2O_4S$ [M+H]$^+$ 581.0407, found 581.0402.
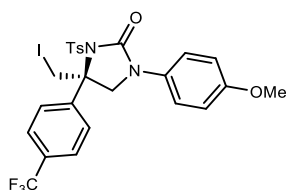
(*R*)-4-(Iodomethyl)-1-(4-methoxyphenyl)-3-tosyl-4-(4-(trifluoromethyl)phenyl)imidazolidin-2-one (121h). Prepared according to the general procedure using the amine (30.7 mg, 100 μmol), and purified by flash column chromatography (SiO$_2$, 15-30% ethyl acetate in hexanes) to afford a white solid (47.4 mg, 75%). The product was determined to be 90% ee by chiral HPLC analysis (Chiralpak IB, 20% EtOH/hexanes, 1.0 mL/min, 30 °C, t_r (major) = 9.7 min, t_r (minor) = 10.6 min); mp = 80-83 °C; [α]$_D^{20}$ +24.8 (c 0.95 CHCl$_3$); R$_f$ = 0.6 (30% EtOAc/hexanes) visualized with UV light or I$_2$; IR (film) 3020, 2933, 2356, 1730, 1513, 1407, 1326, 1252, 1170, 1132 cm^{-1}; ^{1}H NMR (400 MHz, CDCl$_3$) δ 7.59 (app s, 4H), 7.42 (d, J = 9.0 Hz, 2H), 7.40 (d, J = 8.3 Hz, 2H), 7.08 (d, J = 8.1 Hz, 2H), 6.90 (d, J = 9.0 Hz, 2H), 4.47 (d, J = 10.7 Hz, 1H), 4.39 (d, J = 10.7 Hz, 1H), 4.12 (d, J = 9.8 Hz, 1H), 4.05 (d, J = 9.8 Hz, 1H), 3.79 (s, 3H), 2.35 (s, 3H); ^{13}C NMR (100 MHz, CDCl$_3$) ppm 157.1, 151.4, 144.8, 142.8, 153.6, 130.9 ($^2J_{CF}$ = 32.8 Hz), 130.4, 128.9, 128.7, 127.4, 126.6 ($^1J_{CF}$ = 272.3 Hz), 125.6 ($^3J_{CF}$ = 3.5 Hz), 121.4, 114.4, 63.1, 60.8, 55.5, 21.5, 13.1; ^{19}F NMR (376 MHz, CDCl$_3$) ppm -62.5 (s); HRMS (ESI): Exact mass calcd for $C_{25}H_{23}FIN_2O_4S$ [M+H]$^+$ 631.0375, found 631.0373.
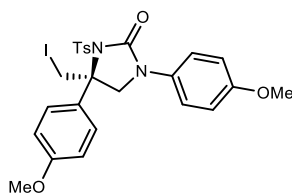
(*R*)-4-(Iodomethyl)-1,4-bis(4-methoxyphenyl)-3-tosylimidazolidin-2-one (121i). Prepared according to the general procedure using the amine (26.9 mg, 100 μmol), and purified by flash column chromatography (SiO$_2$, 20-35% EtOAc/hexanes) to afford a white solid (47.8 mg, 80%). The product was determined to be 90% ee by chiral HPLC analysis (Chiralpak IB, 25% EtOH/hexanes, 1.0 mL/min, 30 °C, t_r (major) = 10.3 min, t_r (minor) = 12.3 min); mp = 56-60 °C; [α]$_D^{20}$ +36.4 (c 1.13 CHCl$_3$); R$_f$ = 0.25 (30% EtOAc/hexanes) visualized with UV light or I$_2$; IR (film) 2933, 2357, 1727, 1604, 1512, 1406, 1358, 1253, 1174 cm^{-1}; ^{1}H NMR (400 MHz, CDCl$_3$) δ 7.43 (dd, J = 8.8, 8.8 Hz, 4H), 7.37 (d, J = 8.9 Hz, 2H), 7.08 (d, J = 8.2 Hz, 2H),

6.88 (d, *J* = 8.9 Hz, 2H), 6.84 (d, *J* = 8.8 Hz, 2H), 4.43 (d, *J* = 11.2 Hz, 1H), 4.40 (d, *J* = 10.6 Hz, 1H), 4.09 (dd, *J* = 9.8, 9.8 Hz, 2H), 3.84 (s, 3H), 3.78 (s, 3H), 2.35 (s, 3H); ^{13}C NMR (100 MHz, CDCl$_3$) ppm 159.6, 156.8, 151.5, 144.3, 135.9, 130.9, 130.7, 128.9, 128.7, 128.3, 121.3, 114.3, 113.9, 63.4, 61.1, 55.5, 55.4, 21.5, 14.3; HRMS (ESI): Exact mass calcd for C$_{25}$H$_{26}$NI$_2$O$_5$S [M+H]$^+$ 593.0607, found 593.0622.
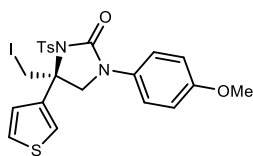
(R)-4-(Iodomethyl)-1-(4-methoxyphenyl)-4-(thiophen-3-yl)-3-tosylimidazolidin-2-one (121j). Prepared according to the general procedure using the amine (24.5 mg, 100 μmol), and purified by flash column chromatography (SiO$_2$, 20-30% ethyl acetate in hexanes) to afford a white solid (53.1 mg, 93%). The product was determined to be 88% ee by chiral HPLC analysis (Chiralpak IB, 25% EtOH/hexanes, 1.0 mL/min, 30 °C, t_r (major) = 9.7 min, t_r (minor) = 11.3 min); mp = 65-68 °C; [α]$_D^{20}$ +13.9 (*c* 1.02 CHCl$_3$); R$_f$ = 0.35 (30% EtOAc/hexanes) visualized with UV light or I$_2$; IR (film) 3108, 2950, 1728, 1512, 1407, 1360, 1253, 1169 cm^{-1}; ^{1}H NMR (400 MHz, CDCl$_3$) δ 7.46 (d, *J* = 8.3 Hz, 2H), 7.44-7.43 (m, 1H), 7.39 (d, *J* = 9.0 Hz, 2H), 7.25 (dd, *J* = 5.0, 2.9 Hz, 1H), 7.11 (d, *J* = 8.2 Hz, 2H), 7.01 (d, *J* = 5.1, 1.2 Hz, 1H), 6.88 (d, *J* = 9.0 Hz, 2H), 4.41 (d, *J* = 10.6 Hz, 1H), 4.37 (d, *J* = 10.6 Hz, 1H), 4.06 (d, *J* = 9.5 Hz, 1H), 4.03 (d, *J* = 9.6 Hz, 1H), 3.78 (s, 3H), 2.35 (s, 3H); ^{13}C NMR (100 MHz, CDCl$_3$) ppm 156.8, 151.4, 144.4, 139.4, 135.7, 130.6, 128.8 (2C), 126.6, 126.2, 124.1, 121.4, 114.3, 61.7, 60.1, 55.4, 21.5, 13.9; HRMS (ESI): Exact mass calcd for C$_{22}$H$_{21}$INaN$_2$O$_4$S$_2$ [M+Na]$^+$ 590.9885, found 590.9886.
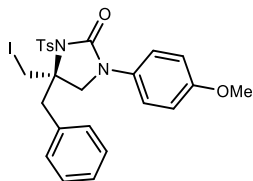
(R)-4-Benzyl-4-(iodomethyl)-1-(4-methoxyphenyl)-3-tosylimidazolidin-2-one (121k). Prepared according to the general procedure using the amine (25.3 mg, 100 μmol), and purified by flash column chromatography (SiO$_2$, 20-30% ethyl acetate in hexanes) to afford a white foam (42.3 mg, 75%). The product was determined to be 49% ee by chiral HPLC analysis (Chiralpak IA, 25% ^{i}PrOH/hexanes, 1.0 mL/min, 30 °C, t_r (minor) = 9.9 min, t_r (major) = 11.2 min); [α]$_D^{20}$ +0.8 (c 1.02 CHCl$_3$); R$_f$ = 0.4 (35% EtOAc/hexanes) visualized with UV light or I$_2$; IR (film) 3023, 2928, 1729, 1512, 1352, 1247 cm^{-1}; ^{1}H NMR (400 MHz, CDCl$_3$) δ 8.06 (d, *J* = 8.8 Hz, 2H), 7.27-7.18 (m, 7H), 6.95 (d, *J* = 9.0 Hz, 2H), 6.69 (d, *J* = 9.0 Hz, 2H), 4.17 (d, *J* = 10.6 Hz, 1H), 3.76 (d, *J* = 10.6 Hz, 1H), 3.68 (d, *J* = 9.5 Hz, 1H), 3.66 (s, 3H), 3.60 (d, *J* = 13.9 Hz, 1H), 3.56 (d, *J* = 9.3 Hz, 1H), 3.55 (d, *J* = 14.0 Hz, 1H), 2.35 (s, 3H); ^{13}C NMR (100 MHz, CDCl$_3$) ppm 156.8, 151.6, 144.8, 136.6, 134.3, 130.4, 130.3, 129.3, 129.2, 128.7, 127.5, 121.6, 114.0, 64.8, 55.3, 54.3, 42.4, 21.6, 15.3; HRMS (ESI): Exact mass calcd for C$_{25}$H$_{26}$IN$_2$O$_4$S [M+H]$^+$ 577.0658, found 577.0667.
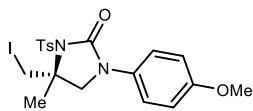
(R)-4-(Iodomethyl)-1-(4-methoxyphenyl)-4-methyl-3-tosylimidazolidin-2-oneone (121l). Prepared according to the general procedure using the amine (17.7 mg, 100 μmol), and purified by flash column chromatography (SiO$_2$, 20-35% EtOAc/hexanes) to afford a colorless oil (46.5 mg, 93%). The product was determined to be 29% ee by chiral HPLC analysis (Chiralpak IA, 25% EtOH/hexanes, 1.0 mL/min, 30 °C, t_r (major) = 12.5 min, t_r (minor) = 17.7 min; [α]$_D^{20}$ +2.3 (*c* 0.98 CHCl$_3$); R$_f$ = 0.25 (35% EtOAc/hexanes) visualized with UV light or I$_2$; IR (film) 2928, 1727, 1513, 1596, 1513, 1410, 1351, 1292, 1158 cm^{-1}; ^{1}H NMR (400 MHz, CDCl$_3$) δ 8.03 (d, *J* = 8.3 Hz, 2H), 7.34 (d, *J* = 9.0 Hz, 2H), 7.31 (d, *J* = 8.2 Hz, 2H), 6.85 (d, *J* = 9.0 Hz, 2H), 3.96 (d, *J* = 10.4 Hz, 1H), 3.86 (d, *J* = 9.6 Hz, 1H), 3.85 (d, *J* = 10.5 Hz, 1H), 3.76 (s, 3H), 3.56 (d, *J* = 9.2 Hz, 1H), 2.41 (s, 3H), 1.99 (s, 3H); ^{13}C NMR (100 MHz, CDCl$_3$) ppm 156.7, 151.4, 144.7, 136.4, 130.8, 129.2, 129.0, 121.0, 114.2, 61.3, 57.8, 55.4, 25.1, 21.6, 15.0; HRMS (ESI): Exact mass calcd for C$_{19}$H$_{21}$IN$_2$NaO$_4$S [M+Na]$^+$ 523.0165, found 523.0145.
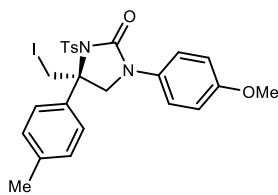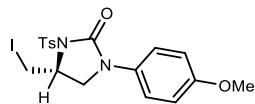
4-(Iodomethyl)-1-(4-methoxyphenyl)-3-tosylimidazolidin-2-one (121m). Prepared according to the general procedure using the amine (16.3 mg, 100 μmol), and purified by flash column chromatography (SiO$_2$, 20-30% EtOAc/hexanes) to afford a white solid (34.1 mg, 70%). The product was determined to be 39% ee by chiral HPLC analysis (Chiralpak IA, 30% EtOH/hexanes, 1.0 mL/min, 30 °C, t_r (minor) = 14.3 min, t_r (major) = 19.3 min); mp = 70-73 °C; [α]$_D^{20}$ -19.8 (*c* 0.82 CHCl$_3$); R$_f$ = 0.25 (30% EtOAc/hexanes) visualized with UV light or I$_2$; IR (film) 2929, 1728, 1596, 1513, 1410, 1352, 1243 cm^{-1}; ^{1}H NMR (400 MHz, CDCl$_3$) δ 7.98 (d, *J* = 8.7 Hz, 2H), 7.34 (d, *J* = 9.1 Hz, 2H), 7.33 (d, *J* = 8.6 Hz, 2H), 6.85 (d, *J* = 9.1 Hz, 2H), 4.48 (dddd, *J* = 8.9, 8.9, 3.5, 3.5 Hz, 1H), 4.03 (dd, *J* = 9.4, 9.4 Hz, 1H), 3.76 (s, 3H), 3.73 (dd, *J* = 10.2, 2.7 Hz, 1H), 3.59 (dd, *J* = 9.6, 3.8 Hz, 1H), 3.52 (dd, *J* = 10.2, 8.2 Hz, 1H), 2.42 (s, 3H); ^{13}C NMR (100 MHz, CDCl$_3$) ppm 156.7, 151.1, 145.0, 135.6, 130.8, 129.6, 128.4, 121.0, 114.2, 55.4, 52.8, 50.0, 21.6, 9.5; HRMS (ESI): Exact mass calcd for C$_{18}$H$_{19}$IN$_2$NaO$_4$S [M+Na]$^+$ 509.0008, found 508.9991.
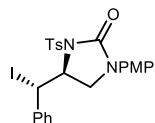
(*S*)-4-((*S*)-Iodo(phenyl)methyl)-1-(4-methoxyphenyl)-3-tosylimidazolidin-2-one (122a). Prepared according to the general procedure using the amine (23.9 mg, 100 μmol), and purified by flash column chromatography (SiO$_2$, 20-30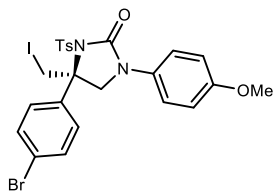% ethyl acetate in hexanes) to afford the imidazolidinone as a white solid (49.0 mg, 92%). The product was determined to be 92% ee by chiral HPLC analysis (Chiralpak AD-H, 25% EtOH/hexanes, 1.0 mL/min, 30 °C, t_r (minor) = 12.2 min, t_r (major) = 13.4 min); mp = 120 °C (dec); [α]$_D^{20}$ +36.4 (*c* 0.84 CHCl$_3$); R$_f$ = 0.4 (30% EtOAc/hexanes) visualized with UV light or I$_2$; IR (film) 2929, 1732, 1596, 1512, 1406, 1355, 1242 cm^{-1}; ^{1}H NMR (400 MHz, CDCl$_3$) δ 7.95 (d, *J* = 8.3 Hz, 2H), 7.41 (d, *J* = 6.8 Hz, 2H), 7.30 (d, *J* = 8.2 Hz, 2H), 7.23-7.13 (m, 3H), 6.84 (d, *J* = 9.1 Hz, 2H), 6.73 (d, *J* = 9.1 Hz, 2H), 5.75 (d, *J* = 3.6 Hz, 1H), 4.98 (ddd, *J* = 8.4, 3.2, 3.2 Hz, 1H), 4.11-4.03 (m, 2H), 3.73 (s, 3H), 2.41 (s, 3H); ^{13}C NMR (100 MHz, CDCl$_3$) ppm 156.7, 150.8, 145.0, 135.8, 134.3, 130.3, 129.8, 129.7, 128.9, 128.5, 128.1, 121.2, 113.9, 59.8, 55.3, 47.0, 33.0, 21.6; HRMS (ESI): Exact mass calcd for C$_{24}$H$_{24}$IN$_2$O$_4$S [M+H]$^+$ 563.0502, found 563.0506.

Absolute Configuration determination of products from (Z)-1,2-disubstituted alkene
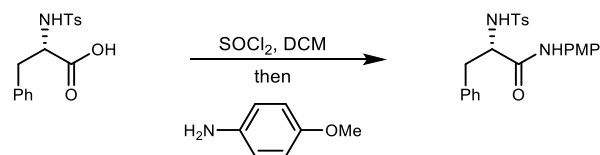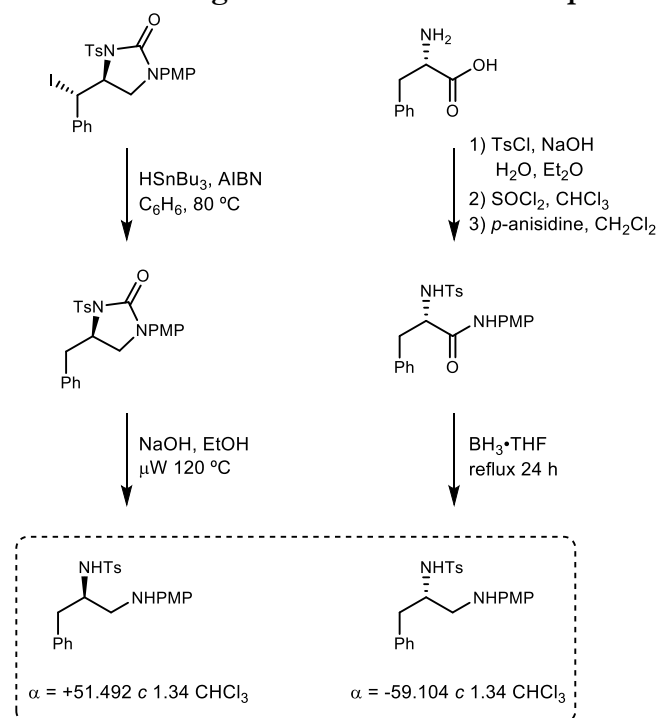
(S)-N-(4-Methoxyphenyl)-2-((4-methylphenyl)sulfonamido)-3-phenylpropanamide. To a flame-dried 50 mL round-bottomed flask charged with a stir bar was added the acid (790 mg, 2.47 mmol) and dichloromethane (8.2 mL), and then thionyl chloride (300 μL, 4.20 mmol) in dichloromethane (8.2 mL) was added dropwise. After stirring for 10 min the white suspension was heated to reflux for 2 h. The reaction mixture was cooled, concentrated, dissolved in dichloromethane (4 mL), and cooled to 0 °C. *p*-Anisidine (304 mg, 2.47 mmol) in dichloromethane (4 mL) was added dropwise and allowed to slowly warm to room temperature over 3 h. The heterogeneous mixture was diluted in dichloromethane, washed with 1 M aq HCl, water, and 1 M NaOH, and the organic layer was then dried and concentrated. The crude product was purified by precipitation from chloroform using hexanes to afford a white solid (465 mg, 44%). $[\alpha]_D^{20}$ -100. (*c* 1.15 CHCl$_3$); R$_f$ = 0.55 (50% EtOAc/hexanes) visualized with UV light; IR (film) 3279, 3027, 2921, 1663, 1514, 1318, 1241, 1159 cm^{-1}; ^{1}H NMR (400 MHz, CDCl$_3$) δ 7.78 (br s, 1H), 7.58 (d, *J* = 8.2 Hz, 2H), 7.24-7.20 (m, 7H), 6.97 (d, *J* = 7.2 Hz, 2H), 6.82 (d, *J* = 9.0 Hz, 2H), 4.96 (d, *J* =6.7 Hz, 1H), 3.97 (dd, *J* = 13.3, 6.6 Hz, 1H), 3.78 (s, 3H), 3.09 (dd, *J* = 13.9, 7.1 Hz, 1H), 2.94 (dd, *J* = 13.9, 6.4 Hz, 1H), 2.41 (s, 3H); ^{13}C NMR (100 MHz, CDCl$_3$) ppm 167.8, 156.8, 144.1, 135.4, 135.1, 129.9, 129.8, 129.2, 129.1, 127.4, 127.2, 122.0, 114.0, 58.2, 55.4, 38.3, 21.5; HRMS (ESI): Exact mass calcd for C$_{23}$H$_{25}$N$_2$O$_4$S [M+H]$^+$ 425.1535, found 425.1530.
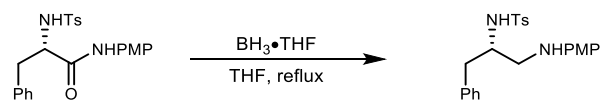
(S)-N-(1-((4-Methoxyphenyl)amino)-3-phenylpropan-2-yl)-4-methylbenzenesulfonamide. To a flame-dried 25 mL round-bottomed flask charged with a stir bar was added the amide (400 mg, 942 μmol) and THF (3.1 mL). The solution was cooled to 0 °C, at which point 1 M BH$_3$•THF (2.8 mL, 2.8 mmol) was added dropwise over 1 min and stirred for an additional 10 min. The reaction mixture was heated to reflux for 24 h, cooled to room

temperature, and quenched with 1 M aq NaOH. The layers were separated and the aqueous layer was extracted with ether, the organic layers were combined, dried and concentrated. The resulting residue was purified by automated flash column chromatography (SiO$_2$, 0-50% ethyl acetate in hexanes). $[\alpha]_D^{20}$ -59.1 (*c* 1.34 CHCl$_3$); R$_f$ = 0.3 (30% EtOAc/hexanes) visualized with UV light; IR (film) 3319, 2923, 1510, 1449, 1311, 1243, 1154 cm^{-1}; ^{1}H NMR (400 MHz, CDCl$_3$) δ 7.61 (d, *J* = 8.2 Hz, 2H), 7.21-7.18 (m, 3H), 7.15 (d, *J* = 8.1 Hz, 2H), 7.03-6.99 (m, 2H), 6.70 (d, *J* = 8.9 Hz, 2H), 6.37 (d, *J* = 8.8 Hz, 2H), 5.13 (d, *J* = 7.2 Hz, 1H), 3.74 (s, 3H), 3.67 (br s, 1H) 3.57 (dddd, *J* = 13.8, 6.9, 6.9, 4.5 Hz, 1H), 3.13 (dd, *J* = 13.0, 4.8 Hz, 1H), 3.00 (dd, *J* = 13.0, 7.1 Hz, 1H) 2.78 (d, *J* = 6.7 Hz, 2H), 2.39 (s, 3H); ^{13}C NMR (100 MHz, CDCl$_3$) ppm 152.1, 143.2, 141.5, 136.8, 136.6, 129.5, 129.1, 128.5, 126.9, 126.6, 114.7, 114.2, 55.6, 54.2, 48.0, 39.5, 21.4; HRMS (ESI): Exact mass calcd for C$_{23}$H$_{27}$N$_2$O$_3$S [M+H]$^+$ 411.1742, found 411.1747.
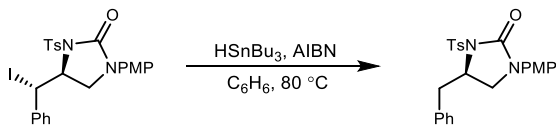
(*R*)-4-Benzyl-1-(4-methoxyphenyl)-3-tosylimidazolidin-2-one. To a flame dried 2-5 mL microwave vial charged with a stir bar was added the urea (40.0 mg, 71.1 μmol, 93% ee), benzene (0.5 mL), and tributyltin hydride (75 μL, 280 μmol). The reaction mixture was degassed (3 freeze-pump-thaw cycles) and backfilled with argon. The colorless suspension was heated to 80 °C for 5 min, and then treated with 3 additions of AIBN (2.0 mg, 12.1 μmol) separated by 45 min. The reaction mixture was then cooled to rt, concentrated to a colorless oil, and purified by flash column chromatography (10% powdered K$_2$CO$_3$ in SiO$_2$, 15-25% ethyl acetate in hexanes)[19] to afford the imidazolidinone as a colorless oil (30.8 mg, 99%). The product was determined to be 91% ee by chiral HPLC analysis (Chiralpak AD-H, 30% EtOH/hexanes, 1.0 mL/min, 30 °C, t_r(minor) = 13.5 min, t_r(major) = 18.6 min); $[\alpha]_D^{20}$ -45.6 (*c* 1.59 CHCl$_3$); R$_f$ = 0.35 (30% EtOAc/hexanes) visualized with UV light; IR (film) 3022, 2924, 1727, 1511, 1406, 1352, 1240 cm^{-1}; ^{1}H NMR (400 MHz, CDCl$_3$) δ 8.03 (d, *J* = 8.2 Hz, 2H), 7.33 (d, *J* = 8.2 Hz, 2H), 7.31 (d, *J* = 7.5 Hz, 2H), 7.27 (dd, *J* = 7.2, 6.8 Hz, 1H), 7.24 (dd, *J* = 7.4, 6.2 Hz, 2H), 7.19 (d, *J* = 9.0 Hz, 2H), 6.80 (d, *J* = 9.0 Hz, 2H), 4.65 (dddd, *J* = 9.4, 9.4, 2.9, 2.9 Hz, 1H), 3.77 (d, *J* = 9.2 Hz, 1H), 3.74 (s, 3H), 3.55 (dd, *J* = 13.3, 3.2 Hz, 1H), 3.47 (dd, *J* = 9.4, 2.7 Hz, 1H), 2.89 (dd, *J* = 13.3, 8.9 Hz, 1H), 2.43 (s, 3H); ^{13}C NMR (100 MHz, CDCl$_3$) ppm 156.5, 151.4, 144.7, 136.3, 135.4, 131.3, 129.5, 129.4, 128.8, 128.3, 127.2, 120.8, 114.0, 55.4, 54.3, 37.5, 40.7, 21.6; HRMS (ESI): Exact mass calcd for C$_{24}$H$_{25}$N$_2$O$_4$S [M+H]$^+$ 437.1535, found 437.1531.

Reaction of 123
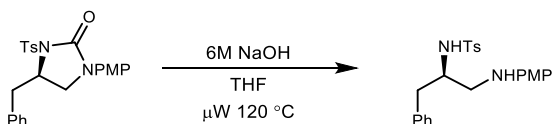
(*R*)-*N*-(1-((4-Methoxyphenyl)amino)-3-phenylpropan-2-yl)-4-methylbenzenesulfonamide. A 0.5-2 mL microwave vial flask charged with a stir bar was charged with the urea (30.0 mg, 68.7 μmol), ethanol (700 μL), and 6 M aq NaOH (50 μL), and then heated to 120 °C under microwave irradiation for 20 min. The reaction mixture was diluted with dichloromethane and washed with satd aq sodium bicarbonate. The aqueous layer was extracted with dichloromethane, the organic layers were combined, dried, and concentrated. The resulting residue was purified by flash column chromatography (SiO$_2$, 23-35% ethyl acetate in hexanes) to afford a white solid. Spectral data matched that of the title compound derived from enantiopure amino acid.

Configuration was determined by optical rotation $[\alpha]_D^{20}$ +51.4 (*c* 1.34 CHCl$_3$).

---

[19] Harrowven, D. C., Curran, D. P., Kostiuk, S. L., Wallis-Guy, I. L., Whiting, S., Stenning, K. J., Tang, B., Packard, E., Nanson, L. *Chemical communications (Cambridge, England),* 2010, *46* (34), 6335-6337.
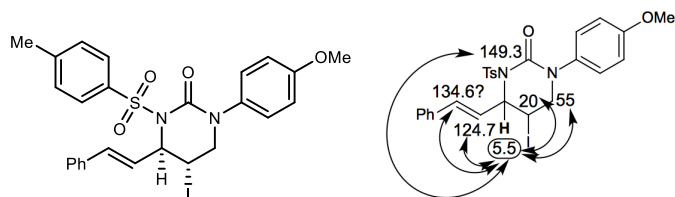
(4*R*,5*S*)-5-iodo-1-(4-methoxyphenyl)-4-((*E*)-styryl)-3-tosyltetrahydropyrimidin-2(1*H*)-one (124a). Prepared according to the general procedure using the amine (265 mg, 1.00 mmol) and a reaction time of 37 h. Purification by flash column chromatography (SiO$_2$, 20-35% ethyl acetate in hexanes) to afford the title compound as a light brown solid (403 mg, 68%). The product was determined to be 92% ee by chiral HPLC analysis (Chiralpak IB, 25% ^{i}PrOH/hexanes, 1.0 mL/min, 30 °C, t_r(major) = 9.3 min, t_r(minor) = 11.6 min); mp = 185-187 °C (dec); [α]$_D^{20}$ +29.3 (*c* 0.82 CHCl$_3$); R$_f$ = 0.3 (35% EtOAc/hexanes) visualized with UV light or I$_2$; IR (film) 3015, 2925, 1675, 1510, 1464, 1422, 1346, 1302, 1245, 1167 cm^{-1}; ^{1}H NMR (600 MHz, CDCl$_3$) δ 7.98 (d, *J* = 8.3 Hz, 2H), 7.40 (d, *J* = 7.1 Hz, 2H), 7.36 (dd, *J* = 7.0, 7.0 Hz, 2H), 7.02 (d, *J* = 7.0 Hz, 1H), 7.33 (d, *J* = 8.1 Hz, 2H), 7.13 (d, *J* = 8.9 Hz, 2H), 6.87 (d, *J* = 14.9 Hz, 1H), 6.84 (d, *J* = 9.1 Hz, 2H), 6.28 (dd, *J* = 15.7, 5.2 Hz, 1H), 5.55 (dd, *J* = 3.6, 1.3 Hz, 1H), 4.65 (dd, *J* = 5.2, 3.1 Hz, 1H), 4.19 (dd, *J* = 14.1, 3.2 Hz, 1H), 3.75 (s, 3H), 3.56 (ddd, *J* = 14.2, 2.1, 2.1 Hz, 1H), 2.39 (s, 3H); ^{13}C NMR (150 MHz, CDCl$_3$) ppm 158.7, 149.3, 144.2, 136.5, 135.3, 134.6, 134.1, 129.7, 128.9, 128.8, 128.7, 128.1, 126.8, 124.7, 114.6, 65.5, 55.5, 55.3, 21.6, 19.6; HRMS (ESI): Exact mass calcd for C$_{26}$H$_{25}$IN$_2$NaO$_4$S [M+Na]$^+$ 611.0478, found 611.0485.
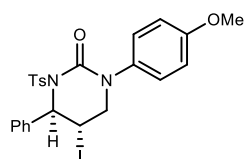
(4*R*,5*S*)-5-Iodo-1-(4-methoxyphenyl)-4-phenyl-3-tosyltetrahydropyrimidin-2(1*H*)-one (124b). Prepared according to the general procedure using the amine (23.9 mg, 100 μmol) for 84 h, and purified by flash column chromatography (SiO$_2$, 20-35% ethyl acetate in hexanes) to afford a white solid (SiO$_2$, 20-35% ethyl acetate in hexanes) to afford the title compound as a light brown solid (34.1 mg, 60%). The product was determined to be 94% ee by chiral HPLC analysis (Chiralpak IB, 25% EtOH/hexanes, 1.0 mL/min, 30 °C, t_r(minor) = 8.0 min, t_r(major) = 8.9 min); mp = 195-197 °C; [α]$_D^{20}$ +14.9 (*c* 1.0 CHCl$_3$); R$_f$ = 0.3 (35% EtOAc/hexanes) visualized with UV light or I$_2$; IR (film) 3019, 2923, 1678, 1604, 1509, 1465, 1350, 1244, 1168 cm^{-1}; ^{1}H NMR (600 MHz, CDCl$_3$) δ 7.86 (d, *J* = 8.3 Hz, 2H), 7.43-7.39 (m, 5H), 7.21 (d, *J* = 8.2 Hz, 2H), 7.15 (d, *J* = 8.8 Hz, 2H), 6.84 (d, *J* = 8.8 Hz, 2H), 5.99 (s, 1H), 4.71 (dd, *J* = 5.5, 2.7 Hz, 1H), 3.79 (dd, *J* = 14.2, 3.0 Hz, 1H), 3.75 (s, 3H), 3.45 (ddd, *J* = 14.2, 2.0, 2.0 Hz, 1H), 2.39 (s, 3H); ^{13}C NMR (150 MHz, CDCl$_3$) ppm 158.6, 149.6, 144.2, 138.7, 136.3, 134.2, 129.6, 129.3, 128.8, 128.7, 128.0, 126.0, 114.6, 67.7, 55.4, 54.4, 21.6, 21.3; HRMS (ESI): Exact mass calcd for C$_{24}$H$_{24}$IN$_2$O$_4$S [M+H]$^+$ 563.0502, found 563.0524.
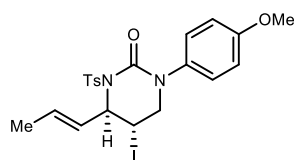
(4*R*,5*S*)-5-Iodo-1-(4-methoxyphenyl)-4-((*E*)-prop-1-en-1-yl)-3-tosyltetrahydropyrimidin-2(1*H*)-one (124c). Prepared according to the general procedure using the amine (17.7 mg, 100 μmol) for 36 h, and purified by flash column chromatography (SiO$_2$, 20-30% ethyl acetate in hexanes) to afford a white solid (21.2 mg, 40%). The product was determined to be 94% ee by chiral HPLC analysis (Chiralpak IB, 25% EtOH/hexanes, 1.0 mL/min, 30 °C, t_r(minor) = 9.3 min, t_r(major) = 9.9 min); mp = 188-190 °C (dec); [α]$_D^{20}$ +41.8 (*c* 0.89 CHCl$_3$); R$_f$ = 0.2 (35% EtOAc/hexanes) visualized by UV or I$_2$; IR (film) 3015, 1674, 1511, 1464, 1346, 1245, 1166 cm^{-1}; ^{1}H NMR (600 MHz, CDCl$_3$) δ 7.96 (d *J* = 8.3 Hz, 2H), 7.24 (d, *J* = 8.1 Hz, 2H), 7.11 (d, *J* = 8.9 Hz, 2H), 6.83 (d, *J* = 8.8 Hz, 2H), 6.06 (dddd, *J* = 13.3, 6.4, 6.4, 1.4 Hz, 1H), 5.62 (ddd, *J* = 15.3, 5.5, 1.6 Hz, 1H), 5.31 (br s, 1H), 4.52 (dd, *J* = 5.2, 3.1 Hz, 1H), 4.15 (dd, *J* = 14.0, 3.1 Hz, 1H), 3.75 (s, 3H), 3.52 (ddd, *J* = 14.1,

1.6, 1.6 Hz, 1H) 2.39 (s, 3H), 1.79 (d, *J* = 6.4 Hz, 3H); ^{13}C NMR (150 MHz, CDCl$_3$) ppm 158.6, 149.2, 144.1, 136.6, 134.2, 131.5, 129.6, 128.8, 128.1, 127.2, 114.6, 65.4, 55.4, 55.1, 21.6, 20.3, 17.9; HRMS (ESI): Exact mass calcd for C$_{21}$H$_{24}$IN$_2$O$_4$S [M+H]$^+$ 527.0502, found 527.0487.
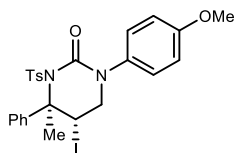
(4*R*,5*S*)-5-Iodo-1-(4-methoxyphenyl)-4-phenyl-3-tosyltetrahydropyrimidin-2(1*H*)-one (124d). Prepared according to the general procedure using the amine (25.3 mg, 100 μmol), and purified by flash column chromatography (SiO$_2$, 20% ethyl acetate in hexanes) to afford a white foam (17.4 mg, 31%). The product was determined to be 86% ee by chiral HPLC analysis (Chiralpak IA, 25% EtOH/hexanes, 1.0 mL/min, 30 °C, *t$_r$* (major) = 10.5 min, *t$_r$* (minor) = 15.1 min); [α]$_D^{20}$ +27.3 (*c* 0.89 CHCl$_3$); R$_f$ = 0.2 (30% EtOAc/hexanes) visualized with UV light or I$_2$; IR (film) 2925, 1679, 1604, 1508, 1461, 1411, 1348, 1299, 1248 cm^{-1}; ^{1}H NMR (400 MHz, CDCl$_3$) δ 7.90 (d, *J* = 9.3 Hz, 2H), 7.62 (d, *J* = 7.4 Hz, 2H), 7.47 (dd, *J* = 7.8, 7.8 Hz, 2H), 7.39 (dd, *J* = 7.2, 7.2 Hz, 1H), 7.29 (d, *J* = 9.6 Hz, 2H), 7.20 (d, *J* = 8.9 Hz, 2H), 6.85 (d, *J* = 8.9 Hz, 2H), 4.63 (dd, *J* = 5.2, 2.7 Hz, 1H), 3.77 (dd, *J* = 13.6, 2.8 Hz, 1H), 3.76 (s, 3H), 3.60 (dd, *J* = 13.6, 5.2 Hz, 1H), 2.48 (s, 3H), 2.39 (s, 3H); ^{13}C NMR (100 MHz, CDCl$_3$) ppm 158.4, 151.4, 143.6, 142.1, 138.6, 134.7, 129.0, 128.9, 128.8, 128.1, 127.7, 125.8, 114.5, 70.3, 55.4, 54.7, 37.8, 31.8, 21.5; HRMS (ESI): Exact mass calcd for C$_{25}$H$_{25}$IN$_2$NaO$_4$S [M+Na]$^+$ 599.0478, found 599.0472.
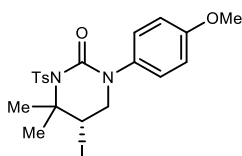
(*S*)-5-Iodo-1-(4-methoxyphenyl)-4,4-dimethyl-3-tosyltetrahydropyrimidin-2(1*H*)-one (124e). Prepared according to the general procedure using the amine (32.2 mg, 168 μmol), and purified by flash column chromatography (SiO$_2$, 20% ethyl acetate in dichloromethane) to afford a white solid (64.7 mg, 75%). The product was determined to be 63% ee by chiral HPLC analysis (Chiralpak IA, 25% EtOH/hexanes, 1.0 mL/min, 30 °C, *t$_r$* (major) = 12.9 min, *t$_r$* (minor) = 18.7 min); mp = 143-147 °C; [α]$_D^{20}$ +33.7 (*c* 1.08 CHCl$_3$); R$_f$ = 0.15 (30% EtOAc/hexanes) visualized with UV light or I$_2$; IR (film) 2919, 1724, 1512, 1409, 1349, 1246 cm^{-1}; ^{1}H NMR (400 MHz, CDCl$_3$) δ 7.93 (d, *J* = 8.3 Hz, 2H), 7.31 (d, *J* = 7.8 Hz, 2H), 7.29 (d, *J* = 9.0 Hz, 2H), 6.85 (d, *J* = 9.0 Hz, 2H), 4.55 (dd, *J* = 8.4, 1.3 Hz, 1H), 4.07 (dd, *J* = 10.3, 8.5 Hz, 1H), 3.90 (dd, *J* = 10.3, 1.4 Hz, 1H), 3.76 (s, 3H), 2.41 (s, 3H), 2.14 (s, 3H), 1.85 (s, 3H); ^{13}C NMR (100 MHz, CDCl$_3$) ppm 156.9, 152.4, 144.9, 135.7, 130.5, 129.6, 128.2, 121.3, 114.3, 63.0, 55.4, 51.3, 51.1, 35.0, 30.7, 21.6; HRMS (ESI): Exact mass calcd for C$_{20}$H$_{23}$IN$_2$NaO$_4$S [M+Na]$^+$ 537.0321, found 537.0313.

Product Derivatization
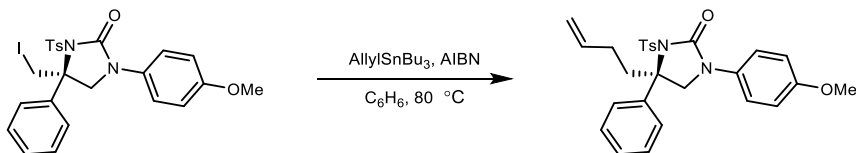
(*R*)-4-(But-3-en-1-yl)-1-(4-methoxyphenyl)-4-phenyl-3-tosylimidazolidin-2-one (126). To a flame dried 2-5 mL microwave vial charged with a stir bar was added the urea (40.0 mg, 71.1 μmol, 92% ee), benzene (0.5 mL), and allyltributylstannane (86 μL, 280 μmol). The reaction mixture was degassed (3 freeze-pump-thaw cycles) and backfilled with argon. The colorless suspension was heated to 80 °C for 5 min followed by 4 additions of AIBN (2.0 mg, 12.1 μmol) separated by 45 min. The reaction mixture was concentrated to a colorless oil and purified by flash column chromatography (10% powdered K$_2$CO$_3$ in SiO$_2$, 15-25% ethyl acetate in hexanes)[20] to afford a colorless oil

---

[20] Harrowven, D. C. *et al. Chem. Comm.* 2010, 46, 6335–6337

(19.9 mg, 60%). The product was determined to be 91% ee by chiral HPLC analysis (Chiralpak IB, 25% EtOH/hexanes, 1.0 mL/min, 30 °C, t_r(major) = 6.1 min, t_r(minor) = 7.7 min); $[\alpha]_D^{20}$ +3.8 (*c* 0.99 CHCl$_3$); R$_f$ = 0.4 (30% EtOAc/hexanes) visualized with UV light; IR (film) 3016, 2924, 2851, 1724, 1511, 1407, 1359, 1250, 1172 cm^{-1}; ^{1}H NMR (400 MHz, CDCl$_3$) δ 7.47 (d, *J* = 8.4 Hz, 2H), 7.46 -7.44 (m, 2H), 7.40 (d, *J* = 9.0 Hz, 2H), 7.37-7.33 (m, 3H), 7.12 (d, *J* = 8.1 Hz, 2H), 6.87 (d, *J* = 9.0 Hz, 2H), 5.95 (dddd, *J* = 16.6, 10.1, 6.2, 6.2 Hz, 1H), 5.16 (d, *J* = 16.7 Hz, 1H), 5.07 (d, *J* = 10.1 Hz, 1H), 3.99 (d, *J* = 9.4 Hz, 1H), 3.89 (d, *J* = 9.5 Hz, 1H), 3.77 (s, 3H), 3.05 (ddd, *J* = 12.1, 12.1, 3.5 Hz, 1H), 2.55-2.45 (m, 1H), 2.42 (dd, *J* = 12.8, 3.1 Hz, 1H), 2.36 (s, 3H), 2.27-2.17 (m, 1H); ^{13}C NMR (100 MHz, CDCl$_3$) ppm 156.6, 152.0, 144.2, 143.0, 136.9, 136.3, 131.1, 129.0, 128.7, 128.6, 128.2, 126.3, 120.8, 115.7, 114.2, 65.1, 58.3, 55.4, 36.6, 27.9, 21.5; HRMS (ESI): Exact mass calcd for C$_{27}$H$_{29}$N$_2$O$_4$S [M+H]$^+$ 477.1848, found 477.1846.
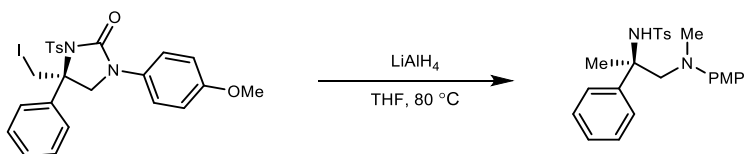
N-(1-((4-Methoxyphenyl)(methyl)amino)-2-phenylpropan-2-yl)-4-methylbenzenesulfonamide (128). To a flame dried 2-5 mL microwave vial charged with a stir bar was added the urea (56.0 mg, 100 μmol), THF (1.6 mL), and LiAlH$_4$ (11.3 mg, 300 μmol). The vial was capped and placed in an oil bath at 80 °C[21] and stirred for 4 hours. The reaction slurry was cooled to room temperature, water was added dropwise then 2 M aq. NaOH (0.5 mL) and ether was added and stirred vigorously for 10 min. The emulsion was filtered through a pad of Celite and the aqueous layer was extracted with ether. The organic layers were combined, dried, and concentrated to afford a yellow oil which was purified by flash column chromatography (SiO$_2$, 10 to 20% EtOAc/hexanes) to afford a white foam (42.4 mg, 60%) IR (film) 3274, 2924, 2357, 1512, 1318, 1247, 1155 cm^{-1}; ^{1}H NMR (600 MHz, CDCl$_3$) δ 7.63 (d, *J* = 8.2 Hz, 2H), 7.41 (d, *J* = 7.6 Hz, 2H), 7.28 (dd, *J* = 7.1, 7.1 Hz, 2H), 7.25 (d, *J* = 7.1 Hz, 1H), 7.23 (d, *J* = 7.1 Hz, 2H), 6.81 (d, *J* = 9.1 Hz, 2H), 6.75 (d, *J* = 9.1 Hz, 2H), 5.62 (br s, 1H), 3.78 (s, 3H), 3.46 (d, *J* = 14.4 Hz, 1H), 3.38 (d, *J* = 14.4 Hz, 1H), 2.42 (s, 6H), 1.73 (s, 3H); ^{13}C NMR (150 MHz, CDCl$_3$) ppm 152.8, 145.6, 144.0, 142.7, 140.5, 129.3, 128.2, 127.0, 126.8, 126.0, 115.6, 114.5, 68.6, 61.9, 55.7, 41.2, 24.1, 21.5; HRMS (ESI): Exact mass calcd for C$_{21}$H$_{28}$N$_2$NaO$_3$S [M+Na]$^+$ 447.1718, found 447.1724.
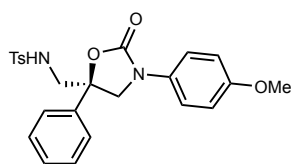
((R)-N-((3-(4-methoxyphenyl)-2-oxo-5-phenyloxazolidin-5-yl)methyl)-4-methylbenzenesulfonamide (129). To a 0.5-2 mL microwave vial charged with a stir vane was added urea (150 mg, 266 μmol, 92% ee), potassium carbonate (73.7 mg, 533 μmol), and methanol (1.3 mL). The heterogeneous suspension was heated to 130 °C in the microwave for 25 min. The reaction mixture was poured into satd aq sodium bicarbonate and extracted with dichloromethane. The organic layers were combined, dried, and concentrated to an off-white solid that was purified by flash column chromatography (SiO$_2$, 20-40% EtOAc/hexanes) to afford a white powder (80.4 mg, 66%). The product was determined to be 85% ee by chiral HPLC analysis (Chiralpak IB, 25% EtOH/hexanes, 1.0 mL/min, 30 °C, t_r(major) = 6.9 min, t_r(minor) = 7.5 min); $[\alpha]_D^{20}$ +13.4 (*c* 1.03 CHCl$_3$); R$_f$ = 0.25 (30% EtOAc/hexanes) visualized with UV light; IR (film) 3253, 2924, 1743, 1512, 1444, 1328, 1246, 1161 cm^{-1}; ^{1}H NMR (400 MHz, CDCl$_3$) δ 7.61 (d, *J* = 8.2 Hz, 2H), 7.34-7.22 (m, 7H), 7.15 (d, *J* = 8.0 Hz, 2H), 6.78 (d, *J* = 9.1 H, 2H), 5.51 (dd, *J* = 8.8, 5.6 Hz, 1H), 4.54 (d, *J* = 8.8 Hz, 1H), 3.96 (d, *J* = 8.8 Hz, 1H), 3.70 (s, 3H), 3.36 (dd, *J* = 13.9, 8.9 Hz, 1H), 3.18 (dd, *J* = 13.8, 5.1 Hz, 1H), 2.30 (s, 3H); ^{13}C NMR (100

---

[21] The reaction setup was placed behind a blast shield in case of pressure buildup in the capped reaction vial. The solvent level was maintained above the oil bath level.

MHz, CDCl$_3$) ppm 156.6, 153.9, 143.6, 140.1, 136.7, 130.7, 129.8, 128.9, 128.7, 126.8, 124.4, 121.0, 114.2, 80.4, 55.4, 54.3, 51.1, 21.5; HRMS (ESI): Exact mass calcd for C$_{24}$H$_{25}$N$_2$O$_5$S [M+H]$^+$ 453.1484, found 453.1490.
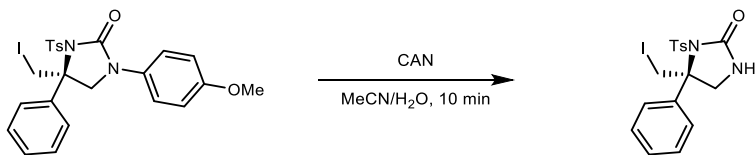
5-(Iodomethyl)-5-phenyl-1-tosylimidazolidin-2-one (131). To a 2-5 mL microwave vial charged with a stir bar was added urea (52.1 mg, 92.6 μmol, 92% ee) and acetonitrile (2.31 mL). Ammonium cerium(IV) nitrate (152 mg, 278 μmol) in water (760 μL) was added dropwise and allowed to stir for 10 min. The reaction mixture was poured into water and extracted with 10:1 ether/dichloromethane, the organic layers were combined, dried, and concentrated to afford a yellow oil which was purified by flash column chromatography (SiO$_2$, 30-45% EtOAc/hexanes) to afford a white solid (35.3 mg, 82%). The product was determined to be 90% ee by chiral HPLC analysis (Chiralpak IB, 25% ^{i}PrOH/hexanes, 1.0 mL/min, 30 °C, t_r(major) = 11.8 min, t_r(minor) = 17.0 min); mp = 178-180 °C; [α]$_D^{20}$ +65.4 (c 1.3 CHCl$_3$); R$_f$ = 0.3 (50% EtOAc/hexanes) visualized with UV light or I$_2$; IR (film) 3310, 3060, 2918, 2357, 1735, 1439, 1359 1279 cm^{-1}; ^{1}H NMR (600 MHz, CDCl$_3$) δ 7.32 (d, J = 8.5 Hz, 2H), 7.35 (dd, J = 7.3, 7.3 Hz, 1H), 7.30 (dd, 7.8, 7.8 Hz, 2H), 7.27-7.25 (m, 2H), 7.03 (d, J = 8.1 Hz, 2H), 5.78 (br s, 1H), 4.39 (d, J = 10.4 Hz, 1H), 4.36 (d, J = 10.5 Hz, 1H), 3.82 (d, J = 10.7 Hz, 1H), 3.73 (d, J = 9.6 Hz, 1H), 2.33 (s, 3H); ^{13}C NMR (150 MHz, CDCl$_3$) ppm 155.6, 144.3, 138.8, 135.9, 128.8, 128.7, 128.6, 127.0, 67.1, 55.6, 21.5, 14.4; HRMS (ESI): Exact mass calcd for C$_{17}$H$_{17}$IN$_2$NaO$_3$S [M+Na]$^+$ 478.9902, found 478.9905.
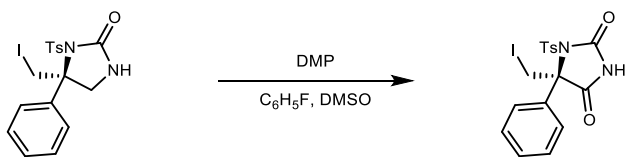
(*R*)-5-(Iodomethyl)-5-phenyl-1-tosylimidazolidine-2,4-dione (132). To a 0.5-2 mL microwave vial charged with a stir bar was added the urea (40.0 mg, 87.6 μmol), DMP (Oakwood Chemicals, 85.5 mg, 201 μmol), fluorobenzene (600 μL), and DMSO was added until all solid was dissolved (18 drops). The reaction mixture was heated to 75 °C for 4 h, and then cooled, quenched with satd aq Na$_2$S$_2$O$_3$, treated with 1 M NaOH, and extracted with diethyl ether. The aqueous layer was acidified to pH~1 and extracted with dichloromethane. The organic layers were combined, washed with satd aq NaHCO$_3$, dried, and concentrated. The crude solid was purified by flash column chromatography (SiO$_2$, 40% ethyl acetate in hexanes) to afford a white solid (39.1 mg, 75%); [α]$_D^{20}$ +2.47 (c 0.85 CHCl$_3$); R$_f$ = 0.5 (50% EtOAc/hexanes) visualized with UV light or I$_2$; IR (film) 3255, 3060, 2924, 1791, 1743, 1363, 1259, 1175 cm^{-1}; ^{1}H NMR (400 MHz, CDCl$_3$) δ 7.53 (d, J = 8.3 Hz, 2H), 7.41-7.32 (m, 5H), 7.18 (d, J = 8.2 Hz, 2H), 4.61 (d, J = 10.4 Hz, 1H), 4.26 (d, J = 10.4 Hz, 1H), 2.40 (s, 3H); ^{13}C NMR (100 MHz, CDCl$_3$) ppm 170.3, 151.5, 145.7, 134.8, 133.0, 129.7, 129.2, 129.1, 129.0, 126.7, 75.5, 21.6, 6.2; HRMS (ESI): Exact mass calcd for C$_{17}$H$_{16}$IN$_2$O$_4$S [M+H]$^+$ 470.9876, found 470.9894.
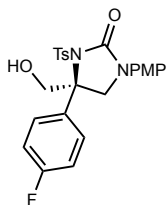
(R)-4-(4-Fluorophenyl)-4-(hydroxymethyl)-1-(4-methoxyphenyl)-3-tosylimidazolidin-2-one (144). To a flame dried-flask was added $NaCNBH_3$ (86.5 mg, 1.37 mmol), the urea (380.0 mg, 665 µmol), and chlorobenezene (3.3 mL), and the headspace was replaced with an oxygen atmosphere by 3 cycles of house vacuum (~60 torr) and refilling with pure oxygen. Oxygen was bubbled through the solution for 10 min, and then tributyltin chloride (18 µL, 6.6 µmol) and 2,2'-azobis(2-methylpropionitrile) (131 mg, 798 µmol) was added. While continuously bubbling oxygen, the mixture was heated to 80 ºC for 2 h. Additional chlorobenze (0.2 mL), $NaCNBH_3$ (10 mg), and AIBN (10 mg) was added and stirred at 80 ºC for 1 h. The reaction was quenched by the addition of methanol (0.5 mL), stirred for 10 min, diluted with dichloromethane, and filtered through a pad of 15% powdered K_2CO_3 in SiO_2 and washed with 50% ethyl acetate in hexanes to afford the crude product as a white foam. The resulting residue was purified by flash column chromatography (SiO_2, 25-40% EtOAc/hexanes) to afford a white foam (172 mg, 55%). The product was determined to be 89% ee by chiral HPLC analysis (Chiralpak IB, 25% EtOH/hexanes, 1.0 mL/min, 30 ºC, t_r (major) = 7.9 min, t_r (minor) = 8.9 min); $[\alpha]_D^{20}$ -8.0 (*c* 0.60 $CHCl_3$); R_f = 0.1 (35% EtOAc/hexanes) visualized with UV light or I_2; IR (film) 3492, 2924, 1720, 1602, 1512, 1246, 1169 cm^{-1}; ^{1}H NMR (400 MHz, $CDCl_3$) δ 7.61 (d, *J* = 8.3 Hz, 2H), 7.38-7.35 (m, 4H), 7.18 (d, *J* = 8.1 Hz, 2H), 7.03 (dd, *J* = 8.6, 8.6 Hz, 2H), 6.84 (d, *J* = 9.1 Hz, 2H) 4.81 (d, , *J* = 11.5 Hz, 1H), 4.35 (d, *J* = 11.5 Hz, 1H), 4.25 (d, *J* = 9.1 Hz, 1H), 3.77 (d, *J* = 9.2 Hz, 1H), 3.75 (s, 3H), 2.71 (br s, 1H), 2.38 (s, 3H); ^{13}C NMR (100 MHz, $CDCl_3$) ppm 162.3 (d, $^1J_{CF}$ = 248.6 Hz), 156.6, 152.0, 144.7, 136.6, 136.5 (d, $^4J_{CF}$ = 3.3 Hz), 131.0, 129.0, 128.7, 127.8 (d, $^3J_{CF}$ = 8.2 Hz), 121.0, 115.7 (d, $^2J_{CF}$ = 21.5 Hz), 114.2, 66.0, 65.1, 56.2, 55.4, 21.5; ^{19}F NMR (376 MHz, $CDCl_3$) ppm -112.8 ; HRMS (ESI): Exact mass calcd for $C_{24}H_{24}FN_2O_5S$ [M+H]$^+$ 471.1390, found 471.1392.
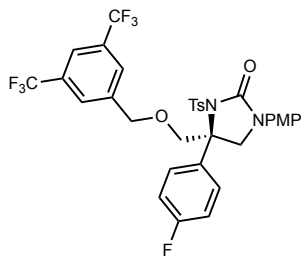
(R)-4-(((3,5-bis(trifluoromethyl)benzyl)oxy)methyl)-4-(4-fluorophenyl)-1-(4-methoxyphenyl)-3-tosylimidazolidin-2-one (150). To a flame-dried 0.5-2 mL microwave vial was added silver trifluoromethanesulfonate (147 mg, 574 µmol), cyclohexane (370 µL), and 3,5-bis(trifluoromethyl)benzyl bromide (122 mg, 382 µmol). To the solution was added the alcohol (90.0 mg, 191 µmol) in dichloromethane (300 µL) dropwise and stirred for 3 h in the dark. The reaction was quenched by filtration of the heterogeneous mixture through a plug of SiO_2 and flushed with 50% EtOAc/hexanes. The crude mixture was purified by flash column chromatography (SiO_2, 0-50% ethyl acetate in hexanes) to afford a white solid (70.4 mg, 53%); mp = 154-157 ºC $[\alpha]_D^{20}$ +2.2 (*c* 0.64 $CHCl_3$); R_f = 0.35 (30% EtOAc/hexanes) visualized with UV light; IR (film) 2927, 1727, 1605, 1512, 1362, 1279, 1170, 1028 cm^{-1}; ^{1}H NMR (400 MHz, $CDCl_3$) δ 7.80 (s, 1H), 7.72 (s, 2H), 7.60 (d, *J* = 8.2 Hz, 2H), 7.43-7.39 (m, 2H), 7.35 (d, *J* = 9.1 Hz, 2H), 7.11 (d, *J* = 8.2 Hz, 2H), 7.08 (dd, *J* = 8.5, 8.5 Hz, 2H), 6.85 (d, *J* = 9.1 Hz, 2H), 4.85 (d, *J* = 12.5 Hz, 1H), 4.80 (d, *J* = 12.6 Hz, 1H), 4.62 (d, *J* = 9.3 Hz, 1H), 4.49 (d, *J* = 9.3 Hz, 1H), 4.20 (d, *J* = 9.3 Hz, 1H), 3.90 (d, *J* = 9.3 Hz, 1H), 3.76 (s, 3H), 2.31 (s, 3H); ^{13}C NMR (100 MHz, $CDCl_3$) ppm 162.4 (d, $^1J_{CF}$ = 248.8 Hz), 156.6, 151.8, 144.5, 139.9, 136.5 (d, $^4J_{CF}$ = 3.4 Hz), 136.2, 131.7 (q, $^2J_{CF}$ = 33.4 Hz), 131.0, 128.9, 128.7, 127.9 (d, $^3J_{CF}$ = 9.5 Hz), 127.1, 122.9 (q, $^1J_{CF}$ = 265.0 Hz), 121.8, 120.8, 115.7, (d, $^2J_{CF}$ = 21.6 Hz), 114.2, 73.2, 72.0, 64.4, 56.9, 55.4, 21.4; ^{19}F NMR (376 MHz, $CDCl_3$) ppm –62.8 (s, 6F), -112.7 (s, 1F) HRMS (ESI): Exact mass calcd for $C_{33}H_{28}F_7N_2O_5S$ [M+H]$^+$ 697.1602, found 697.1600
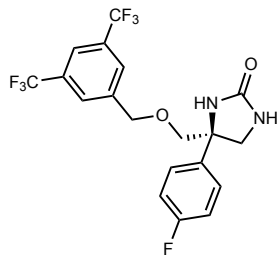
(*R*)-4-(((3,5-bis(Trifluoromethyl)benzyl)oxy)methyl)-4-(4-fluorophenyl)imidazolidin-2-one (151). To a 2-5 mL microwave vial was added the urea xx (56.0 mg, 80.0 µmol) and acetonitrile (2.6 mL). Ammonium cerium(IV) nitrate (176 mg, 321 µmol) in water (610 µL) was added dropwise and allowed to stir for 10 min. The reaction mixture was diluted with water and extracted with ethyl acetate. The organic layers were dried and concentrated to afford an orange solid. Quinone byproduct was removed by a silica plug, first eluting the quinone with 20% EtOAc/hexanes then eluting the product with 50% EtOAc/hexanes to afford an off white solid. The atmosphere of the 25 mL round bottomed flask with the off white solid was replaced with nitrogen by 4 cycles of high vacuum and filling with dry nitrogen. 0.1 Molar samarium(II) diiodide in THF (3 mL) was added in one portion and stirred for 3 min. Triethylamine (100 µL, 1.30 mmol) and water (20 µL, 1.10 mmol) were added and the mixture turned from dark blue to white immediately. The white suspension was stirred with 10% aqueous rochelles salt and sodium carbonate for 5 min and extracted with 5:1 diethyl ether and dichloromethane. The organic layers were combined, dried with magnesium sulfate, and concentrated. The resulting brown oil was purified by a silia plug eluting byproducts with 50% EtOAc/hexanes and the desired product with 10% MeOH/DCM to afford an off white foam (25.0 mg, 71%) $[\alpha]_D^{20}$ -49.3 (*c* 1.10 CHCl$_3$); R$_f$ = 0.4 (10% MeOH/DCM) visualized with UV light; IR (film) 3228, 2872, 1707, 1509, 1361, 1280, 1133 cm^{-1}; ^{1}H NMR (600 MHz, CDCl$_3$) δ 7.76 (s, 1H), 7.59 (s, 2H), 7.30 (dd, $^3J_{HH}$ = 8.8 Hz, $^4J_{HF}$ = 5.1 Hz, 2H), 7.05 (dd, $^3J_{HH}$ = 8.5 Hz, $^3J_{HF}$ = 8.5 Hz, 2H), 6.29 (s, 1H), 5.32 (s, 1H), 4.63 (d, *J* = 13.1 Hz, 1H), 4.53 (d, *J* = 13.1 Hz, 1H), 3.79 (d, *J* = 9.2 Hz, 1H), 3.77 (d, *J* = 9.1 Hz, 1H), 3.68 (d, *J* = 8.9 Hz, 1H), 3.51 (d, *J* = 8.8 Hz, 1H); ^{13}C NMR (150 MHz, CDCl$_3$) ppm 162.9, 162.1 (d, $^1J_{CF}$ = 247.3 Hz), 140.2, 138.1 (d, $^4J_{CF}$ = 3.4 Hz), 131.7 (q, $^2J_{CF}$ = 33.3 Hz), 127.0, 126.9 (d, $^3J_{CF}$ = 8.0 Hz), 123.1 (q, $^1J_{CF}$ = 272.3 Hz), 121.6, 115.5 (d, $^2J_{CF}$ = 22.1 Hz), 76.3, 71.9, 62.9, 50.6; HRMS (ESI): Exact mass calcd for C$_{19}$H$_{16}$F$_7$N$_2$O$_2$ [M+H]$^+$ 437.1095, found 437.1092

NMR Studies on CO$_2$ Capture by Amine Substrate in the Absence and Presence of Catalyst 7c

To a J. Young NMR tube was added *N*-benzyl-3-phenylbut-3-en-1-amine 7**8** (R = Ph) (11.8 mg, 50.0 µmol) and anhydrous toluene-d_8 (1.5 mL). The sample was loaded into a precooled (-20 °C) NMR bore (Bruker DRX-500, 500 MHz). After 20 minutes the first ^{1}H NMR spectrum was collected (**1a**, Figure 1). This same NMR tube was purged with CO$_2$ gas for 15 seconds and cooled again to -20 °C. Both ^{1}H NMR (**1b**, Figure 1) and ^{13}C NMR (**1b**, Figure 2) spectra were collected. To this sample was added ^{7}MeOStilbPBAM•HNTf$_2$ (47.2 mg, 50.0 µmol) and the tube was purged with CO$_2$ and again cooled to -20 °C. A considerable amount of white precipitate was noted, despite mixing, which was allowed to settle prior to recording ^{1}H NMR (**1c**, Figure 1). The low solubility of a stoichiometric amount of ^{7}MeOStilbPBAM•HNTf$_2$ at this concentration (necessary for ^{13}C collection in the prior experiments) should be considered when interpreting **1c**. No ^{13}C data was collected for **1c** due to the severe broadening.

Figure 1. ^{1}H NMR (500 MHz, -20 °C, tol-d_8) studies of amine (expt 1a), amine/CO_2 (expt 1b), and amine/CO_2/catalyst (expt 1c).
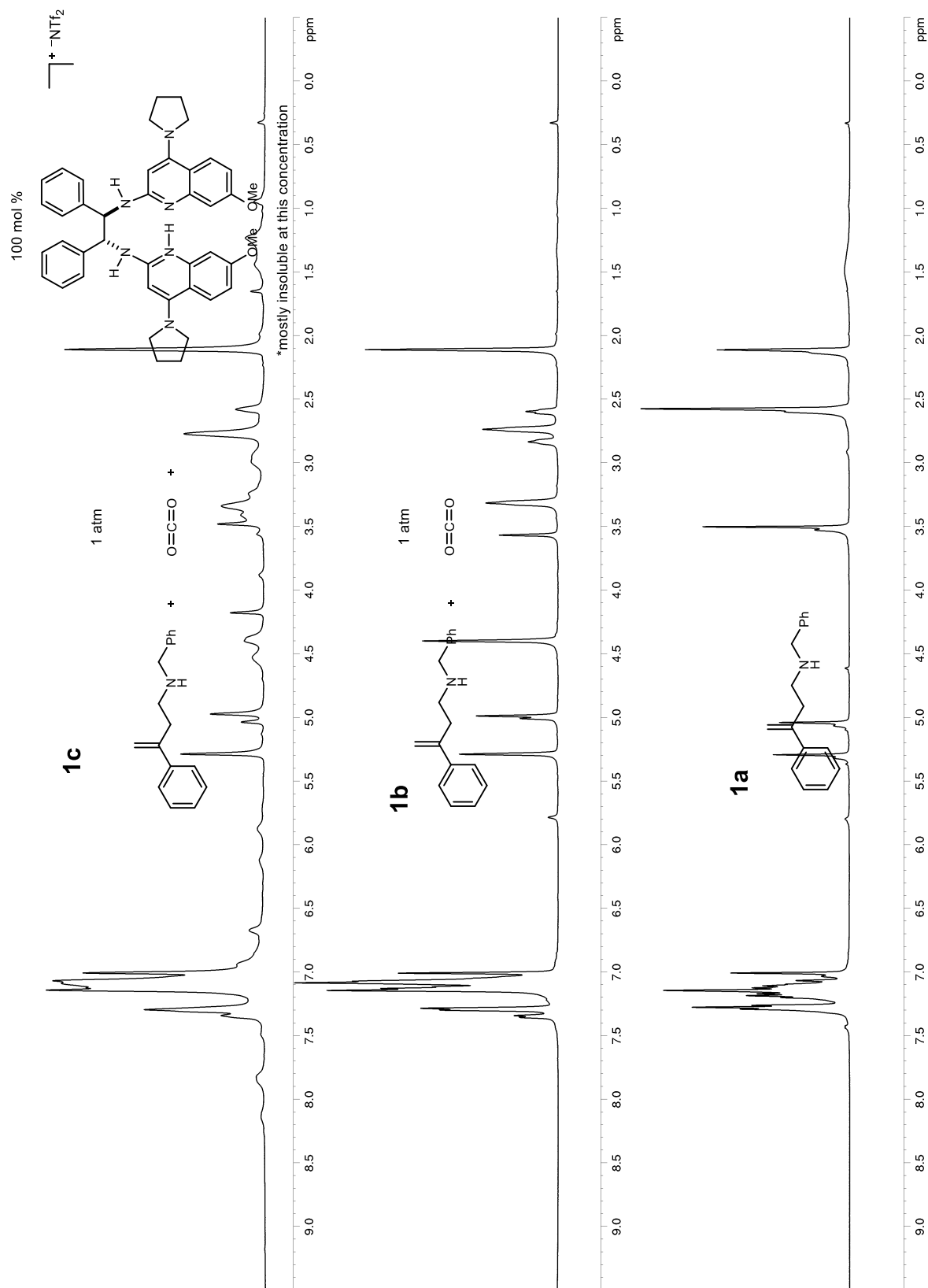
Figure 2. ^{13}C NMR (125 MHz, -20 °C, tol-d_8) of amine (expt 1a), amine/CO_2 (expt 1b).
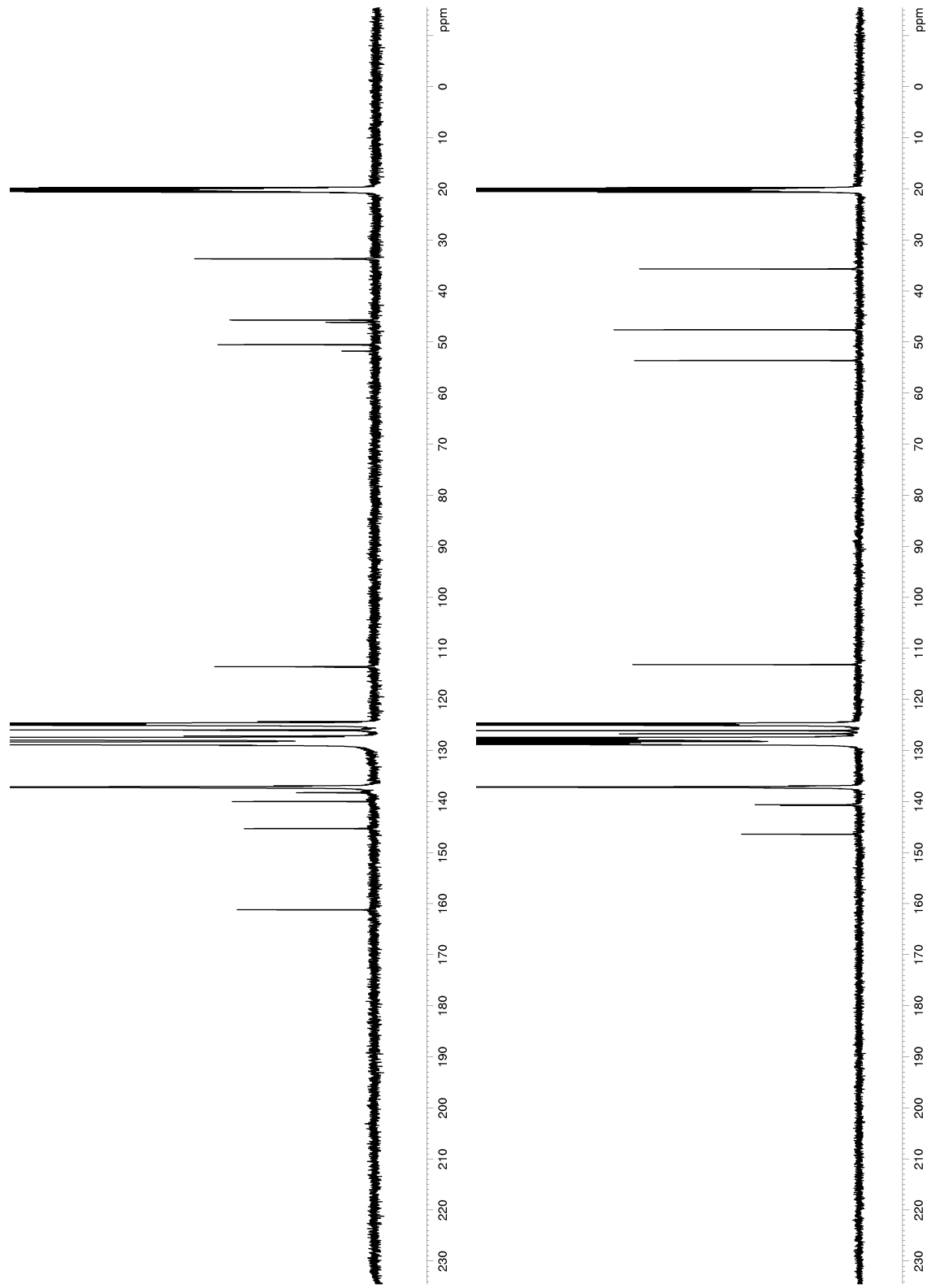
pK$_a$ Studies

To a dry NMR tube was added catalyst (50.0 µmol), 1-formyl piperazine (5.6 mg, 50.0 µmol), TMS (5 µL) and anhydrous DMSO-d_6 (1.25 g). The mixture was titrated with 0.05 M anhydrous TFA in DMSO-d_6 in 4 µL increments and the peaks were measured relative to TMS internal standard (Bruker AV-II, 600 MHz).

Summary of NMR titrations

^{7}*MeOStilbPBAM (7c)*

	-LOG(slope)	pKa piperazine + -log(slope)
Titration 1	-0.2323	8.0477
Titration 2	-0.2404	8.0396
Titration 3	-0.2398	8.0402
Average	-0.2418	8.0425
Standard Deviation	0.0037	0.0037

StilbPBAM (7a)

	-LOG(slope)	pKa piperazine + -log(slope)
Titration 1	-0.3932	7.8868
Titration 2	-0.3818	7.8982
Titration 3	-0.3979	7.8821
Average	-0.3910	7.8890
Standard Deviation	0.0083	0.0083

Titration 1 of ^{7}OMeStilbPBAM vs. 1-formylpiperazine

Titre #	∂a (StilbPBAM)	∂b (formyl piperazine)	$\partial a-\partial A\degree$	$\partial b-\partial B\degree$	$\partial AH-\partial a$	$\partial BH-\partial b$	$(\partial a-\partial A\degree)*(\partial BH-\partial b)$	$(\partial b-\partial B\degree)*(\partial AH-\partial a)$
0	7.7935	2.5983	0	0	0.2851	0.4864	0	0
1	7.7992	2.6258	0.0057	0.0275	0.2794	0.4589	0.002616	0.007683
2	7.8138	2.6573	0.0203	0.059	0.2648	0.4274	0.008676	0.015623
3	7.8338	2.7006	0.0403	0.1023	0.2448	0.3841	0.015479	0.025043
4	7.8433	2.7248	0.0498	0.1265	0.2353	0.3599	0.017923	0.029765
5	7.8579	2.7587	0.0644	0.1604	0.2207	0.326	0.020994	0.0354
6	7.8728	2.7926	0.0793	0.1943	0.2058	0.2921	0.023164	0.039987
7	7.8879	2.826	0.0944	0.2277	0.1907	0.2587	0.024421	0.043422
8	7.908	2.8562	0.1145	0.2579	0.1706	0.2285	0.026163	0.043998
9	7.919	2.8903	0.1255	0.292	0.1596	0.1944	0.024397	0.046603
10	7.936	2.9189	0.1425	0.3206	0.1426	0.1658	0.023627	0.045718
11	7.9518	2.9246	0.1583	0.3263	0.1268	0.1601	0.025344	0.041375
12	7.9703	2.9774	0.1768	0.3791	0.1083	0.1073	0.018971	0.041057
13	7.9854	2.9978	0.1919	0.3995	0.0932	0.0869		
14	8.0008	3.0239	0.2073	0.4256	0.0778	0.0608	0.012604	0.033112
15	8.0263	3.0416	0.2328	0.4433	0.0523	0.0431	0.010034	0.023185
16	8.0452	3.0596	0.2517	0.4613	0.0334	0.0251	0.006318	0.015407
17	8.0601	3.0725	0.2666	0.4742	0.0185	0.0122	0.003253	0.008773
18	8.0764	3.0841	0.2829	0.4858	0.0022	0.0006	0.00017	0.001069
19	8.0774	3.0842	0.2839	0.4859	0.0012	0.0005	0.000142	0.000583
20	8.0786	3.0847	0.2851	0.4864	0	0	0	0

Titration 1 of 7OMeStilbPBAM vs 1-formyl piperazine

$y = 1.7074x + 0.0023$
$R^2 = 0.95714$

Titration 2 of ^{7}OMeStilbPBAM vs. 1-formylpiperazine

Titre #	∂a (StilbPBAM)	∂b (formyl piperazine)	$\partial a - \partial A°$	$\partial b - \partial B°$	$\partial AH - \partial a$	$\partial BH - \partial b$	$(\partial a - \partial A°)*(\partial BH - \partial b)$	$(\partial b - \partial B°)*(\partial AH - \partial a)$
0	7.7982	2.5853	0	0	0.3015	0.4987	0	0
1	7.8017	2.5913	0.0035	0.006	0.298	0.4927	0.00172445	0.001788
2	7.8122	2.6129	0.014	0.0276	0.2875	0.4711	0.0065954	0.007935
3	7.8271	2.6475	0.0289	0.0622	0.2726	0.4365	0.01261485	0.01695572
4	7.8366	2.669	0.0384	0.0837	0.2631	0.415	0.015936	0.02202147
5	7.8577	2.7157	0.0595	0.1304	0.242	0.3683	0.02191385	0.0315568
6	7.8751	2.7572	0.0769	0.1719	0.2246	0.3268	0.02513092	0.03860874
7	7.89	2.7932	0.0918	0.2079	0.2097	0.2908	0.02669544	0.04359663
8	7.9037	2.824	0.1055	0.2387	0.196	0.26	0.02743	0.0467852
9	7.9159	2.8508	0.1177	0.2655	0.1838	0.2332	0.02744764	0.0487989
10	7.9254	2.8727	0.1272	0.2874	0.1743	0.2113	0.02687736	0.05009382
11	7.9447	2.908	0.1465	0.3227	0.155	0.176	0.025784	0.0500185
12	7.9578	2.9301	0.1596	0.3448	0.1419	0.1539	0.02456244	0.04892712
13	7.9756	2.9609	0.1774	0.3756	0.1241	0.1231	0.02183794	0.04661196
14	7.9927	2.985	0.1945	0.3997	0.107	0.099	0.0192555	0.0427679
15	8.0123	3.0096	0.2141	0.4243	0.0874	0.0744	0.01592904	0.03708382
16	8.0173	3.0302	0.2191	0.4449	0.0824	0.0538	0.01178758	0.03665976
17	8.0272	3.0403	0.229	0.455	0.0725	0.0437	0.0100073	0.0329875
18	8.0562	3.0537	0.258	0.4684	0.0435	0.0303	0.0078174	0.0203754
19	8.083	3.074	0.2848	0.4887	0.0167	0.01	0.002848	0.00816129
20	8.0947	3.0817	0.2965	0.4964	0.005	0.0023	0.00068195	0.002482
21	8.0989	3.0843	0.3007	0.499	0.0008	-0.0003	-9.021E-05	0.0003992
22	8.099	3.0839	0.3008	0.4986	0.0007	0.0001	3.008E-05	0.00034902
23	8.0997	3.084	0.3015	0.4987	0	0	0	0

Titration 2 of 7OMeStilbPBAM vs 1-formyl piperazine

y = 1.7396x + 0.0023
R² = 0.89582

y-axis: (∂b-∂B°)*(∂AH-∂a)
x-axis: (∂a-∂A°)*(∂BH-∂b)

Titration 3 of [7]OMeStilbPBAM vs. 1-formylpiperazine

Titre #	∂a (StilbPBAM)	∂b (formyl piperazine)	$\partial a\text{-}\partial A°$	$\partial b\text{-}\partial B°$	$\partial AH\text{-}\partial a$	$\partial BH\text{-}\partial b$	$(\partial a\text{-}\partial A°)*(\partial BH\text{-}\partial b)$	$(\partial b\text{-}\partial B°)*(\partial AH\text{-}\partial a)$
0	7.7997	2.5866	0	0	0.2966	0.4972	0	0
1	7.8032	2.5936	0.0035	0.007	0.2931	0.4902	0.001716	0.002052
2	7.8172	2.6241	0.0175	0.0375	0.2791	0.4597	0.008045	0.010466
3	7.8306	2.6544	0.0309	0.0678	0.2657	0.4294	0.013268	0.018014
4	7.8427	2.6823	0.043	0.0957	0.2536	0.4015	0.017265	0.02427
5	7.8579	2.7209	0.0582	0.1343	0.2384	0.3629	0.021121	0.032017
6	7.8725	2.756	0.0728	0.1694	0.2238	0.3278	0.023864	0.037912
7	7.8863	2.786	0.0866	0.1994	0.21	0.2978	0.025789	0.041874
8	7.901	2.8186	0.1013	0.232	0.1953	0.2652	0.026865	0.04531
9	7.9119	2.8368	0.1122	0.2502	0.1844	0.247	0.027713	0.046137
10	7.9239	2.8692	0.1242	0.2826	0.1724	0.2146	0.026653	0.04872
11	7.9452	2.913	0.1455	0.3264	0.1511	0.1708	0.024851	0.049319
12	7.9566	2.931	0.1569	0.3444	0.1397	0.1528	0.023974	0.048113
13	7.9709	2.9545	0.1712	0.3679	0.1254	0.1293	0.022136	0.046135
14	7.9838	2.9766	0.1841	0.39	0.1125	0.1072	0.019736	0.043875
15	8.0018	2.9915	0.2021	0.4049	0.0945	0.0923	0.018654	0.038263
16	8.0177	3.0155	0.218	0.4289	0.0786	0.0683	0.014889	0.033712
17	8.0256	3.0259	0.2259	0.4393	0.0707	0.0579	0.01308	0.031059
18	8.0435	3.0479	0.2438	0.4613	0.0528	0.0359	0.008752	0.024357
19	8.0694	3.0613	0.2697	0.4747	0.0269	0.0225	0.006068	0.012769
20	8.0818	3.0751	0.2821	0.4885	0.0145	0.0087	0.002454	0.007083
21	8.094	3.0825	0.2943	0.4959	0.0023	0.0013	0.000383	0.001141
22	8.0963	3.0838	0.2966	0.4972	0	0	0	0

Titration 3 of 7OMeStilbPBAM vs 1-formyl piperazine

$y = 1.7374x + 0.0018$
$R^2 = 0.91156$

Titration 1 of StilbPBAM vs. 1-formylpiperazine

Titre #	∂a (StilbPBAM)	∂b (formyl piperazine)	∂a- $\partial A°$	∂b- $\partial B°$	∂AH- ∂a	∂BH- ∂b	(∂a- $\partial A°$)*(∂BH- ∂b)	(∂b- $\partial B°$)*(∂AH- ∂a)
0	7.1692	2.5886	0	0	0.061	0.4838	0	0
1	7.1695	2.5889	0.0003	0.0003	0.0607	0.4835	0.00014505	1.821E-05
2	7.1719	2.6126	0.0027	0.024	0.0583	0.4598	0.00124146	0.0013992
3	7.1753	2.6779	0.0061	0.0893	0.0549	0.3945	0.00240645	0.00490257
4	7.1808	2.7517	0.0116	0.1631	0.0494	0.3207	0.00372012	0.00805714
5	7.1838	2.7837	0.0146	0.1951	0.0464	0.2887	0.00421502	0.00905264
6	7.186	2.8152	0.0168	0.2266	0.0442	0.2572	0.00432096	0.01001572
7	7.1884	2.8386	0.0192	0.25	0.0418	0.2338	0.00448896	0.01045
8	7.1917	2.8732	0.0225	0.2846	0.0385	0.1992	0.004482	0.0109571
9	7.194	2.9058	0.0248	0.3172	0.0362	0.1666	0.00413168	0.01148264
10	7.1982	2.9253	0.029	0.3367	0.032	0.1471	0.0042659	0.0107744
11	7.2012	2.9504	0.032	0.3618	0.029	0.122	0.003904	0.0104922
12	7.2033	2.9678	0.0341	0.3792	0.0269	0.1046	0.00356686	0.01020048
13	7.209	3.0016	0.0398	0.413	0.0212	0.0708	0.00281784	0.0087556
14	7.2122	3.0162	0.043	0.4276	0.018	0.0562	0.0024166	0.0076968
15	7.214	3.025	0.0448	0.4364	0.0162	0.0474	0.00212352	0.00706968
16	7.2209	3.0452	0.0517	0.4566	0.0093	0.0272	0.00140624	0.00424638
17	7.2264	3.0632	0.0572	0.4746	0.0038	0.0092	0.00052624	0.00180348
18	7.2292	3.0705	0.06	0.4819	0.001	0.0019	0.000114	0.0004819
19	7.2295	3.0713	0.0603	0.4827	0.0007	0.0011	6.633E-05	0.00033789
20	7.2303	3.0729	0.0611	0.4843	-1E-04	-0.0005	-3.055E-05	-4.843E-05
21	7.2311	3.0734	0.0619	0.4848	-0.0009	-0.001	-6.19E-05	-0.0004363
22	7.2302	3.0724	0.061	0.4838	0	0	0	0

Titration 1 of StilbPBAM vs 1-formyl piperazine

$y = 2.4776x + 0.0001$
$R^2 = 0.95187$

y-axis: $(\partial b - \partial B°)*(\partial AH - \partial a)$

x-axis: $(\partial a - \partial A°)*(\partial BH - \partial b)$

Appendix 4.1-149

Titration 2 of StilbPBAM vs. 1-formylpiperazine

Titre #	∂a (StilbPBAM)	∂b (formyl piperazine)	$\partial a-\partial A°$	$\partial b-\partial B°$	$\partial AH-\partial a$	$\partial BH-\partial b$	$(\partial a-\partial A°)*(\partial BH-\partial b)$	$(\partial b-\partial B°)*(\partial AH-\partial a)$
0	7.1662	2.586	0	0	0.0807	0.4976	0	0
1	7.1669	2.5906	0.0007	0.0046	0.08	0.493	0.0003451	0.000368
2	7.1761	2.708	0.0099	0.122	0.0708	0.3756	0.00371844	0.0086376
3	7.1791	2.7335	0.0129	0.1475	0.0678	0.3501	0.00451629	0.0100005
4	7.1856	2.8002	0.0194	0.2142	0.0613	0.2834	0.00549796	0.01313046
5	7.188	2.8161	0.0218	0.2301	0.0589	0.2675	0.0058315	0.01355289
6	7.1913	2.8477	0.0251	0.2617	0.0556	0.2359	0.00592109	0.01455052
7	7.1996	2.9106	0.0334	0.3246	0.0473	0.173	0.0057782	0.01535358
8	7.2064	2.9581	0.0402	0.3721	0.0405	0.1255	0.0050451	0.01507005
9	7.2098	2.9795	0.0436	0.3935	0.0371	0.1041	0.00453876	0.01459885
10	7.2143	3.0008	0.0481	0.4148	0.0326	0.0828	0.00398268	0.01352248
11	7.2257	3.0451	0.0595	0.4591	0.0212	0.0385	0.00229075	0.00973292
12	7.2291	3.0546	0.0629	0.4686	0.0178	0.029	0.0018241	0.00834108
13	7.234	3.0657	0.0678	0.4797	0.0129	0.0179	0.00121362	0.00618813
14	7.2417	3.0817	0.0755	0.4957	0.0052	0.0019	0.00014345	0.00257764
15	7.2423	3.082	0.0761	0.496	0.0046	0.0016	0.00012176	0.0022816
16	7.2428	3.0821	0.0766	0.4961	0.0041	0.0015	0.0001149	0.00203401
17	7.2436	3.0824	0.0774	0.4964	0.0033	0.0012	9.288E-05	0.00163812
18	7.2443	3.0825	0.0781	0.4965	0.0026	0.0011	8.591E-05	0.0012909
19	7.2451	3.0828	0.0789	0.4968	0.0018	0.0008	6.312E-05	0.00089424
20	7.2456	3.083	0.0794	0.497	0.0013	0.0006	4.764E-05	0.0006461
21	7.2461	3.0832	0.0799	0.4972	0.0008	0.0004	3.196E-05	0.00039776
22	7.2469	3.0836	0.0807	3.0836	0	0	0	0

Titration 2 of StilbPBAM vs 1-formyl piperazine

$y = 2.409x + 0.0014$
$R^2 = 0.92603$

y-axis: $(\partial b-\partial B°)*(\partial AH-\partial a)$
x-axis: $(\partial a-\partial A°)*(\partial BH-\partial b)$
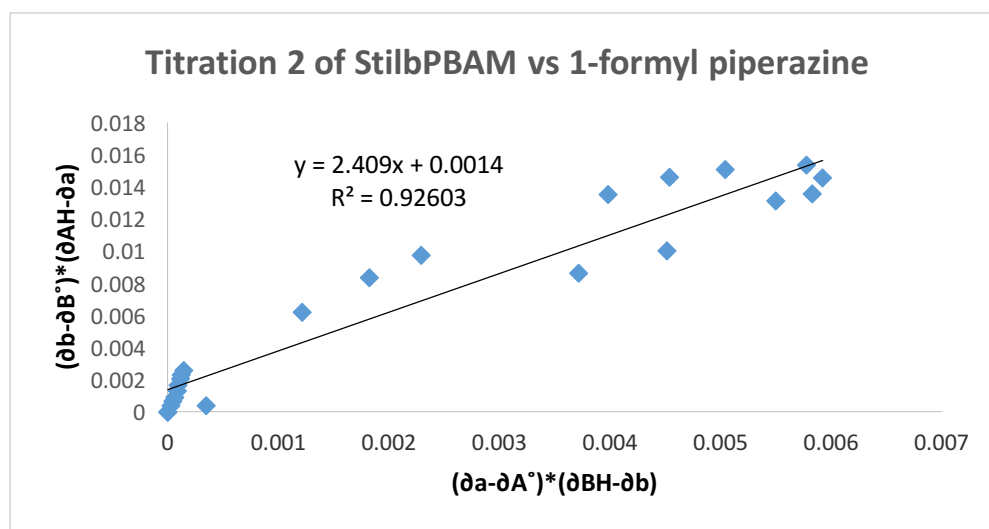
Titration 3 of StilbPBAM vs. 1-formylpiperazine

Titre #	∂a (StilbPBAM)	∂b (formyl piperazine)	$\partial a - \partial A°$	$\partial b - \partial B°$	$\partial AH - \partial a$	$\partial BH - \partial b$	$(\partial a - \partial A°)*(\partial BH - \partial b)$	$(\partial b - \partial B°)*(\partial AH - \partial a)$
0	7.1671	2.5869	0	0	0.076	0.4945	0	0
1	7.1671	2.5872	0	0.0003	0.076	0.4942	0	2.28E-05
2	7.1674	2.5894	0.0003	0.0025	0.0757	0.492	0.0001476	0.00018925
3	7.1697	2.604	0.0026	0.0171	0.0734	0.4774	0.00124124	0.00125514
4	7.1764	2.7022	0.0093	0.1153	0.0667	0.3792	0.00352656	0.00769051
5	7.1793	2.7321	0.0122	0.1452	0.0638	0.3493	0.00426146	0.00926376
6	7.1806	2.7411	0.0135	0.1542	0.0625	0.3403	0.00459405	0.0096375
7	7.1872	2.8062	0.0201	0.2193	0.0559	0.2752	0.00553152	0.01225887
8	7.1882	2.8242	0.0211	0.2373	0.0549	0.2572	0.00542692	0.01302777
9	7.1923	2.861	0.0252	0.2741	0.0508	0.2204	0.00555408	0.01392428
10	7.1954	2.8865	0.0283	0.2996	0.0477	0.1949	0.00551567	0.01429092
11	7.1998	2.9193	0.0327	0.3324	0.0433	0.1621	0.00530067	0.01439292
12	7.1982	2.9165	0.0311	0.3296	0.0449	0.1649	0.00512839	0.01479904
13	7.2092	2.9761	0.0421	0.3892	0.0339	0.1053	0.00443313	0.01319388
14	7.2132	2.9979	0.0461	0.411	0.0299	0.0835	0.00384935	0.0122889
15	7.2177	3.0157	0.0506	0.4288	0.0254	0.0657	0.00332442	0.01089152
16	7.2206	3.0269	0.0535	0.44	0.0225	0.0545	0.00291575	0.0099
17	7.2224	3.0306	0.0553	0.4437	0.0207	0.0508	0.00280924	0.00918459
18	7.2256	3.0407	0.0585	0.4538	0.0175	0.0407	0.00238095	0.0079415
19	7.2334	3.0633	0.0663	0.4764	0.0097	0.0181	0.00120003	0.00462108
20	7.2383	3.0744	0.0712	0.4875	0.0048	0.007	0.0004984	0.00234
21	7.2409	3.0793	0.0738	0.4924	0.0022	0.0021	0.00015498	0.00108328
22	7.2424	3.081	0.0753	0.4941	0.0007	0.0004	3.012E-05	0.00034587
23	7.243	3.0814	0.0759	0.4945	1E-04	0	0	4.945E-05
24	7.2431	3.0814	0.076	0.4945	0	0	0	0

Appendix 4.1-151
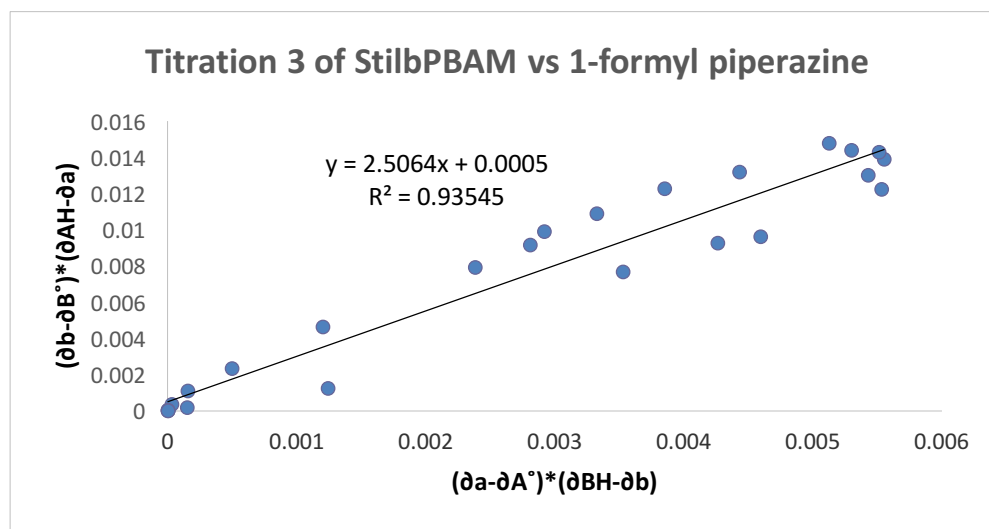
Diffusion NMR experiments: (ref: *Org. Lett.* 2015, *17*, 1429)

The ^{19}F DOSY experiments were run on Bruker DRX-500 (500 MHz) spectrometer equipped with Multinuclear Broadband Fluorine Observe (BBFO^{PLUS}) probe with z-axis gradient coil. The standard Bruker pulse sequence (ledbpgp2s) incorporating longitudinal eddy current delay was used for ^{19}F DOSY experiments. For ^{19}F diffusion measurements, the delay was set to 700-1200 µs and Δ was set to 80-100 ms. The individual slices of pseudo-2D diffusion spectra were phased. The diffusion coefficients were calculated from the signal attenuation curves of individual DOSY peaks. The formula weights were obtained by the linear regression analysis of log D vs log FW^3 where D is the experimentally calculated diffusion coefficients and FW is the formula weight of the compound. 1,4-Bis(trifluoromethyl)benzene, methyl trifluoroacetate and 3-bromobenzotrifluoride were chosen as internal standards for this DOSY study.

To a J. Young NMR tube was added *N*-benzyl-3-(4-(trifluoromethyl)phenyl)but-3-en-1-amine **78** (R = $^{P}CF_3C_6H_4$) (3.9 mg, 12.6 µmol), 1,4-bis(trifluoromethyl)benzene (2.8 mg, 12.6 µmol), methyl trifluoroacetate (1.6 mg, 12.6 µmol), 3-bromobenzotrifluoride (2.9 mg, 12.6 µmol) and anhydrous toluene-d_8 (0.7 mL). The tube was purged with CO_2 and loaded into a precooled (-20 °C) NMR bore (Bruker DRX-500, 500 MHz). After 20 minutes the first DOSY experiment data was collected.
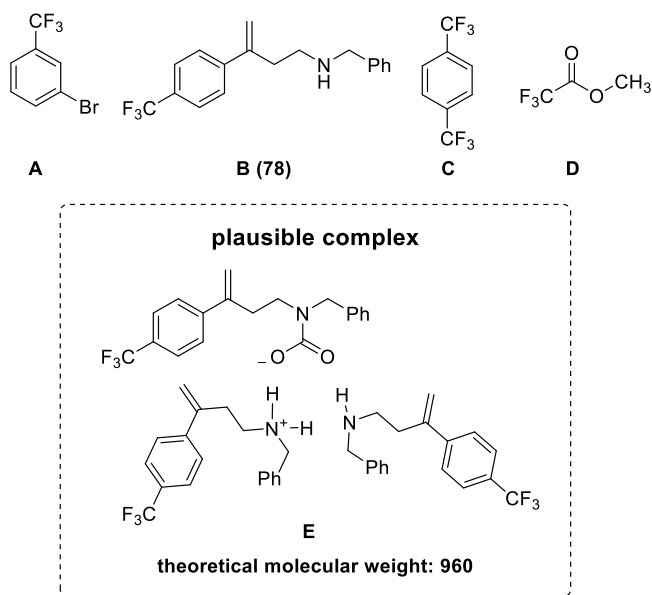
^{19}F DOSY Experiment (78)+CO_2

Compound	chemical shift	D (diffusion)	MW	LogD	LogMW	calculated MW (expt)	error %
A	-56.04	6.921E-10	225.01	-9.15983	2.35	222.85	0.96
B	-60.19	Not observed	305.34	-9.46332	N/A	N/A	N/A
C	-61.16	7.019E-10	214.11	-9.15372	2.33	216.28	1.01
D	-73.11	8.984E-10	128.05	-9.04653	2.11	127.91	0.11
E	-60.22	3.441E-10	960.04	-9.46332	N/A	985.96	-2.70

log D versus log FW analysis of 19F DOSY

$y = -0.4699x - 8.0565$
$R^2 = 0.999$
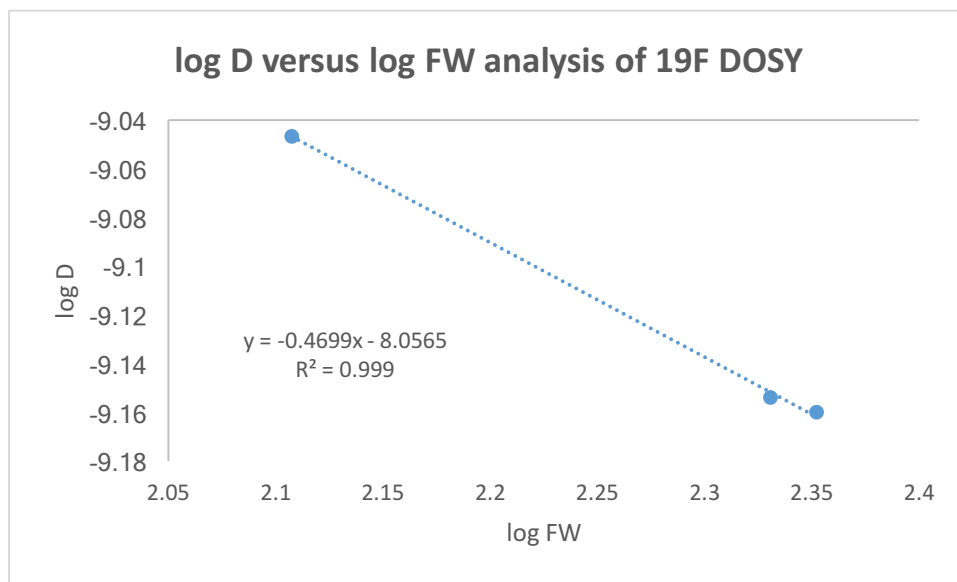
Figure 3. ^{19}F DOSY (470 MHz, -20 °C, tol-d_8) amine **78**/CO_2
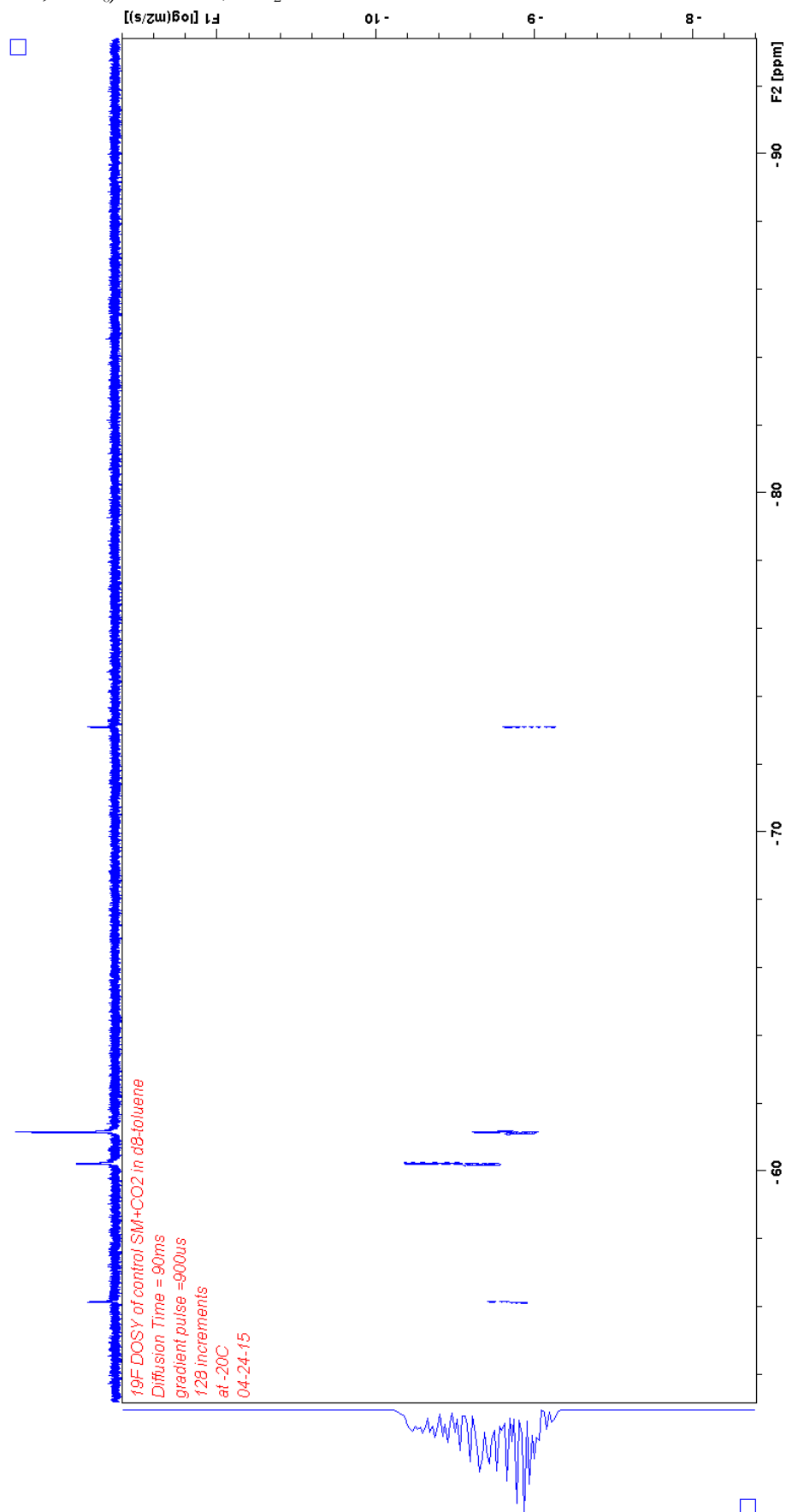
Figure 4. Signal attenuation curve of A in a mixture of B (**78**)/CO_2 in d_6-toluene.
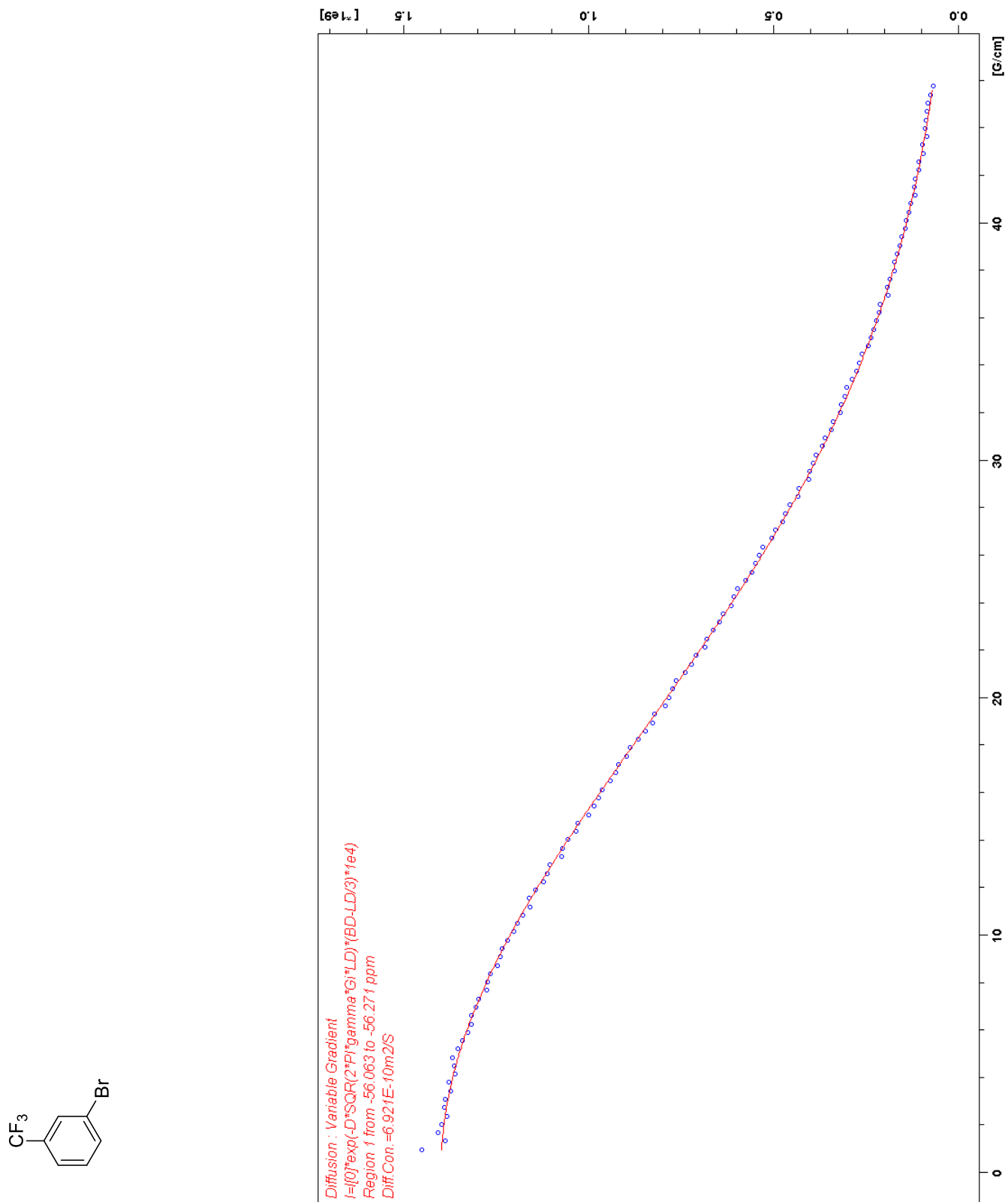
Figure 5. Signal attenuation curve of B (**78**) in a mixture of B (**78**)/CO_2 in d_6-toluene.

Diffusion : Variable Gradient
*I=I[0]*exp(-D*SQR(2*PI*gamma*G*LD)*(BD-LD/3)*1e4)*
Region 1 from -59.787 to -60.563 ppm
Diff.Con.=3.441E-10m2/S
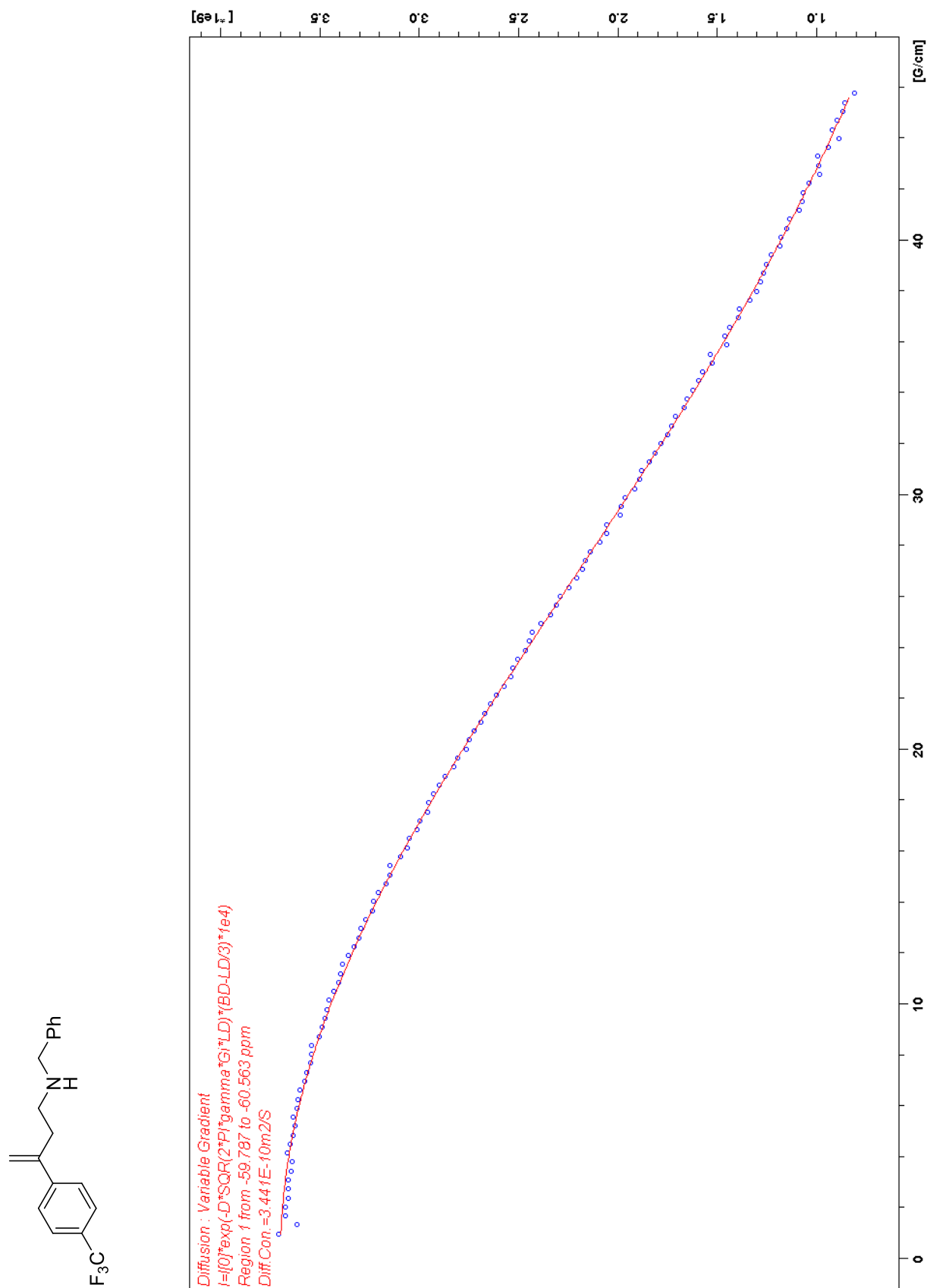
Figure 6. Signal attenuation curve of C in a mixture of B (**78**)/CO_2 in d_6-toluene.
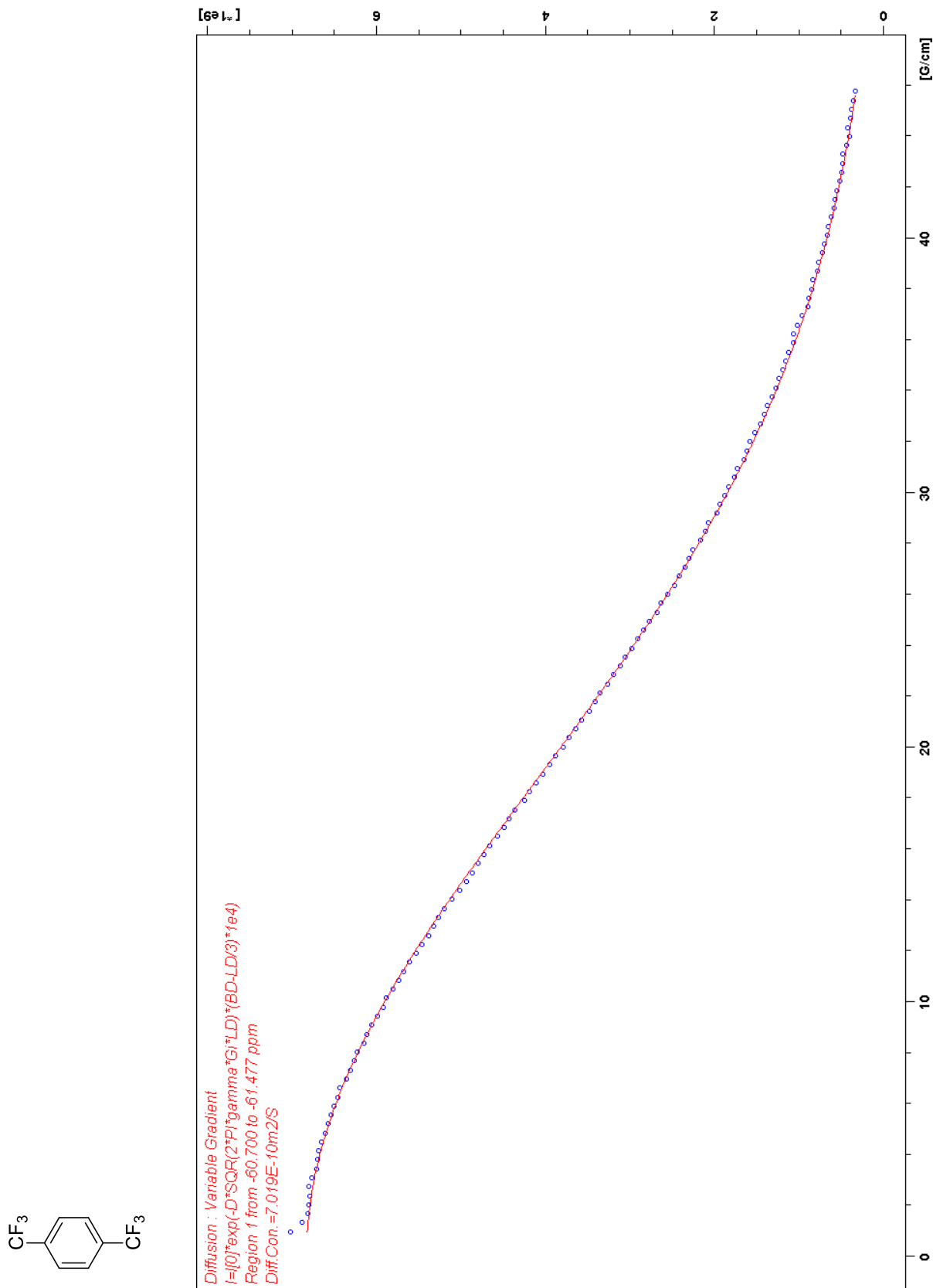
Figure 7. Signal attenuation curve of D in a mixture of B (**78**)/CO$_2$ in d_6-toluene.
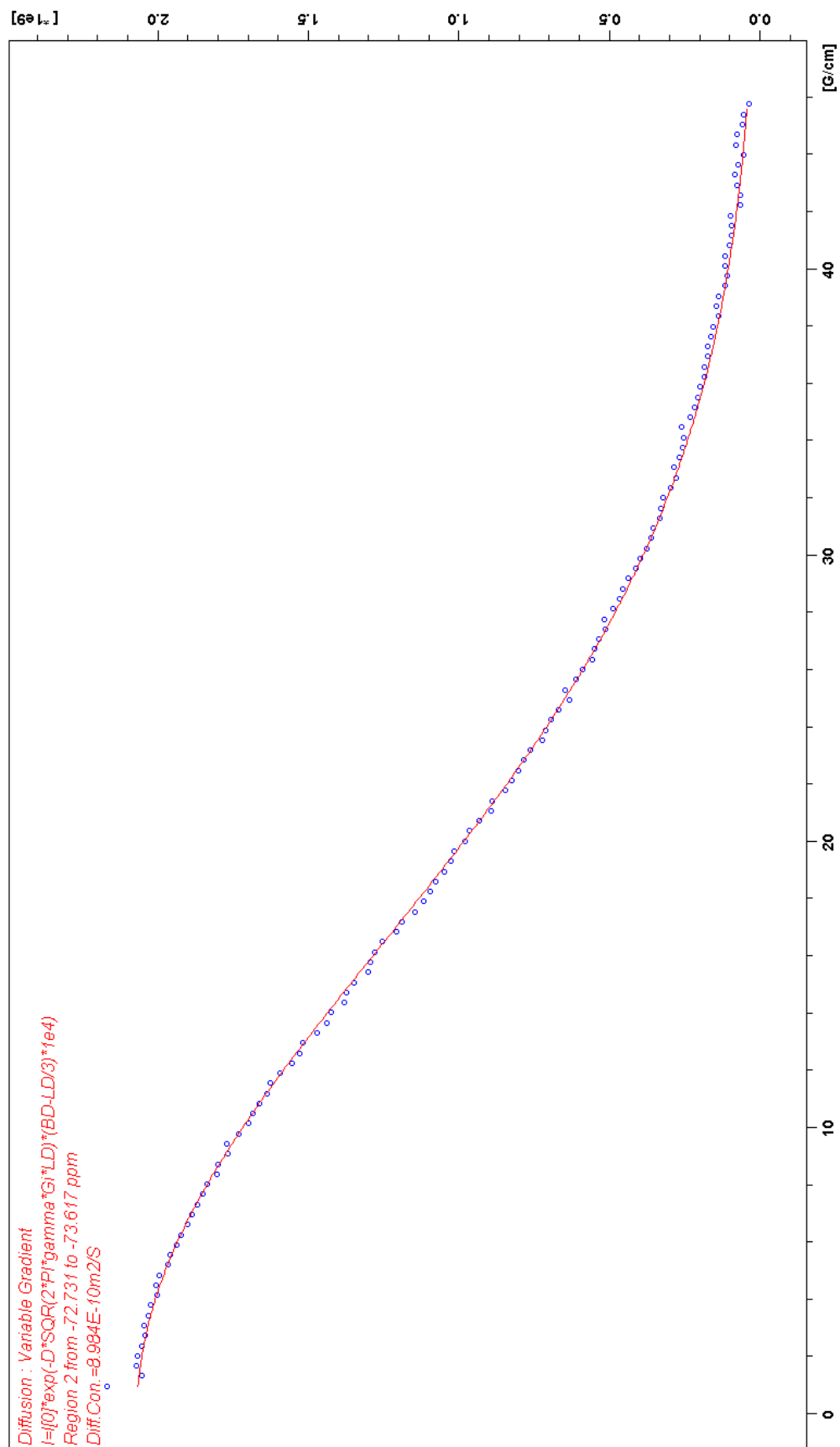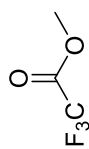
Diffusion : Variable Gradient
I=I[0]*exp(-D*SQR(2*PI*gamma*Gi*LD)*(BD-LD/3)*1e4)
Region 2 from -72.731 to -73.617 ppm
Diff.Con.=8.984E-10m2/S

To a J. Young NMR tube was added *N*-benzyl-3-(4-(trifluoromethyl)phenyl)but-3-en-1-amine **78** (R = $^pCF_3C_6H_4$) (3.9 mg, 12.6 µmol), 1,4-bis(trifluoromethyl)benzene (2.8 mg, 12.6 µmol), methyl trifluoroacetate (1.6 mg, 12.6 µmol), 3-bromobenzotrifluoride (2.9 mg, 12.6 µmol), ^{7}MeOStilbPBAM•HNTf$_2$ **42** (12.0 mg, 12.6 µmol) and anhydrous toluene-d_8 (0.7 mL). The tube was purged with CO_2 and loaded into a precooled (-20 °C) NMR bore (Bruker DRX-500, 500 MHz). After 20 minutes the first DOSY experiment data was collected.
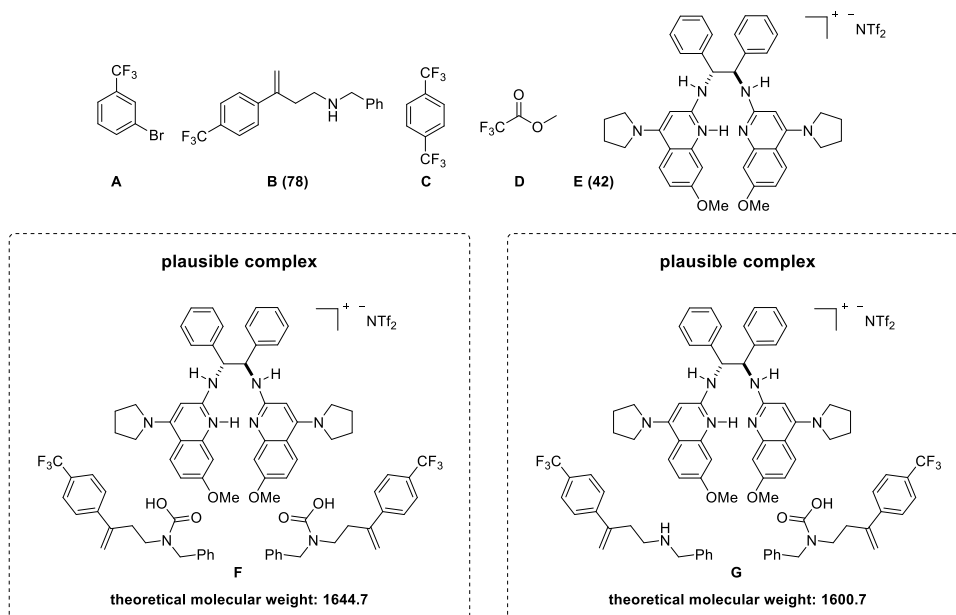
^{19}F DOSY Experiment (28a)+(7c•HNTf$_2$)+CO$_2$

Compound	chemical shift	D (diffusion)	MW	LogD	LogMW	calculated MW	error %
A	-56.28	5.549E-10	225.01	-9.2557853	2.35	219.58	2.41
B	-60.19	not observed	305.34	N/A	N/A	N/A	N/A
F	-60.23	1.595E-10	1644.7	-9.7972393	N/A	1485.21	9.70
G	-60.23	1.595E-10	1600.7	-9.7972393	N/A	1485.21	7.22
C	-61.48	5.543E-10	214.11	-9.2562551	2.33	219.94	2.72
D	-73.36	7.9E-10	128.05	-9.1023729	2.11	127.75	0.23
E	-77.01	not observed	945.99	N/A	N/A	N/A	N/A
G	-77.01	1.495E-10	1600.7	-9.8253588	N/A	1640.22	2.47
F	-77.01	1.495E-10	1644.7	-9.8253588	N/A	1640.22	-0.27

log D versus log FW analysis of 19F DOSY

$$y = -0.6522x - 7.7286$$
$$R^2 = 0.99325$$
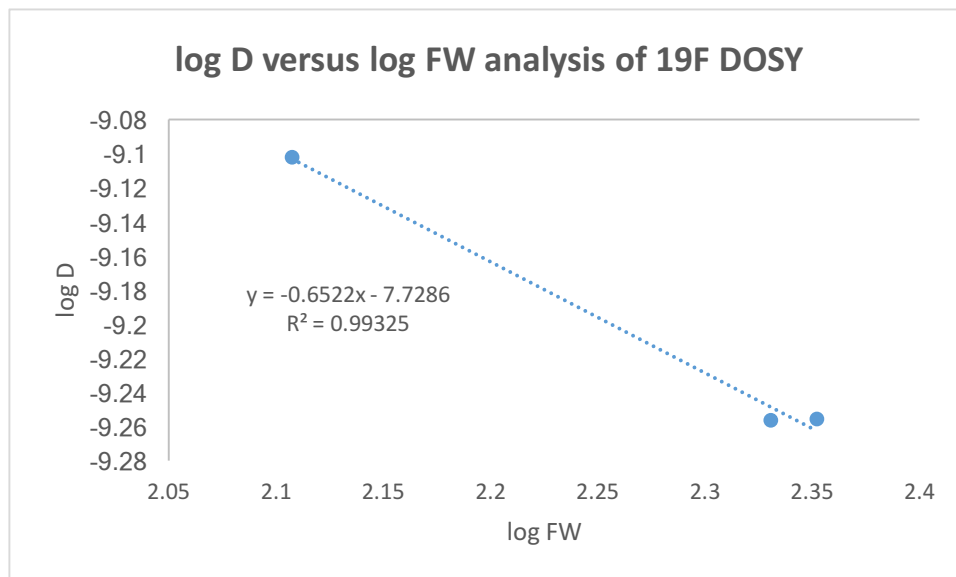
Figure 8. ^{19}F DOSY (470 MHz, -20 °C, tol-d_8) studies of amine **78**/CO_2/catalyst **42**.

19F DOSY of SM/CO2 + catalyst in d8-toluene
Diffusion Time = 90ms
gradient pulse =900us
128 increments
at -20C better shimming RG = 4k
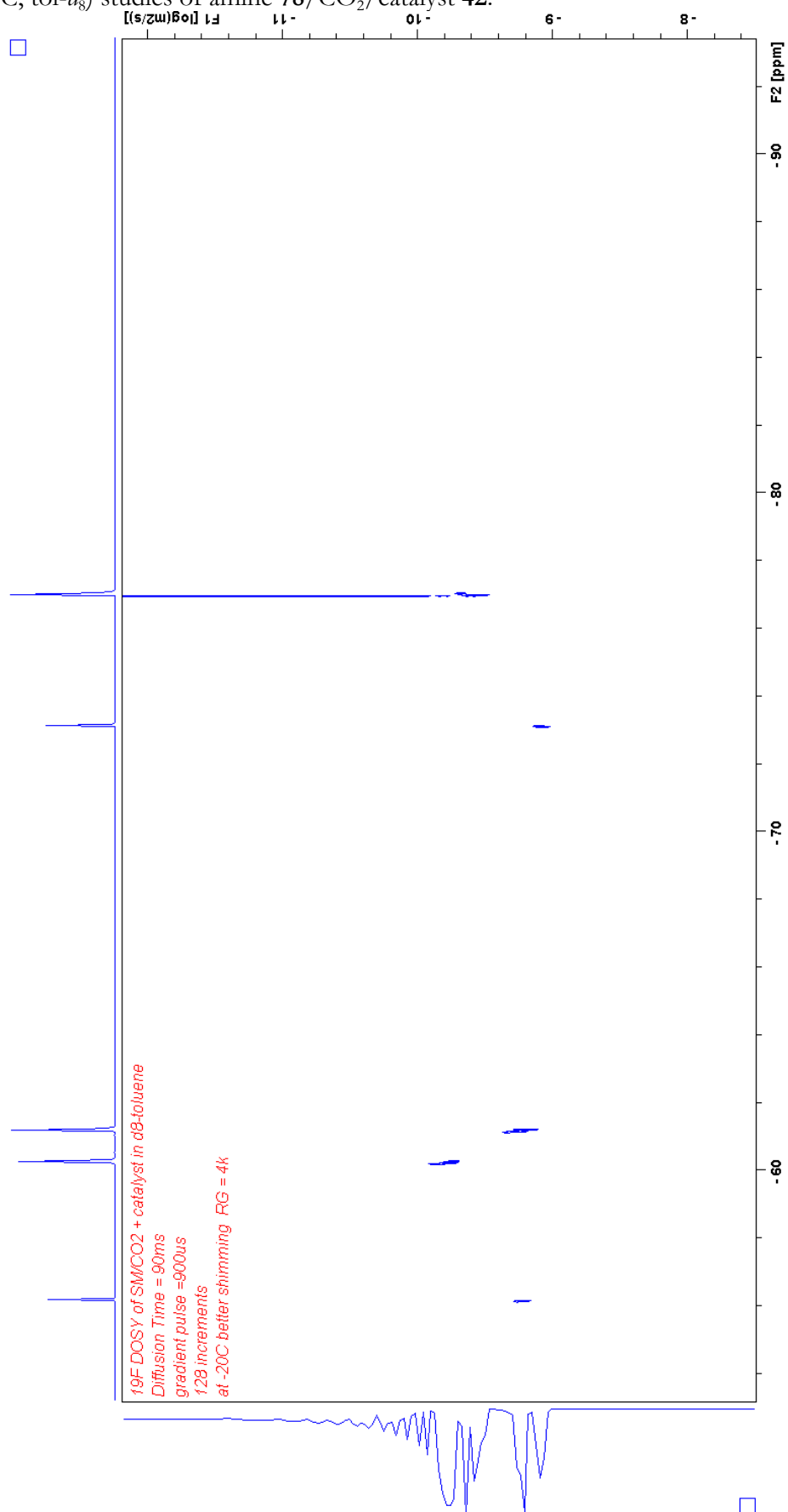
Figure 9. Signal attenuation curve of A in a mixture of **78**/CO_2/**42** in d_6-toluene.
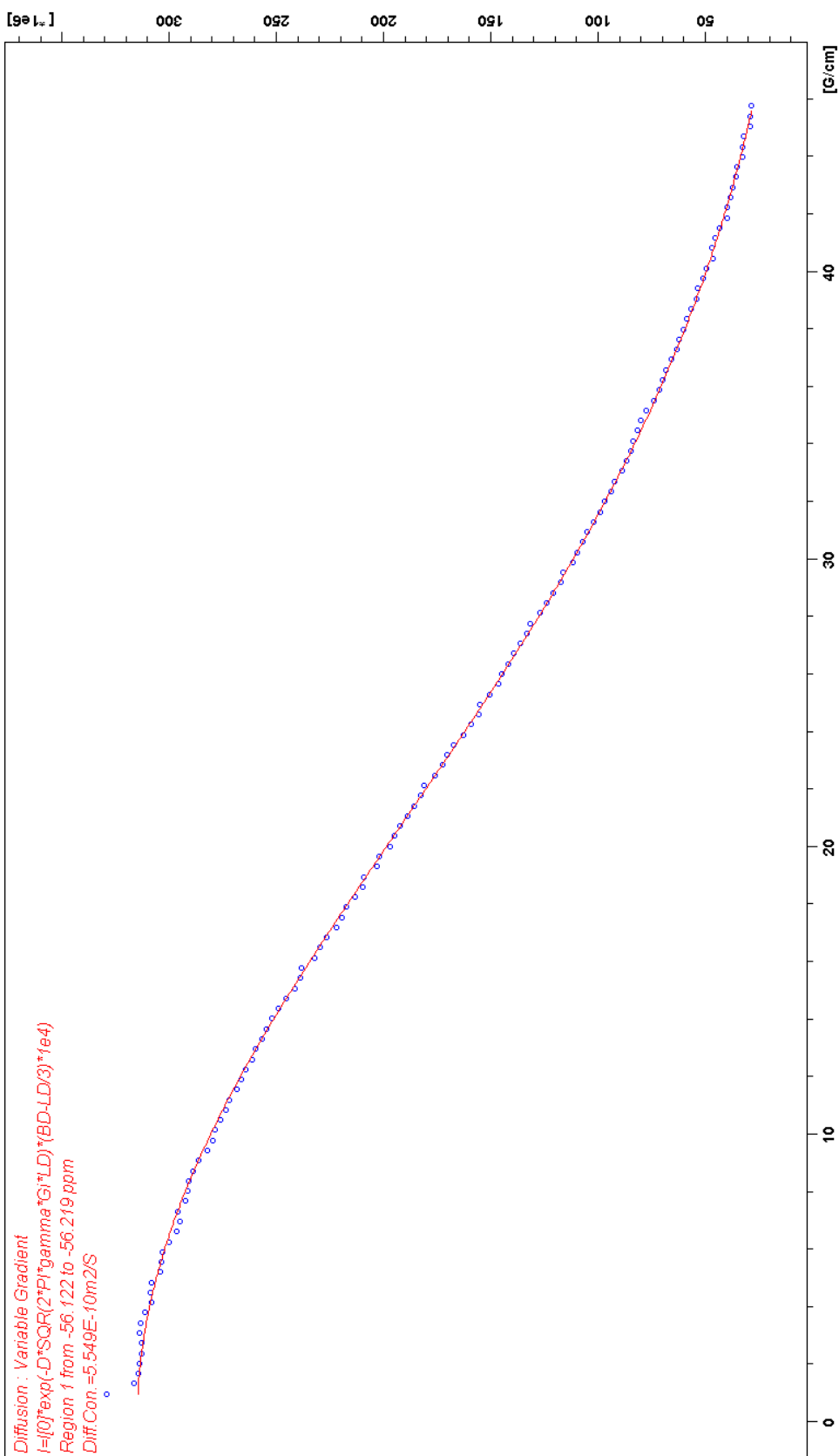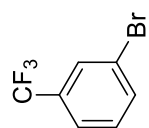
Figure 10. Signal attenuation curve of B (**78**) in a mixture of **78**/CO_2/**42** in d_6-toluene.
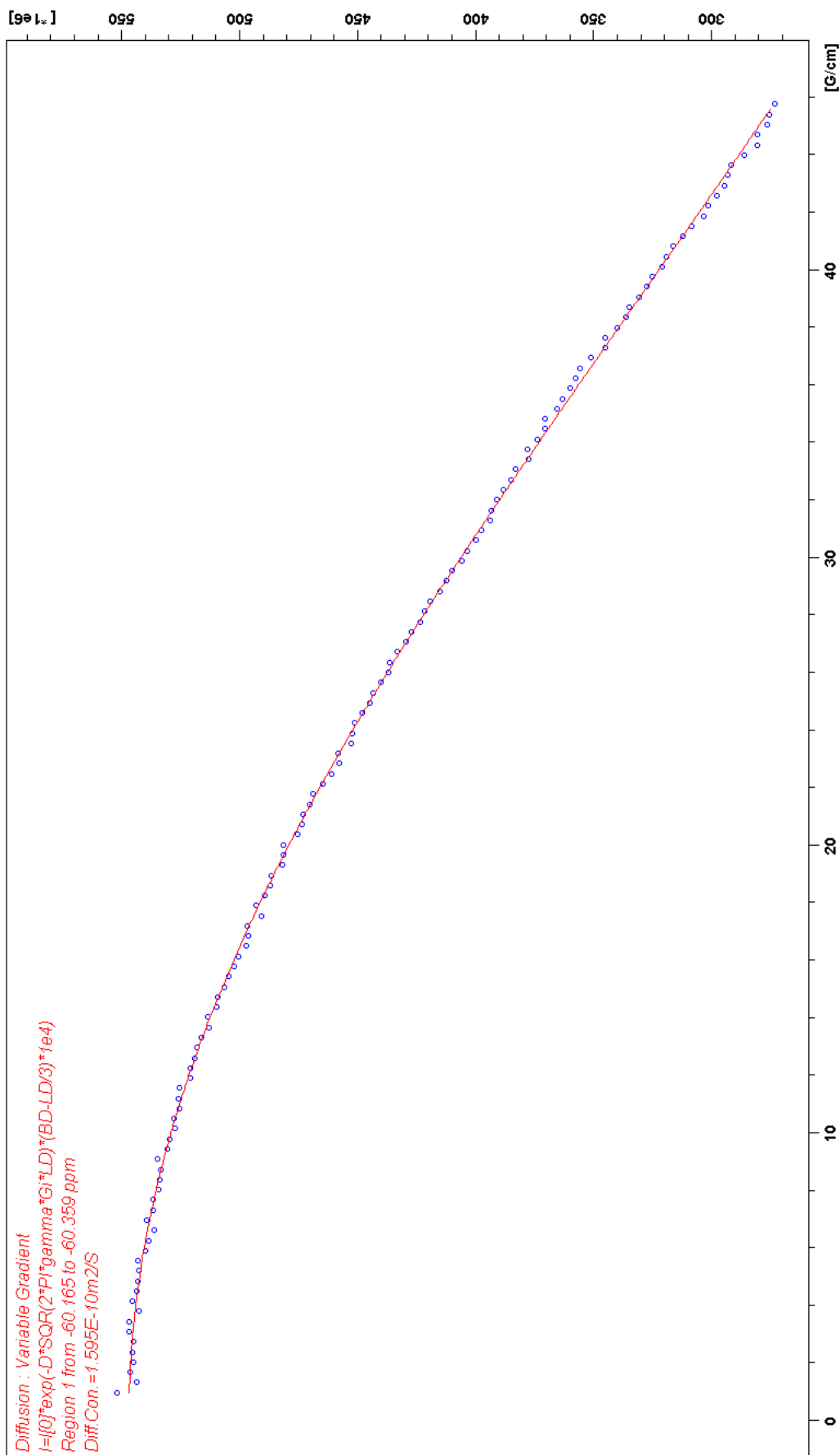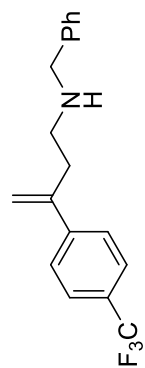
Figure 11. Signal attenuation curve of C in a mixture of **78**/CO$_2$/**42** in d_6-toluene.

Diffusion : Variable Gradient
I=I[0]*exp(-D*SQR(2*PI*gamma*Gi*LD)*(BD-LD/3)*1e4)
Region 1 from -61.119 to -61.279 ppm
Diff.Con.=-5.543E-10m2/S
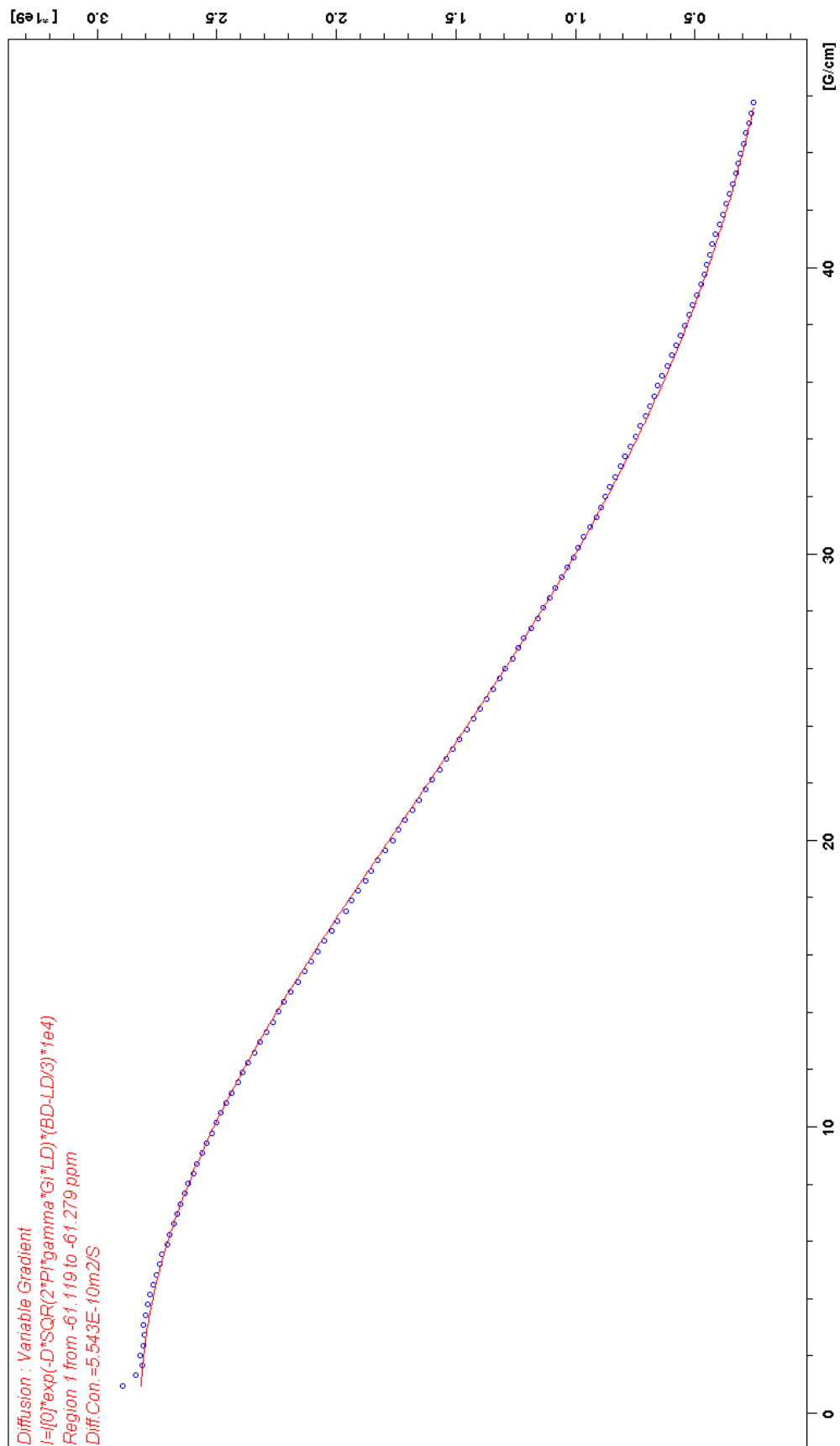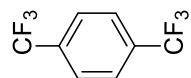
Appendix 4.1-165

Figure 12. Signal attenuation curve of D in a mixture of **78**/CO_2/**42** in d_6-toluene.
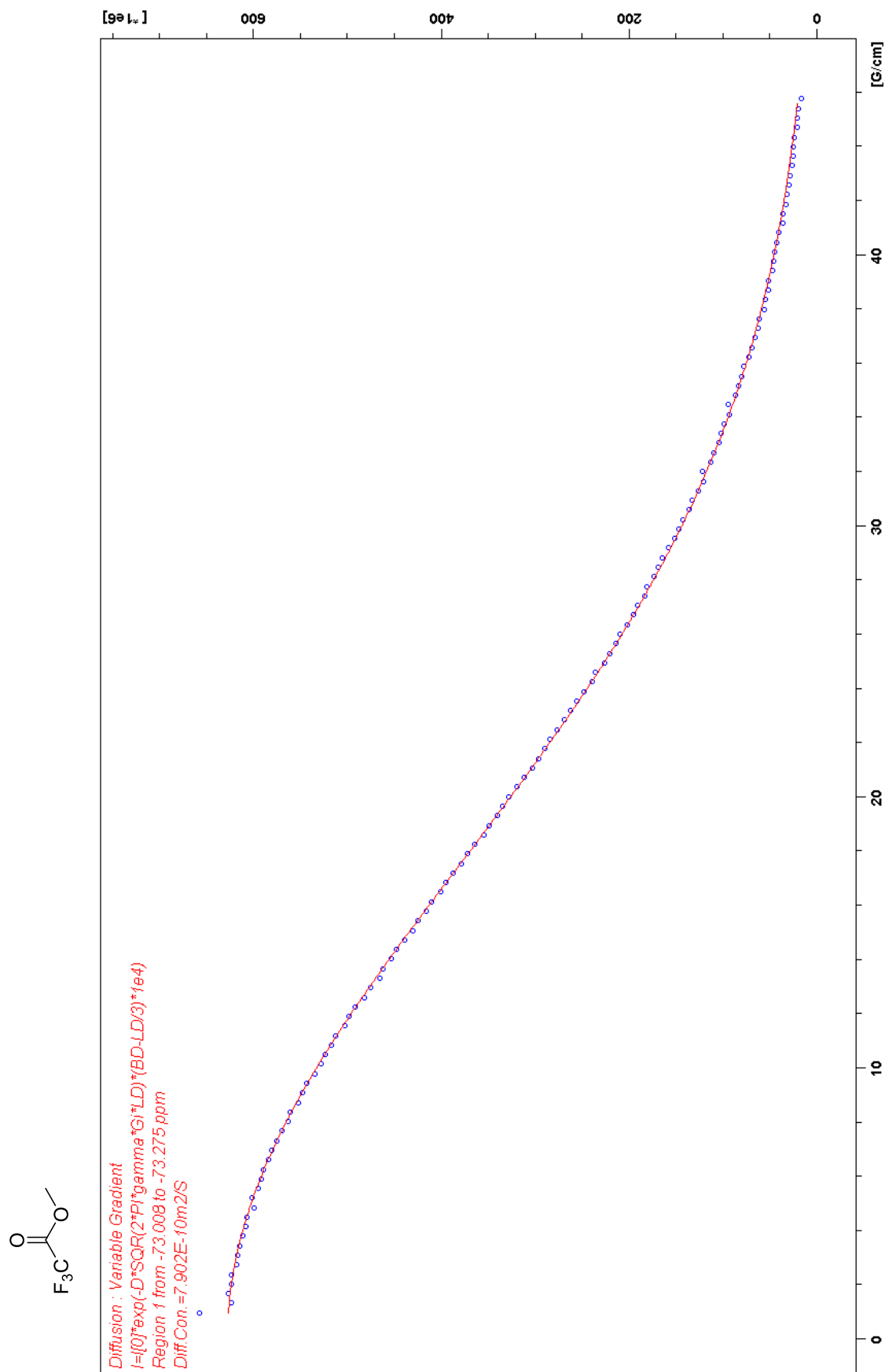
Figure 13. Signal attenuation curve of E (**42**) in a mixture of **78**/CO_2/**42** in d_6-toluene.
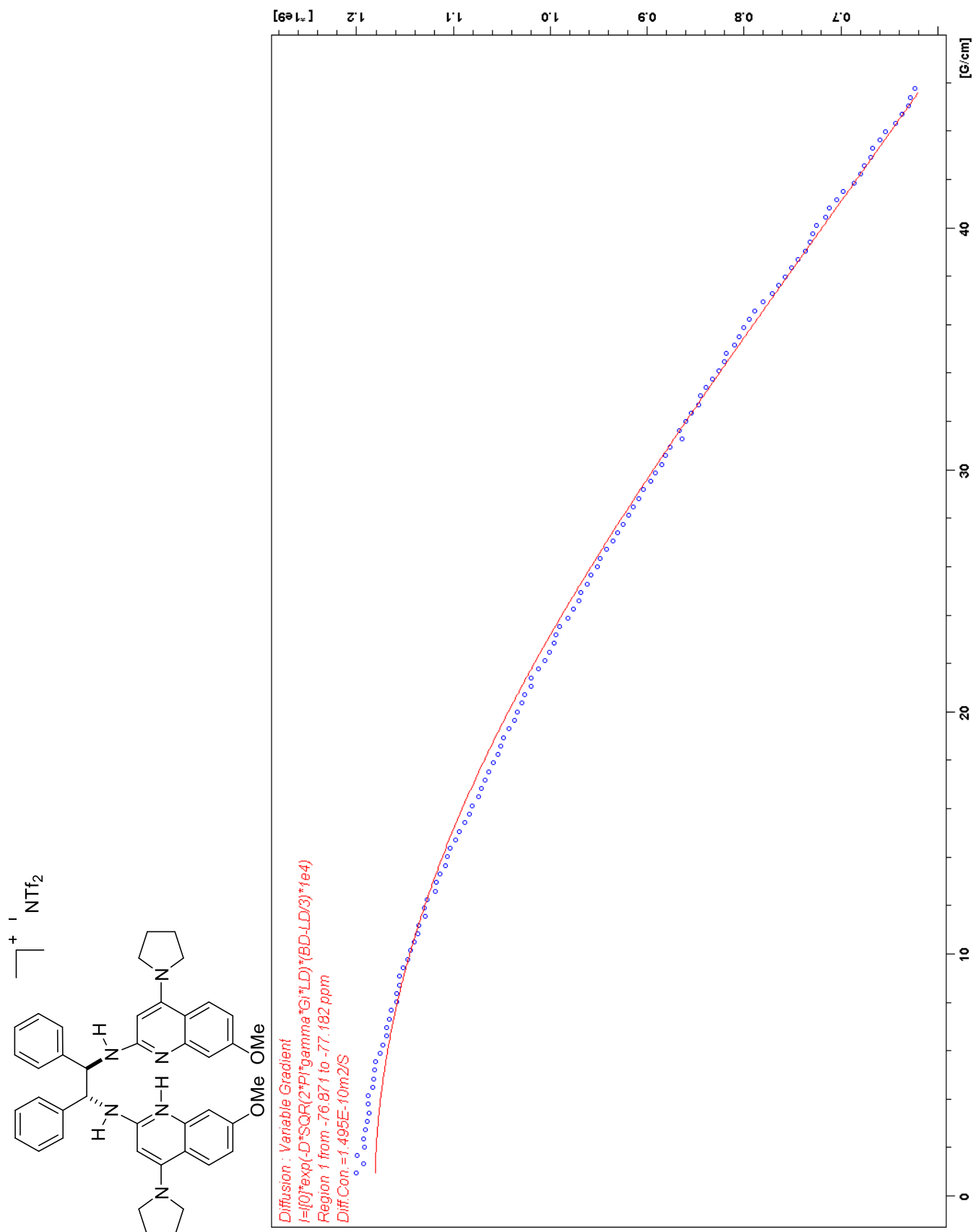
This page intentionally left blank

Appendix 4.2.1: Spectral data for iodocarbonation chemistry

Thomas J. Struble

Figure 1. ^{1}H NMR (400 MHz, CDCl$_3$) of **31.**
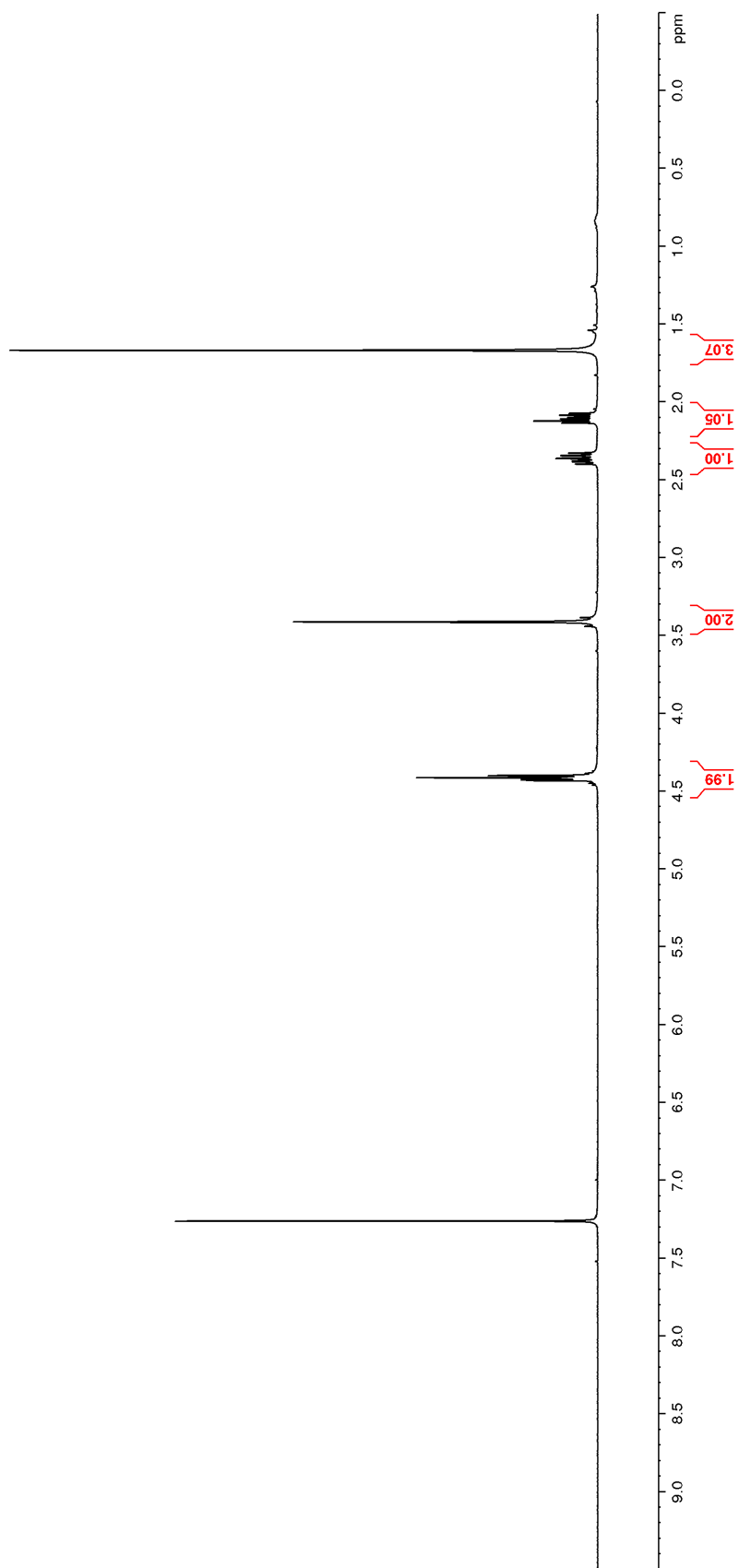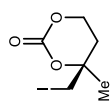
Figure 2. HPLC trace of **31.**
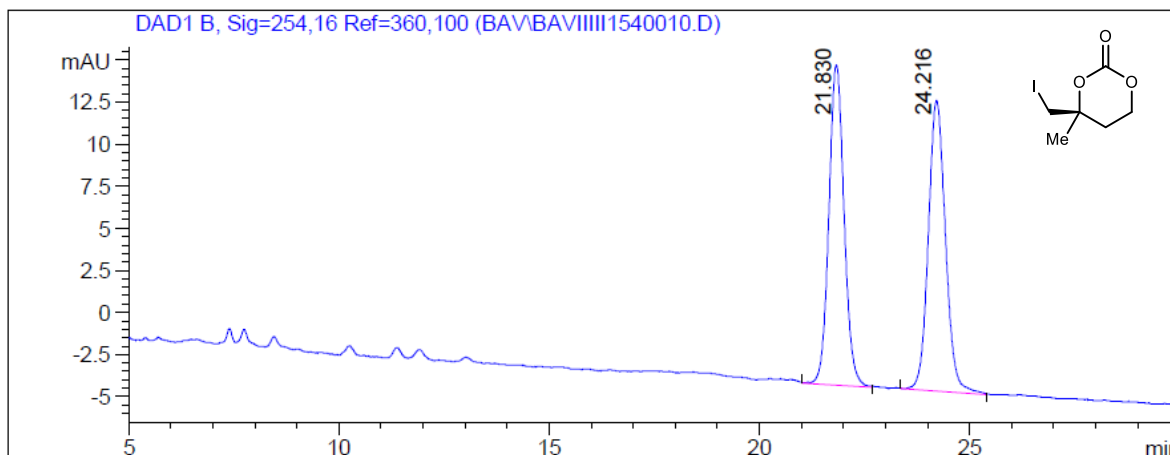

```
Signal  1: DAD1 B, Sig=254,16 Ref=360,100

       Peak    RT      Width      Area      Area %
       #      [min]   [min]
       ------------------------------------------
        1    21.830   0.421    480.205    49.53
        2    24.216   0.473    489.319    50.47
```
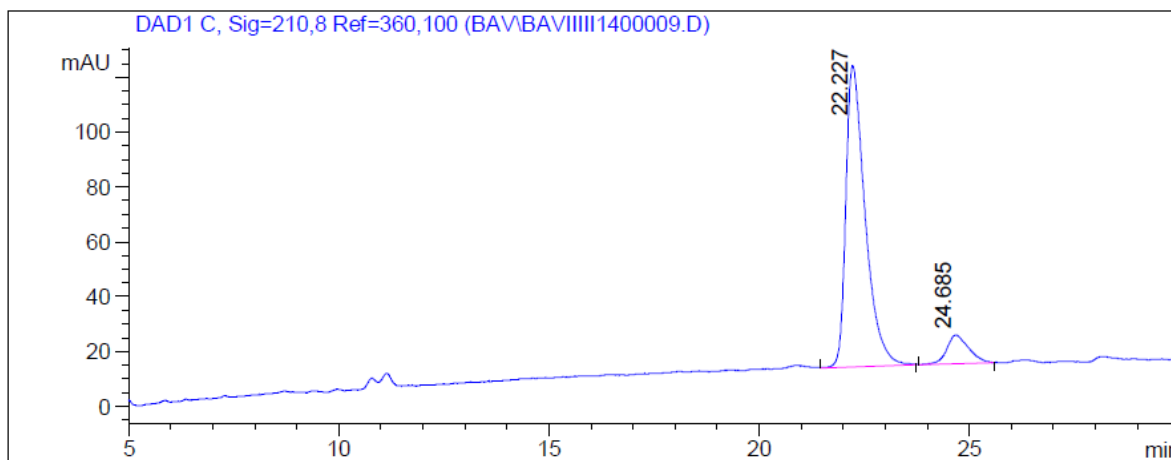


```
Signal  1: DAD1 C, Sig=210,8 Ref=360,100

       Peak    RT      Width      Area      Area %
       #      [min]   [min]
       ------------------------------------------
        1    22.227   0.531   3501.574    90.17
        2    24.685   0.603    381.613     9.83
       ------------------------------------------
```

Figure 3. ^{1}H NMR (400 MHz, CDCl$_3$) of **44.**
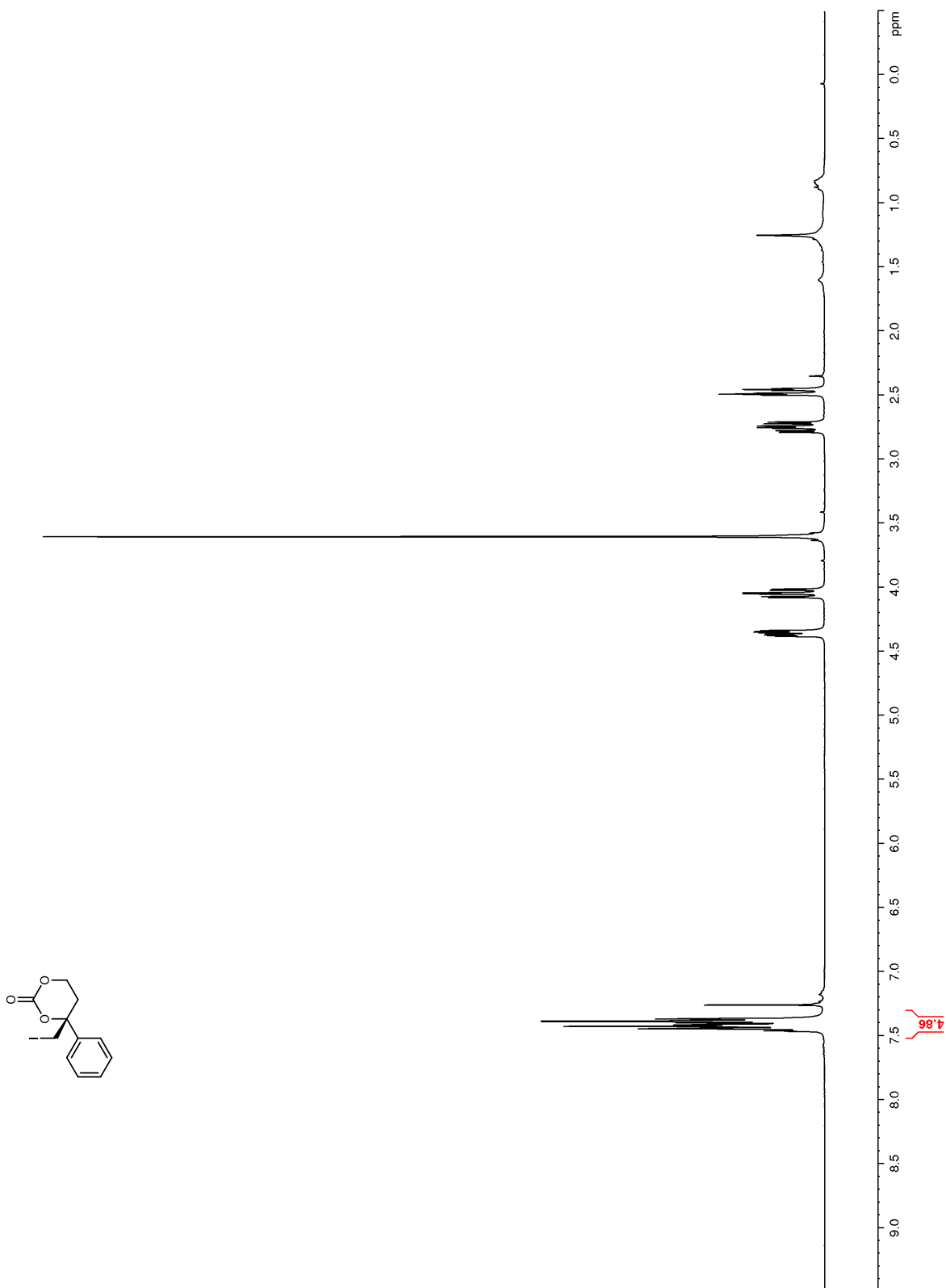
Figure 4. ^{13}C NMR (400 MHz, CDCl$_3$) of **44.**
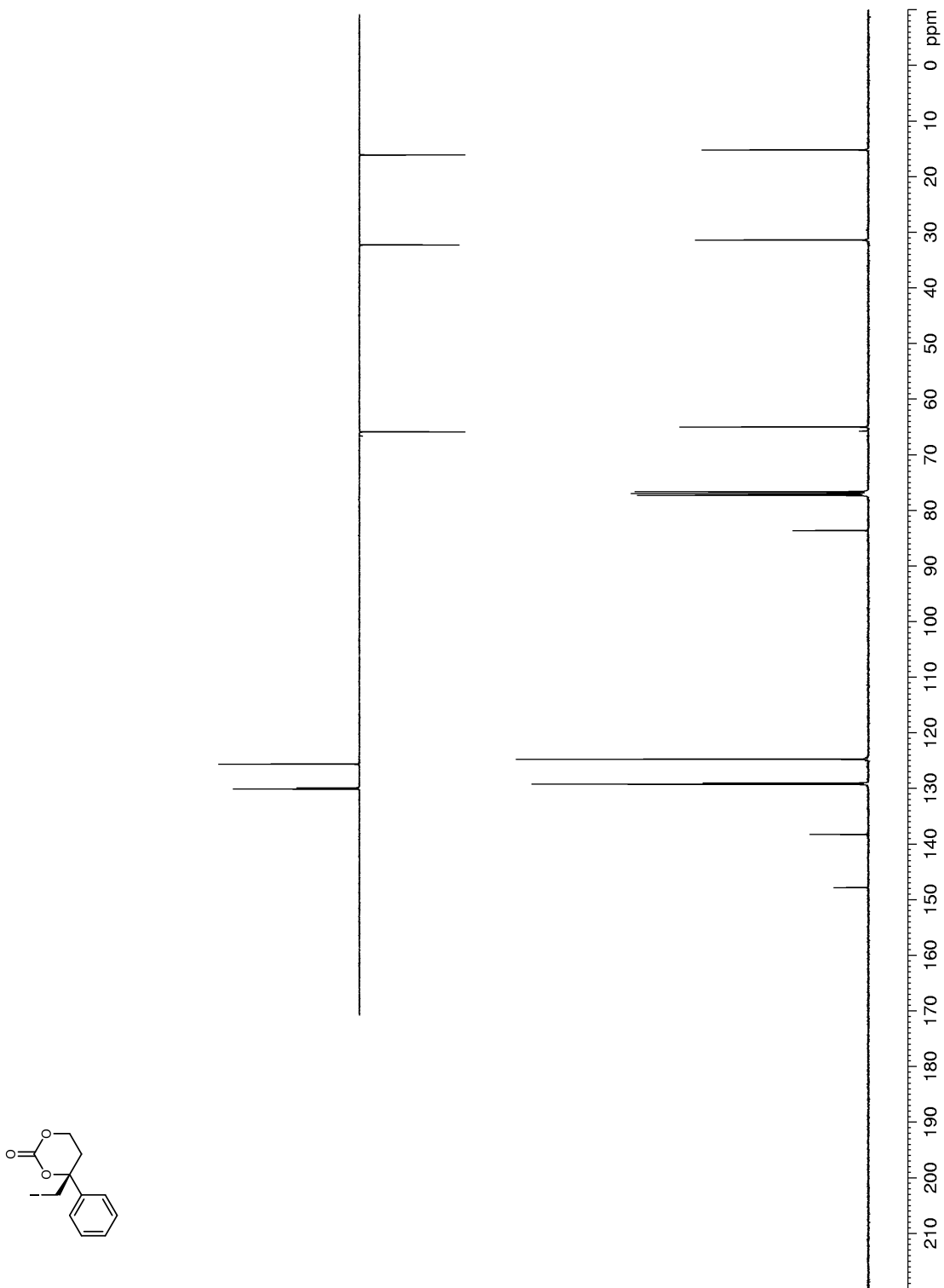
Figure 5. HPLC trace of **44.**
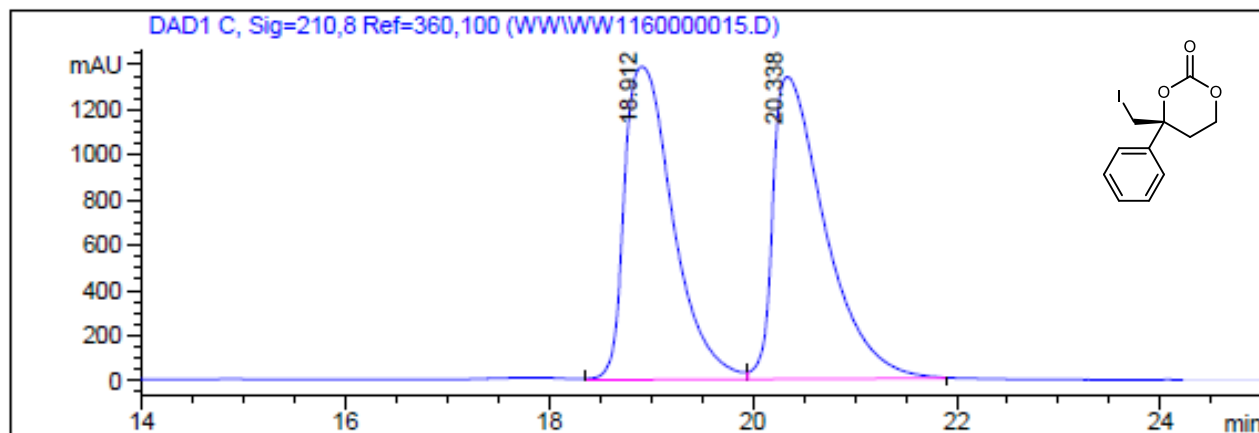
Signal 1: DAD1 C, Sig=210,8 Ref=360,100

```
    Peak    RT      Width      Area      Area %
    #      [min]    [min]
    ------------------------------------------------
     1     18.912  0.553  45973.105    49.13
     2     20.338  0.593  47610.668    50.87
    ------------------------------------------------
```
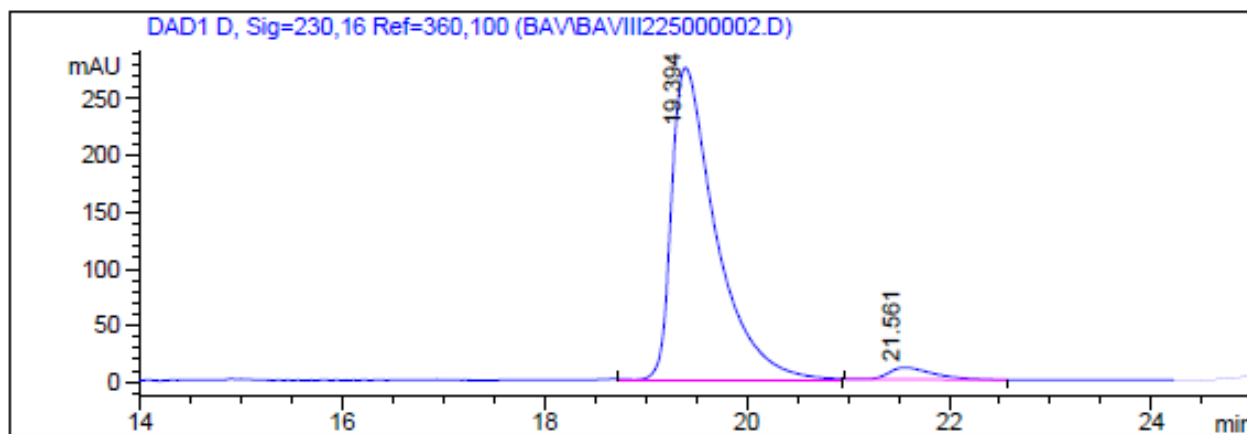

Signal 1: DAD1 D, Sig=230,16 Ref=360,100

```
    Peak    RT      Width      Area      Area %
    #      [min]    [min]
    ------------------------------------------------
     1     19.394  0.506   8346.550    96.21
     2     21.561  0.519    328.357     3.79
    ------------------------------------------------
```

Figure 6. ^{1}H NMR (400 MHz, CDCl$_3$) of **45.**
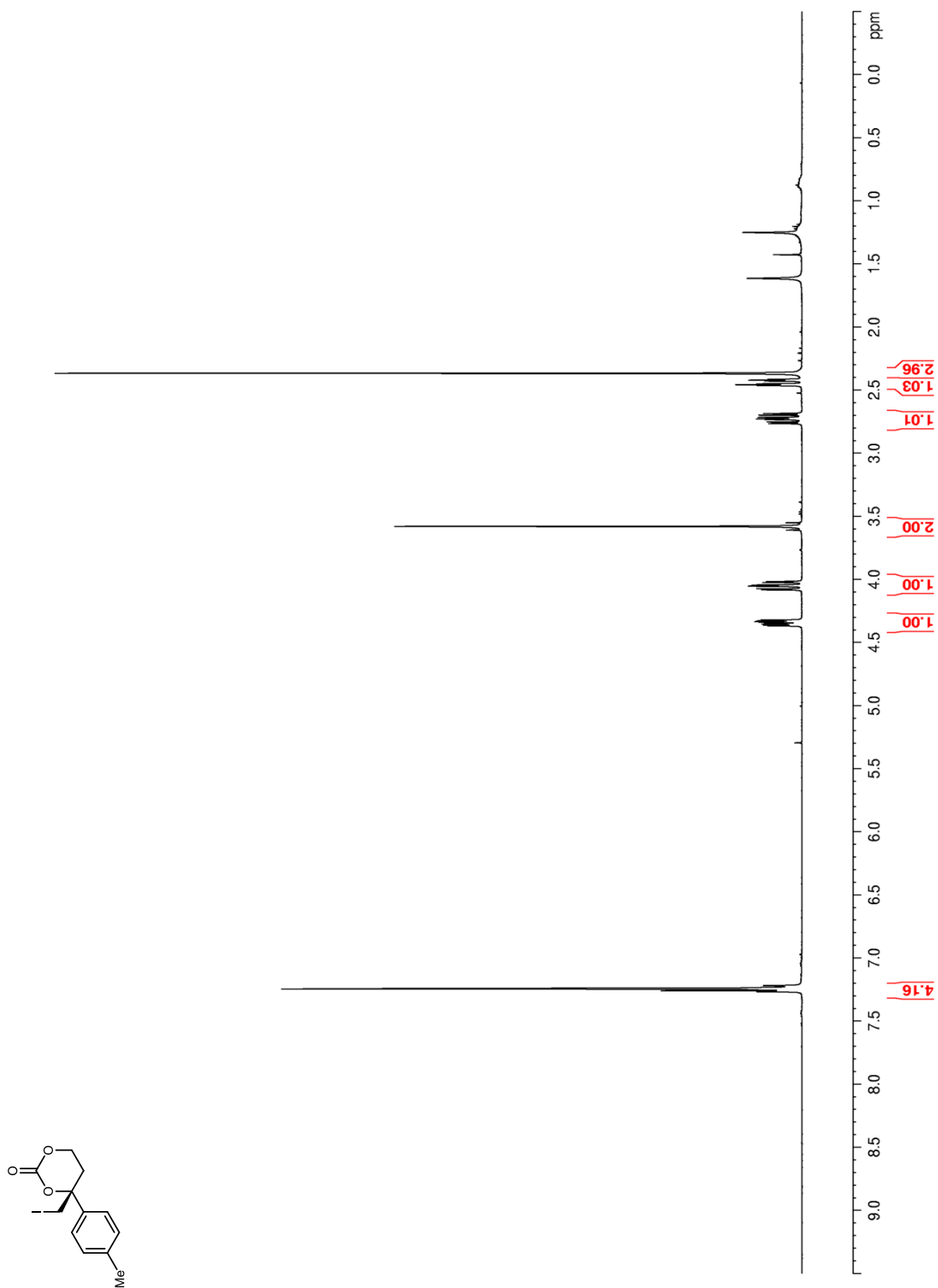
Figure 7. ^{13}C NMR (100MHz, CDCl$_3$) of **45.**
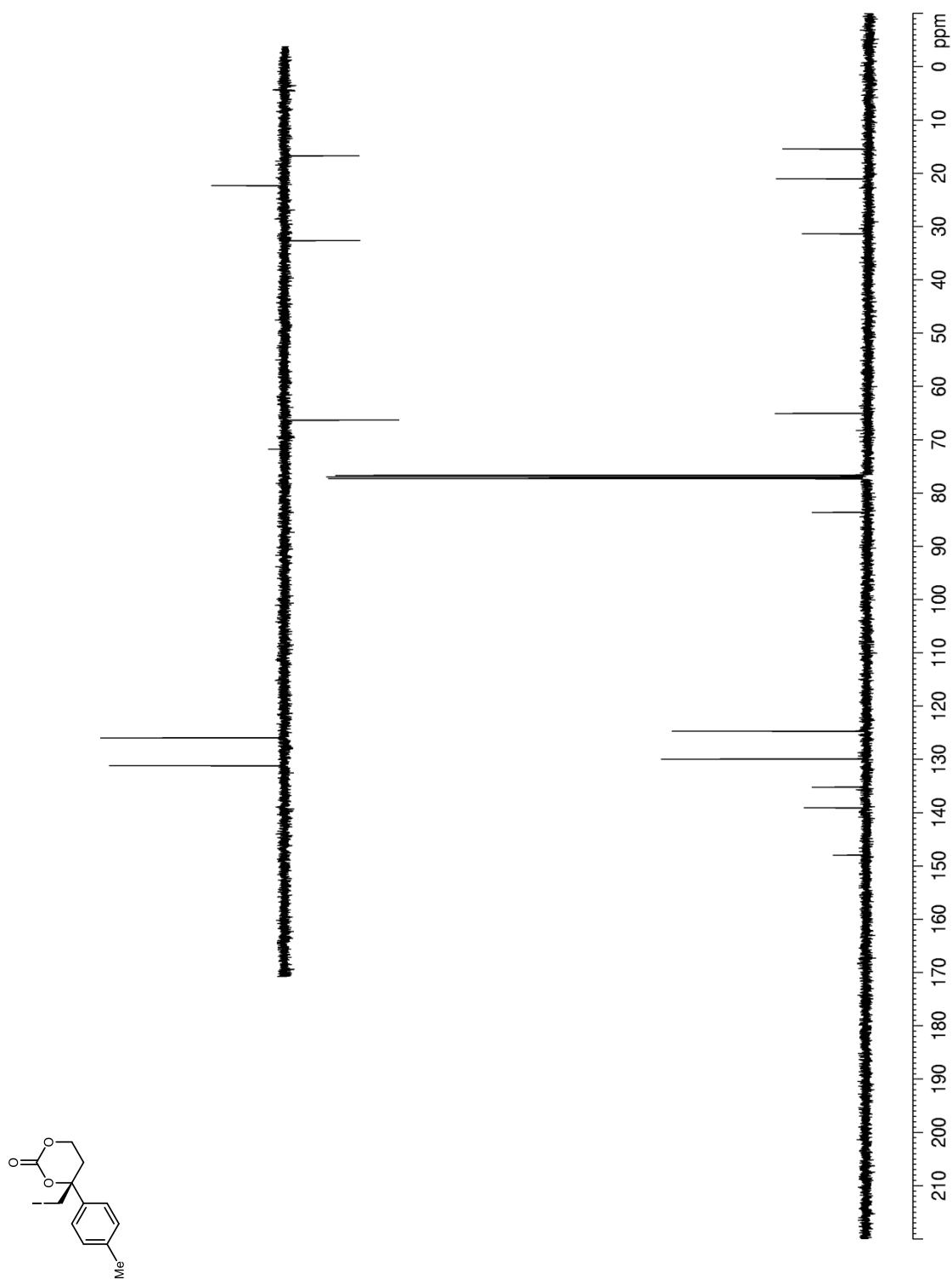
Figure 8. HPLC trace of **45.**
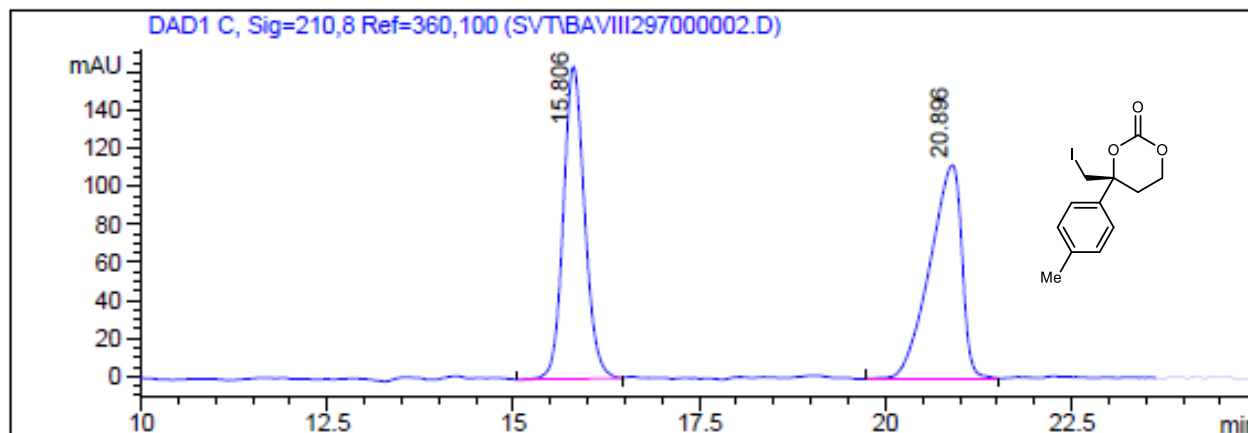

```
Signal  1: DAD1 C, Sig=210,8 Ref=360,100

   Peak   RT      Width     Area      Area %
   #      [min]   [min]

   ------------------------------------------
   1    15.806   0.331   3268.098    49.30
   2    20.896   0.498   3360.896    50.70
   ------------------------------------------
```
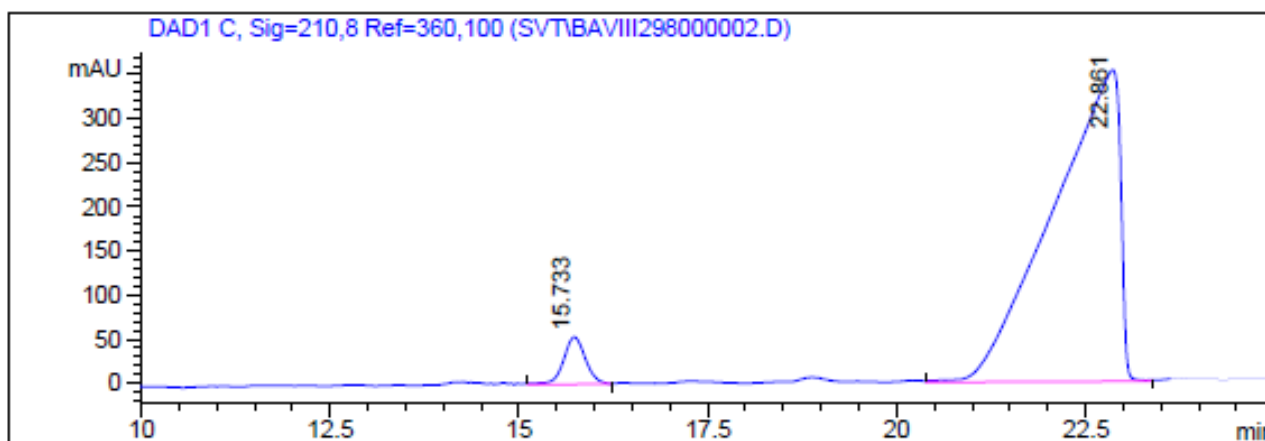


```
Signal  1: DAD1 C, Sig=210,8 Ref=360,100

   Peak   RT      Width     Area      Area %
   #      [min]   [min]

   ------------------------------------------
   1    15.733   0.336    1075.862    4.70
   2    22.861   1.030  21816.816   95.30
   ------------------------------------------
```

Figure 9. ^{1}H NMR (400 MHz, CDCl$_3$) of **46.**
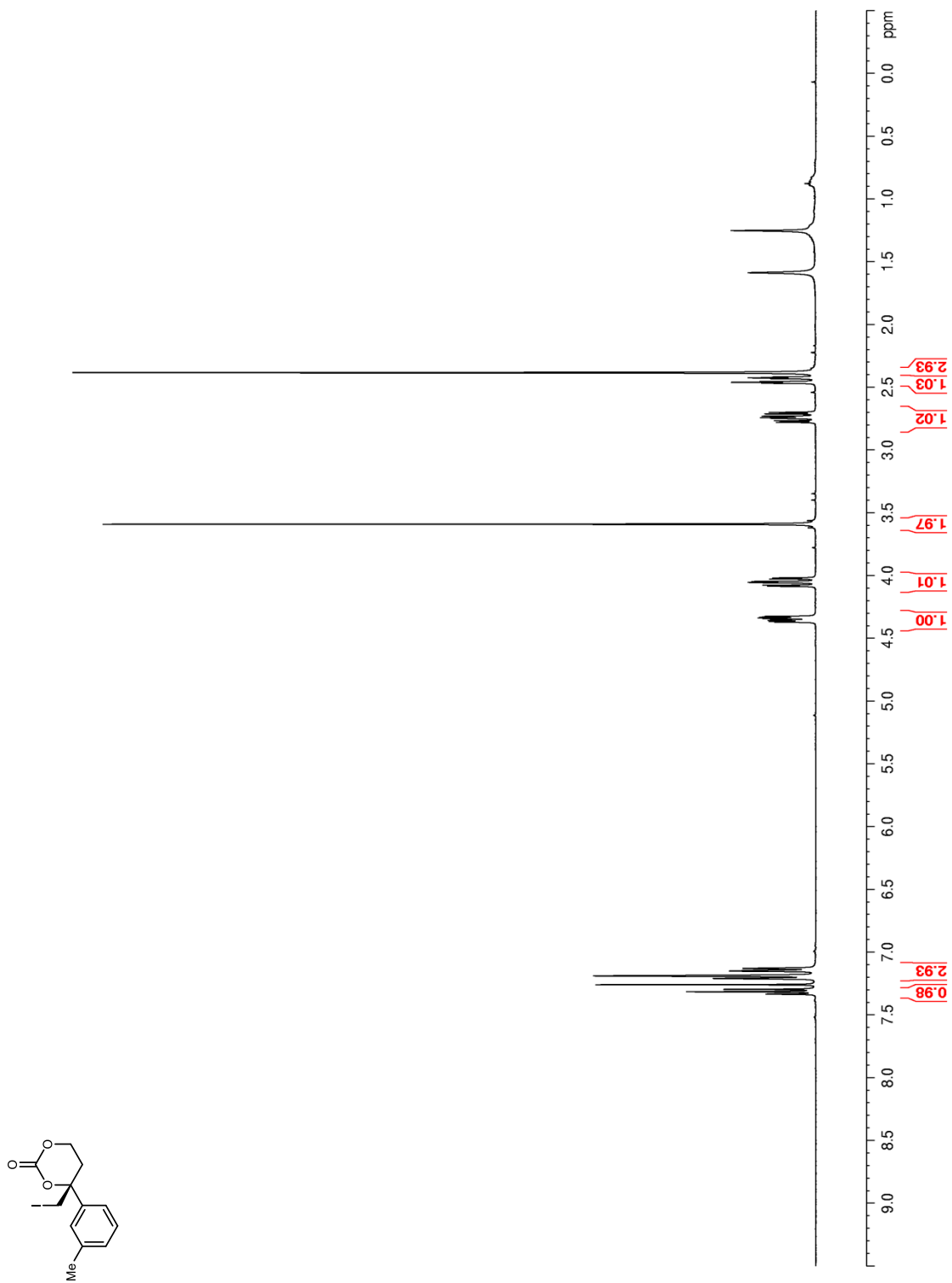
Figure 10. ^{13}C NMR (100 MHz, CDCl$_3$) of **46.**
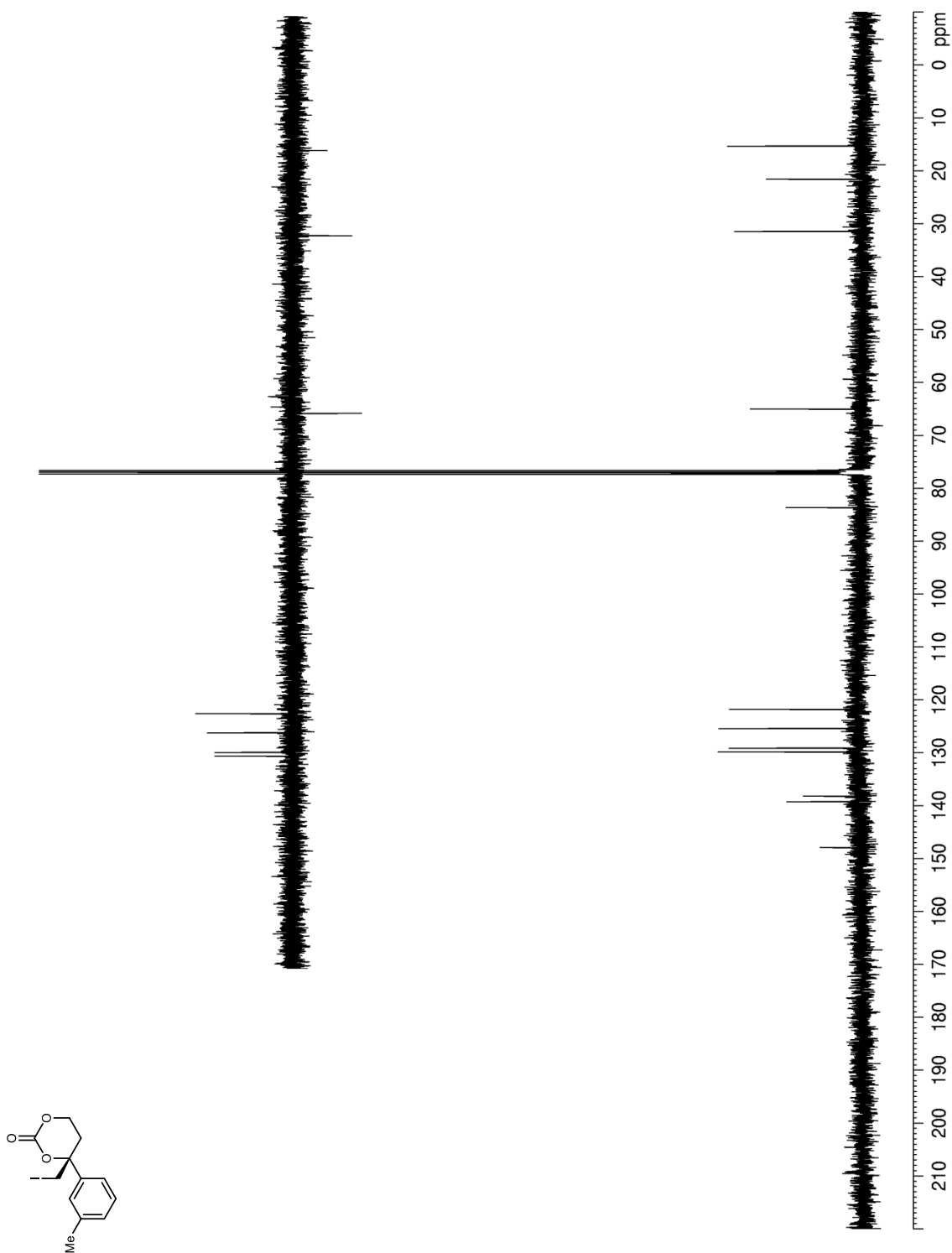
Figure 11. HPLC trace of **46.**
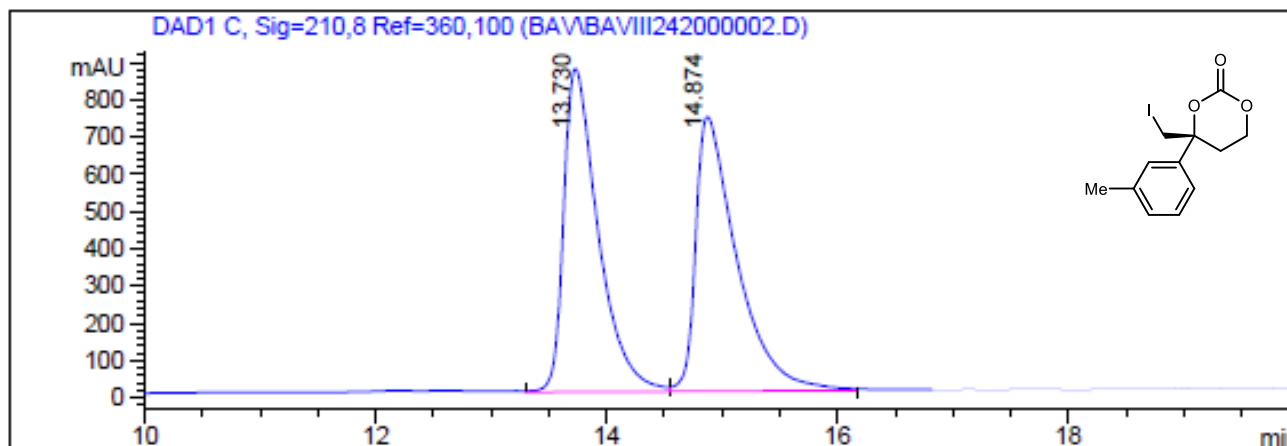

```
Signal  1: DAD1 C, Sig=210,8 Ref=360,100

    Peak    RT      Width      Area      Area %
    #      [min]    [min]
    ---------------------------------------------
    1     13.730   0.347   18033.313    49.69
    2     14.874   0.413   18255.705    50.31
    ---------------------------------------------
```
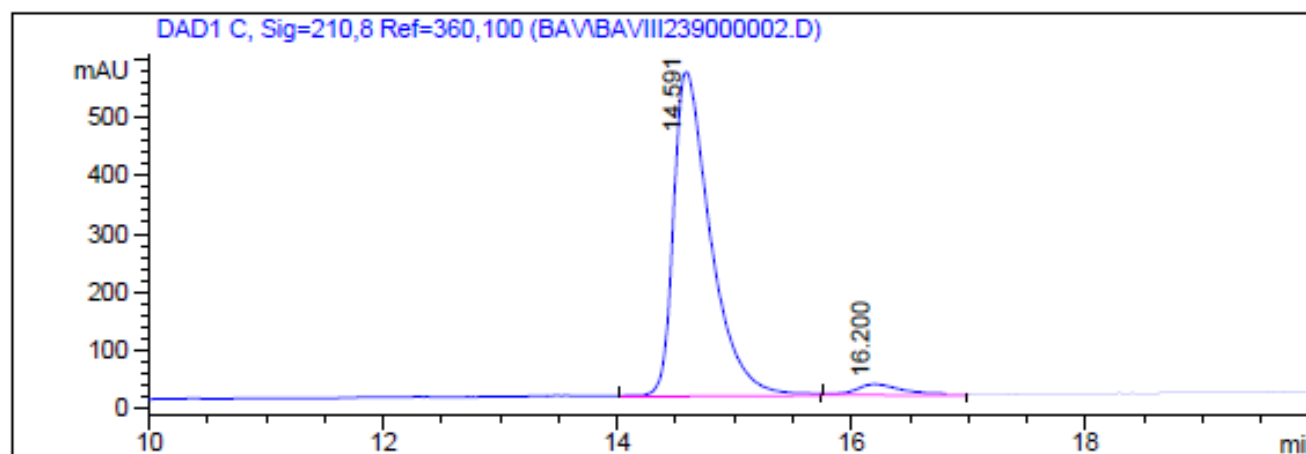


```
Signal  1: DAD1 C, Sig=210,8 Ref=360,100

    Peak    RT      Width      Area      Area %
    #      [min]    [min]
    ---------------------------------------------
    1     14.591   0.367   12271.151    95.67
    2     16.200   0.495     554.742     4.33
    ---------------------------------------------
```

Figure 12. ^{1}H NMR (500 MHz, CDCl$_3$) of **48.**

Figure 13. ^{13}C NMR (126 MHz, CDCl$_3$) of **48.**
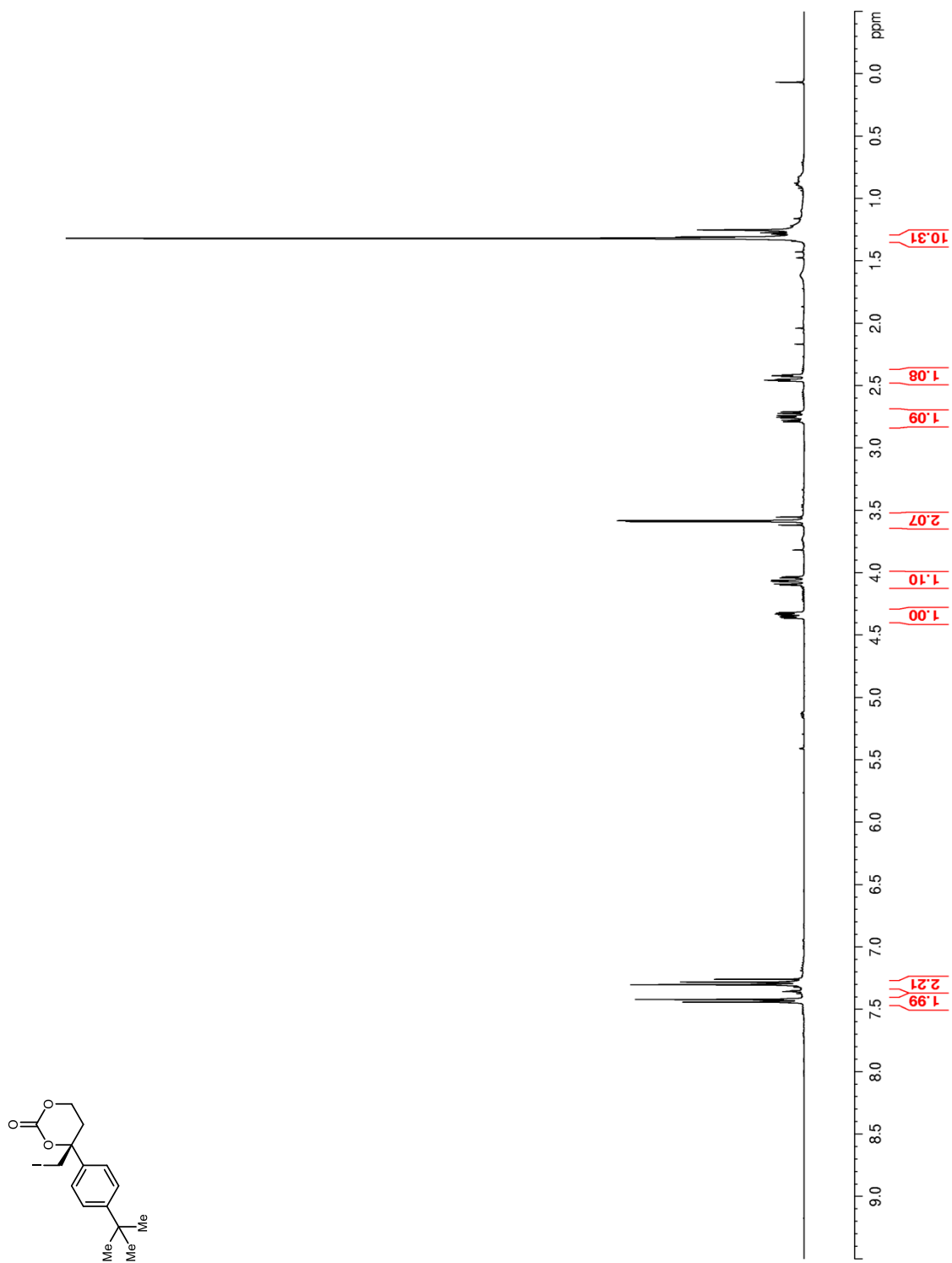
Figure 14. HPLC trace of **48.**
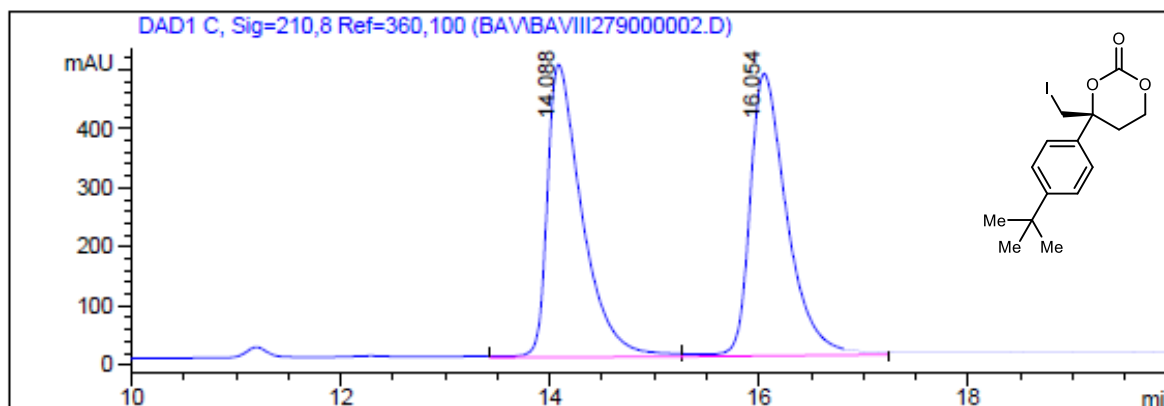
Signal 1: DAD1 C, Sig=210,8 Ref=360,100

```
Peak    RT      Width     Area      Area %
 #     [min]    [min]
---------------------------------------------
 1    14.088   0.386  11486.315    49.32
 2    16.054   0.412  11803.989    50.68
---------------------------------------------
```
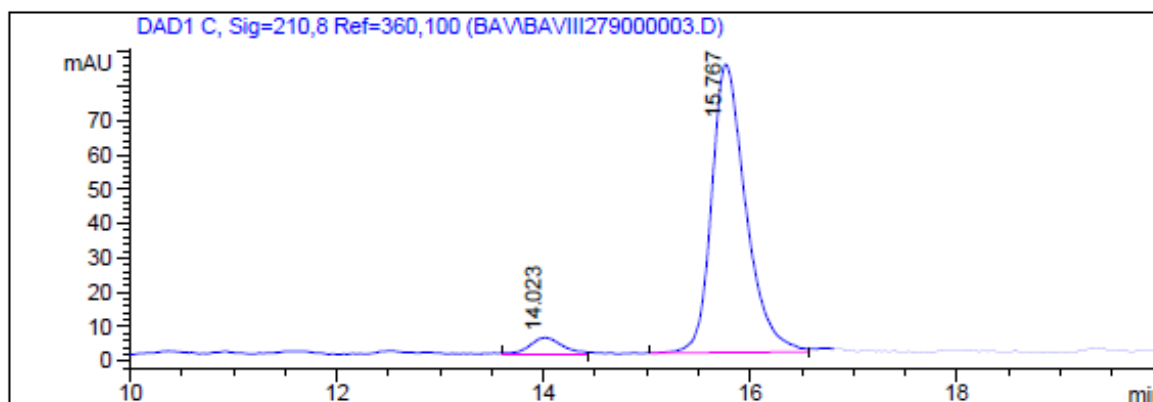

Signal 1: DAD1 C, Sig=210,8 Ref=360,100

```
Peak    RT      Width     Area      Area %
 #     [min]    [min]
---------------------------------------------
 1    14.023   0.355    98.501     4.85
 2    15.767   0.384  1930.406    95.15
---------------------------------------------
```

Figure 15. ^{1}H NMR (400 MHz, CDCl$_3$) of **49.**
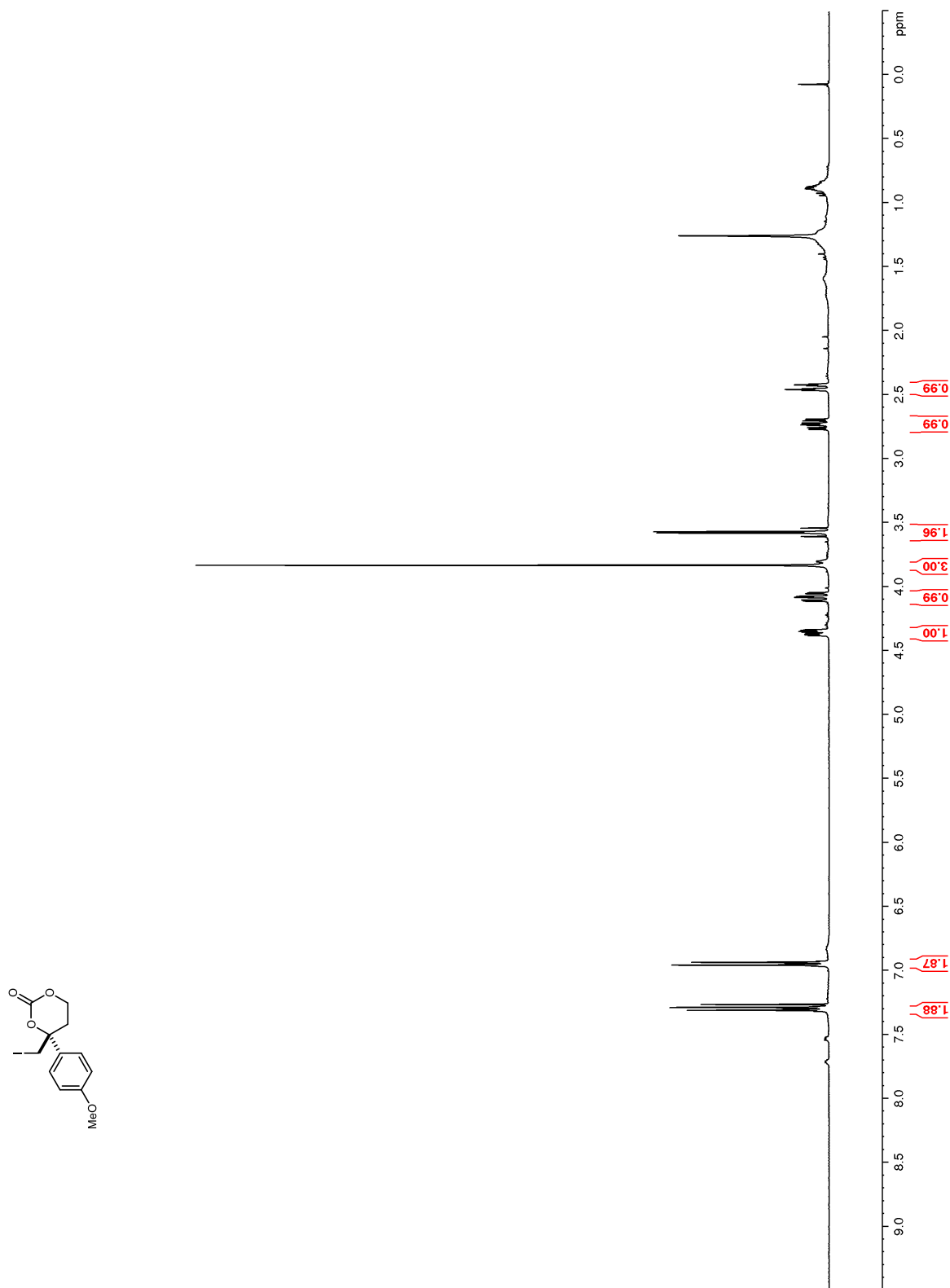
Figure 16. ^{13}C NMR (100 MHz, CDCl$_3$) of **49.**
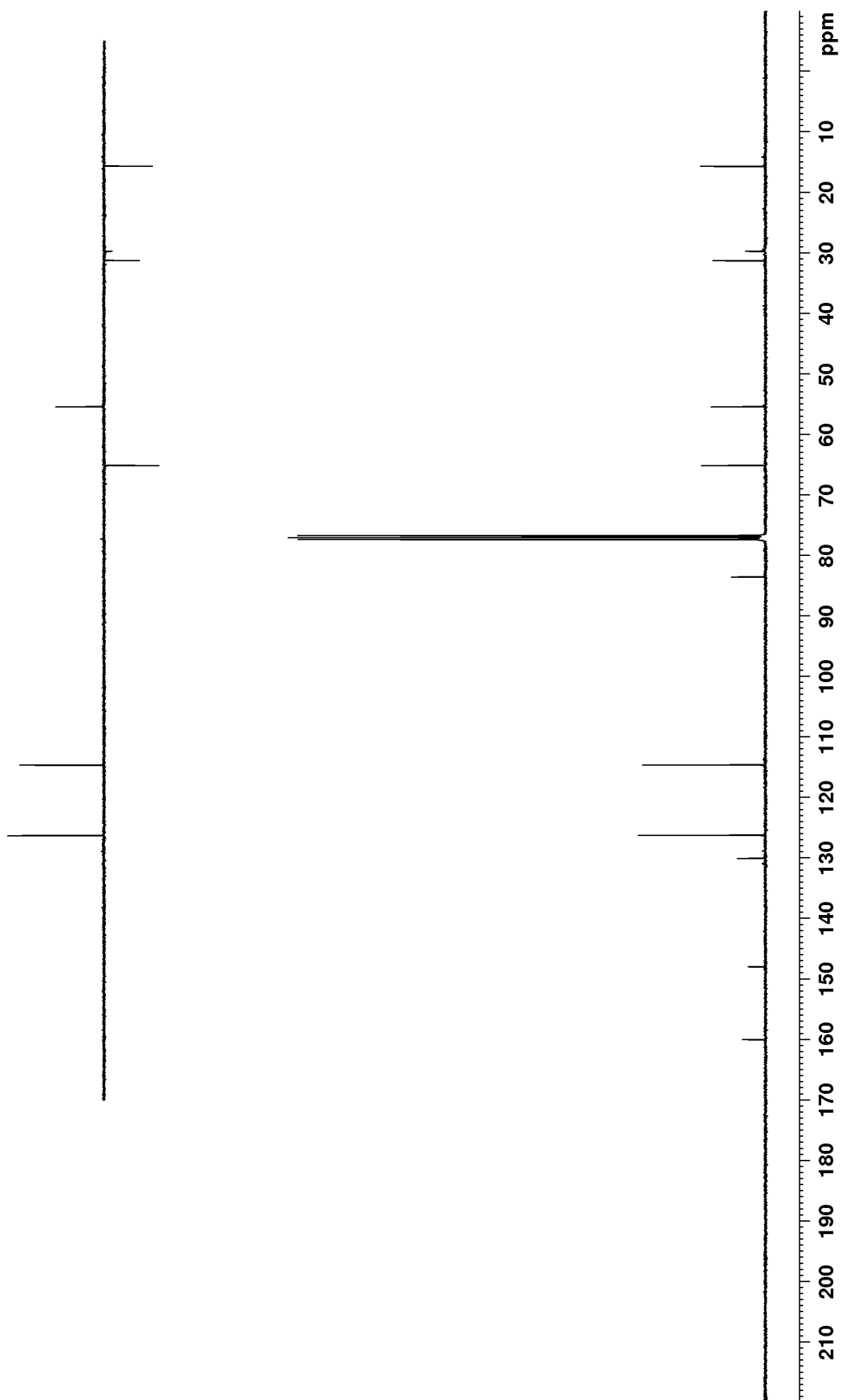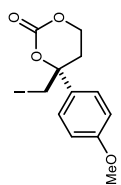
Figure 17. HPLC trace of **49.**
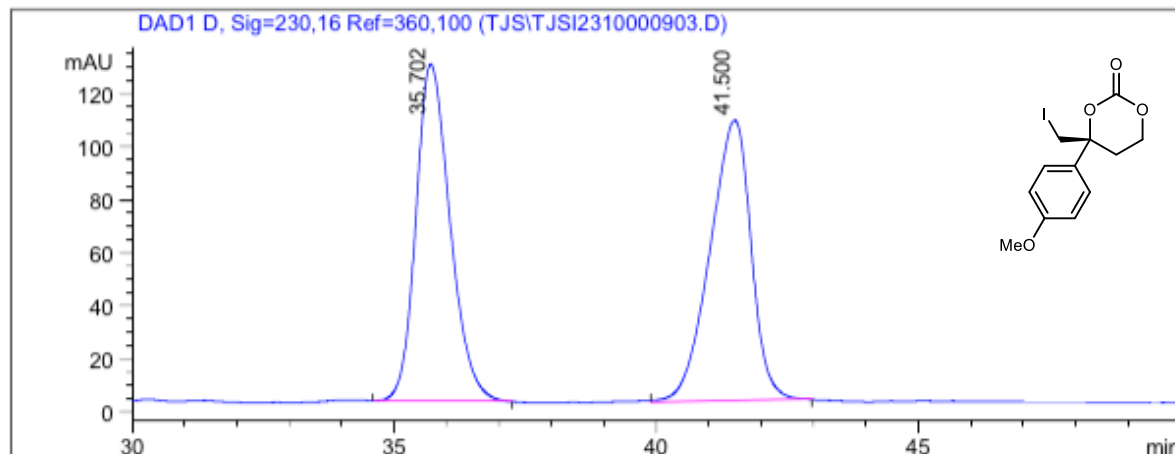

```
Signal  1: DAD1 D, Sig=230,16 Ref=360,100

  Peak    RT      Width      Area       Area %
  #      [min]   [min]
  --------------------------------------------
   1    35.702  0.754    5742.137     49.82
   2    41.500  0.913    5784.685     50.18
  --------------------------------------------
```
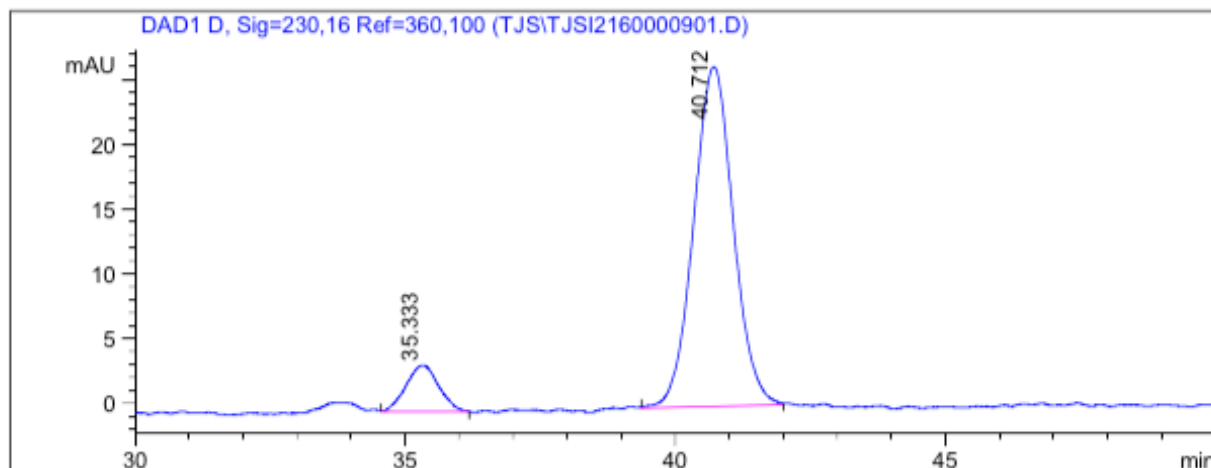


```
Signal  1: DAD1 D, Sig=230,16 Ref=360,100

  Peak    RT      Width      Area       Area %
  #      [min]   [min]
  --------------------------------------------
   1    35.333  0.703     150.324     10.10
   2    40.712  0.853    1338.295     89.90
  --------------------------------------------
```

Figure 18. ^{1}H NMR (400 MHz, CDCl3) of **50.**
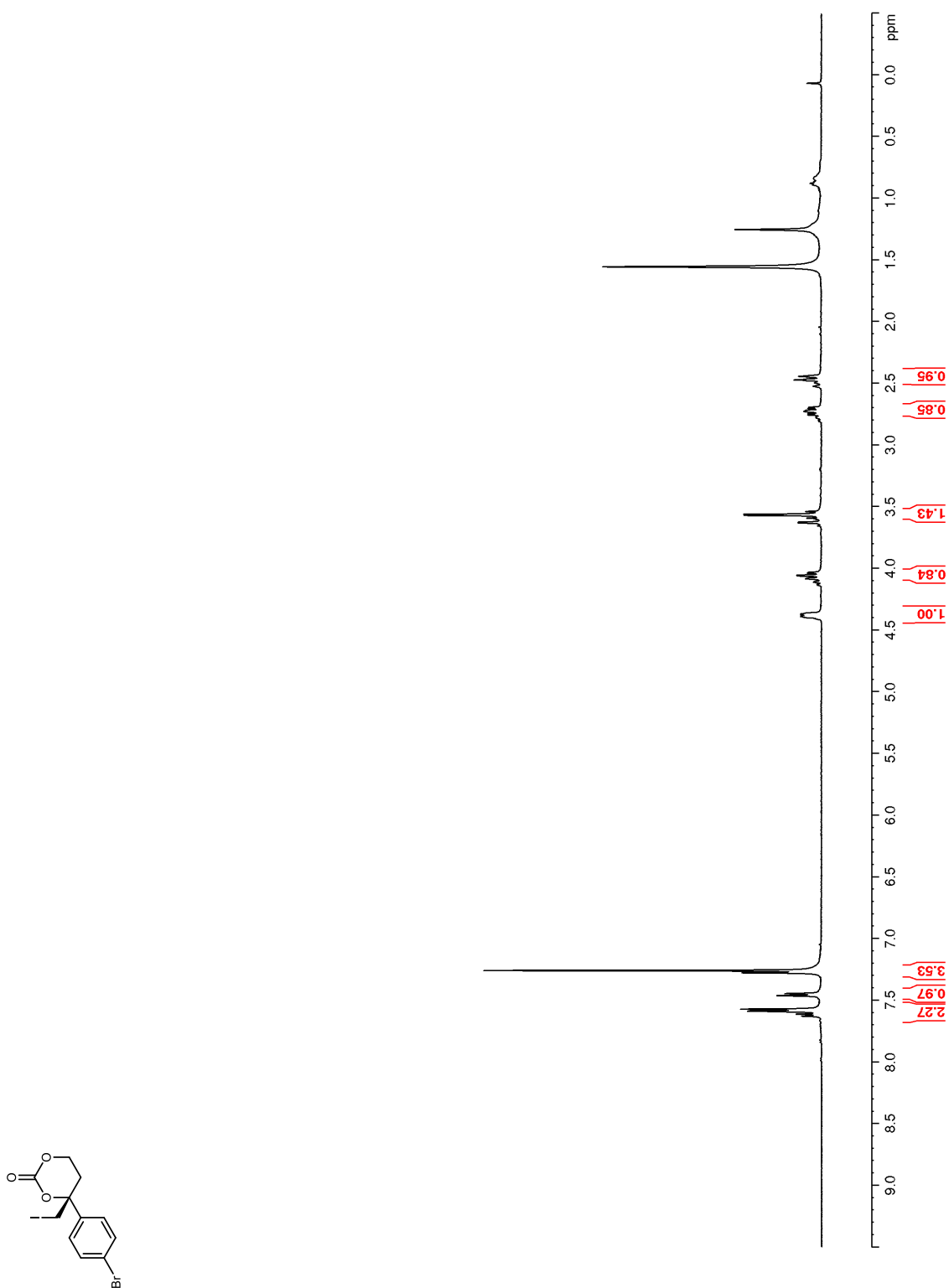
Figure 19. ^{13}C NMR (100 MHz, CDCl$_3$) of **50.**
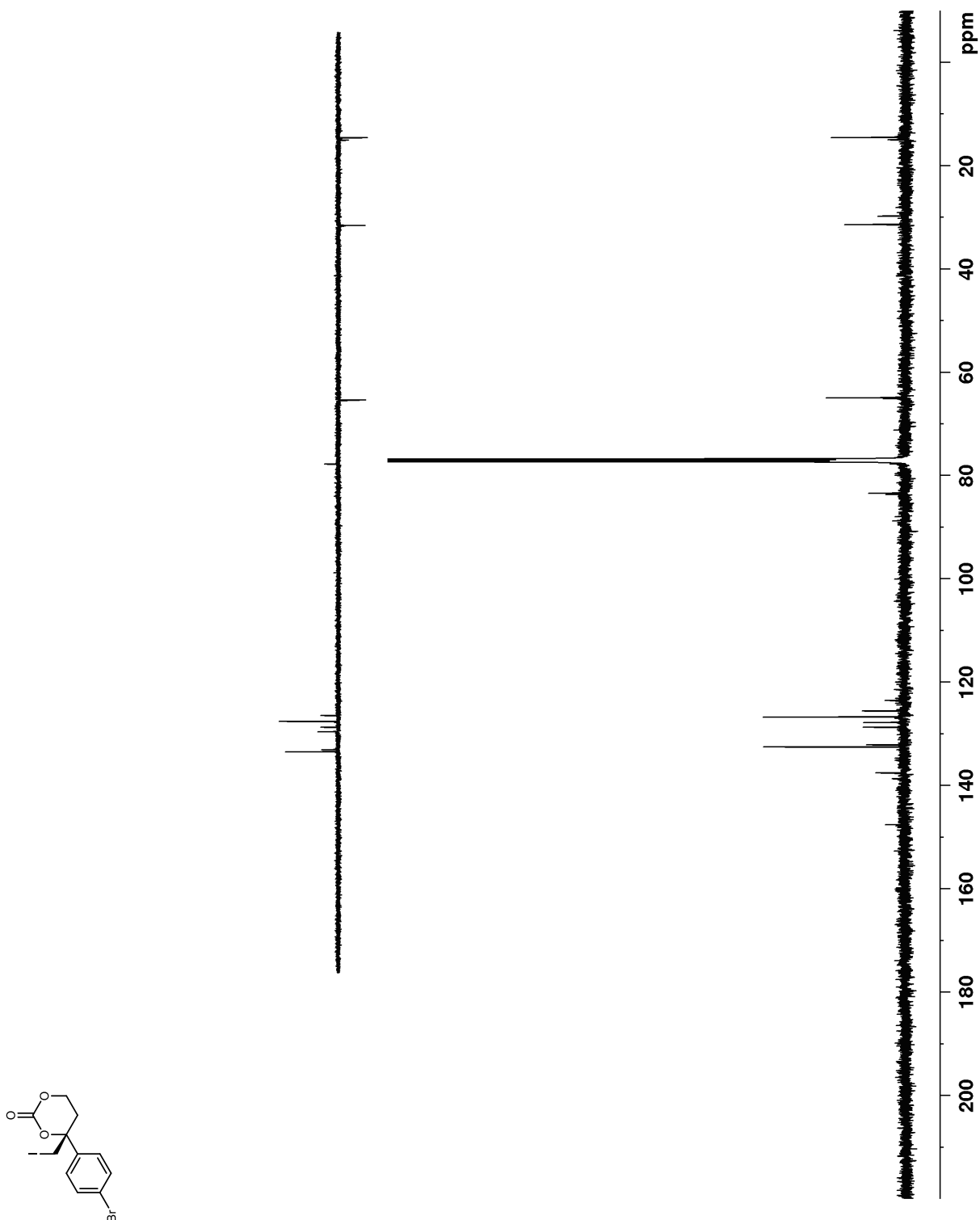
Figure 20. HPLC trace of **50.**
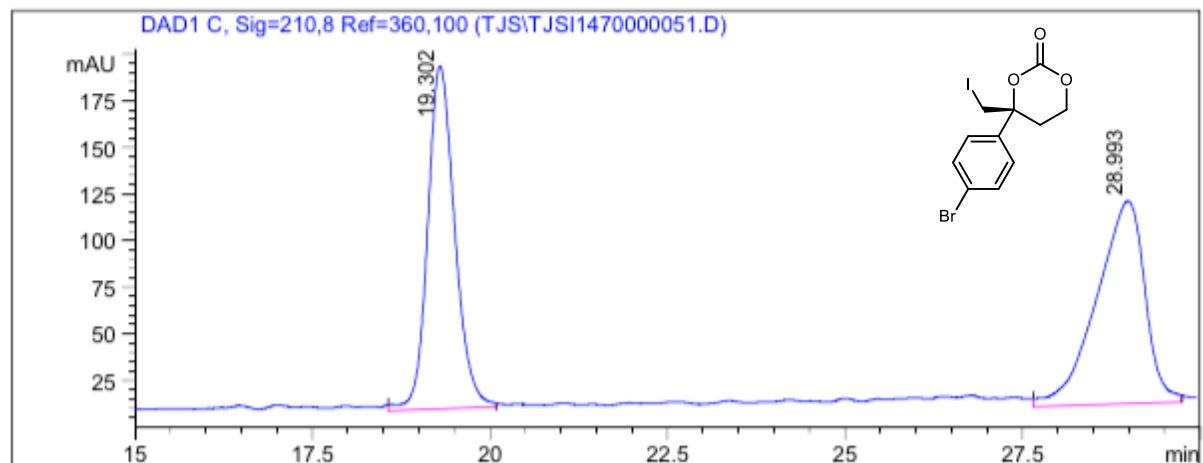

```
Signal  1: DAD1 C, Sig=210,8 Ref=360,100

   Peak    RT      Width     Area      Area %
    #     [min]    [min]
  -----------------------------------------------
    1    19.302   0.444   4894.816    48.61
    2    28.993   0.793   5175.311    51.39
  -----------------------------------------------
```
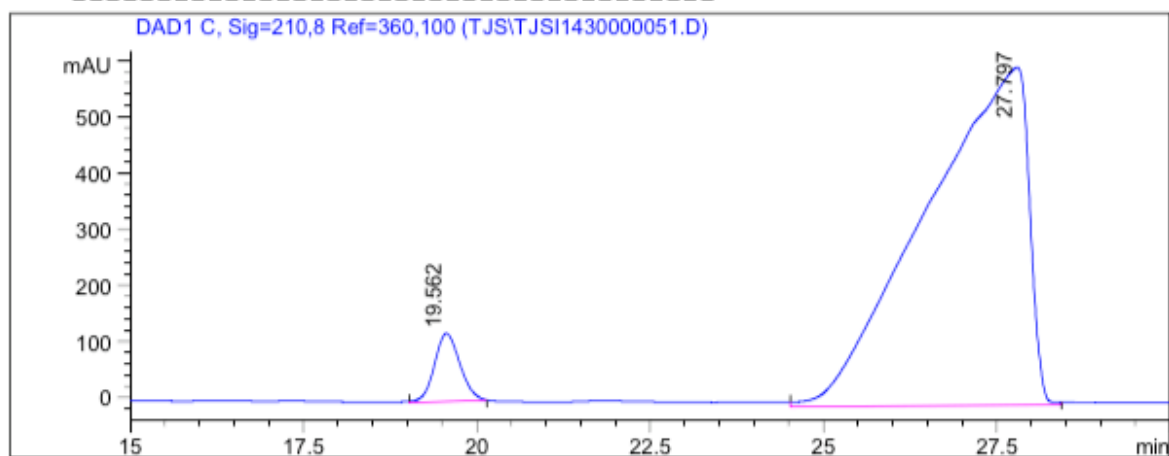


```
Signal  1: DAD1 C, Sig=210,8 Ref=360,100

   Peak    RT      Width     Area      Area %
    #     [min]    [min]
  -----------------------------------------------
    1    19.562   0.427   3097.948     4.76
    2    27.797   1.722  62043.488    95.24
  -----------------------------------------------
```

Figure 21. ^{1}H NMR (400 MHz, CDCl$_3$) of **51.**
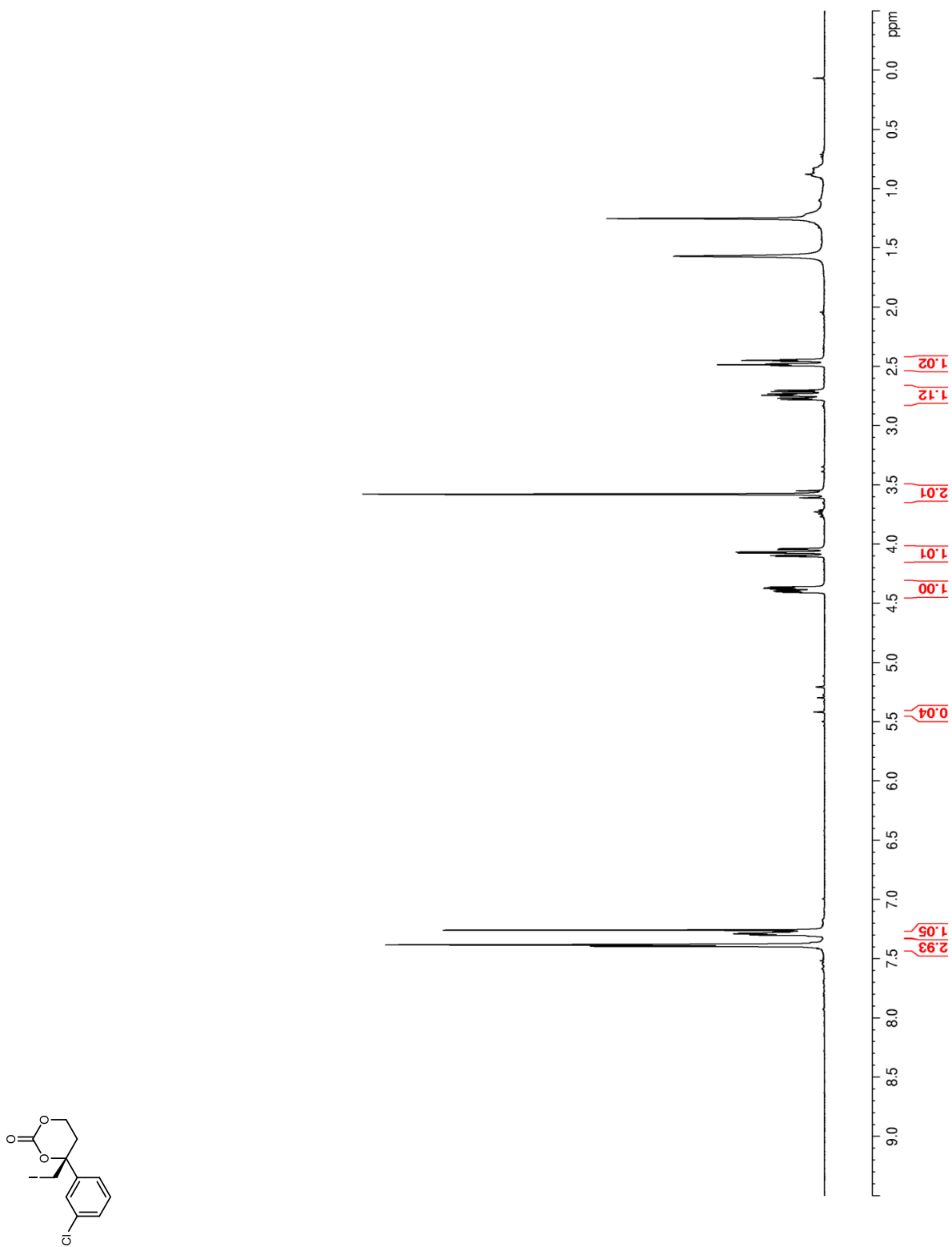
Figure 22. ^{13}C NMR (100 MHz, CDCl$_3$) of **51.**
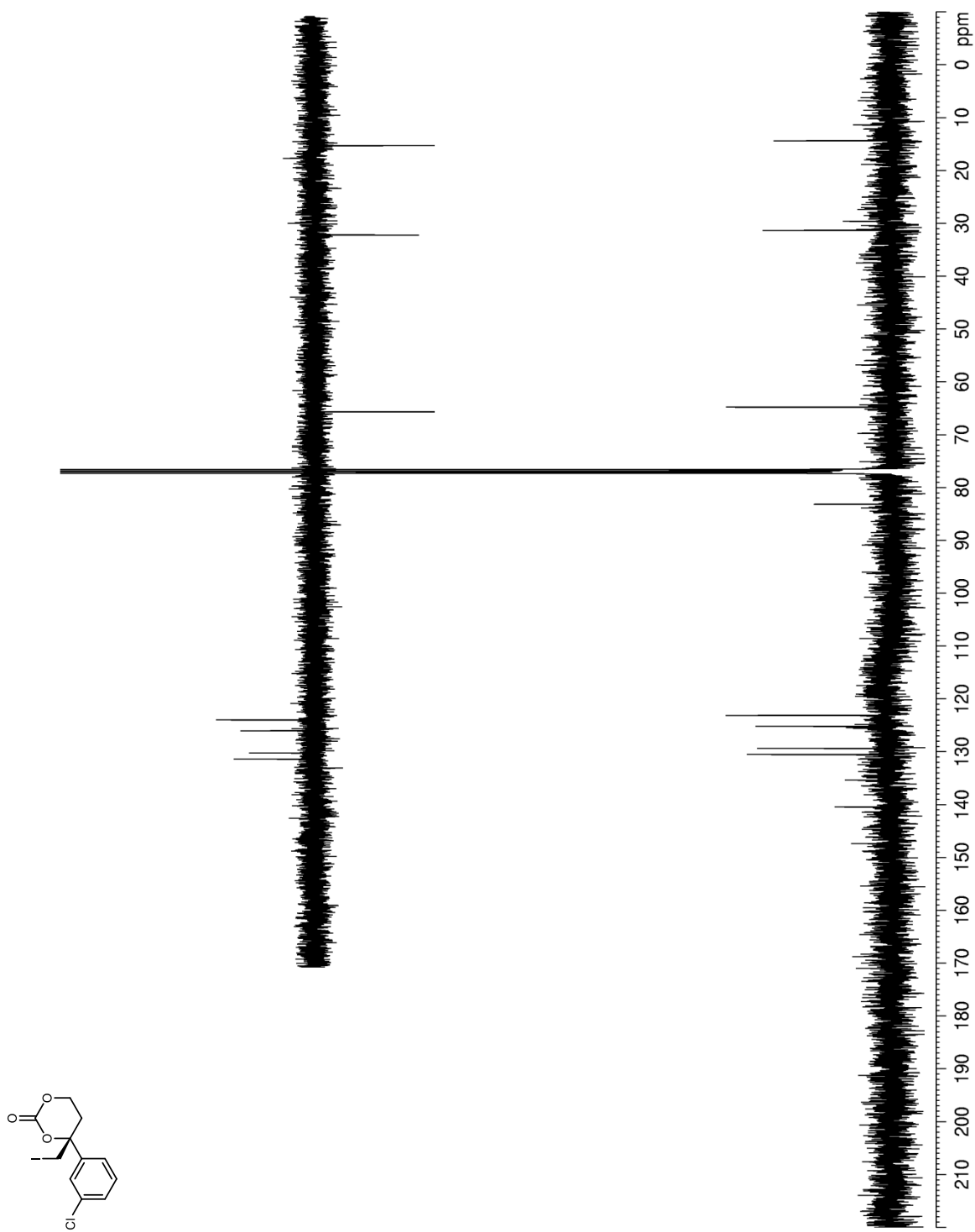
Figure 23. HPLC trace of **51.**
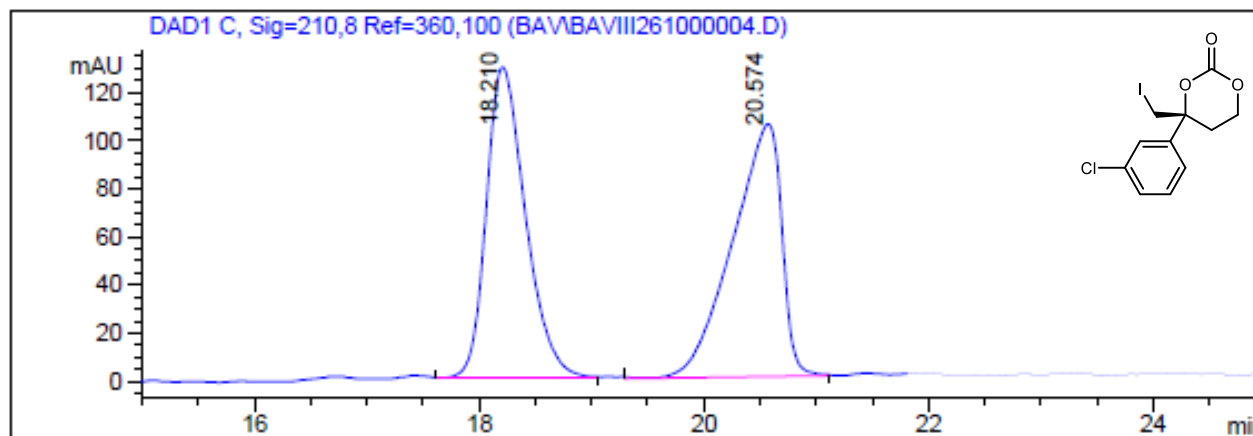

```
Signal  1: DAD1 C, Sig=210,8 Ref=360,100

    Peak    RT      Width     Area      Area %
    #      [min]    [min]
    ----------------------------------------------
      1    18.210   0.407   3165.705    49.66
      2    20.574   0.509   3208.489    50.34
    ----------------------------------------------
```
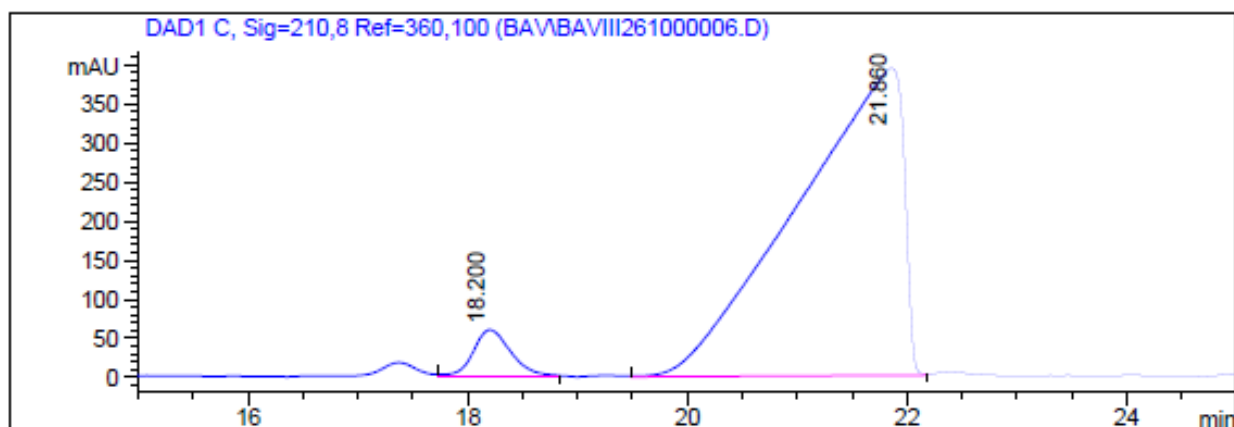


```
Signal  1: DAD1 C, Sig=210,8 Ref=360,100

    Peak    RT      Width      Area       Area %
    #      [min]    [min]
    -------------------------------------------------
      1    18.200   0.396    1408.968      5.06
      2    21.860   1.121   26446.949     94.94
    -------------------------------------------------
```

Figure **24**. ^{1}H NMR (400 MHz, CDCl$_3$) of **52.**
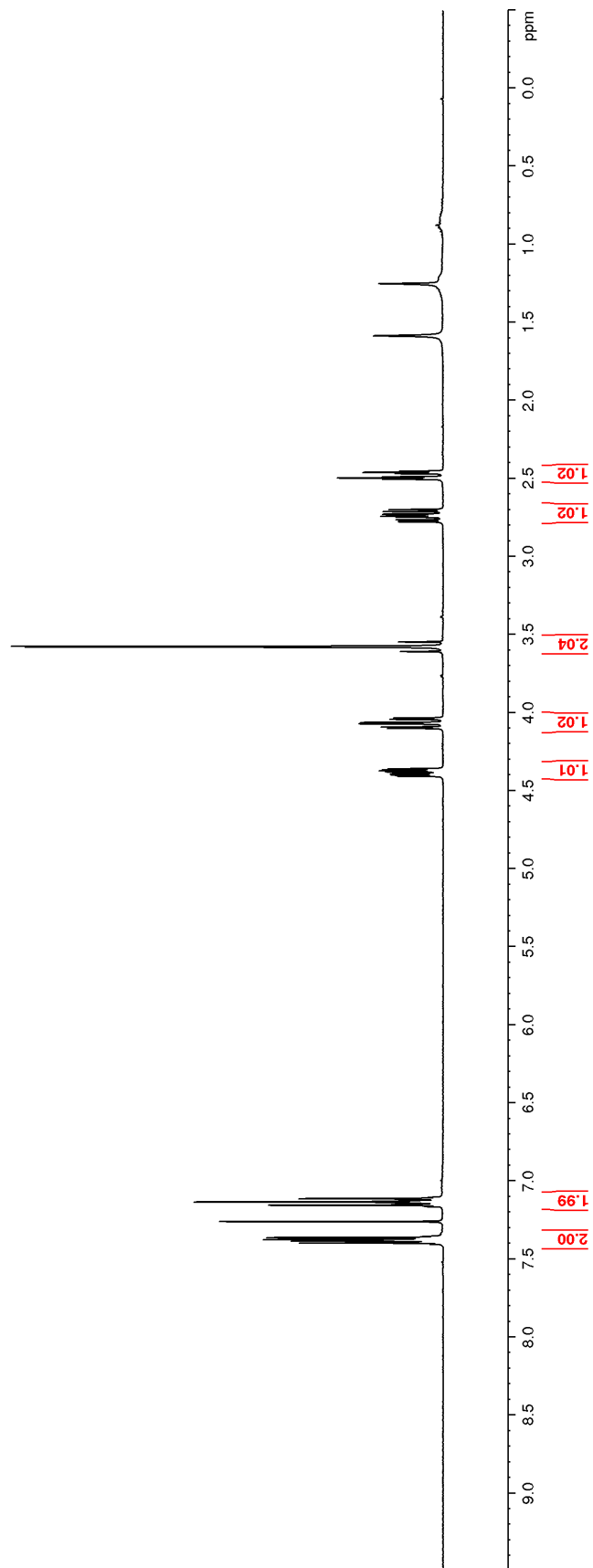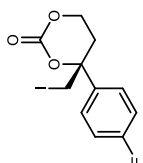
Figure **25**. ^{13}C NMR (100 MHz, CDCl$_3$) of **52.**
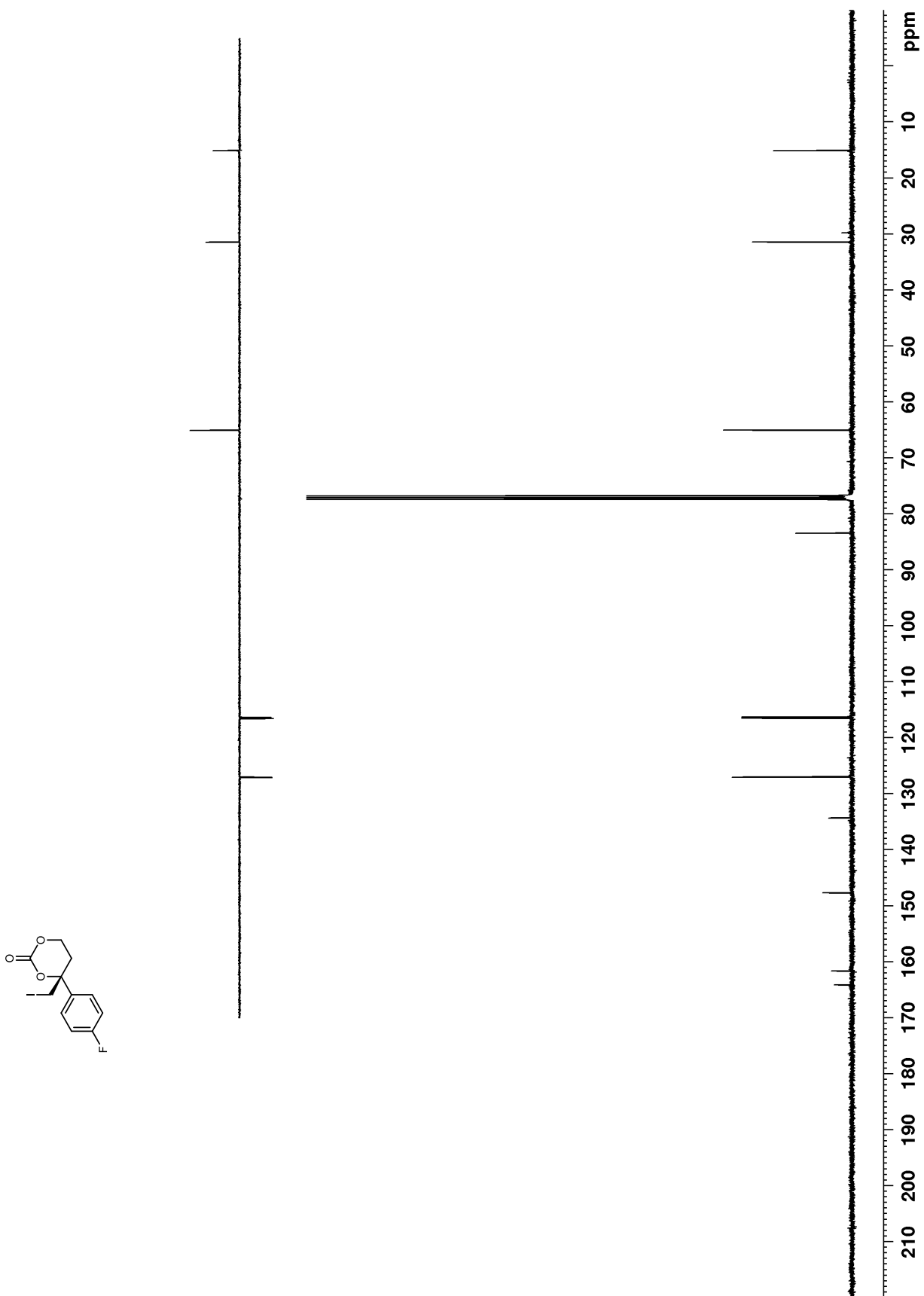
Figure 26. HPLC trace of **52.**
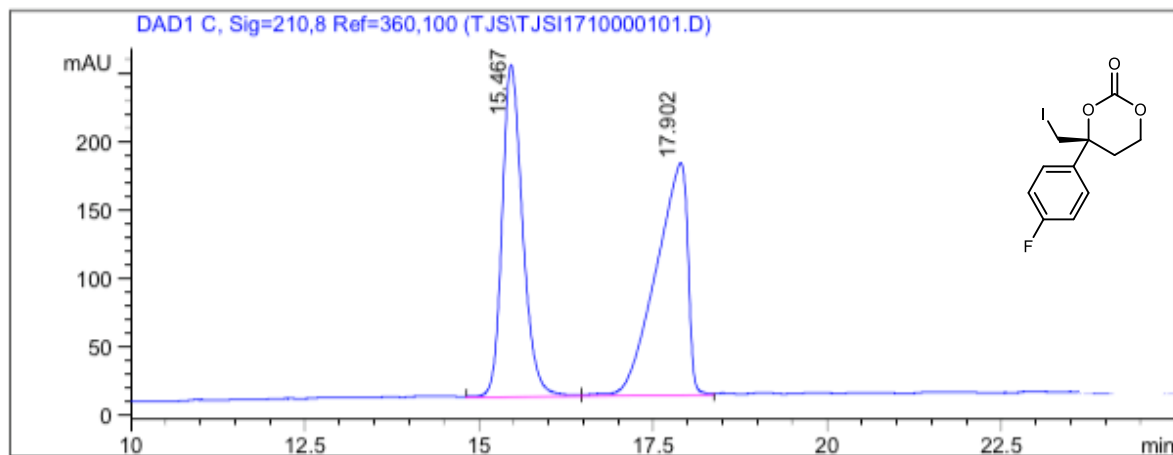

```
Signal  1: DAD1 C, Sig=210,8 Ref=360,100


   Peak    RT      Width     Area      Area %
   #      [min]    [min]

 ----------------------------------------
    1    15.467   0.342   4983.125    47.94
    2    17.902   0.532   5411.033    52.06
 ----------------------------------------
```
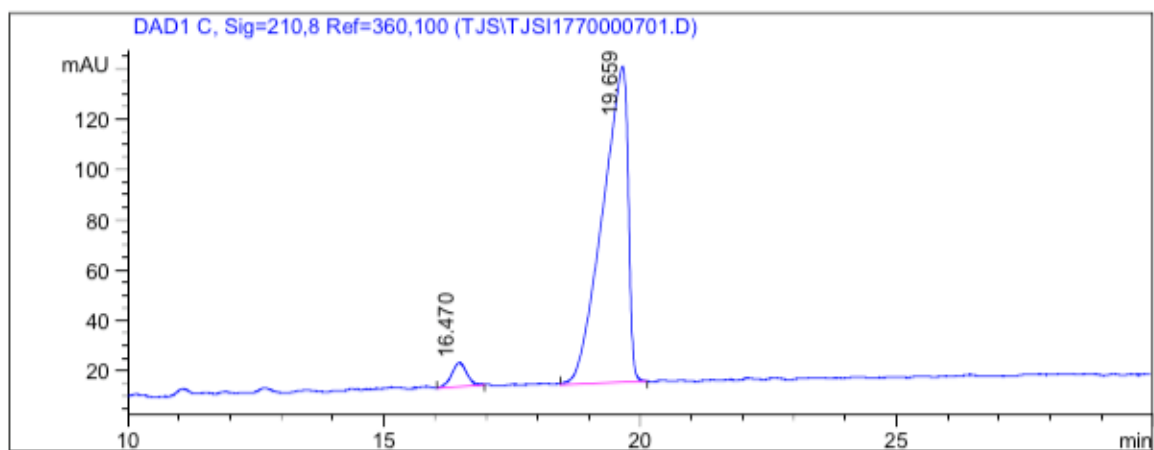


```
Signal  1: DAD1 C, Sig=210,8 Ref=360,100


   Peak    RT      Width     Area      Area %
   #      [min]    [min]

 ----------------------------------------
    1    16.470   0.350    201.689     4.43
    2    19.659   0.579   4354.841    95.57
 ----------------------------------------
```

Figure 27. ^{1}H NMR (400 MHz, CDCl$_3$) of **53.**
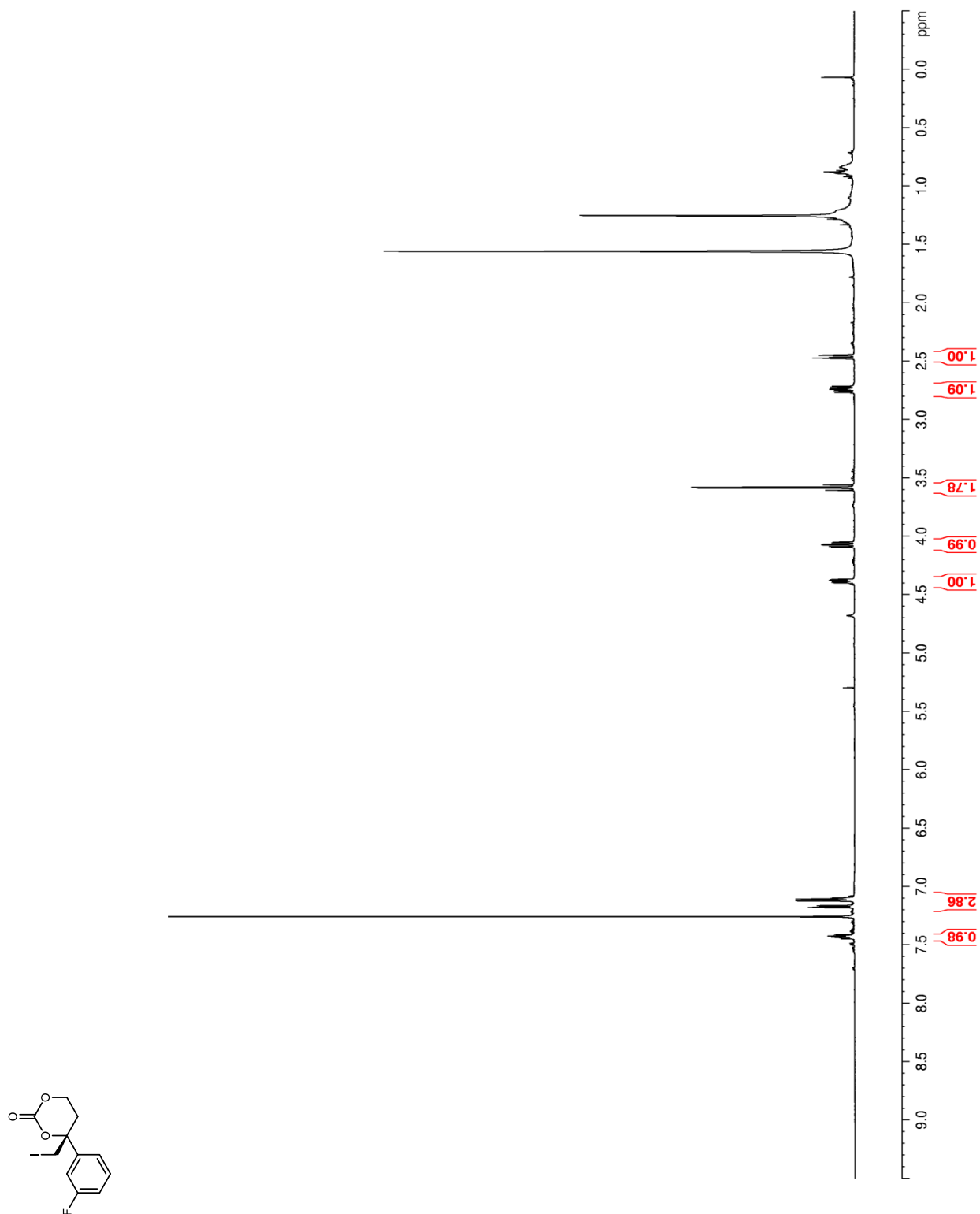
Figure 28. ^{13}C NMR (126 MHz, CDCl$_3$) of **53.**
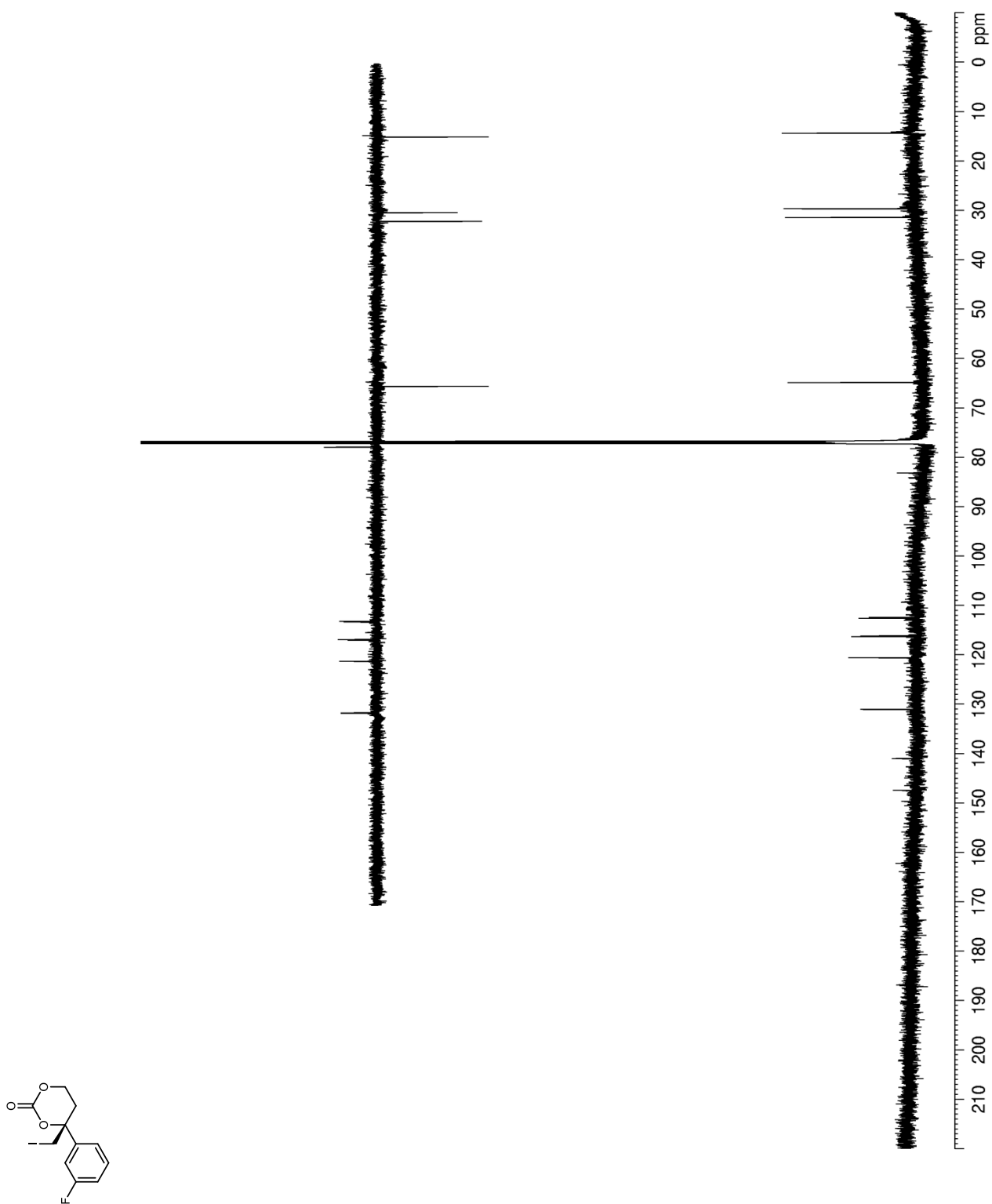
Figure 29. HPLC trace of **53.**
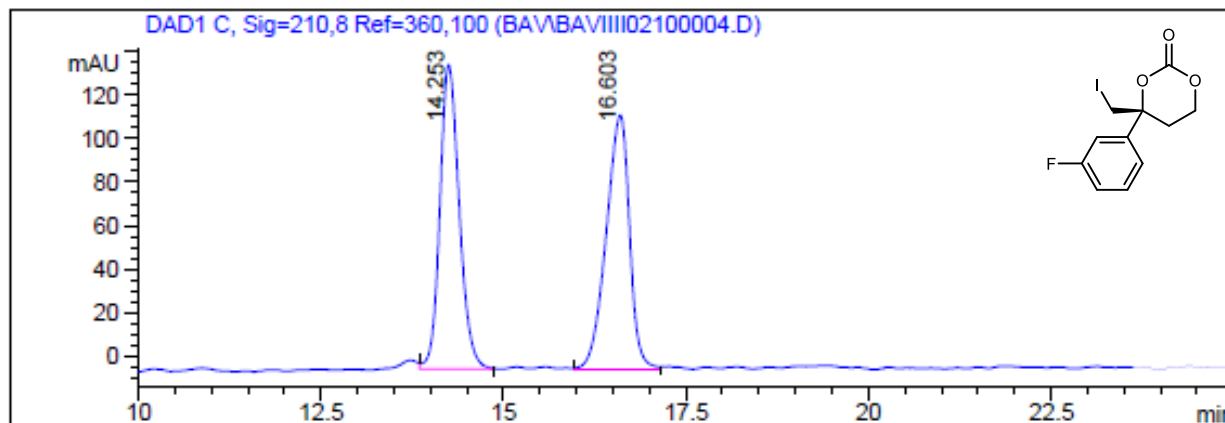

```
Signal  1: DAD1 C, Sig=210,8 Ref=360,100

    Peak    RT      Width       Area      Area %
    #      [min]    [min]
    ----------------------------------------------
     1    14.253   0.308    2582.281    49.84
     2    16.603   0.371    2598.957    50.16
    ----------------------------------------------
```
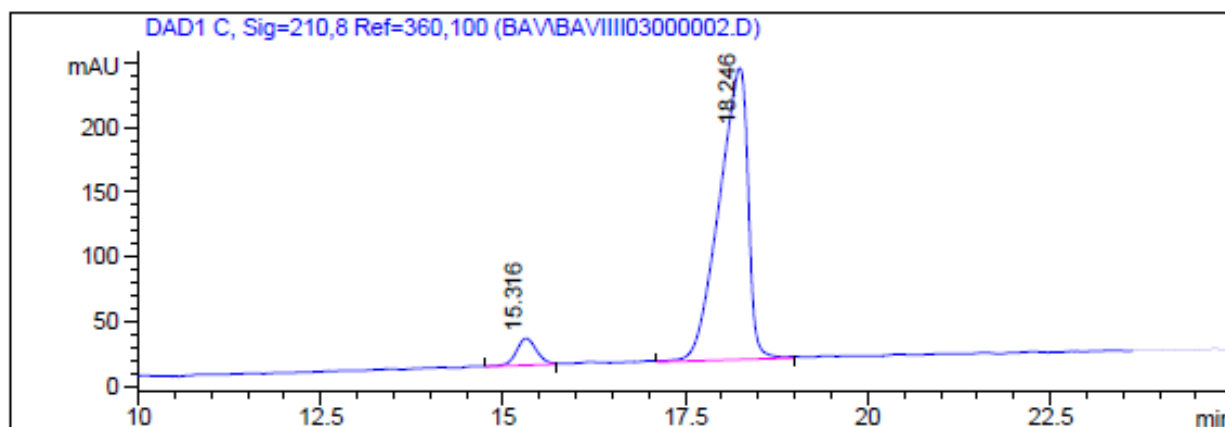


```
Signal  1: DAD1 C, Sig=210,8 Ref=360,100

    Peak    RT      Width       Area      Area %
    #      [min]    [min]
    ----------------------------------------------
     1    15.316   0.320     396.090     5.98
     2    18.246   0.460    6226.796    94.02
    ----------------------------------------------
```

Figure 30. ^{1}H NMR (400 MHz, CDCl$_3$) of **54.**
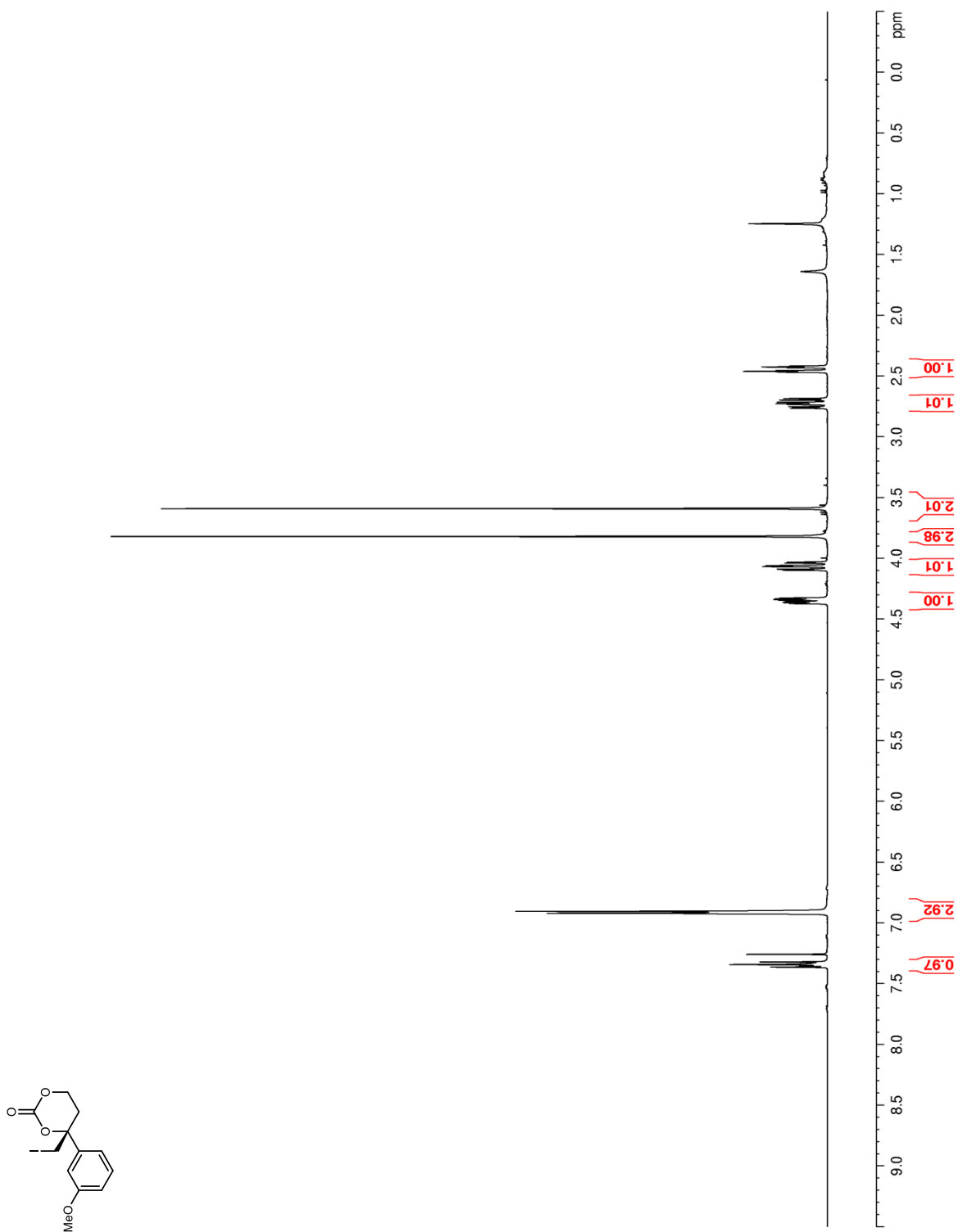
Figure 31. ^{13}C NMR (100 MHz, CDCl$_3$) of **54.**
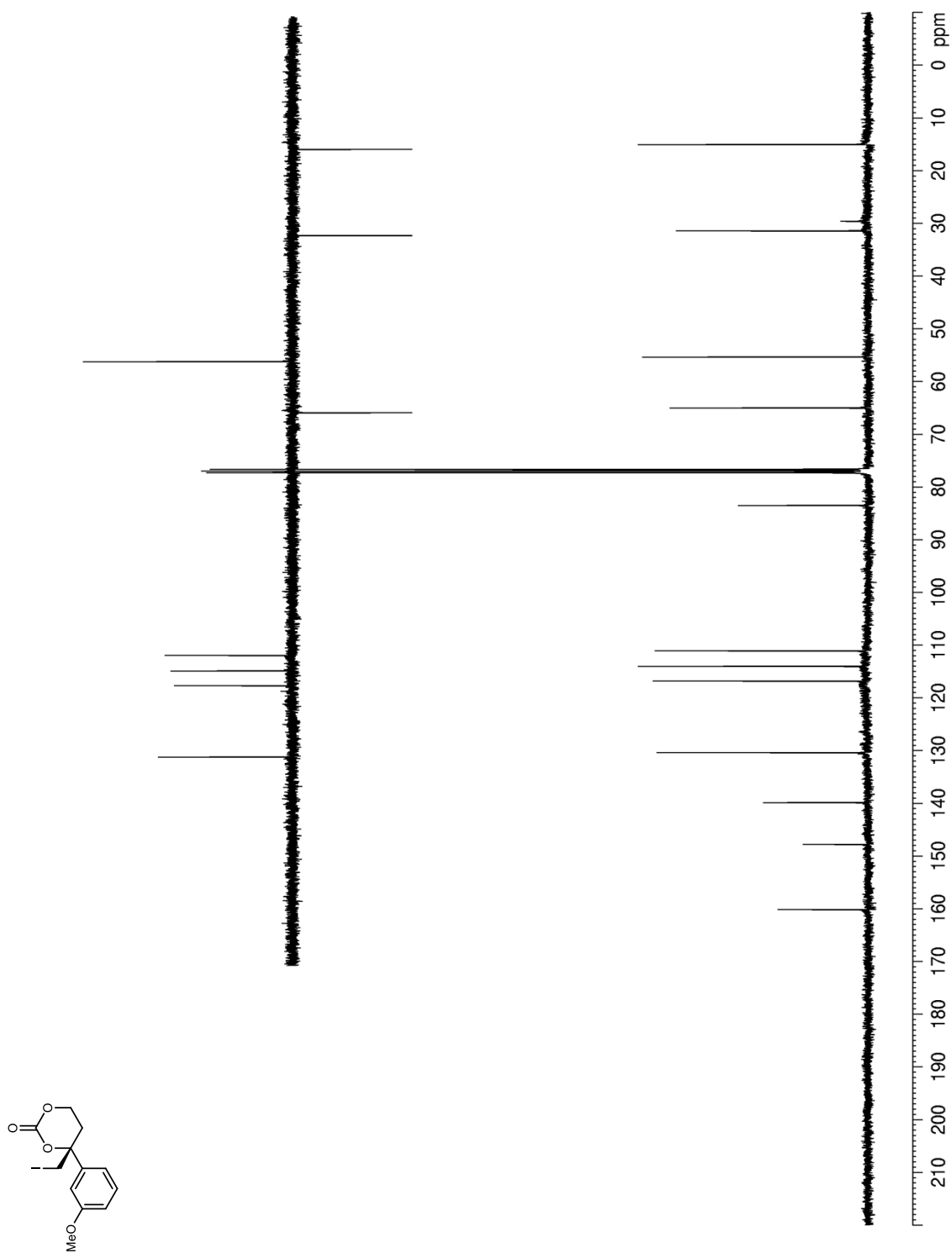
Figure 32. HPLC trace of **54.**
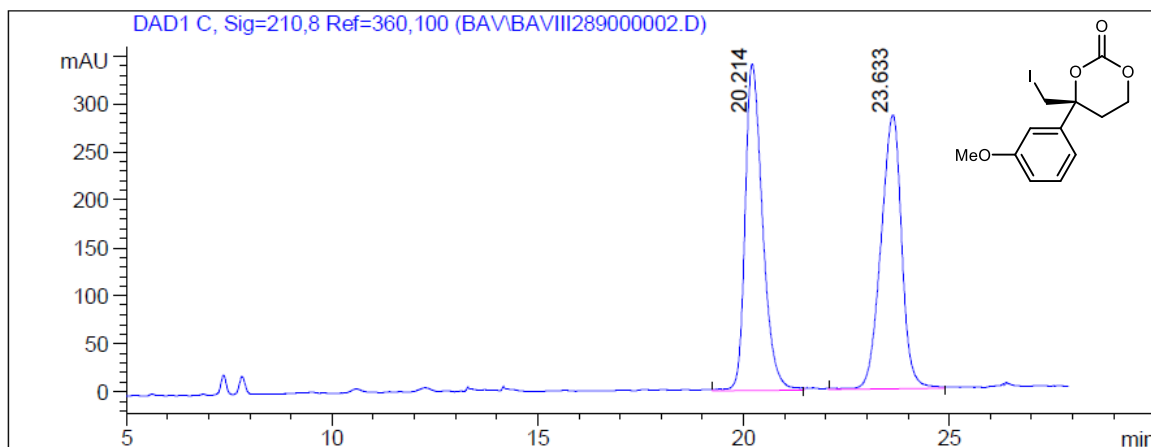

```
Signal   1: DAD1 C, Sig=210,8 Ref=360,100


   Peak    RT      Width      Area      Area %
    #     [min]    [min]
  -------------------------------------------
    1    20.214   0.490  10007.156    49.99
    2    23.633   0.584  10009.657    50.01
  -------------------------------------------
```
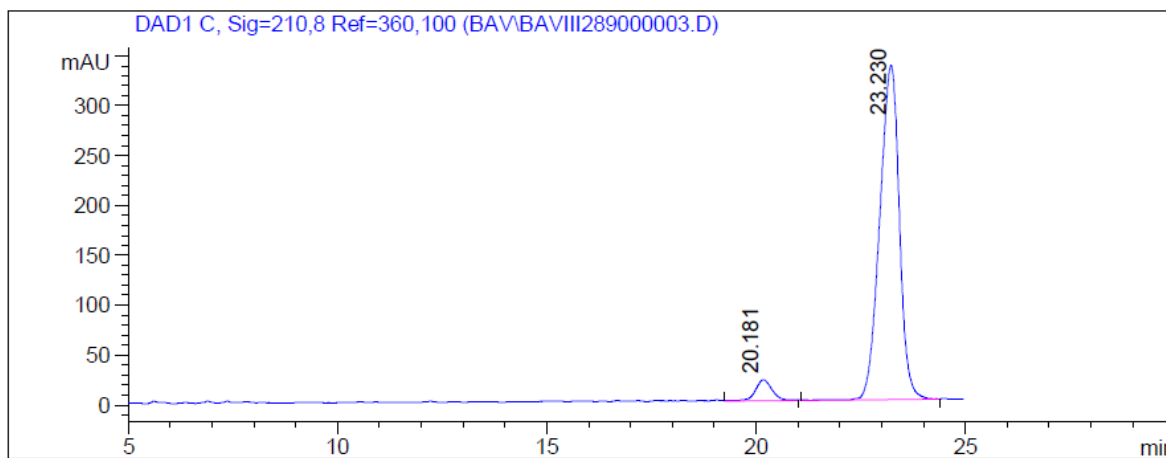


```
Signal   1: DAD1 C, Sig=210,8 Ref=360,100


   Peak    RT      Width      Area      Area %
    #     [min]    [min]
  -------------------------------------------
    1    20.181   0.471    603.124     5.24
    2    23.230   0.542  10897.025    94.76
  -------------------------------------------
```

Figure 33. ^{1}H NMR (400 MHz, CDCl$_3$) of **59.**
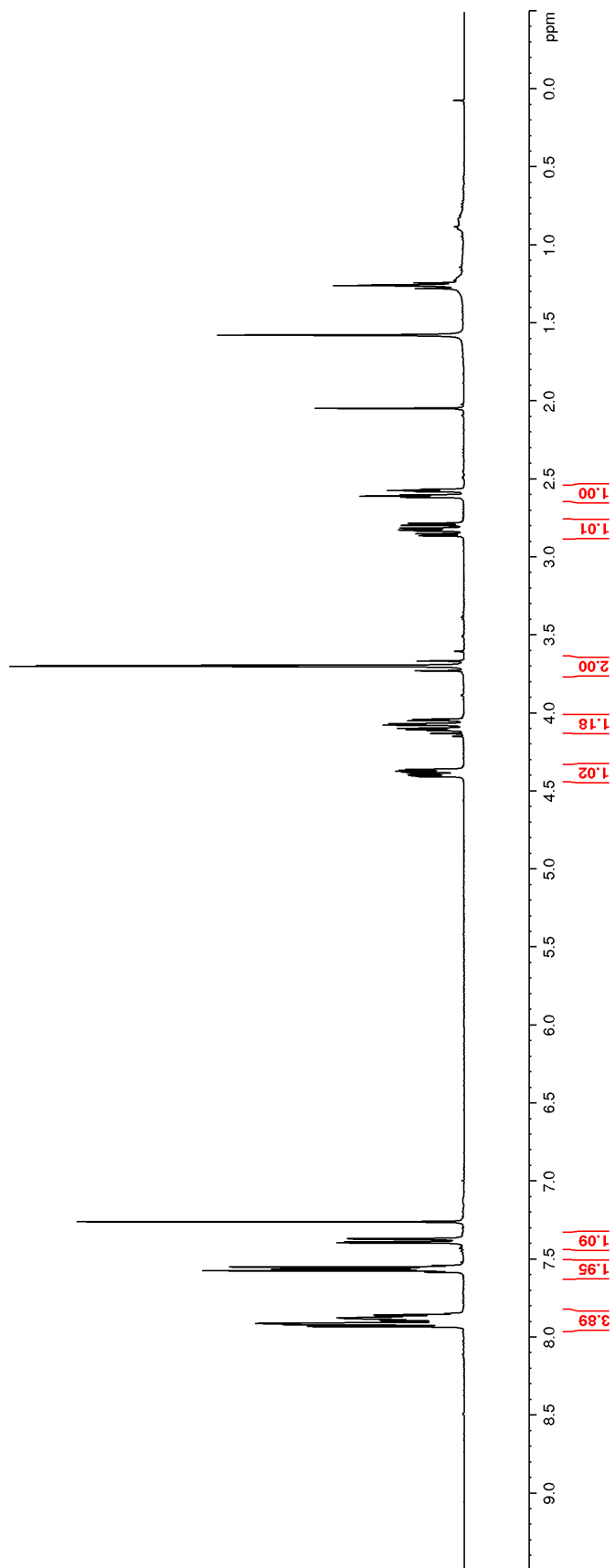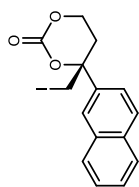
Figure 34. ^{13}C NMR (100 MHz, CDCl$_3$) of **59.**
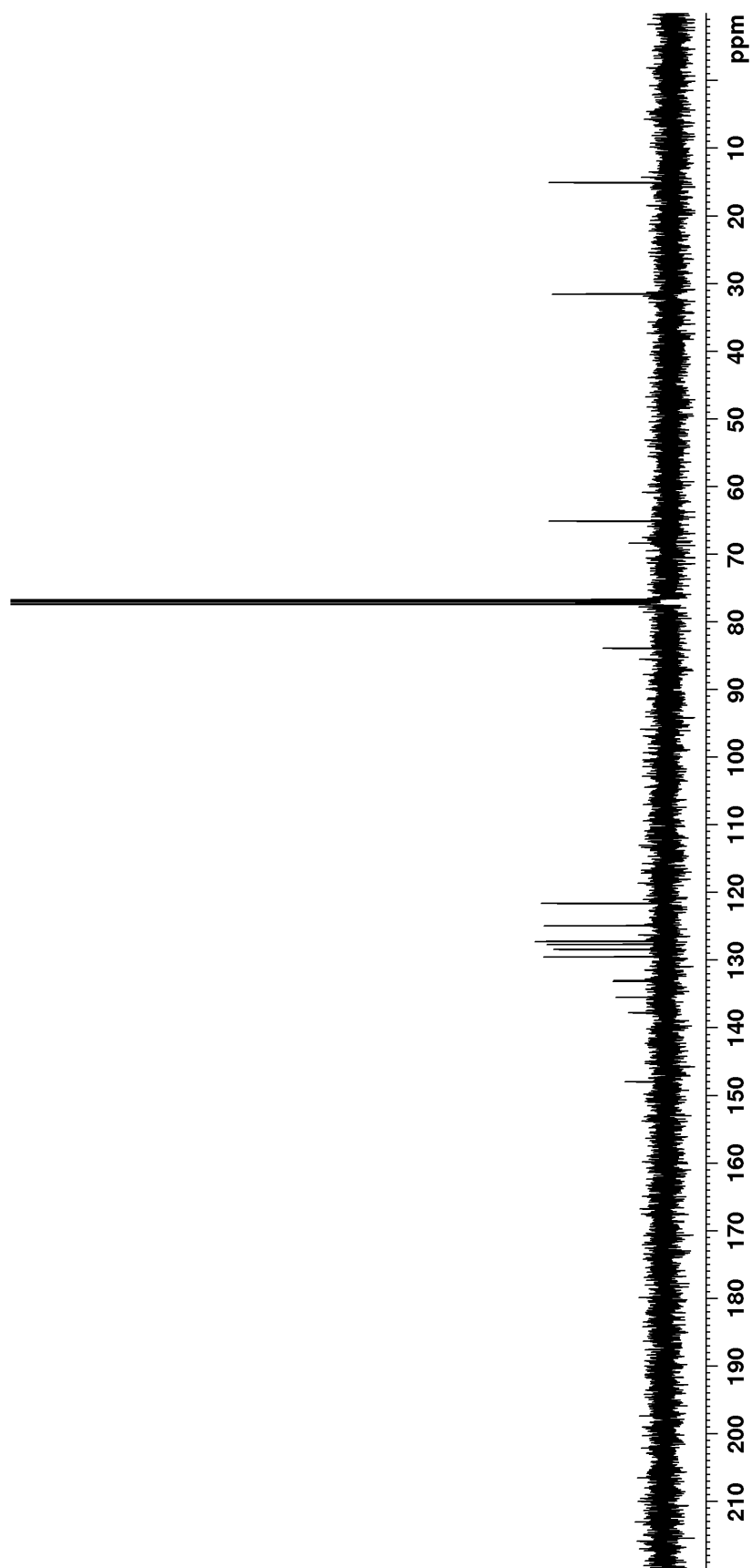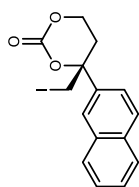
Figure 35. HPLC trace of **59.**
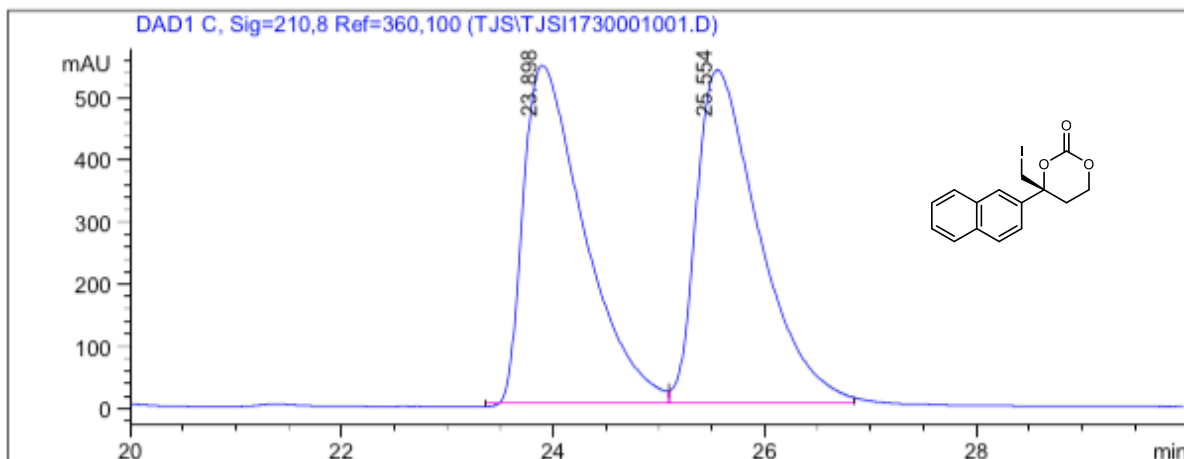

```
Signal   1: DAD1 C, Sig=210,8 Ref=360,100


    Peak    RT      Width      Area      Area %
     #     [min]    [min]
    ----|--------|--------|----------|---------
     1    23.898   0.664   21630.357   49.52
     2    25.554   0.686   22052.986   50.48
    ----|--------|--------|----------|---------
```
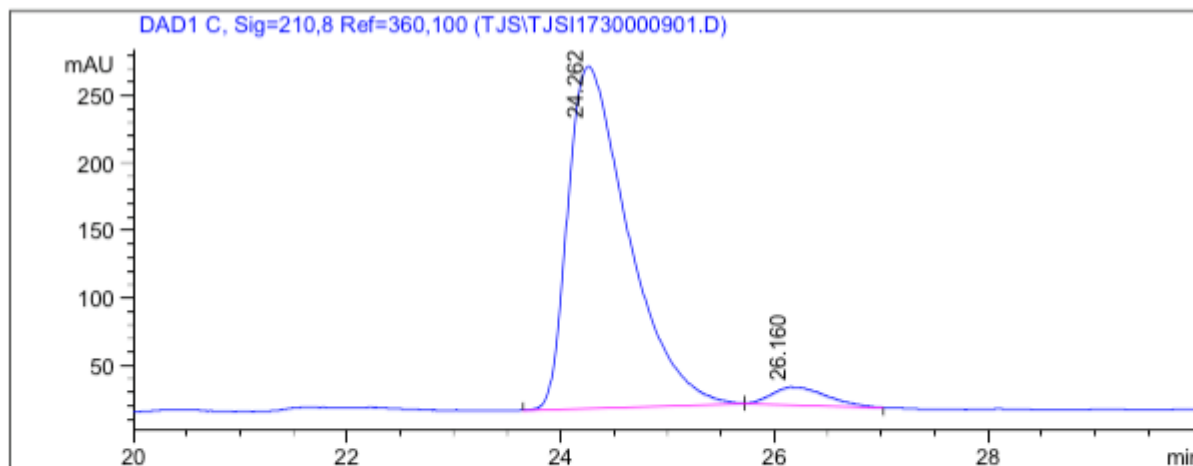


```
Signal   1: DAD1 C, Sig=210,8 Ref=360,100


    Peak    RT      Width      Area      Area %
     #     [min]    [min]
    ----|--------|--------|----------|---------
     1    24.262   0.657   9983.698    95.27
     2    26.160   0.607    495.495     4.73
    ----|--------|--------|----------|---------
```

Figure 36. ^{1}H NMR (400 MHz, CDCl$_3$) of **62.**
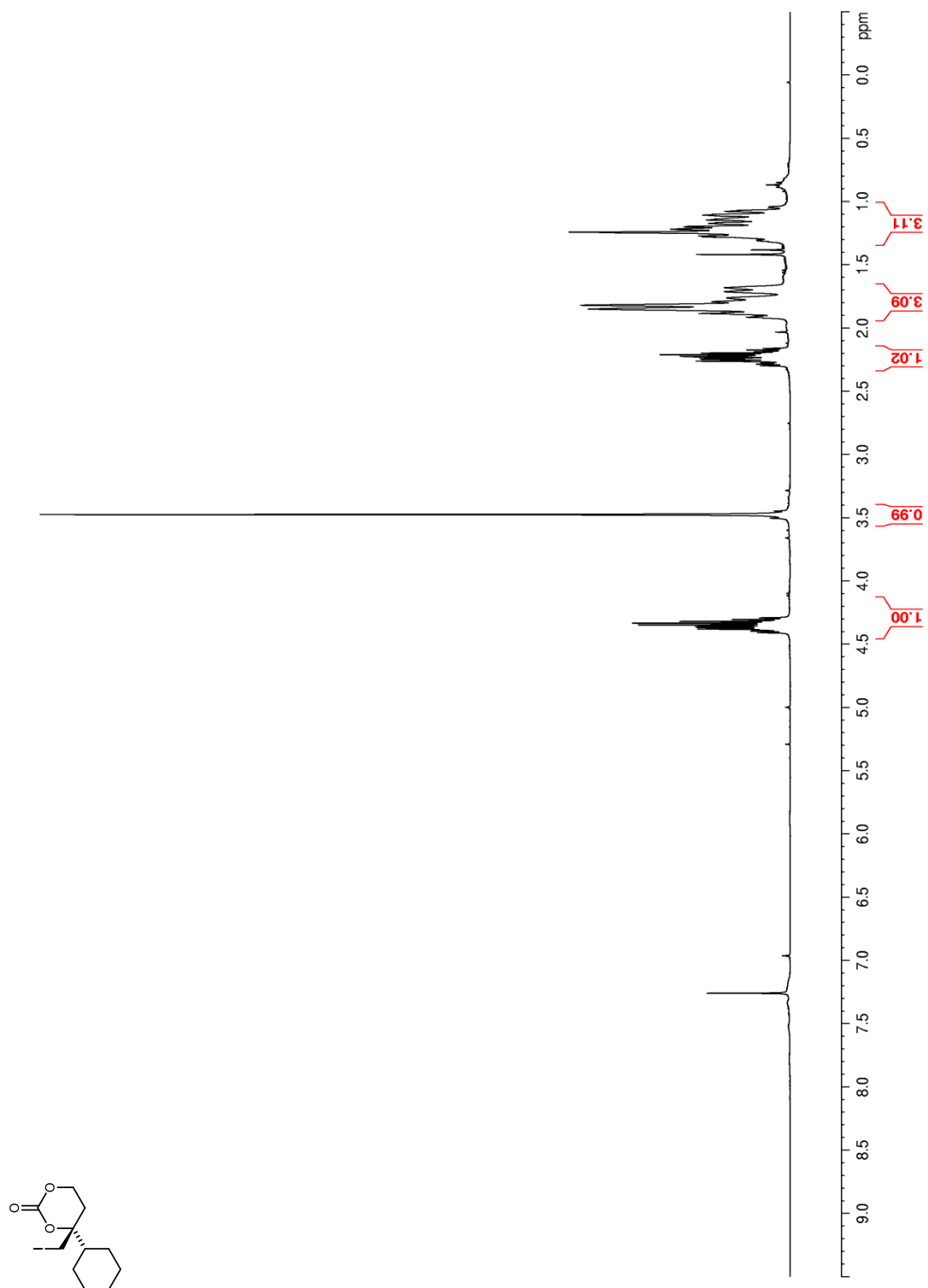
Figure 37. ^{13}C NMR (100 MHz, CDCl$_3$) of **62.**
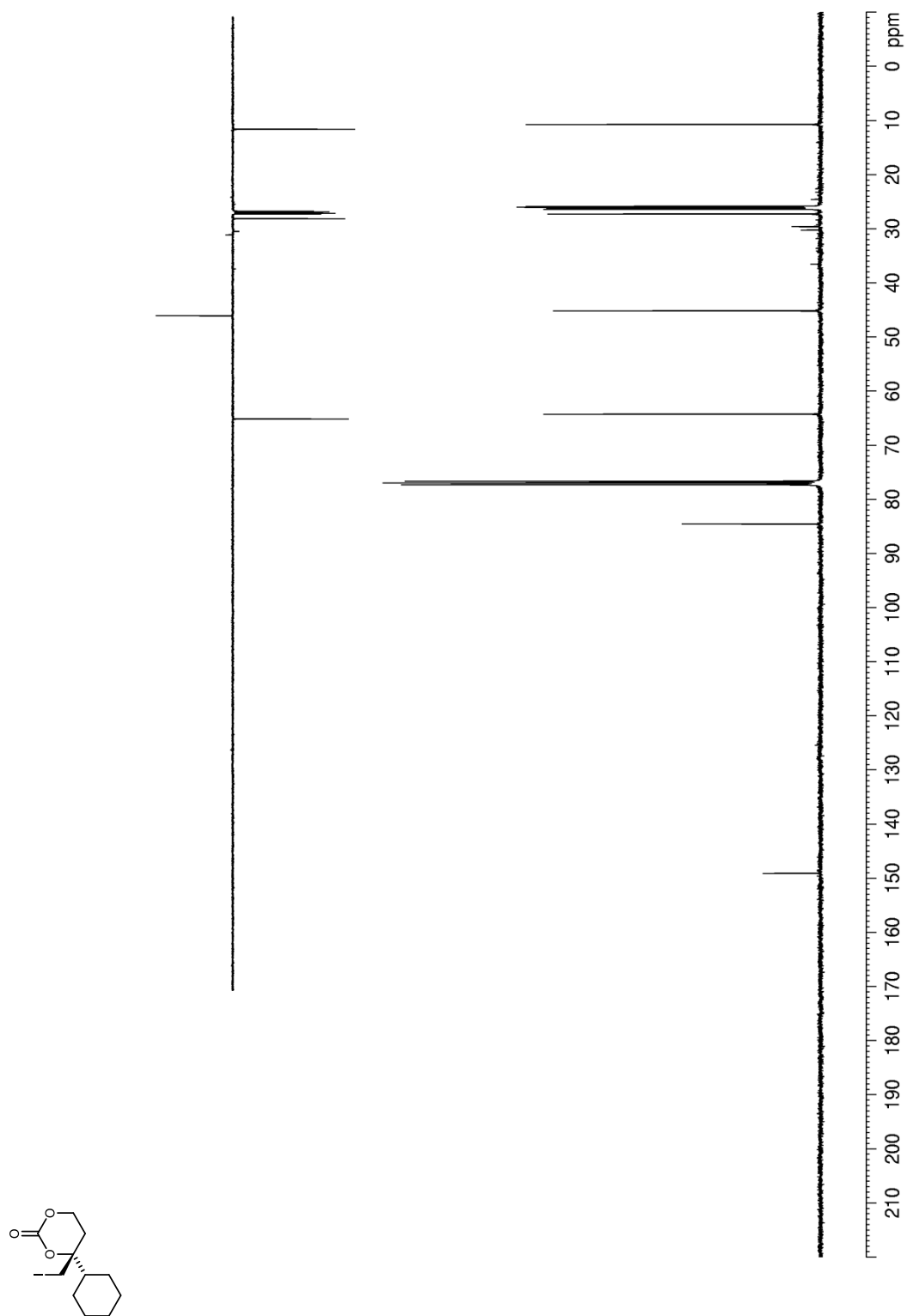
Figure 38. HPLC trace of **62.**
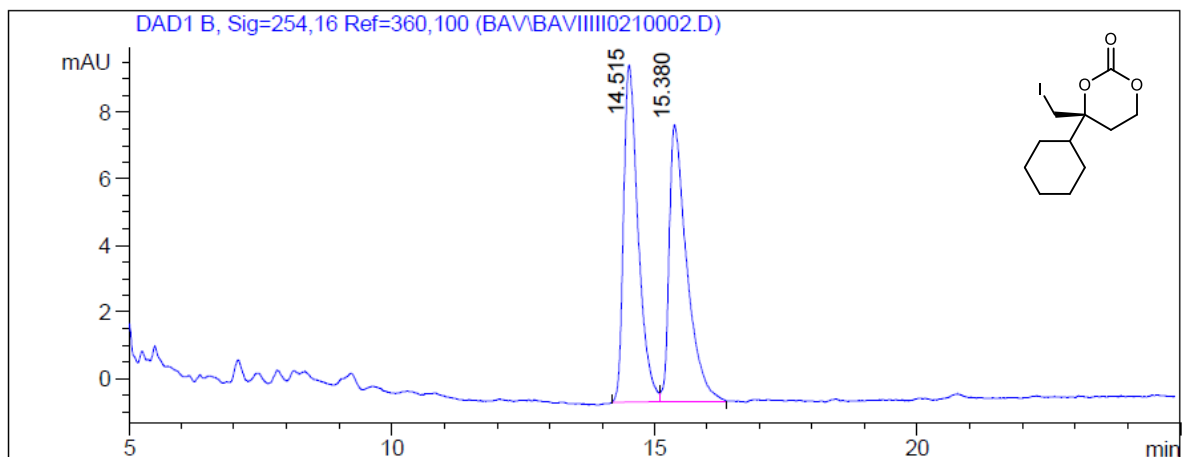

```
Signal  1: DAD1 B,  Sig=254,16 Ref=360,100

    Peak    RT      Width     Area      Area %
     #     [min]    [min]
    ---------------------------------------------
     1    14.515   0.322    195.534    50.17
     2    15.380   0.390    194.172    49.83
    ---------------------------------------------
```
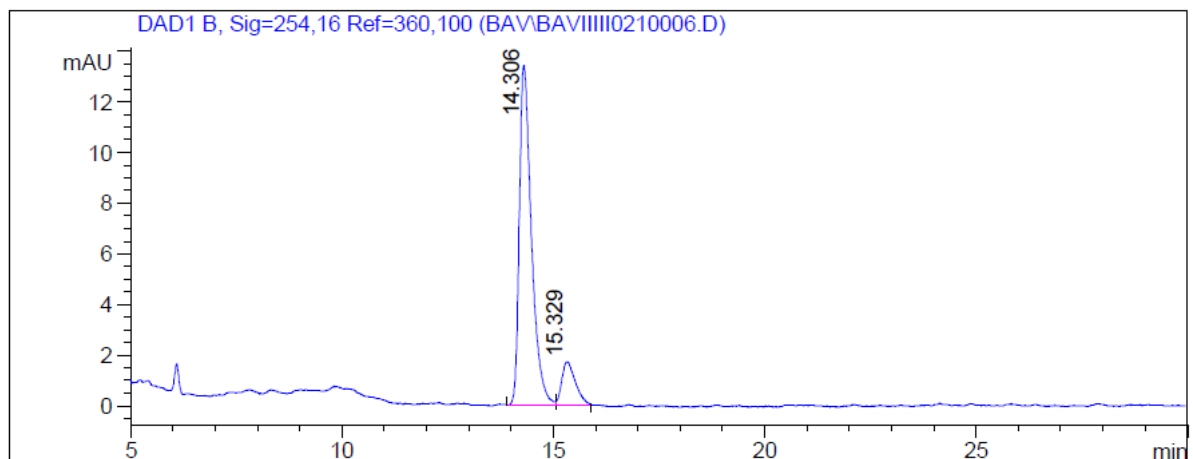


```
Signal  1: DAD1 B,  Sig=254,16 Ref=360,100

    Peak    RT      Width     Area      Area %
     #     [min]    [min]
    ---------------------------------------------
     1    14.306   0.330    265.550    87.39
     2    15.329   0.373     38.330    12.61
    ---------------------------------------------
```

Figure 39. ^{1}H NMR (400 MHz, CDCl$_3$) of **63.**
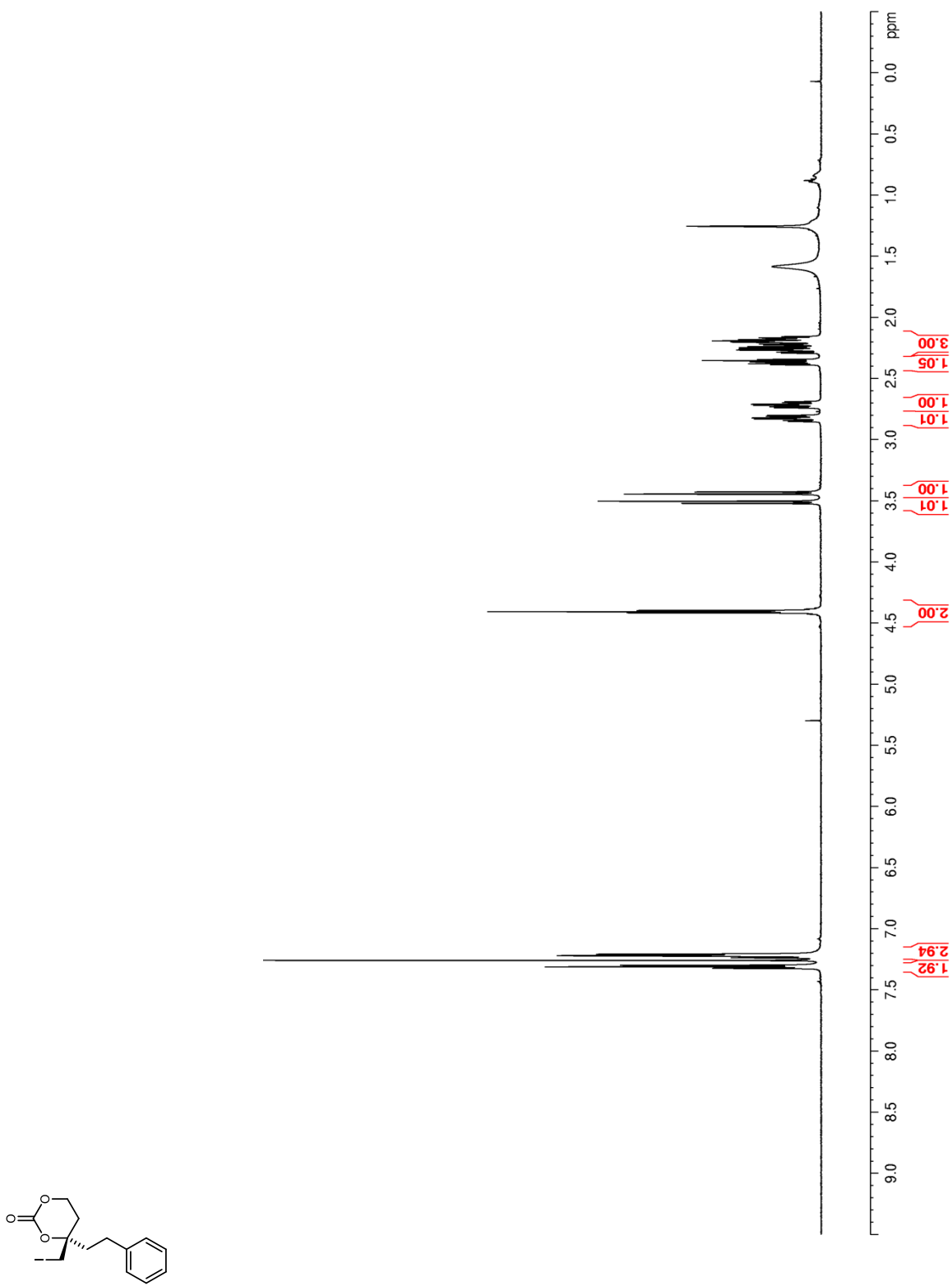
Figure 40. ^{13}C NMR (100 MHz, CDCl$_3$) of **63.**
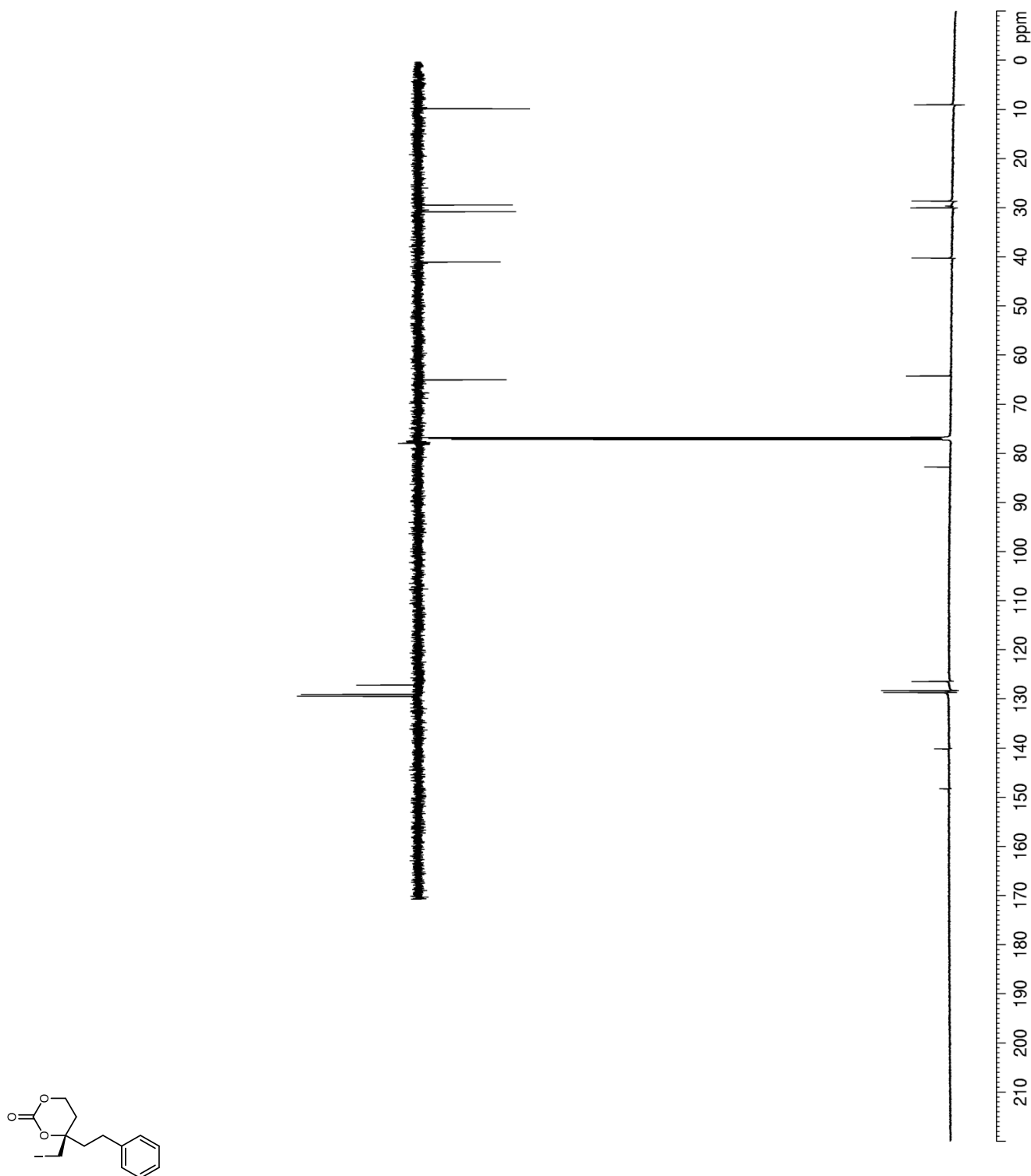
Figure 41. HPLC trace of **63.**
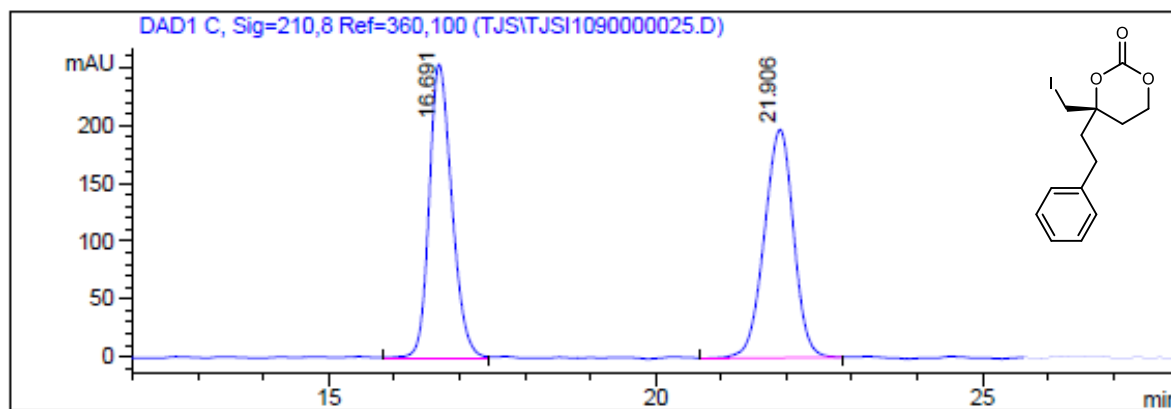

```
Signal  1: DAD1 C, Sig=210,8 Ref=360,100

    Peak    RT      Width     Area      Area %
    #     [min]    [min]
    ----------------------------------------------
    1    16.691   0.402   6122.921   49.85
    2    21.906   0.521   6160.588   50.15
    ----------------------------------------------
```
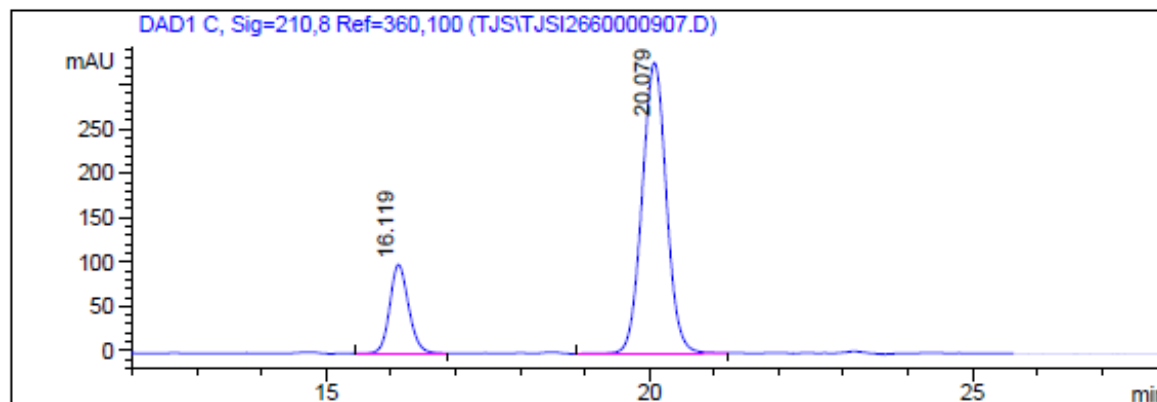


```
Signal  1: DAD1 C, Sig=210,8 Ref=360,100

    Peak    RT      Width     Area      Area %
    #     [min]    [min]
    ----------------------------------------------
    1    16.119   0.341   2053.020   19.25
    2    20.079   0.437   8611.422   80.75
    ----------------------------------------------
```

Figure 42. ^{1}H NMR (400 MHz, CDCl$_3$) of **64.**
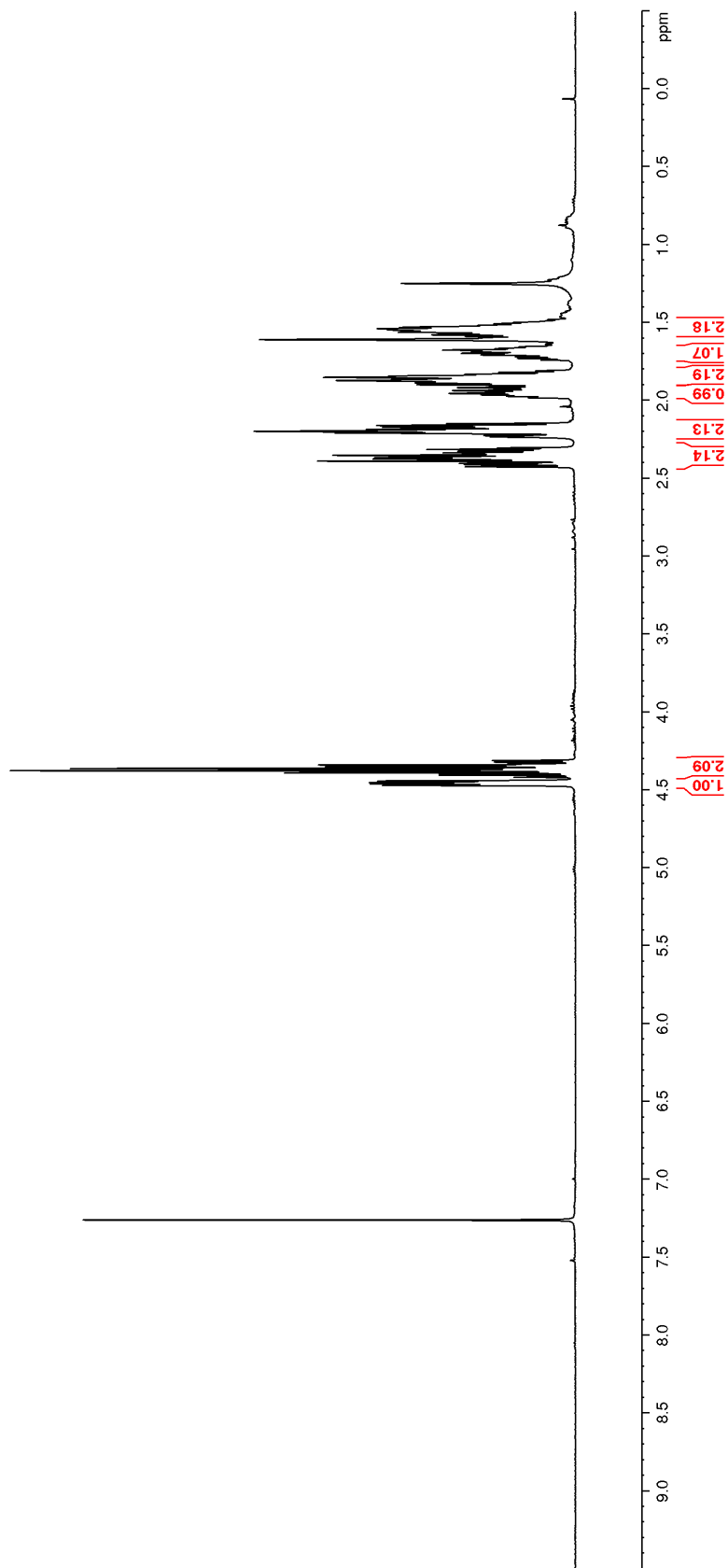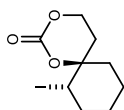
Figure **43**. ^{13}C NMR (125 MHz, CDCl$_3$) of **64.**
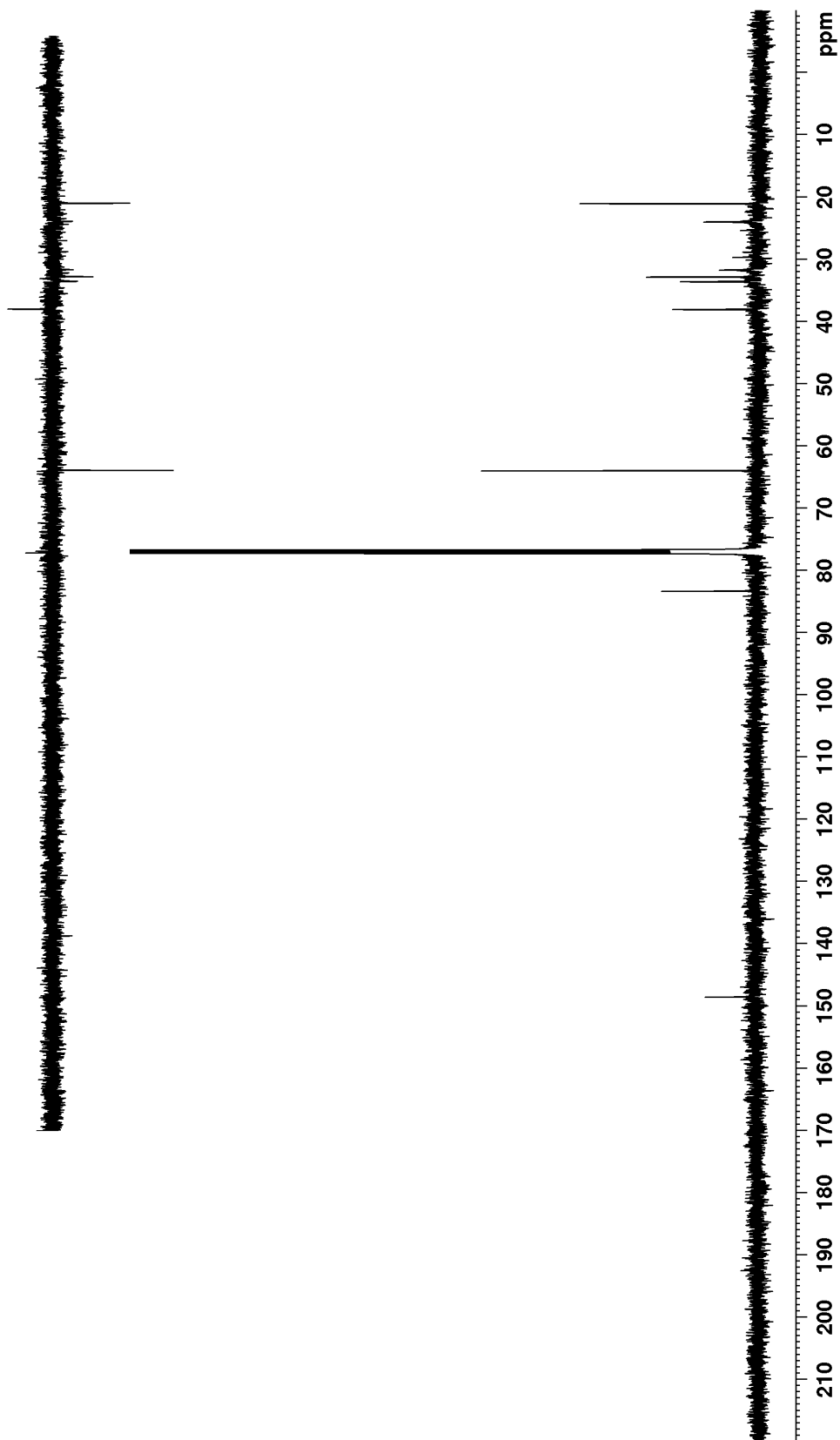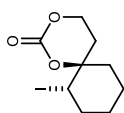
Figure 44. HPLC trace of **64.**
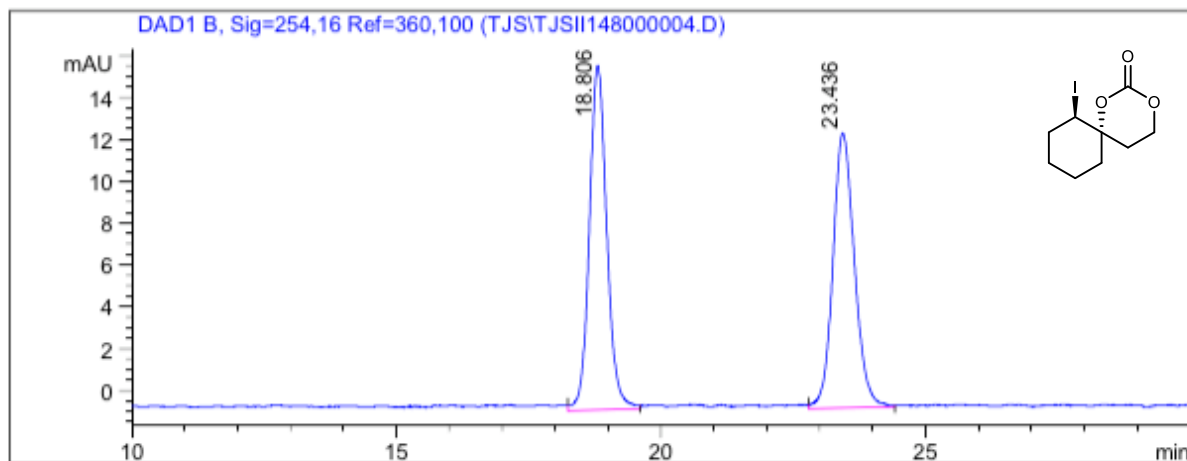

```
Signal  1: DAD1 B, Sig=254,16 Ref=360,100


   Peak    RT      Width      Area      Area %
    #     [min]    [min]

  ------------------------------------------------
    1    18.806   0.381    376.608    50.31
    2    23.436   0.472    371.940    49.69
```
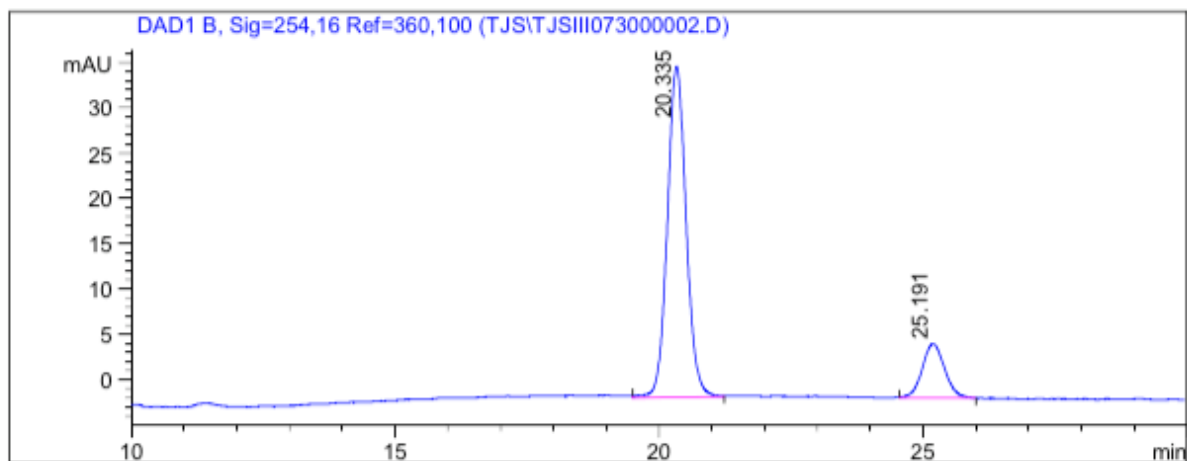


```
Signal  1: DAD1 B, Sig=254,16 Ref=360,100


   Peak    RT      Width      Area      Area %
    #     [min]    [min]

  ------------------------------------------------
    1    20.335   0.414    907.381    83.51
    2    25.191   0.497    179.122    16.49
  ------------------------------------------------
```

Figure 45. ^{1}H NMR (400 MHz, CDCl$_3$) of **68.**
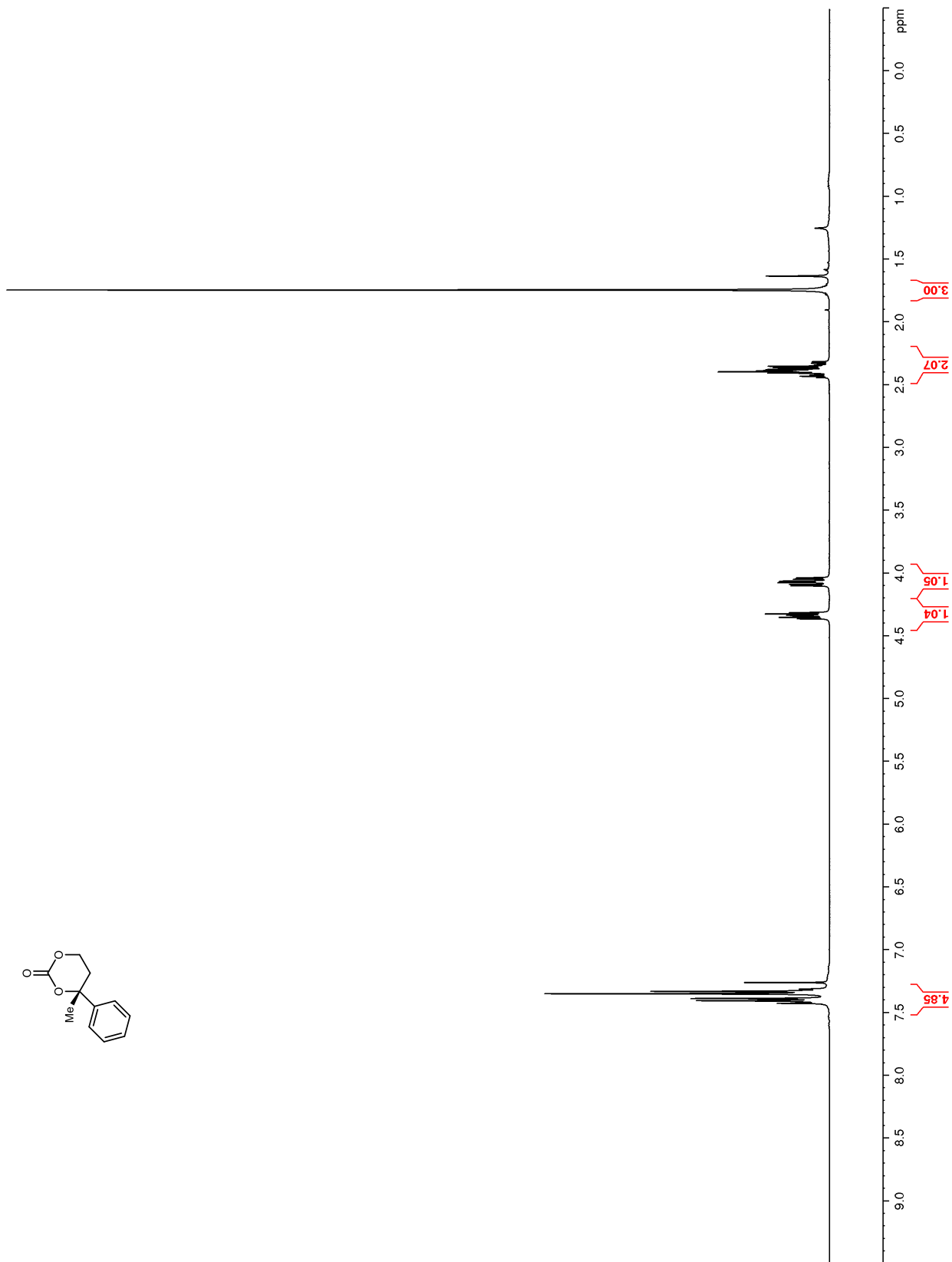
Figure 46. HPLC trace of **68.**
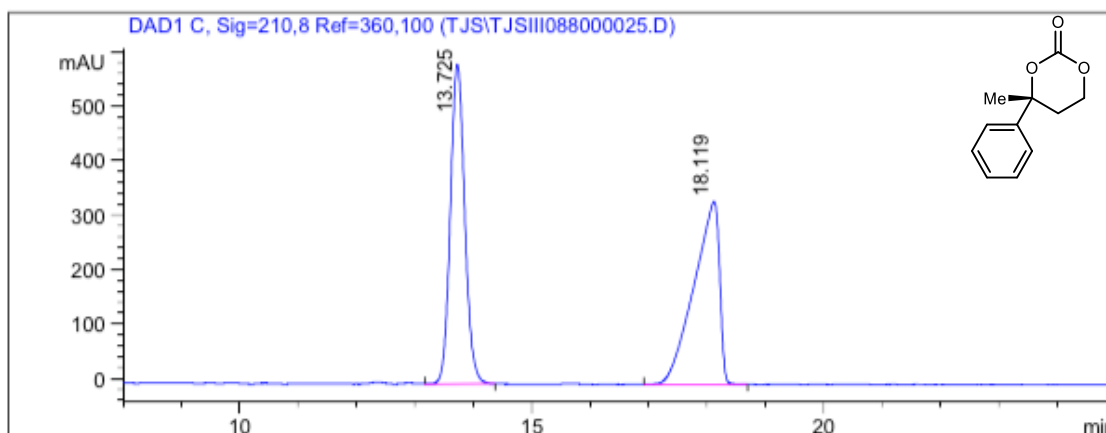

```
Signal  1: DAD1 C, Sig=210,8 Ref=360,100

    Peak    RT      Width     Area       Area %
    #       [min]   [min]
    -----------------------------------------
    1     13.725   0.285   10035.506    49.44
    2     18.119   0.509   10263.197    50.56
    -----------------------------------------
```
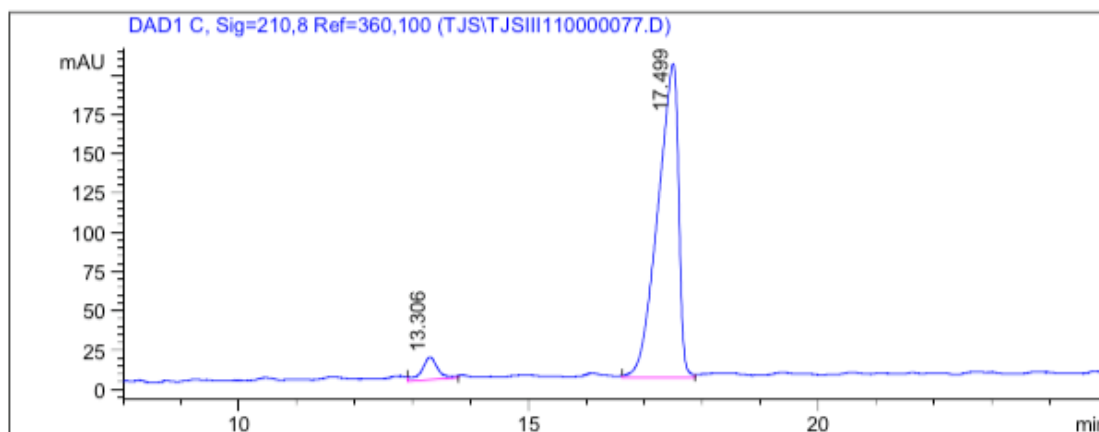


```
Signal  1: DAD1 C, Sig=210,8 Ref=360,100

    Peak    RT      Width     Area      Area %
    #       [min]   [min]
    -----------------------------------------
    1     13.306   0.320    274.621     5.23
    2     17.499   0.416   4981.165    94.77
    -----------------------------------------
```

Figure 47. ^{1}H NMR (400 MHz, CDCl$_3$) of **70.**
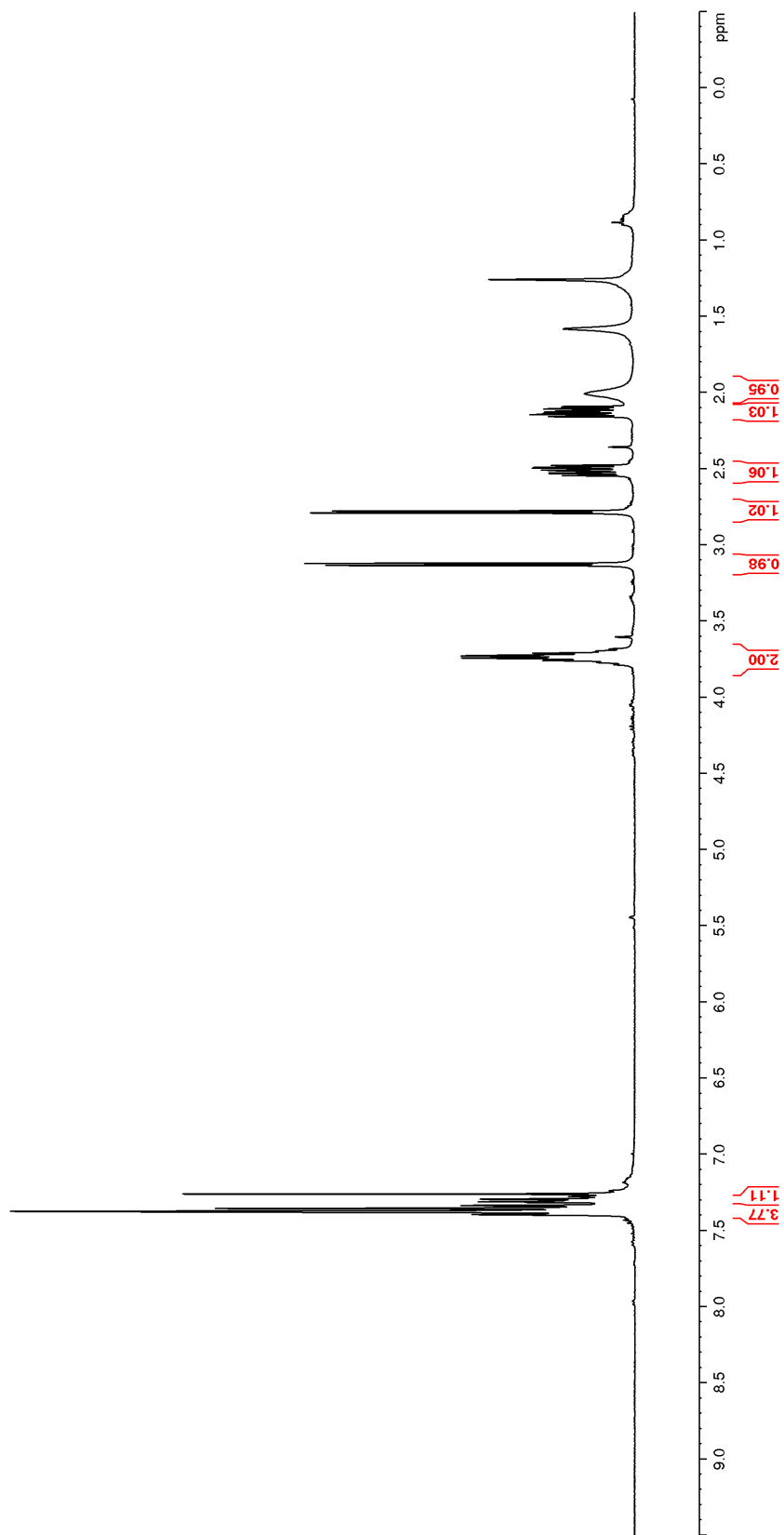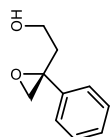
Figure 48. ^{1}H NMR (600 MHz, CDCl$_3$) of **69.**
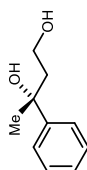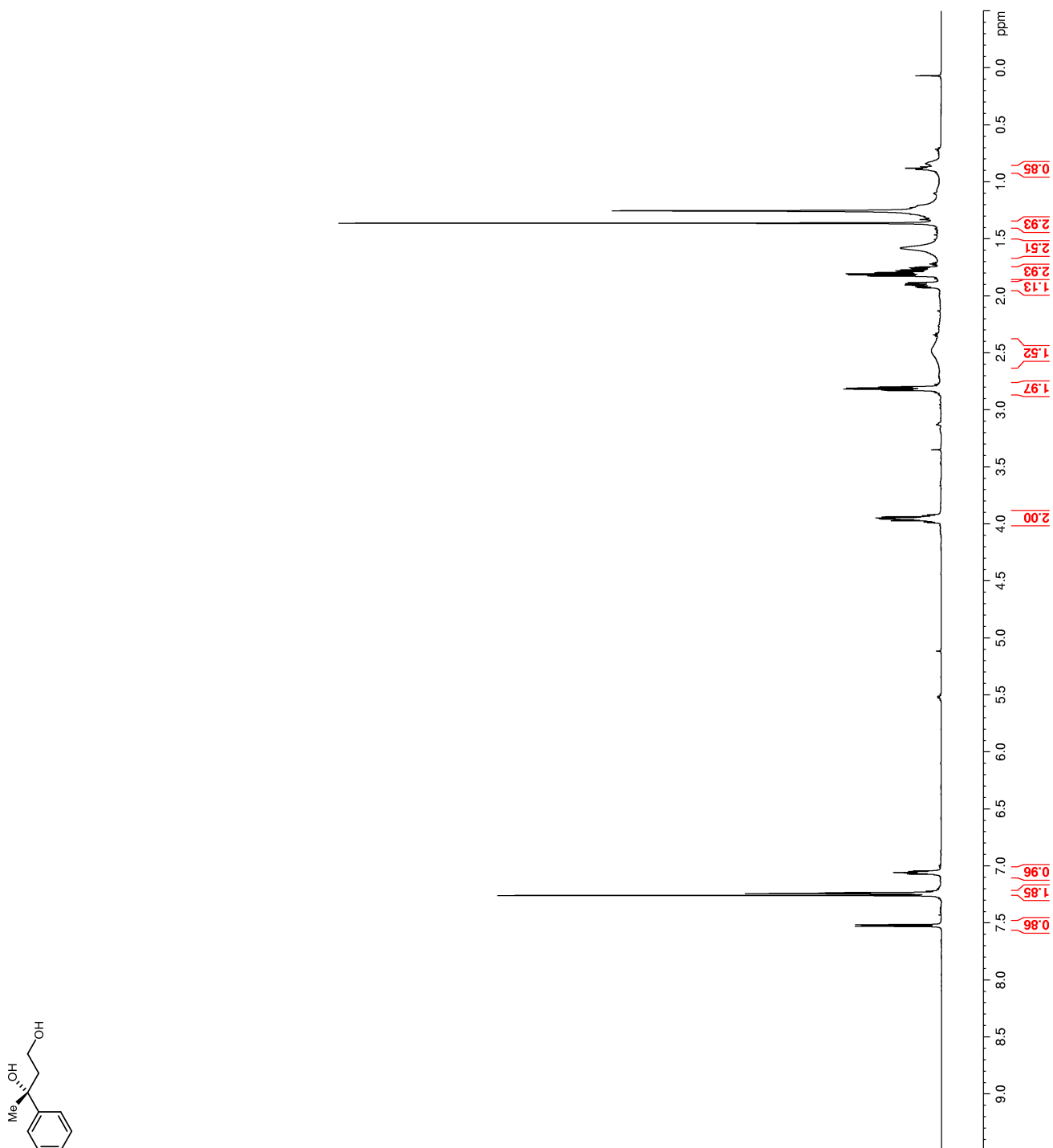
Figure 49. ^{13}C NMR (150 MHz, CDCl$_3$) of **69.**
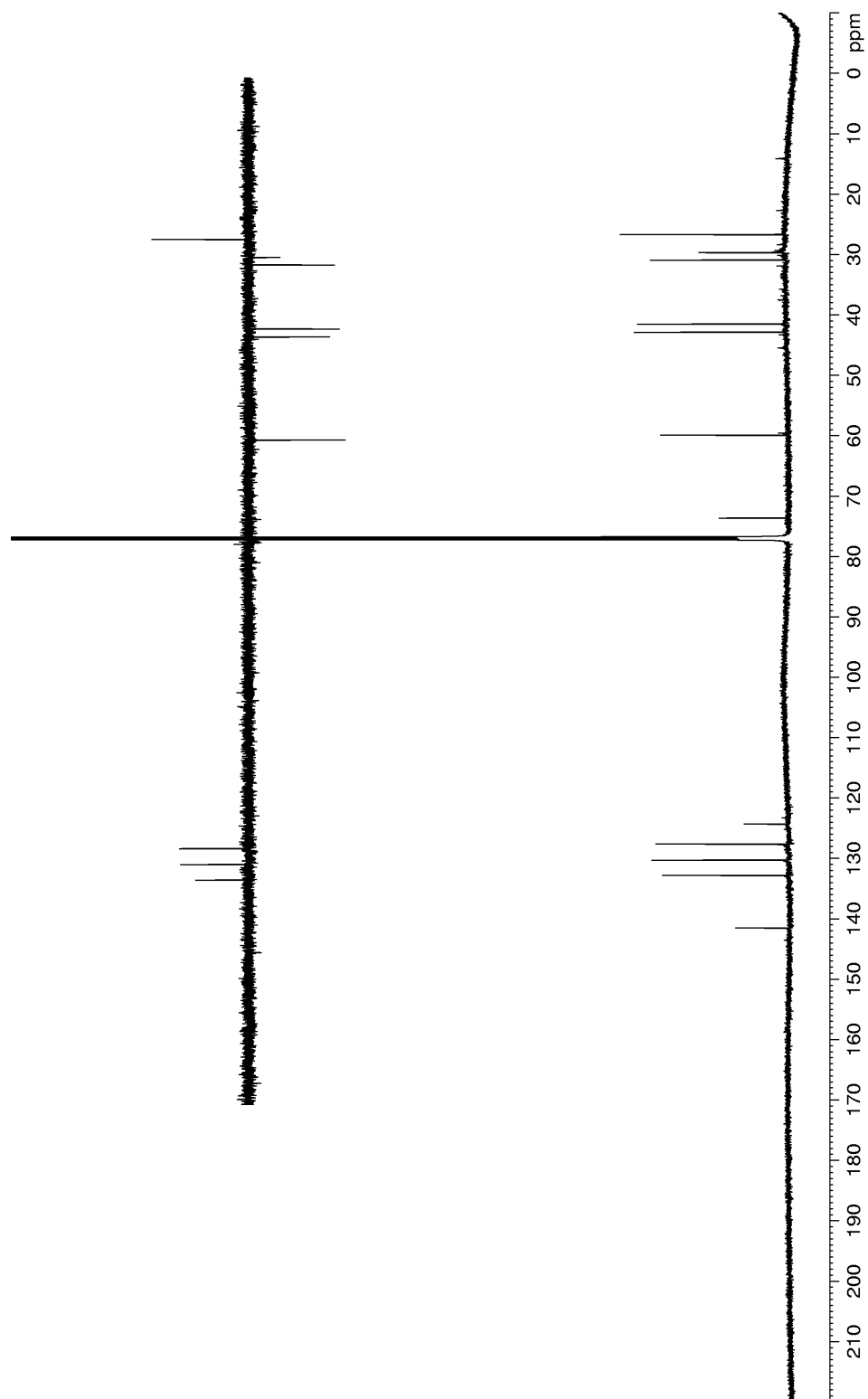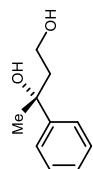
Figure 50. HPLC trace of **69.**
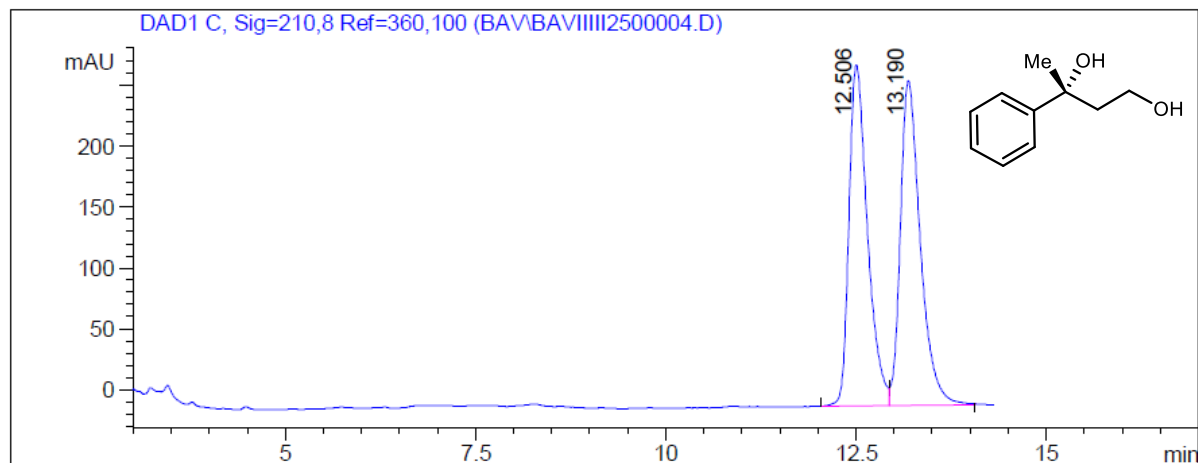

```
Signal  1: DAD1 C, Sig=210,8 Ref=360,100


   Peak    RT      Width     Area      Area %
    #     [min]    [min]
   ----------------------------------------
    1    12.506   0.282    4730.385    49.48
    2    13.190   0.303    4829.833    50.52
   ----------------------------------------
```
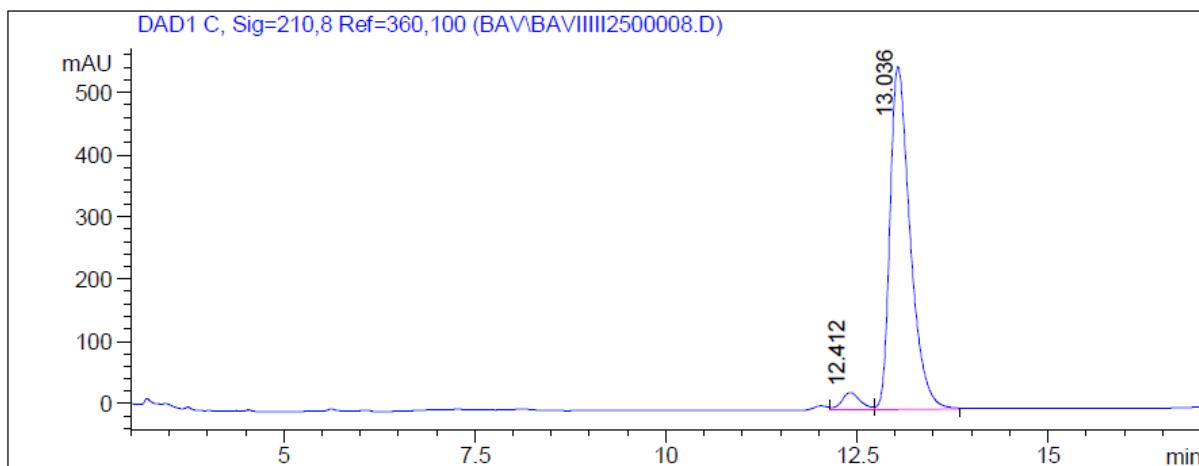


```
Signal  1: DAD1 C, Sig=210,8 Ref=360,100


   Peak    RT      Width     Area      Area %
    #     [min]    [min]
   ----------------------------------------
    1    12.412   0.284     474.696     4.48
    2    13.036   0.306   10117.824    95.52
   ----------------------------------------
```

Figure 51. HPLC trace of **70.**

Trace of the epoxide racemate is known and ee obtained by comparison.

Yamamoto *et al. J. Am. Chem. Soc.* **2010** 132, 7878–7880.
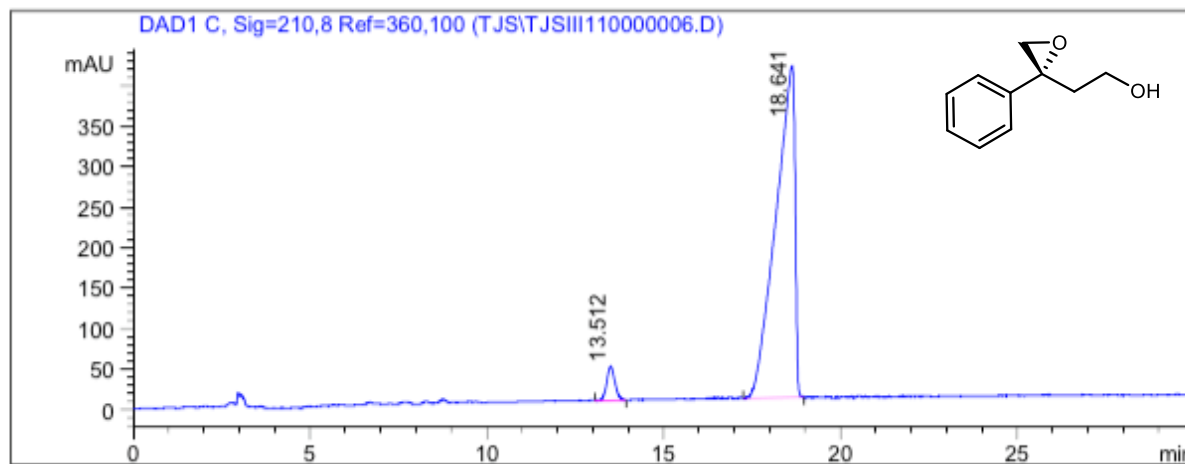

```
Signal   1: DAD1 C, Sig=210,8 Ref=360,100


     Peak    RT      Width     Area      Area %
     #      [min]    [min]

     ------------------------------------------------

      1    13.512   0.273     684.913      4.25
      2    18.641   0.629  15449.646     95.75

     ------------------------------------------------
```

Appendix 4.2.2: Spectral data for iodourea chemistry

Thomas J. Struble

Figure 62. ^{1}H NMR (400 MHz, CDCl$_3$) of **120a**
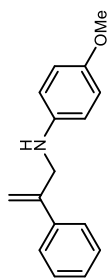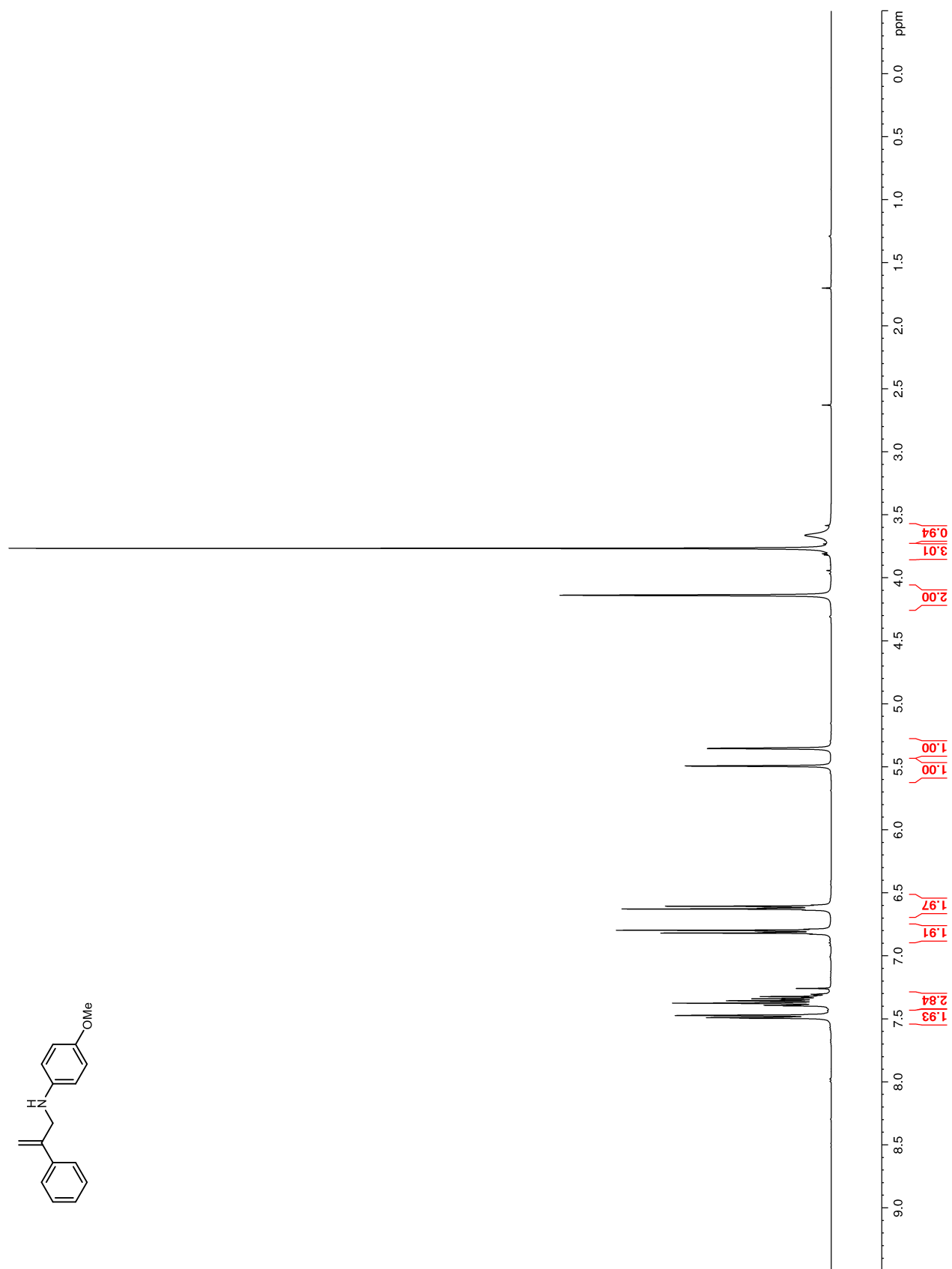
Figure 63. ^{13}C NMR (100 MHz, CDCl$_3$) of **120a**
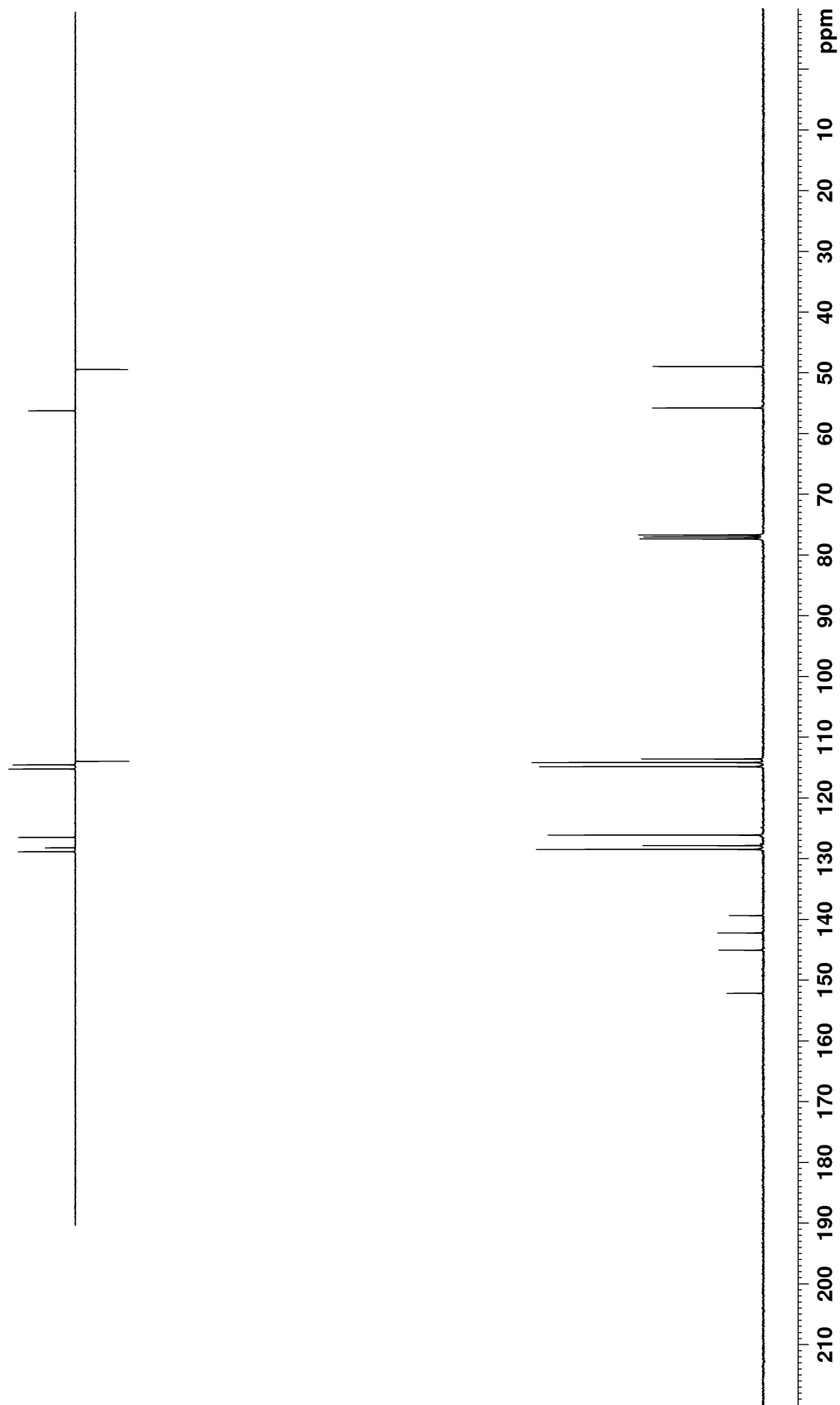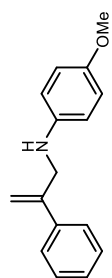
Figure 64. ^{1}H NMR (400 MHz, CDCl$_3$) of **120c**
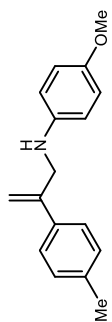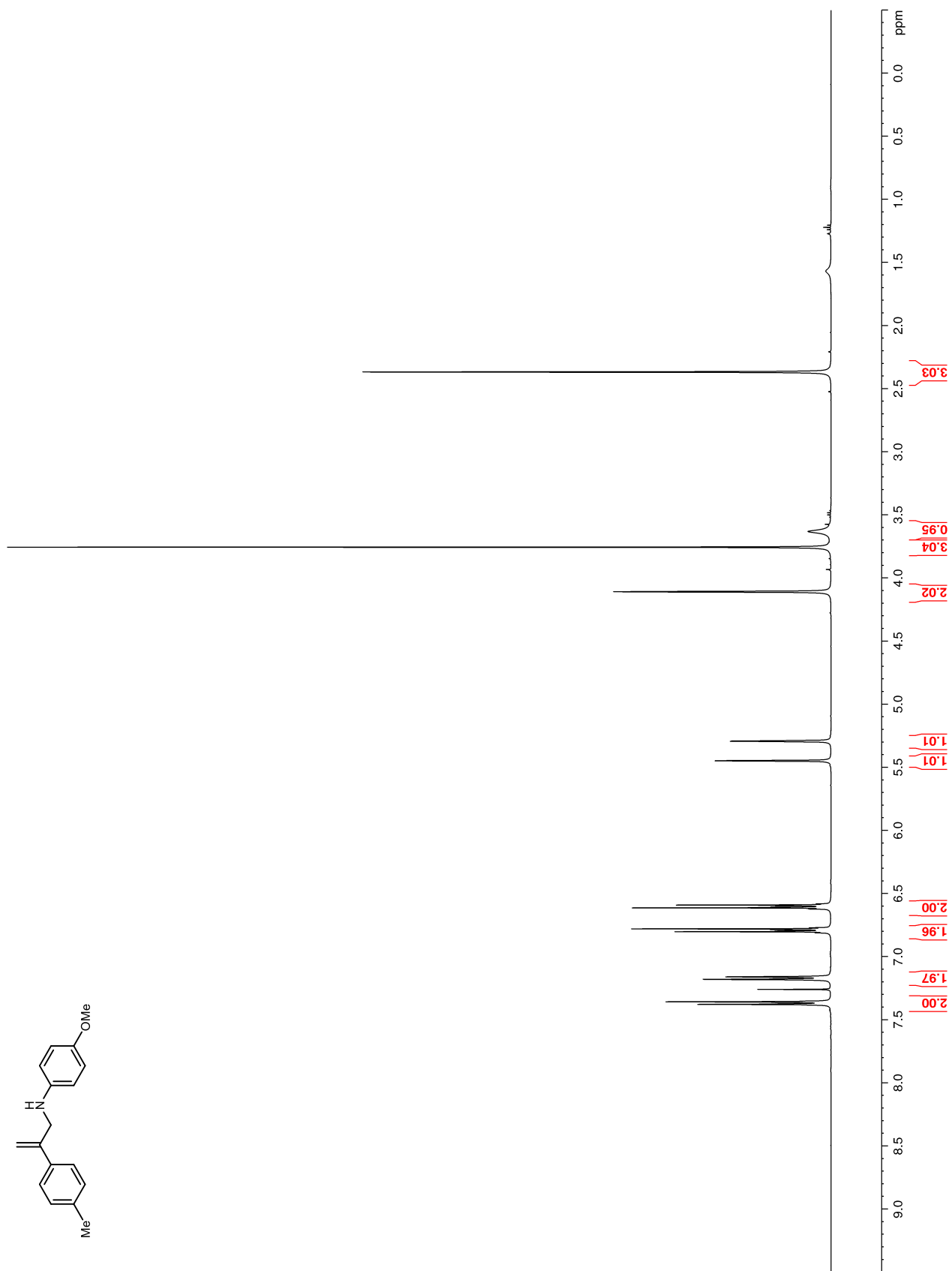
Figure 65. ^{13}C NMR (100 MHz, CDCl$_3$) of **120c**
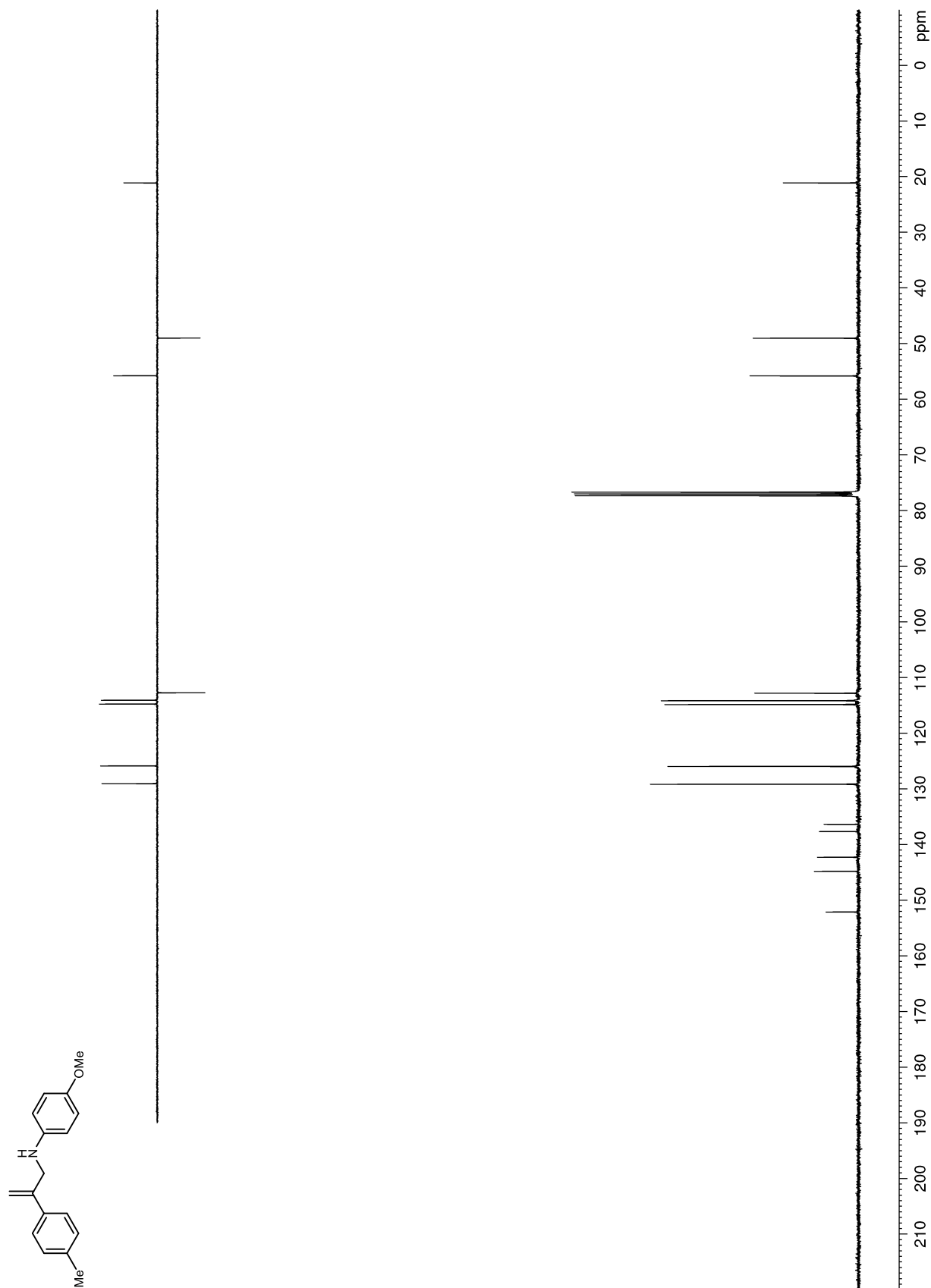
Figure 66. ^{1}H NMR (400 MHz, CDCl$_3$) of **120e**
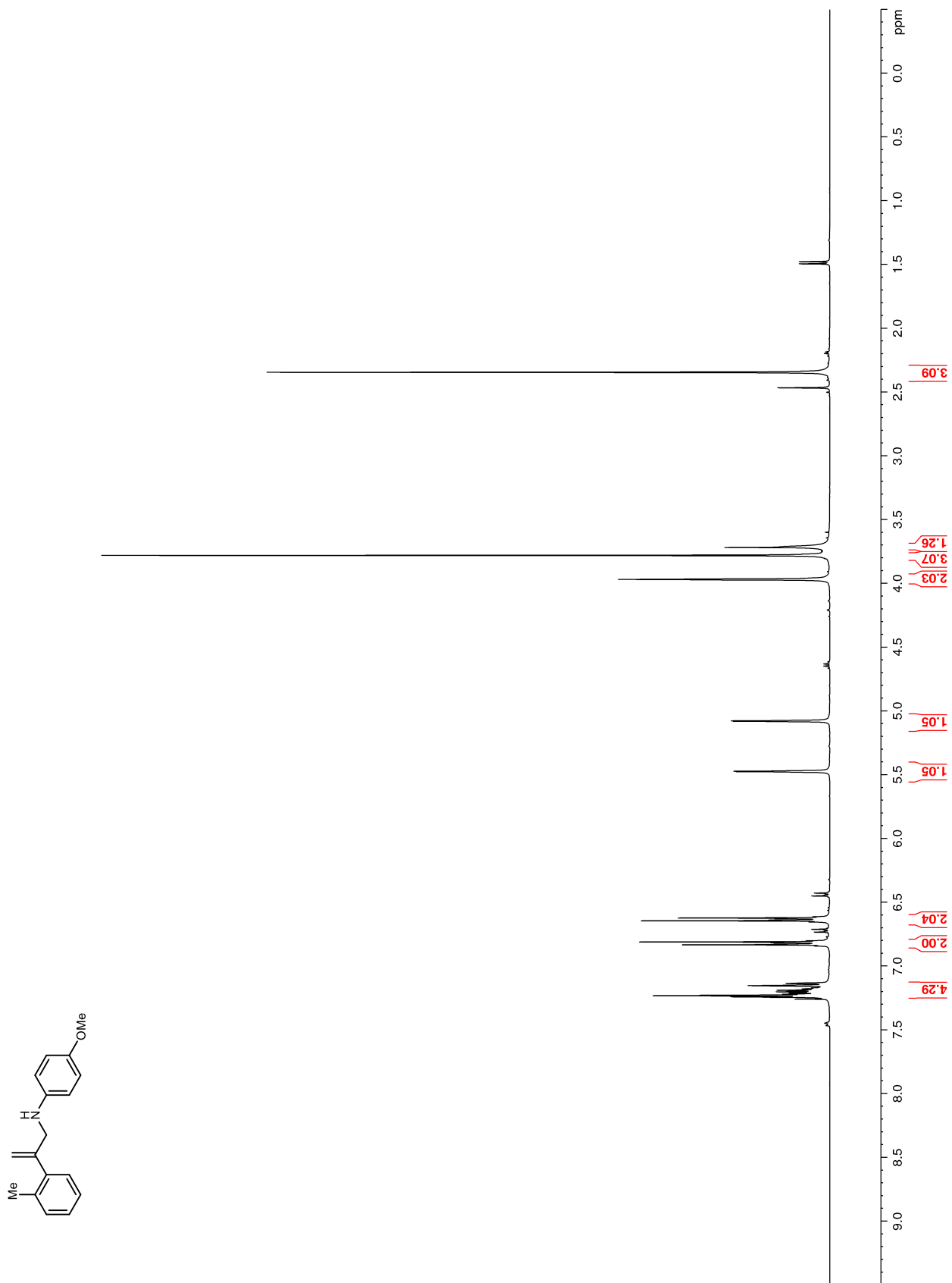
Figure 67. ^{13}C NMR (100 MHz, CDCl$_3$) of **120e**
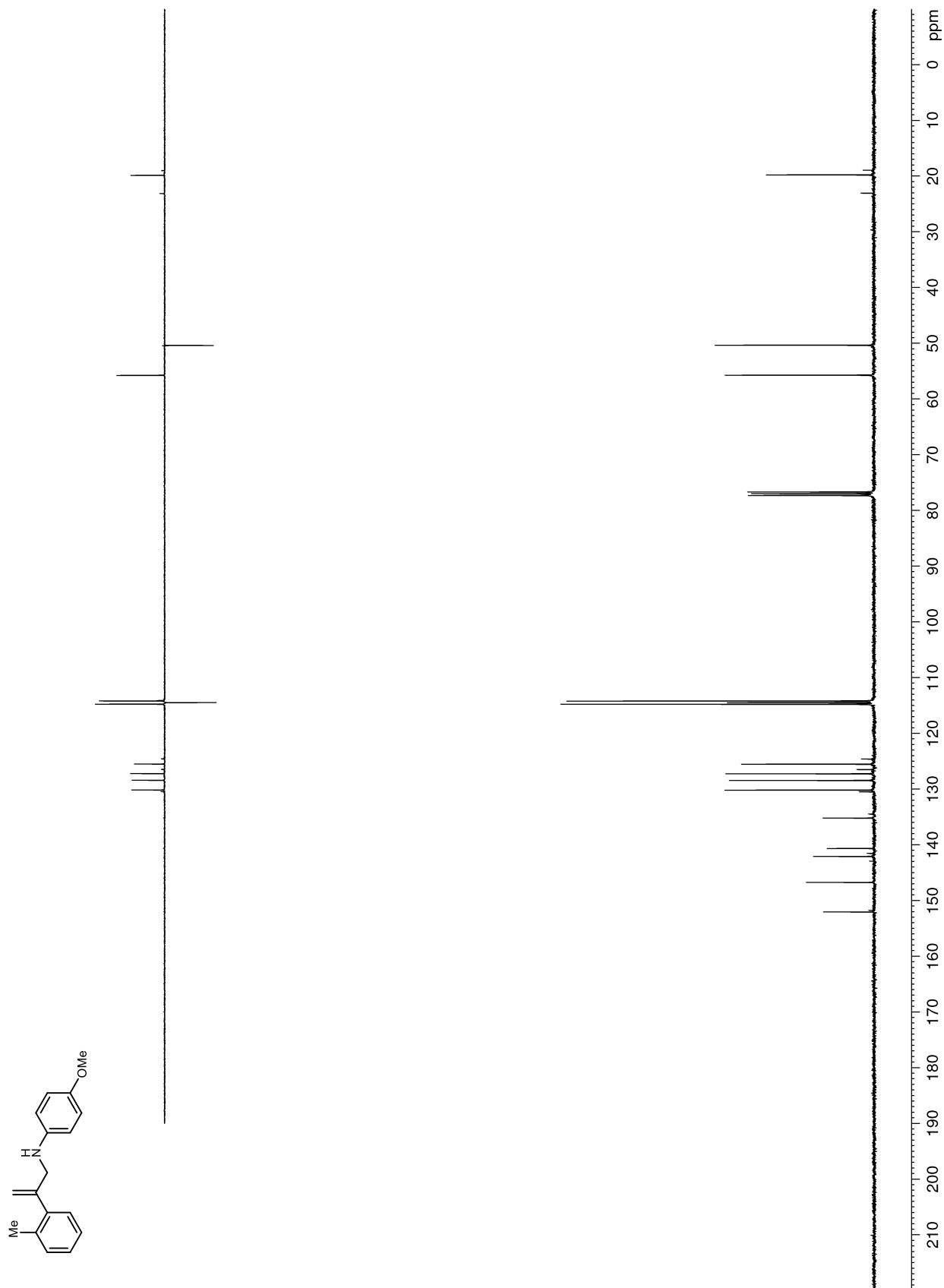
Figure 68. ^{1}H NMR (400 MHz, CDCl$_3$) of **120f**
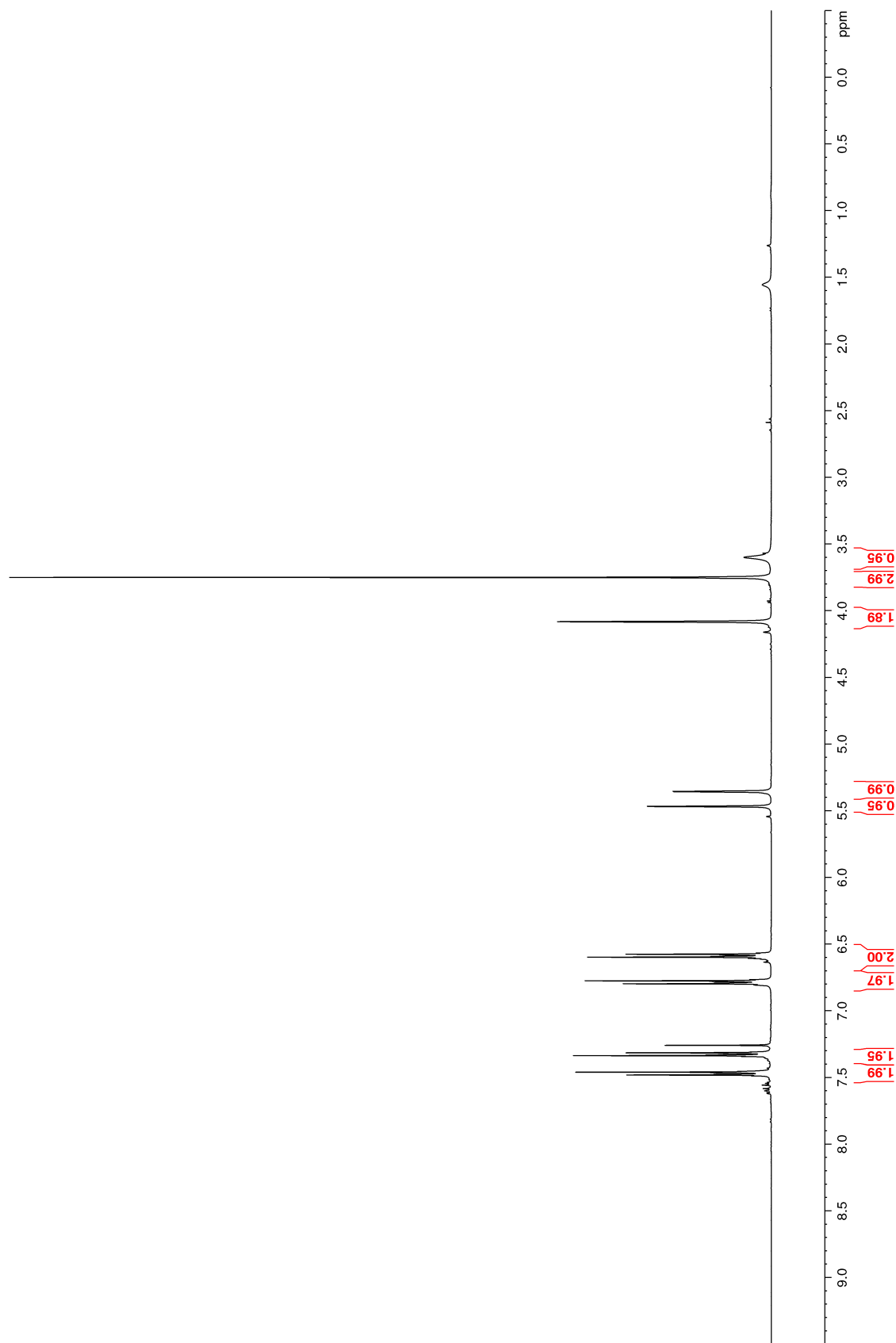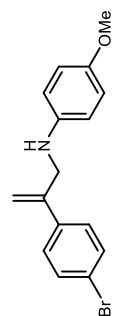
Figure 69. ^{13}C NMR (100 MHz, CDCl$_3$) of **120f**
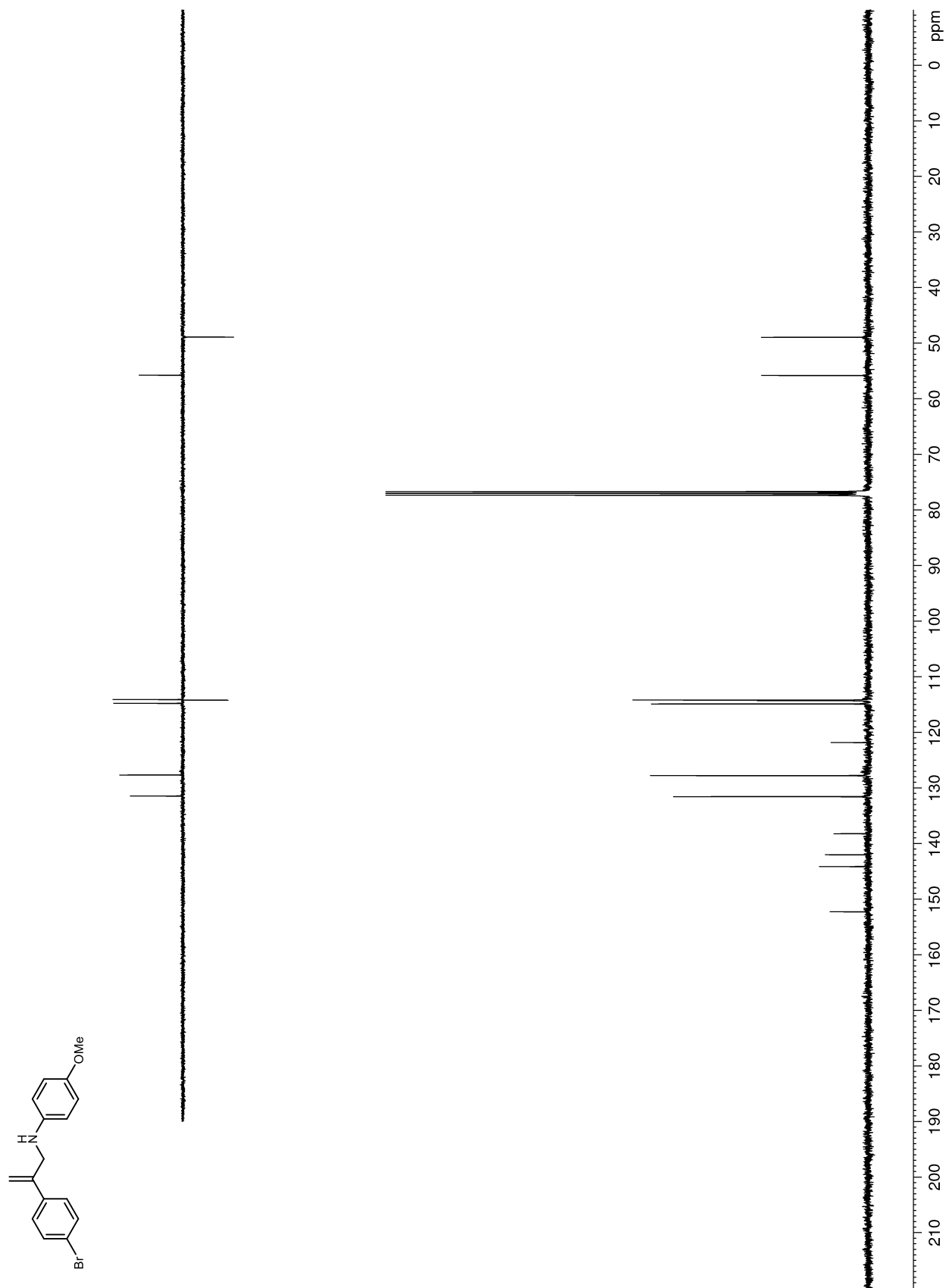
Figure 70. ^{1}H NMR (400 MHz, CDCl$_3$) of **120g**
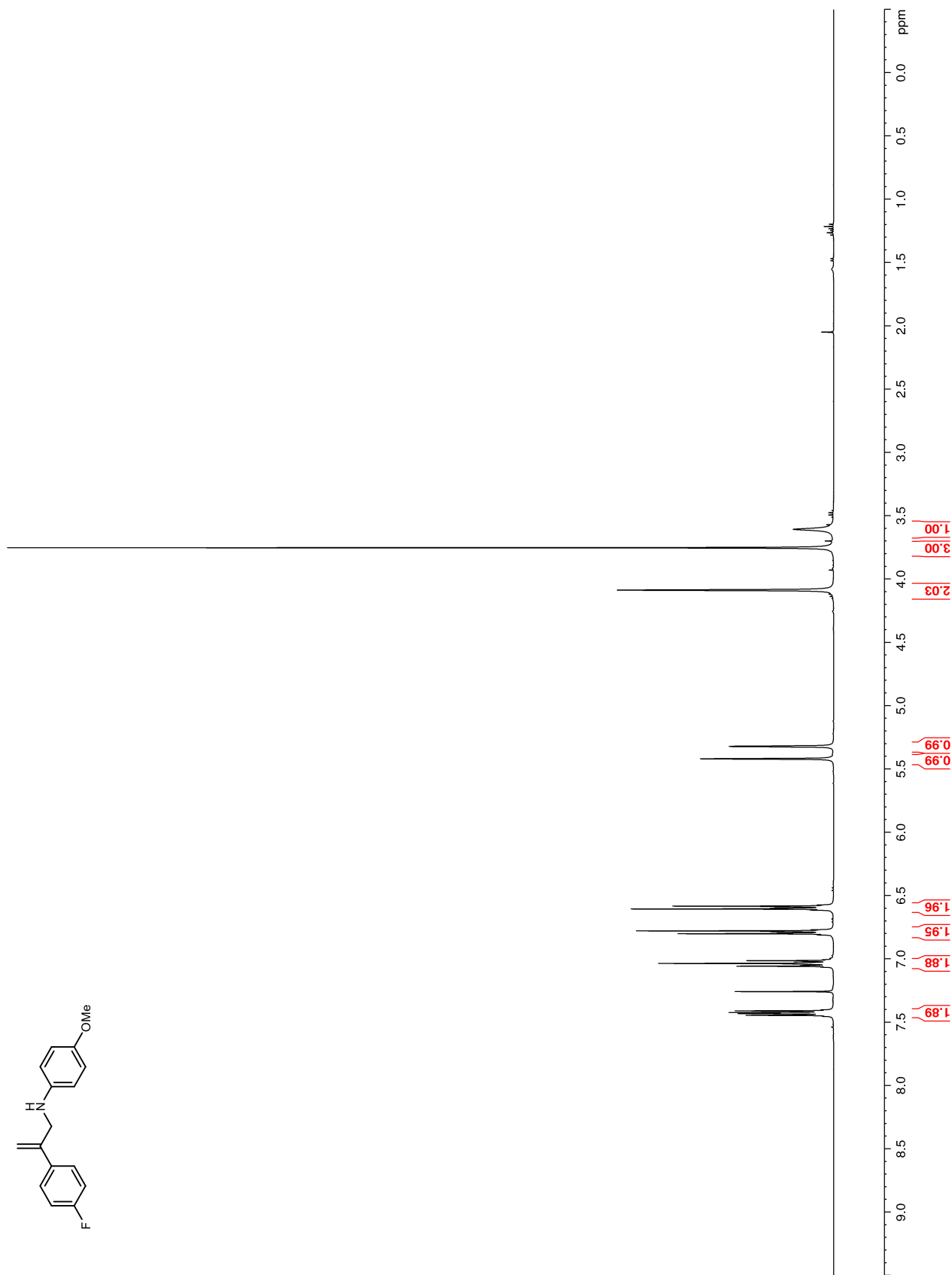
Figure 71. ^{13}C NMR (100 MHz, CDCl$_3$) of **120g**
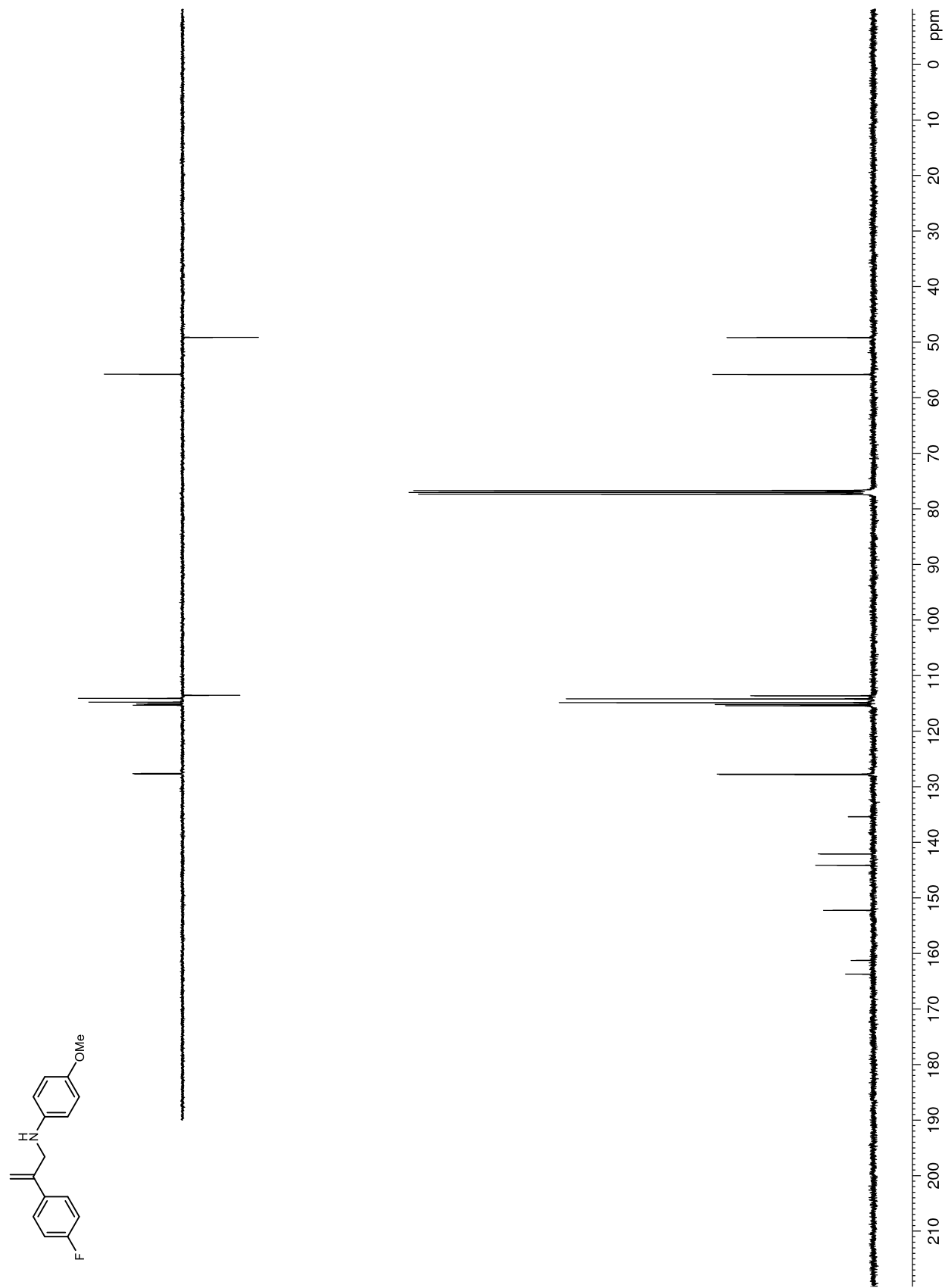
Figure 72. ^{19}F NMR (376 MHz, CDCl$_3$) of **120g**
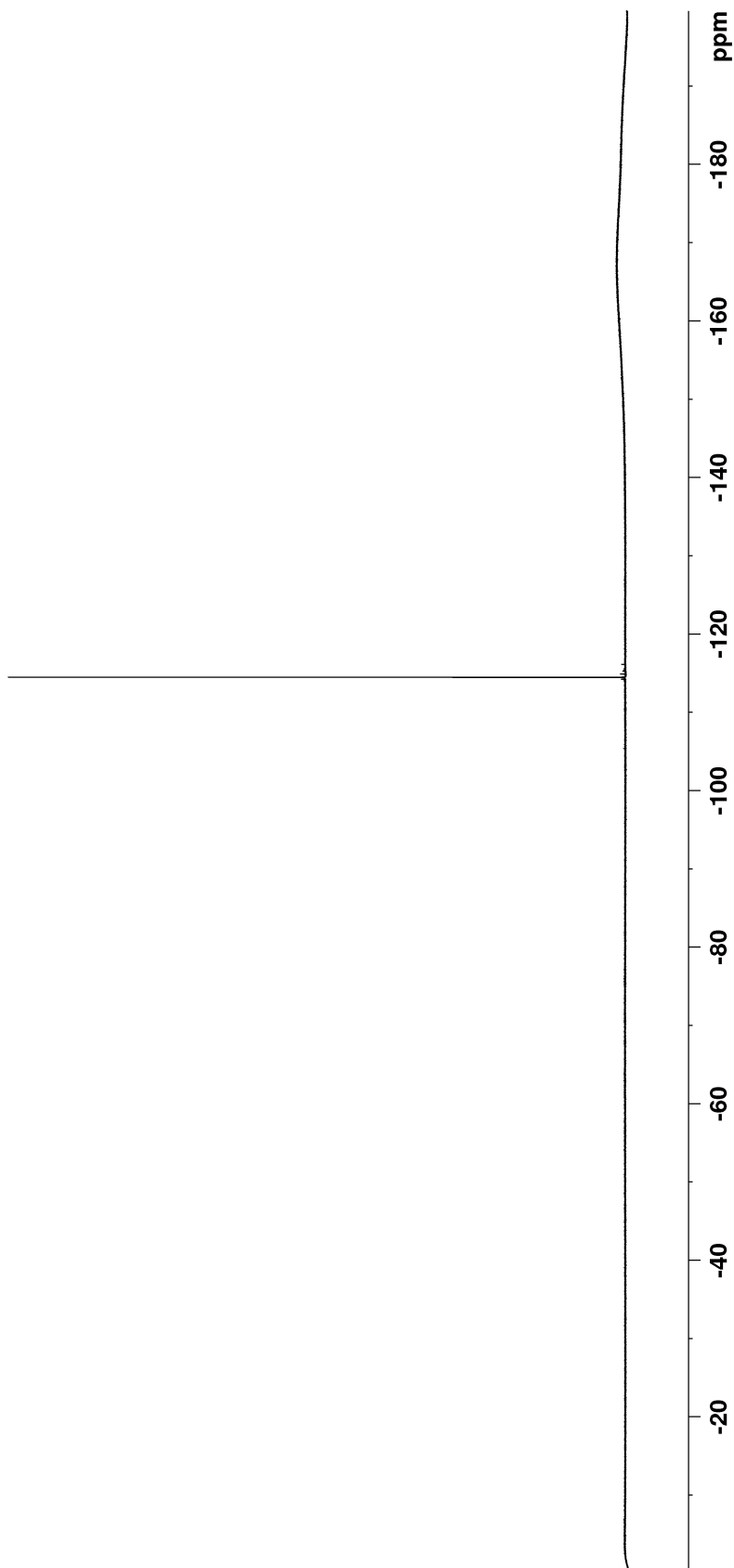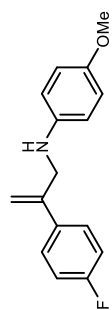
Figure 73. ¹H NMR (400 MHz, CDCl₃) of **120h**
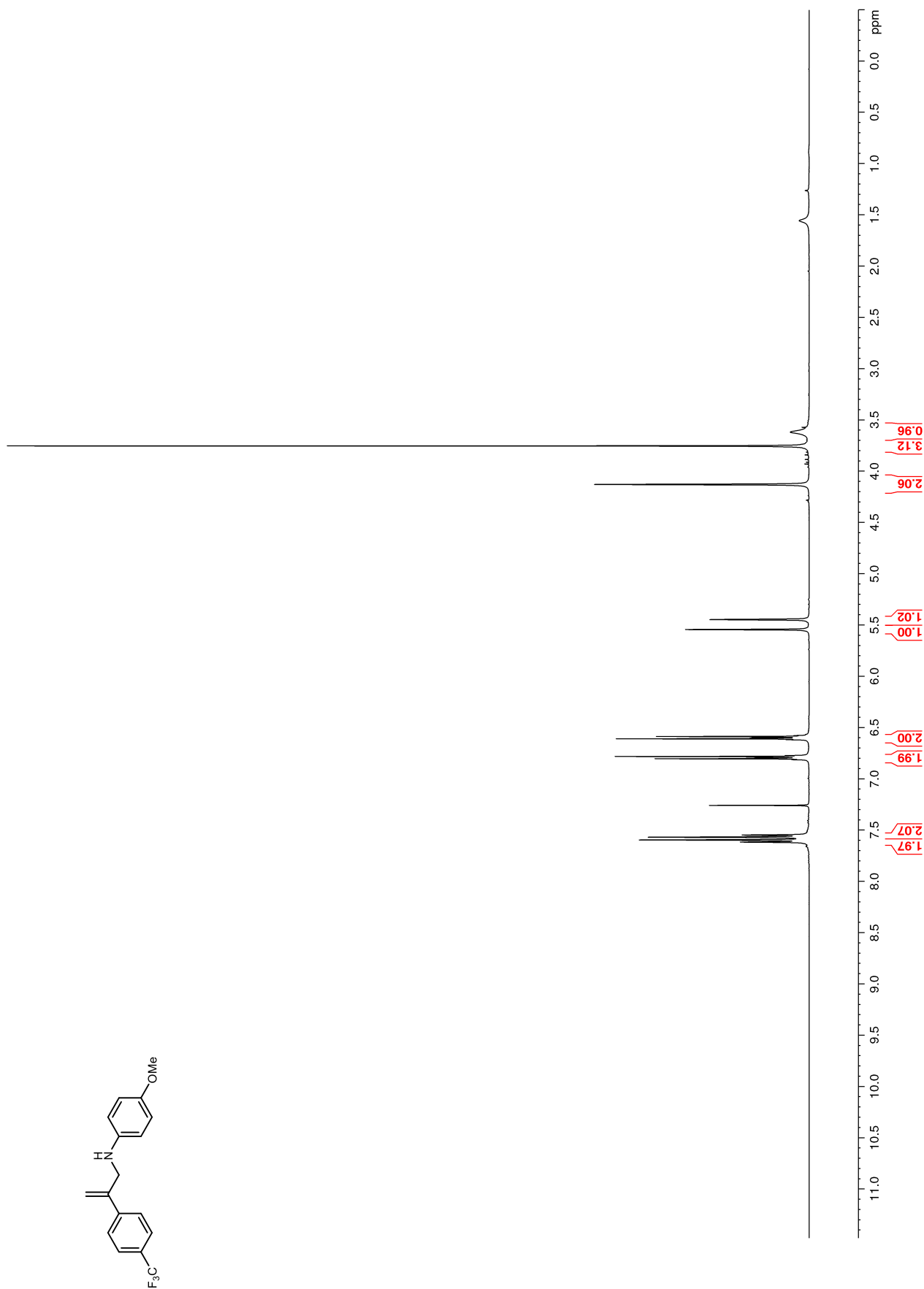
Figure 74. ^{13}C NMR (100 MHz, CDCl$_3$) of **120h**
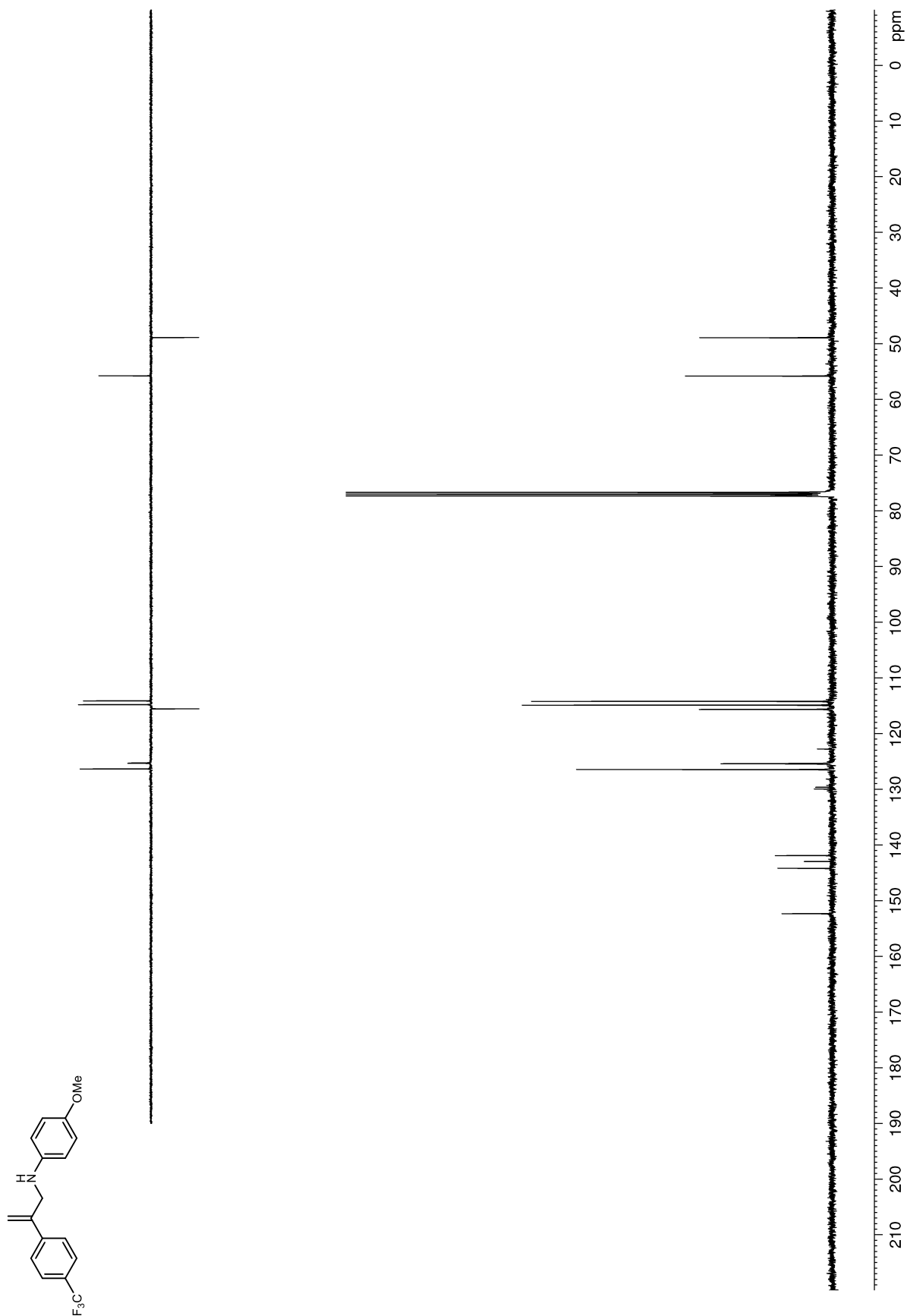
Figure 75. ^{19}F NMR (376 MHz, CDCl$_3$) of **120h**
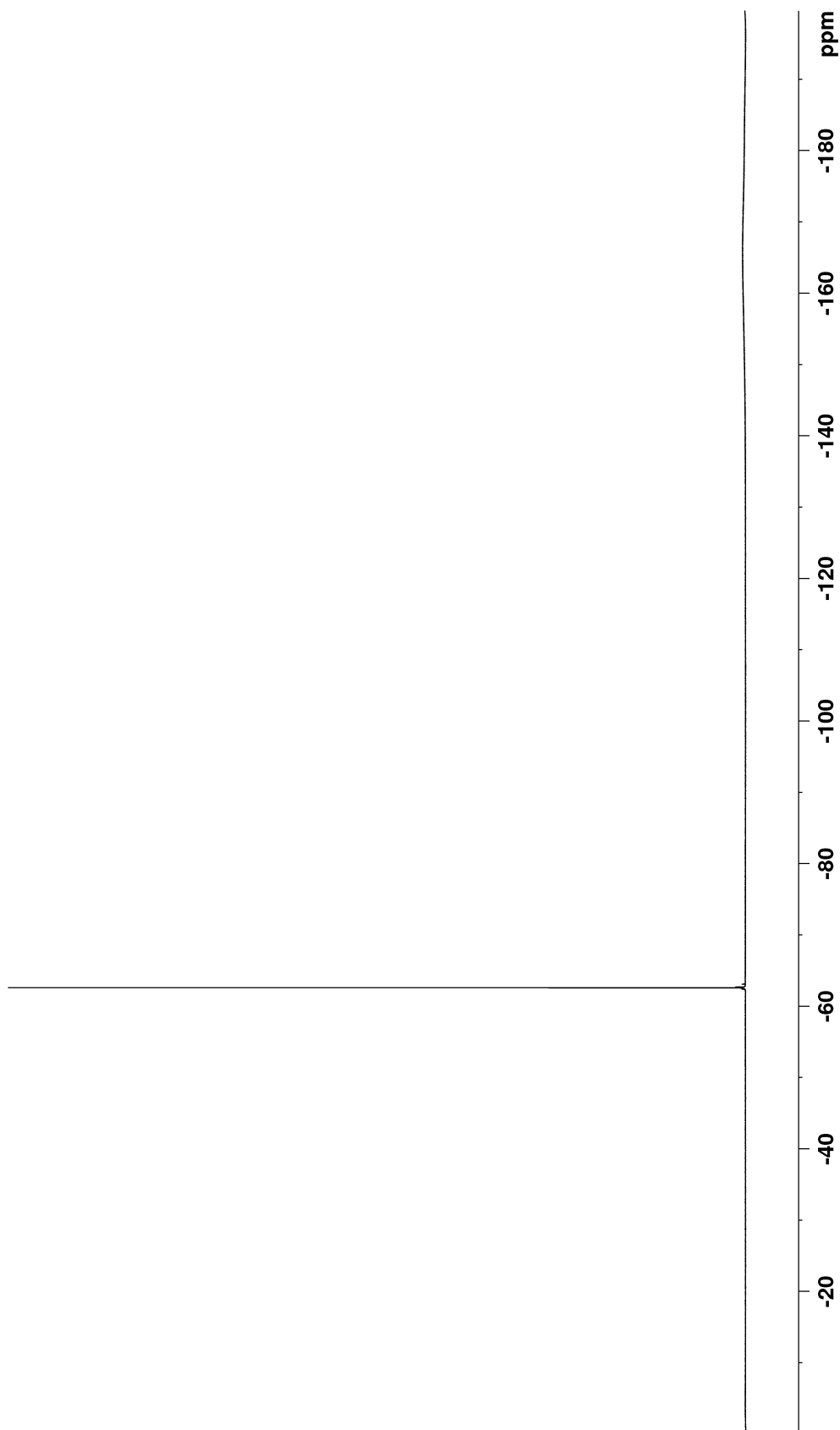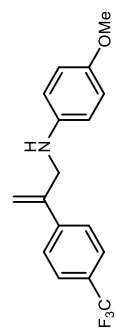
Figure 76. ^{1}H NMR (400 MHz, CDCl$_3$) of **120i**
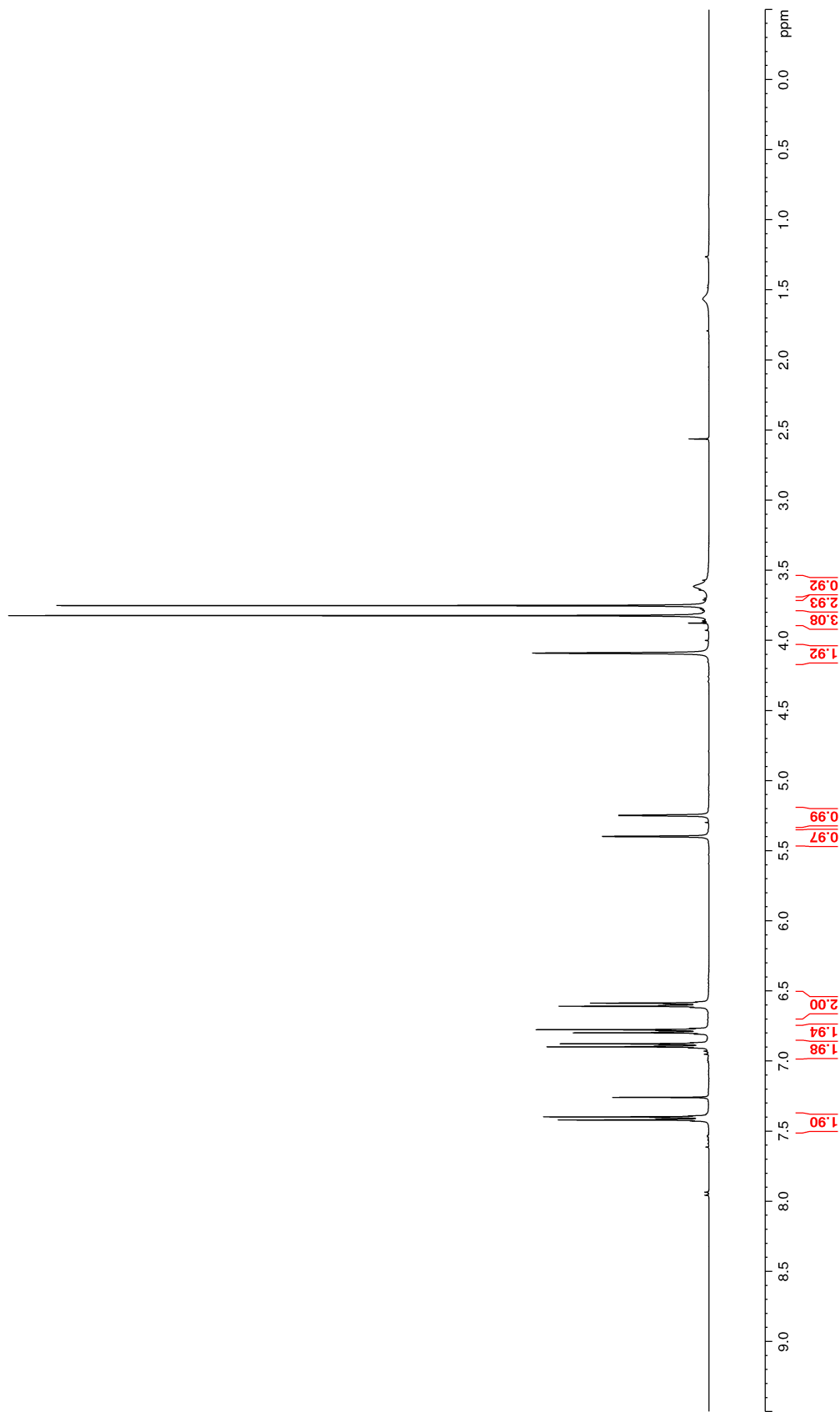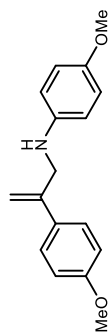
Figure 77. ^{13}C NMR (100 MHz, CDCl$_3$) of **120i**
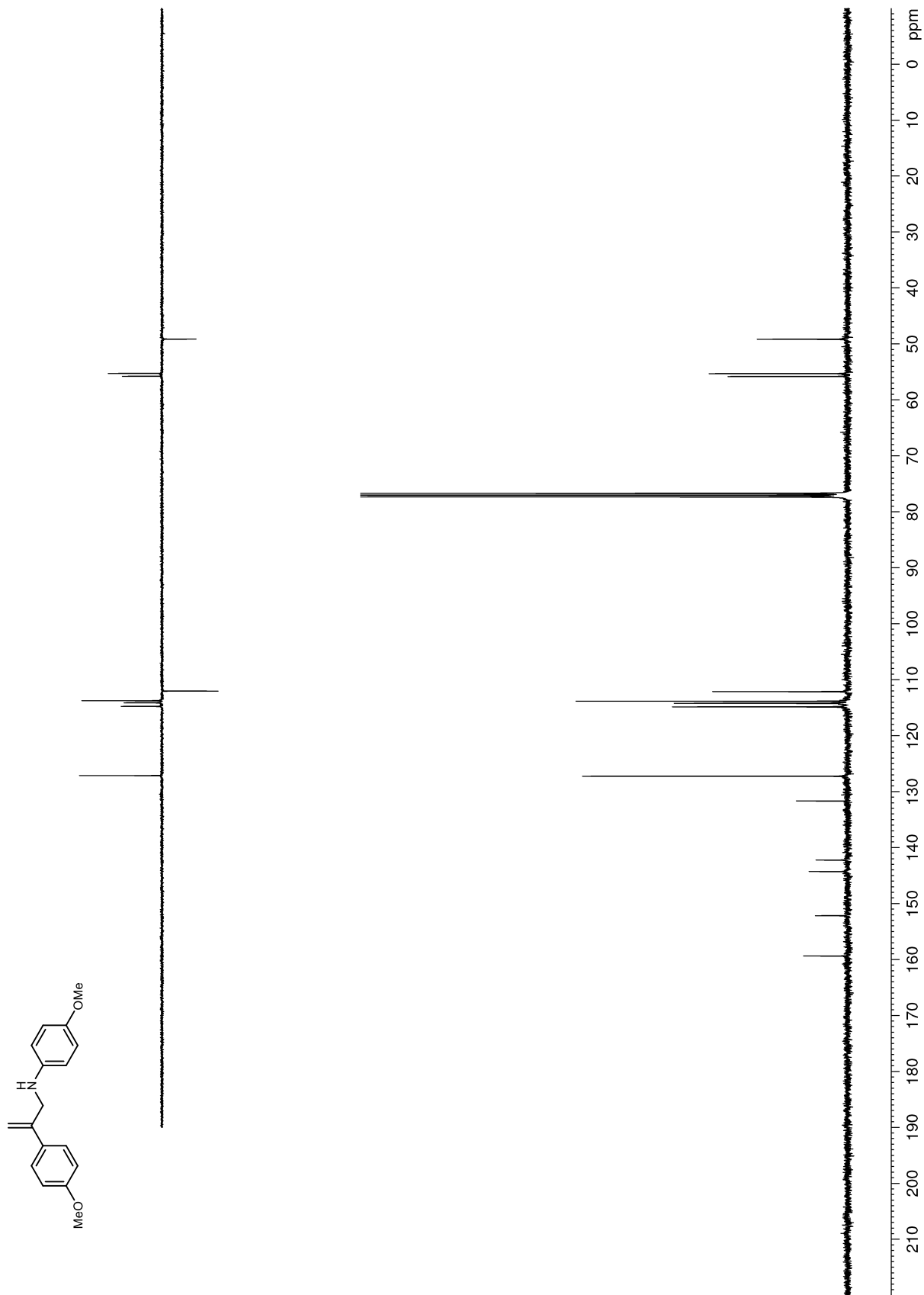
Figure 78. ^{1}H NMR (400 MHz, CDCl$_3$) of **120j**
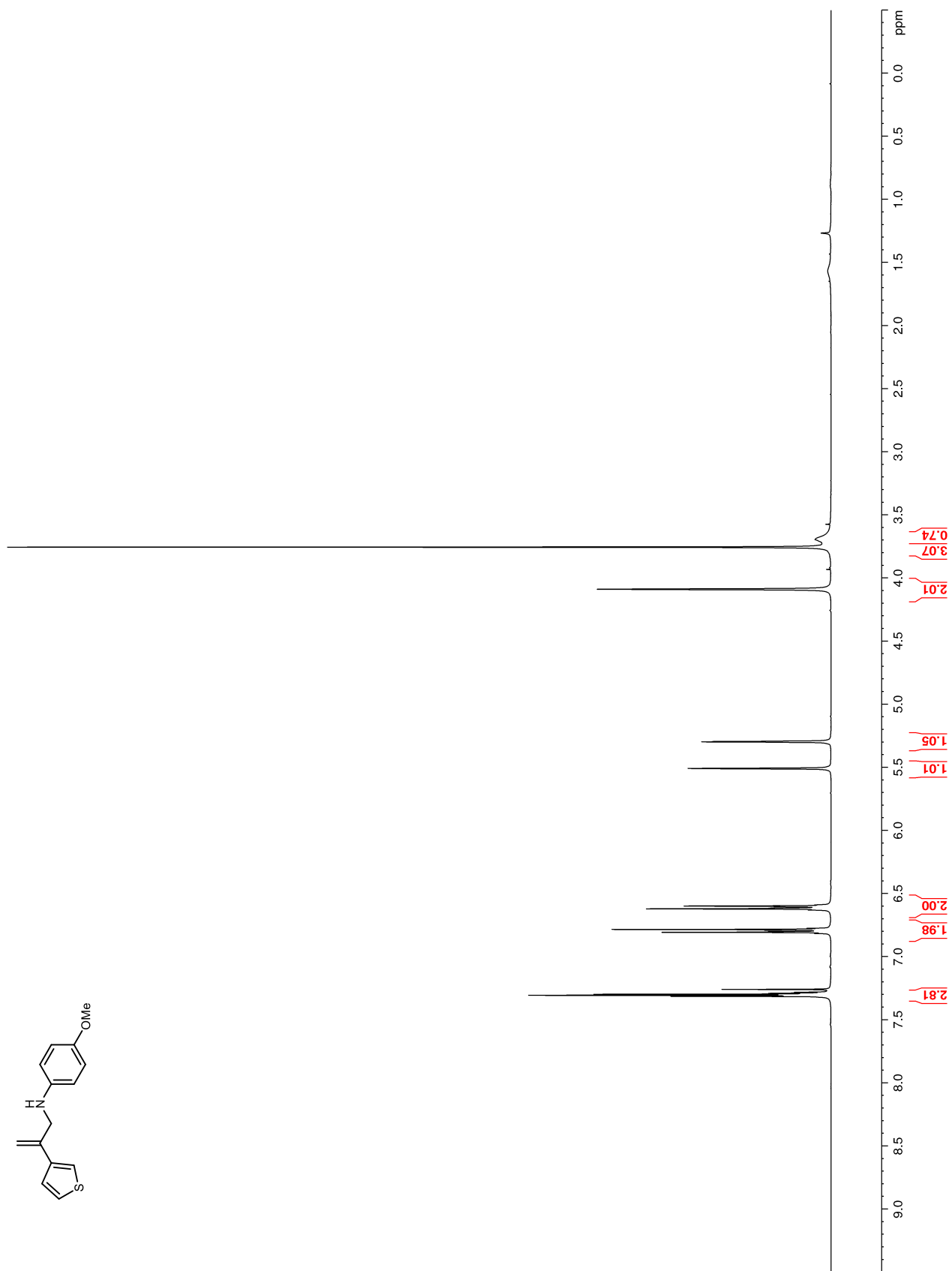
Figure 79. ^{13}C NMR (100 MHz, CDCl$_3$) of **120j**
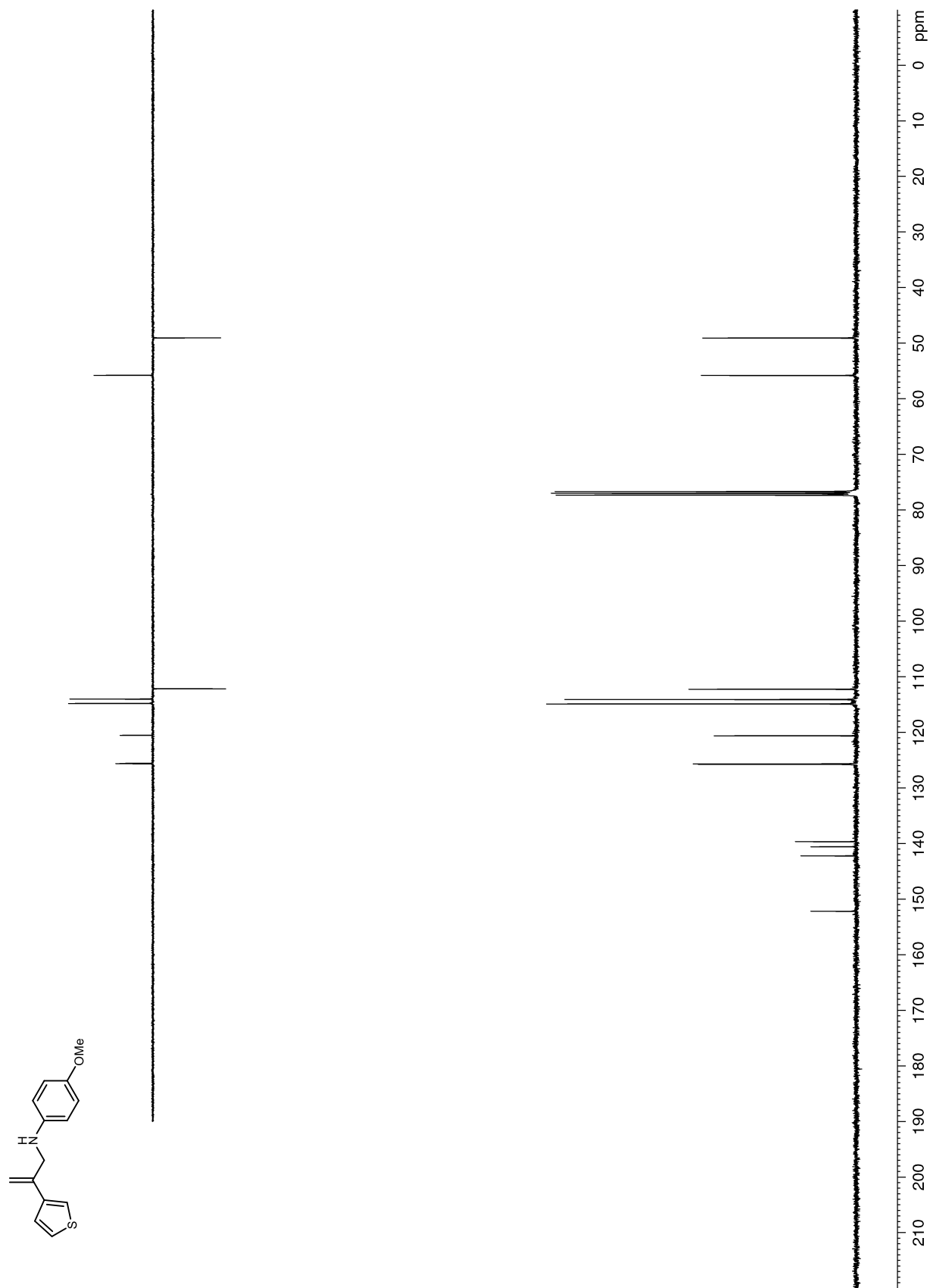
Figure 80. ^{1}H NMR (400 MHz, CDCl$_3$) of **120k**
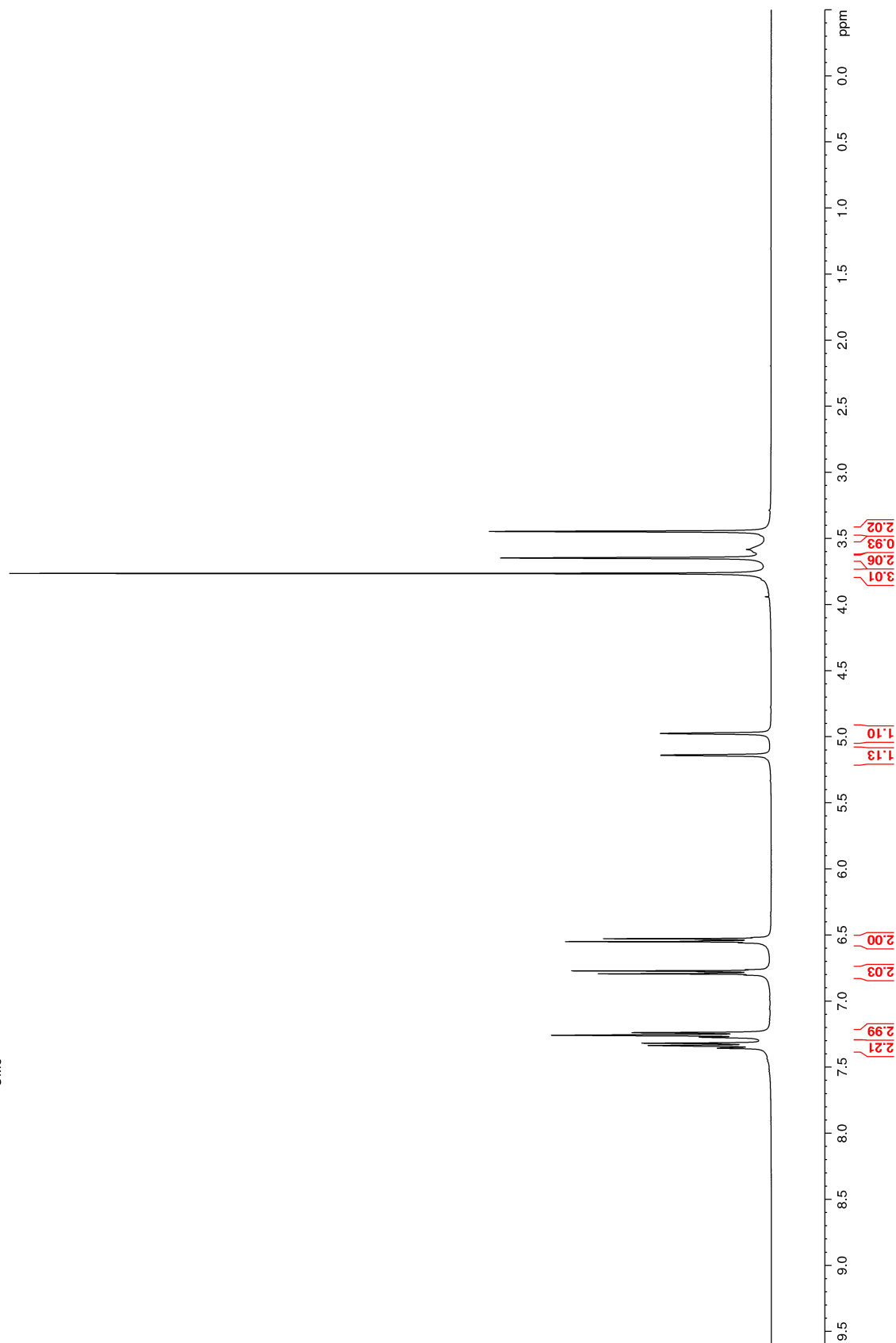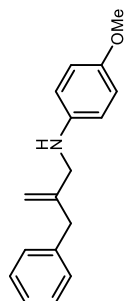
Figure 81. ^{13}C NMR (100 MHz, CDCl$_3$) of **120k**
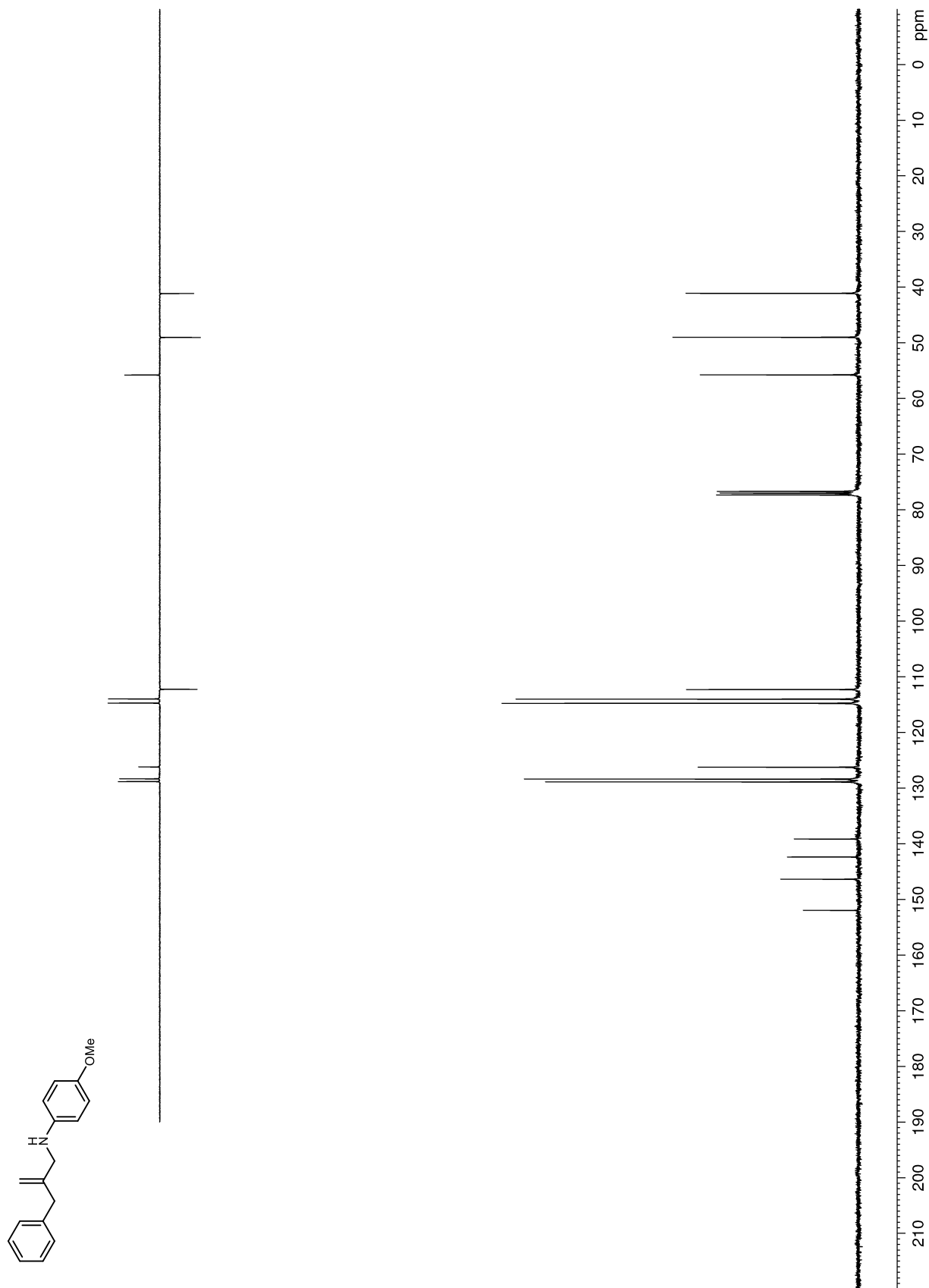
Figure 82. ^{1}H NMR (400 MHz, CDCl$_3$)
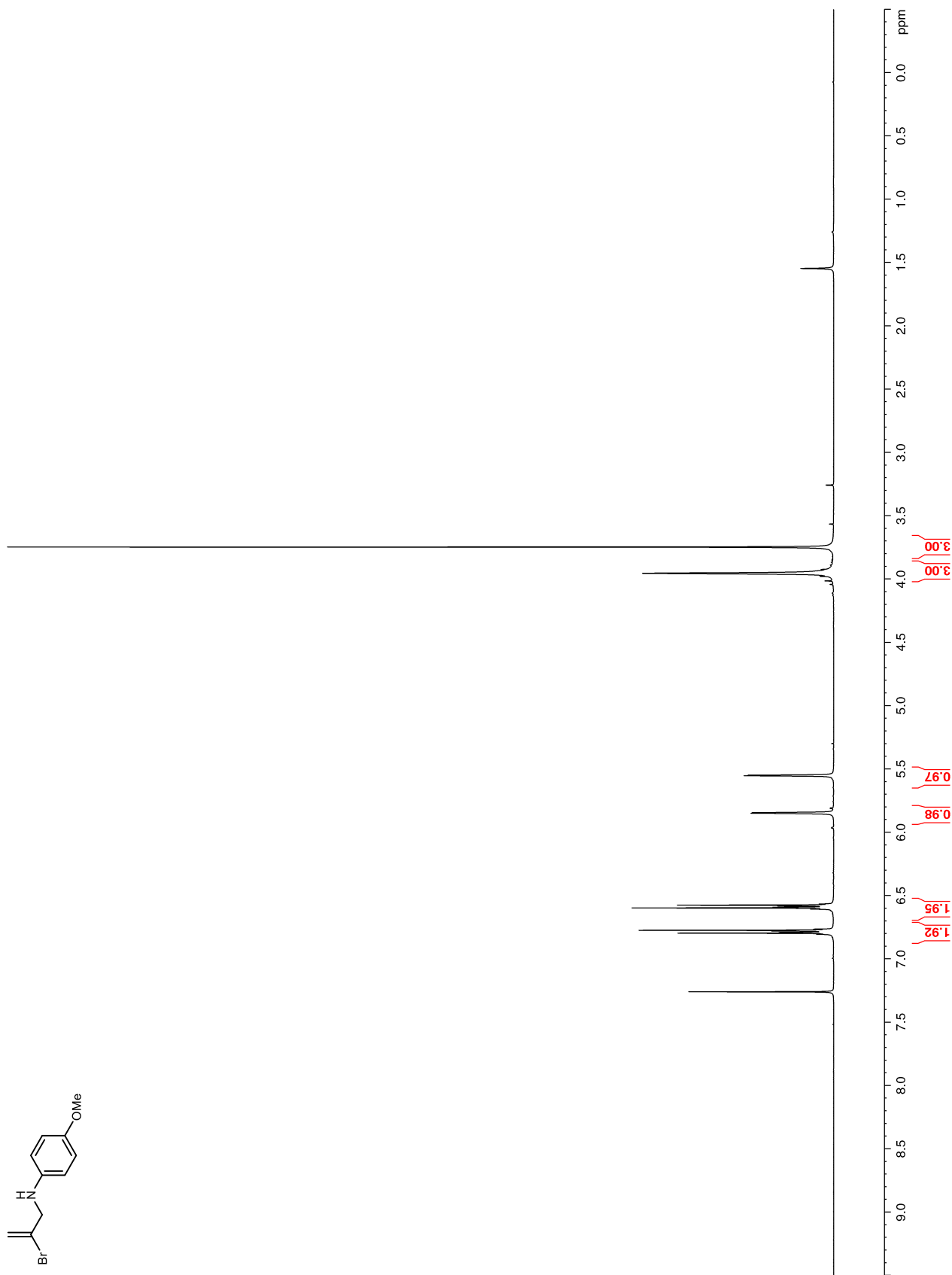
Figure 83. ^{13}C NMR (100 MHz, CDCl$_3$)
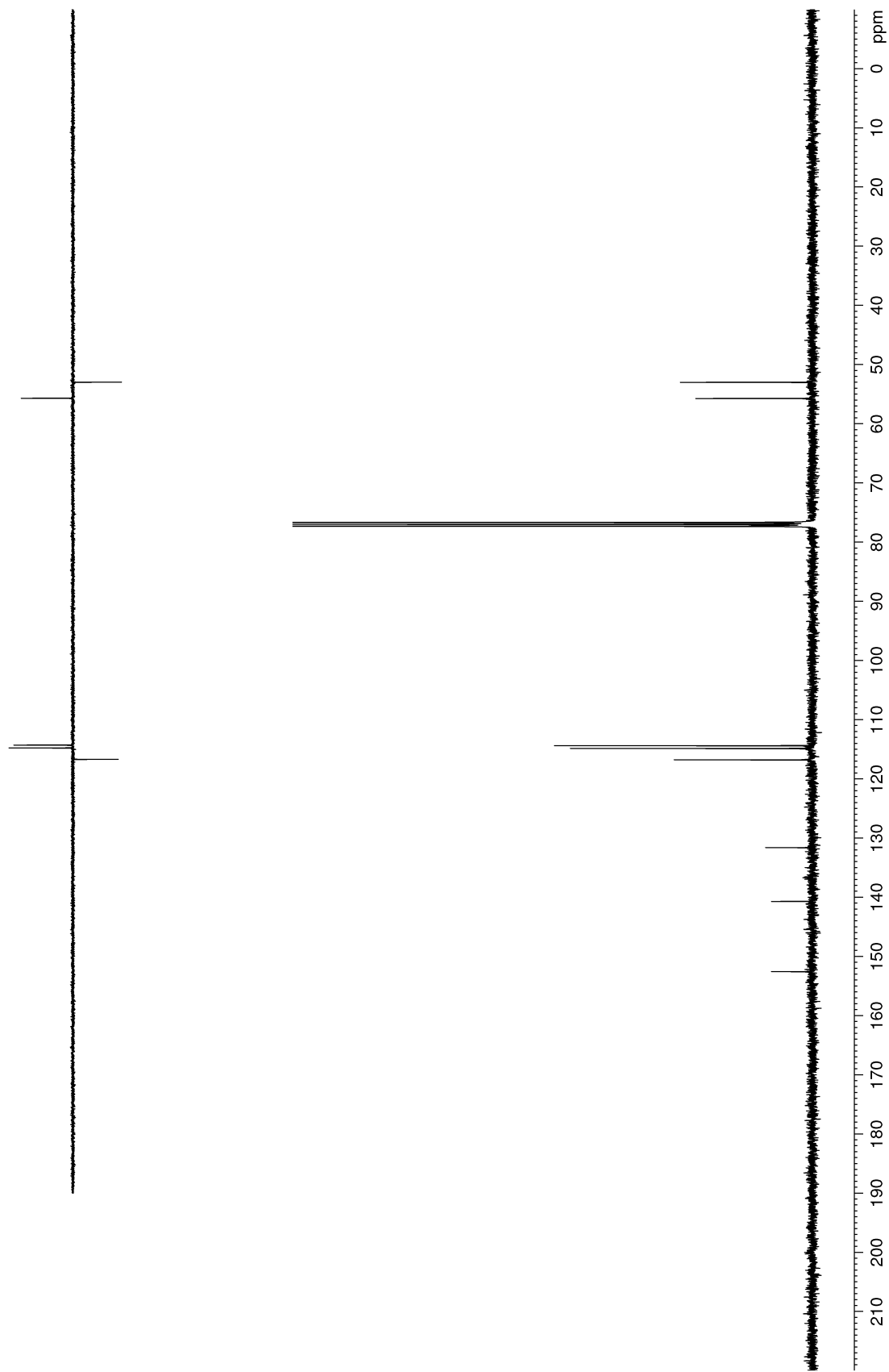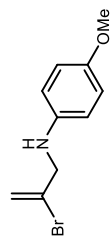
Figure 84. ^{1}H NMR (400 MHz, CDCl$_3$)
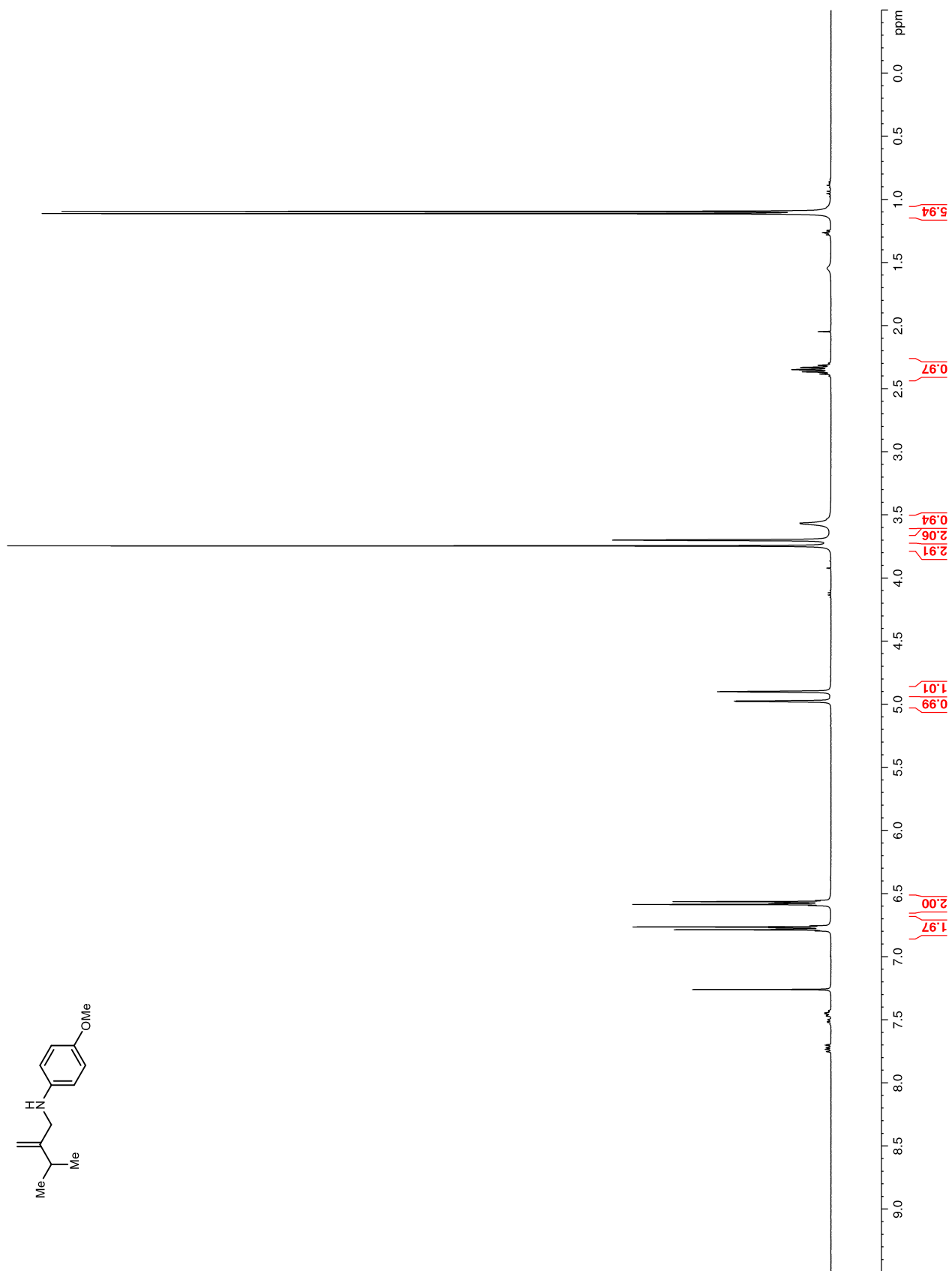
Figure 85. ^{13}C NMR (100 MHz, CDCl$_3$)
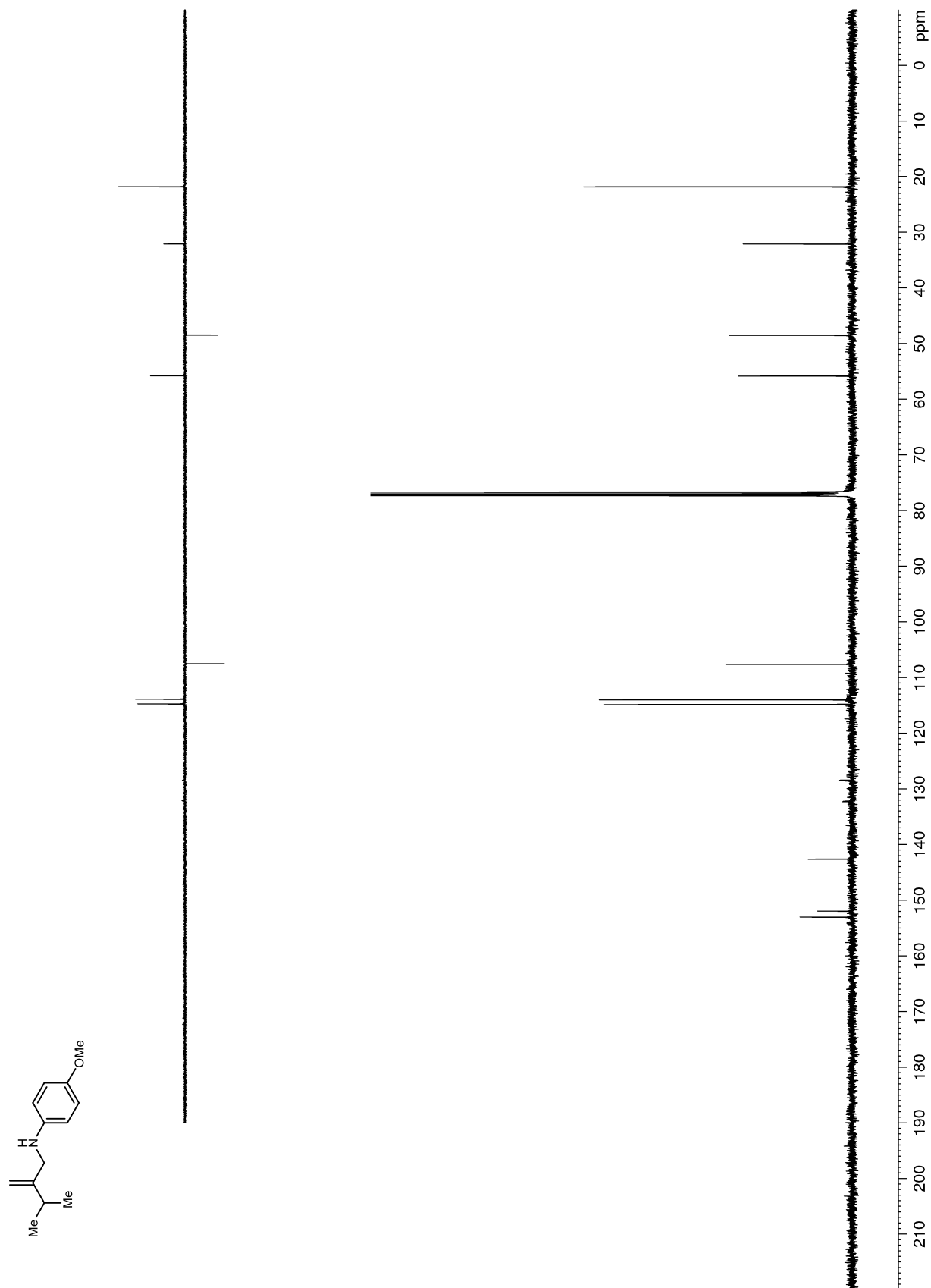
Figure 86. ^{1}H NMR (400 MHz, CDCl$_3$) of **125a**
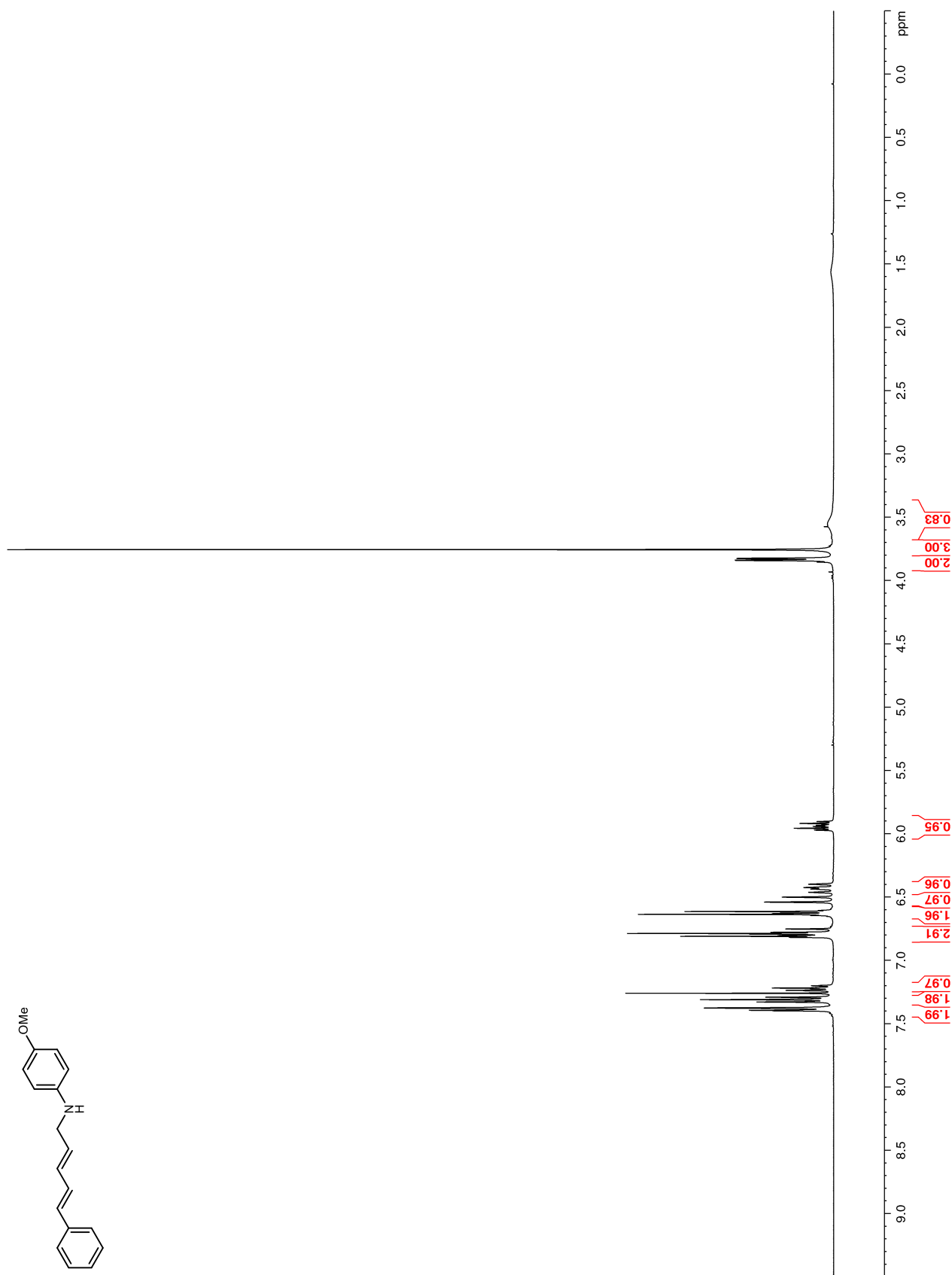
Figure 87. ^{13}C NMR (100 MHz, CDCl$_3$) of **125a**
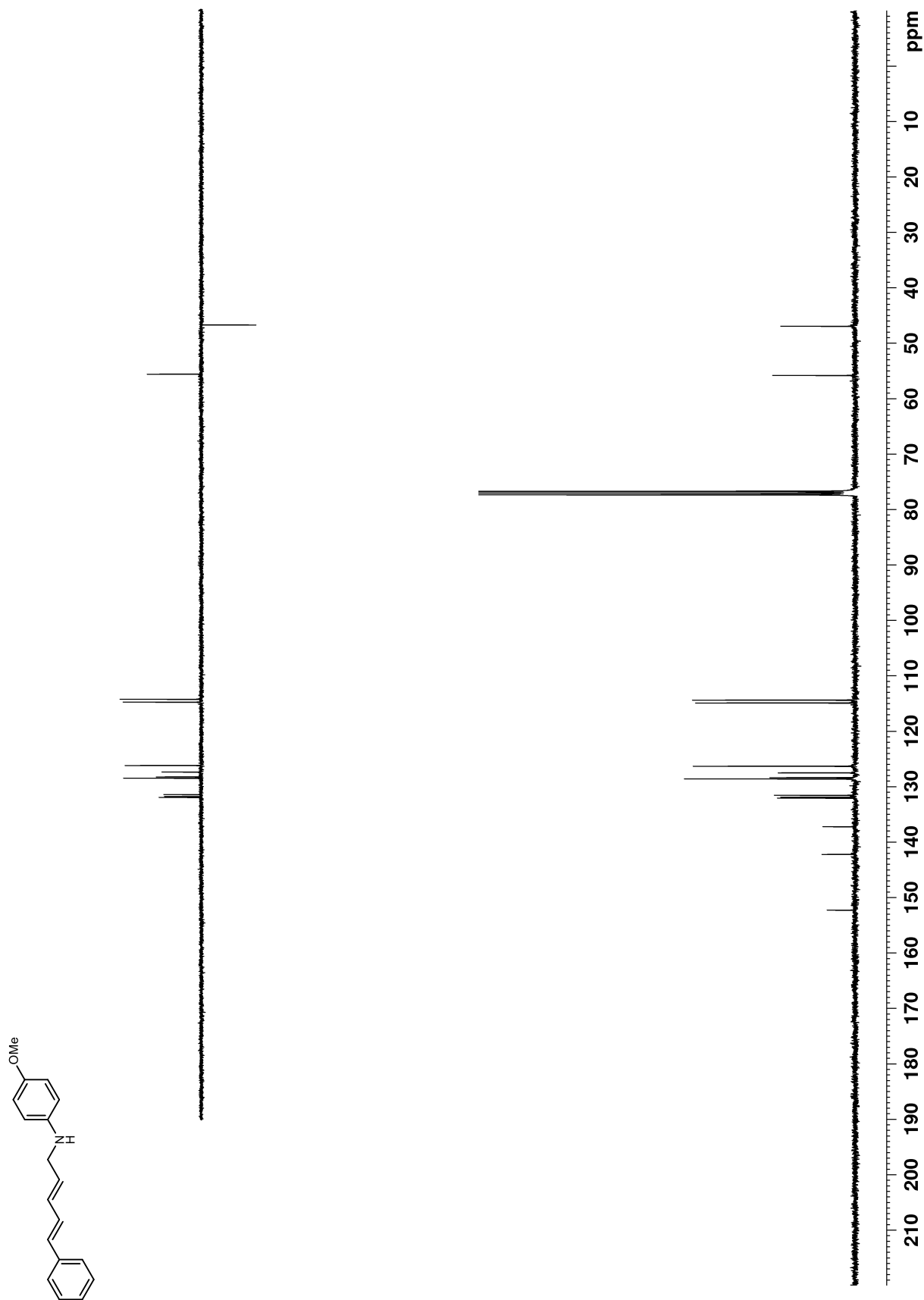
Figure 88. ^{1}H NMR (400 MHz, CDCl$_3$) of **125c**
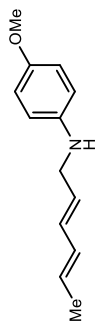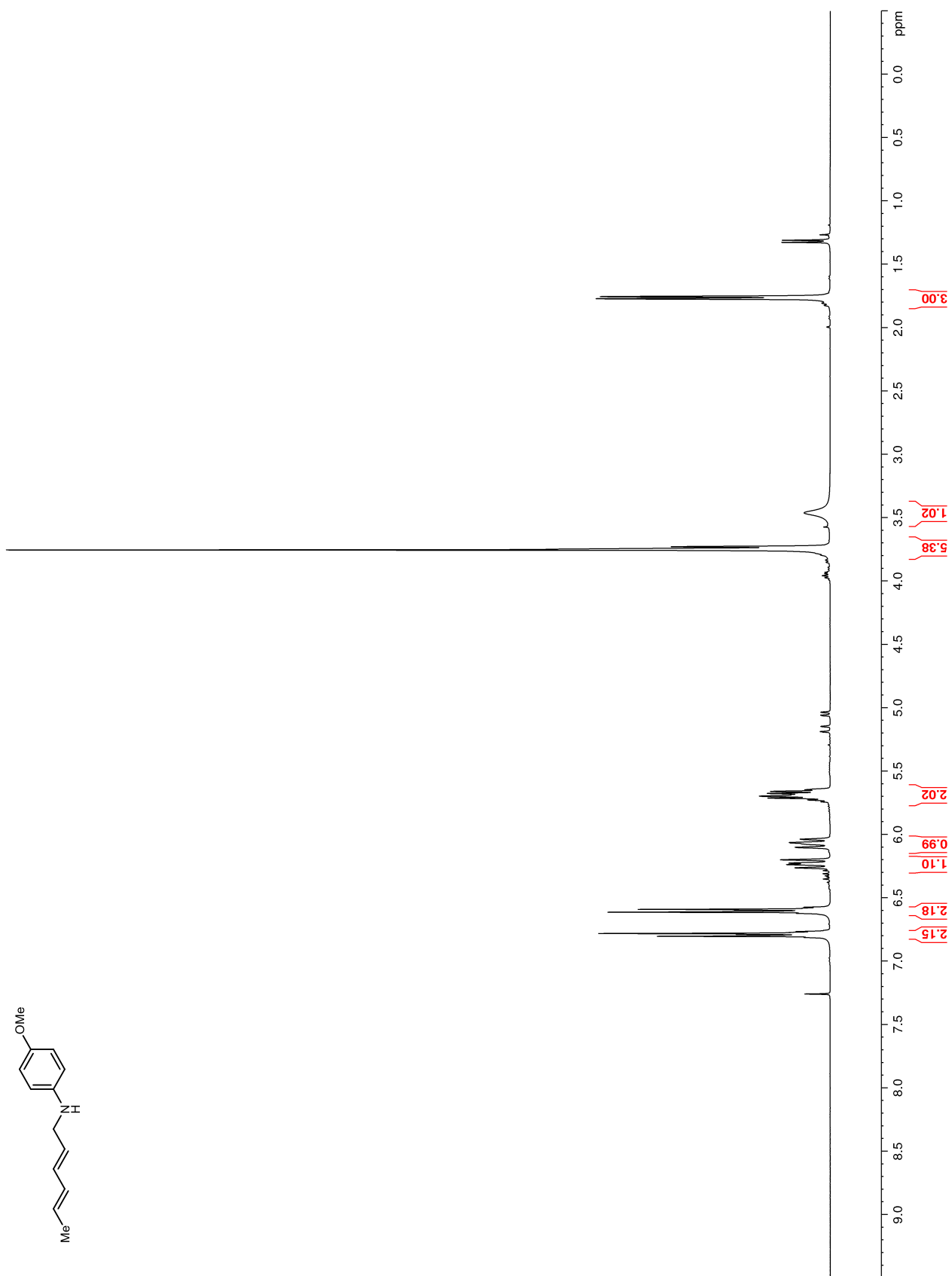
Figure 89. ^{13}C NMR (100 MHz, CDCl$_3$) of **125c**
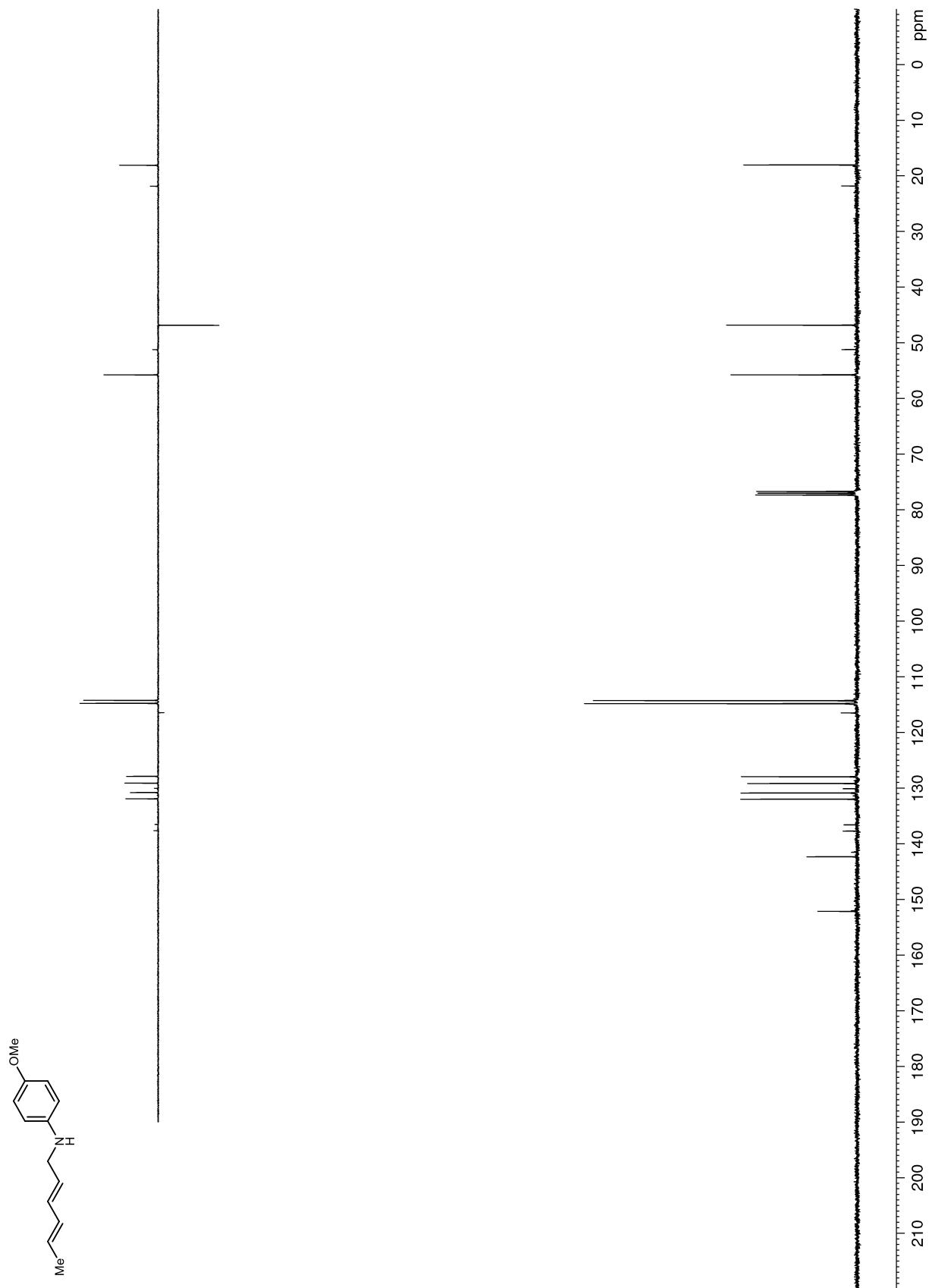
Figure 90. ^{1}H NMR (400 MHz, CDCl$_3$) of **125d**
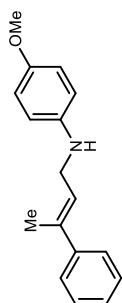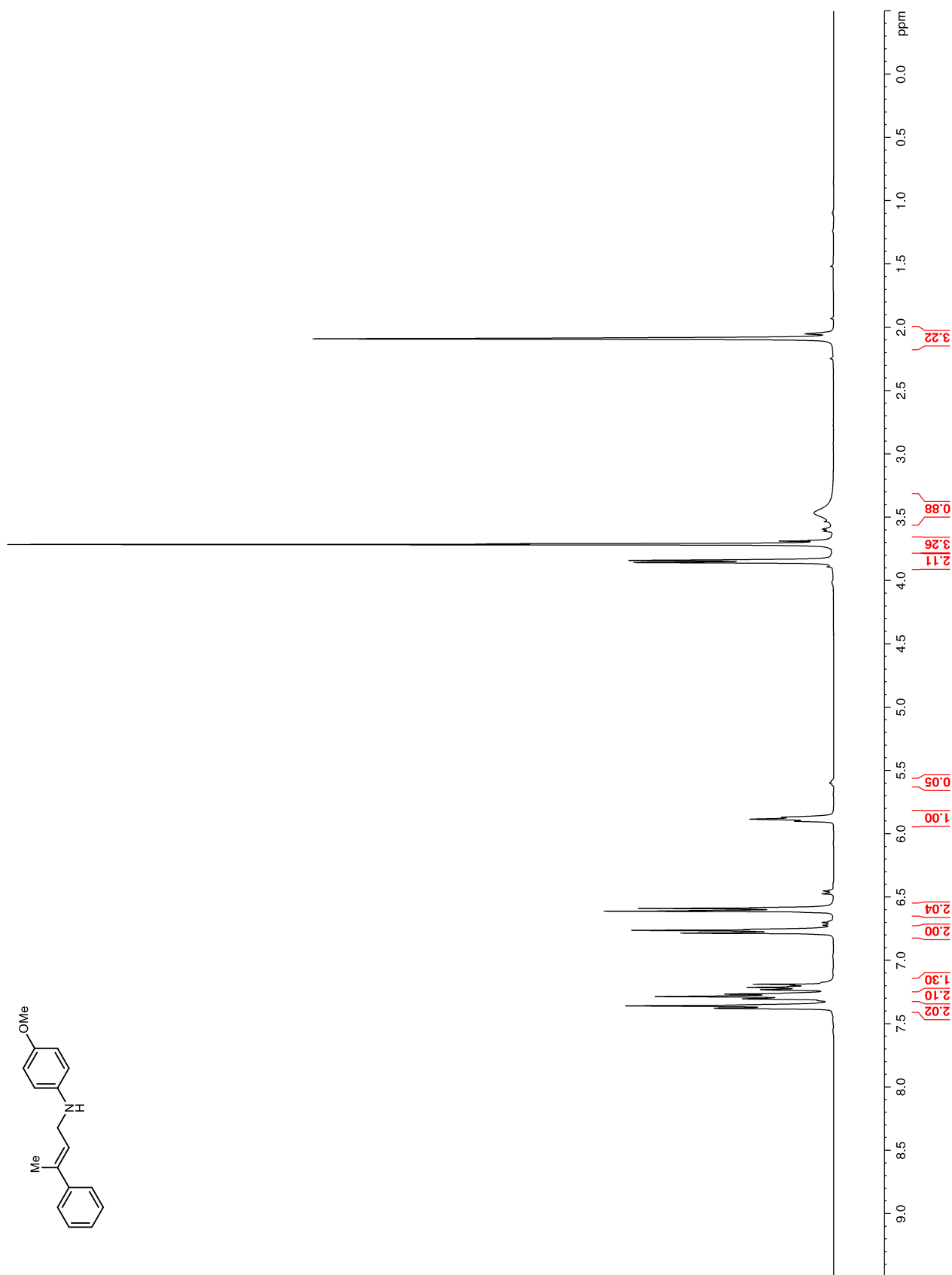
Figure 91. ^{13}C NMR (100 MHz, CDCl$_3$) of **125d**
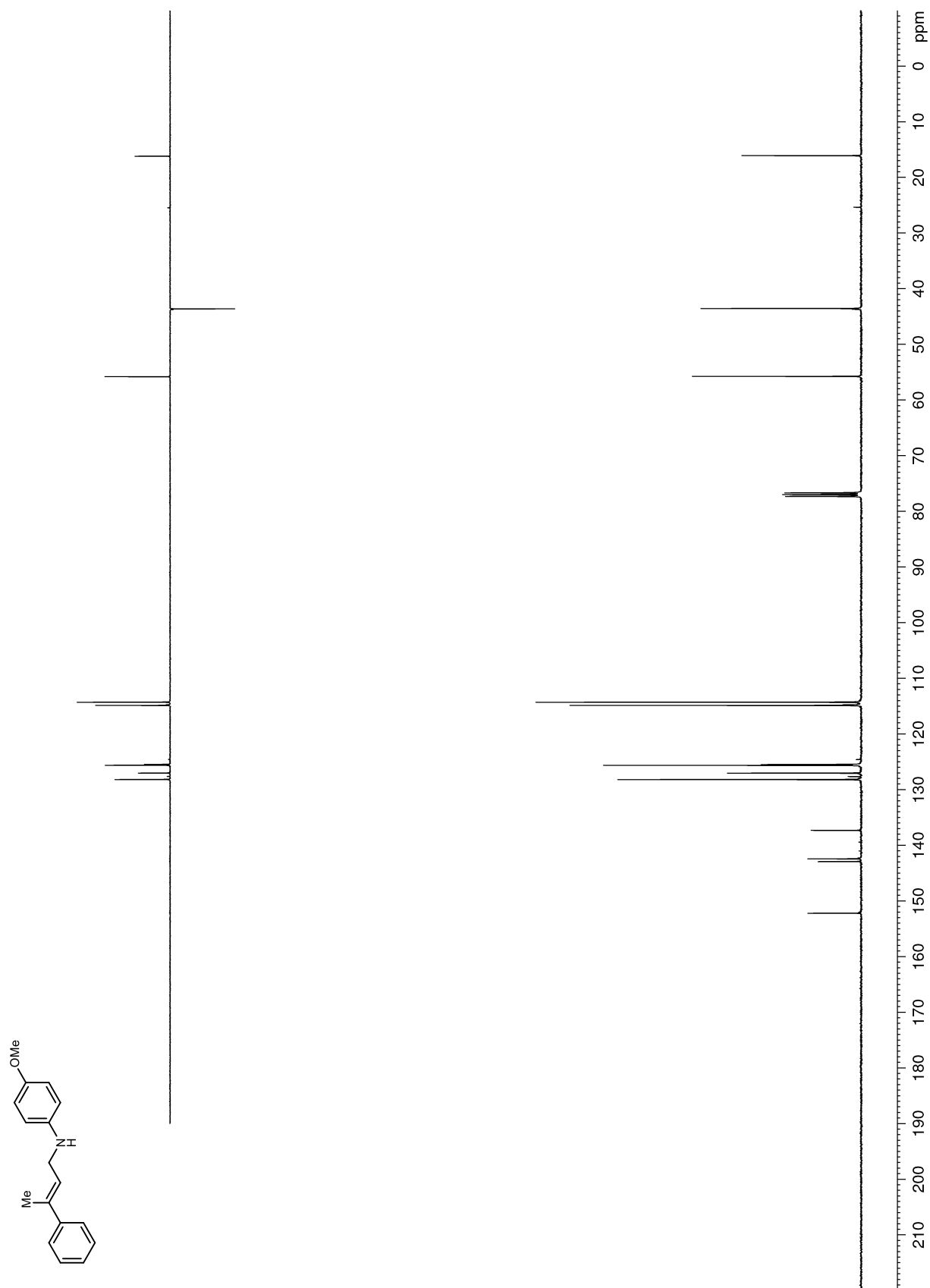
Figure 92. ^{1}H NMR (400 MHz, CDCl$_3$) of **121a**
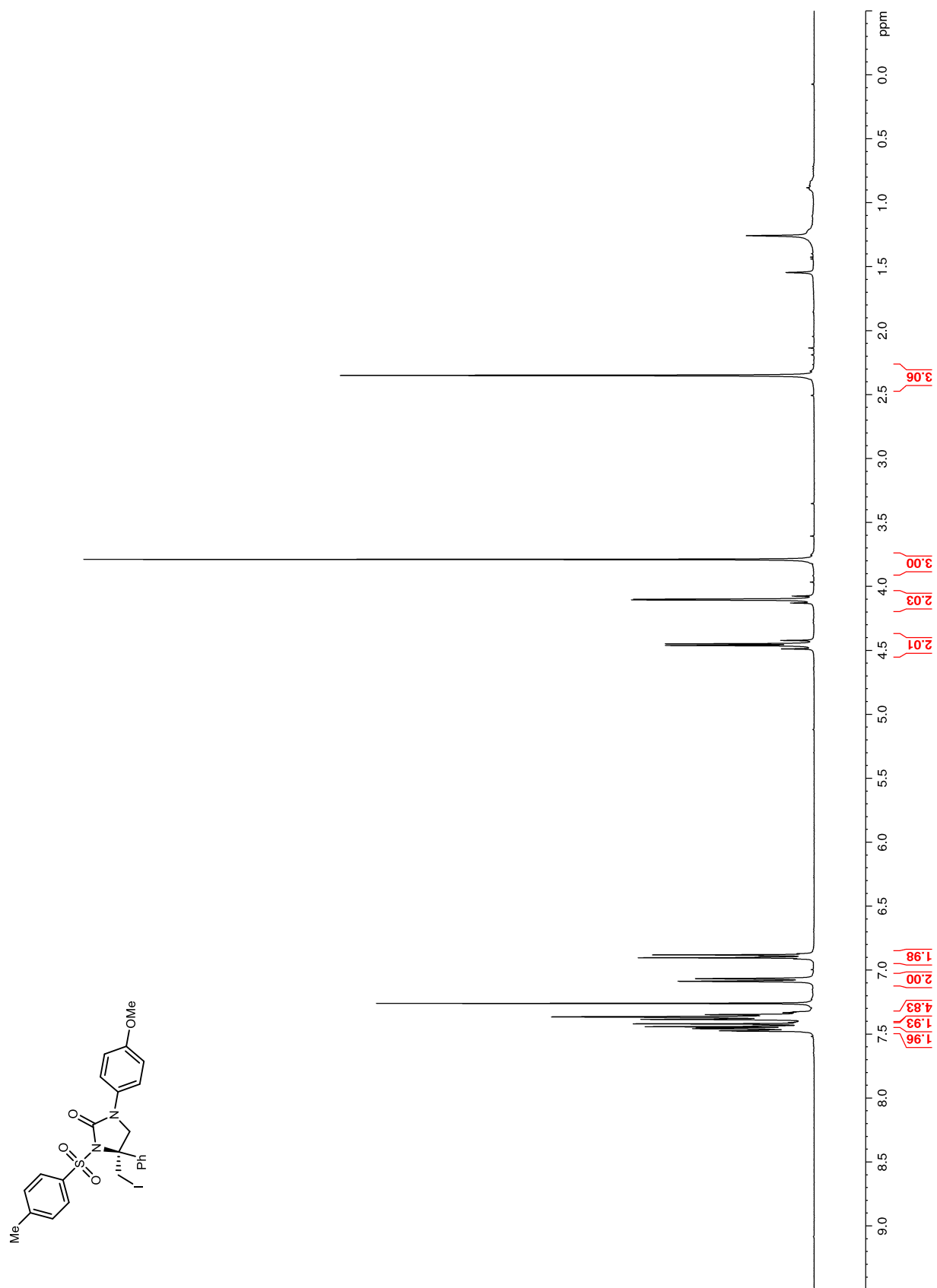
Figure 93. ^{13}C NMR (100 MHz, CDCl$_3$) of **121a**
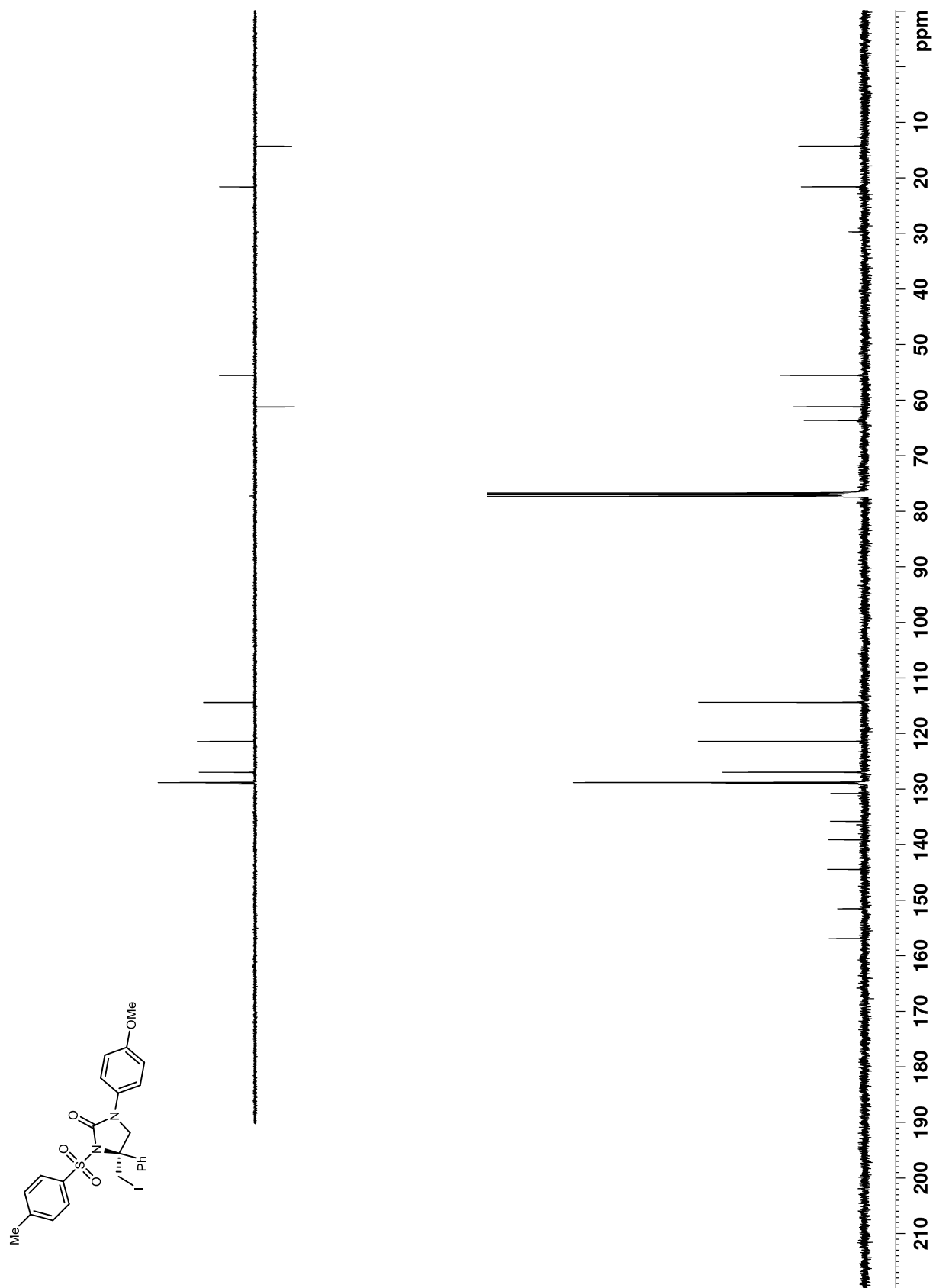
Figure 94. HPLC trace of **121a**. Chiralcel IB 25% EtOH/hexanes, 1.0 mL/min, 30 ºC
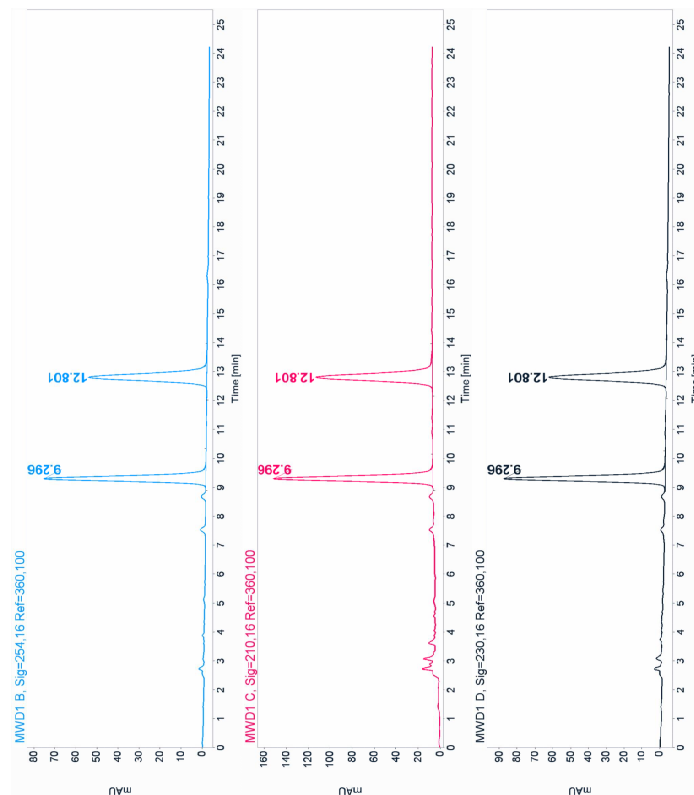
Signal: MWD1 B, Sig=254,16 Ref=360,100

RT [min]	Type	Width [min]	Area	Height	Area% Name
9.296	MF	0.2149	993.6379	77.0763	49.8733
12.801	FM	0.2970	998.6868	56.0471	50.1267
		Sum	1992.3247		

Signal: MWD1 C, Sig=210,16 Ref=360,100

RT [min]	Type	Width [min]	Area	Height	Area% Name
9.296	MF	0.2160	1876.8495	144.8276	49.7624
12.801	FM	0.2995	1894.7690	105.4569	50.2376
		Sum	3771.6185		

Signal: MWD1 D, Sig=230,16 Ref=360,100

RT [min]	Type	Width [min]	Area	Height	Area% Name
9.296	MF	0.2169	1178.6044	90.5626	49.9259
12.801	FM	0.2993	1182.1024	65.8272	50.0741
		Sum	2360.7068		

Signal: MWD1 B, Sig=254,16 Ref=360,100

RT [min]	Type	Width [min]	Area	Height	Area% Name
9.245	MF	0.2141	903.9155	70.3762	98.4540
12.688	FM	0.3205	14.1939	0.7382	1.5460
		Sum	918.1094		

Signal: MWD1 C, Sig=210,16 Ref=360,100

RT [min]	Type	Width [min]	Area	Height	Area% Name
9.245	MF	0.2153	1712.3983	132.5459	97.6011
12.694	FM	0.4196	42.0892	1.6716	2.3989
		Sum	1754.4876		

Signal: MWD1 D, Sig=230,16 Ref=360,100

RT [min]	Type	Width [min]	Area	Height	Area% Name
9.245	MF	0.2144	1063.5018	82.6792	98.3021
12.690	FM	0.3398	18.3696	0.9011	1.6979
		Sum	1081.8714		

Appendix 4.2-254
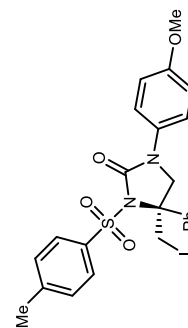
Figure 95. ^{1}H NMR (400 MHz, CDCl$_3$) of **121b**
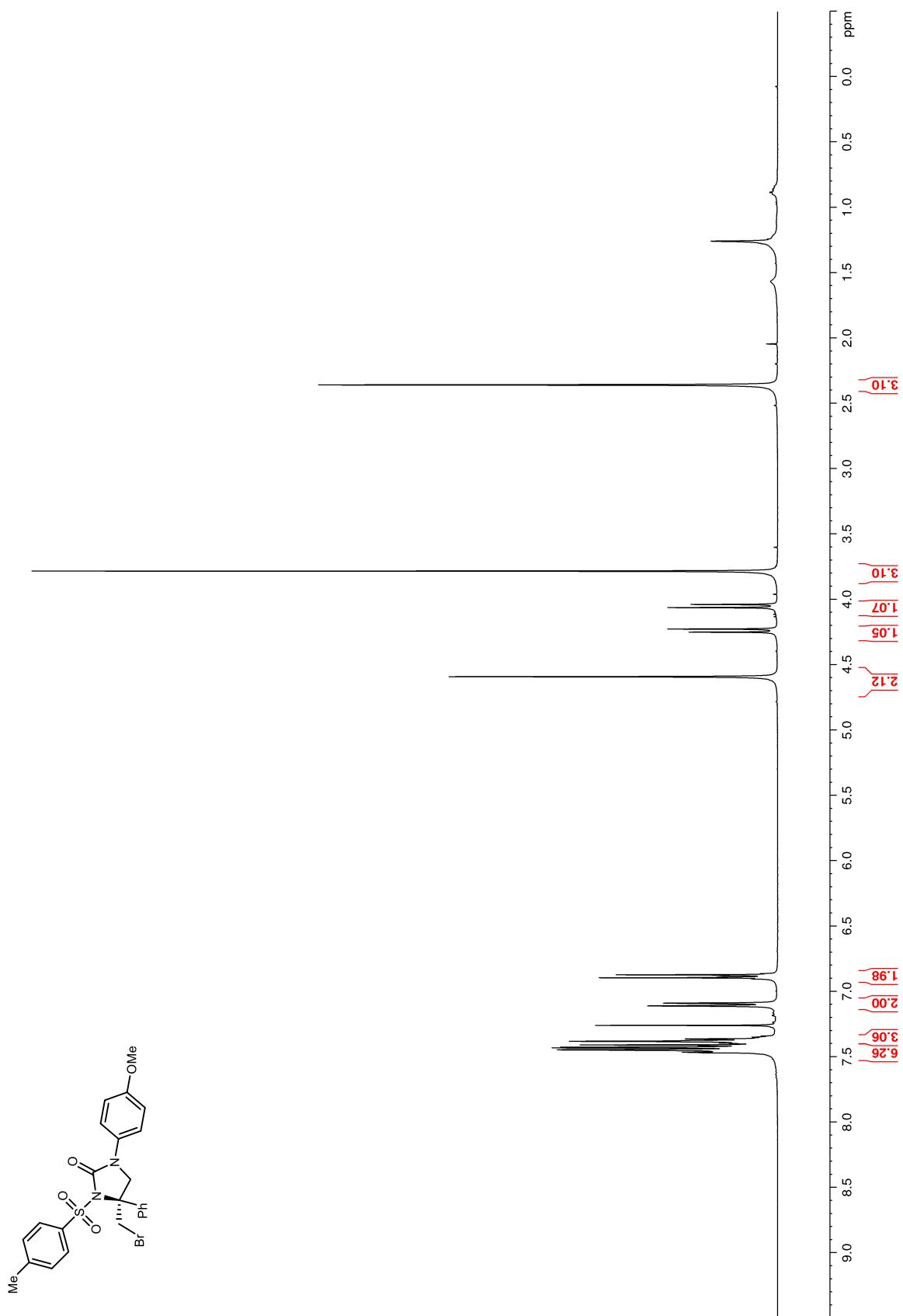
Figure 96. ^{13}C NMR (100 MHz, CDCl$_3$) of **121b**

Figure 97. HPLC trace of **121b**. Chiralcel IB 25% EtOH/hexanes, 1.0 mL/min, 30 ºC
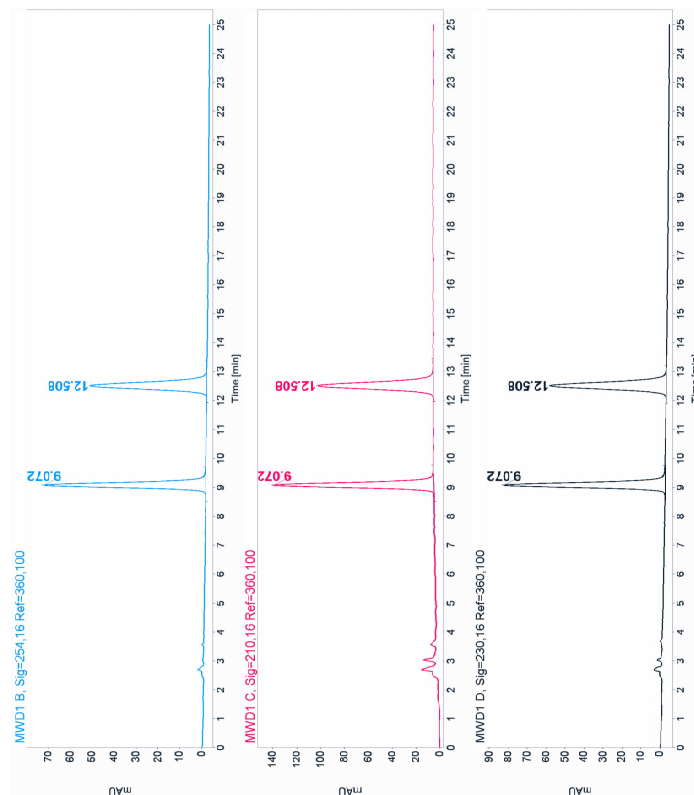
Signal: MWD1 B, Sig=254,16 Ref=360,100

RT [min]	Type	Width [min]	Area	Height	Area%	Name
9.072	MM	0.2082	923.8829	73.9411	50.3484	
12.508	MM	0.2855	911.0981	53.1826	49.6516	
		Sum	1834.9810			

Signal: MWD1 C, Sig=210,16 Ref=360,100

RT [min]	Type	Width [min]	Area	Height	Area%	Name
9.072	MM	0.2080	1676.1353	134.2877	50.0794	
12.508	MM	0.2874	1670.8180	96.9075	49.9206	
		Sum	3346.9532			

Signal: MWD1 D, Sig=230,16 Ref=360,100

RT [min]	Type	Width [min]	Area	Height	Area%	Name
9.072	MM	0.2090	1069.7747	85.3212	50.3280	
12.508	MM	0.2865	1055.8318	61.4245	49.6720	
		Sum	2125.6064			

Signal: MWD1 B, Sig=254,16 Ref=360,100

RT [min]	Type	Width [min]	Area	Height	Area%	Name
9.052	MM	0.2094	734.8335	58.4928	78.0572	
12.463	MM	0.2905	206.5707	11.8531	21.9428	
		Sum	941.4042			

Signal: MWD1 C, Sig=210,16 Ref=360,100

RT [min]	Type	Width [min]	Area	Height	Area%	Name
9.052	MM	0.2073	1322.2778	106.3031	77.3330	
12.463	MM	0.2982	387.5716	21.6617	22.6670	
		Sum	1709.8494			

Signal: MWD1 D, Sig=230,16 Ref=360,100

RT [min]	Type	Width [min]	Area	Height	Area%	Name
9.052	MM	0.2079	841.8255	67.4801	77.9553	
12.463	MM	0.2905	238.0563	13.6573	22.0447	
		Sum	1079.8818			

Appendix 4.2-257
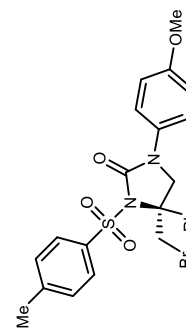
Figure 98. ^{1}H NMR (400 MHz, CDCl$_3$) of **121c**
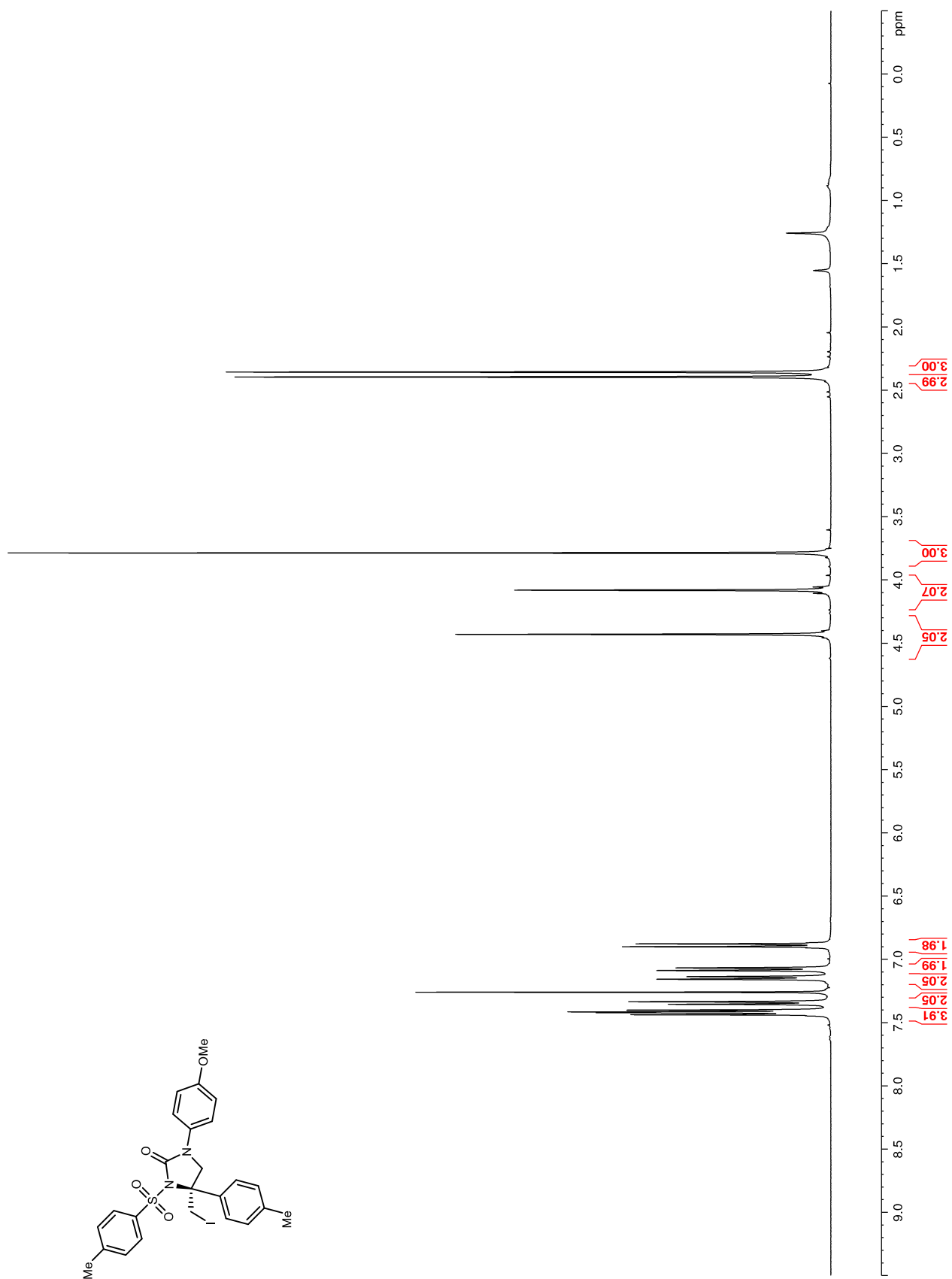
Figure 99. ^{13}C NMR (100 MHz, CDCl$_3$) of **121c**
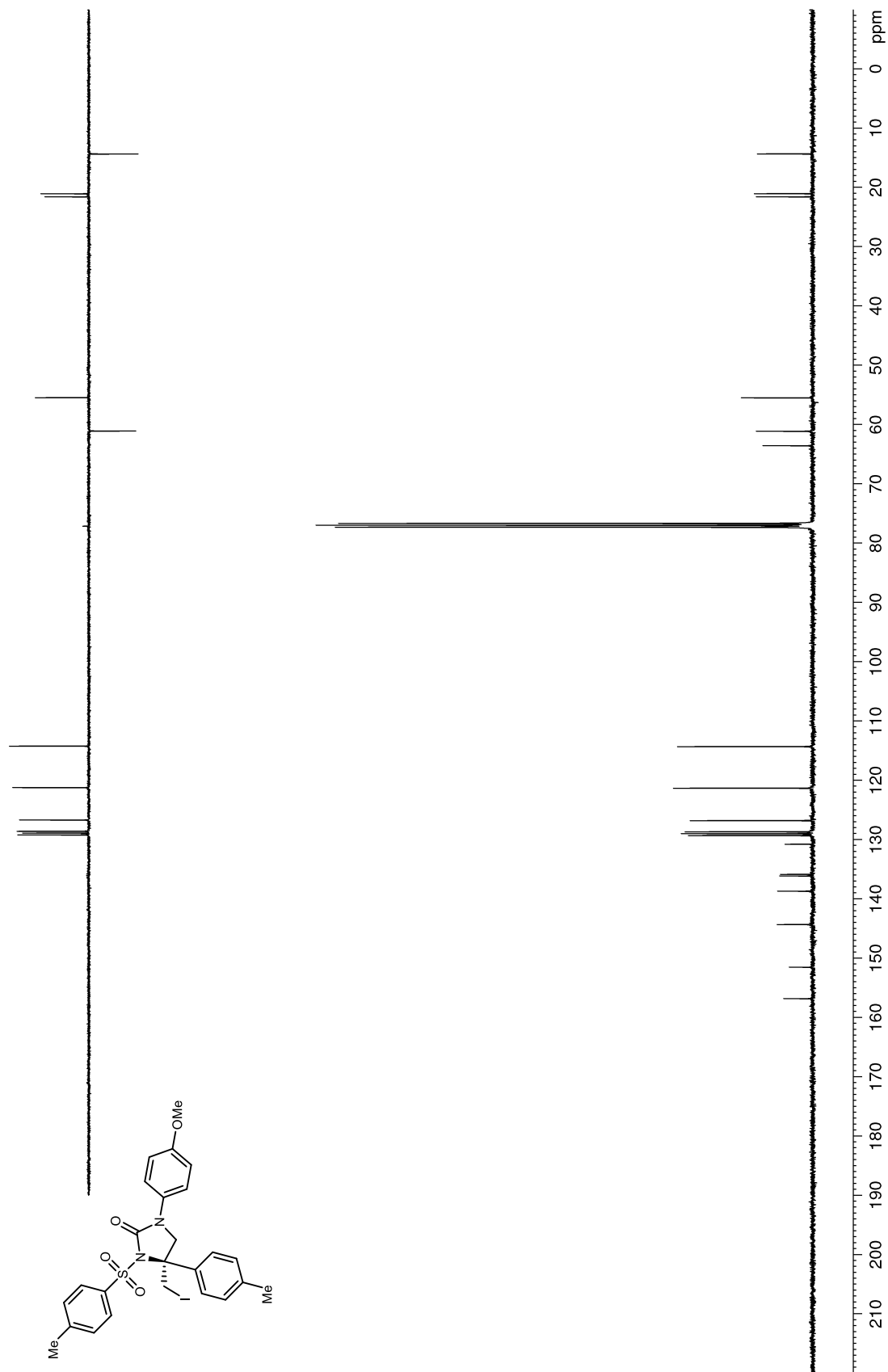
Figure 100. HPLC trace of **121c**. Chiralcel IB 25% EtOH/hexanes, 1.0 mL/min, 30 ºC
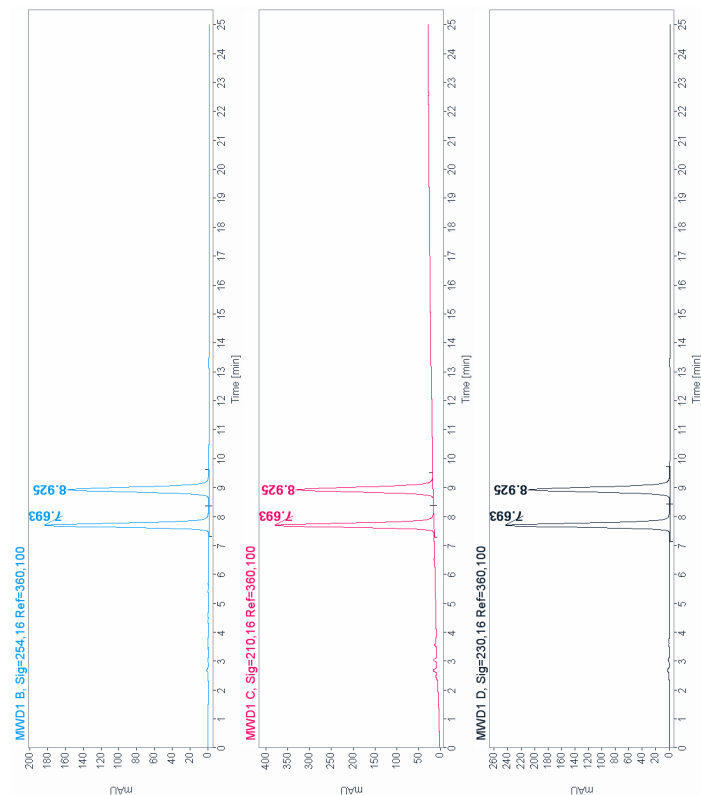
Signal: MWD1 B, Sig=254,16 Ref=360,100

RT [min]	Type	Width [min]	Area	Height	Area% Name
7.693	MF	0.1756	1946.9960	184.7690	50.0197
8.925	FM	0.2051	1945.4602	158.0783	49.9803
		Sum	3892.4562		

Signal: MWD1 C, Sig=210,16 Ref=360,100

RT [min]	Type	Width [min]	Area	Height	Area% Name
7.693	MF	0.1742	3808.7175	364.3750	50.1701
8.925	FM	0.2022	3782.8911	311.8689	49.8299
		Sum	7591.6086		

Signal: MWD1 D, Sig=230,16 Ref=360,100

RT [min]	Type	Width [min]	Area	Height	Area% Name
7.693	MF	0.1739	2547.8103	244.1781	50.1017
8.925	FM	0.2024	2537.4668	208.9040	49.8983
		Sum	5085.2771		

Signal: MWD1 B, Sig=254,16 Ref=360,100

RT [min]	Type	Width [min]	Area	Height	Area% Name
7.670	MF	0.1731	2146.4287	206.7096	96.4467
8.917	FM	0.2117	79.0793	6.2267	3.5533
		Sum	2225.5080		

Signal: MWD1 C, Sig=210,16 Ref=360,100

RT [min]	Type	Width [min]	Area	Height	Area% Name
7.669	MF	0.1739	4253.0596	407.7130	96.5846
8.917	FM	0.2046	150.3962	12.2497	3.4154
		Sum	4403.4558		

Signal: MWD1 D, Sig=230,16 Ref=360,100

RT [min]	Type	Width [min]	Area	Height	Area% Name
7.670	MF	0.1731	2845.0537	273.9561	96.2397
8.917	FM	0.2208	111.1636	8.3898	3.7603
		Sum	2956.2173		

Appendix 4.2-260

Figure 101. ^{1}H NMR (400 MHz, CDCl$_3$) of **121d**

Figure 102. ^{13}C NMR (100 MHz, CDCl$_3$) of **121d**

Figure 103. HPLC trace of **121d**. Chiralcel IB 25% EtOH/hexanes, 1.0 mL/min, 30 ºC

Signal: MWD1 B, Sig=254,16 Ref=360,100

RT [min]	Type	Width [min]	Area	Height	Area%	Name
8.669	MF	0.2044	1004.7476	81.9076	50.1124	
10.481	FM	0.2496	1000.2404	66.7996	49.8876	
	Sum		2004.9879			

Signal: MWD1 C, Sig=210,16 Ref=360,100

RT [min]	Type	Width [min]	Area	Height	Area%	Name
8.669	MF	0.2050	2007.8997	163.2151	50.2689	
10.481	FM	0.2489	1986.4158	133.0383	49.7311	
	Sum		3994.3154			

Signal: MWD1 D, Sig=230,16 Ref=360,100

RT [min]	Type	Width [min]	Area	Height	Area%	Name
8.669	MF	0.2038	1131.8381	92.5488	50.1941	
10.481	FM	0.2481	1123.0845	75.4344	49.8059	
	Sum		2254.9226			

Signal: MWD1 B, Sig=254,16 Ref=360,100

RT [min]	Type	Width [min]	Area	Height	Area%	Name
8.697	MF	0.2022	2666.5383	219.7627	80.0209	
10.542	FM	0.2510	665.7635	44.1992	19.9791	
	Sum		3332.3019			

Signal: MWD1 C, Sig=210,16 Ref=360,100

RT [min]	Type	Width [min]	Area	Height	Area%	Name
8.697	MF	0.2031	5280.9023	433.3150	79.9058	
10.542	FM	0.2509	1328.0077	88.2294	20.0942	
	Sum		6608.9100			

Signal: MWD1 D, Sig=230,16 Ref=360,100

RT [min]	Type	Width [min]	Area	Height	Area%	Name
8.697	MF	0.2027	3020.6863	248.3285	79.9328	
10.542	FM	0.2524	758.3480	50.0833	20.0672	
	Sum		3779.0342			

Appendix 4.2-263

Figure 104. ^{1}H NMR (400 MHz, CDCl$_3$) of **121e**

Figure 105. ^{13}C NMR (100 MHz, CDCl$_3$) of **121e**

Figure 106. HPLC trace of **121e**. Chiralcel IB 25% EtOH/hexanes, 1.0 mL/min, 30 ºC

Signal: MWD1 B, Sig=254,16 Ref=360,100

RT [min]	Type	Width [min]	Area	Height	Area%	Name
7.770	MF	0.1783	632.6559	59.1361	50.3206	
8.557	FM	0.1958	624.5956	53.1588	49.6794	
		Sum	1257.2515			

Signal: MWD1 C, Sig=210,16 Ref=360,100

RT [min]	Type	Width [min]	Area	Height	Area%	Name
7.770	MF	0.1794	1329.8820	123.5331	50.3729	
8.557	FM	0.1963	1310.1930	111.2191	49.6271	
		Sum	2640.0750			

Signal: MWD1 D, Sig=230,16 Ref=360,100

RT [min]	Type	Width [min]	Area	Height	Area%	Name
7.770	MF	0.1794	768.2528	71.3728	50.2653	
8.557	FM	0.1972	760.1434	64.2415	49.7347	
		Sum	1528.3962			

Signal: MWD1 B, Sig=254,16 Ref=360,100

RT [min]	Type	Width [min]	Area	Height	Area%	Name
7.732	MF	0.1774	2423.0400	227.6145	95.9699	
8.536	FM	0.2132	101.7507	7.9554	4.0301	
		Sum	2524.7908			

Signal: MWD1 C, Sig=210,16 Ref=360,100

RT [min]	Type	Width [min]	Area	Height	Area%	Name
7.732	MF	0.1797	5068.3418	470.1022	95.9810	
8.536	FM	0.2132	212.2278	16.5941	4.0190	
		Sum	5280.5696			

Signal: MWD1 D, Sig=230,16 Ref=360,100

RT [min]	Type	Width [min]	Area	Height	Area%	Name
7.732	MF	0.1793	2957.7556	274.9801	95.8123	
8.536	FM	0.2191	129.2769	9.8324	4.1877	
		Sum	3087.0325			

Appendix 4.2-266

Figure 107. ^{1}H NMR (400 MHz, CDCl$_3$) of **121f**

Figure 108. ^{13}C NMR (100 MHz, CDCl$_3$) of **121f**

Figure 109. HPLC trace of **121f**. Chiralcel IB 25% *i*PrOH/hexanes, 1.0 mL/min, 30 ºC
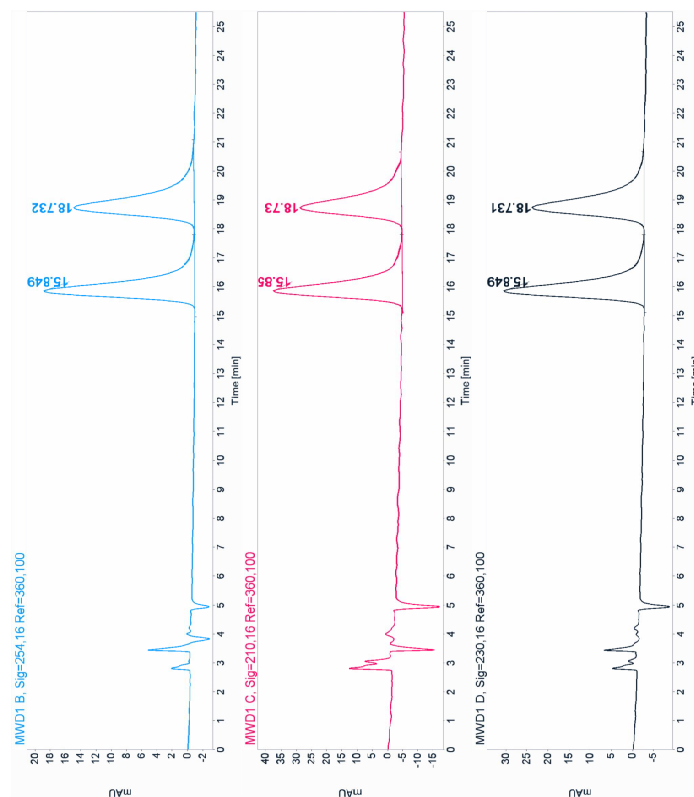
Signal: MWD1 B, Sig=254,16 Ref=360,100

RT [min]	Type	Width [min]	Area	Height	Area%	Name
15.849	MF	0.6284	746.0493	19.7865	50.7710	
18.732	FM	0.7665	723.3918	15.7296	49.2290	
		Sum	1469.4410			

Signal: MWD1 C, Sig=210,16 Ref=360,100

RT [min]	Type	Width [min]	Area	Height	Area%	Name
15.850	MF	0.6347	1611.2145	42.3072	51.3985	
18.730	FM	0.7601	1523.5377	33.4045	48.6015	
		Sum	3134.7522			

Signal: MWD1 D, Sig=230,16 Ref=360,100

RT [min]	Type	Width [min]	Area	Height	Area%	Name
15.849	MF	0.6299	1262.4985	33.4046	50.8396	
18.731	FM	0.7665	1220.7980	26.5451	49.1604	
		Sum	2483.2965			

Signal: MWD1 B, Sig=254,16 Ref=360,100

RT [min]	Type	Width [min]	Area	Height	Area%	Name
15.912	MM	0.6263	943.4529	25.1049	94.2022	
18.941	MM	0.8429	58.0662	1.1481	5.7978	
		Sum	1001.5191			

Signal: MWD1 C, Sig=210,16 Ref=360,100

RT [min]	Type	Width [min]	Area	Height	Area%	Name
15.912	MM	0.6260	1993.5515	53.0783	94.4294	
18.947	MM	0.7777	117.6039	2.5202	5.5706	
		Sum	2111.1554			

Signal: MWD1 D, Sig=230,16 Ref=360,100

RT [min]	Type	Width [min]	Area	Height	Area%	Name
15.912	MM	0.6197	1567.4626	42.1585	95.5018	
18.948	MM	0.7194	73.8292	1.7103	4.4982	
		Sum	1641.2919			

Appendix 4.2-269
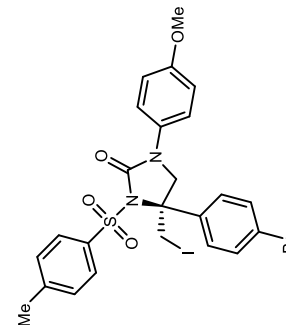
Figure 110. ^{1}H NMR (400 MHz, CDCl$_3$) of **121g**
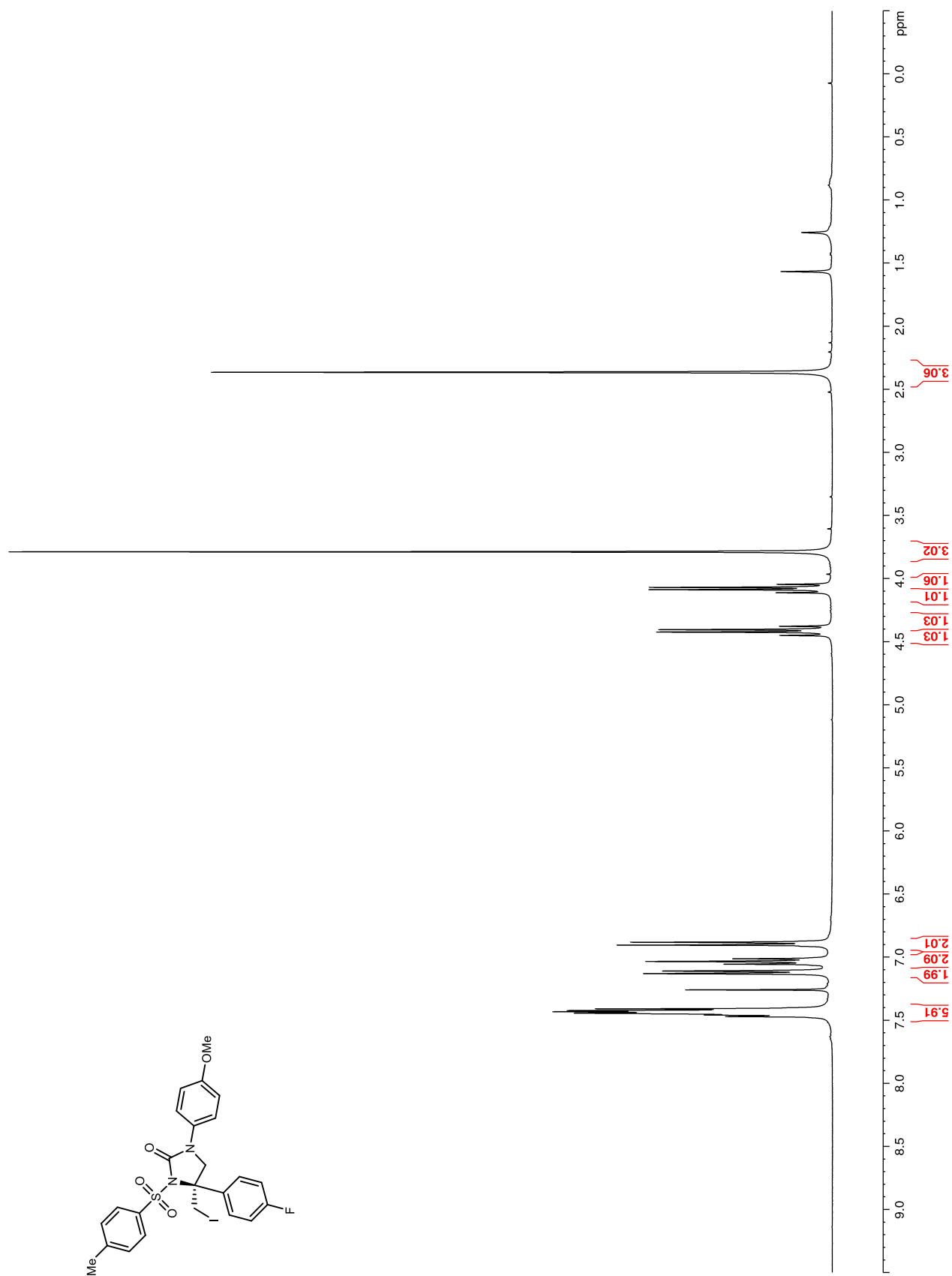
Figure 111. ^{13}C NMR (100 MHz, CDCl$_3$) of **121g**
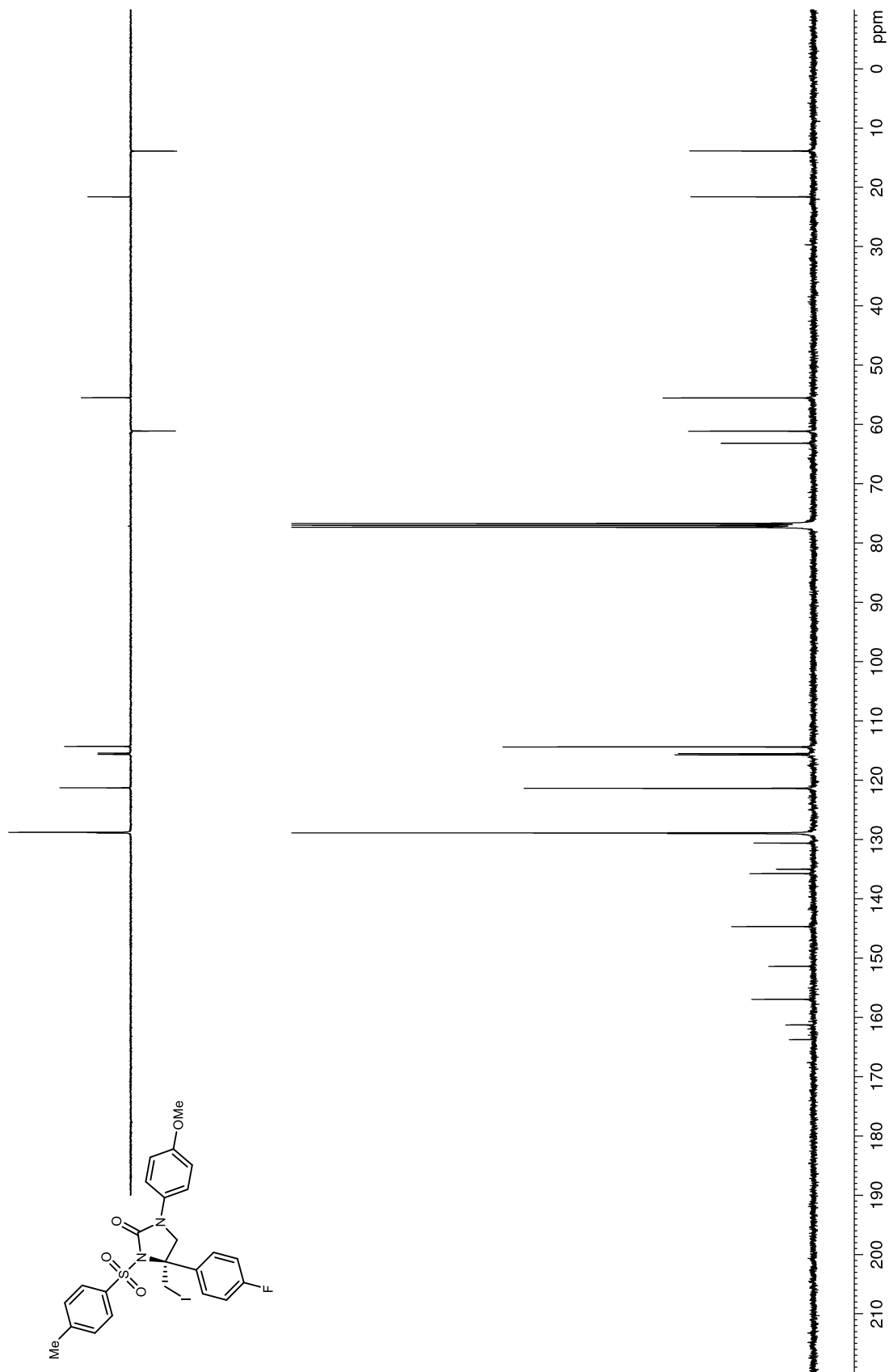
Figure 112. ^{19}F NMR (376 MHz, CDCl$_3$) of **121g**

Figure 113. HPLC trace of **121g**. Chiralcel IB 25% EtOH/hexanes, 1.0 mL/min, 30 ºC
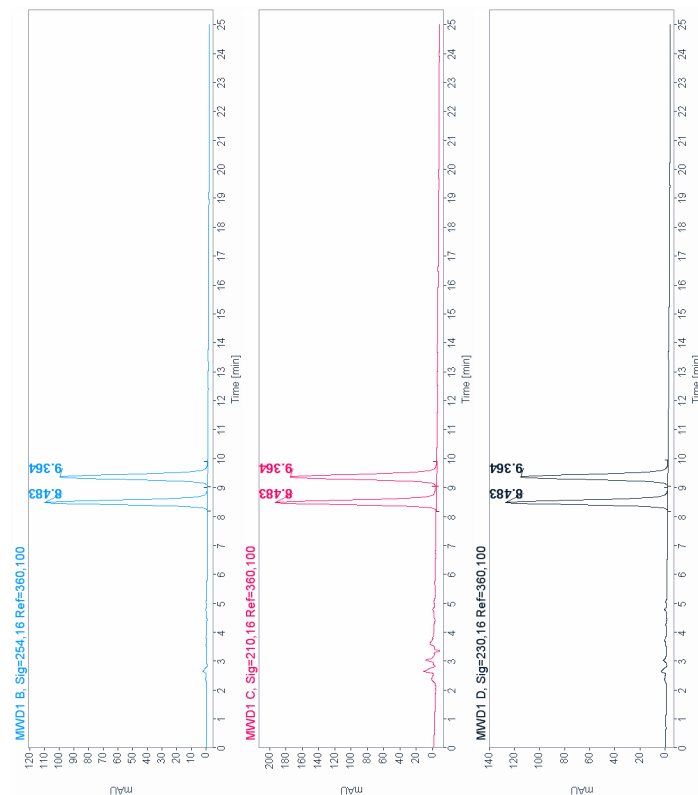
Signal: MWD1 B, Sig=254,16 Ref=360,100

RT [min]	Type	Width [min]	Area	Height	Area%	Name
8.483	BB	0.1775	1267.2739	110.7557	50.0451	
9.364	BB	0.1946	1264.9904	100.6440	49.9549	
		Sum	2532.2643			

Signal: MWD1 C, Sig=210,16 Ref=360,100

RT [min]	Type	Width [min]	Area	Height	Area%	Name
8.483	VV	0.1795	2301.4839	198.1845	50.1404	
9.364	VB	0.1960	2288.5974	180.3466	49.8596	
		Sum	4590.0813			

Signal: MWD1 D, Sig=230,16 Ref=360,100

RT [min]	Type	Width [min]	Area	Height	Area%	Name
8.483	VB	0.1776	1479.3574	129.1860	50.0687	
9.364	BB	0.1946	1475.2994	117.4075	49.9313	
		Sum	2954.6569			

Signal: MWD1 B, Sig=254,16 Ref=360,100

RT [min]	Type	Width [min]	Area	Height	Area%	Name
8.434	BB	0.1749	2232.0583	195.9812	94.7406	
9.328	BB	0.1978	123.9091	9.6505	5.2594	
		Sum	2355.9674			

Signal: MWD1 C, Sig=210,16 Ref=360,100

RT [min]	Type	Width [min]	Area	Height	Area%	Name
8.434	BV	0.1775	3992.9102	348.8686	94.3907	
9.327	VB	0.2051	237.2853	17.8531	5.6093	
		Sum	4230.1954			

Signal: MWD1 D, Sig=230,16 Ref=360,100

RT [min]	Type	Width [min]	Area	Height	Area%	Name
8.434	BB	0.1750	2604.6919	228.5615	94.6980	
9.328	BB	0.1986	145.8329	11.2998	5.3020	
		Sum	2750.5248			
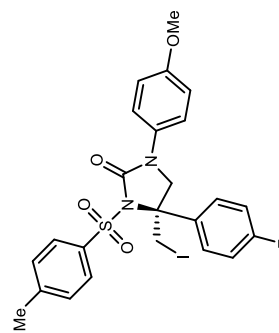
Figure 114. ^{1}H NMR (400 MHz, CDCl$_3$) of **121h**
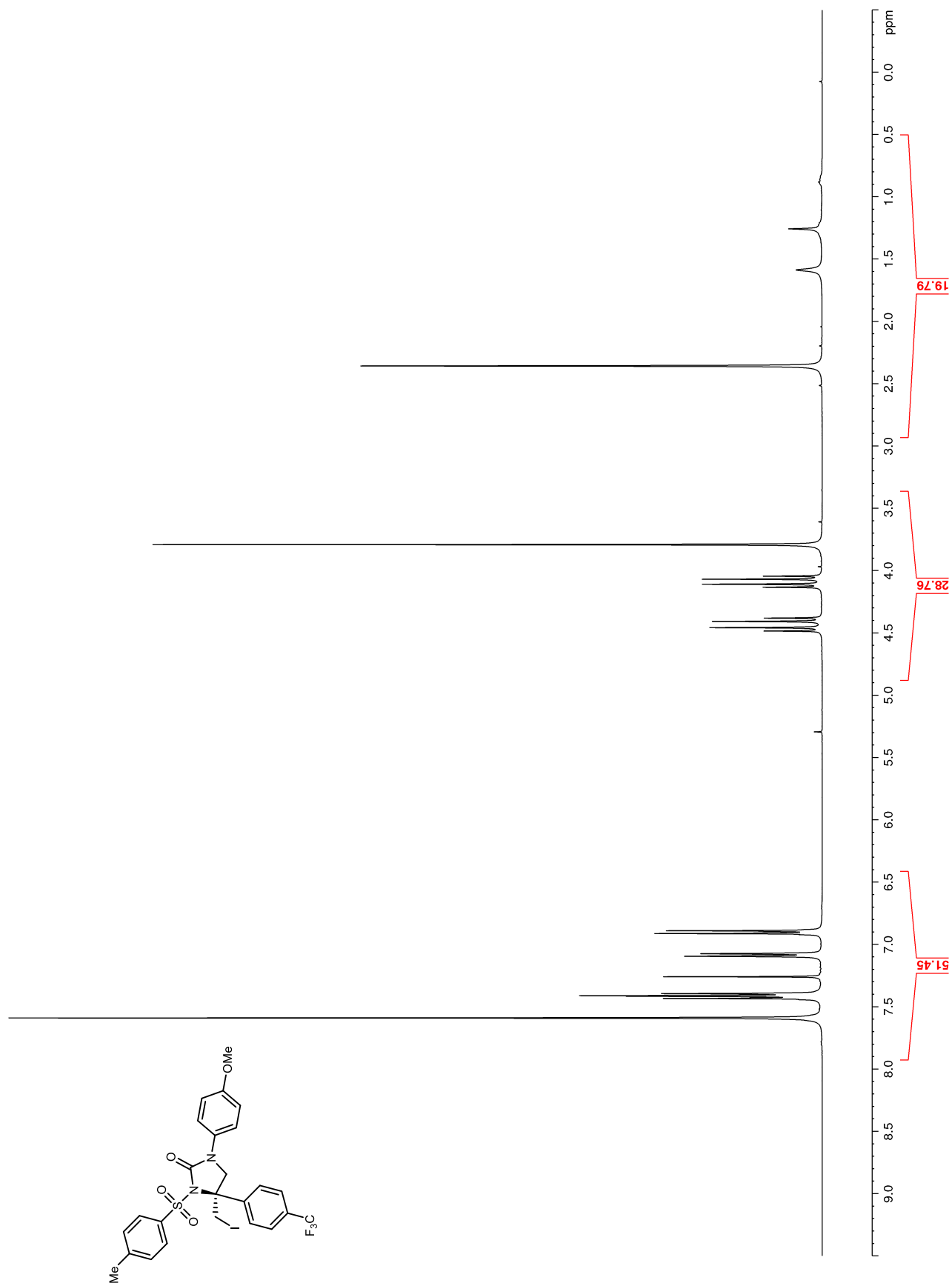
Figure 115. ^{13}C NMR (100 MHz, CDCl$_3$) of **121h**
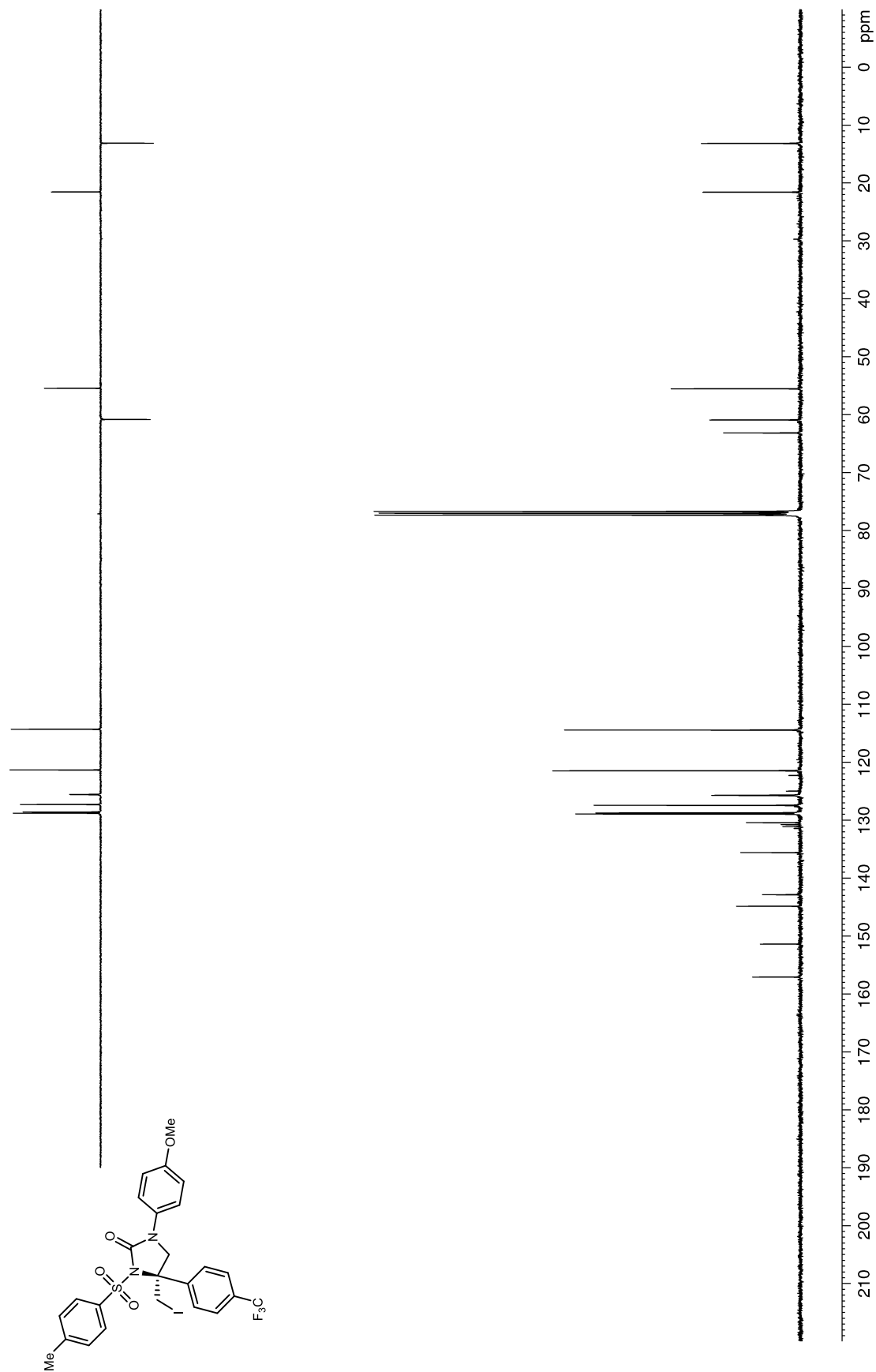
Figure 116. ^{19}F NMR (376 MHz, CDCl$_3$) of **121h**
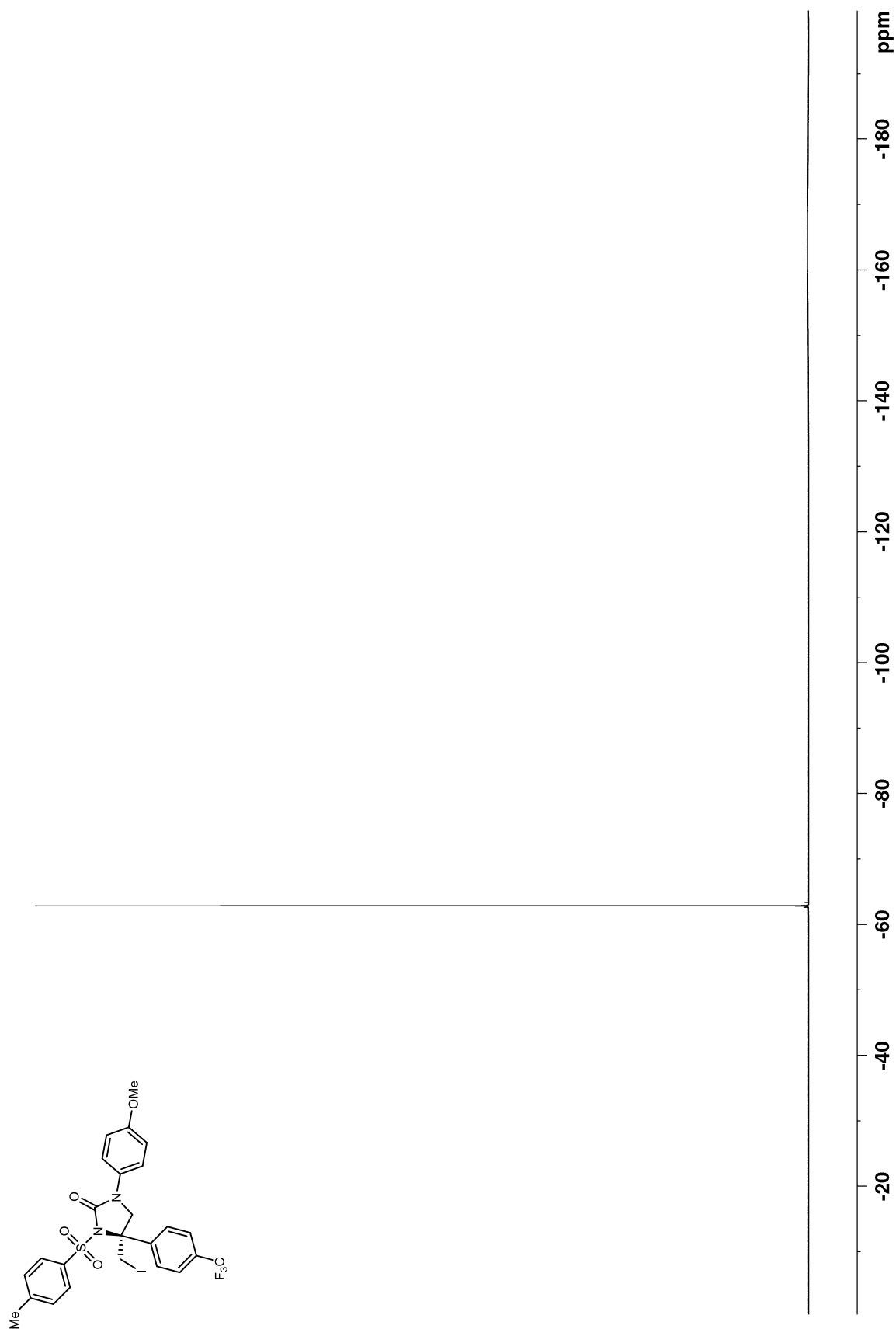
Figure 117. HPLC trace of **121h**. Chiralcel IB 20% EtOH/hexanes, 1.0 mL/min, 30 ºC
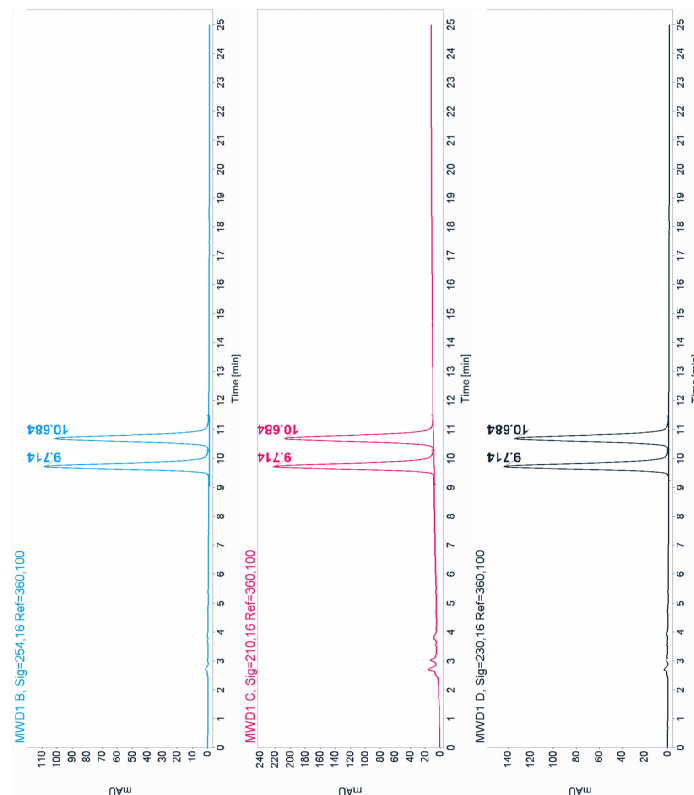
Signal: MWD1 B, Sig=254,16 Ref=360,100

RT [min]	Type	Width [min]	Area	Height	Area%	Name
9.714	MF	0.2394	1578.4957	109.9144	49.9561	
10.684	FM	0.2583	1581.2712	102.0278	50.0439	
		Sum	3159.7670			

Signal: MWD1 C, Sig=210,16 Ref=360,100

RT [min]	Type	Width [min]	Area	Height	Area%	Name
9.714	MF	0.2387	3065.9697	214.0329	49.9834	
10.684	FM	0.2573	3068.0007	198.7006	50.0166	
		Sum	6133.9705			

Signal: MWD1 D, Sig=230,16 Ref=360,100

RT [min]	Type	Width [min]	Area	Height	Area%	Name
9.714	MF	0.2355	2043.7488	144.6201	49.9672	
10.684	FM	0.2541	2046.4326	134.2133	50.0328	
		Sum	4090.1814			

Signal: MWD1 B, Sig=254,16 Ref=360,100

RT [min]	Type	Width [min]	Area	Height	Area%	Name
9.690	MF	0.2370	975.9741	68.6255	95.5253	
10.668	FM	0.2696	45.7174	2.8265	4.4747	
		Sum	1021.6915			

Signal: MWD1 C, Sig=210,16 Ref=360,100

RT [min]	Type	Width [min]	Area	Height	Area%	Name
9.690	MF	0.2365	1901.0802	133.9766	95.6185	
10.669	FM	0.2636	87.1121	5.5078	4.3815	
		Sum	1988.1923			

Signal: MWD1 D, Sig=230,16 Ref=360,100

RT [min]	Type	Width [min]	Area	Height	Area%	Name
9.690	MF	0.2367	1287.7213	90.6613	95.4794	
10.668	FM	0.2712	60.9695	3.7464	4.5206	
		Sum	1348.6909			

Appendix 4.2-277
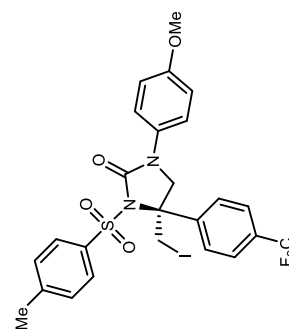
Figure 118. ^{1}H NMR (400 MHz, CDCl$_3$) of **121i**
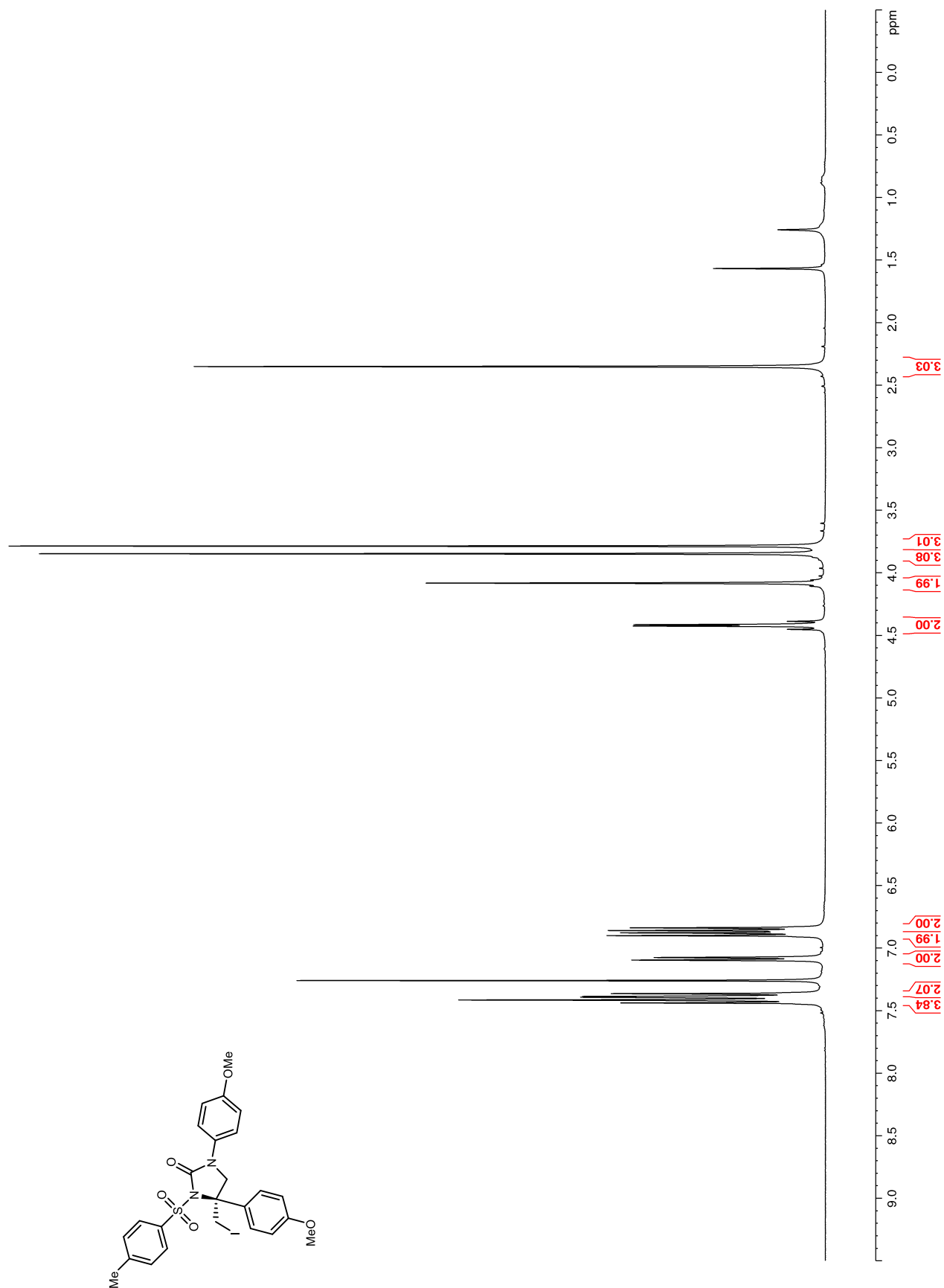
Figure 119. ^{13}C NMR (100 MHz, CDCl$_3$) of **121i**
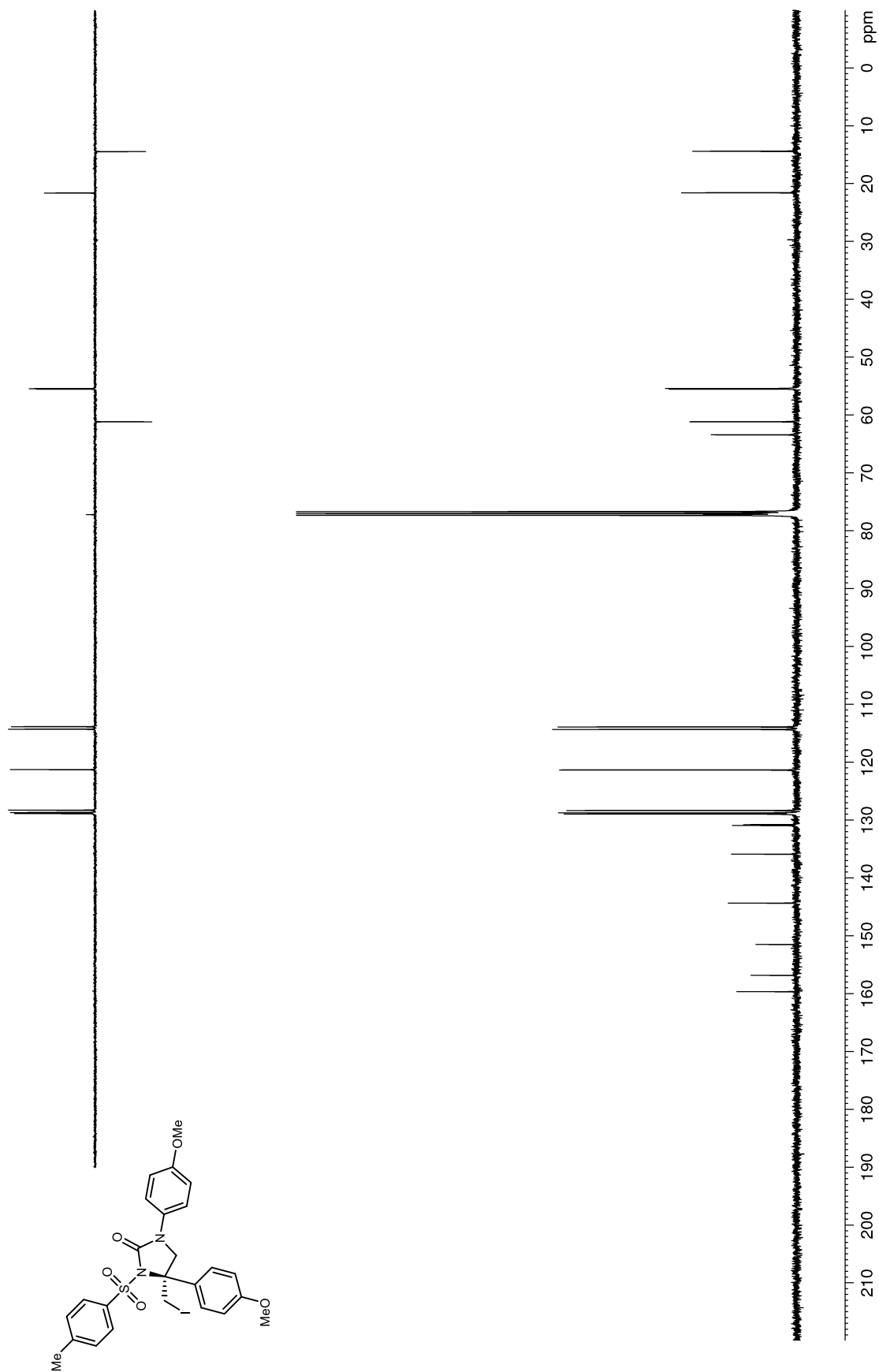
Figure 120. HPLC trace of **121i**. Chiralcel IB 25% EtOH/hexanes, 1.0 mL/min, 30 ºC
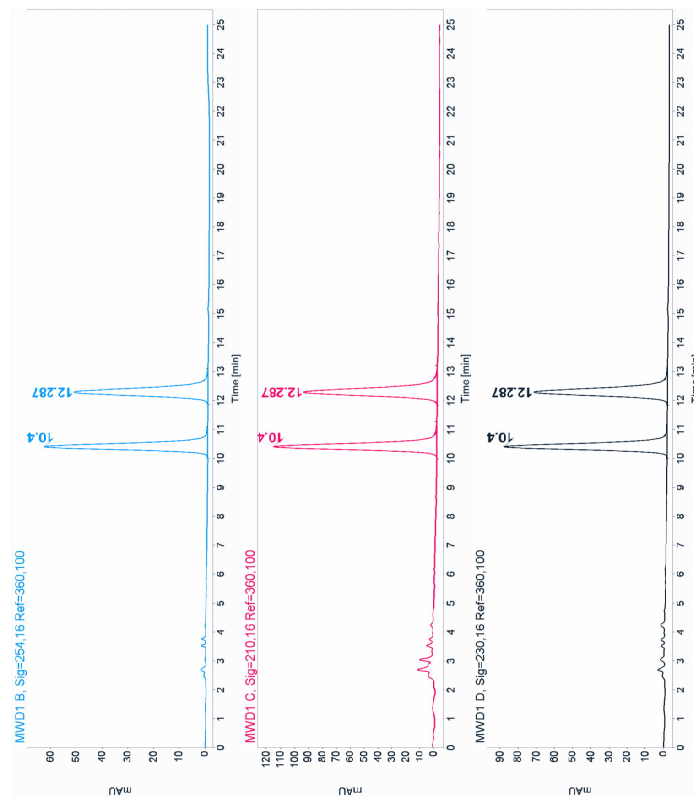
Signal: MWD1 B, Sig=254,16 Ref=360,100

RT [min]	Type	Width [min]	Area	Height	Area%	Name
10.400	BB	0.2347	976.2837	63.7514	50.1379	
12.287	BB	0.2854	970.9115	52.1137	49.8621	
		Sum	1947.1952			

Signal: MWD1 C, Sig=210,16 Ref=360,100

RT [min]	Type	Width [min]	Area	Height	Area%	Name
10.400	BB	0.2355	1797.7905	116.8468	50.2250	
12.287	BB	0.2857	1781.6818	95.4963	49.7750	
		Sum	3579.4723			

Signal: MWD1 D, Sig=230,16 Ref=360,100

RT [min]	Type	Width [min]	Area	Height	Area%	Name
10.400	BB	0.2351	1382.1316	90.0439	50.1729	
12.287	BB	0.2856	1372.6044	73.5958	49.8271	
		Sum	2754.7360			

Signal: MWD1 B, Sig=254,16 Ref=360,100

RT [min]	Type	Width [min]	Area	Height	Area%	Name
10.365	BB	0.2327	5554.5752	366.7061	95.4614	
12.315	BB	0.2898	264.0872	14.0142	4.5386	
		Sum	5818.6624			

Signal: MWD1 C, Sig=210,16 Ref=360,100

RT [min]	Type	Width [min]	Area	Height	Area%	Name
10.365	BB	0.2367	10009.4971	653.4316	95.3545	
12.315	BB	0.2908	487.6450	25.7676	4.6455	
		Sum	10497.1420			

Signal: MWD1 D, Sig=230,16 Ref=360,100

RT [min]	Type	Width [min]	Area	Height	Area%	Name
10.365	BB	0.2329	7836.1377	516.7186	95.4404	
12.315	BB	0.2904	374.3697	19.8139	4.5596	
		Sum	8210.5074			
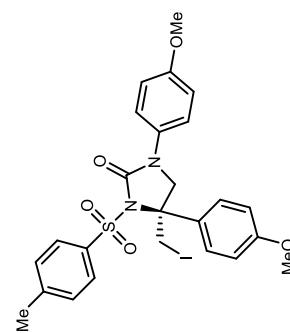
Figure 121. ^{1}H NMR (400 MHz, CDCl$_3$) of **121j**
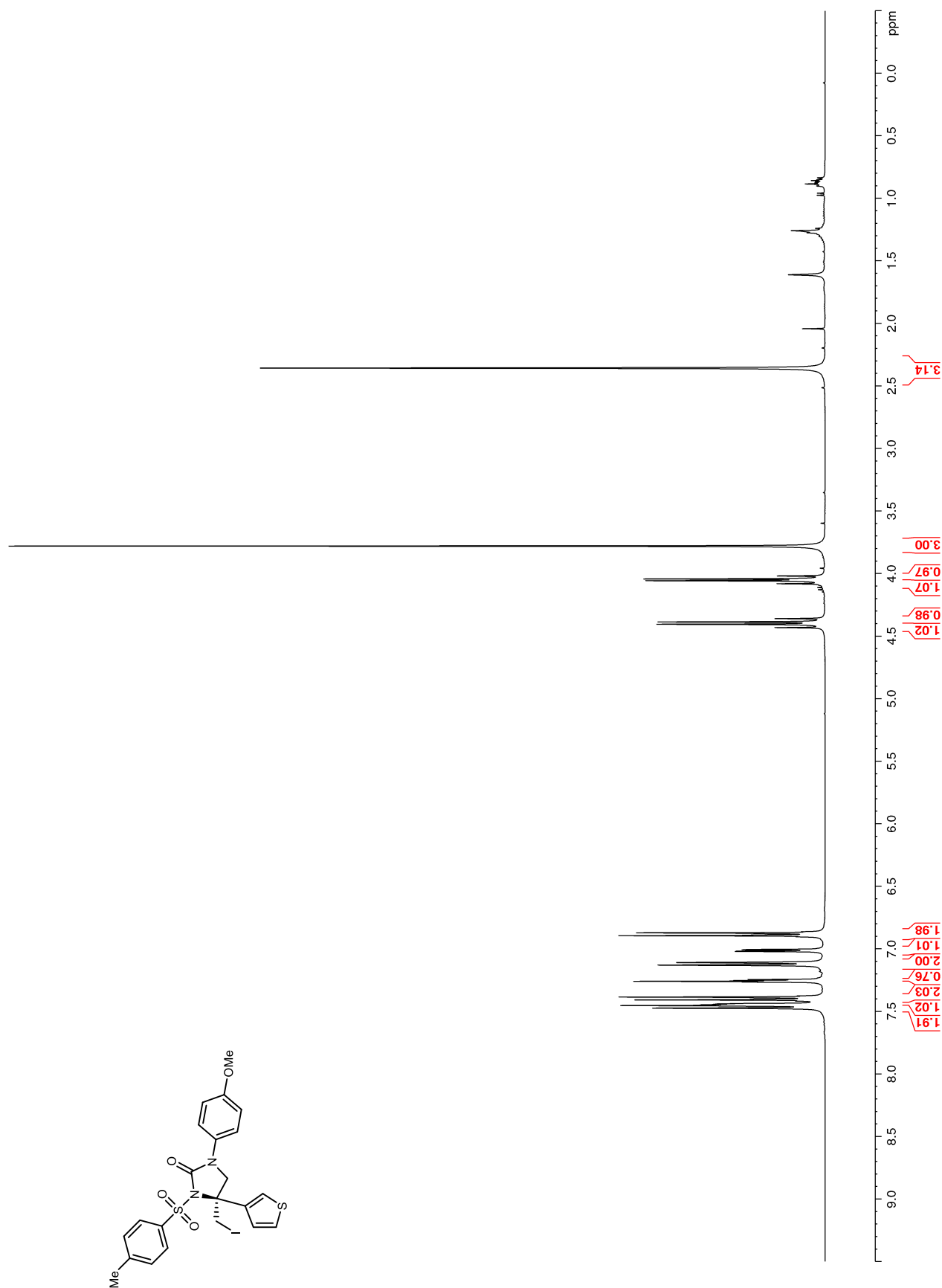
Figure 122. ^{13}C NMR (100 MHz, CDCl$_3$) of **121j**
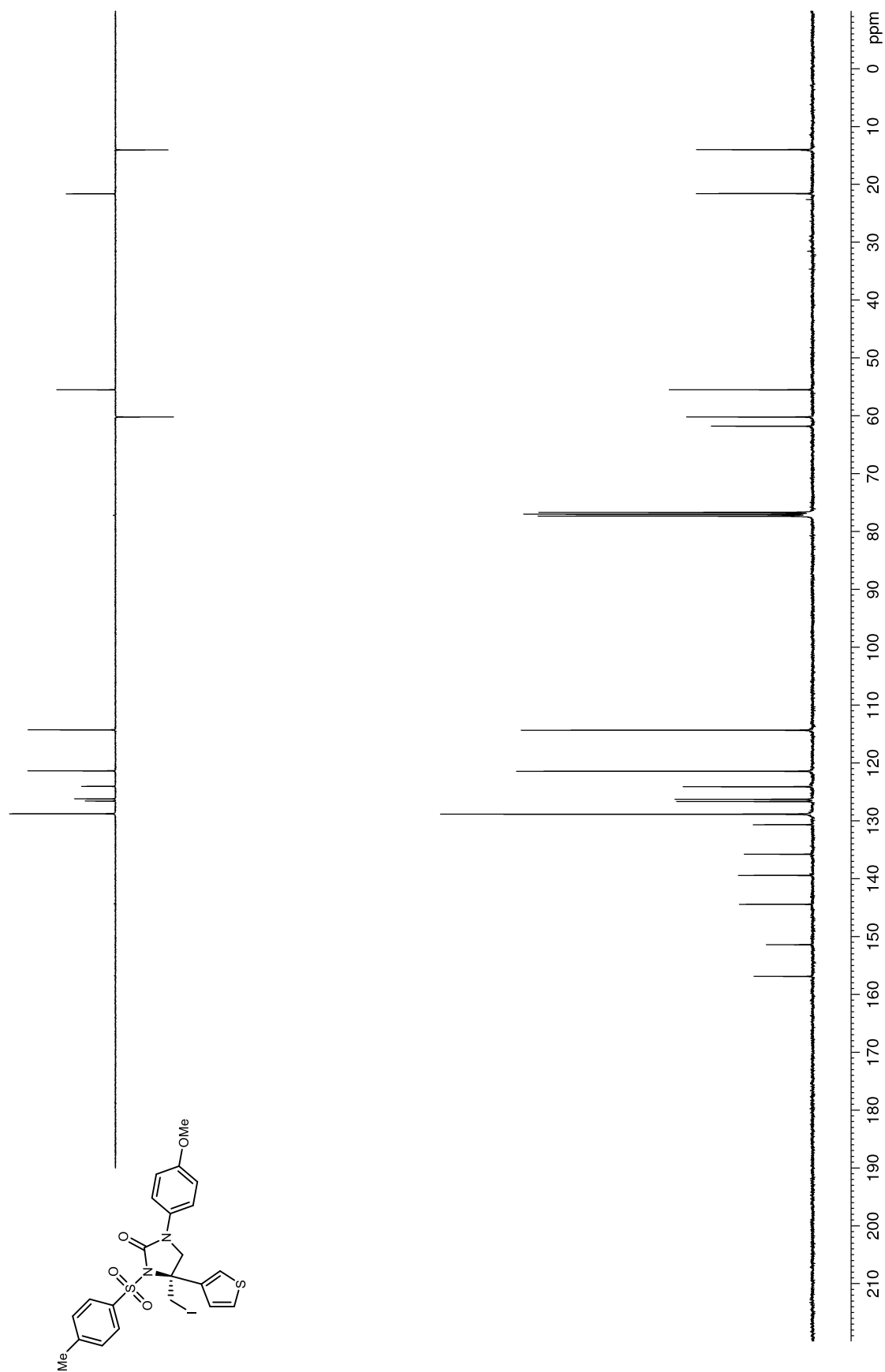
Figure 123. HPLC trace of **121j**. Chiralcel IB 25% EtOH/hexanes, 1.0 mL/min, 30 ºC

Signal: MWD1 B, Sig=254,16 Ref=360,100

RT [min]	Type	Width [min]	Area	Height	Area%	Name
9.721	MM	0.2222	4077.7439	305.9200	94.1485	
11.346	FM	0.2736	253.4397	15.4409	5.8515	
		Sum	4331.1836			

Signal: MWD1 C, Sig=210,16 Ref=360,100

RT [min]	Type	Width [min]	Area	Height	Area%	Name
9.721	MF	0.2225	5898.0503	441.8351	94.4284	
11.346	FM	0.2625	348.0050	22.0987	5.5716	
		Sum	6246.0553			

Signal: MWD1 D, Sig=230,16 Ref=360,100

RT [min]	Type	Width [min]	Area	Height	Area%	Name
9.721	MF	0.2218	5162.4336	387.9008	94.4598	
11.346	FM	0.2626	302.7834	19.2194	5.5402	
		Sum	5465.2169			

Signal: MWD1 B, Sig=254,16 Ref=360,100

RT [min]	Type	Width [min]	Area	Height	Area%	Name
9.731	MF	0.2203	1234.4429	93.3880	50.1540	
11.323	FM	0.2561	1226.8606	79.8573	49.8460	
		Sum	2461.3035			

Signal: MWD1 C, Sig=210,16 Ref=360,100

RT [min]	Type	Width [min]	Area	Height	Area%	Name
9.731	MF	0.2219	1818.7166	136.5827	50.2756	
11.323	FM	0.2567	1798.7770	116.8051	49.7244	
		Sum	3617.4935			

Signal: MWD1 D, Sig=230,16 Ref=360,100

RT [min]	Type	Width [min]	Area	Height	Area%	Name
9.731	MF	0.2210	1574.6379	118.7288	50.3608	
11.323	FM	0.2553	1552.0751	101.3354	49.6392	
		Sum	3126.7130			

Appendix 4.2-283

Figure 124. ^{1}H NMR (400 MHz, CDCl$_3$) of **121k**
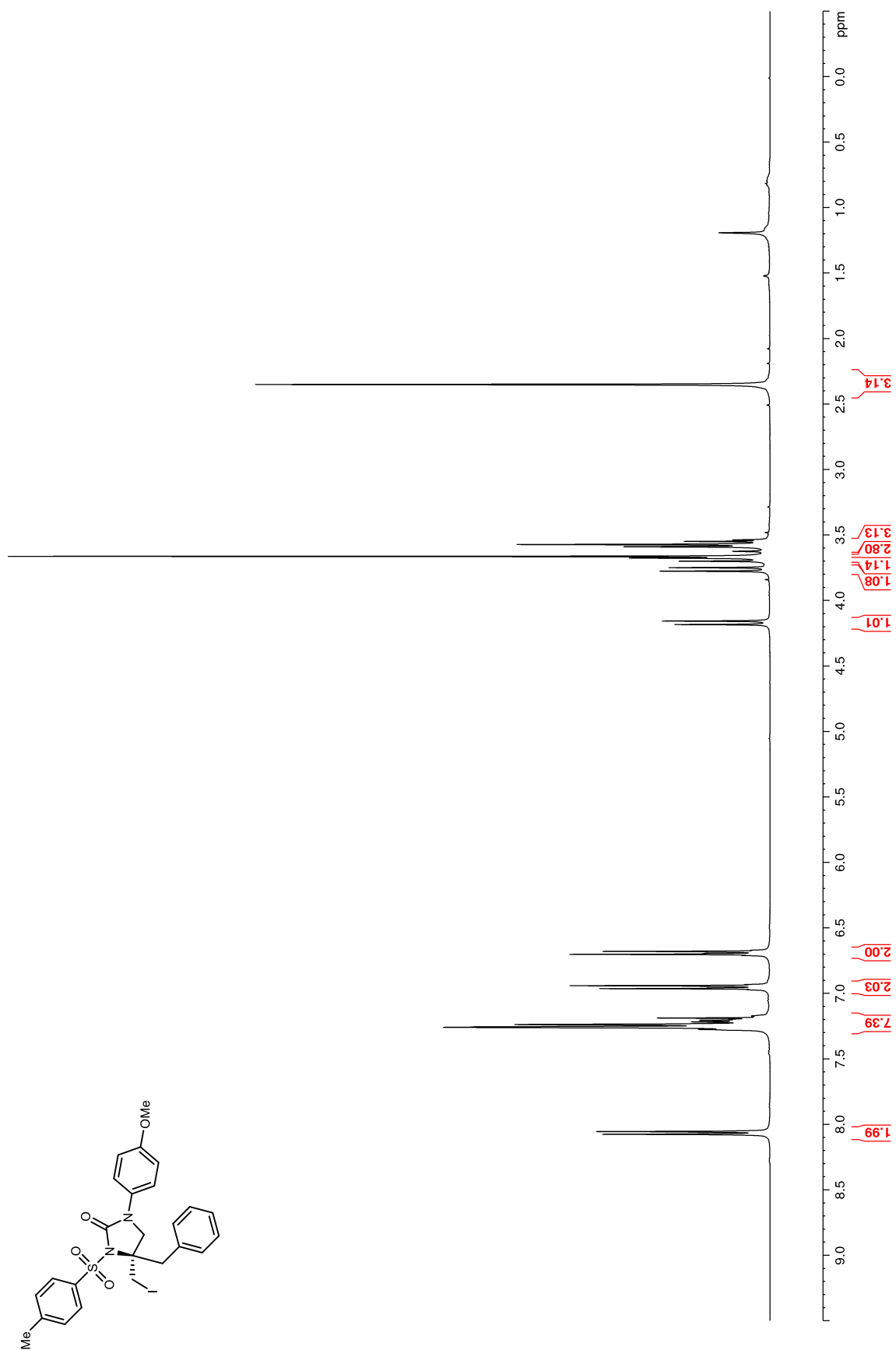
Figure 125. ^{13}C NMR (100 MHz, CDCl$_3$) of **121k**
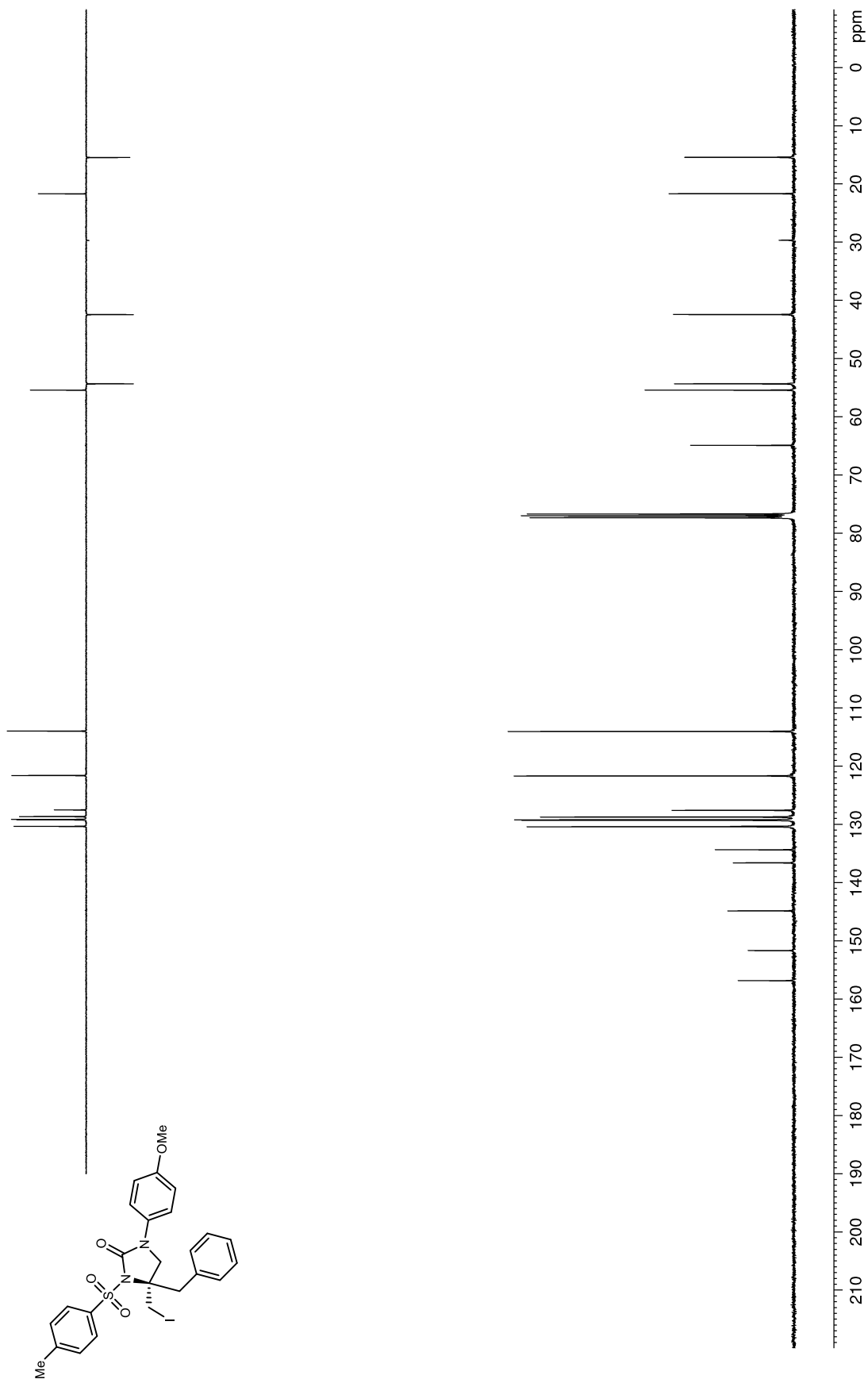
Figure 126. HPLC trace of **121k**. Chiralcel IB 25% EtOH/hexanes, 1.0 mL/min, 30 ºC

Signal: MWD1 B, Sig=254,16 Ref=360,100

RT [min]	Type	Width [min]	Area	Height	Area%	Name
10.037	MF	0.2691	295.5872	18.3072	49.6704	
11.372	FM	0.3159	299.5103	15.8002	50.3296	
		Sum	595.0975			

Signal: MWD1 C, Sig=210,16 Ref=360,100

RT [min]	Type	Width [min]	Area	Height	Area%	Name
10.038	MM	0.2640	523.6517	33.0572	49.1530	
11.374	MM	0.3142	541.6979	28.7347	50.8470	
		Sum	1065.3497			

Signal: MWD1 D, Sig=230,16 Ref=360,100

RT [min]	Type	Width [min]	Area	Height	Area%	Name
10.037	MF	0.2740	368.2639	22.4002	50.5225	
11.373	FM	0.3132	360.6461	19.1890	49.4775	
		Sum	728.9101			

Signal: MWD1 B, Sig=254,16 Ref=360,100

RT [min]	Type	Width [min]	Area	Height	Area%	Name
9.984	MF	0.2655	1315.3895	82.5817	25.0255	
11.290	FM	0.3001	3940.8081	218.8960	74.9745	
		Sum	5256.1976			

Signal: MWD1 C, Sig=210,16 Ref=360,100

RT [min]	Type	Width [min]	Area	Height	Area%	Name
9.984	MF	0.2702	2461.2319	151.7897	25.8039	
11.290	FM	0.2988	7076.9751	394.6943	74.1961	
		Sum	9538.2070			

Signal: MWD1 D, Sig=230,16 Ref=360,100

RT [min]	Type	Width [min]	Area	Height	Area%	Name
9.984	MF	0.2667	1613.1456	100.7964	25.1155	
11.290	FM	0.3004	4809.7695	266.8728	74.8845	
		Sum	6422.9152			

Appendix 4.2-286

Figure 127. ^{1}H NMR (400 MHz, CDCl$_3$) of **121l**
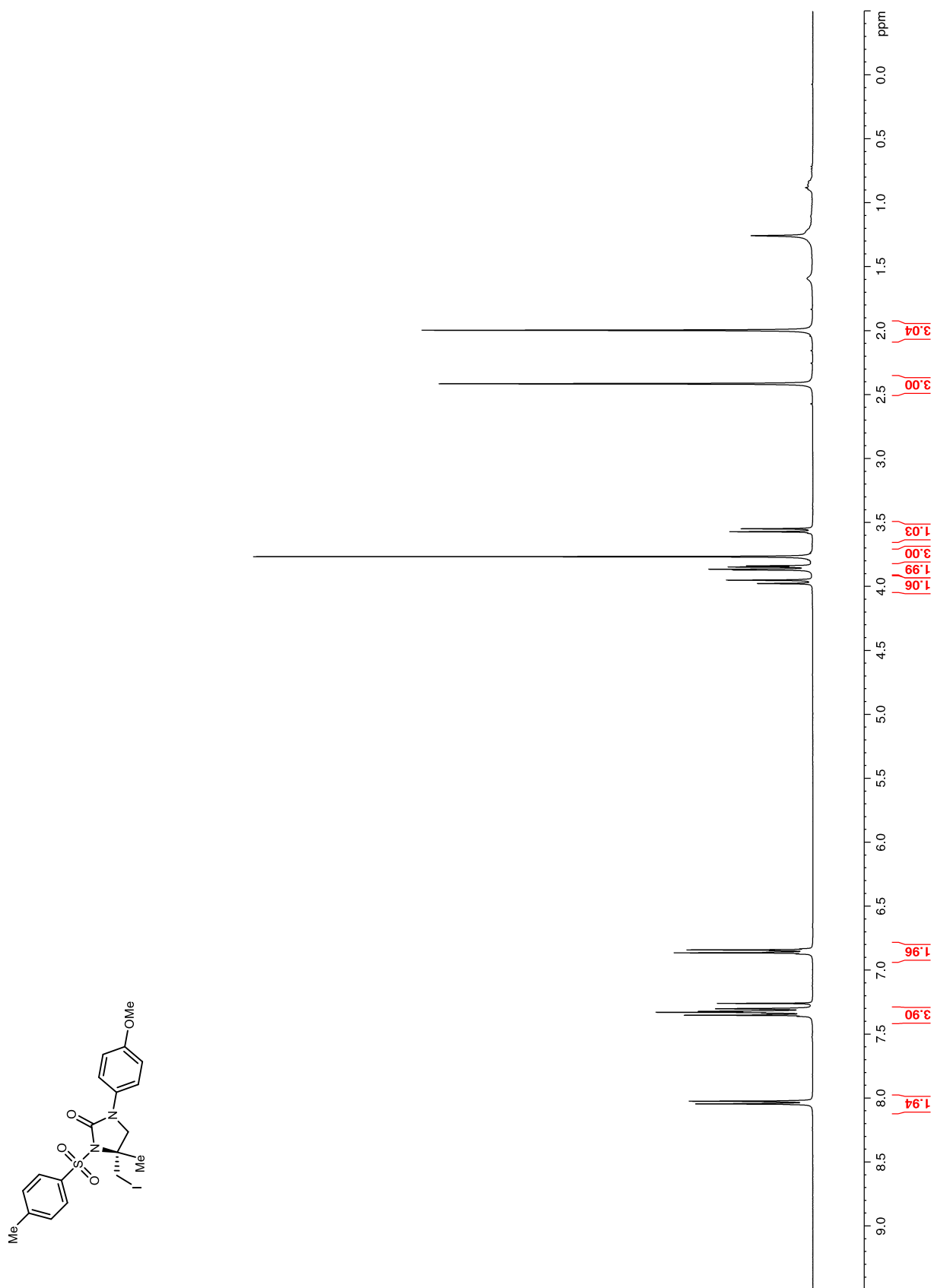
Figure 128. ^{13}C NMR (100 MHz, CDCl$_3$) of **121l**
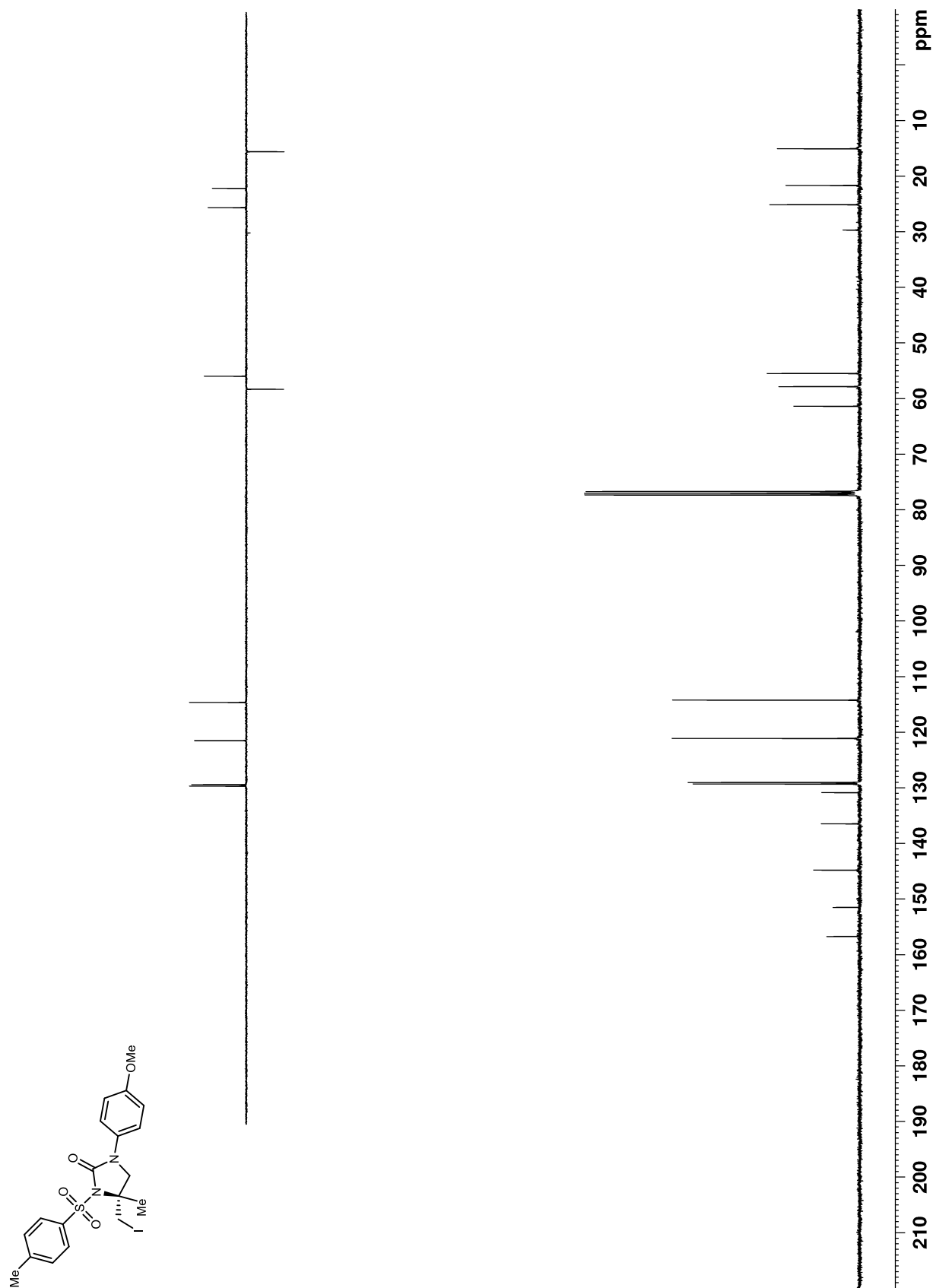
Figure 129. HPLC trace of **121l**. Chiralcel IB 25% EtOH/hexanes, 1.0 mL/min, 30 ºC

Signal: MWD1 B, Sig=254,16 Ref=360,100

RT [min]	Type	Width [min]	Area	Height	Area%	Name
12.538	MF	0.3004	2515.4871	139.5644	64.6682	
17.728	FM	0.4256	1374.3505	53.8261	35.3318	
		Sum	3889.8375			

Signal: MWD1 C, Sig=210,16 Ref=360,100

RT [min]	Type	Width [min]	Area	Height	Area%	Name
12.538	MF	0.3020	3132.2681	172.8539	64.4193	
17.728	FM	0.4302	1730.0421	67.0271	35.5807	
		Sum	4862.3102			

Signal: MWD1 D, Sig=230,16 Ref=360,100

RT [min]	Type	Width [min]	Area	Height	Area%	Name
12.538	MF	0.3026	2705.1016	148.9944	64.5753	
17.728	FM	0.4295	1483.9614	57.5819	35.4247	
		Sum	4189.0630			

Signal: MWD1 B, Sig=254,16 Ref=360,100

RT [min]	Type	Width [min]	Area	Height	Area%	Name
12.556	MM	0.3035	952.1183	52.2856	50.2798	
17.752	MM	0.4261	941.5204	36.8278	49.7202	
		Sum	1893.6387			

Signal: MWD1 C, Sig=210,16 Ref=360,100

RT [min]	Type	Width [min]	Area	Height	Area%	Name
12.556	MM	0.3032	1181.9719	64.9795	50.2208	
17.752	MM	0.4267	1171.5789	45.7598	49.7792	
		Sum	2353.5508			

Signal: MWD1 D, Sig=230,16 Ref=360,100

RT [min]	Type	Width [min]	Area	Height	Area%	Name
12.556	MM	0.3027	1012.8427	55.7632	50.1136	
17.752	MM	0.4272	1008.2509	39.3335	49.8864	
		Sum	2021.0936			

Appendix 4.2-289

Figure 130. ^{1}H NMR (400 MHz, CDCl$_3$) of **121m**

Figure 131. ^{13}C NMR (100 MHz, CDCl$_3$) of **121m**
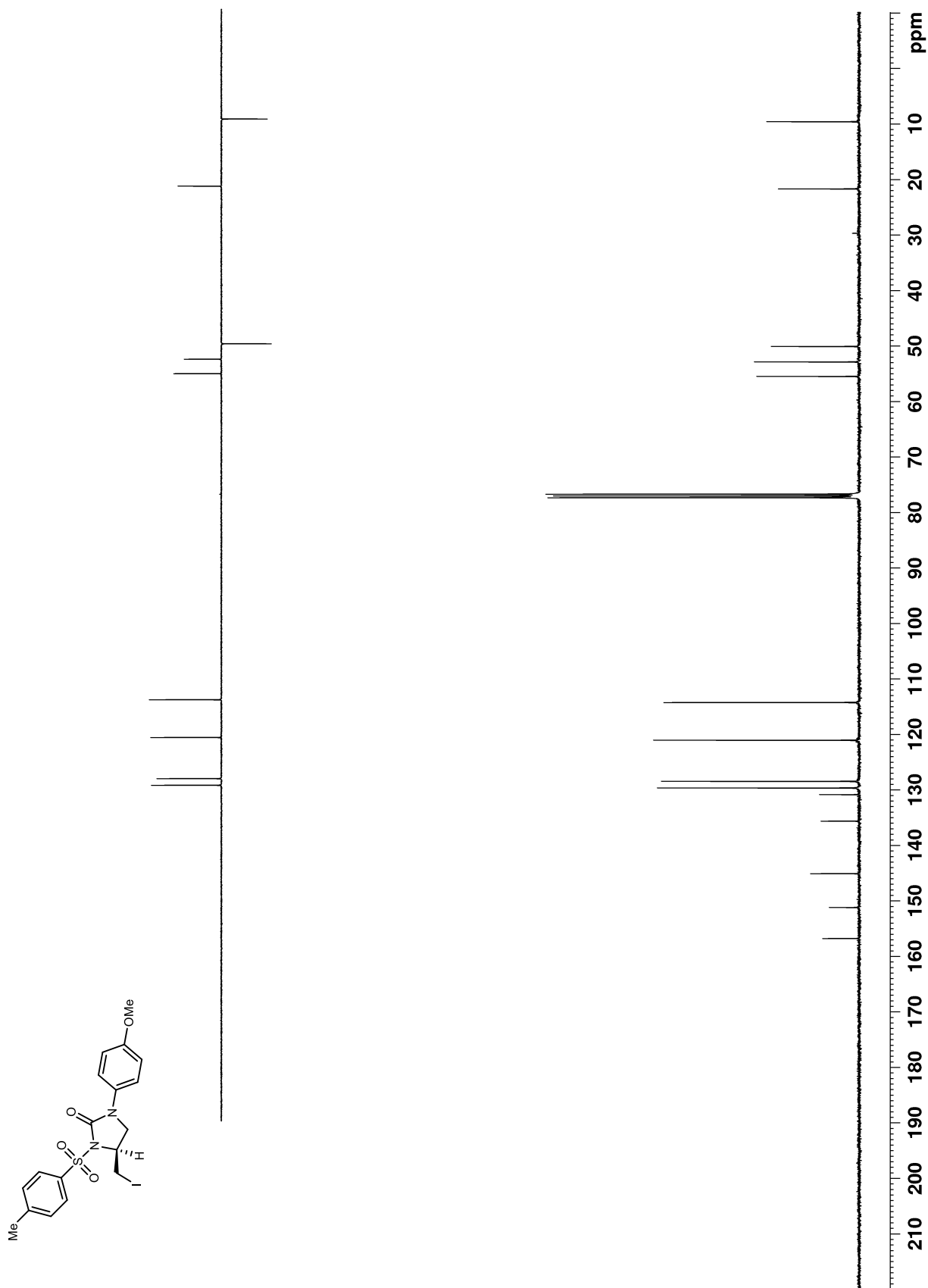
Figure 132. HPLC trace of **121m**. Chiralcel IB 30% EtOH/hexanes, 1.0 mL/min, 30 ºC
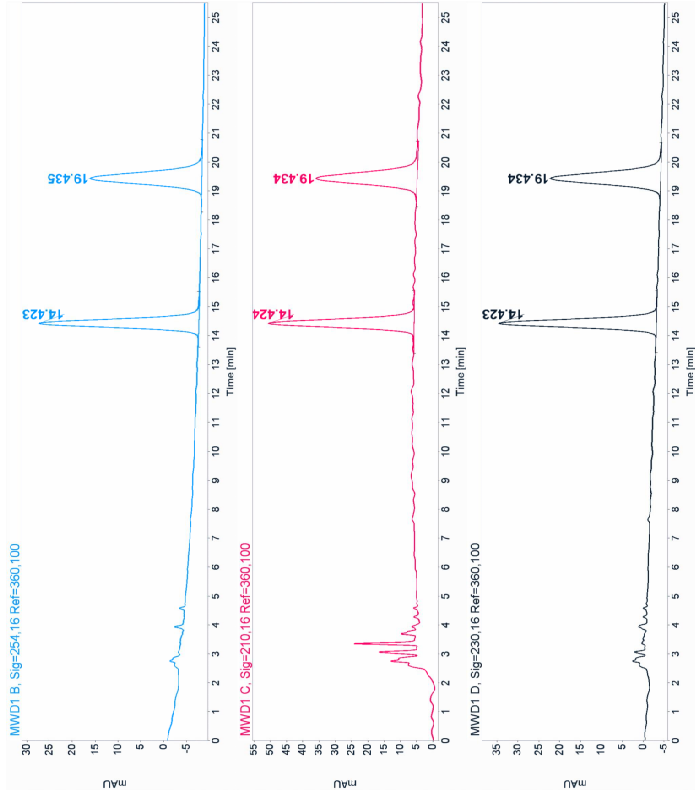
Signal: MWD1 B, Sig=254,16 Ref=360,100

RT [min]	Type	Width [min]	Area	Height	Area%	Name
14.423	MM	0.3366	707.8035	35.0463	50.0428	
19.435	MM	0.4820	706.5922	24.4307	49.9572	
		Sum	1414.3957			

Signal: MWD1 C, Sig=210,16 Ref=360,100

RT [min]	Type	Width [min]	Area	Height	Area%	Name
14.424	MM	0.3416	916.4442	44.7123	49.9714	
19.434	MM	0.4903	917.4943	31.1892	50.0286	
		Sum	1833.9385			

Signal: MWD1 D, Sig=230,16 Ref=360,100

RT [min]	Type	Width [min]	Area	Height	Area%	Name
14.423	MM	0.3367	761.5370	37.6937	49.5517	
19.434	MM	0.4898	775.3162	26.3828	50.4483	
		Sum	1536.8531			
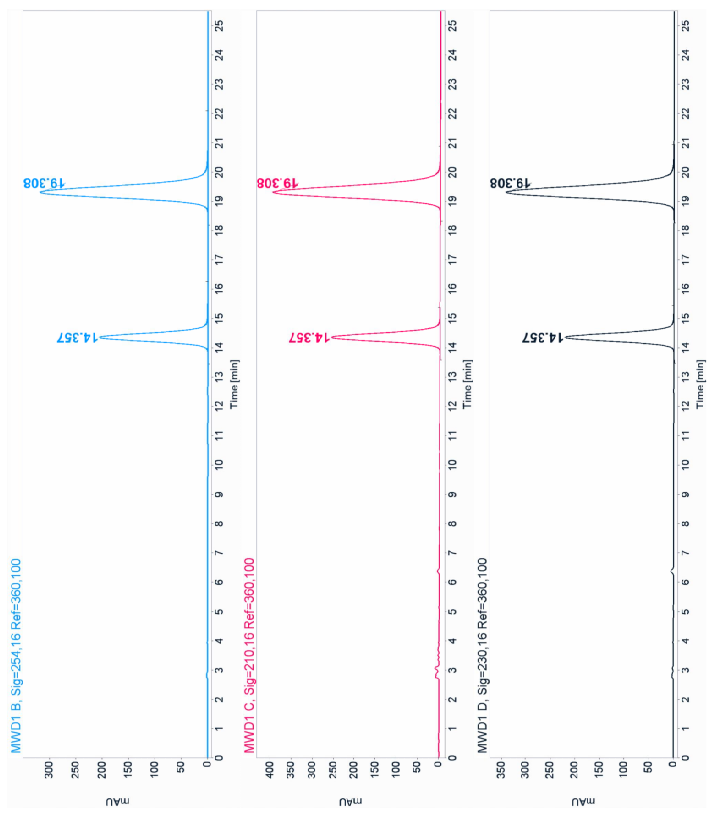
Signal: MWD1 B, Sig=254,16 Ref=360,100

RT [min]	Type	Width [min]	Area	Height	Area%	Name
14.357	MM	0.3373	4151.7793	205.1759	30.7650	
19.308	MM	0.4890	9343.3564	318.4436	69.2350	
		Sum	13495.1357			

Signal: MWD1 C, Sig=210,16 Ref=360,100

RT [min]	Type	Width [min]	Area	Height	Area%	Name
14.357	MM	0.3400	5269.8516	258.3383	30.9722	
19.308	MM	0.4921	11744.9463	397.7429	69.0278	
		Sum	17014.7979			

Signal: MWD1 D, Sig=230,16 Ref=360,100

RT [min]	Type	Width [min]	Area	Height	Area%	Name
14.357	MM	0.3410	4521.5674	220.9697	30.9913	
19.308	MM	0.4904	10068.2080	342.1633	69.0087	
		Sum	14589.7754			

Appendix 4.2-292
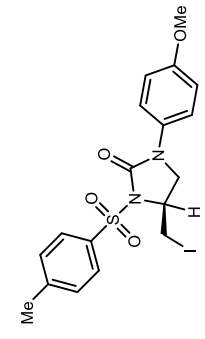
Figure 133. ^{1}H NMR (400 MHz, CDCl$_3$) of **122a**
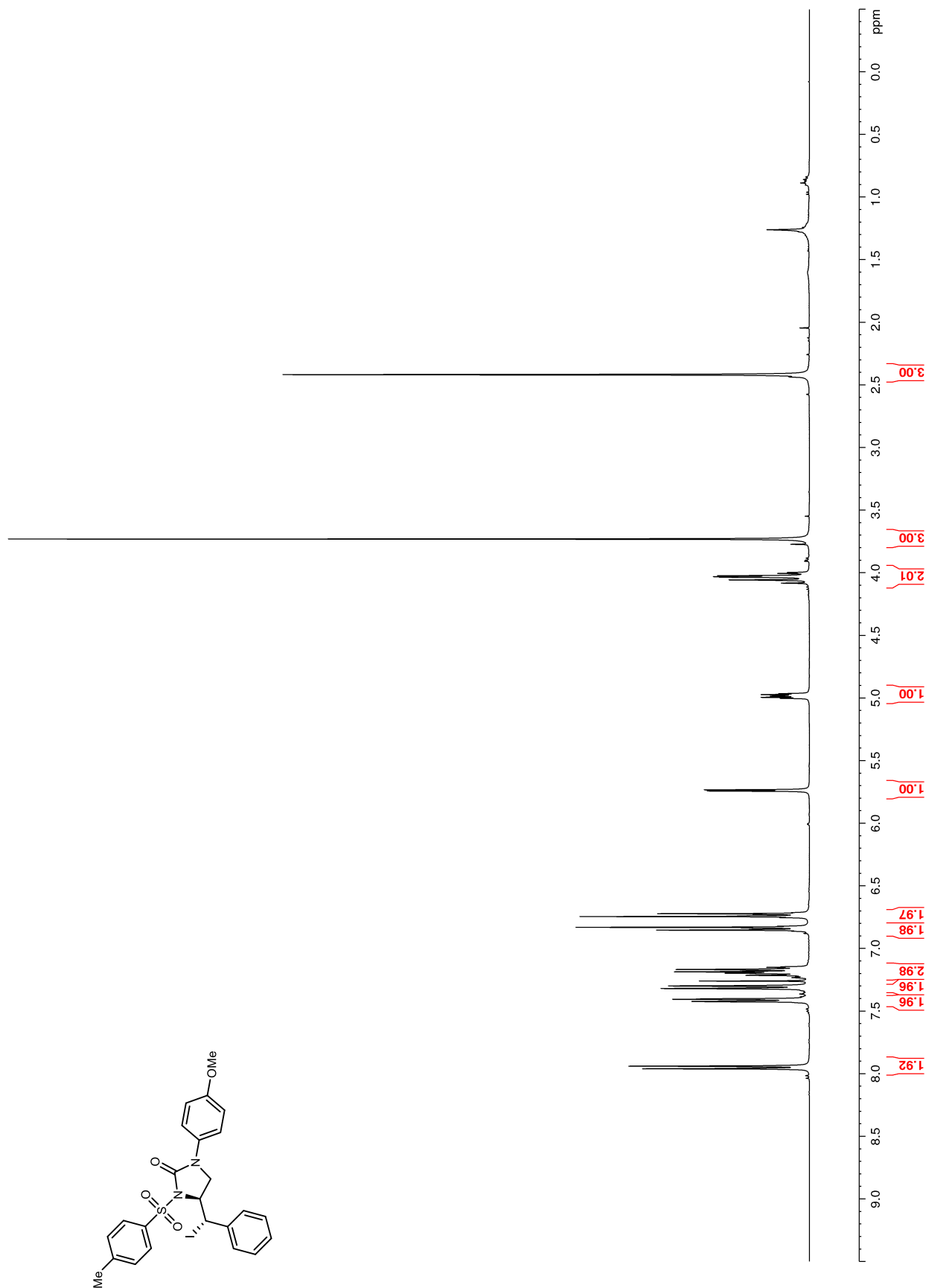
Figure 134. ^{13}C NMR (100 MHz, CDCl$_3$) of **122a**
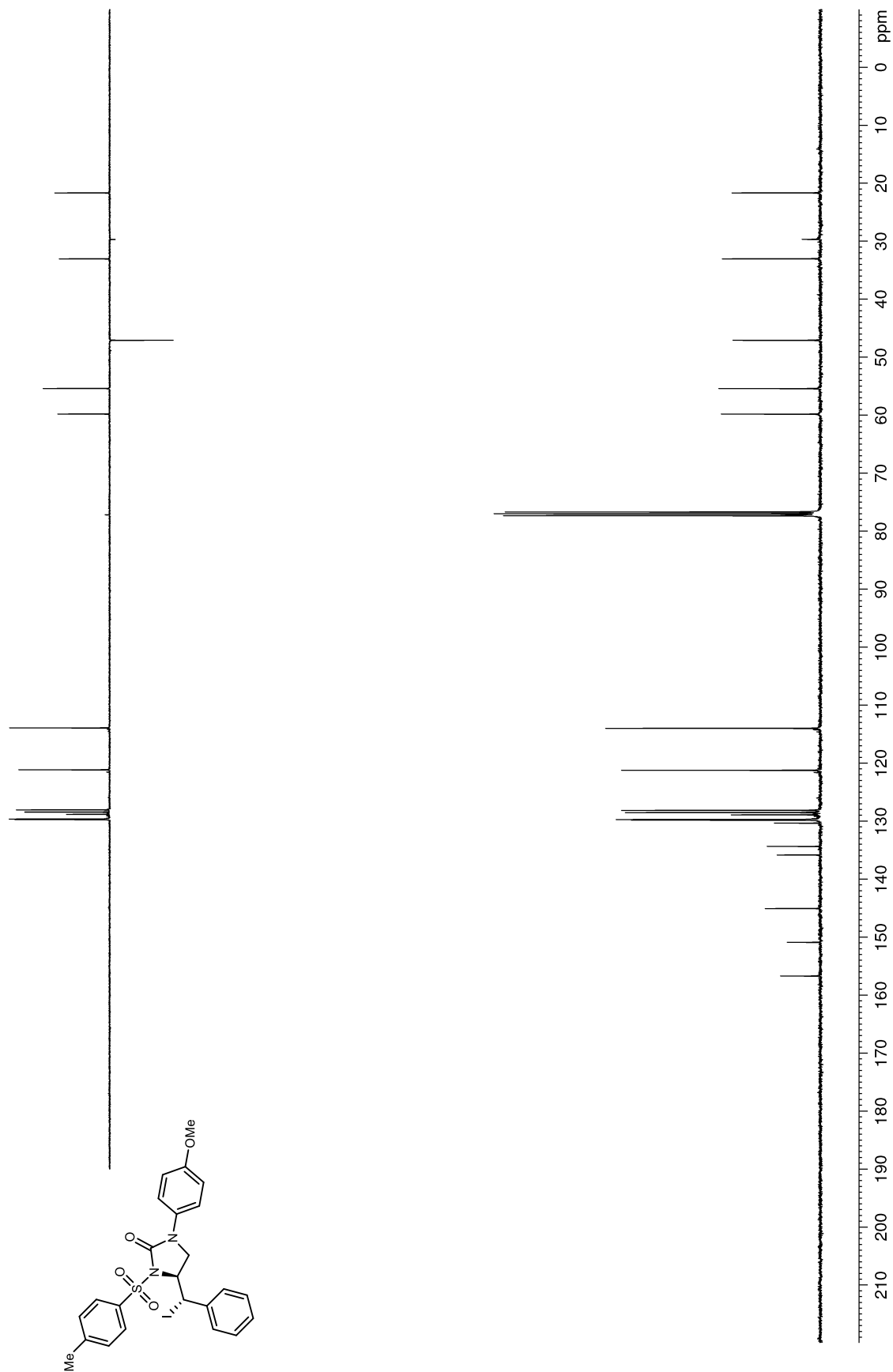
Figure 135. HPLC trace of **122a**. Chiralcel IB 25% EtOH/hexanes, 1.0 mL/min, 30 ºC
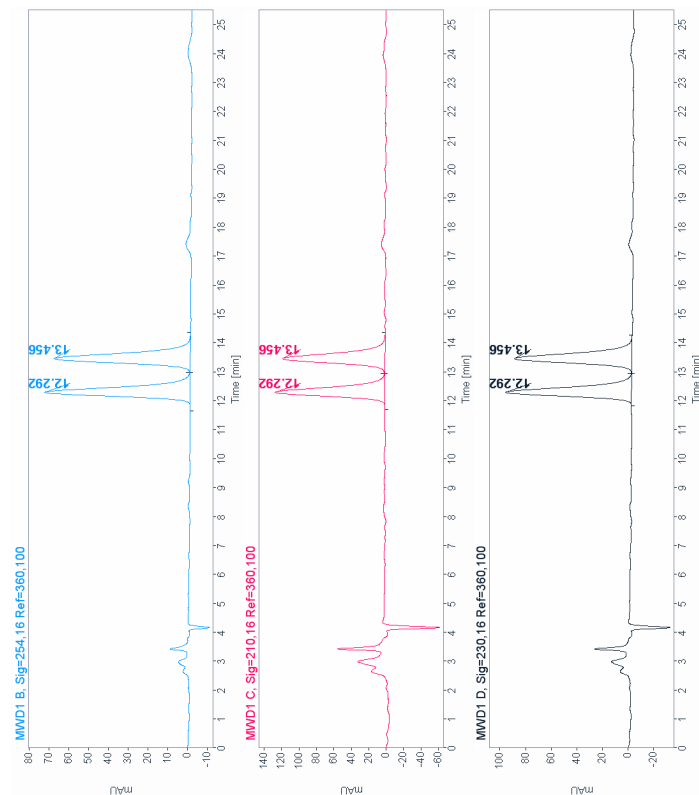
Signal: MWD1 B, Sig=254,16 Ref=360,100

RT [min]	Type	Width [min]	Area	Height	Area%	Name
12.292	MF	0.3528	1553.3883	73.3790	49.7917	
13.456	FM	0.3800	1566.3881	68.6971	50.2083	
		Sum	3119.7764			

Signal: MWD1 C, Sig=210,16 Ref=360,100

RT [min]	Type	Width [min]	Area	Height	Area%	Name
12.292	MF	0.3536	2671.4849	125.9131	49.5241	
13.456	FM	0.3850	2722.8279	117.8647	50.4759	
		Sum	5394.3127			

Signal: MWD1 D, Sig=230,16 Ref=360,100

RT [min]	Type	Width [min]	Area	Height	Area%	Name
12.292	MF	0.3519	2073.7358	98.2214	49.7915	
13.456	FM	0.3794	2091.1045	91.8602	50.2085	
		Sum	4164.8403			
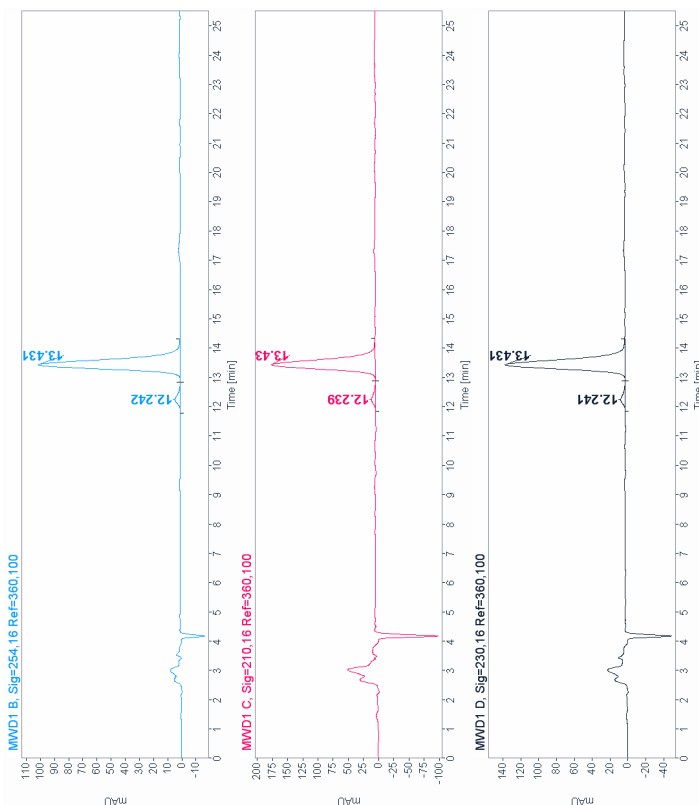
Signal: MWD1 B, Sig=254,16 Ref=360,100

RT [min]	Type	Width [min]	Area	Height	Area%	Name
12.242	MF	0.3898	88.3492	3.7771	3.7805	
13.431	FM	0.3730	2248.6033	100.4806	96.2195	
		Sum	2336.9524			

Signal: MWD1 C, Sig=210,16 Ref=360,100

RT [min]	Type	Width [min]	Area	Height	Area%	Name
12.239	MF	0.4157	172.1056	6.8997	4.2975	
13.430	FM	0.3735	3832.7073	171.0341	95.7025	
		Sum	4004.8129			

Signal: MWD1 D, Sig=230,16 Ref=360,100

RT [min]	Type	Width [min]	Area	Height	Area%	Name
12.241	MF	0.4025	124.5204	5.1561	3.9648	
13.431	FM	0.3734	3016.1372	134.6341	96.0352	
		Sum	3140.6576			
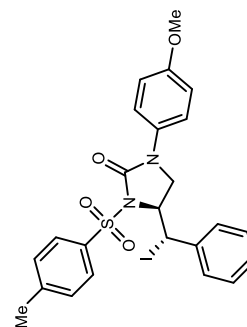
Figure 136. ^{1}H NMR (600 MHz, CDCl$_3$) of **124a**
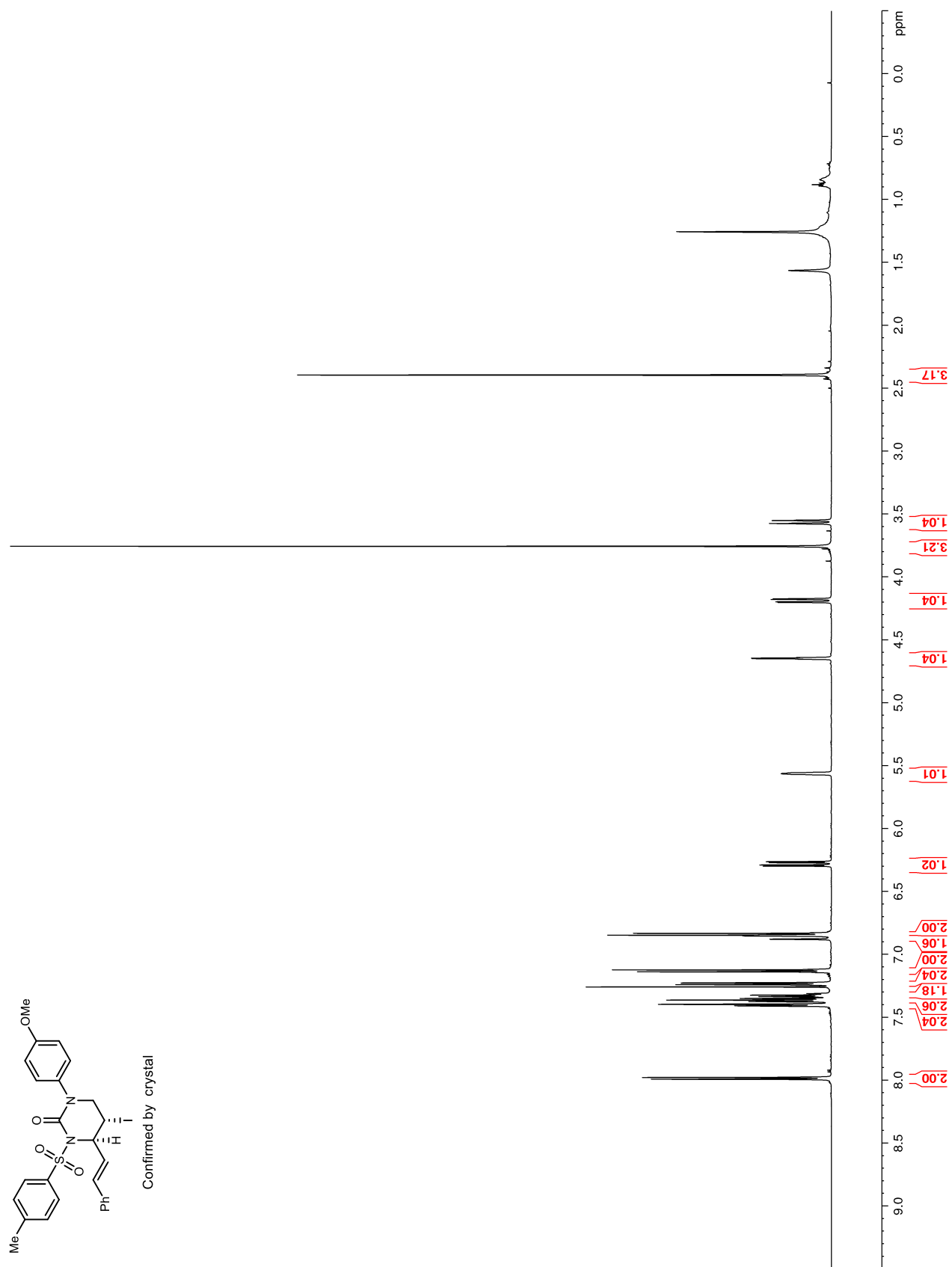
Figure 137. ^{13}C NMR (150 MHz, CDCl$_3$) of **124a**

Figure 138**.** HMBC of **124a**
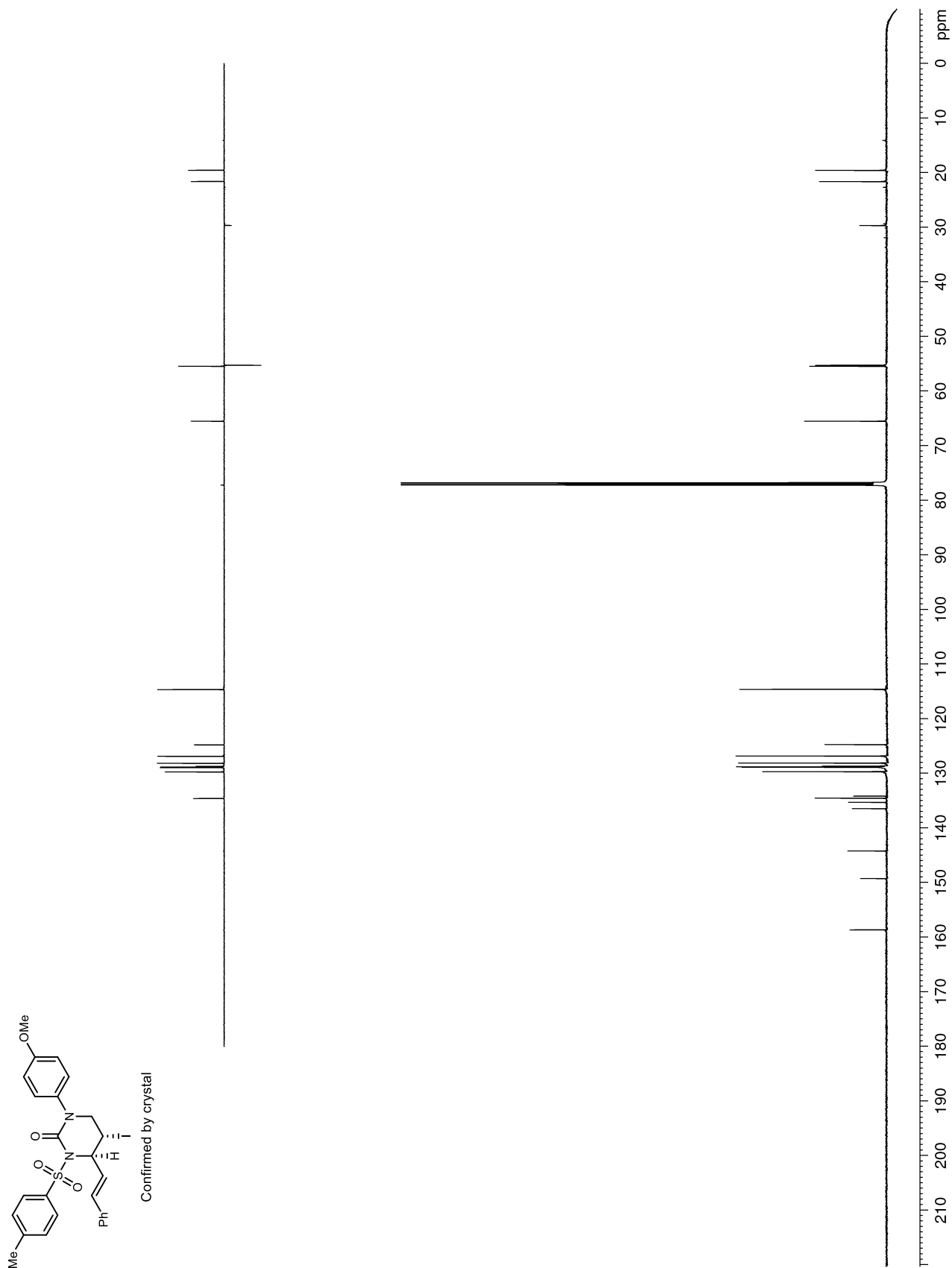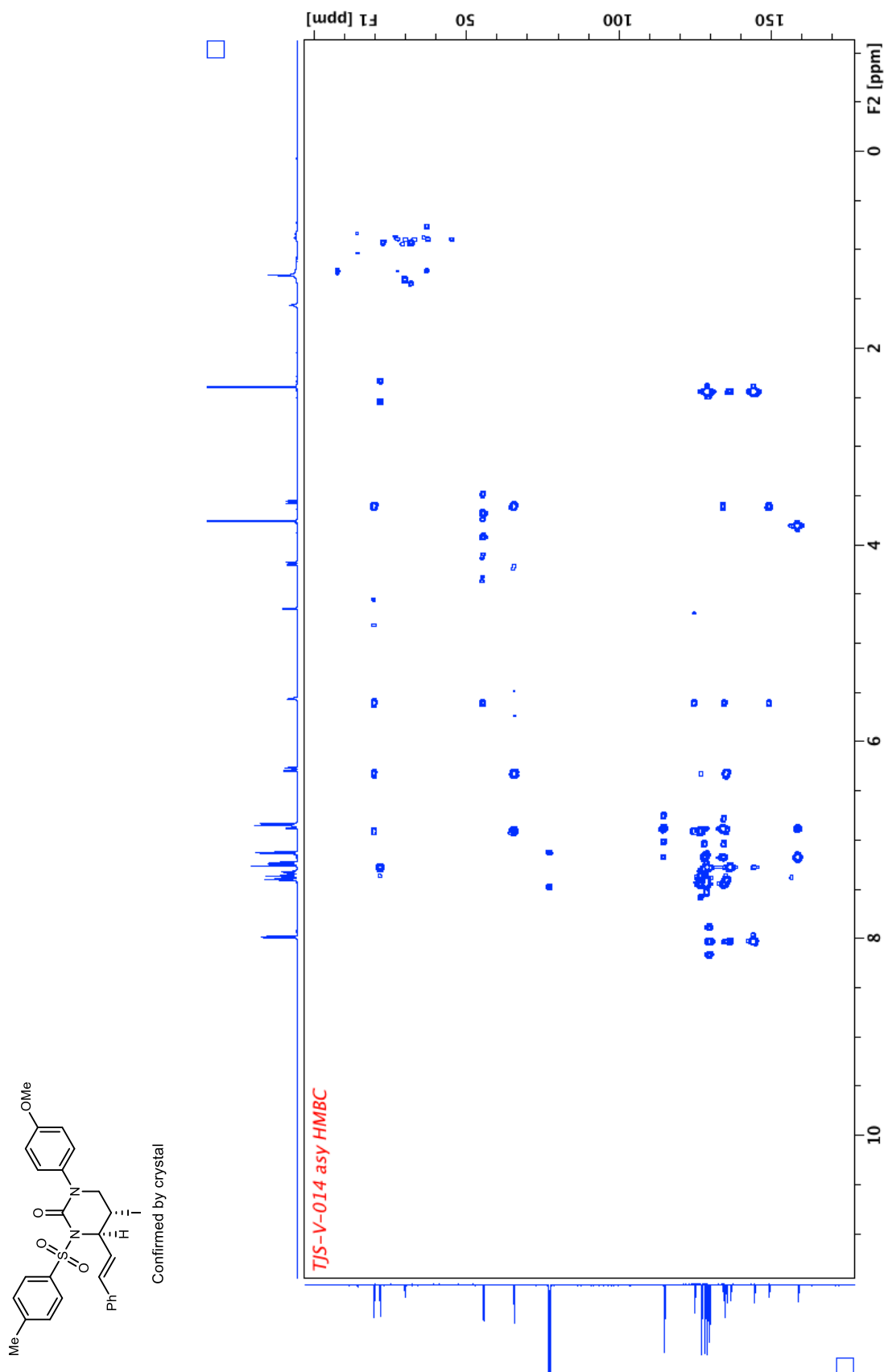
Figure 139. HPLC trace of **124a**. Chiralcel IB 25% EtOH/hexanes, 1.0 mL/min, 30 ºC

Signal: MWD1 B, Sig=254,16 Ref=360,100

RT [min]	Type	Width [min]	Area	Height	Area% Name
9.325	MF	0.2526	4294.7803	283.4146	96.8690
11.649	FM	0.3468	138.8156	6.6712	3.1310
		Sum	4433.5958		

Signal: MWD1 C, Sig=210,16 Ref=360,100

RT [min]	Type	Width [min]	Area	Height	Area% Name
9.325	MF	0.2547	7067.4790	462.4039	96.5674
11.647	FM	0.3724	251.2237	11.2437	3.4326
		Sum	7318.7027		

Signal: MWD1 D, Sig=230,16 Ref=360,100

RT [min]	Type	Width [min]	Area	Height	Area% Name
9.325	MF	0.2531	4929.2134	324.6240	96.4750
11.648	FM	0.3830	180.1024	7.8383	3.5250
		Sum	5109.3158		

Signal: MWD1 B, Sig=254,16 Ref=360,100

RT [min]	Type	Width [min]	Area	Height	Area% Name
9.323	MF	0.2564	1618.8982	105.2441	49.6563
11.559	FM	0.3413	1641.3097	80.1385	50.3437
		Sum	3260.2079		

Signal: MWD1 C, Sig=210,16 Ref=360,100

RT [min]	Type	Width [min]	Area	Height	Area% Name
9.323	MF	0.2577	2673.4941	172.9185	49.9026
11.558	FM	0.3406	2683.9321	131.3339	50.0974
		Sum	5357.4263		

Signal: MWD1 D, Sig=230,16 Ref=360,100

RT [min]	Type	Width [min]	Area	Height	Area% Name
9.323	MF	0.2562	1855.2292	120.6930	49.9562
11.558	FM	0.3384	1858.4803	91.5426	50.0438
		Sum	3713.7096		

Confirmed by crystal

Appendix 4.2-299

Figure 140. ^{1}H NMR (600 MHz, CDCl$_3$) of **124b**
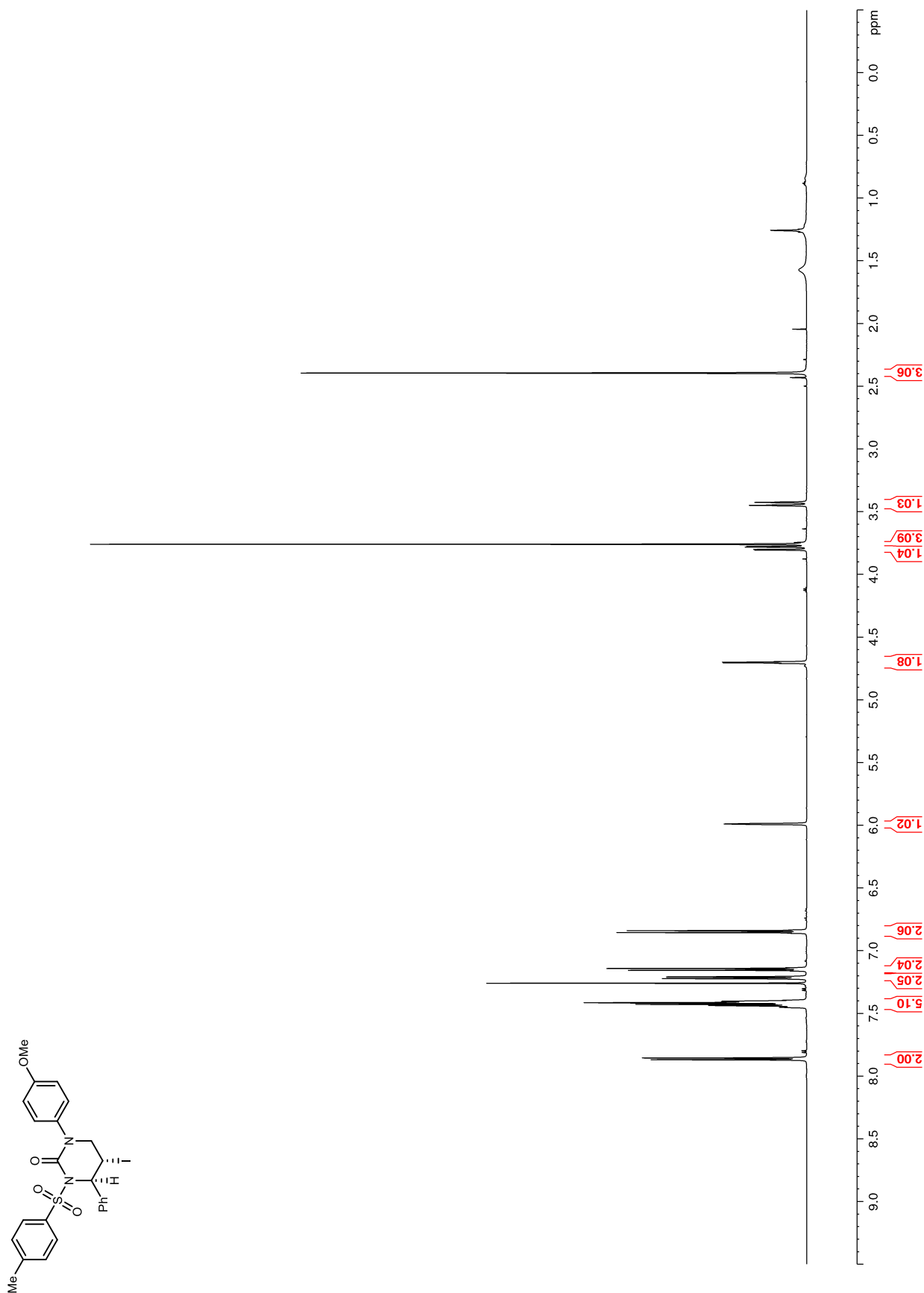
Figure 141. ^{13}C NMR (150 MHz, CDCl$_3$) of **124b**
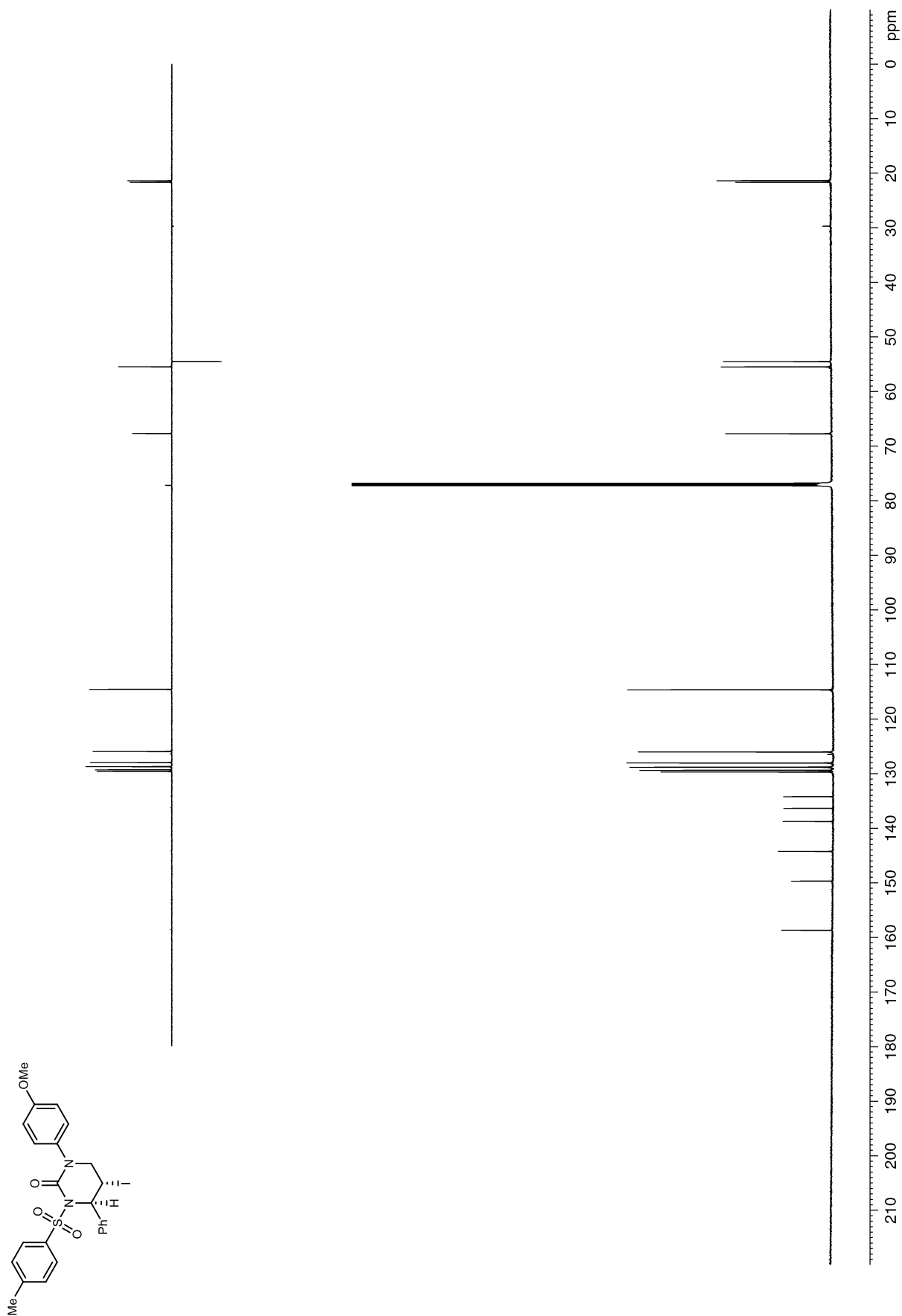
Figure 142. HPLC trace of **124b**. Chiralcel IB 25% EtOH/hexanes, 1.0 mL/min, 30 ºC
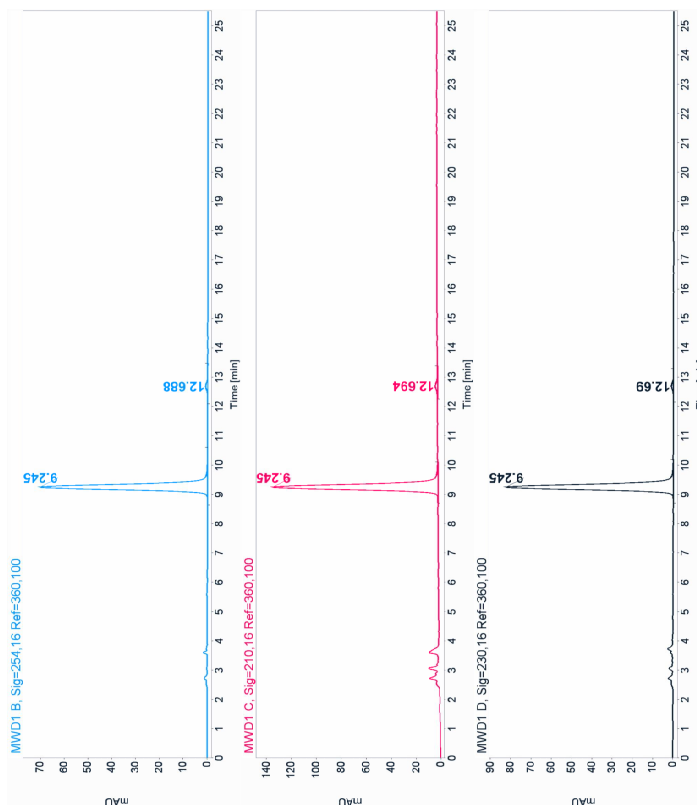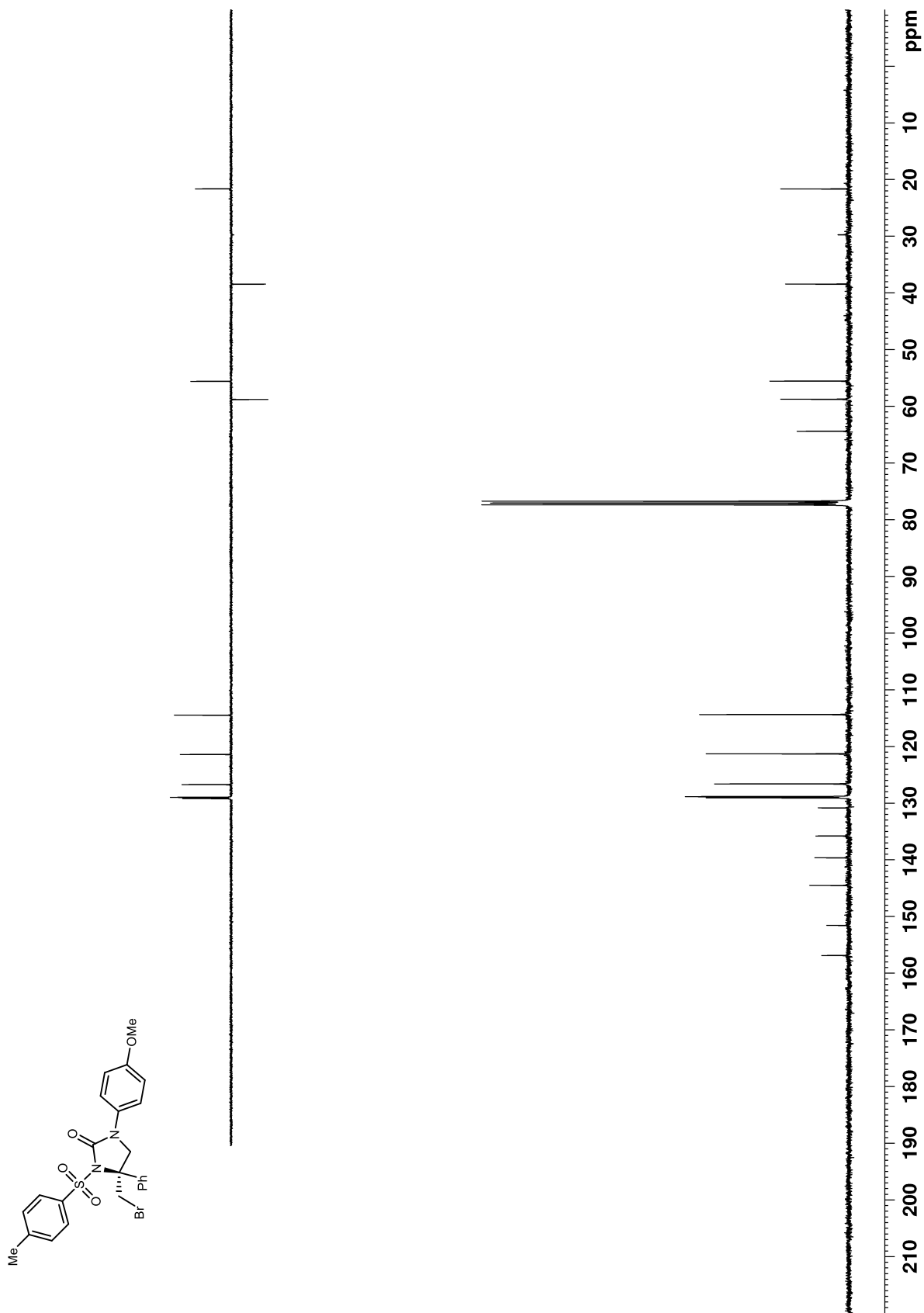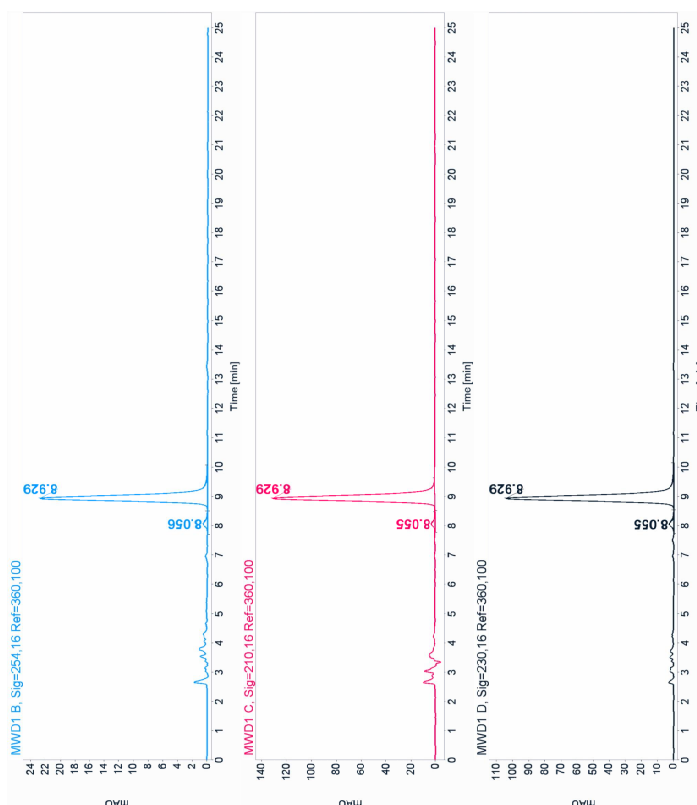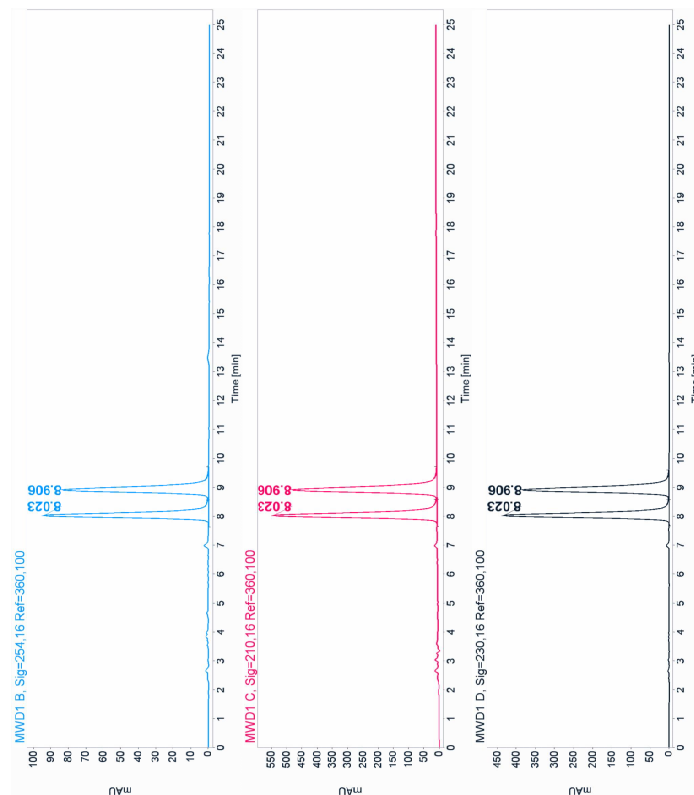

Signal: MWD1 B, Sig=254,16 Ref=360,100

RT [min]	Type	Width [min]	Area	Height	Area%	Name
8.023	MF	0.2021	1145.2716	94.4343	49.7763	
8.906	FM	0.2305	1155.5648	83.5446	50.2237	
		Sum	2300.8364			

Signal: MWD1 C, Sig=210,16 Ref=360,100

RT [min]	Type	Width [min]	Area	Height	Area%	Name
8.023	MF	0.2018	6483.1147	535.3854	49.8374	
8.906	FM	0.2292	6525.4287	474.4708	50.1626	
		Sum	13008.5435			

Signal: MWD1 D, Sig=230,16 Ref=360,100

RT [min]	Type	Width [min]	Area	Height	Area%	Name
8.023	MF	0.2005	5217.0542	433.7766	49.8920	
8.906	FM	0.2278	5239.6348	383.4114	50.1080	
		Sum	10456.6890			
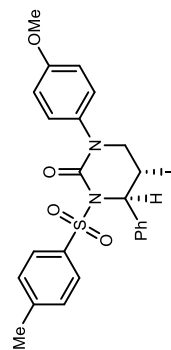
Signal: MWD1 B, Sig=254,16 Ref=360,100

RT [min]	Type	Width [min]	Area	Height	Area%	Name
8.056	MF	0.2349	7.9561	0.5645	2.4220	
8.929	FM	0.2340	320.5404	22.8327	97.5780	
		Sum	328.4965			

Signal: MWD1 C, Sig=210,16 Ref=360,100

RT [min]	Type	Width [min]	Area	Height	Area%	Name
8.055	MM	0.2497	50.2722	3.3552	2.6934	
8.929	MM	0.2316	1816.2095	130.6881	97.3066	
		Sum	1866.4817			

Signal: MWD1 D, Sig=230,16 Ref=360,100

RT [min]	Type	Width [min]	Area	Height	Area%	Name
8.055	MF	0.2274	35.2206	2.5810	2.3641	
8.929	FM	0.2326	1454.5864	104.4243	97.6359	
		Sum	1489.8070			

Appendix 4.2-302

Figure 143. ^{1}H NMR (600 MHz, CDCl$_3$) of **124c**
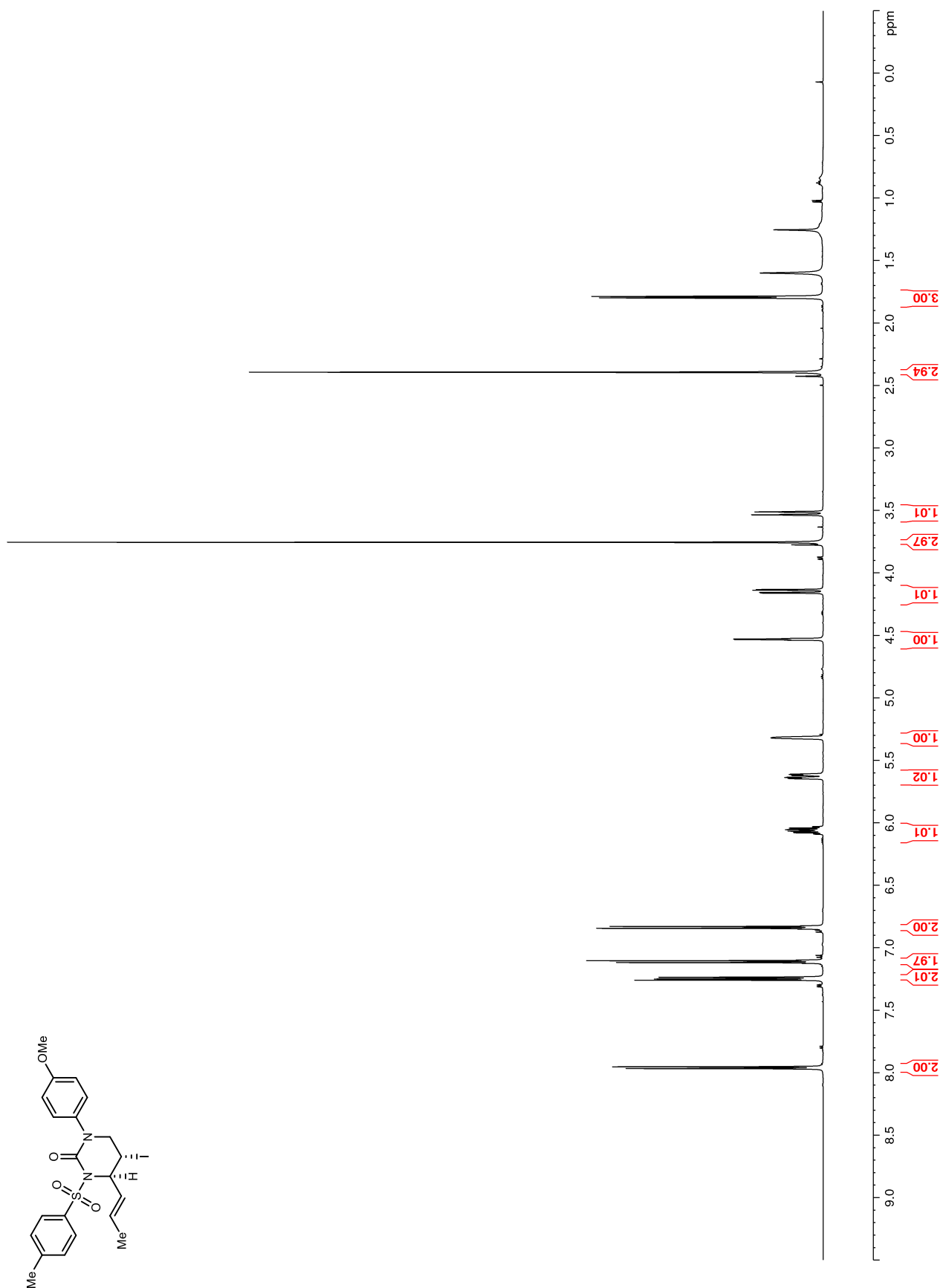
**Figure** 144. ^{13}C NMR (150 MHz, CDCl$_3$) of **124c**
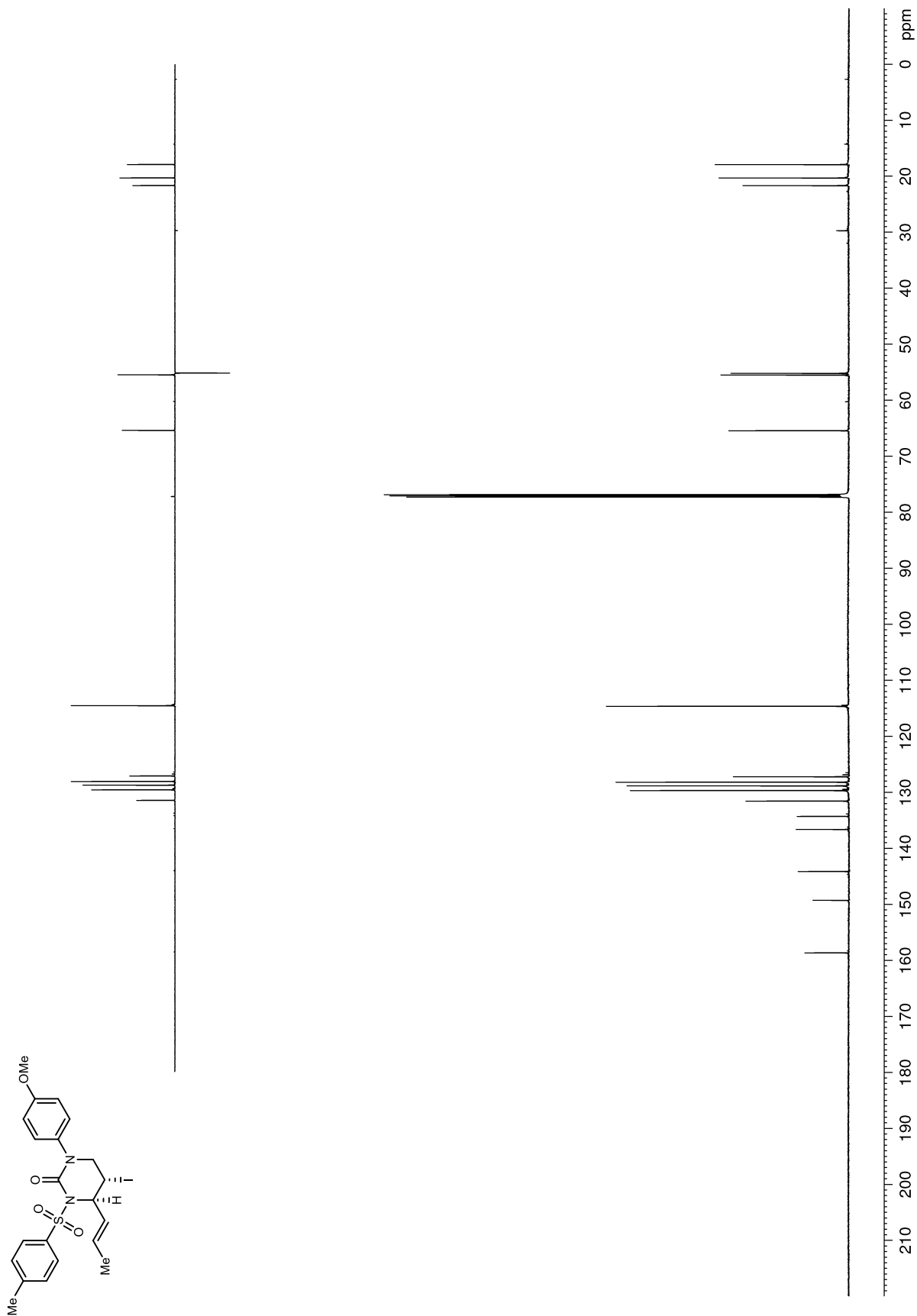
Figure 145. HPLC trace of **124c**. Chiralcel IB 25% EtOH/hexanes, 1.0 mL/min, 30 ºC
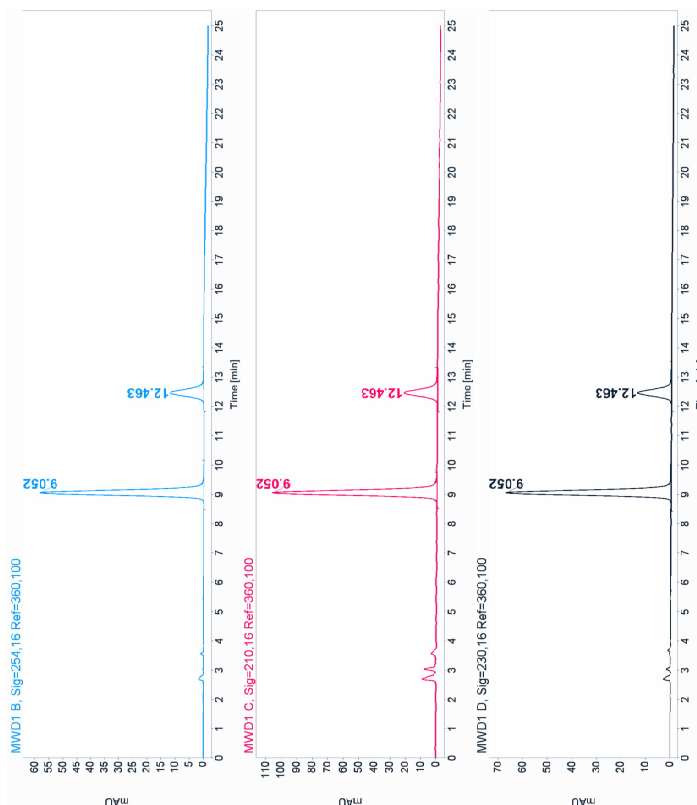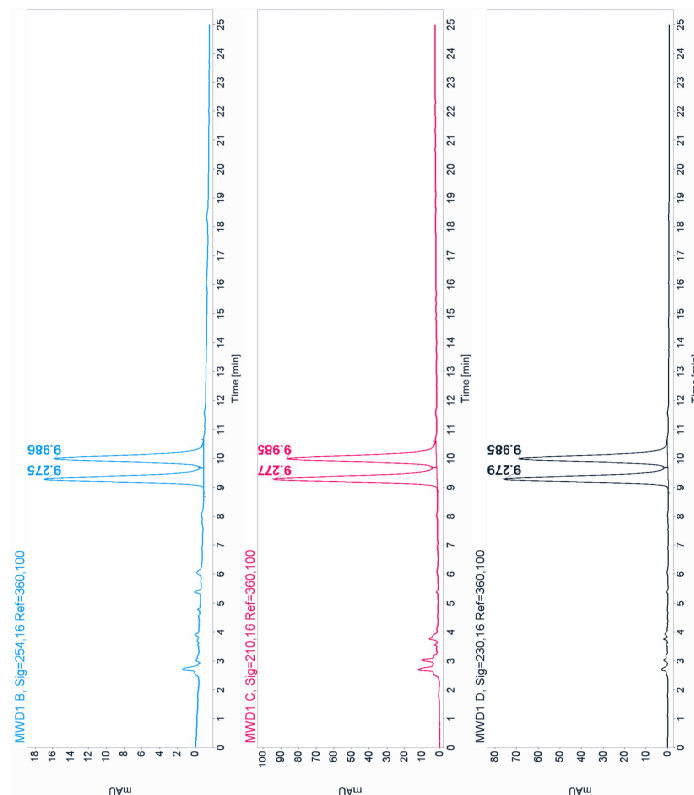

Signal: MWD1 B, Sig=254,16 Ref=360,100

RT [min]	Type	Width [min]	Area	Height	Area% Name
9.275	MF	0.2423	260.8529	17.9432	49.7710
9.986	FM	0.2625	263.2536	16.7161	50.2290
		Sum	524.1065		

Signal: MWD1 C, Sig=210,16 Ref=360,100

RT [min]	Type	Width [min]	Area	Height	Area% Name
9.277	MF	0.2439	1351.9000	92.3911	50.3201
9.985	FM	0.2629	1334.6996	84.6271	49.6799
		Sum	2686.5996		

Signal: MWD1 D, Sig=230,16 Ref=360,100

RT [min]	Type	Width [min]	Area	Height	Area% Name
9.279	MF	0.2451	1120.4932	76.1975	50.7645
9.985	FM	0.2627	1086.7428	68.9536	49.2355
		Sum	2207.2360		
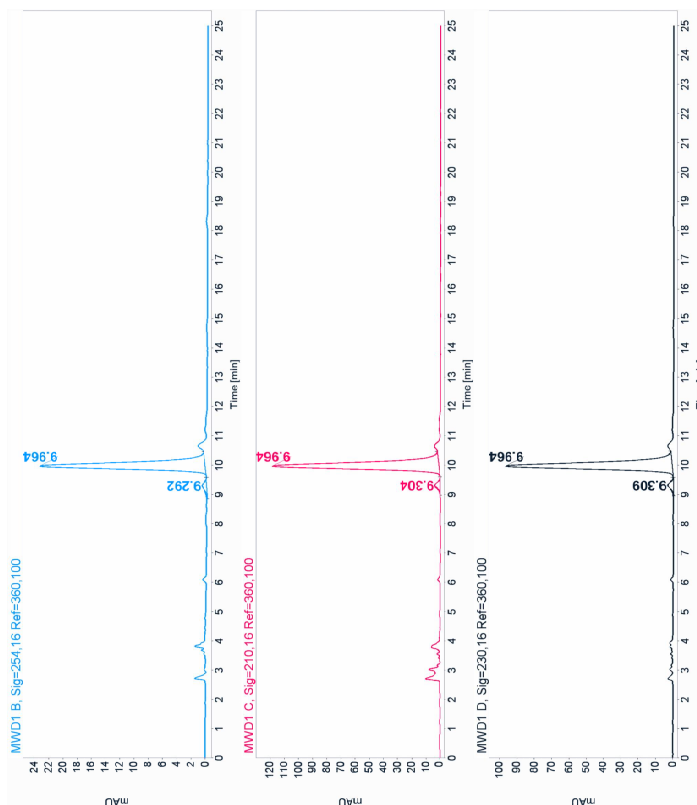
Signal: MWD1 B, Sig=254,16 Ref=360,100

RT [min]	Type	Width [min]	Area	Height	Area% Name
9.292	MM	0.3094	10.9742	0.5911	3.0138
9.964	MM	0.2532	353.1626	23.247	96.9862
		Sum	364.1368		

Signal: MWD1 C, Sig=210,16 Ref=360,100

RT [min]	Type	Width [min]	Area	Height	Area% Name
9.304	MM	0.2428	48.2297	3.3102	2.6233
9.964	MM	0.2539	1790.3162	117.5339	97.3767
		Sum	1838.5458		

Signal: MWD1 D, Sig=230,16 Ref=360,100

RT [min]	Type	Width [min]	Area	Height	Area% Name
9.309	MM	0.2678	51.2458	3.1892	3.3693
9.964	MM	0.2550	1469.7328	96.0732	96.6307
		Sum	1520.9786		

Appendix 4.2-305

Figure 146. ^{1}H NMR (400 MHz, CDCl$_3$) of **124d**

Figure 147. ^{13}C NMR (100 MHz, CDCl$_3$) of **124d**

Figure 148. HPLC trace of **124d**. Chiralcel IA 25% EtOH/hexanes, 1.0 mL/min, 30 ºC
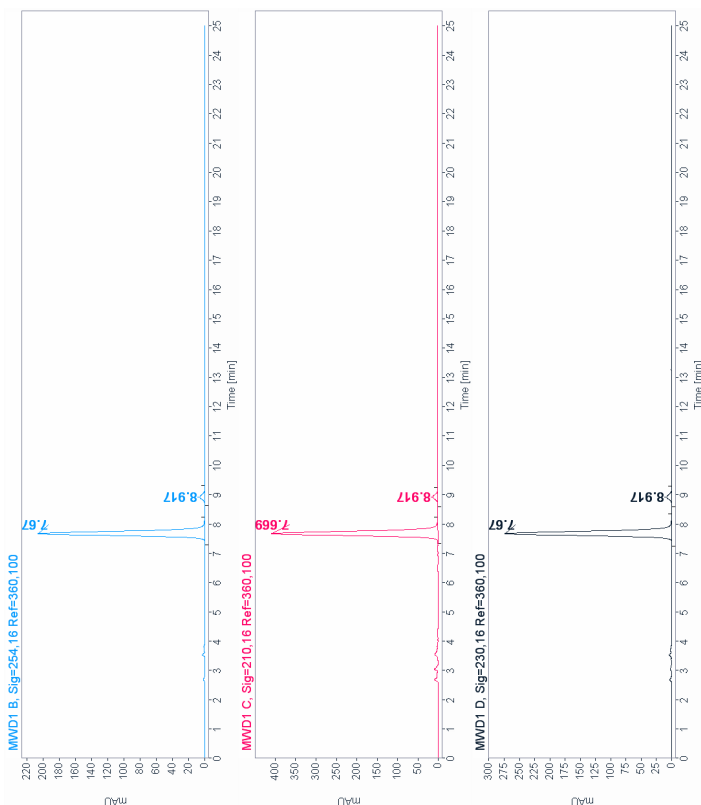

Signal: MWD1 B, Sig=254,16 Ref=360,100

RT [min]	Type	Width [min]	Area	Height	Area% Name
10.518	MM	0.2886	262.2847	15.1445	48.7454
15.052	MM	0.4925	275.7856	9.3319	51.2546
		Sum	538.0703		

Signal: MWD1 C, Sig=210,16 Ref=360,100

RT [min]	Type	Width [min]	Area	Height	Area% Name
10.518	MM	0.2895	1296.0388	74.6095	49.7898
15.052	MM	0.4771	1306.9799	45.6532	50.2102
		Sum	2603.0187		

Signal: MWD1 D, Sig=230,16 Ref=360,100

RT [min]	Type	Width [min]	Area	Height	Area% Name
10.518	MM	0.2906	998.3164	57.2587	49.8992
15.053	MM	0.4765	1002.3508	35.0564	50.1008
		Sum	2000.6672		

Signal: MWD1 B, Sig=254,16 Ref=360,100

RT [min]	Type	Width [min]	Area	Height	Area% Name
10.519	MM	0.2908	528.3113	30.2743	92.5906
15.100	MM	0.5401	42.2773	1.3047	7.4094
		Sum	570.5886		

Signal: MWD1 C, Sig=210,16 Ref=360,100

RT [min]	Type	Width [min]	Area	Height	Area% Name
10.519	MM	0.2908	2593.7051	148.6719	93.0897
15.100	MM	0.5118	192.5389	6.2705	6.9103
		Sum	2786.2439		

Signal: MWD1 D, Sig=230,16 Ref=360,100

RT [min]	Type	Width [min]	Area	Height	Area% Name
10.519	MM	0.2914	1996.3925	114.1927	93.9359
15.101	MM	0.4720	128.8786	4.5503	6.0641
		Sum	2125.2711		

Figure 149. ^{1}H NMR (400 MHz, CDCl$_3$) of **124e**
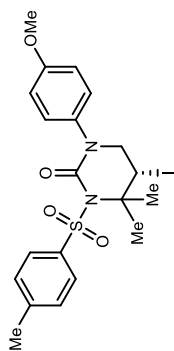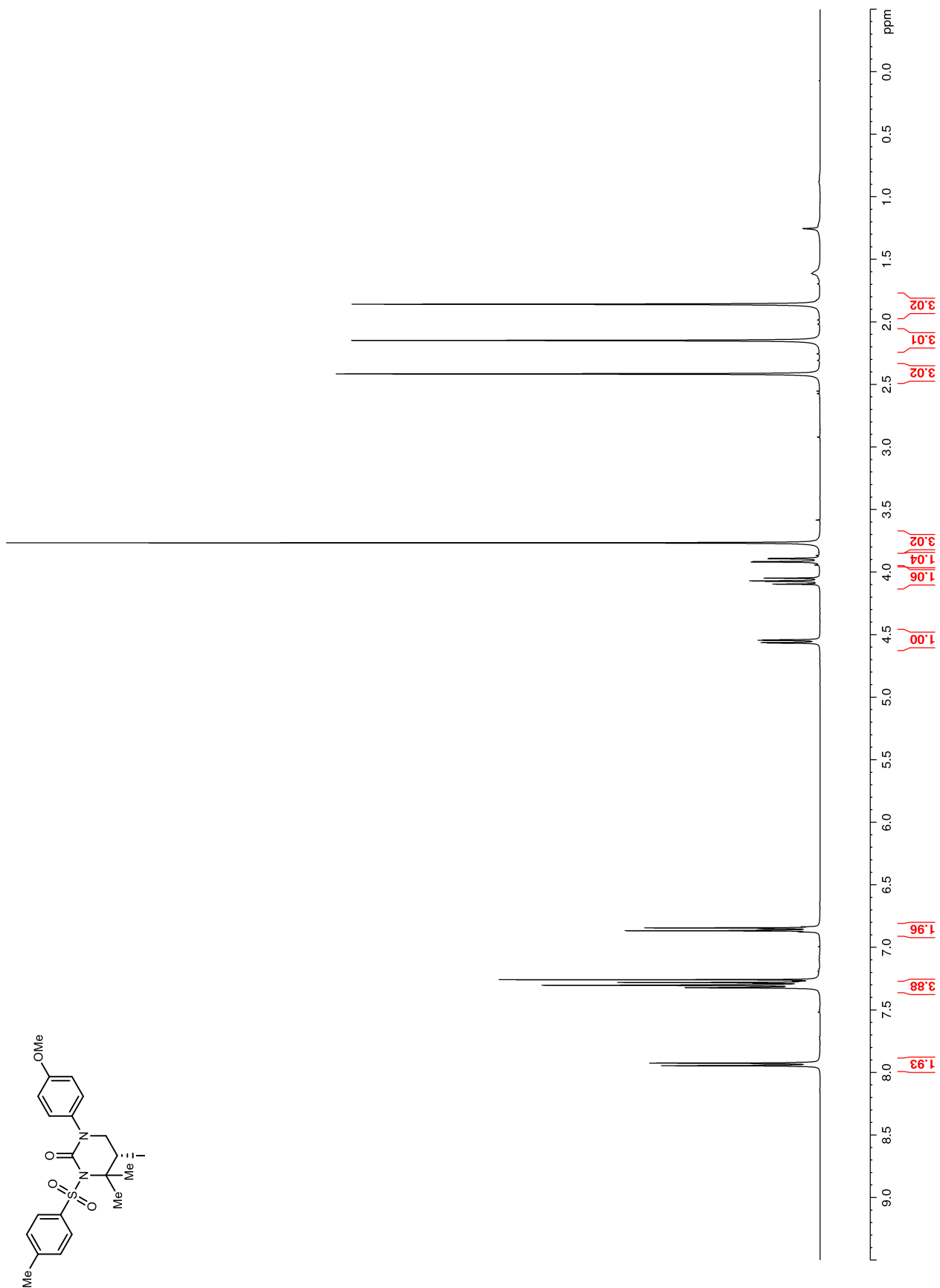
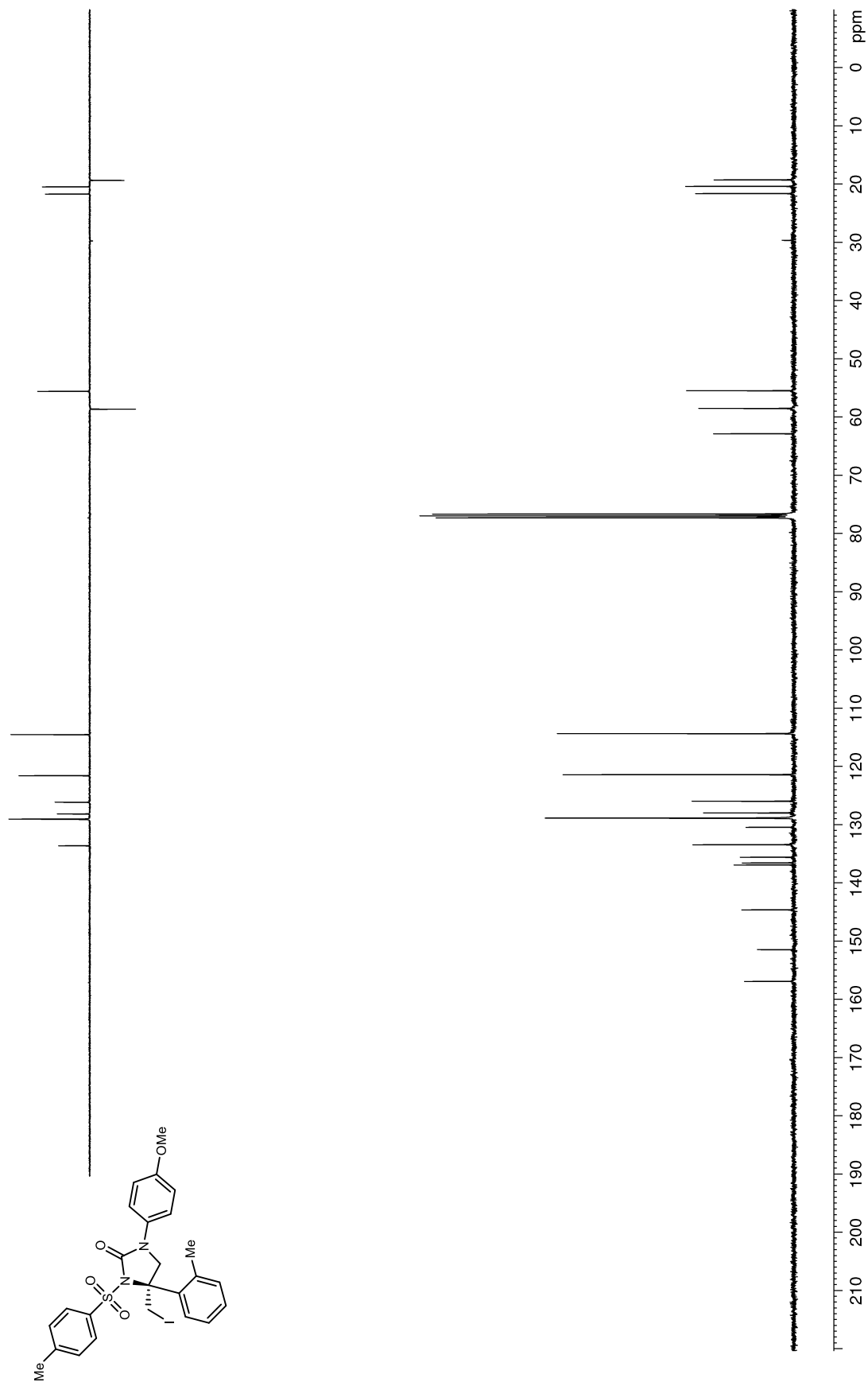**Figure** 150. ^{13}C NMR (100 MHz, CDCl$_3$) of **124e**
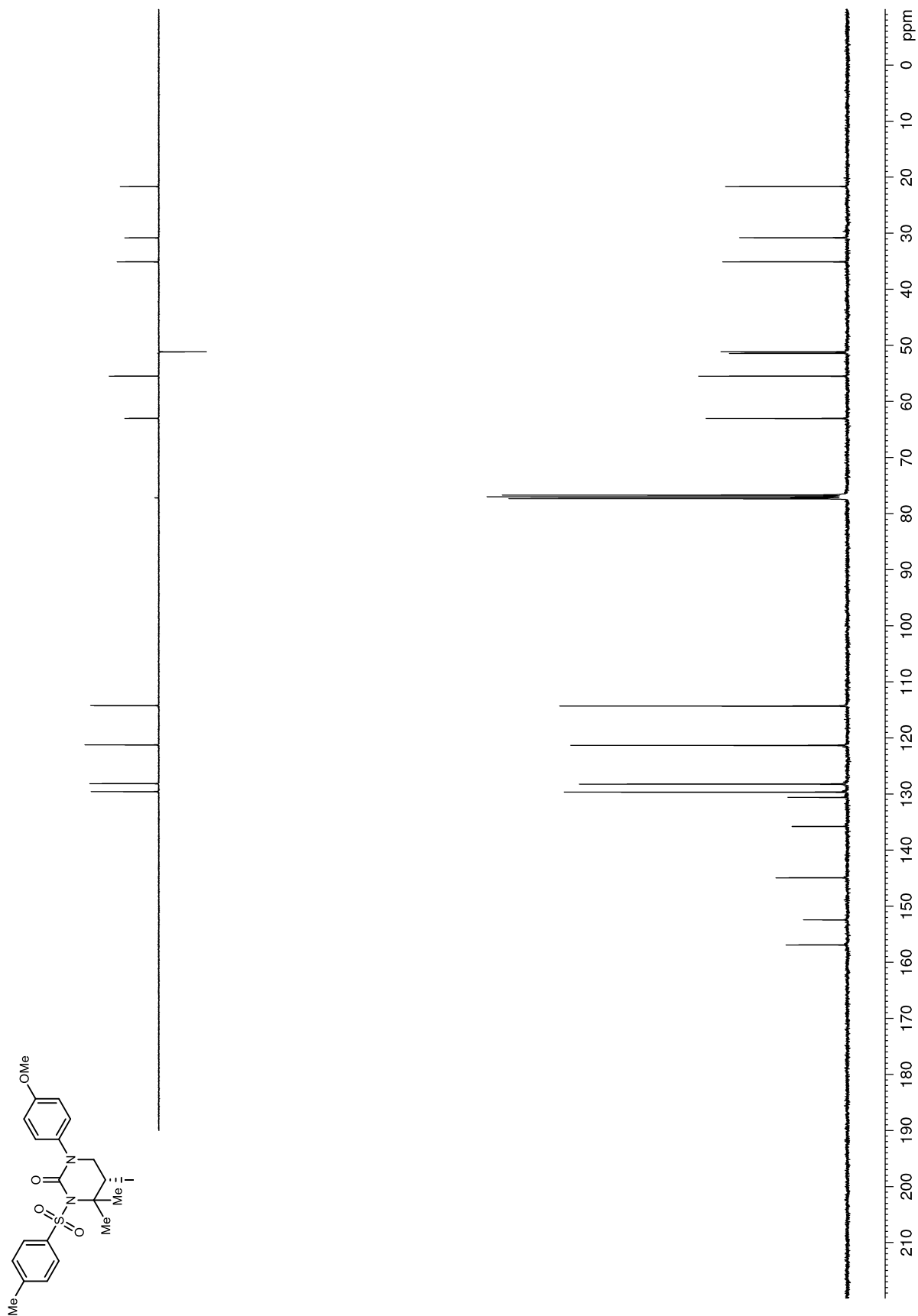
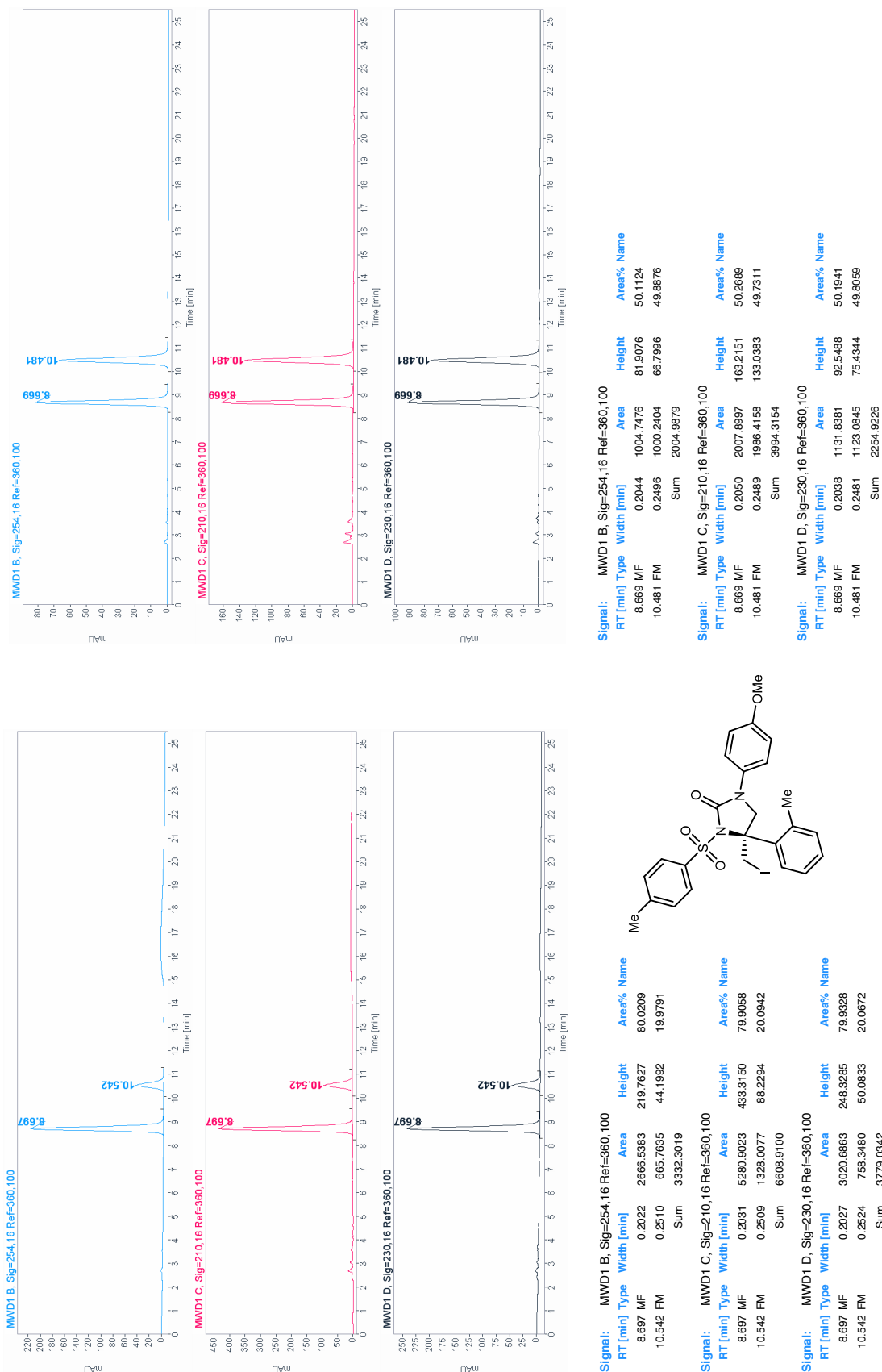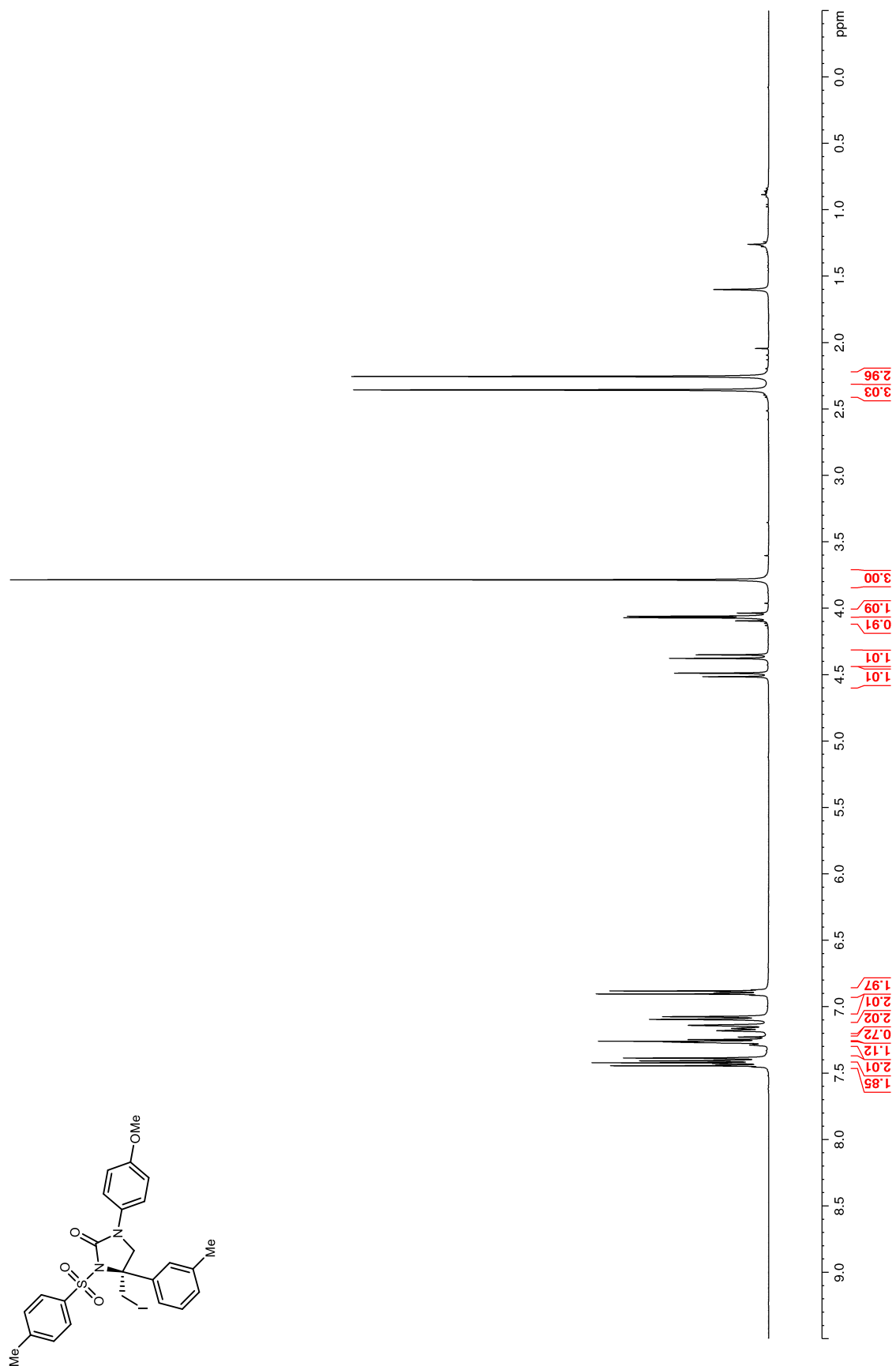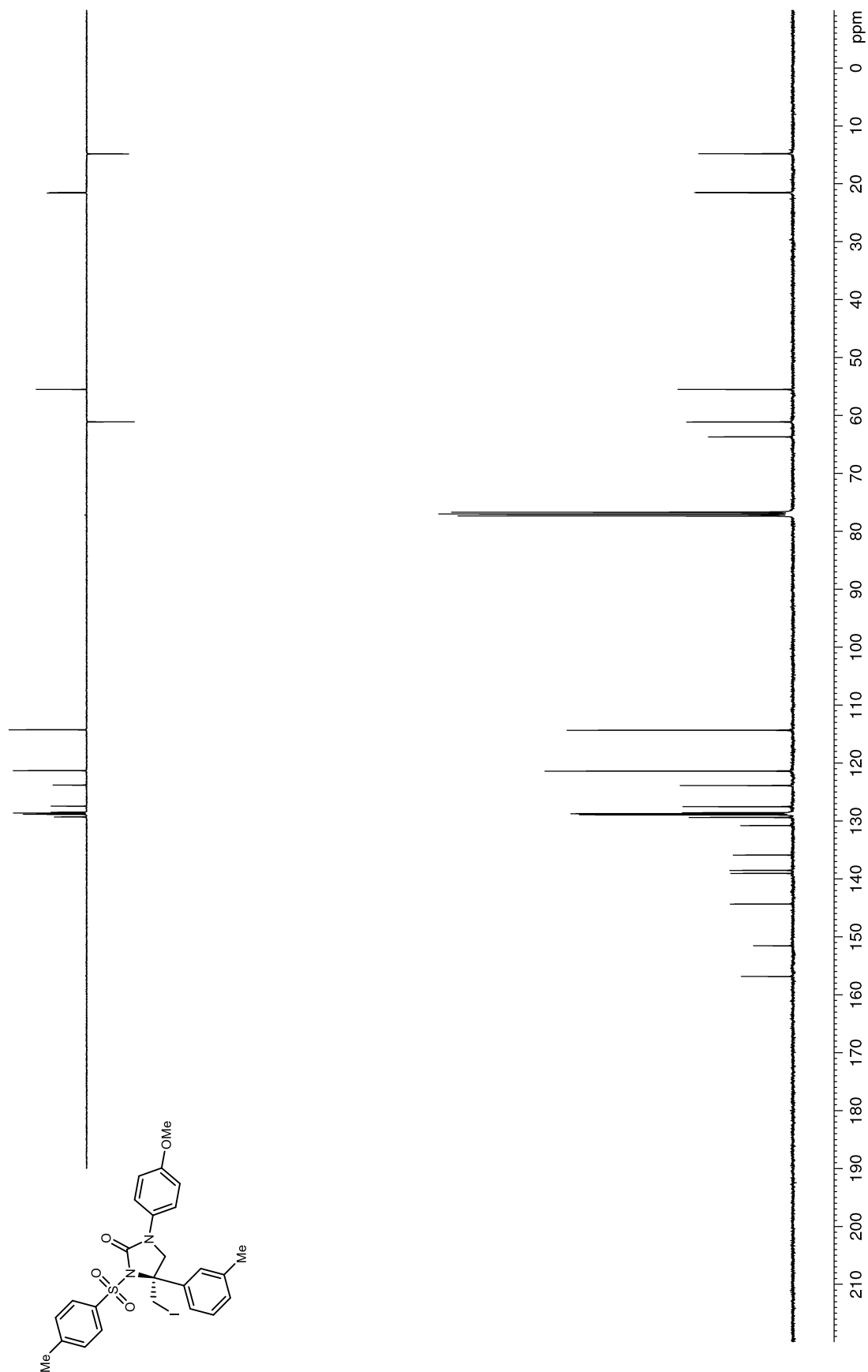**Figure 151.** HPLC trace of **124e**. Chiralcel IA 25% EtOH/hexanes, 1.0 mL/min, 30 ºC

Signal: MWD1 B, Sig=254,16 Ref=360,100

RT [min]	Type	Width [min]	Area	Height	Area%	Name
13.068	MM	0.3438	723.1289	35.0525	50.1160	
18.884	MM	0.4517	719.7824	26.5575	49.8840	
		Sum	1442.9113			

Signal: MWD1 C, Sig=210,16 Ref=360,100

RT [min]	Type	Width [min]	Area	Height	Area%	Name
13.067	MM	0.3541	1082.6597	50.9590	46.6120	
18.883	MM	0.5108	1240.0453	40.4625	53.3880	
		Sum	2322.7050			

Signal: MWD1 D, Sig=230,16 Ref=360,100

RT [min]	Type	Width [min]	Area	Height	Area%	Name
13.068	MM	0.3437	850.3733	41.2323	49.9094	
18.884	MM	0.4539	853.4617	31.3401	50.0906	
		Sum	1703.8350			

Signal: MWD1 B, Sig=254,16 Ref=360,100

RT [min]	Type	Width [min]	Area	Height	Area%	Name
12.994	MM	0.3449	2249.5066	108.6964	81.1288	
18.749	MM	0.4654	523.2546	18.7398	18.8712	
		Sum	2772.7612			

Signal: MWD1 C, Sig=210,16 Ref=360,100

RT [min]	Type	Width [min]	Area	Height	Area%	Name
12.994	MM	0.3659	3429.9592	156.2400	80.4091	
18.749	MM	0.4959	835.6754	28.0838	19.5909	
		Sum	4265.6346			

Signal: MWD1 D, Sig=230,16 Ref=360,100

RT [min]	Type	Width [min]	Area	Height	Area%	Name
12.994	MM	0.3498	2685.9207	127.9652	81.5469	
18.750	MM	0.4611	607.7919	21.9673	18.4531	
		Sum	3293.7125			

Appendix 4.2-311

Figure 152. ^{1}H NMR (400 MHz, CDCl$_3$) comparison for absolute stereochemistry determination of **122a**

Figure 153. ^{1}H NMR (400 MHz, CDCl$_3$) of **126**
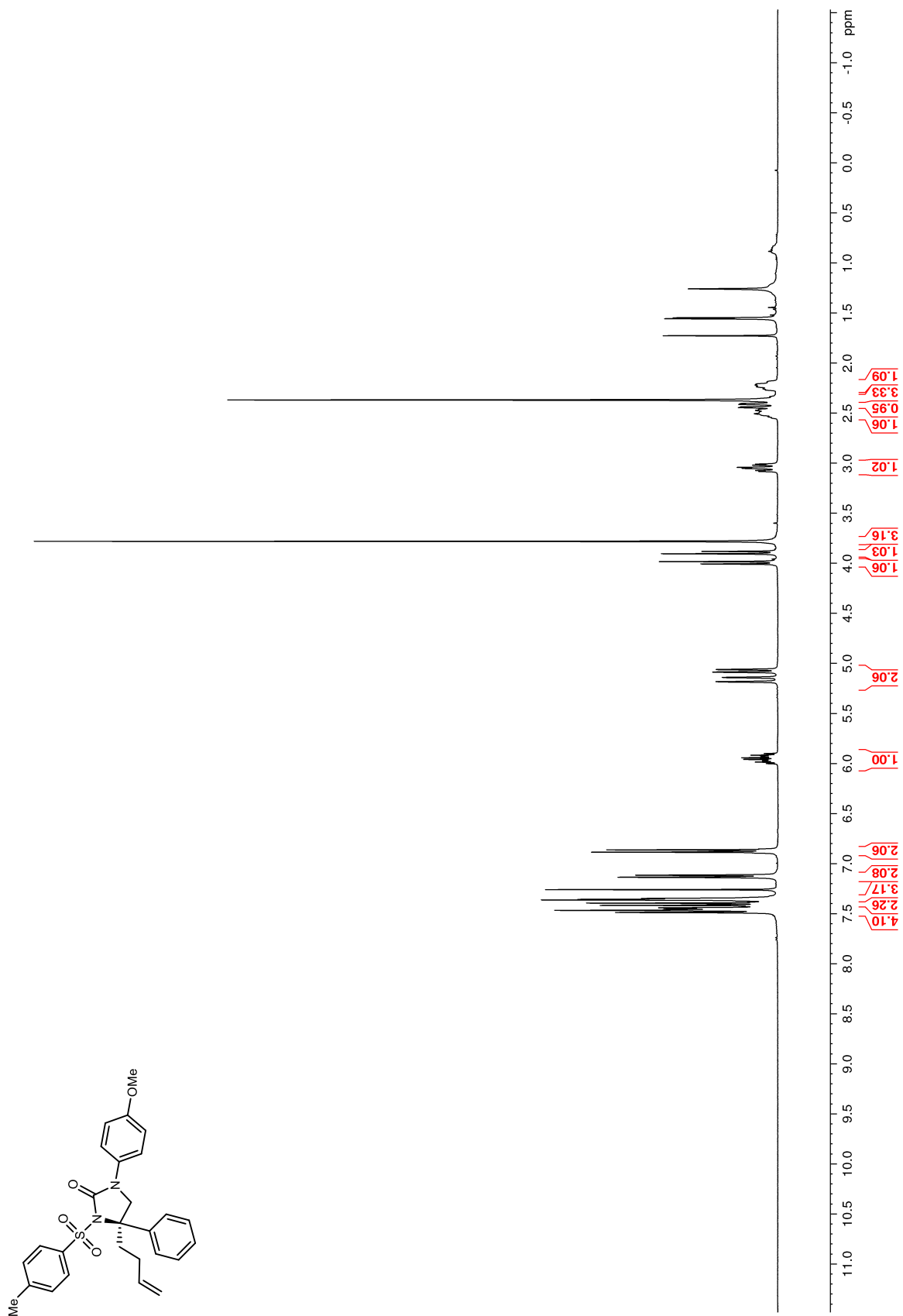
Figure 154. ^{13}C NMR (100 MHz, CDCl$_3$) of **126**
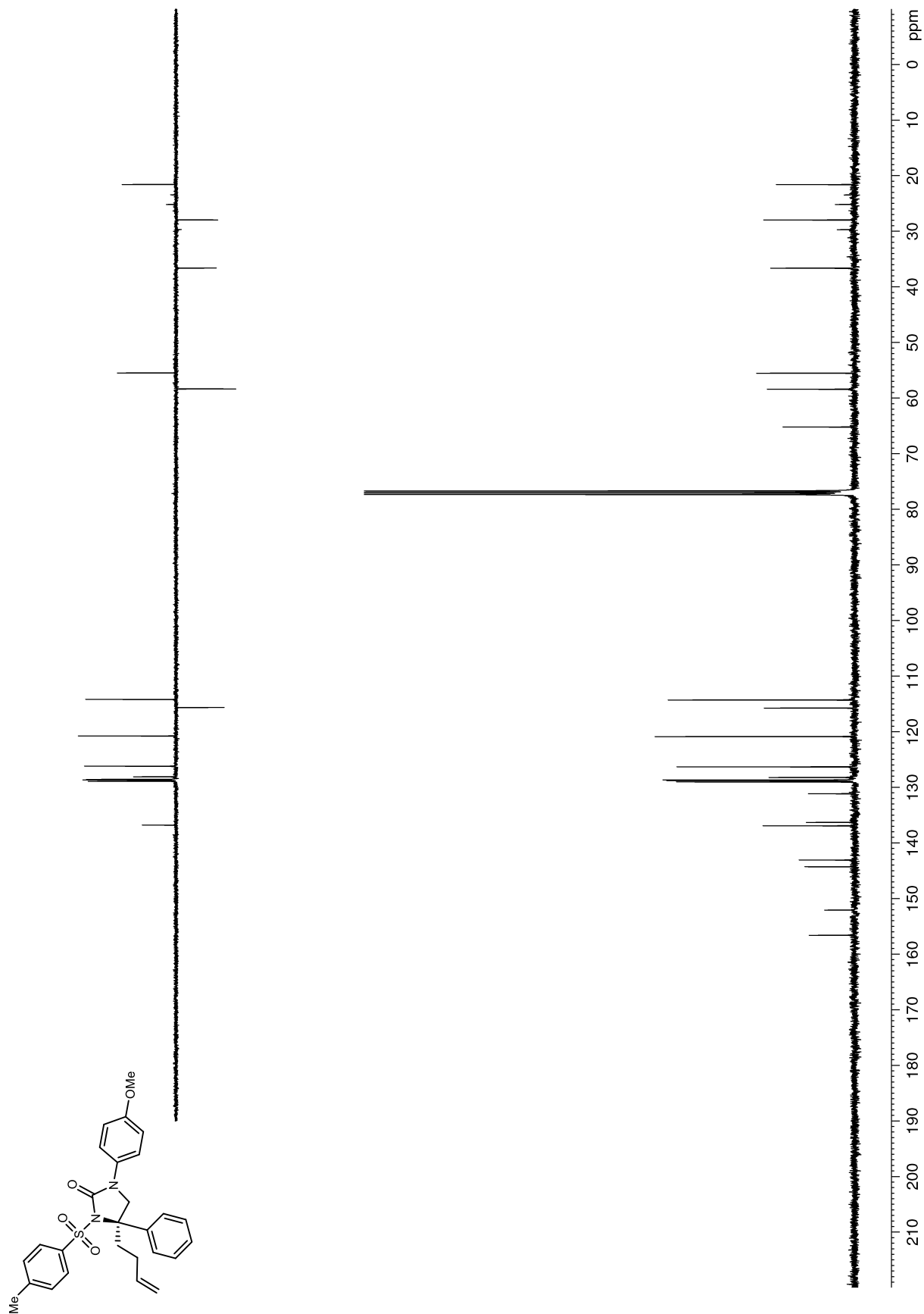
Figure 155. HPLC trace of **126**. Chiralcel IB 20% EtOH/hexanes, 1.0 mL/min, 30 ºC
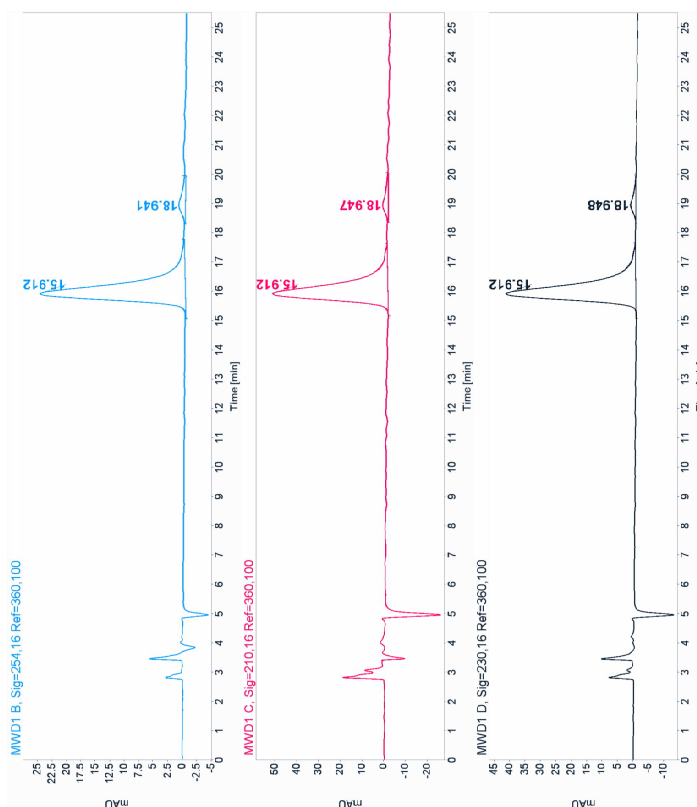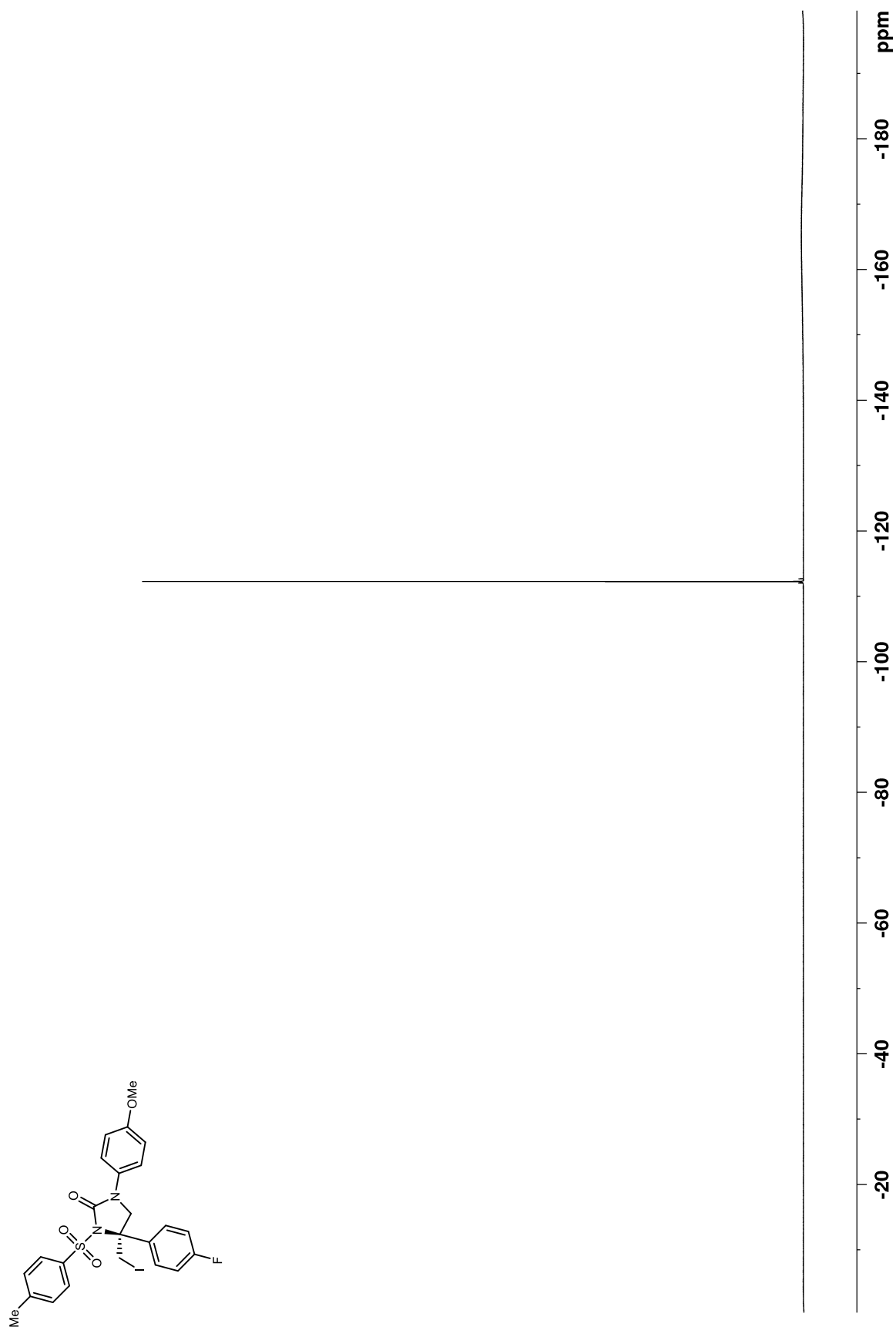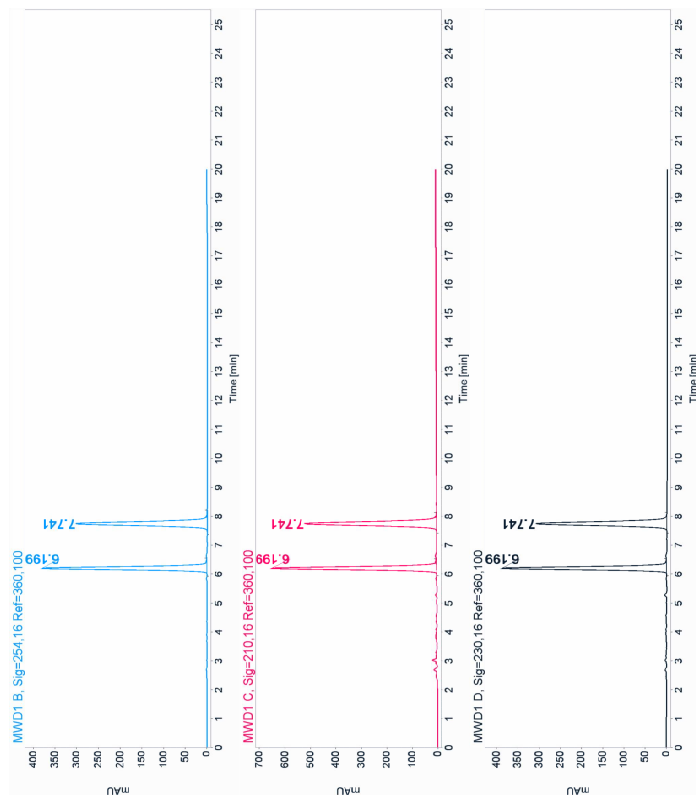

Signal: MWD1 B, Sig=254,16 Ref=360,100

RT [min]	Type	Width [min]	Area	Height	Area% Name
6.199	MM	0.1259	2881.0586	381.4461	49.6862
7.741	MM	0.1610	2917.4465	301.9373	50.3138
		Sum	5798.5051		

Signal: MWD1 C, Sig=210,16 Ref=360,100

RT [min]	Type	Width [min]	Area	Height	Area% Name
6.199	MM	0.1268	4927.9966	647.5181	49.6190
7.741	MM	0.1616	5003.6831	515.9415	50.3810
		Sum	9931.6797		

Signal: MWD1 D, Sig=230,16 Ref=360,100

RT [min]	Type	Width [min]	Area	Height	Area% Name
6.199	MM	0.1257	2937.0176	389.5063	49.8046
7.741	MM	0.1601	2960.0674	308.1173	50.1954
		Sum	5897.0850		
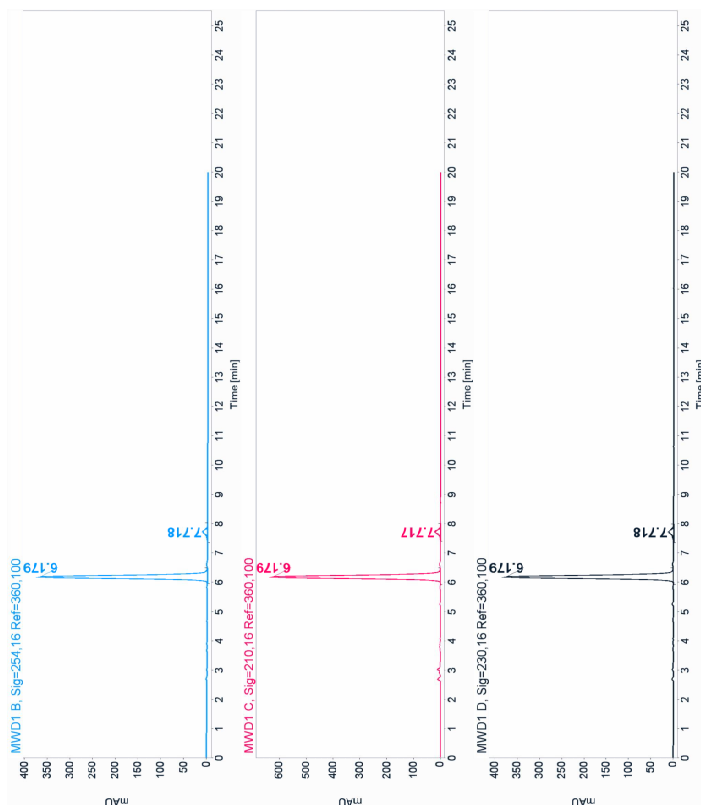
Signal: MWD1 B, Sig=254,16 Ref=360,100

RT [min]	Type	Width [min]	Area	Height	Area% Name
6.179	VV	0.1184	2787.4946	367.9214	96.1459
7.718	BB	0.1644	111.7404	10.3130	3.8541
		Sum	2899.2350		

Signal: MWD1 C, Sig=210,16 Ref=360,100

RT [min]	Type	Width [min]	Area	Height	Area% Name
6.179	MM	0.1272	4781.3511	626.2761	95.2379
7.717	MM	0.2035	239.0774	19.5826	4.7621
		Sum	5020.4285		

Signal: MWD1 D, Sig=230,16 Ref=360,100

RT [min]	Type	Width [min]	Area	Height	Area% Name
6.179	MM	0.1258	2837.5044	375.9621	95.8045
7.718	MM	0.1906	124.2605	10.8632	4.1955
		Sum	2961.7649		

Appendix 4.2-315
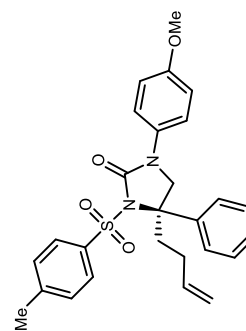
Figure 156. ^{1}H NMR (400 MHz, CDCl$_3$) of **129**
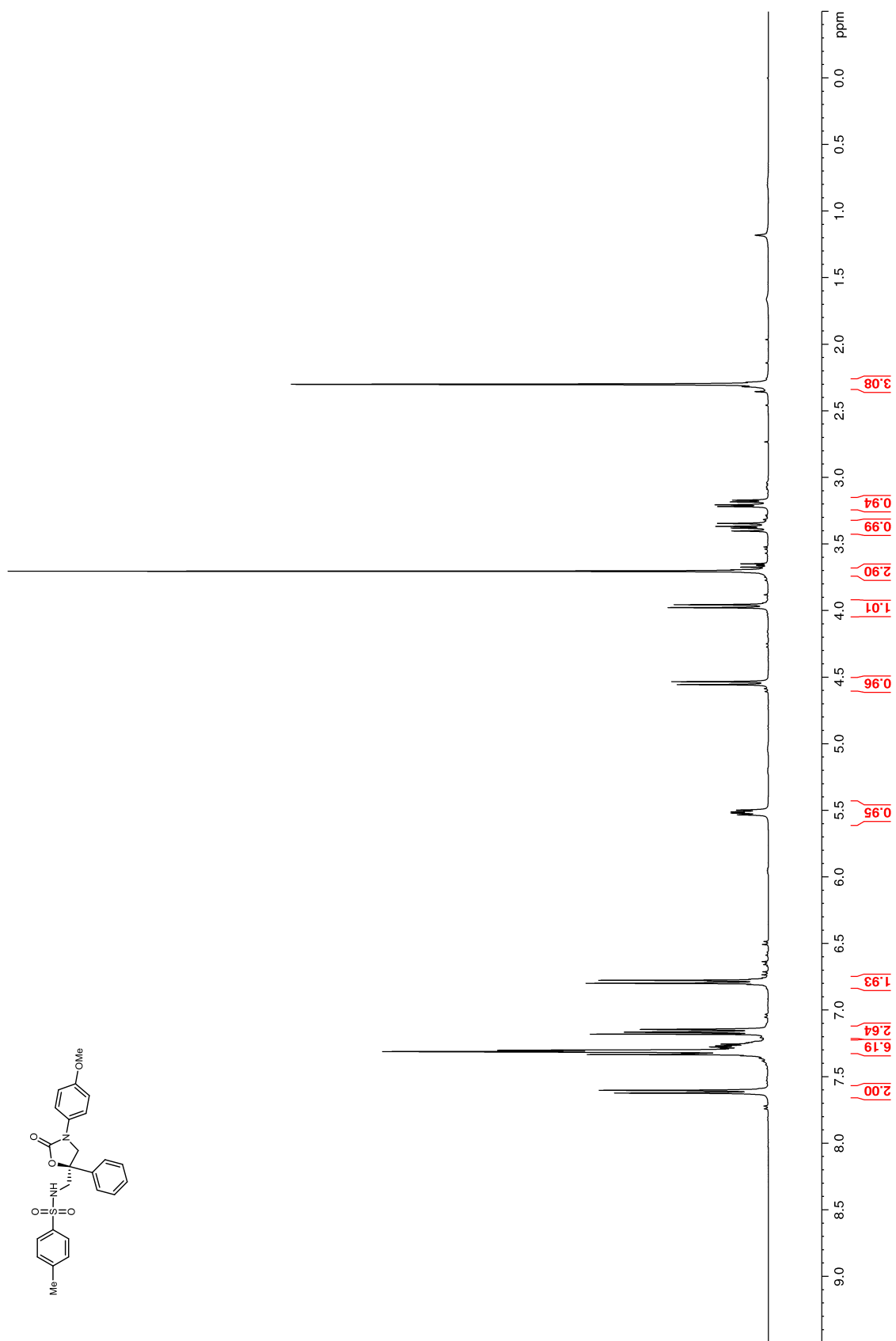
**Figure** 157. ^{13}C NMR (100 MHz, CDCl$_3$) of **129**
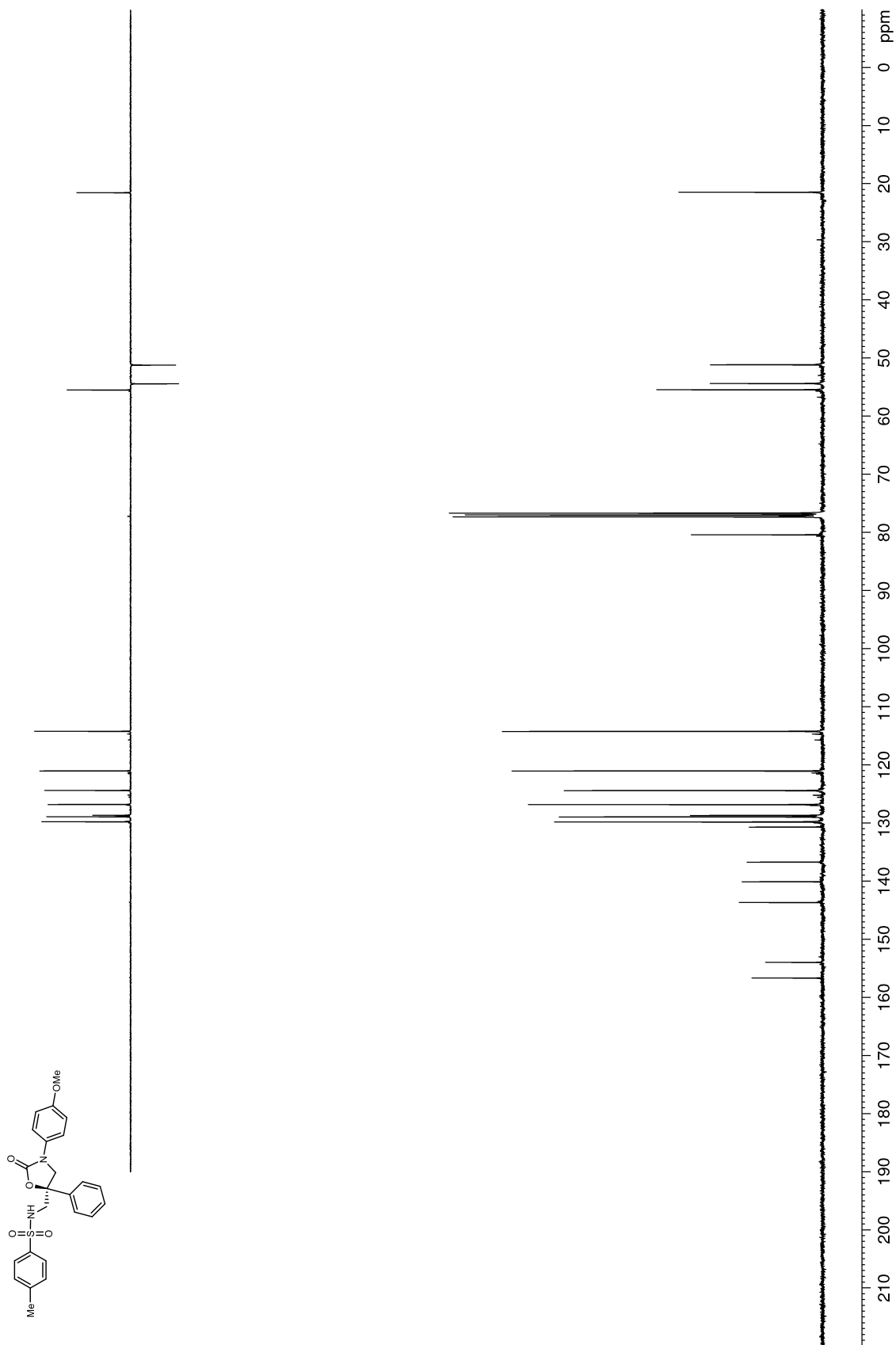
Figure 158. HPLC trace of **129**. Chiralcel IB 25% EtOH/hexanes, 1.0 mL/min, 30 ºC
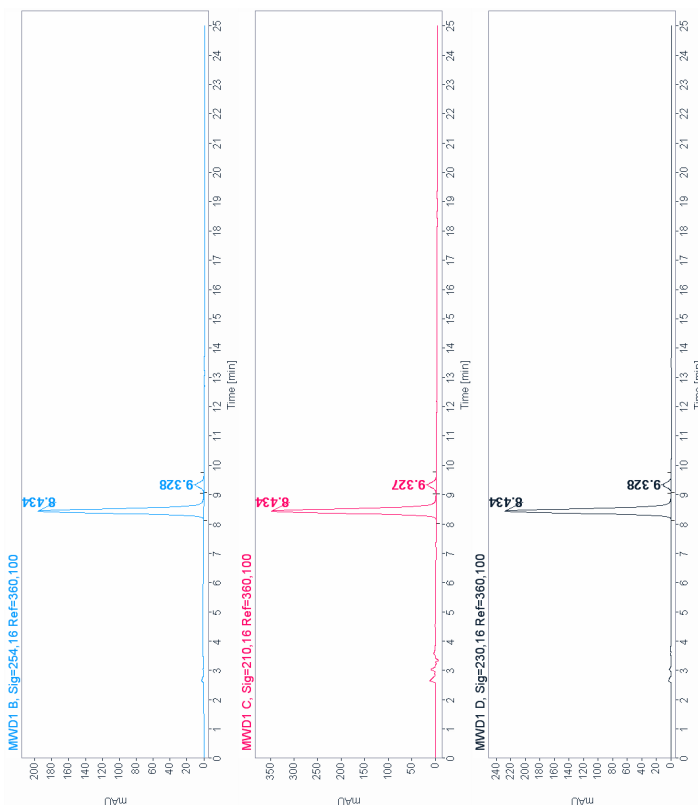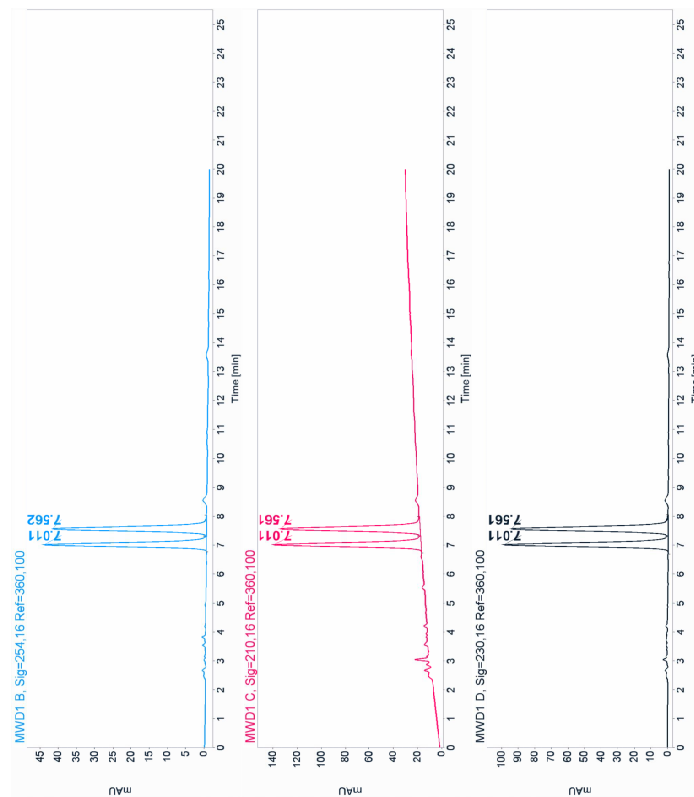

Signal: MWD1 B, Sig=254,16 Ref=360,100

RT [min]	Type	Width [min]	Area	Height	Area%	Name
7.011	BV	0.1511	440.2968	44.6384	49.2560	
7.562	VB	0.1652	453.5972	42.2828	50.7440	
		Sum	893.8940			

Signal: MWD1 C, Sig=210,16 Ref=360,100

RT [min]	Type	Width [min]	Area	Height	Area%	Name
7.011	MF	0.1638	1204.4648	122.5326	48.8612	
7.561	FM	0.1803	1260.6117	116.5176	51.1388	
		Sum	2465.0765			

Signal: MWD1 D, Sig=230,16 Ref=360,100

RT [min]	Type	Width [min]	Area	Height	Area%	Name
7.011	MF	0.1644	977.9402	99.1355	48.8296	
7.561	FM	0.1808	1024.8212	94.4453	51.1704	
		Sum	2002.7614			
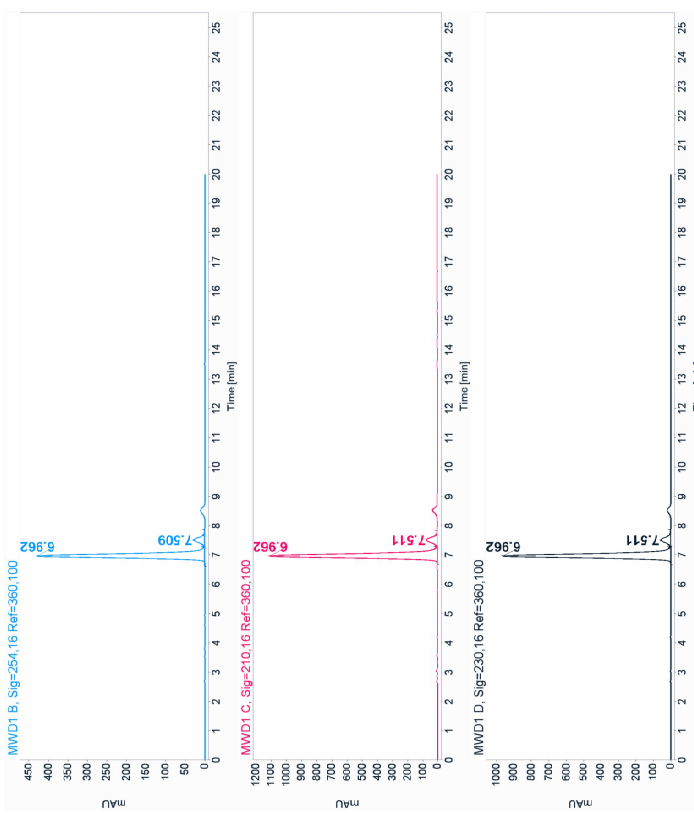
Signal: MWD1 B, Sig=254,16 Ref=360,100

RT [min]	Type	Width [min]	Area	Height	Area%	Name
6.962	MF	0.1592	4100.5801	429.1677	92.1554	
7.509	FM	0.2079	349.0557	27.9838	7.8446	
		Sum	4449.6357			

Signal: MWD1 C, Sig=210,16 Ref=360,100

RT [min]	Type	Width [min]	Area	Height	Area%	Name
6.962	MF	0.1638	10875.7090	1106.6172	92.3073	
7.511	FM	0.2082	906.3648	72.5575	7.6927	
		Sum	11782.0738			

Signal: MWD1 D, Sig=230,16 Ref=360,100

RT [min]	Type	Width [min]	Area	Height	Area%	Name
6.962	MF	0.1588	9172.5059	962.4373	92.9049	
7.511	FM	0.2043	700.5038	57.1370	7.0951	
		Sum	9873.0096			

Appendix 4.2-318
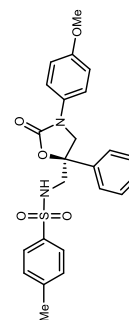
Figure 159. ^{1}H NMR (400 MHz, DMSO-d_3) of **130**
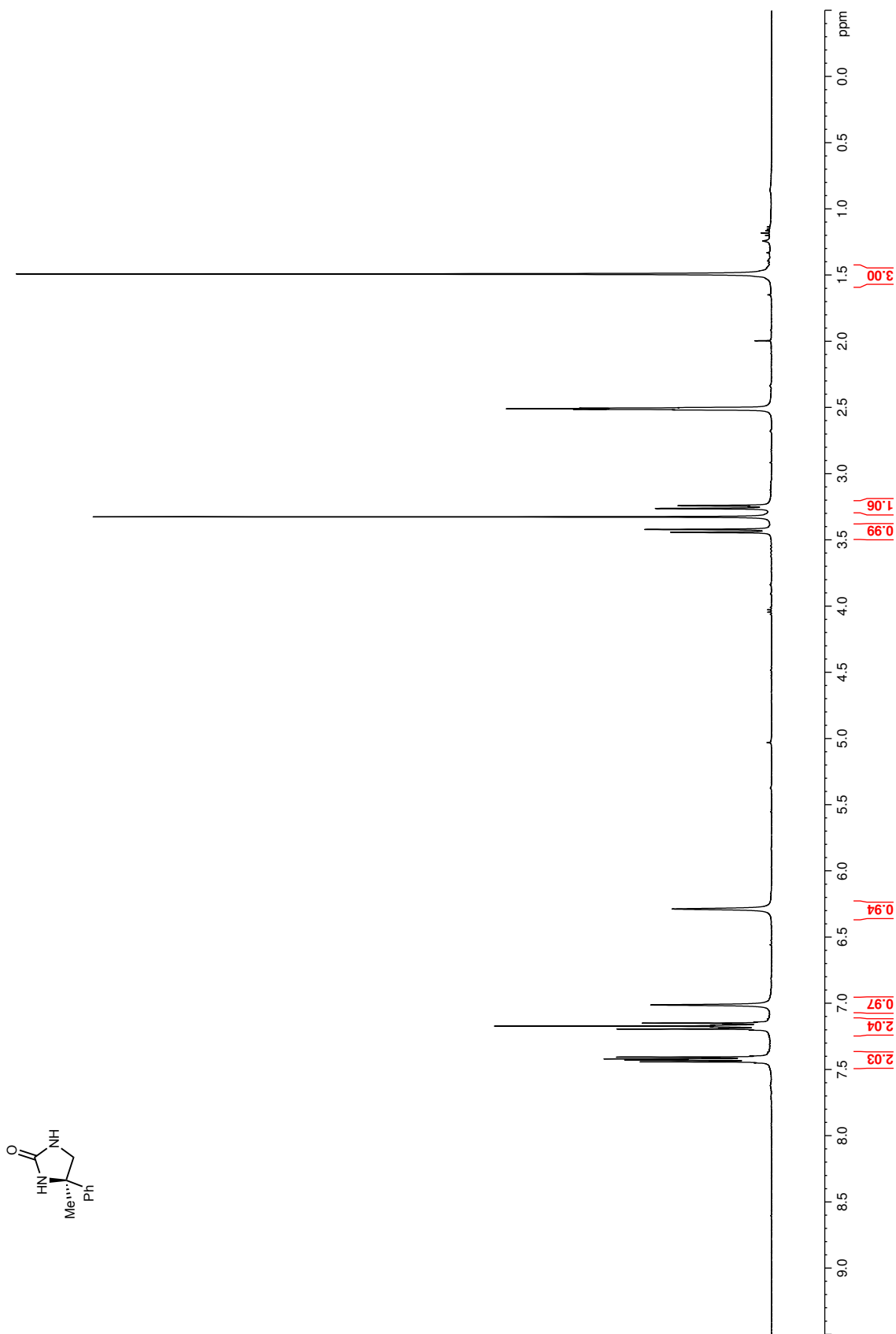
Figure 160. ^{1}H NMR (600 MHz, CDCl$_3$) of **131**

**Figure** 161. ^{13}C NMR (150 MHz, CDCl$_3$) of **131**
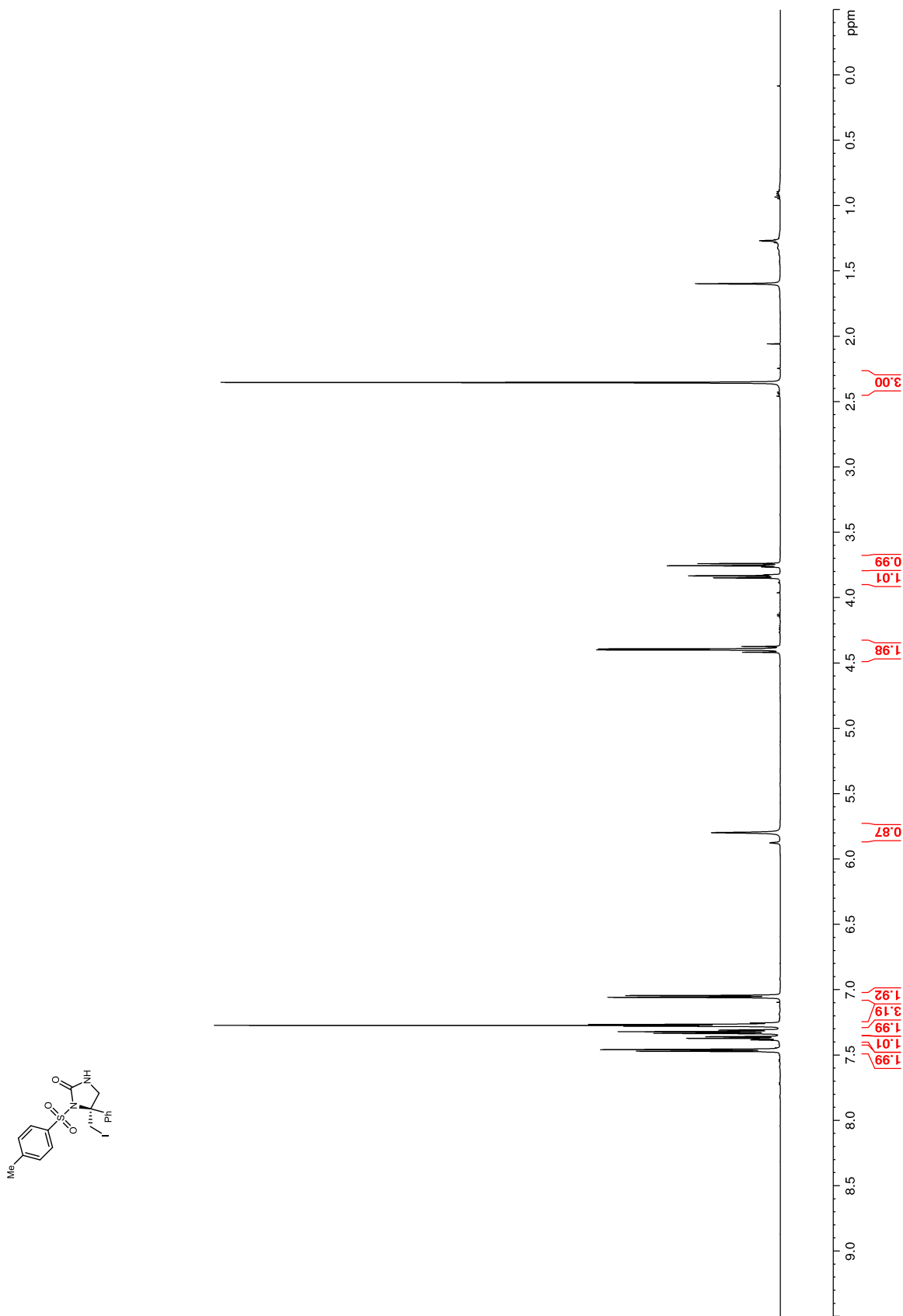
Figure 162. HPLC trace of **131**. Chiralcel IA 25% iPrOH/hexanes, 1.0 mL/min, 30 ºC
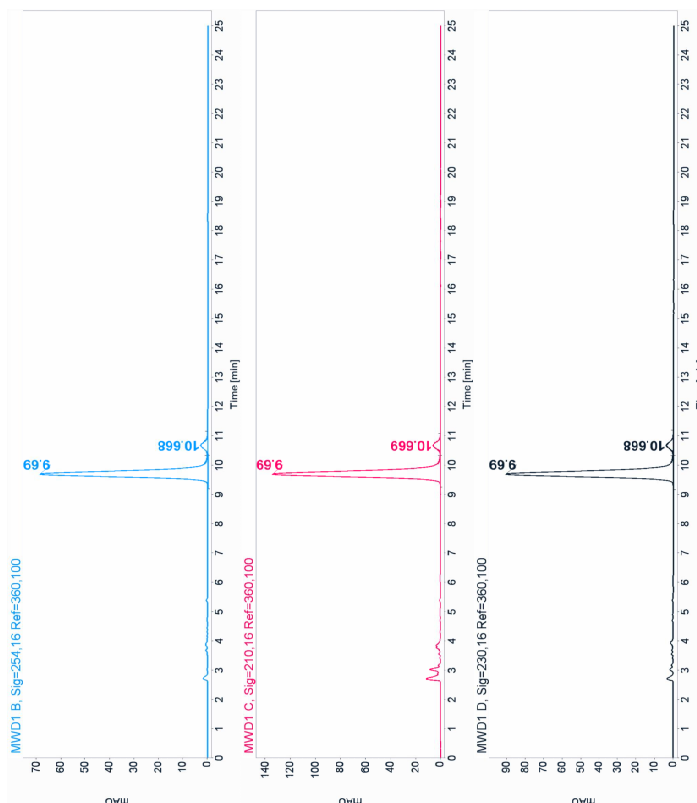

Signal: MWD1 B, Sig=254,16 Ref=360,100

RT [min]	Type	Width [min]	Area	Height	Area%	Name
11.925	MF	0.4367	323.5465	12.3468	50.7966	
16.852	FM	0.6581	313.3992	7.9370	49.2034	
		Sum	636.9457			

Signal: MWD1 C, Sig=210,16 Ref=360,100

RT [min]	Type	Width [min]	Area	Height	Area%	Name
11.925	MF	0.4268	2446.3716	95.5254	51.3742	
16.853	FM	0.6310	2315.4990	61.1597	48.6258	
		Sum	4761.8706			

Signal: MWD1 D, Sig=230,16 Ref=360,100

RT [min]	Type	Width [min]	Area	Height	Area%	Name
11.925	MF	0.4291	1633.3107	63.4426	50.0108	
16.853	FM	0.6634	1632.6044	41.0139	49.9892	
		Sum	3265.9150			

Signal: MWD1 B, Sig=254,16 Ref=360,100

RT [min]	Type	Width [min]	Area	Height	Area%	Name
11.842	MF	0.3864	780.0839	33.6443	95.8198	
17.044	FM	0.7806	34.0316	0.7266	4.1802	
		Sum	814.1155			

Signal: MWD1 C, Sig=210,16 Ref=360,100

RT [min]	Type	Width [min]	Area	Height	Area%	Name
11.842	MM	0.3871	6098.2188	262.5729	93.1884	
17.034	MM	0.9377	445.7494	7.9229	6.8116	
		Sum	6543.9681			

Signal: MWD1 D, Sig=230,16 Ref=360,100

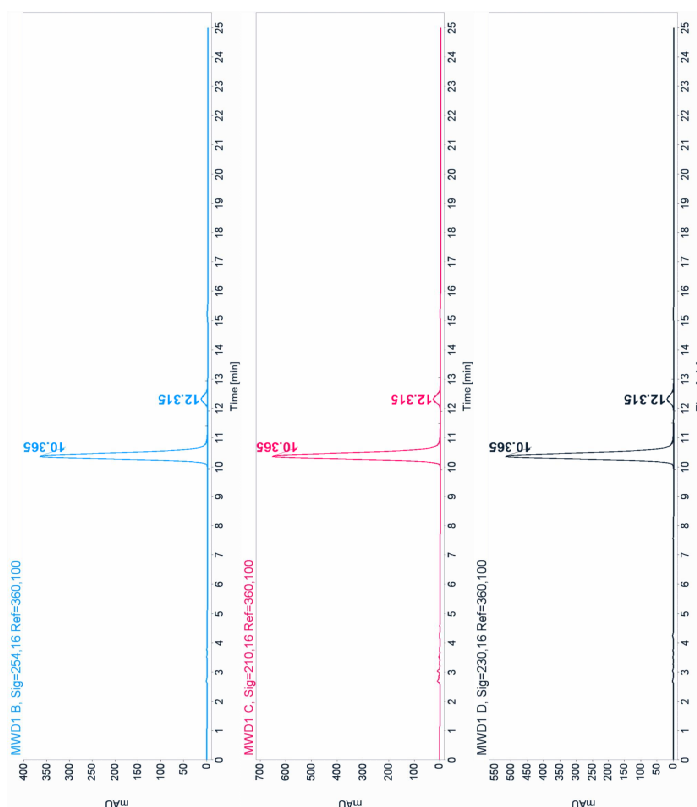| RT [min]	Type	Width [min]	Area	Height	Area%	Name
11.842	MF	0.3930	4128.5645	175.1070	95.3461	
17.031	FM	0.8357	201.5157	4.0188	4.6539	
		Sum	4330.0802			

Figure 163. ^{1}H NMR (400 MHz, CDCl$_3$) of **132**
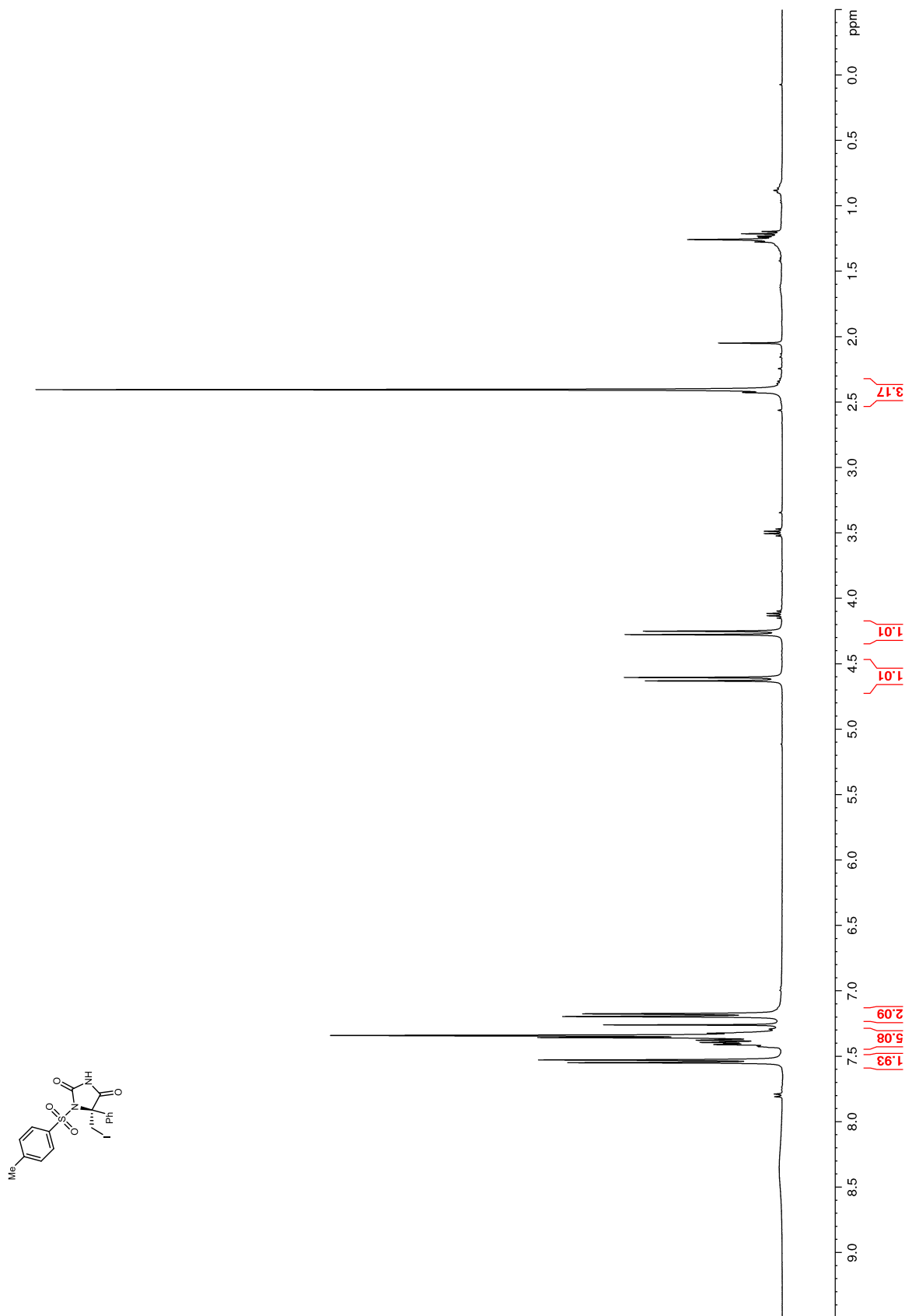
Figure 164. ^{13}C NMR (100 MHz, CDCl$_3$) of **132**
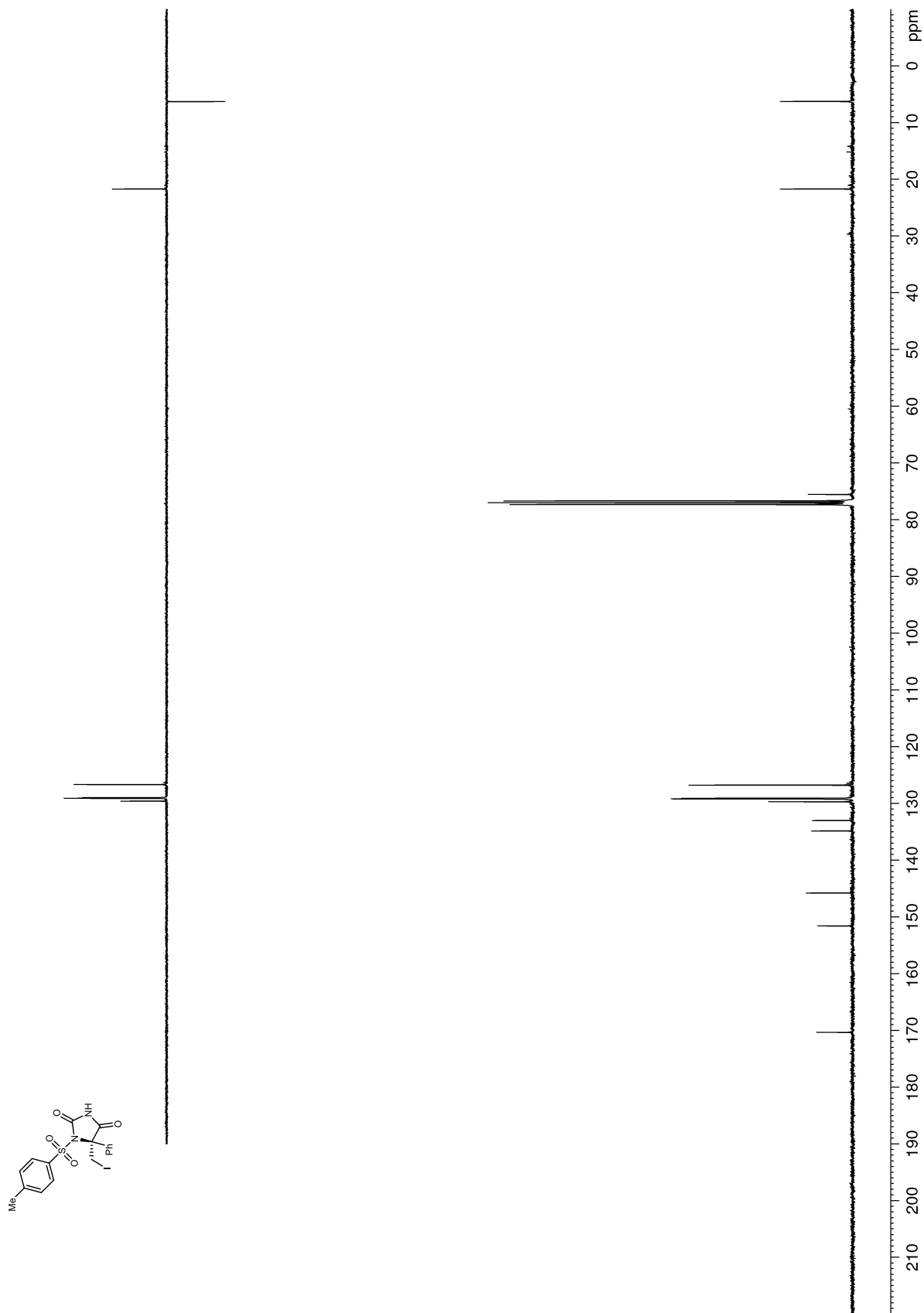
Figure 165. ^{1}H NMR (400 MHz, CDCl$_3$) of derivative of **122a**
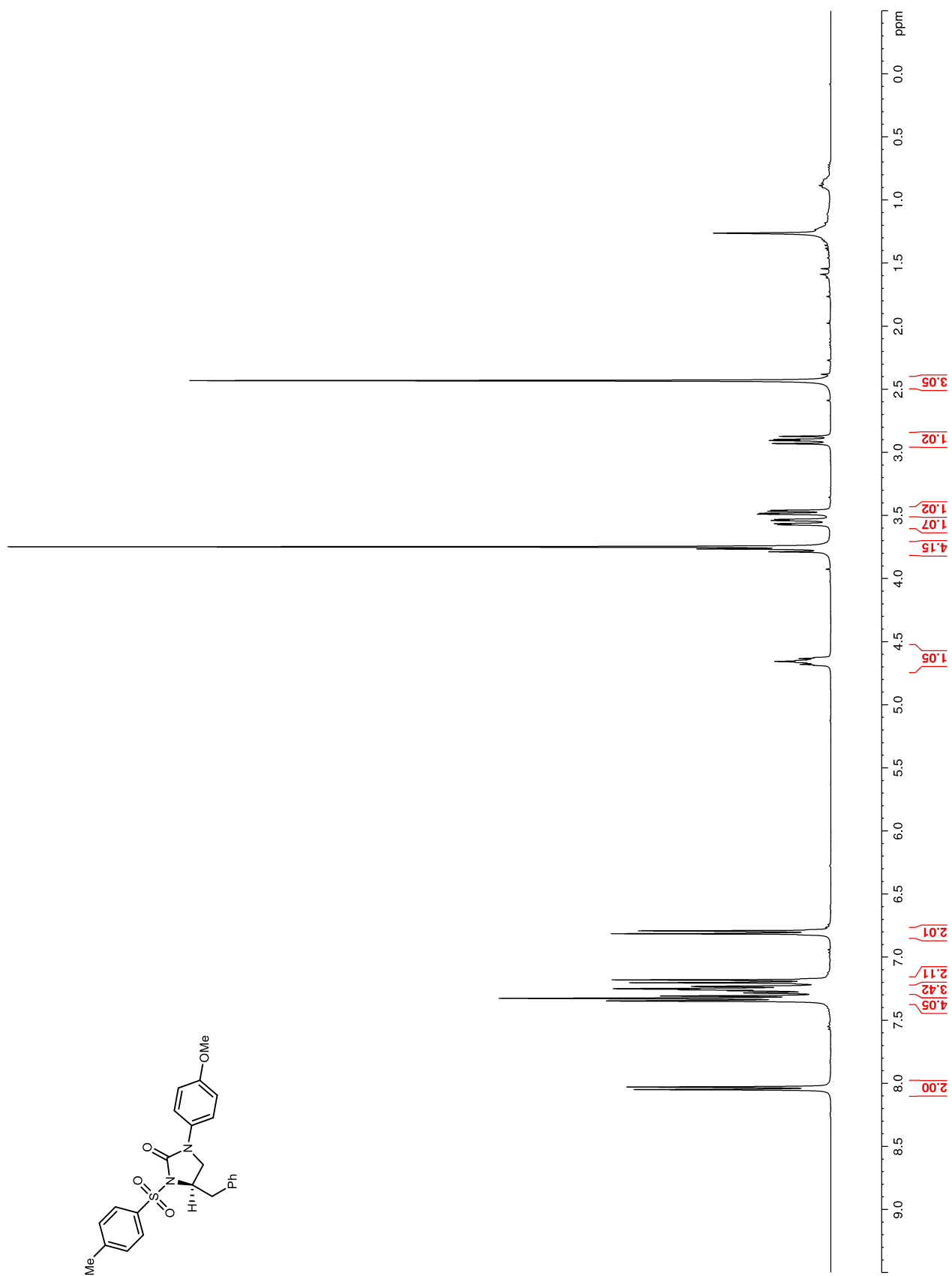
Figure 166. ^{13}C NMR (100 MHz, CDCl$_3$) of derivative of **122a**
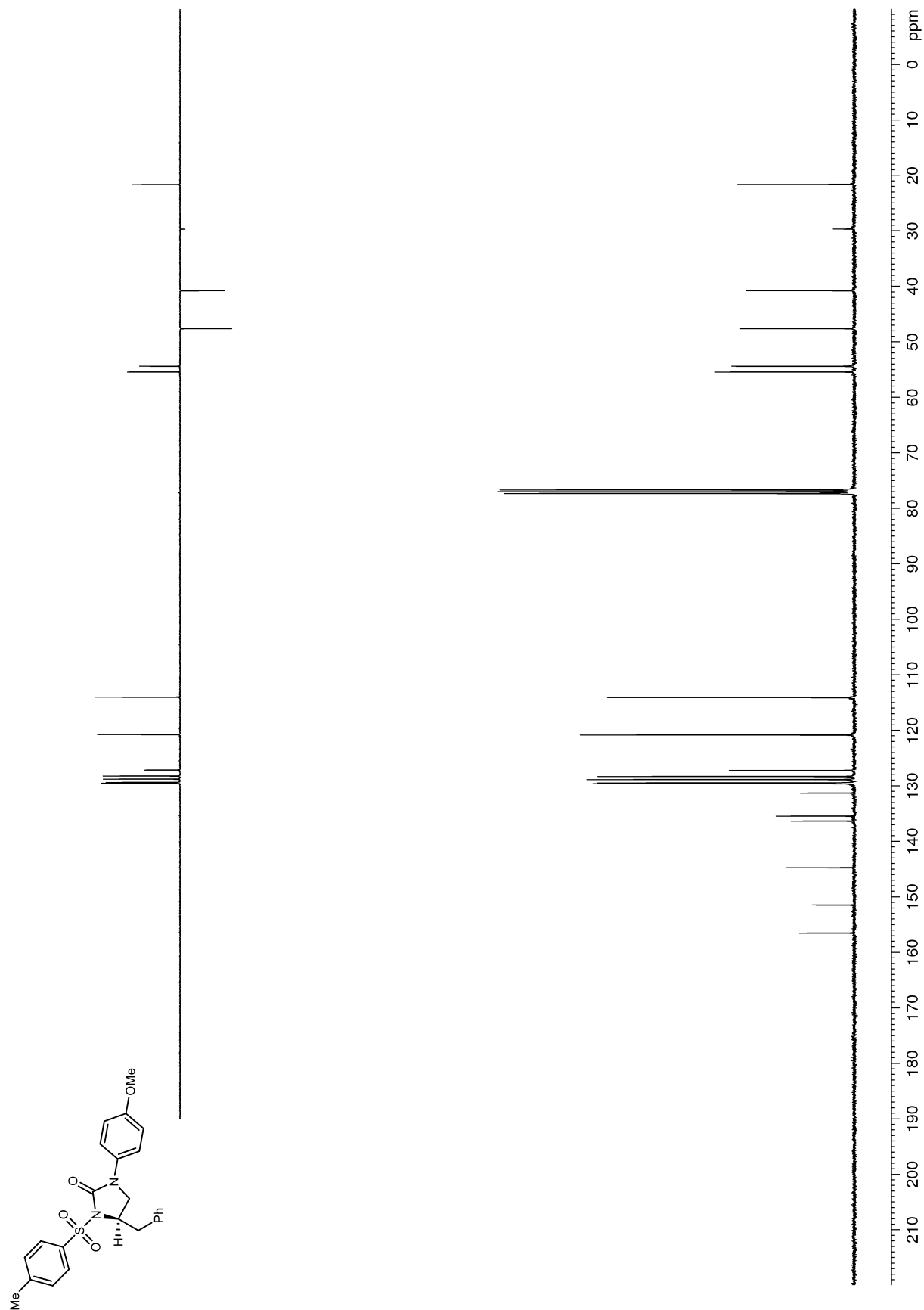
Figure 167. HPLC trace of derivative of **122a**. Chiralcel IB 30% EtOH/hexanes, 1.0 mL/min, 30 ºC

Signal: MWD1 B, Sig=254,16 Ref=360,100

RT [min]	Type	Width [min]	Area	Height	Area%	Name
13.571	MM	0.3524	1766.7405	83.5551	45.3252	
18.651	MM	0.5283	2131.1775	67.2339	54.6748	
	Sum		3897.9180			

Signal: MWD1 C, Sig=210,16 Ref=360,100

RT [min]	Type	Width [min]	Area	Height	Area%	Name
13.571	MM	0.3666	2468.0386	112.2109	44.4627	
18.651	MM	0.5498	3082.7742	93.4466	55.5373	
	Sum		5550.8127			

Signal: MWD1 D, Sig=230,16 Ref=360,100

RT [min]	Type	Width [min]	Area	Height	Area%	Name
13.571	MM	0.3577	1991.3799	92.7874	45.6874	
18.651	MM	0.5277	2367.3269	74.7696	54.3126	
	Sum		4358.7068			

Signal: MWD1 B, Sig=254,16 Ref=360,100

RT [min]	Type	Width [min]	Area	Height	Area%	Name
13.530	MM	0.3745	27.9241	1.2426	3.5800	
18.597	MM	0.5156	752.0798	24.3119	96.4200	
	Sum		780.0038			

Signal: MWD1 C, Sig=210,16 Ref=360,100

RT [min]	Type	Width [min]	Area	Height	Area%	Name
13.524	MM	0.3888	52.7526	2.2913	4.1884	
18.597	MM	0.5119	1206.7378	39.2912	95.8116	
	Sum		1259.4904			

Signal: MWD1 D, Sig=230,16 Ref=360,100

RT [min]	Type	Width [min]	Area	Height	Area%	Name
13.530	MM	0.4772	47.6662	1.6647	5.5243	
18.597	MM	0.5070	815.1851	26.7978	94.4757	
	Sum		862.8512			

Appendix 4.2-327
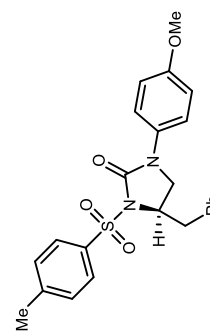
Figure 168. HPLC trace of derivative of **123a**. Chiralcel IB 30% EtOH/hexanes, 1.0 mL/min, 30 ºC

Signal: MWD1 B, Sig=254,16 Ref=360,100

RT [min]	Type	Width [min]	Area	Height	Area%	Name
13.571	MM	0.3524	1766.7405	83.5551	45.3252	
18.651	MM	0.5283	2131.1775	67.2339	54.6748	
		Sum	3897.9180			

Signal: MWD1 C, Sig=210,16 Ref=360,100

RT [min]	Type	Width [min]	Area	Height	Area%	Name
13.571	MM	0.3666	2468.0386	112.2109	44.4627	
18.651	MM	0.5498	3082.7742	93.4466	55.5373	
		Sum	5550.8127			

Signal: MWD1 D, Sig=230,16 Ref=360,100

RT [min]	Type	Width [min]	Area	Height	Area%	Name
13.571	MM	0.3577	1991.3799	92.7874	45.6874	
18.651	MM	0.5277	2367.3269	74.7696	54.3126	
		Sum	4358.7068			

Signal: MWD1 B, Sig=254,16 Ref=360,100

RT [min]	Type	Width [min]	Area	Height	Area%	Name
13.476	MM	0.3790	1082.6852	47.6055	38.6619	
18.470	MM	0.5139	1717.7058	55.7063	61.3381	
		Sum	2800.3910			

Signal: MWD1 C, Sig=210,16 Ref=360,100

RT [min]	Type	Width [min]	Area	Height	Area%	Name
13.476	MM	0.4020	1855.0883	76.9012	38.7211	
18.470	MM	0.5421	2935.8147	90.2572	61.2789	
		Sum	4790.9030			

Signal: MWD1 D, Sig=230,16 Ref=360,100

RT [min]	Type	Width [min]	Area	Height	Area%	Name
13.476	MM	0.3758	1190.4923	52.7914	36.9207	
18.470	MM	0.5379	2033.9691	63.0247	63.0793	
		Sum	3224.4614			

Appendix 4.2-328

Figure 169. ^{1}H NMR (400 MHz, CDCl$_3$) of **144**
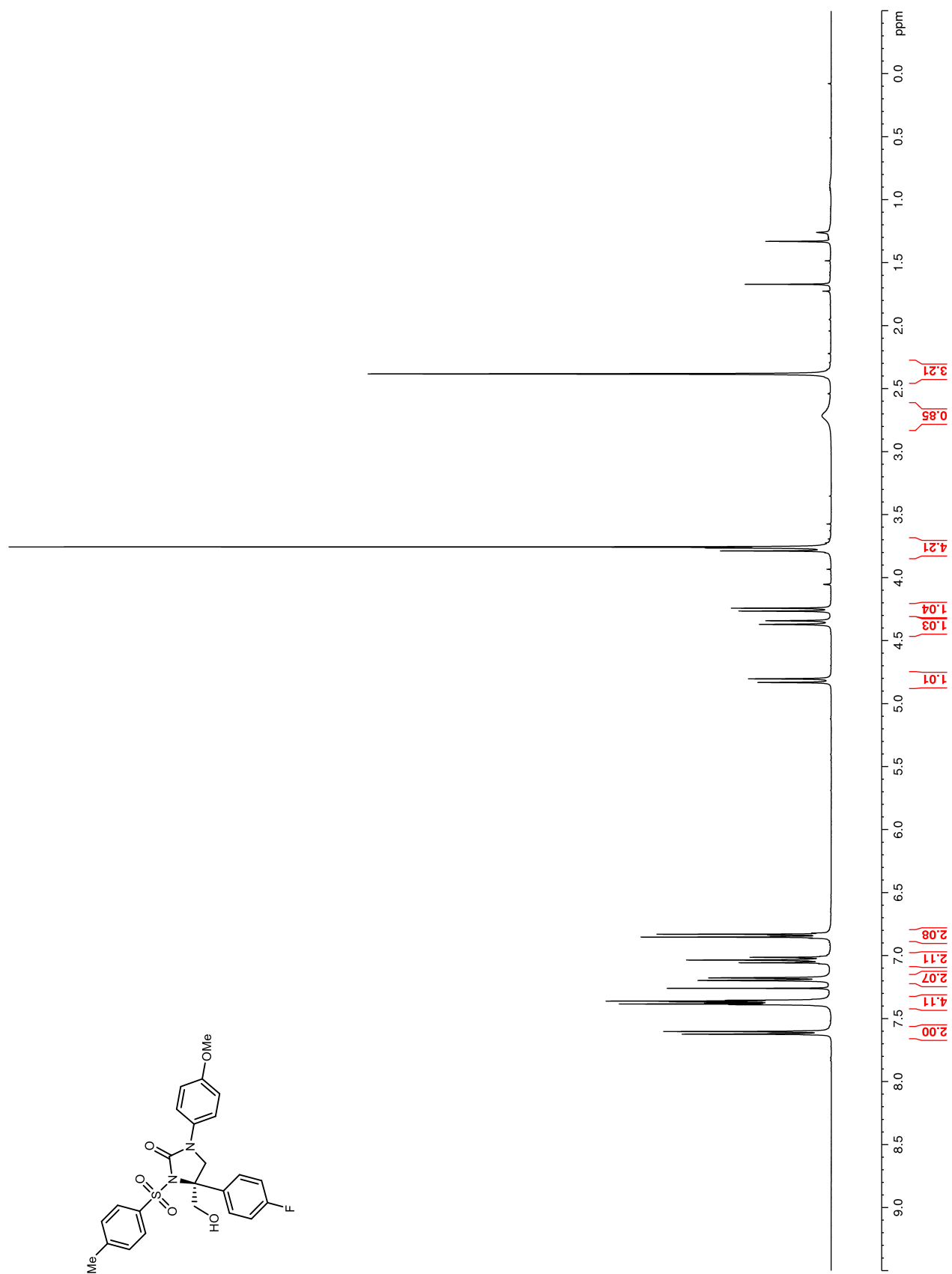
Figure 170. ^{13}C NMR (100 MHz, CDCl$_3$) of **144**
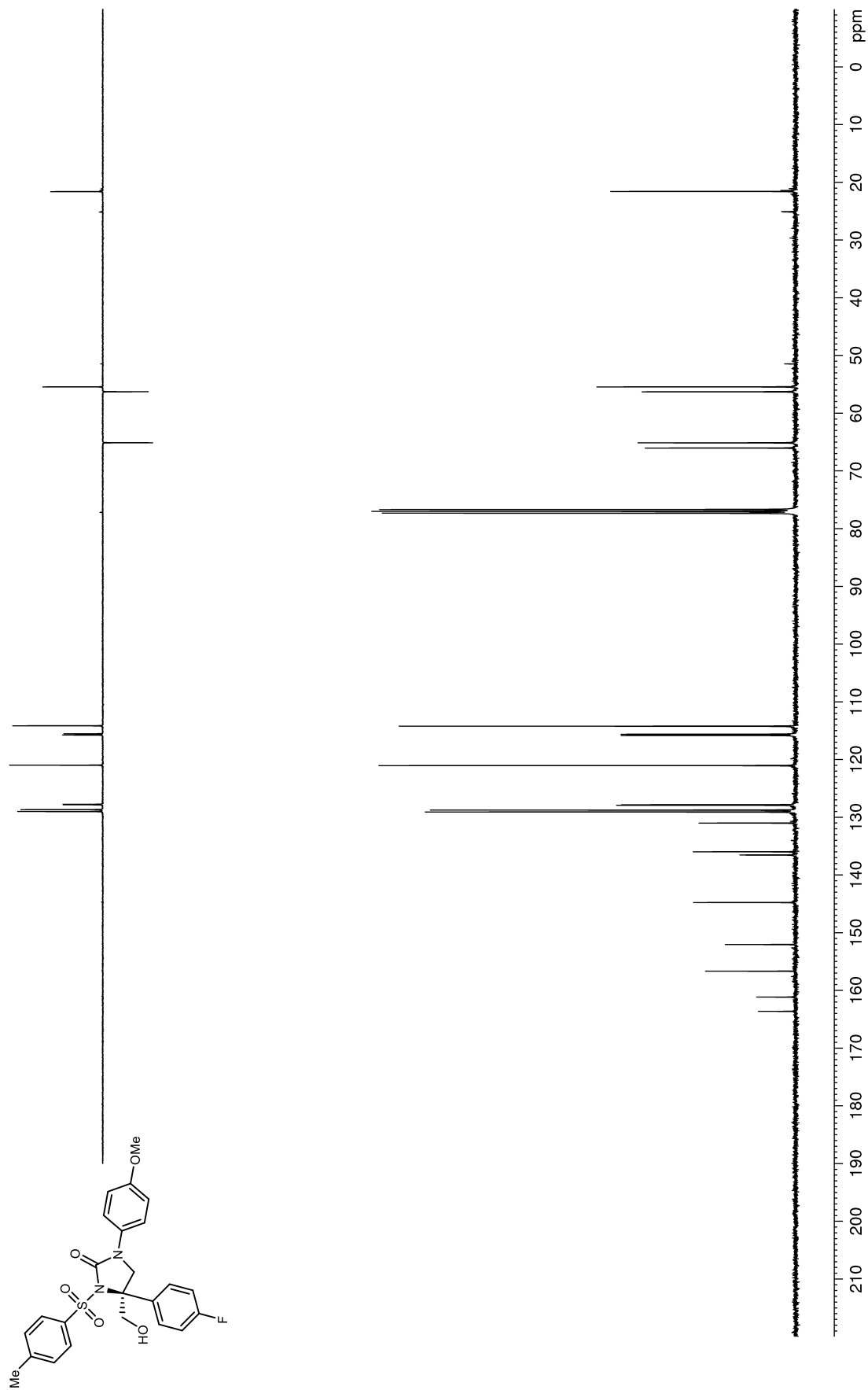
Figure 171. ^{19}F NMR (376 MHz, CDCl$_3$) of **144**

−112.79

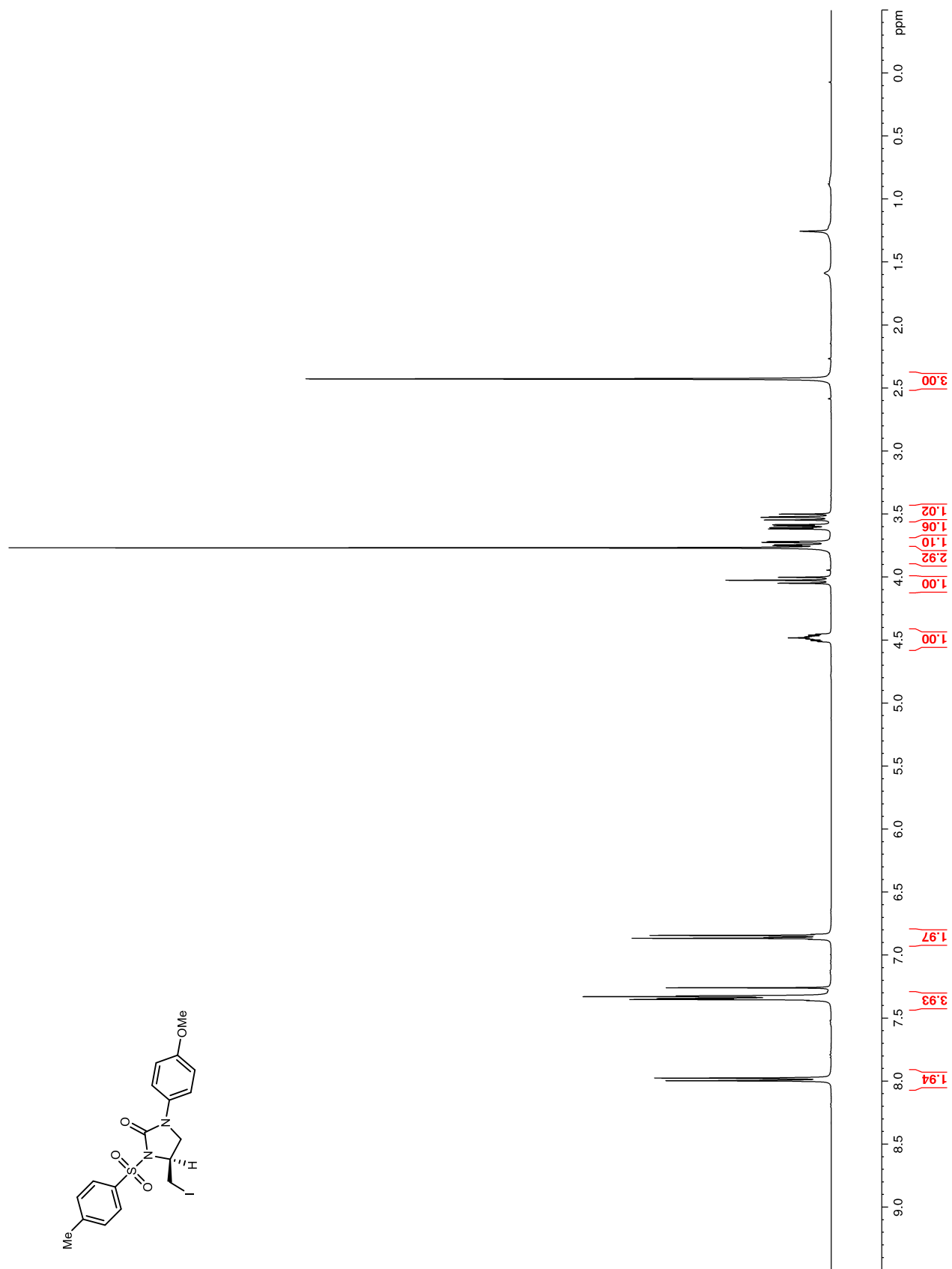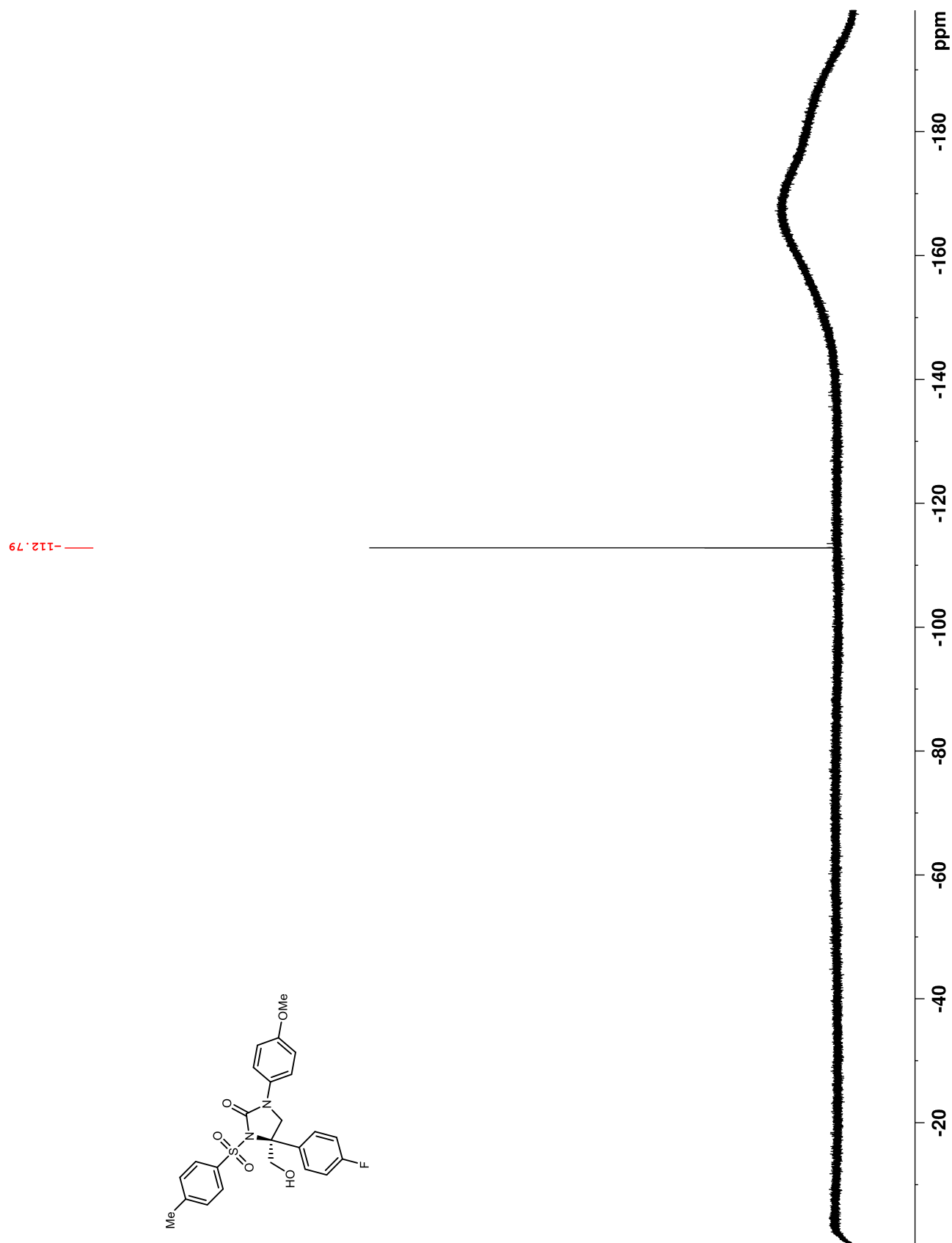**Figure 172.** HPLC trace of **144**. Chiralcel IB 25% EtOH/hexanes, 1.0 mL/min, 30 ºC
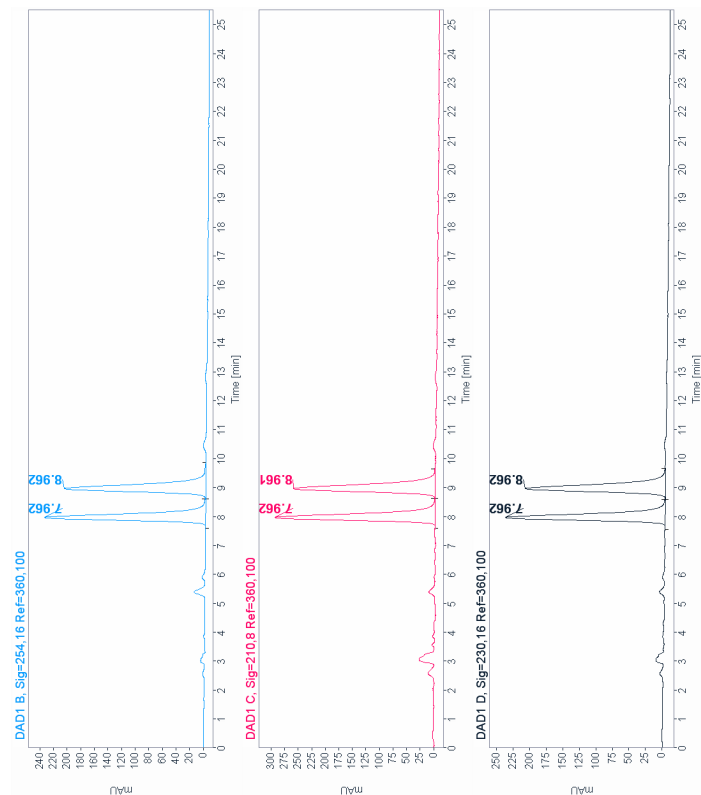
Signal: DAD1 B, Sig=254,16 Ref=360,100

RT [min]	Type	Width [min]	Area	Height	Area% Name
7.962	MF	0.2518	3572.0159	236.3964	50.0631
8.962	FM	0.2855	3563.0059	207.9736	49.9369
		Sum	7135.0217		

Signal: DAD1 C, Sig=210,8 Ref=360,100

RT [min]	Type	Width [min]	Area	Height	Area% Name
7.962	MF	0.2581	4576.9795	295.5295	50.2316
8.961	FM	0.2888	4534.7769	261.7307	49.7684
		Sum	9111.7563		

Signal: DAD1 D, Sig=230,16 Ref=360,100

RT [min]	Type	Width [min]	Area	Height	Area% Name
7.962	MF	0.2527	3664.8511	241.7523	50.1894
8.962	FM	0.2853	3637.1970	212.4919	49.8106
		Sum	7302.0481		
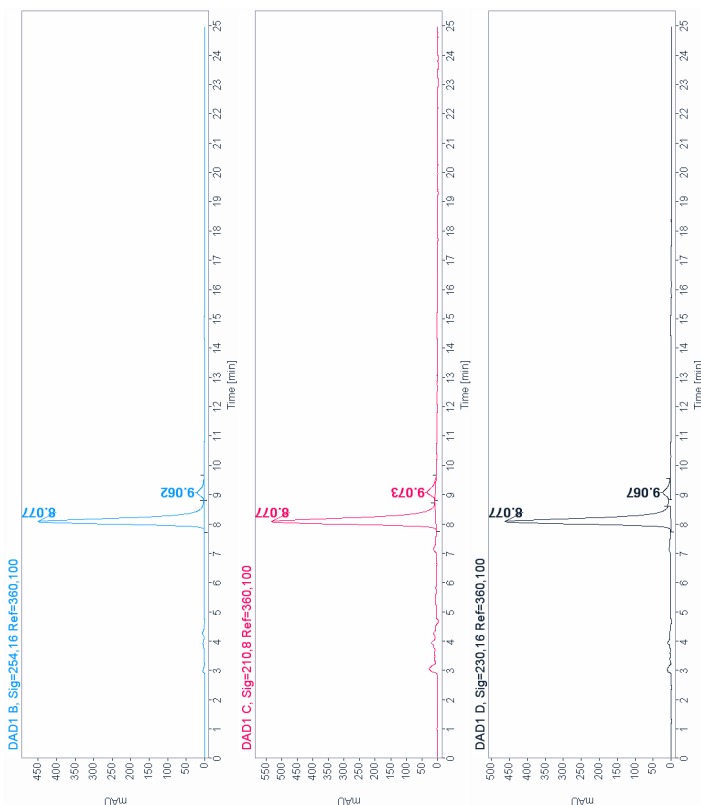
Signal: DAD1 B, Sig=254,16 Ref=360,100

RT [min]	Type	Width [min]	Area	Height	Area% Name
8.077	MF	0.2422	6527.2783	449.1498	94.8717
9.062	FM	0.3086	352.8338	19.0541	5.1283
		Sum	6880.1122		

Signal: DAD1 C, Sig=210,8 Ref=360,100

RT [min]	Type	Width [min]	Area	Height	Area% Name
8.077	MM	0.2591	8203.9395	527.7134	94.6079
9.073	MM	0.3060	467.5771	25.4670	5.3921
		Sum	8671.5165		

Signal: DAD1 D, Sig=230,16 Ref=360,100

RT [min]	Type	Width [min]	Area	Height	Area% Name
8.077	MF	0.2435	6728.2939	460.5094	94.5470
9.067	FM	0.3150	388.0536	20.5323	5.4530
		Sum	7116.3476		

Appendix 4.2-332
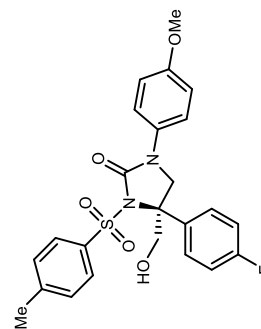
Figure 173. ^{1}H NMR (400 MHz, CDCl$_3$) of **150**
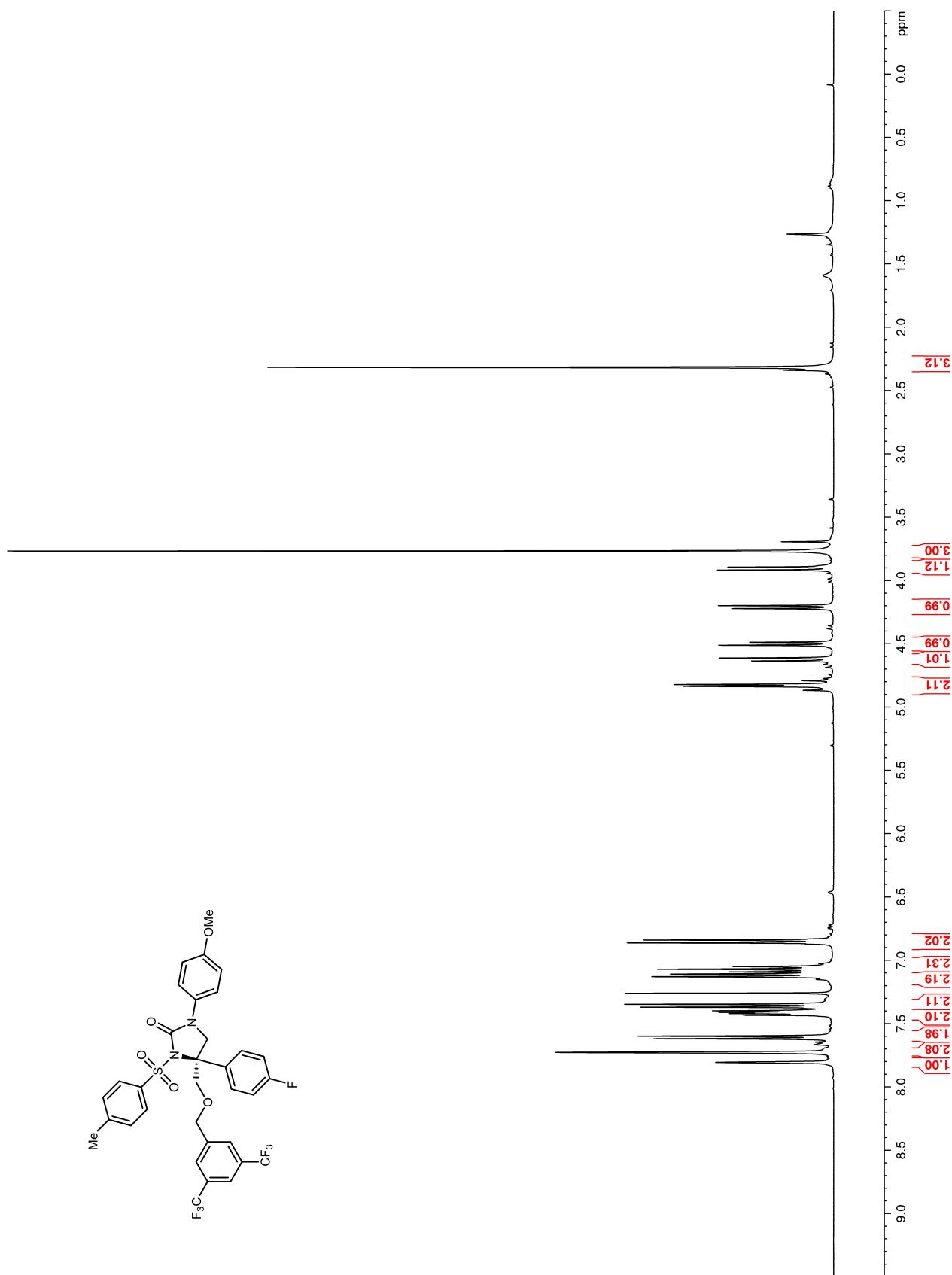
Figure 174. ^{13}C NMR (100 MHz, CDCl$_3$) of **150**
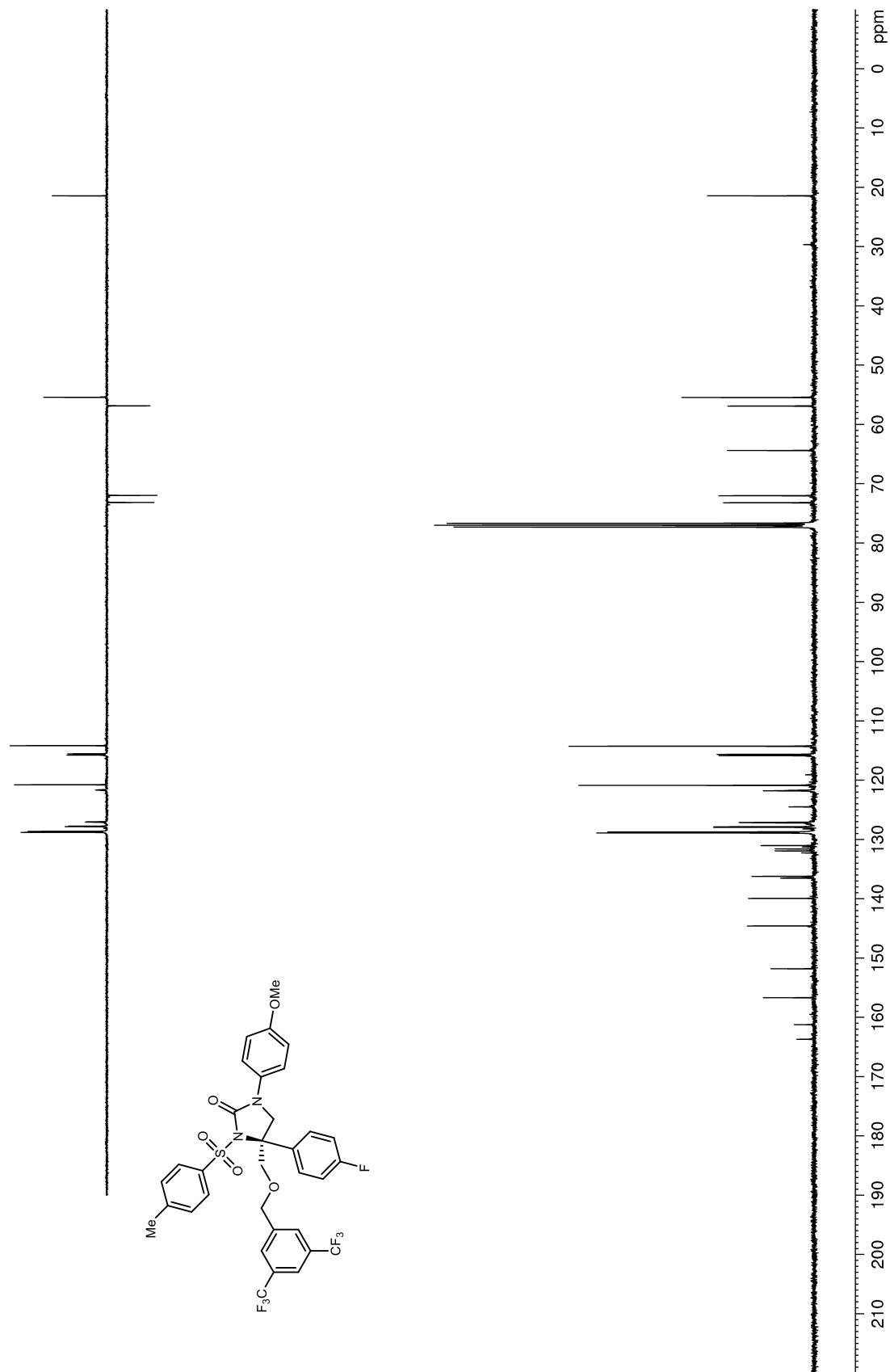
Figure 175. ^{19}F NMR (376 MHz, CDCl$_3$) of **150**

Figure 176**.** HMBC of **151**
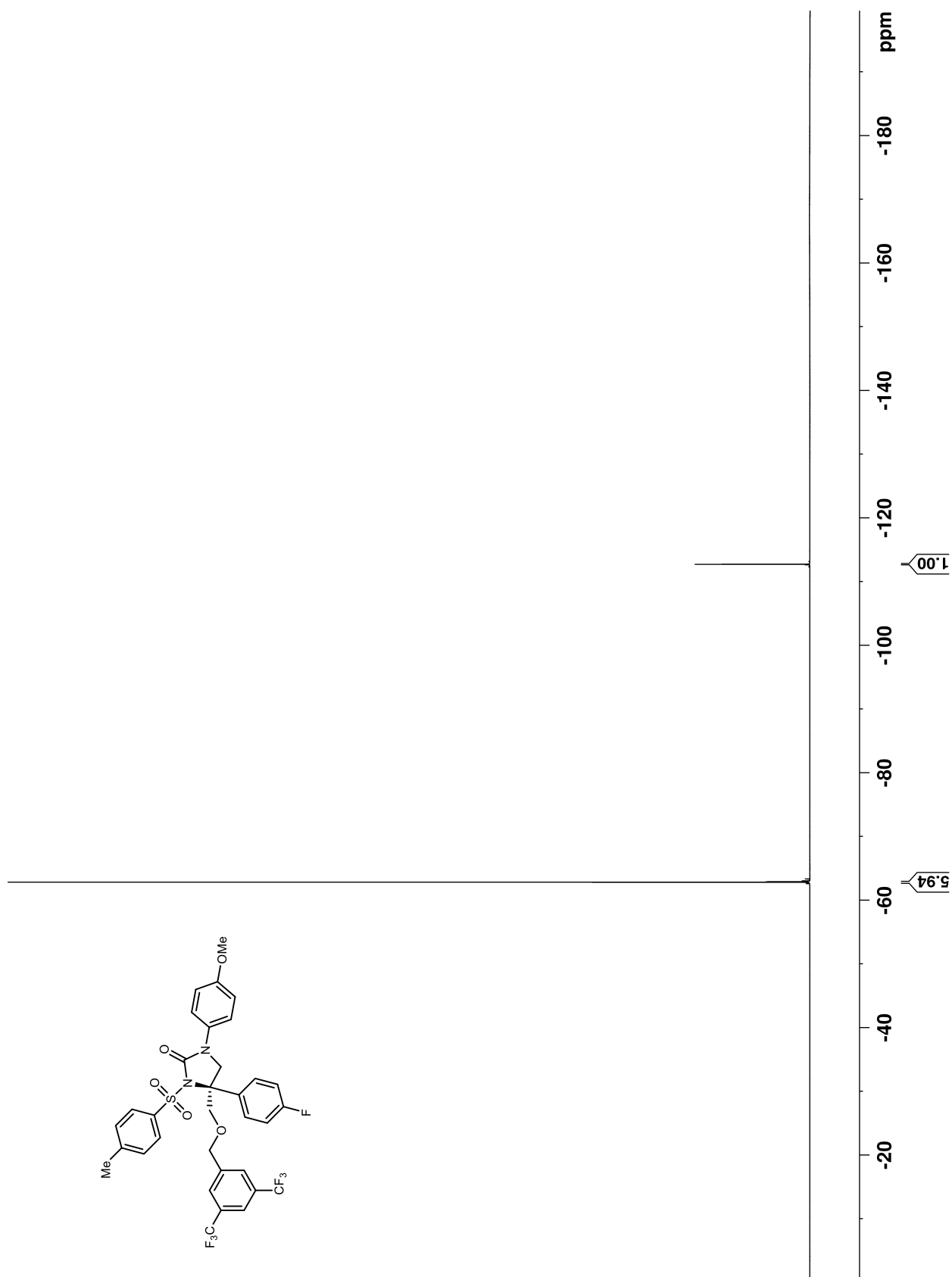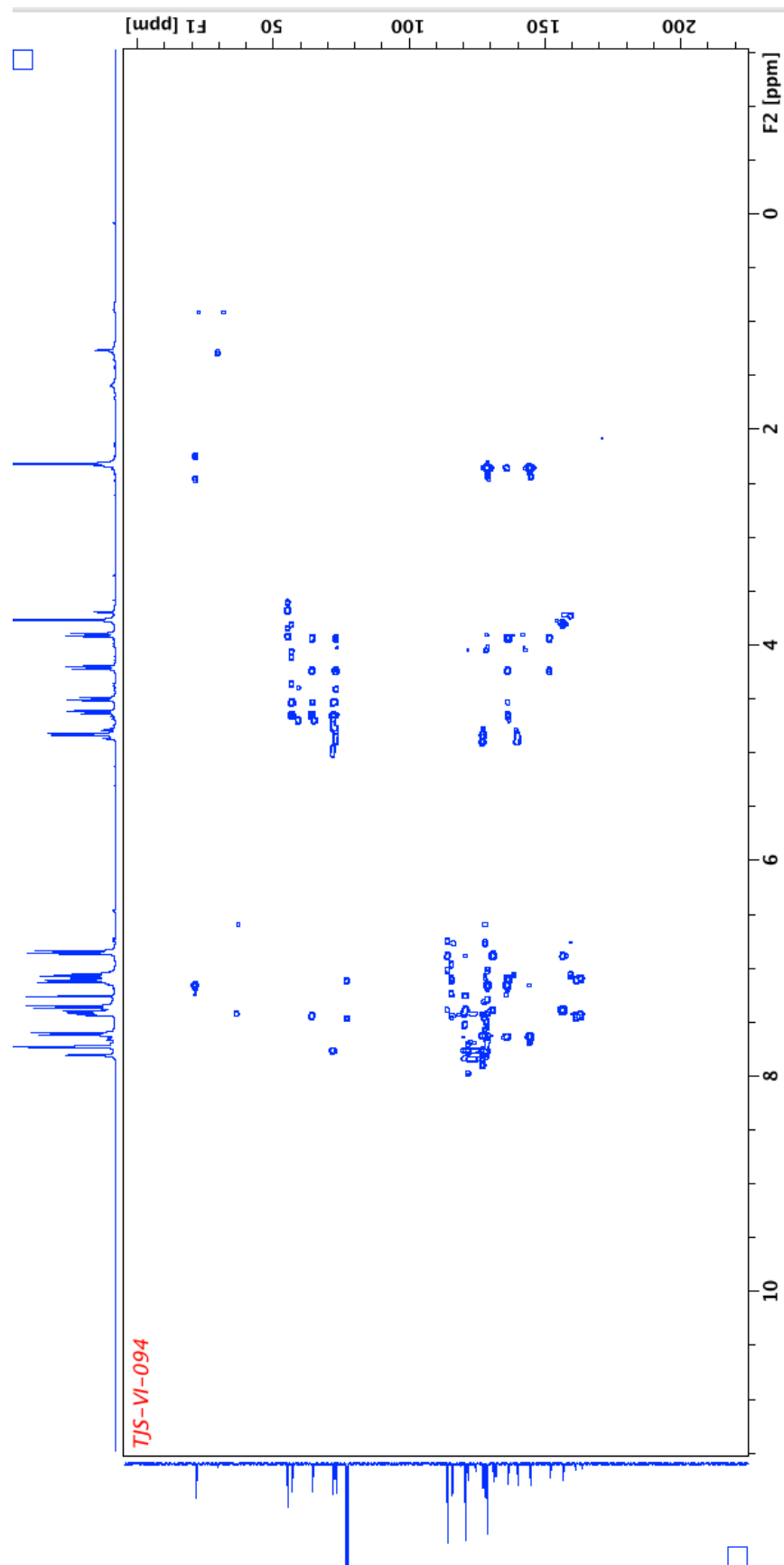
Figure 177. ^{1}H NMR (600 MHz, CDCl$_3$) of **151**
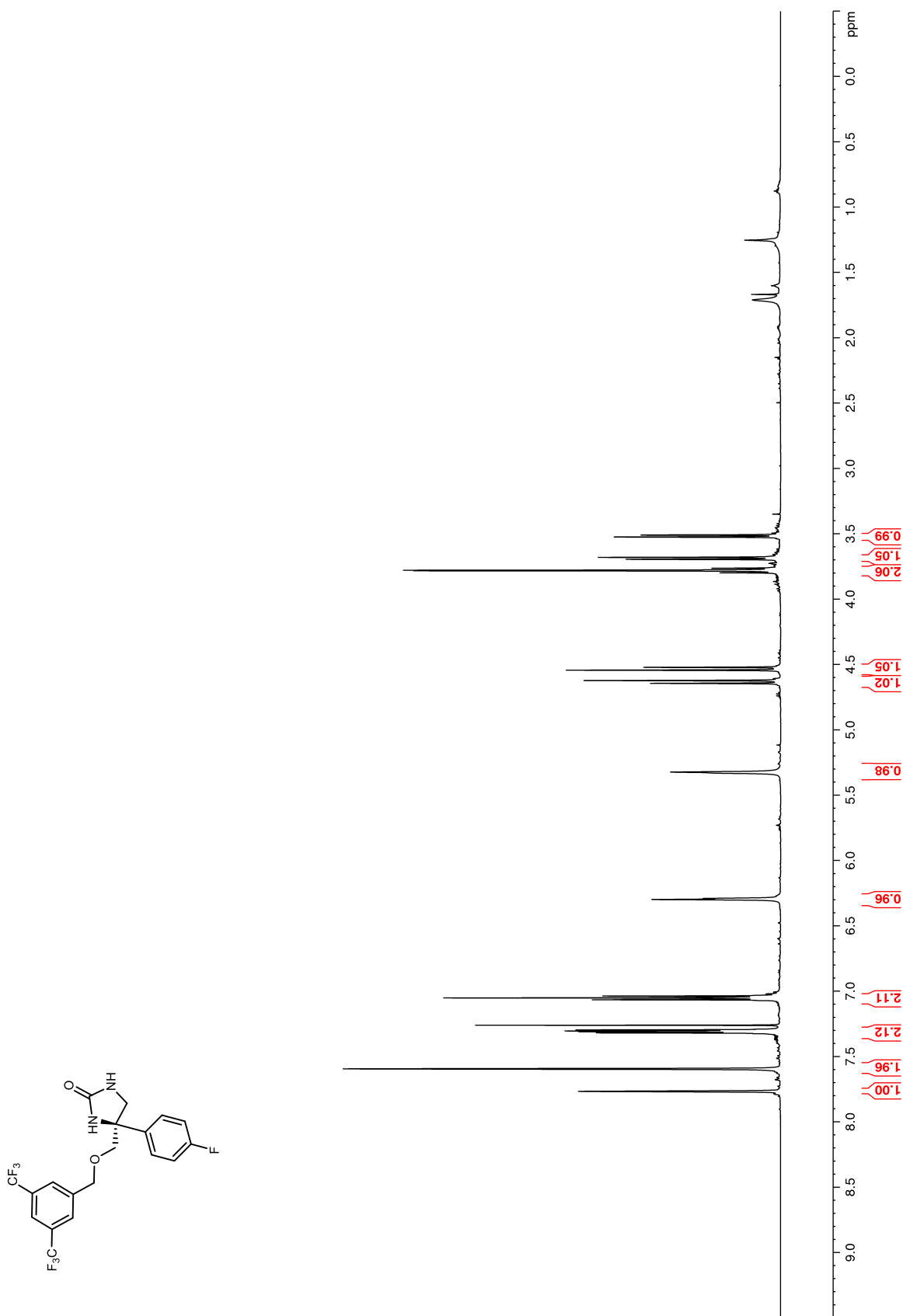
Figure 178. ^{13}C NMR (150 MHz, CDCl$_3$) of **151**
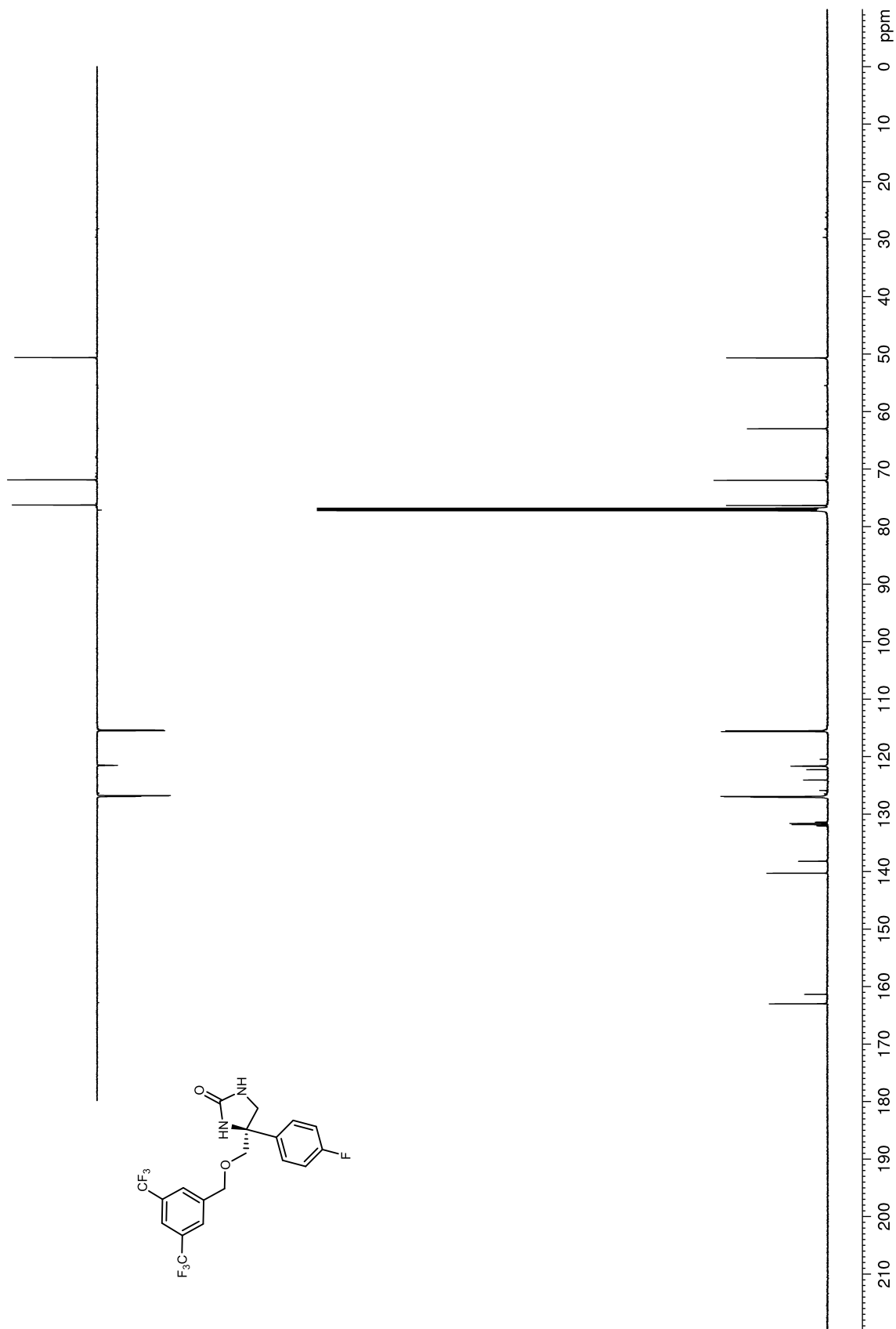
Figure 179. ^{19}F NMR (376 MHz, CDCl$_3$) of **151**

Figure 180**.** HMBC of **151**
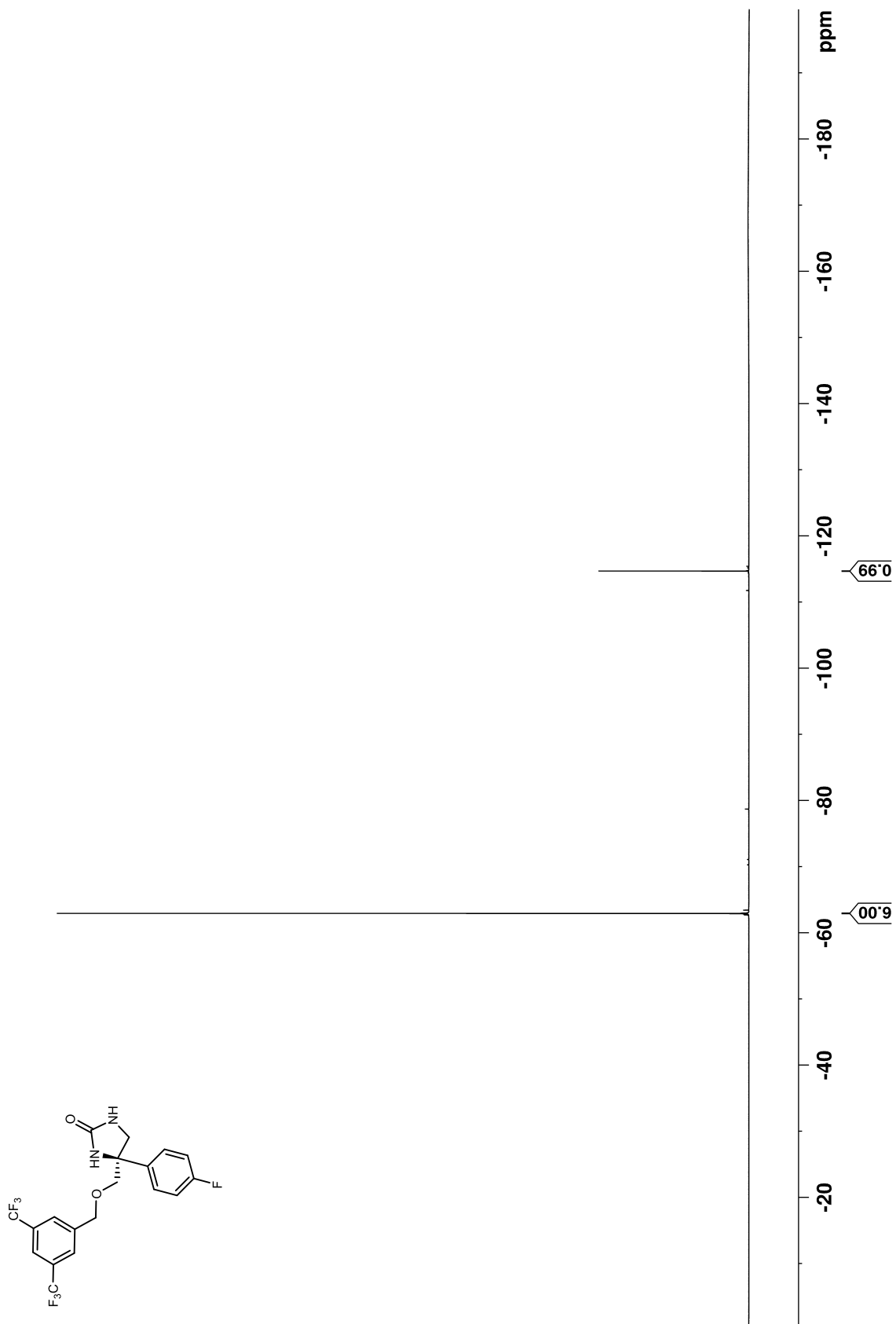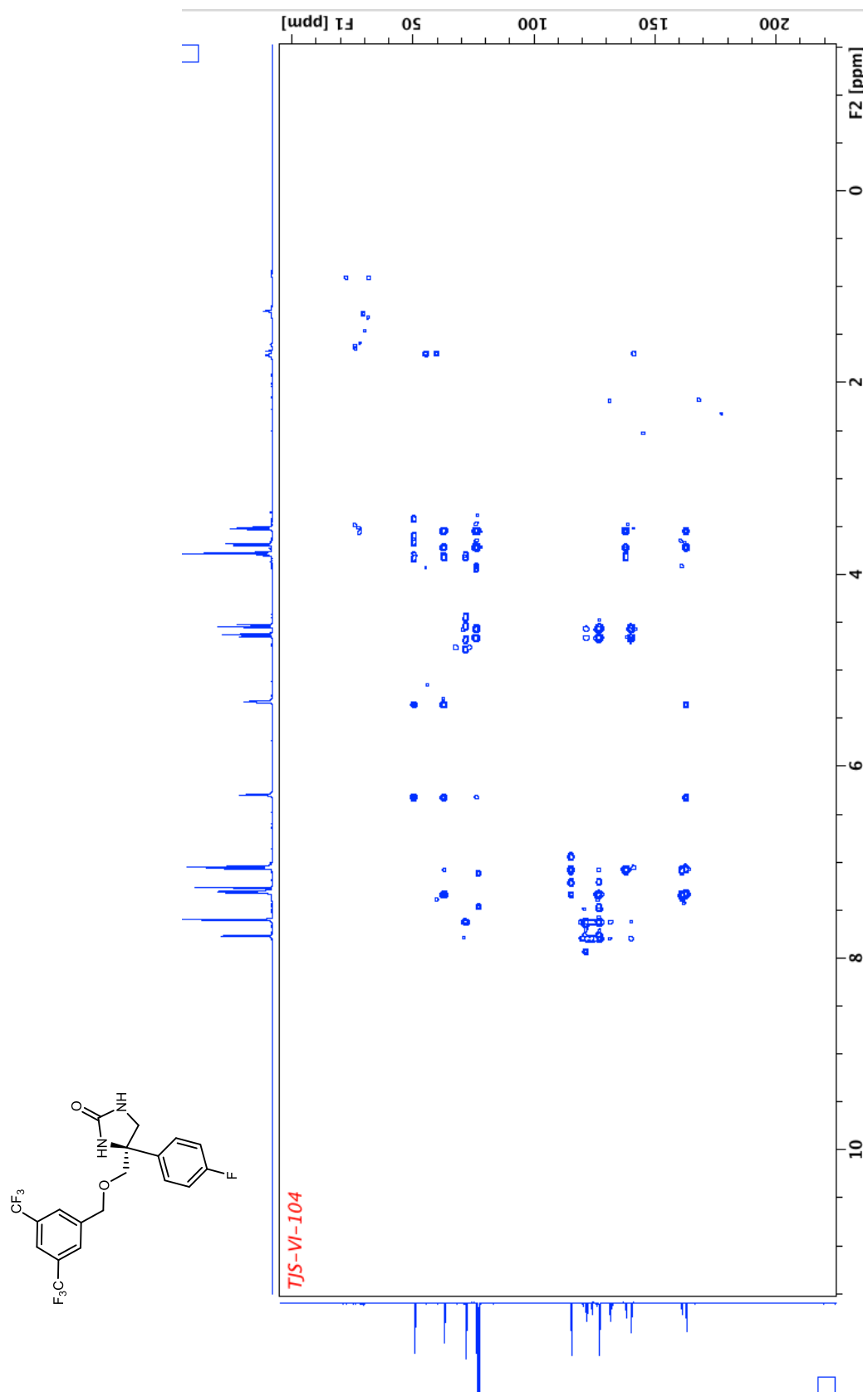
Determination of the Absolute Configuration (Single Crystal X-ray)

A single crystal of purified iodocarbonate **44** was grown by the vapor-diffusion method in diethyl ether under hexanes atmosphere, and the absolute stereochemistry was determined by X-ray crystallography.

Crystal data

$C_{11}H_{11}IO_3$

$M_r = 318.10$

Orthorhombic, $P2_12_12_1$

$a = 7.4336 (3)$ Å

$b = 8.2693 (3)$ Å

$c = 18.5884 (7)$ Å

$V = 1142.64 (8)$ Å^3

$Z = 4$

$F(000) = 616$

$D_x = 1.849$ Mg m^{-3}

Mo $K\alpha$ radiation, $\lambda = 0.71073$ Å

Cell parameters from 9901 reflections

$\theta = 2.7–30.1°$

$\mu = 2.79$ mm^{-1}

$T = 150$ K

Block, yellowish

$0.31 \times 0.29 \times 0.22$ mm

Data collection

Kappa diffractometer

Radiation source: fine-focus sealed tube

Graphite monochromator

Detector resolution: 83.33 pixels mm^{-1}

ω and phi scans

Absorption correction: multi-scan *SADABS*, R. Blessing; 1995

$T_{min} = 0.479$, $T_{max} = 0.579$

15981 measured reflections

3365 independent reflections

3318 reflections with $I > 2\sigma(I)$

$R_{int} = 0.028$

$\theta_{max} = 30.1°$, $\theta_{min} = 2.2°$

$h = -10 \rightarrow 10$

$k = -11 \rightarrow 11$

$l = -26 \rightarrow 19$

Refinement

Refinement on F^2

Least-squares matrix: full

$R[F^2 > 2\sigma(F^2)] = 0.015$

$wR(F^2) = 0.038$

$S = 1.16$

3365 reflections

136 parameters

0 restraints

Secondary atom site location: difference Fourier map

Hydrogen site location: inferred from neighboring sites

H-atom parameters constrained

$w = 1/[\sigma^2(F_o^2) + (0.0143P)^2 + 0.2525P]$ where $P = (F_o^2 + 2F_c^2)/3$

$(\Delta/\sigma)_{max} = 0.001$

$\Delta\rho_{max} = 0.35$ e Å^{-3}

$\Delta\rho_{min} = -0.61$ e Å^{-3}

Absolute structure: Flack H D (1983), Acta Cryst.

A39, 876-881

Primary atom site location: structure-invariant direct methods

Absolute structure parameter: 0.004 (14)

Special details

 Geometry. All esds (except the esd in the dihedral angle between two l.s. planes) are estimated using the full covariance matrix. The cell esds are taken into account individually in the estimation of esds in distances, angles and torsion angles; correlations between esds in cell parameters are only used when they are defined by crystal symmetry. An approximate (isotropic) treatment of cell esds is used for estimating esds involving l.s. planes.

Refinement. Refinement of F^2 against ALL reflections. The weighted R-factor wR and goodness of fit S are based on F^2, conventional R-factors R are based on F, with F set to zero for negative F^2. The threshold expression of $F^2 > 2\text{sigma}(F^2)$ is used only for calculating R-factors(gt) etc. and is not relevant to the choice of reflections for refinement. R-factors based on F^2 are statistically about twice as large as those based on F, and R- factors based on ALL data will be even larger.
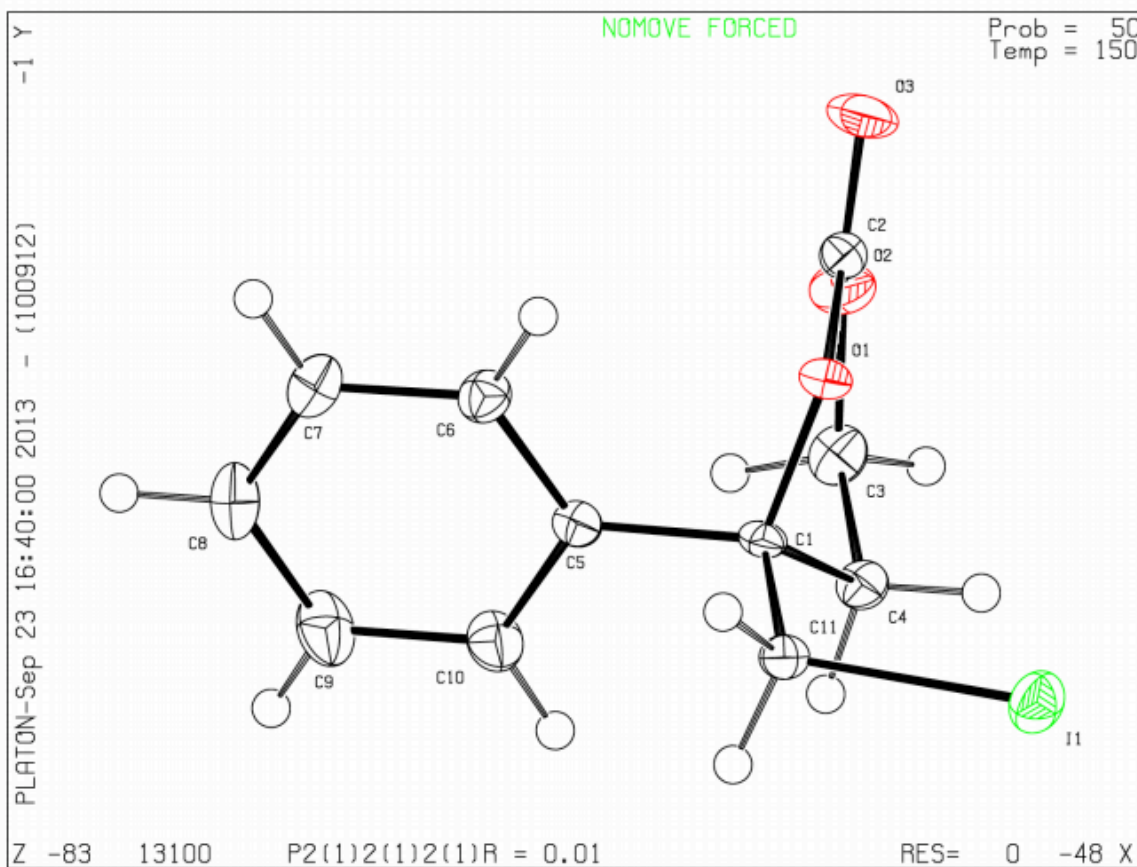
Crystal Structures
A single crystal of purified urea **121f** was grown by the vapor-diffusion method in dichloromethane under hexanes atmosphere, and the absolute stereochemistry was determined by X-ray crystallography

INDIANA UNIVERSITY DEPARTMENT OF CHEMISTRY

Molecular Structure Center

Report No. 16055
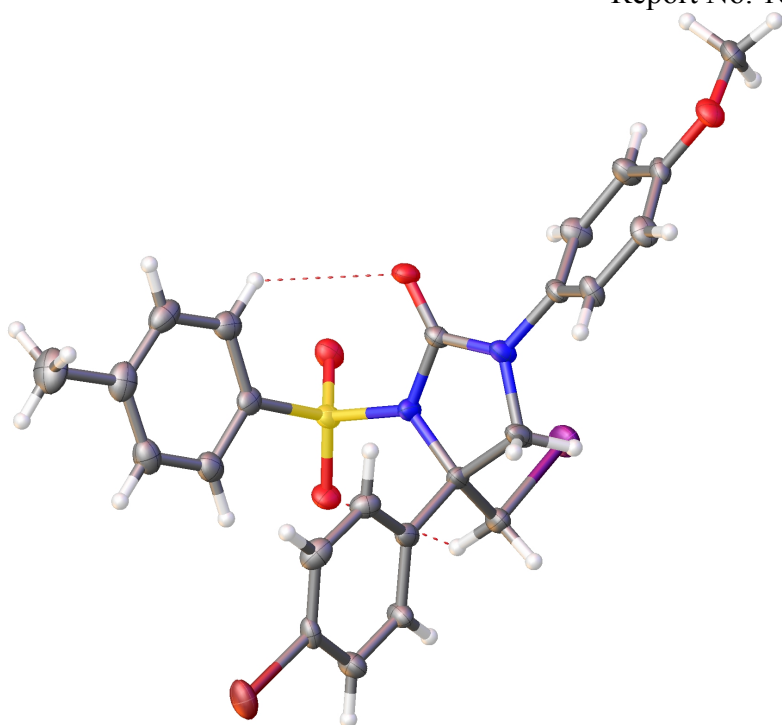
C$_{24}$H$_{22}$BrIN$_2$O$_4$S (XX)

Prepared for:

Thomas Struble and Professor J. Johnston

By M. Pink,
June 21, 2016

ΨMSC
Molecular Structure Center

The sample was submitted by Thomas Struble (research group of Jeffrey Johnston, Department of Chemistry, Vanderbilt University). A colorless crystal (approximate dimensions $0.31 \times 0.21 \times 0.05$ mm^3) was placed onto the tip of a 0.05 mm diameter glass capillary and mounted on a Bruker APEX II Kappa Duo diffractometer equipped with an APEX II detector at 150(2) K.

Data collection

The data collection was carried out using Mo Kα radiation (graphite monochromator) with a frame time of 10 seconds and a detector distance of 40 mm. A collection strategy was calculated and complete data to a resolution of 0.70 Å with a redundancy of 4 were collected. Four major sections of frames were collected with 0.50º ω and ϕ scans. The total exposure time was 3.34 hours. The frames were integrated with the Bruker SAINT software package[1] using a narrow-frame algorithm. The integration of the data using an orthorhombic unit cell yielded a total of 22668 reflections to a maximum θ angle of 27.53° (0.77 Å resolution), of which 5492 were independent (average redundancy 4.127, completeness = 99.6%, R_{int} = 3.77%, R_{sig} = 4.14%) and 5092 (92.72%) were greater than 2σ(F2). The final cell constants of a = 7.4546(12) Å, b = 13.367(2) Å, c = 24.063(4) Å, volume = 2397.8(7) Å3, are based upon the refinement of the XYZ-centroids of 9880 reflections above 20 σ(I) with 5.721° < 2θ < 55.01°. Data were corrected for absorption effects using the multi-scan method (SADABS[2]). The ratio of minimum to maximum apparent transmission was 0.686. The calculated minimum and maximum transmission coefficients (based on crystal size) are 0.4440 and 0.8590. Please refer to Table 1 for additional crystal and refinement information.

Structure solution and refinement

The space group $P2_12_12_1$ was determined based on intensity statistics and systematic absences. The structure was solved and refined using the SHELX suite of programs.[3] An intrinsic-methods solution was calculated, which provided most non-hydrogen atoms from the E-map. Full-matrix least squares / difference Fourier cycles were performed, which located the remaining non-hydrogen atoms. All non-hydrogen atoms were refined with anisotropic displacement parameters. The hydrogen atoms were placed in ideal positions and refined as riding atoms with relative isotropic displacement parameters. The final anisotropic full-matrix least-squares refinement on F2 with 300 variables converged at R1 = 2.84%, for the observed data and wR2 = 6.94% for all data. The goodness-of-fit was 1.050. The largest peak in the final difference electron density synthesis was 1.041 e$^-$/Å^3 and the largest hole was -0.496 e$^-$/Å^3 with an RMS deviation of 0.078 e$^-$/Å^3. On the basis of the final model, the calculated density was 1.777 g/cm^3 and F(000), 1264 e$^-$.

1 SAINT, Bruker Analytical X-Ray Systems, Madison, WI, current version.
2 SADABS, Bruker Analytical X-Ray Systems, Madison, WI, current version.
3 A short history of *SHELX*, G. M. Sheldrick, *Acta Cryst*. A64, 112 - 122 (2008).
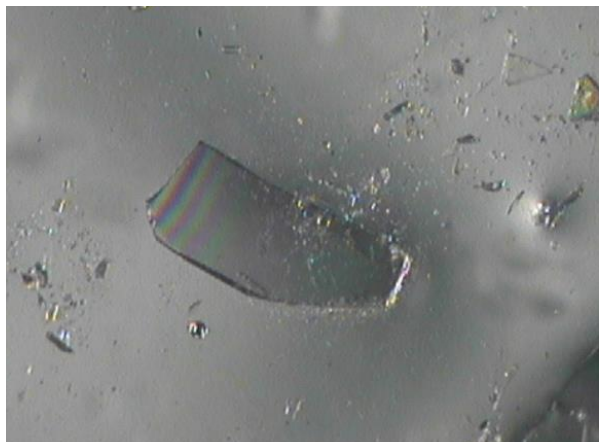
Bulk material.
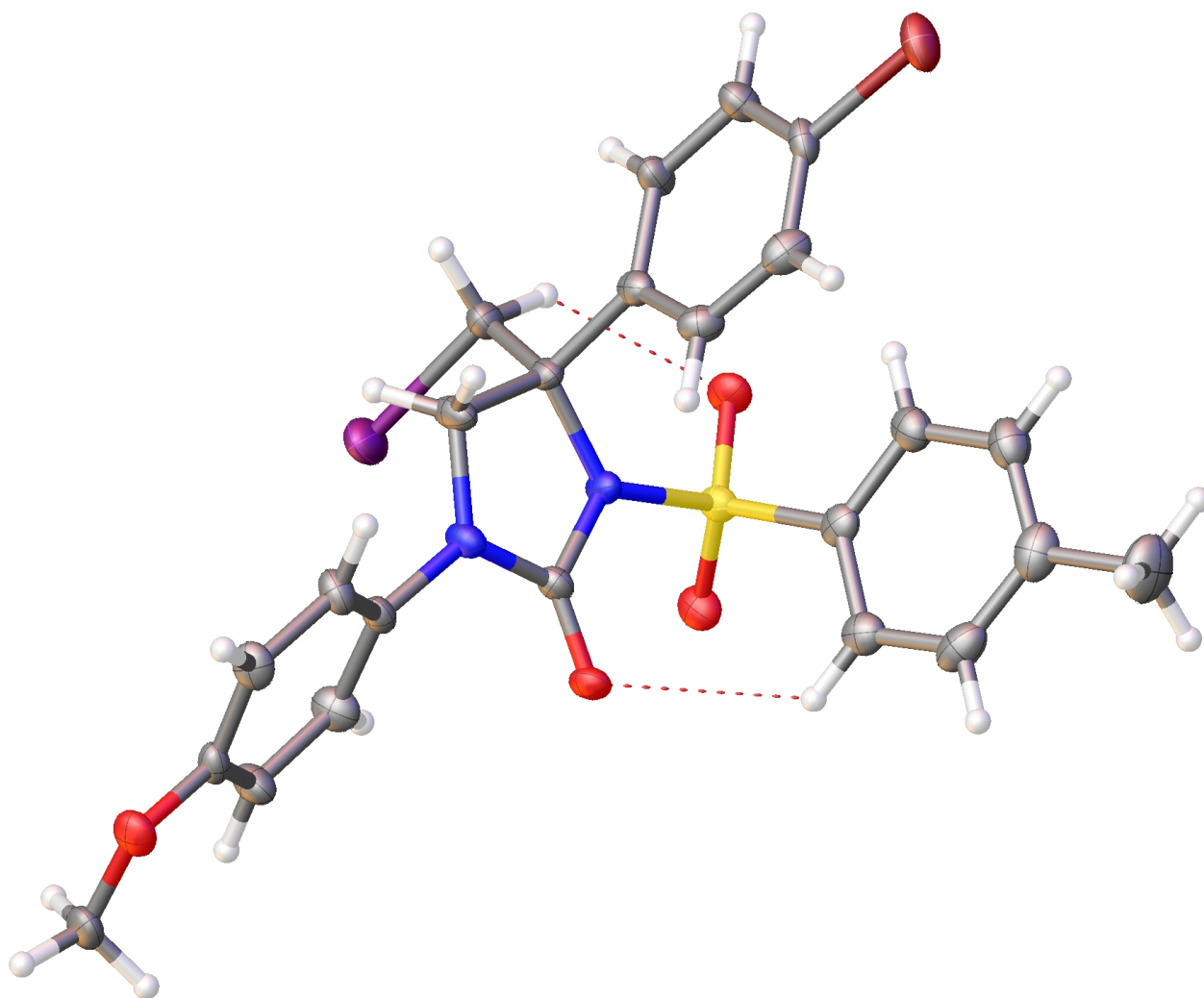
Formula unit.
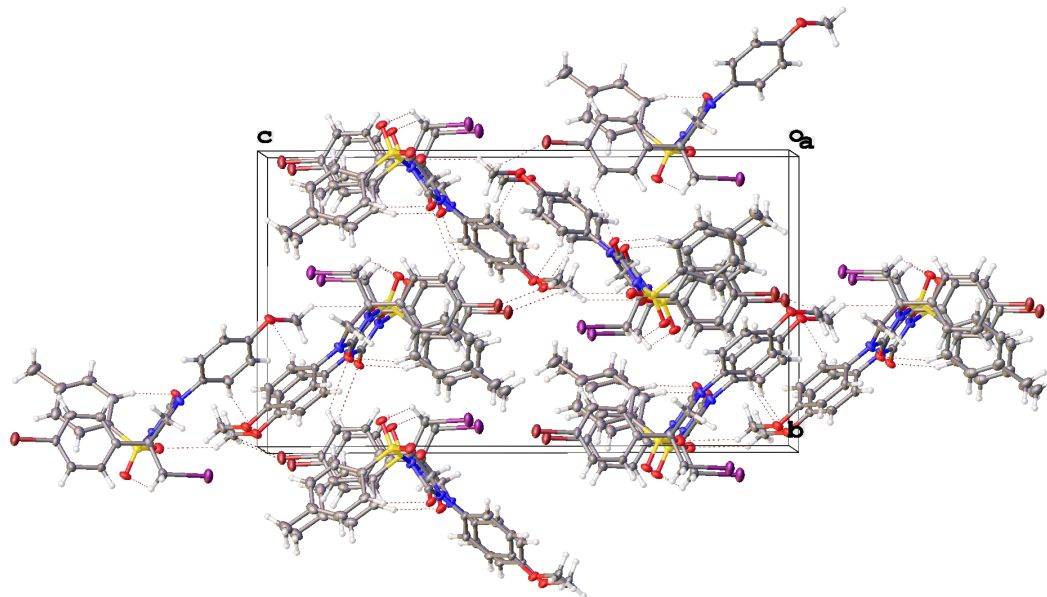
Cell plot, view along *a*.
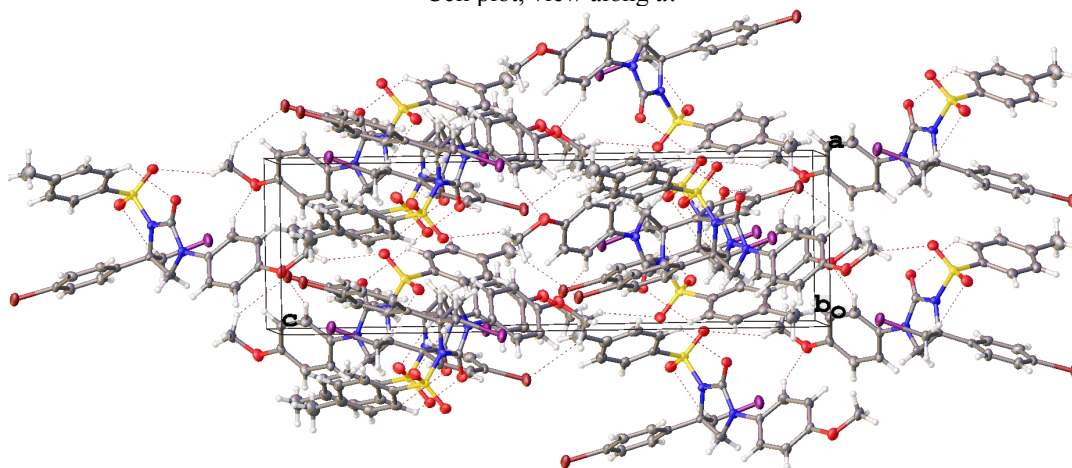
Cell plot, view along *b*.
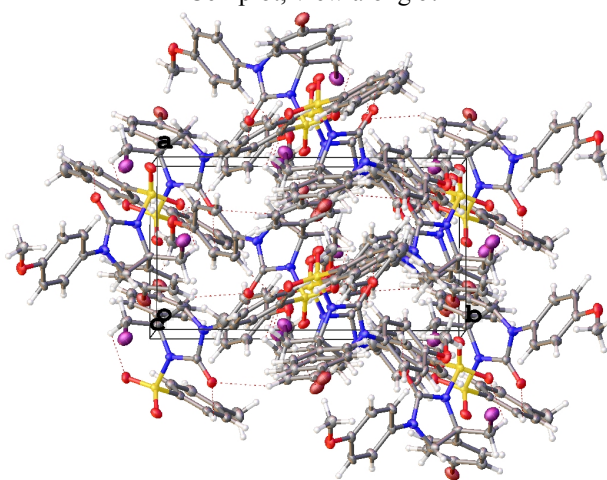
Cell plot, view along *c*.

Table 1. Crystal data and structure refinement for 16055.

Empirical formula	C24 H22 Br I N2 O4 S
Formula weight	641.30
Crystal color, shape, size	colorless plate, $0.31 \times 0.21 \times 0.05$ mm^3
Temperature	150(2) K
Wavelength	0.71073 Å
Crystal system, space group	Orthorhombic, P2$_1$2$_1$2$_1$
Unit cell dimensions	a = 7.4546(12) Å α= 90°.
	b = 13.367(2) Å β= 90°.
	c = 24.063(4) Å γ = 90°.
Volume	2397.7(7) Å^3
Z	4
Density (calculated)	1.777 Mg/m^3
Absorption coefficient	3.123 mm^{-1}
F(000)	1264

Data collection

Diffractometer	APEX II Kappa Duo, Bruker
Theta range for data collection	1.743 to 27.529°.
Index ranges	-9<=h<=9, -17<=k<=16, -31<=l<=31
Reflections collected	22668
Independent reflections	5492 [R$_{int}$ = 0.0377]
Observed Reflections	5092
Completeness to theta = 25.242°	99.6 %

Solution and Refinement

Absorption correction	Semi-empirical from equivalents
Max. and min. transmission	0.7456 and 0.5118
Solution	Intrinsic methods
Refinement method	Full-matrix least-squares on F^2
Weighting scheme	w = [σ^2Fo^2+ AP^2+ BP]$^{-1}$, with
	P = (Fo^2+ 2 Fc^2)/3, A = 0.0344, B = 0.0995
Data / restraints / parameters	5492 / 0 / 300
Goodness-of-fit on F^2	1.050
Final R indices [I>2sigma(I)]	R1 = 0.0284, wR2 = 0.0682
R indices (all data)	R1 = 0.0322, wR2 = 0.0694
Absolute structure parameter	0.027(5)
Largest diff. peak and hole	1.041 and -0.496 e.Å^{-3}

Goodness-of-fit = $[\Sigma[w(F_o^2 - F_c^2)^2]/N_{observns} - N_{params})]^{1/2}$, all data.

R1 = $\Sigma(|F_o| - |F_c|) / \Sigma |F_o|$. wR2 = $[\Sigma[w(F_o^2 - F_c^2)^2] / \Sigma [w(F_o^2)^2]]^{1/2}$.

Table 2. Atomic coordinates (× 10^4) and equivalent isotropic displacement parameters (Å^2 × 10^3) for 16055. U(eq) is defined as one third of the trace of the orthogonalized U^{ij} tensor.

	x	y	z	U(eq)
I1	5213(1)	10878(1)	1015(1)	37(1)
Br1	1955(1)	9681(1)	4592(1)	34(1)
S1	7989(1)	9867(1)	2407(1)	20(1)
O1	7392(4)	10809(2)	2617(1)	26(1)
O2	9481(4)	9833(2)	2033(1)	26(1)
O3	7701(4)	8051(2)	1673(1)	23(1)
O4	3484(4)	5621(2)	-176(1)	28(1)
N1	6209(4)	9391(3)	2076(1)	20(1)
N2	4667(4)	8330(3)	1550(1)	22(1)
C1	4347(5)	9790(4)	2113(2)	21(1)
C2	6346(5)	8526(3)	1747(2)	18(1)
C3	3299(5)	8999(4)	1766(2)	28(1)
C4	4186(6)	10830(4)	1852(2)	25(1)
C5	3703(5)	9790(3)	2721(2)	21(1)
C6	3793(5)	8906(4)	3022(2)	25(1)
C7	3285(6)	8866(4)	3581(2)	28(1)
C8	2644(5)	9723(4)	3831(2)	23(1)
C9	2512(6)	10618(4)	3542(2)	25(1)
C10	3046(6)	10639(3)	2987(2)	23(1)
C11	8389(5)	9048(3)	2965(2)	22(1)
C12	9310(5)	8159(3)	2891(2)	25(1)
C13	9616(6)	7544(4)	3345(2)	33(1)
C14	9016(6)	7810(4)	3877(2)	33(1)
C15	8064(6)	8691(4)	3938(2)	31(1)
C16	7739(6)	9318(4)	3487(2)	28(1)
C17	9445(8)	7163(4)	4379(2)	45(1)
C18	4357(5)	7650(3)	1099(2)	19(1)
C19	5501(6)	7636(4)	652(2)	27(1)
C20	5259(6)	6965(4)	220(2)	26(1)
C21	3822(6)	6315(3)	229(2)	21(1)
C22	2612(6)	6354(3)	664(2)	25(1)
C23	2876(6)	7008(3)	1105(2)	24(1)
C24	4628(6)	5640(4)	-653(2)	31(1)

Table 3. Bond lengths [Å] and angles [°] for 16055.

Bond	Length	Bond	Length
I1-C4	2.156(4)	Br1-C8	1.902(4)
S1-O1	1.428(3)	S1-O2	1.431(3)
S1-N1	1.673(3)	S1-C11	1.758(5)
O3-C2	1.206(5)	O4-C21	1.368(5)
O4-C24	1.431(5)	N1-C2	1.405(5)
N1-C1	1.490(5)	N2-C2	1.364(5)
N2-C18	1.435(5)	N2-C3	1.453(5)
C1-C4	1.530(7)	C1-C5	1.539(5)
C1-C3	1.557(6)	C3-H3A	0.9900
C3-H3B	0.9900	C4-H4A	0.9900
C4-H4B	0.9900	C5-C6	1.388(6)
C5-C10	1.392(6)	C6-C7	1.397(6)
C6-H6	0.9500	C7-C8	1.381(6)
C7-H7	0.9500	C8-C9	1.387(6)
C9-C10	1.394(6)	C9-H9	0.9500
C10-H10	0.9500	C11-C12	1.384(6)
C11-C16	1.394(6)	C12-C13	1.387(7)
C12-H12	0.9500	C13-C14	1.401(7)
C13-H13	0.9500	C14-C15	1.382(7)
C14-C17	1.519(7)	C15-C16	1.392(7)
C15-H15	0.9500	C16-H16	0.9500
C17-H17A	0.9800	C17-H17B	0.9800
C17-H17C	0.9800	C18-C19	1.372(6)
C18-C23	1.398(6)	C19-C20	1.384(6)
C19-H19	0.9500	C20-C21	1.379(6)
C20-H20	0.9500	C21-C22	1.384(6)
C22-C23	1.389(6)	C22-H22	0.9500
C23-H23	0.9500	C24-H24A	0.9800
C24-H24B	0.9800	C24-H24C	0.9800

Angle	Value	Angle	Value
O1-S1-O2	119.50(19)	O1-S1-N1	104.84(18)
O2-S1-N1	107.76(17)	O1-S1-C11	109.4(2)
O2-S1-C11	109.18(19)	N1-S1-C11	105.18(19)
C21-O4-C24	116.7(3)	C2-N1-C1	113.3(3)
C2-N1-S1	121.6(3)	C1-N1-S1	125.1(3)
C2-N2-C18	122.2(3)	C2-N2-C3	113.7(3)
C18-N2-C3	123.2(3)	N1-C1-C4	111.9(3)
N1-C1-C5	110.4(3)	C4-C1-C5	111.4(3)
N1-C1-C3	101.1(3)	C4-C1-C3	110.9(3)
C5-C1-C3	110.7(3)	O3-C2-N2	128.0(4)
O3-C2-N1	125.2(4)	N2-C2-N1	106.7(3)
N2-C3-C1	104.9(3)	N2-C3-H3A	110.8
C1-C3-H3A	110.8	N2-C3-H3B	110.8
C1-C3-H3B	110.8	H3A-C3-H3B	108.8
C1-C4-I1	112.5(3)	C1-C4-H4A	109.1
I1-C4-H4A	109.1	C1-C4-H4B	109.1
I1-C4-H4B	109.1	H4A-C4-H4B	107.8
C6-C5-C10	118.1(4)	C6-C5-C1	118.7(4)
C10-C5-C1	123.2(4)	C5-C6-C7	121.4(4)
C5-C6-H6	119.3	C7-C6-H6	119.3
C8-C7-C6	118.8(4)	C8-C7-H7	120.6
C6-C7-H7	120.6	C7-C8-C9	121.4(4)
C7-C8-Br1	119.3(3)	C9-C8-Br1	119.3(3)
C8-C9-C10	118.5(4)		

Angle	Value	Angle	Value
C8-C9-H9	120.8	C10-C9-H9	120.8
C5-C10-C9	121.7(4)	C5-C10-H10	119.2
C9-C10-H10	119.2	C12-C11-C16	117.9(4)
C12-C11-S1	121.3(3)	C16-C11-S1	119.2(4)
C11-C12-C13	120.4	C11-C12-H12	120.4
C13-C12-H12	119.4	C12-C13-C14	121.1(5)
C12-C13-H13	119.4	C14-C13-H13	119.4
C15-C14-C13	118.5(4)	C15-C14-C17	121.2(4)
C13-C14-C17	121.0(5)	C14-C15-C16	119.4
C14-C15-H15	119.4	C16-C15-H15	119.4
C15-C16-C11	120.5	C15-C16-H16	120.5
C11-C16-H16	120.5	C14-C17-H17A	109.5
C14-C17-H17B	109.5	H17A-C17-H17B	109.5
C14-C17-H17C	109.5	H17A-C17-H17C	109.5
H17B-C17-H17C	109.5	C19-C18-C23	119.4(4)
C19-C18-N2	120.1(4)	C23-C18-N2	120.5(4)
C18-C19-C20	121.1(4)	C18-C19-H19	119.5
C20-C19-H19	119.5	C21-C20-C19	119.9(4)
C21-C20-H20	120.1	C19-C20-H20	120.1
O4-C21-C20	124.0(4)	O4-C21-C22	116.4(4)
C20-C21-C22	119.6(4)	C21-C22-C23	120.6(4)
C21-C22-H22	119.7	C23-C22-H22	119.7
C22-C23-C18	119.3(4)	C22-C23-H23	120.3
C18-C23-H23	120.3	O4-C24-H24A	109.5
O4-C24-H24B	109.5	H24A-C24-H24B	109.5
O4-C24-H24C	109.5	H24A-C24-H24C	109.5
H24B-C24-H24C	109.5		

Table 4. Anisotropic displacement parameters ($Å^2 \times 10^3$) for 16055. The anisotropic displacement factor exponent takes the form: $-2\pi^2[h^2 a^{*2}U^{11} + ... + 2 h k a^* b^* U^{12}]$

	U^{11}	U^{22}	U^{33}	U^{23}	U^{13}	U^{12}
I1	42(1)	48(1)	20(1)	2(1)	4(1)	9(1)
Br1	38(1)	44(1)	19(1)	3(1)	-2(1)	-12(1)
S1	19(1)	18(1)	22(1)	-5(1)	-1(1)	-3(1)
O1	29(1)	18(2)	31(2)	-8(1)	-4(1)	-1(1)
O2	23(1)	28(2)	27(2)	-4(1)	0(1)	-7(1)
O3	23(1)	21(2)	25(2)	-9(1)	1(1)	2(1)
O4	36(2)	22(2)	27(2)	-8(1)	-5(1)	-3(1)
N1	16(2)	22(2)	23(2)	-8(2)	-4(1)	1(1)
N2	20(2)	24(2)	23(2)	-9(2)	1(1)	-2(2)
C1	15(2)	26(2)	21(2)	-6(2)	-2(1)	3(2)
C2	21(2)	16(2)	18(2)	-3(2)	1(2)	-2(2)
C3	20(2)	35(3)	29(2)	-17(2)	0(2)	0(2)
C4	29(2)	29(2)	19(2)	-3(2)	-1(2)	6(2)
C5	16(2)	24(2)	24(2)	-7(2)	-3(2)	-1(2)
C6	22(2)	21(2)	31(2)	-2(2)	3(2)	-1(2)
C7	23(2)	22(2)	39(2)	6(2)	2(2)	-3(2)
C8	23(2)	31(2)	14(2)	2(2)	-3(1)	-6(2)
C9	30(2)	25(2)	21(2)	-4(2)	2(2)	-1(2)
C10	33(2)	18(2)	18(2)	0(2)	0(2)	3(2)
C11	18(2)	21(2)	28(2)	-4(2)	-6(2)	-5(2)
C12	21(2)	24(2)	31(2)	-5(2)	-2(2)	-5(2)
C13	24(2)	24(2)	50(3)	1(2)	-8(2)	-2(2)
C14	29(2)	31(3)	38(3)	9(2)	-7(2)	-12(2)
C15	29(2)	38(3)	26(2)	1(2)	-2(2)	-9(2)
C16	24(2)	32(3)	27(2)	-5(2)	-3(2)	-5(2)
C17	53(3)	36(3)	47(3)	17(3)	-10(3)	-8(3)
C18	25(2)	16(2)	16(2)	-3(2)	-2(2)	0(2)
C19	26(2)	24(2)	32(2)	-5(2)	3(2)	-9(2)
C20	26(2)	30(2)	22(2)	-7(2)	3(2)	-4(2)
C21	27(2)	17(2)	18(2)	-2(2)	-7(2)	-1(2)
C22	30(2)	18(2)	27(2)	-2(2)	-3(2)	-9(2)
C23	27(2)	28(2)	17(2)	-2(2)	-1(2)	-8(2)
C24	36(2)	34(3)	22(2)	-12(2)	-8(2)	5(2)

Table 5. Hydrogen coordinates ($\times 10^4$) and isotropic displacement parameters ($\mathring{A}^2 \times 10^3$) for 16055.

	x	y	z	U(eq)
H3A	2438	8630	2003	34
H3B	2633	9324	1459	34
H4A	4853	11316	2084	30
H4B	2909	11033	1850	30
H6	4209	8315	2845	30
H7	3379	8259	3784	34
H9	2067	11204	3719	31
H10	2960	11247	2785	28
H12	9728	7972	2532	31
H13	10242	6932	3295	39
H15	7623	8871	4295	37
H16	7084	9921	3535	33
H17A	9196	7540	4720	67
H17B	10714	6974	4370	67
H17C	8700	6559	4370	67
H19	6475	8093	639	33
H20	6082	6952	-81	31
H22	1591	5928	662	30
H23	2058	7020	1408	29
H24A	4157	5183	-936	46
H24B	5839	5429	-546	46
H24C	4672	6321	-804	46

Table 6. Torsion angles [°] for 16055.

Torsion	Angle	Torsion	Angle
O1-S1-N1-C2	171.0(3)	O2-S1-N1-C2	42.7(4)
C11-S1-N1-C2	-73.7(4)	O1-S1-N1-C1	-11.8(4)
O2-S1-N1-C1	-140.1(3)	C11-S1-N1-C1	103.5(4)
C2-N1-C1-C4	-116.0(4)	S1-N1-C1-C4	66.6(4)
C2-N1-C1-C5	119.3(4)	S1-N1-C1-C5	-58.1(5)
C2-N1-C1-C3	2.0(4)	S1-N1-C1-C3	-175.3(3)
C18-N2-C2-O3	-16.8(7)	C3-N2-C2-O3	173.9(4)
C18-N2-C2-N1	165.0(4)	C3-N2-C2-N1	-4.3(5)
C1-N1-C2-O3	-177.1(4)	S1-N1-C2-O3	0.4(6)
C1-N1-C2-N2	1.2(5)	S1-N1-C2-N2	178.7(3)
C2-N2-C3-C1	5.5(5)	C18-N2-C3-C1	-163.7(4)
N1-C1-C3-N2	-4.2(4)	C4-C1-C3-N2	114.6(4)
C5-C1-C3-N2	-121.2(4)	N1-C1-C4-I1	52.7(4)
C5-C1-C4-I1	176.8(2)	C3-C1-C4-I1	-59.4(4)
N1-C1-C5-C6	-53.8(5)	C4-C1-C5-C6	-178.8(4)
C3-C1-C5-C6	57.3(5)	N1-C1-C5-C10	125.6(4)
C4-C1-C5-C10	0.6(5)	C3-C1-C5-C10	-123.3(4)
C10-C5-C6-C7	-1.6(6)	C1-C5-C6-C7	177.9(4)
C5-C6-C7-C8	1.4(6)	C6-C7-C8-C9	-0.6(6)
C6-C7-C8-Br1	-179.8(3)	C7-C8-C9-C10	-0.1(6)
Br1-C8-C9-C10	179.1(3)	C6-C5-C10-C9	0.9(6)
C1-C5-C10-C9	-178.5(4)	C8-C9-C10-C5	-0.1(6)
O1-S1-C11-C12	-167.0(3)	O2-S1-C11-C12	-34.5(4)
N1-S1-C11-C12	80.9(4)	O1-S1-C11-C16	13.4(4)
O2-S1-C11-C16	145.9(3)	N1-S1-C11-C16	-98.7(3)
C16-C11-C12-C13	-1.3(6)	S1-C11-C12-C13	179.1(3)
C11-C12-C13-C14	-0.3(6)	C12-C13-C14-C15	1.8(7)
C12-C13-C14-C17	-176.5(4)	C13-C14-C15-C16	-1.6(7)
C17-C14-C15-C16	176.7(4)	C14-C15-C16-C11	0.0(6)
C12-C11-C16-C15	1.5(6)	S1-C11-C16-C15	-178.9(3)
C2-N2-C18-C19	-39.7(6)	C3-N2-C18-C19	128.6(5)
C2-N2-C18-C23	141.2(4)	C3-N2-C18-C23	-50.5(6)
C23-C18-C19-C20	-3.0(7)	N2-C18-C19-C20	178.0(4)
C18-C19-C20-C21	1.7(7)	C24-O4-C21-C20	-5.2(6)
C24-O4-C21-C22	174.2(4)	C19-C20-C21-O4	-179.3(4)
C19-C20-C21-C22	1.2(7)	O4-C21-C22-C23	177.7(4)
C20-C21-C22-C23	-2.9(7)	C21-C22-C23-C18	1.6(7)
C19-C18-C23-C22	1.3(6)	N2-C18-C23-C22	-179.6(4)

Table 7. Hydrogen bonds for 16055 [Å and °].

D-H...A	d(D-H)	d(H...A)	d(D...A)	<(DHA)
C4-H4A...O1	0.99	2.39	3.016(5)	120.9
C9-H9...O3#1	0.95	2.65	3.297(6)	125.9
C12-H12...O3	0.95	2.56	3.168(5)	121.8
C19-H19...O4#2	0.95	2.54	3.419(5)	154.4
C24-H24A...I1#3	0.98	3.27	3.963(5)	129.3
C24-H24A...O2#3	0.98	2.65	3.382(5)	131.6
C24-H24B...Br1#4	0.98	3.00	3.828(5)	143.4

Symmetry transformations used to generate equivalent atoms:

#1 -x+1,y+1/2,-z+1/2   #2 x+1/2,-y+3/2,-z   #3 x-1/2,-y+3/2,-z   #4 -x+1,y-1/2,-z+1/2

A single crystal of purified urea **124a** was grown by the vapor-diffusion method in dichloromethane under hexanes atmosphere, and the absolute stereochemistry was determined by X-ray crystallography

INDIANA UNIVERSITY DEPARTMENT OF CHEMISTRY

Molecular Structure Center

Report No. 16052
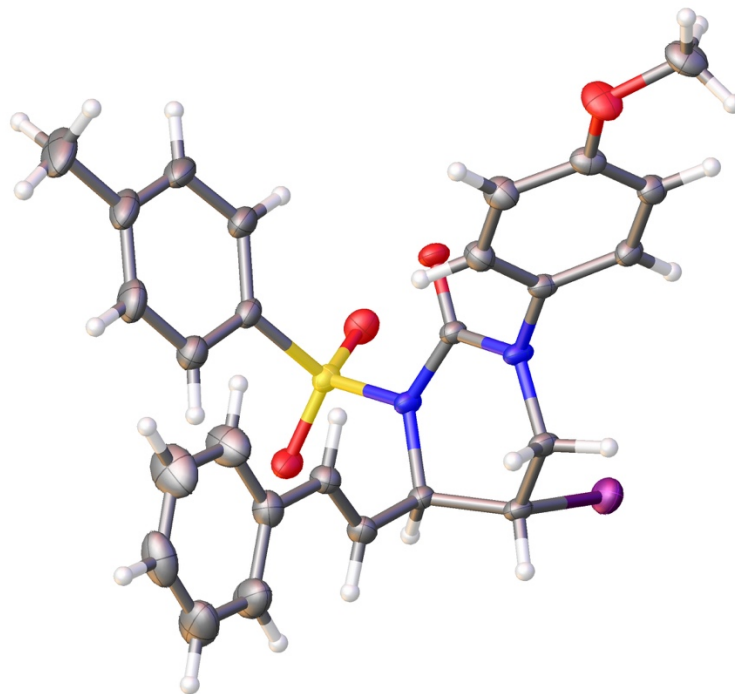
C$_{26}$H$_{25}$IN$_2$O$_4$S (XX)

Prepared for

Thomas Struble and Professor J. Johnston

M. Pink, May 31, 2016

The sample was submitted by Thomas Struble (research group of Jeffrey Johnston, Department of Chemistry, Vanderbilt University). A light yellow crystal (approximate dimensions 0.32 × 0.28 × 0.23 mm^3) was placed onto the tip of a 0.05 mm diameter glass capillary and mounted on a Bruker APEX II Kappa Duo diffractometer equipped with an APEX II detector at 150(2) K.

Data collection. The data collection was carried out using Mo Kα radiation (graphite monochromator) with a frame time of 20 seconds and a detector distance of 40 mm. A collection strategy was calculated and complete data to a resolution of 0.70 Å with a redundancy of 4 were collected. Six major sections of frames were collected with 0.50º ω and φ scans; details are below.

Axis	2θ/°	ω/°	φ/°	χ/°	Frames
Phi	42.00	-7.54	-344.91	34.46	739
Omega	37.00	-39.88	-192.49	93.16	95
Phi	4.50	134.67	-231.70	-81.54	209
Phi	-38.00	318.20	-46.30	-81.54	733
Omega	-40.50	-43.49	83.13	-99.40	129
Phi	-20.50	-18.90	-290.48	96.27	681

A total of 2586 frames were collected. The total exposure time was 14.37 hours. The frames were integrated with the Bruker SAINT software package[1] using a narrow-frame algorithm. The integration of the data using a monoclinic unit cell yielded a total of 25107 reflections to a maximum θ angle of 30.10° (0.71 Å resolution), of which 7073 were independent (average redundancy 3.550, completeness = 99.4%, R$_{int}$ = 3.21%, R$_{sig}$ = 2.81%) and 6970 (98.54%) were greater than 2σ(F2). The final cell constants of a = 6.8374(3) Å, b = 14.8665(6) Å, c = 12.6176(6) Å, β = 105.7165(15)°, volume = 1234.61(9) Å^3, are based upon the refinement of the XYZ-centroids of 9817 reflections above 20 σ(I) with 4.330° < 2θ < 60.09°. Data were corrected for absorption effects using the multi-scan method (SADABS[2]). The ratio of minimum to maximum apparent transmission was 0.854. The calculated minimum and maximum transmission coefficients (based on crystal size) are 0.6371 and 0.7460. Please refer to Table 1 for additional crystal and refinement information.

Structure solution and refinement. The space group P2$_1$ was determined based on intensity statistics and systematic absences. The structure was solved and refined using the SHELX suite of programs.[3] An intrinsic-methods solution was calculated, which provided most non-hydrogen atoms from the E-map. Full-matrix least squares / difference Fourier cycles were performed, which located the remaining non-hydrogen atoms. All non-hydrogen atoms were refined with anisotropic displacement parameters. The hydrogen atoms were placed in ideal positions and refined as riding atoms with relative isotropic displacement parameters. The final anisotropic full-matrix least-squares refinement on F2 with 309 variables converged at R1 = 2.00%, for the observed data and wR2 = 5.27% for all data. The goodness-of-fit was 1.082. The largest peak in the final difference electron density synthesis was 0.655 e$^-$/Å^3 and the largest hole was -0.290 e$^-$/Å^3 with an RMS deviation of 0.051 e$^-$/Å^3. On the basis of the final model, the calculated density was 1.583 g/cm^3 and F(000), 592 e$^-$. The absolute configuration was determined based on anomalous scattering.

1 SAINT, Bruker Analytical X-Ray Systems, Madison, WI, current version.
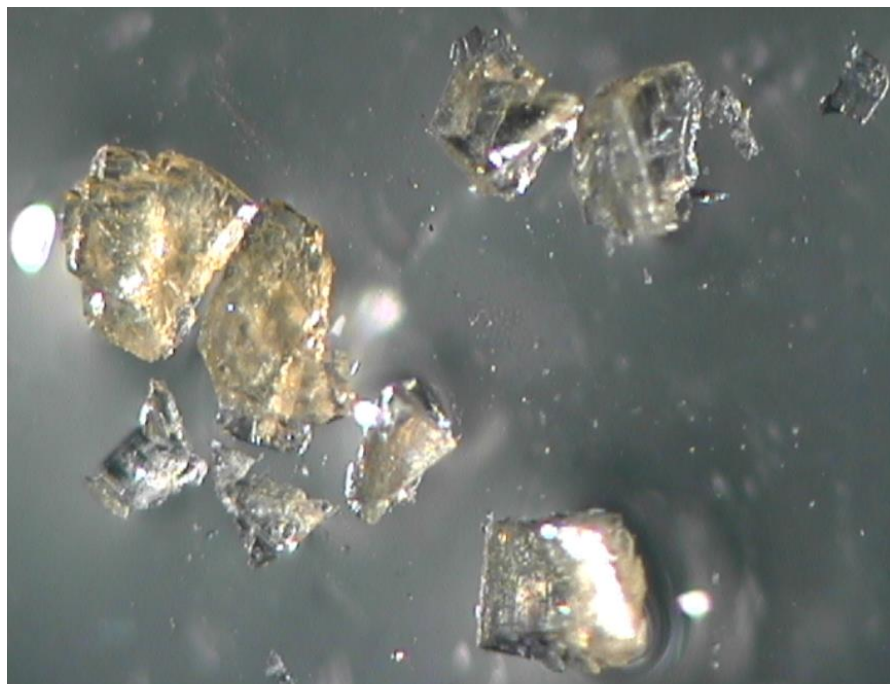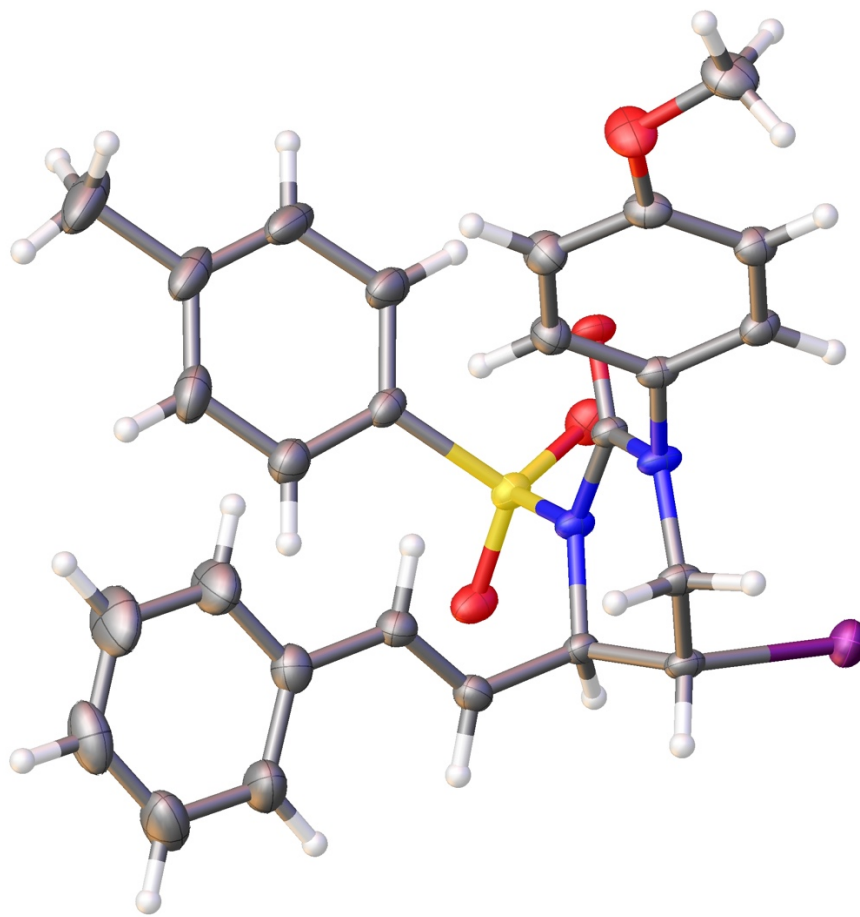
2 SADABS, Bruker Analytical X-Ray Systems, Madison, WI, current version.
3 A short history of *SHELX*, G. M. Sheldrick, *Acta Cryst*. A64, 112 - 122 (2008).

Bulk material.

Formula unit.
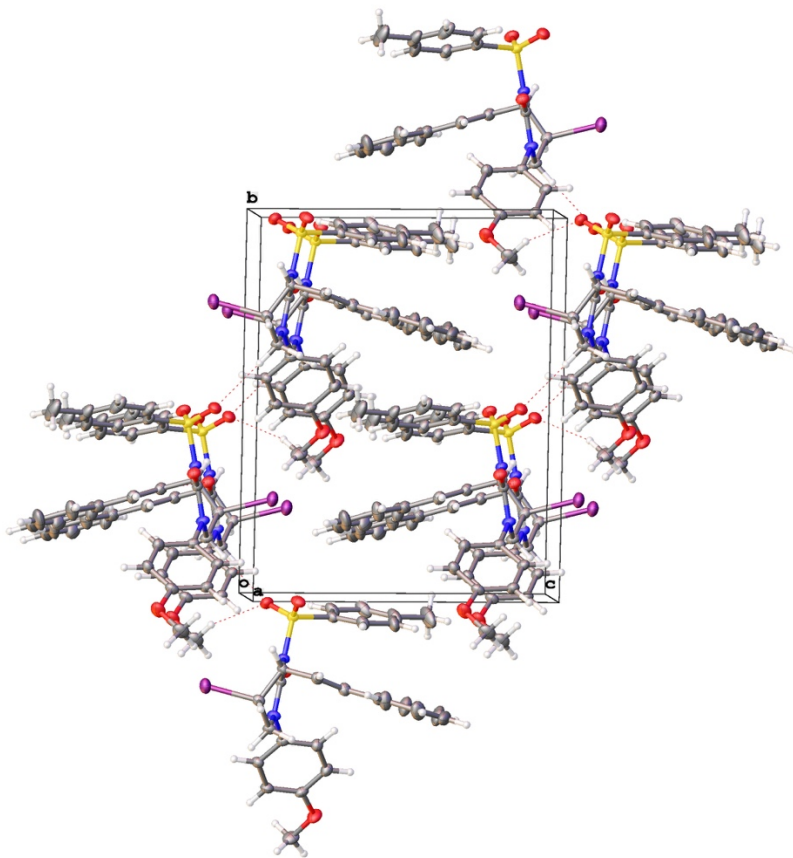
Cell plot, view along *a*.
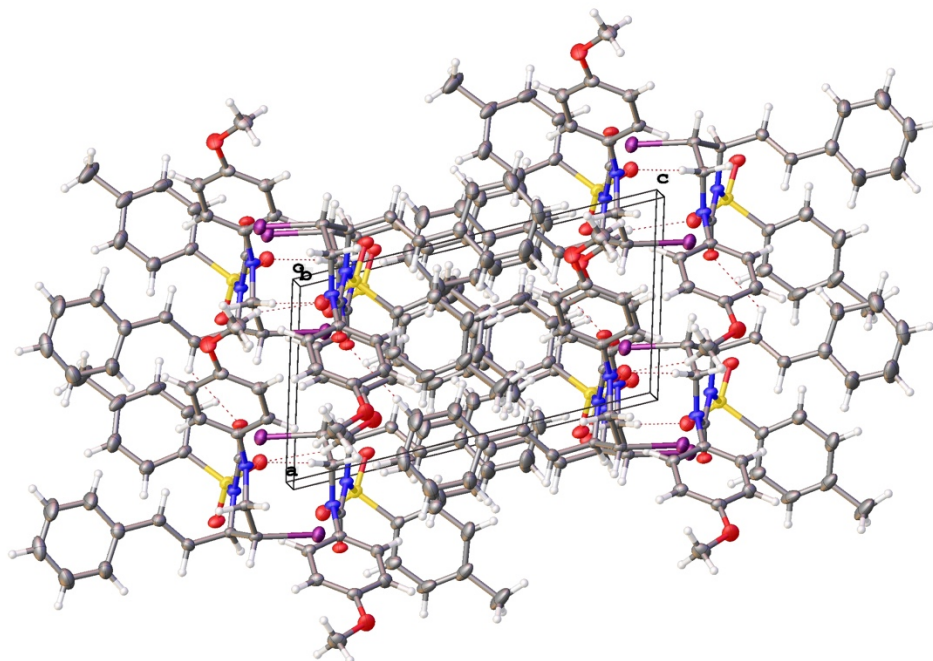
Cell plot, view along *b*.
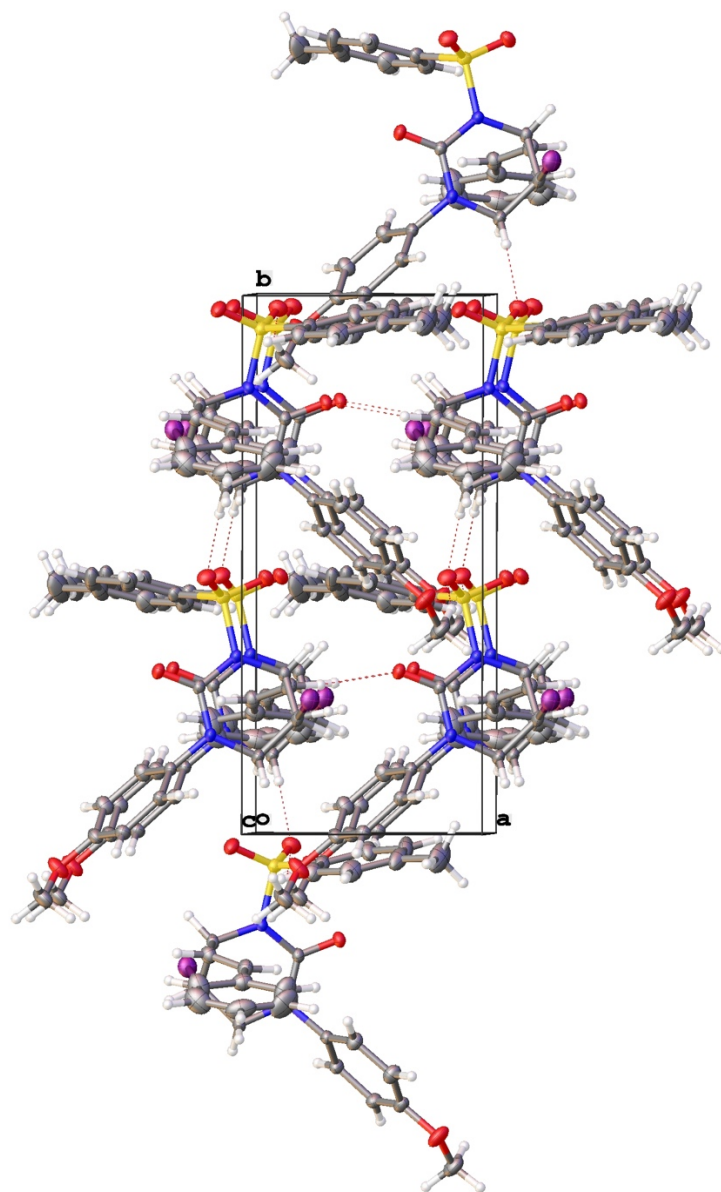
Cell plot, view along *c*.

Table 1. Crystal data and structure refinement for 16052.cif.

Empirical formula	C26 H25 I N2 O4 S
Formula weight	588.44
Crystal color, shape, size	light yellow block, $0.32 \times 0.28 \times 0.23$ mm^3
Temperature	150(2) K
Wavelength	0.71073 Å
Crystal system, space group	Monoclinic, P2$_1$

Unit cell dimensions
$a = 6.8374(3)$ Å $\alpha = 90°$.
$b = 14.8665(6)$ Å $\beta = 105.7165(15)°$.
$c = 12.6176(6)$ Å $\gamma = 90°$.

Volume	1234.61(9) Å^3
Z	2
Density (calculated)	1.583 Mg/m^3
Absorption coefficient	1.417 mm^{-1}
F(000)	592

Data collection

Diffractometer	APEX II Kappa Duo, Bruker
Theta range for data collection	2.165 to 30.103°.
Index ranges	-9<=h<=9, -20<=k<=19, -17<=l<=17
Reflections collected	25107
Independent reflections	7073 [R(int) = 0.0321]
Observed Reflections	6970
Completeness to theta = 25.242°	99.9 %

Solution and Refinement

Absorption correction	Semi-empirical from equivalents
Max. and min. transmission	0.7460 and 0.6371
Solution	Intrinsic methods
Refinement method	Full-matrix least-squares on F^2
Weighting scheme	$w = [\sigma^2Fo^2 + AP^2 + BP]^{-1}$, with
	$P = (Fo^2 + 2 Fc^2)/3$, A = 0.0241, B = 0.1906
Data / restraints / parameters	7073 / 1 / 309
Goodness-of-fit on F^2	1.082
Final R indices [I>2sigma(I)]	R1 = 0.0200, wR2 = 0.0526
R indices (all data)	R1 = 0.0204, wR2 = 0.0527
Absolute structure parameter	0.009(5)
Largest diff. peak and hole	0.655 and -0.290 e.Å^{-3}

Goodness-of-fit = $[\Sigma[w(F_o^2 - F_c^2)^2]/N_{observns} - N_{params})]^{1/2}$, all data.

$R1 = \Sigma(|F_o| - |F_c|) / \Sigma |F_o|$. $wR2 = [\Sigma[w(F_o^2 - F_c^2)^2] / \Sigma [w(F_o^2)^2]]^{1/2}$.

Table 2. Atomic coordinates ($\times 10^4$) and equivalent isotropic displacement parameters ($\text{Å}^2 \times 10^3$) for 16052.cif. U(eq) is defined as one third of the trace of the orthogonalized U^{ij} tensor.

	x	y	z	U(eq)
I1	12885(1)	2505(1)	10896(1)	32(1)
S1	9104(1)	4395(1)	8262(1)	20(1)
O1	6446(2)	3024(1)	8613(1)	22(1)
O2	8470(3)	4768(1)	9156(2)	28(1)
O3	10886(3)	4753(1)	8014(2)	27(1)
O4	2248(3)	-629(2)	7735(2)	36(1)
N1	9669(3)	3298(1)	8505(2)	18(1)
N2	8622(3)	1837(1)	8836(2)	21(1)
C1	11685(3)	2977(2)	8437(2)	19(1)
C2	8144(3)	2728(1)	8656(2)	18(1)
C3	10610(3)	1441(2)	8880(2)	22(1)
C4	12257(3)	2148(2)	9172(2)	21(1)
C5	11792(4)	2740(2)	7295(2)	24(1)
C6	10217(3)	2490(2)	6468(2)	26(1)
C7	10271(4)	2246(2)	5348(2)	30(1)
C8	12063(5)	2155(2)	5040(2)	43(1)
C9	12034(6)	1900(3)	3970(3)	50(1)
C10	10202(6)	1749(2)	3194(2)	46(1)
C11	8422(7)	1848(3)	3488(3)	57(1)
C12	8450(5)	2089(3)	4559(3)	46(1)
C13	7050(4)	4444(2)	7070(2)	24(1)
C14	7387(4)	4281(2)	6049(2)	31(1)
C15	5749(5)	4306(2)	5113(2)	40(1)
C16	3800(5)	4531(2)	5184(3)	41(1)
C17	3538(4)	4723(2)	6220(3)	40(1)
C18	5133(4)	4669(2)	7166(2)	32(1)
C19	2024(5)	4556(4)	4168(3)	62(1)
C20	6953(3)	1210(1)	8608(2)	20(1)
C21	5730(4)	1136(2)	7538(2)	25(1)
C22	4153(4)	528(2)	7282(2)	28(1)
C23	3814(4)	-37(2)	8098(2)	24(1)
C24	5015(4)	33(2)	9174(2)	24(1)
C25	6586(3)	666(2)	9429(2)	22(1)
C26	1669(5)	-1187(2)	8518(3)	37(1)

Table 3. Bond lengths [Å] and angles [°] for 16052.cif.

I1-C4	2.166(2)	S1-O2	1.4255(19) S1-O3
1.4399(19)	S1-N1	1.6844(19)	S1-C13 1.759(2)
O1-C2	1.228(3)	O4-C23	1.365(3) O4-C26
1.425(4)	N1-C2	1.397(3)	N1-C1 1.483(3)
N2-C2	1.369(3)	N2-C20	1.441(3) N2-C3
1.468(3)	C1-C5	1.504(3)	C1-C4 1.528(3)
C1-H1	1.0000	C3-C4	1.511(3) C3-H3A
0.9900	C3-H3B	0.9900	C4-H4 1.0000 C5-C6
1.334(3)	C5-H5A	0.9500	C6-C7 1.469(3)
C6-H6	0.9500	C7-C12	1.387(4) C7-C8
1.389(4)	C8-C9	1.397(4)	C8-H8 0.9500 C9-C10
1.383(5)	C9-H9	0.9500	C10-C11 1.373(6)
C10-H10	0.9500	C11-C12	1.394(4) C11-
H11	0.9500	C12-H12	0.9500 C13-C18
1.390(4)	C13-C14	1.390(4)	C14-C15 1.391(4)
C14-H14A	0.9500	C15-C16	1.400(5) C15-
H15	0.9500	C16-C17	1.396(5) C16-
C19	1.509(4)	C17-C18	1.384(4) C17-
H17	0.9500	C18-H18	0.9500 C19-H19A
0.9800	C19-H19B	0.9800	C19-H19C 0.9800 C20-
C21	1.386(3)	C20-C25	1.389(3) C21-
C22	1.377(3)	C21-H21	0.9500 C22-C23
1.396(4)	C22-H22	0.9500	C23-C24 1.388(3)
C24-C25	1.399(3)	C24-H24	0.9500 C25-H25
0.9500	C26-H26B	0.9800	C26-H26C 0.9800 C26-
H26D	0.9800		
O2-S1-O3	119.03(12)	O2-S1-N1	109.69(10) O3-S1-
N1	103.34(10)	O2-S1-C13	108.48(12) O3-S1-
C13	108.95(11)	N1-S1-C13	106.65(11) C23-O4-
C26	118.9(2)	C2-N1-C1	123.53(18) C2-N1-
S1	117.97(14)	C1-N1-S1	118.22(15) C2-N2-
C20	116.88(18)	C2-N2-C3	124.87(19) C20-N2-
C3	115.04(18)	N1-C1-C5	114.72(18) N1-C1-
C4	108.30(17)	C5-C1-C4	108.74(18) N1-C1-
H1	108.3	C5-C1-H1	108.3 C4-C1-H1
108.3	O1-C2-N2	122.3(2)	O1-C2-N1
120.56(18)	N2-C2-N1	117.14(19)	N2-C3-C4
110.59(18)	N2-C3-H3A	109.5	C4-C3-H3A 109.5
N2-C3-H3B	109.5	C4-C3-H3B	109.5 H3A-C3-H3B
108.1	C3-C4-C1	111.20(18)	C3-C4-I1 110.30(15)
C1-C4-I1	111.11(16)	C3-C4-H4	108.0 C1-C4-H4
108.0	I1-C4-H4	108.0	C6-C5-C1 125.2(2)
C6-C5-H5A	117.4	C1-C5-H5A	117.4 C5-C6-C7

126.6(2)	C5-C6-H6 116.7	C7-C6-H6	116.7
C12-C7-C8	118.1(3)	C12-C7-C6	118.7(3) C8-C7-C6
123.2(2)	C7-C8-C9	120.9(3)	C7-C8-H8 119.5
C9-C8-H8	119.5	C10-C9-C8	120.1(3) C10-C9-H9
120.0	C8-C9-H9	120.0	C11-C10-C9 119.4(3)
C11-C10-H10	120.3	C9-C10-H10	120.3 C10-C11-C12
120.6(3)	C10-C11-H11	119.7	C12-C11-H11 119.7
C7-C12-C11	120.9(3)	C7-C12-H12	119.6 C11-C12-H12
119.6	C18-C13-C14	121.3(2)	C18-C13-S1
119.23(19)	C14-C13-S1	119.42(19)	C13-C14-C15 119.0(3)
C13-C14-H14A	120.5	C15-C14-H14A	120.5 C14-C15-C16
120.9(3)	C14-C15-H15	119.5	C16-C15-H15 119.5
C17-C16-C15	118.3(2)	C17-C16-C19	120.8(3) C15-C16-C19
120.8(3)	C18-C17-C16	121.7(3)	C18-C17-H17 119.2
C16-C17-H17	119.2	C17-C18-C13	118.7(3) C17-C18-H18
120.7	C13-C18-H18	120.7	C16-C19-H19A 109.5
C16-C19-H19B	109.5	H19A-C19-H19B	109.5 C16-C19-H19C
109.5	H19A-C19-H19C	109.5	H19B-C19-H19C 109.5
C21-C20-C25	119.8(2)	C21-C20-N2	118.8(2) C25-C20-N2
121.4(2)	C22-C21-C20	120.5(2)	C22-C21-H21 119.7
C20-C21-H21	119.7	C21-C22-C23	119.9(2) C21-C22-H22
120.1	C23-C22-H22	120.1	O4-C23-C24 125.4(2)
O4-C23-C22	114.4(2)	C24-C23-C22	120.3(2) C23-C24-C25
119.3(2)	C23-C24-H24	120.3	C25-C24-H24 120.3
C20-C25-C24	120.2(2)	C20-C25-H25	119.9 C24-C25-H25
119.9	O4-C26-H26B	109.5	O4-C26-H26C 109.5
H26B-C26-H26C	109.5	O4-C26-H26D	109.5 H26B-C26-H26D
109.5	H26C-C26-H26D	109.5	

Table 4. Anisotropic displacement parameters ($\text{Å}^2 \times 10^3$) for 16052.cif. The anisotropic displacement factor exponent takes the form: $-2\pi^2[\ h^2\ a^{*2}U^{11} + ... + 2\ h\ k\ a^*\ b^*\ U^{12}\ ]$

	U^{11}	U^{22}	U^{33}	U^{23}	U^{13}	U^{12}
I1	31(1)	40(1)	23(1)	2(1)	3(1)	2(1)
S1	18(1)	16(1)	24(1)	1(1)	2(1)	0(1)
O1	14(1)	22(1)	31(1)	3(1)	6(1)	3(1)
O2	31(1)	24(1)	29(1)	-4(1)	6(1)	3(1)
O3	21(1)	23(1)	36(1)	6(1)	4(1)	-4(1)
O4	35(1)	36(1)	36(1)	-7(1)	7(1)	-20(1)
N1	14(1)	16(1)	25(1)	2(1)	5(1)	2(1)
N2	12(1)	17(1)	32(1)	3(1)	5(1)	1(1)
C1	14(1)	22(1)	20(1)	3(1)	4(1)	2(1)
C2	14(1)	19(1)	20(1)	1(1)	3(1)	1(1)
C3	15(1)	19(1)	31(1)	2(1)	6(1)	3(1)
C4	14(1)	23(1)	27(1)	3(1)	5(1)	3(1)
C5	22(1)	26(1)	24(1)	2(1)	9(1)	3(1)
C6	21(1)	30(1)	26(1)	3(1)	7(1)	-2(1)
C7	35(1)	27(1)	26(1)	2(1)	7(1)	-1(1)
C8	41(2)	62(2)	27(1)	2(1)	9(1)	9(1)
C9	60(2)	60(2)	34(1)	3(1)	21(2)	14(2)
C10	79(3)	35(2)	27(1)	-5(1)	18(1)	-10(2)
C11	64(2)	71(2)	29(1)	-13(2)	2(1)	-26(2)
C12	42(2)	65(2)	29(1)	-9(1)	5(1)	-15(2)
C13	20(1)	22(1)	25(1)	6(1)	1(1)	-1(1)
C14	29(1)	33(1)	29(1)	6(1)	4(1)	1(1)
C15	43(2)	44(2)	25(1)	10(1)	-2(1)	-4(1)
C16	30(1)	45(2)	39(1)	19(1)	-8(1)	-10(1)
C17	19(1)	49(2)	49(2)	23(1)	1(1)	-1(1)
C18	23(1)	34(1)	36(1)	13(1)	4(1)	4(1)
C19	42(2)	78(3)	49(2)	29(2)	-18(2)	-15(2)
C20	14(1)	17(1)	28(1)	1(1)	6(1)	0(1)
C21	24(1)	28(1)	24(1)	1(1)	7(1)	-3(1)
C22	28(1)	30(1)	26(1)	-5(1)	6(1)	-6(1)
C23	21(1)	21(1)	31(1)	-6(1)	8(1)	-5(1)
C24	22(1)	20(1)	30(1)	3(1)	6(1)	-1(1)
C25	18(1)	20(1)	26(1)	4(1)	3(1)	0(1)
C26	34(2)	33(1)	47(2)	-5(1)	15(1)	-15(1)

Table 5. Hydrogen coordinates (× 10^4) and isotropic displacement parameters (Å^2 × 10 ^{3}) for 16052.cif.

	x	y	z	U(eq)
H1	12707	3459	8732	22
H3A	10574	1174	8157	26
H3B	10915	955	9438	26
H4	13522	1885	9047	25
H5A	13085	2770	7152	28
H6	8929	2469	6618	31
H8	13326	2268	5564	52
H9	13274	1831	3776	60
H10	10177	1579	2465	55
H11	7159	1750	2956	68
H12	7205	2148	4752	56
H14A	8716	4155	5991	37
H15	5955	4169	4416	48
H17	2233	4895	6277	49
H18	4921	4783	7868	38
H19A	2506	4444	3516	93
H19B	1376	5149	4106	93
H19C	1038	4092	4223	93
H21	5982	1508	6977	30
H22	3297	493	6552	34
H24	4771	-344	9733	29
H25	7404	725	10165	27
H26B	534	-1573	8138	56
H26C	1252	-810	9055	56
H26D	2825	-1562	8899	56

Table 6. Torsion angles [°] for 16052.cif.

Torsion angle	Value	Torsion angle	Value
O2-S1-N1-C2	58.97(19)	O3-S1-N1-C2	-173.11(16)
C13-S1-N1-C2	-58.33(19)	O2-S1-N1-C1	-126.91(17)
O3-S1-N1-C1	1.00(18)	C13-S1-N1-C1	115.79(17)
C2-N1-C1-C5	89.2(2)	S1-N1-C1-C5	-84.5(2)
C2-N1-C1-C4	-32.4(3)	S1-N1-C1-C4	153.82(16)
C20-N2-C2-O1	20.4(3)	C3-N2-C2-O1	179.1(2)
C20-N2-C2-N1	-158.67(19)	C3-N2-C2-N1	0.0(3)
C1-N1-C2-O1	-173.81(19)	S1-N1-C2-O1	0.0(3)
C1-N1-C2-N2	5.3(3)	S1-N1-C2-N2	179.03(16)
C2-N2-C3-C4	23.4(3)	C20-N2-C3-C4	-177.55(19)
N2-C3-C4-C1	-50.4(2)	N2-C3-C4-I1	73.3(2)
N1-C1-C4-C3	54.2(2)	C5-C1-C4-C3	-71.1(2)
N1-C1-C4-I1	-69.13(19)	C5-C1-C4-I1	165.61(15)
N1-C1-C5-C6	-25.1(3)	C4-C1-C5-C6	96.3(3)
C1-C5-C6-C7	-179.3(2)	C5-C6-C7-C12	-173.6(3)
C5-C6-C7-C8	6.9(5)	C12-C7-C8-C9	-1.0(5)
C6-C7-C8-C9	178.5(3)	C7-C8-C9-C10	1.1(6)
C8-C9-C10-C11	-0.3(6)	C9-C10-C11-C12	-0.6(6)
C8-C7-C12-C11	0.0(5)	C6-C7-C12-C11	-179.4(3)
C10-C11-C12-C7	0.7(6)	O2-S1-C13-C18	-10.5(2)
O3-S1-C13-C18	-141.5(2)	N1-S1-C13-C18	107.6(2)
O2-S1-C13-C14	167.8(2)	O3-S1-C13-C14	36.8(2)
N1-S1-C13-C14	-74.1(2)	C18-C13-C14-C15	-2.8(4)
S1-C13-C14-C15	178.9(2)	C13-C14-C15-C16	2.8(4)
C14-C15-C16-C17	-0.5(4)	C14-C15-C16-C19	-179.9(3)
C15-C16-C17-C18	-2.0(5)	C19-C16-C17-C18	177.5(3)
C16-C17-C18-C13	2.1(5)	C14-C13-C18-C17	0.4(4)
S1-C13-C18-C17	178.7(2)	C2-N2-C20-C21	62.9(3)
C3-N2-C20-C21	-97.9(2)	C2-N2-C20-C25	-118.9(2)
C3-N2-C20-C25	80.4(3)	C25-C20-C21-C22	0.0(4)
N2-C20-C21-C22	178.3(2)	C20-C21-C22-C23	-1.8(4)
C26-O4-C23-C24	4.5(4)	C26-O4-C23-C22	-175.0(2)
C21-C22-C23-O4	-178.1(2)	C21-C22-C23-C24	2.4(4)
O4-C23-C24-C25	179.4(2)	C22-C23-C24-C25	-1.1(4)
C21-C20-C25-C24	1.3(3)	N2-C20-C25-C24	-176.9(2)
C23-C24-C25-C20	-0.8(4)		

Table 7. Hydrogen bonds for 16052.cif [Å and °].

D-H...A	d(D-H)	d(H...A)	d(D...A)	<(DHA)
C3-H3B...O2#1	0.99	2.46	3.446(3)	177.4
C5-H5A...O1#2	0.95	2.55	3.194(3)	124.8
C26-H26B...I1#3	0.98	3.22	3.908(3)	128.6
C26-H26C...O2#3	0.98	2.37	3.285(4)	154.4
C26-H26D...I1#1	0.98	3.19	4.086(3)	152.6

Symmetry transformations used to generate equivalent atoms: #1 -x+2,y-1/2,-z+2, #2 x+1,y,z, #3 -x+1,y-1/2,-z+2

Appendix 4.4 DFT transition state structures and coordinates

Thomas Struble

DFT Calculations

Complex 178
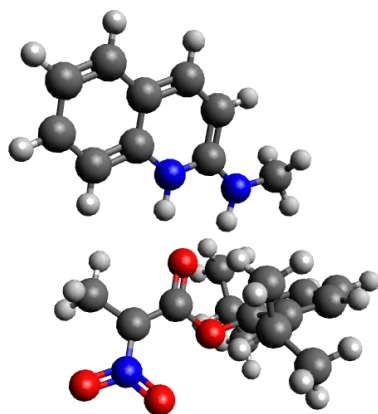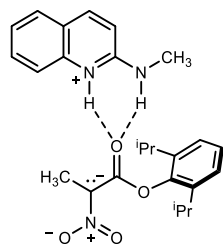
#T B3LYP/6-31G* opt freq=noraman scrf=(iefpcm,solvent=toluene,smd) temperature=253

Zero-point correction=   0.526909 (Hartree/Particle)
 Thermal correction to Energy=   0.551269
 Thermal correction to Enthalpy=   0.552070
 Thermal correction to Gibbs Free Energy=   0.473579
 Sum of electronic and zero-point Energies=   -1435.924142
 Sum of electronic and thermal Energies=   -1435.899781
 Sum of electronic and thermal Enthalpies=   -1435.898980
 Sum of electronic and thermal Free Energies=   -1435.977471

Charge = 0 Multiplicity = 1

C	3.22147	-2.74772	-0.03020
C	4.50697	-2.30705	0.08518
C	4.82750	-0.91499	0.05998
C	3.75909	0.00549	-0.09361
N	2.47157	-0.48121	-0.21312
C	2.15657	-1.80000	-0.18453
N	0.87479	-2.14950	-0.29801
C	0.39597	-3.52449	-0.28784

C	4.00853	1.38878	-0.12177
C	6.14494	-0.41911	0.18014
C	6.38597	0.94138	0.14979
C	5.31188	1.84175	-0.00088
H	2.98535	-3.80351	-0.00818
H	5.31420	-3.02547	0.20081
H	1.67766	0.17614	-0.34511
H	0.19520	-1.38416	-0.39017
H	0.80308	-4.09642	-1.12939
H	0.65376	-4.03287	0.64806
H	-0.68999	-3.49610	-0.37643
H	3.18265	2.08319	-0.23756
H	6.96093	-1.12715	0.29624
H	7.39933	1.31950	0.24197
H	5.50561	2.91015	-0.02260
O	-1.10850	4.94254	-0.57989
N	-1.49548	3.77466	-0.31759
O	-2.58996	3.56935	0.25183
C	-0.62366	2.73054	-0.66750
C	-0.91030	1.36924	-0.46688
C	0.68520	3.15423	-1.26990
O	-2.20093	1.03590	-0.14448
C	-2.50900	-0.27273	0.21331
O	-0.06037	0.44271	-0.61207
C	-2.95948	-1.15754	-0.78210
C	-3.36484	-2.43662	-0.37362
C	-3.32917	-2.80970	0.96966
C	-2.89742	-1.89983	1.93473
C	-2.49076	-0.60681	1.58058
C	-2.04962	0.40910	2.63008
C	-3.02042	0.48226	3.82146
C	-0.61295	0.12742	3.11160
C	-3.02303	-0.74522	-2.24902
C	-2.00845	-1.52951	-3.10221
C	-4.44656	-0.88089	-2.82023
H	1.32847	3.68880	-0.55568
H	1.22421	2.27813	-1.63862
H	0.52817	3.83825	-2.11133
H	-3.72444	-3.14336	-1.11739
H	-3.65205	-3.80450	1.26652
H	-2.89172	-2.19343	2.98089
H	-2.05484	1.39144	2.14814
H	-2.72321	1.29223	4.49839
H	-4.04537	0.68309	3.48976

H	-3.03084	-0.44537	4.40681
H	-0.28952	0.89385	3.82676
H	0.09447	0.12743	2.27506
H	-0.54514	-0.84752	3.61164
H	-2.75239	0.31300	-2.30493
H	-2.03988	-1.19014	-4.14497
H	-0.98743	-1.38306	-2.73263
H	-2.22425	-2.60553	-3.09709
H	-4.47823	-0.50918	-3.85171
H	-5.16780	-0.30228	-2.23214
H	-4.78456	-1.92442	-2.83455

Complex 179
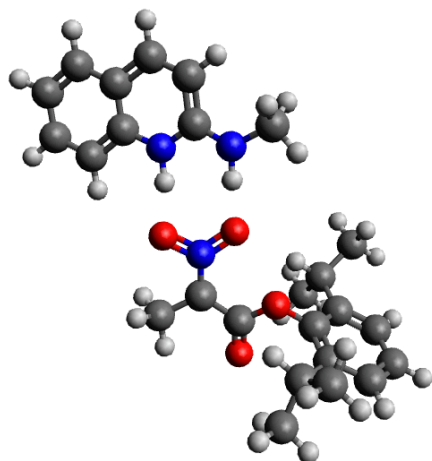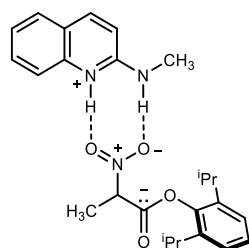
#T B3LYP/6-31G* opt freq=noraman scrf=(iefpcm,solvent=toluene,smd) temperature=253

Zero-point correction=	0.526785 (Hartree/Particle)
Thermal correction to Energy=	0.550880
Thermal correction to Enthalpy=	0.551681
Thermal correction to Gibbs Free Energy=	0.474758
Sum of electronic and zero-point Energies=	-1435.942964
Sum of electronic and thermal Energies=	-1435.918869
Sum of electronic and thermal Enthalpies=	-1435.918068
Sum of electronic and thermal Free Energies=	-1435.994991

Charge = 0 Multiplicity = 1

C	-4.74524	2.10082	1.35839
C	-5.97103	1.65792	0.95525
C	-6.12486	0.44069	0.22194
C	-4.95030	-0.29756	-0.07417
N	-3.72943	0.18447	0.34510
C	-3.57325	1.33631	1.03804
N	-2.33589	1.69011	1.38281
C	-1.99547	2.90010	2.11350
C	-5.02662	-1.50947	-0.78643
C	-7.37225	-0.05654	-0.21781
C	-7.44307	-1.24619	-0.91801
C	-6.26525	-1.96967	-1.19920
H	-4.63491	3.02498	1.91117
H	-6.85853	2.23873	1.19265
H	-2.87066	-0.40580	0.15563
H	-1.56131	1.10428	1.01469
H	-2.25766	3.80511	1.55184
H	-2.48942	2.93254	3.09107
H	-0.91612	2.89463	2.27438
H	-4.11589	-2.05991	-1.00217
H	-8.27126	0.51163	0.00602
H	-8.40306	-1.62574	-1.25429
H	-6.32847	-2.90399	-1.74953
O	-1.65486	-1.50306	-0.03322
N	-0.47139	-0.98705	-0.13695
O	-0.31725	0.25411	0.12942
C	0.52362	-1.79219	-0.55737
C	1.92142	-1.38818	-0.64255
C	0.14731	-3.18008	-0.98795
O	2.24954	-0.26023	0.06601
C	3.55796	0.22701	-0.02966
O	2.76202	-2.03241	-1.25627
C	4.52077	-0.22571	0.88671
C	5.79551	0.35267	0.81779
C	6.08837	1.34299	-0.11740
C	5.10409	1.77955	-1.00285
C	3.81438	1.23387	-0.97655
C	2.73579	1.68679	-1.95506
C	2.63840	3.21750	-2.06938
C	2.95406	1.04442	-3.33956
C	4.20831	-1.31642	1.90478
C	4.90306	-2.63878	1.52627

C	4.56477	-0.89340	3.34082
H	-0.61707	-3.16497	-1.77498
H	1.03412	-3.68891	-1.36852
H	-0.26815	-3.76481	-0.15753
H	6.56808	0.02228	1.50698
H	7.08358	1.77892	-0.15356
H	5.34109	2.55642	-1.72459
H	1.77680	1.32834	-1.56817
H	1.79278	3.49342	-2.71136
H	2.48294	3.68453	-1.08969
H	3.53966	3.65838	-2.51208
H	2.14056	1.31578	-4.02439
H	2.98906	-0.04766	-3.26624
H	3.89742	1.38266	-3.78693
H	3.12843	-1.49155	1.87792
H	4.62955	-3.43433	2.23107
H	4.61035	-2.95616	0.52053
H	5.99529	-2.53457	1.54750
H	4.25802	-1.67014	4.05213
H	4.05975	0.03834	3.62163
H	5.64336	-0.74111	3.46740

Complex 180
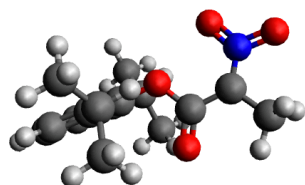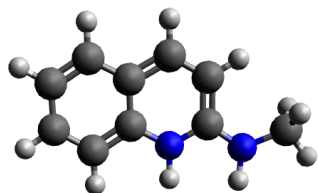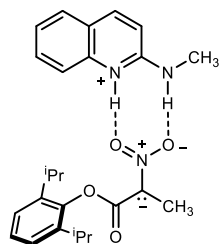
#T B3LYP/6-31G* opt freq=noraman scrf=(iefpcm,solvent=toluene,smd) temperature=253

Zero-point correction=	0.526437 (Hartree/Particle)	
Thermal correction to Energy=	0.550640	
Thermal correction to Enthalpy=	0.551441	

Thermal correction to Gibbs Free Energy=   0.474046
Sum of electronic and zero-point Energies=   -1435.943674
Sum of electronic and thermal Energies=   -1435.919471
Sum of electronic and thermal Enthalpies=   -1435.918670
Sum of electronic and thermal Free Energies=   -1435.996065

Charge = 0 Multiplicity = 1

C	-5.55741	-0.15058	0.16332
C	-5.61135	1.21254	0.21267
C	-4.42616	2.01083	0.24041
C	-3.18120	1.33139	0.22864
N	-3.16853	-0.04505	0.18858
C	-4.28266	-0.80973	0.14284
N	-4.12236	-2.13279	0.08274
C	-5.21073	-3.08992	-0.03372
C	-1.96996	2.04884	0.25343
C	-4.43063	3.42355	0.28034
C	-3.24007	4.12524	0.30512
C	-2.01128	3.43178	0.29169
H	-6.46018	-0.74740	0.13379
H	-6.57646	1.71224	0.22524
H	-2.23049	-0.53634	0.23148
H	-3.15453	-2.47931	-0.06221
H	-5.90485	-3.01546	0.81053
H	-5.77197	-2.96155	-0.96783
H	-4.77293	-4.08960	-0.02891
H	-1.02861	1.50752	0.23930
H	-5.38420	3.94489	0.28969
H	-3.24660	5.21057	0.33452
H	-1.07980	3.99021	0.31012
O	-1.55570	-2.96483	-0.67070
N	-0.56156	-2.21333	-0.35640
O	-0.76775	-1.21832	0.43485
C	0.65438	-2.52862	-0.84570
C	1.85650	-1.72949	-0.65232
C	0.75584	-3.80258	-1.63266
O	1.66091	-0.47625	-0.12437
C	2.78856	0.31539	0.12201
O	2.97081	-2.12116	-0.97517
C	3.34322	0.28753	1.41308
C	4.42010	1.14574	1.66937
C	4.90930	2.00222	0.68418
C	4.32354	2.01677	-0.57990

C	3.24673	1.17507	-0.88934
C	2.62528	1.17721	-2.28176
C	2.20002	2.58611	-2.73171
C	3.57648	0.52912	-3.30629
C	2.81349	-0.66684	2.47827
C	3.73184	-1.89866	2.60852
C	2.61120	0.01566	3.84202
H	0.15762	-3.76162	-2.55212
H	1.79890	-3.97787	-1.89948
H	0.38640	-4.65945	-1.05598
H	4.88147	1.14391	2.65300
H	5.74670	2.65989	0.90333
H	4.70998	2.68797	-1.34233
H	1.71940	0.56449	-2.24066
H	1.69579	2.53697	-3.70465
H	1.50597	3.04274	-2.01606
H	3.05914	3.25861	-2.84125
H	3.10547	0.48395	-4.29647
H	3.83534	-0.49022	-3.00250
H	4.50656	1.10328	-3.40367
H	1.83227	-1.01581	2.14093
H	3.31932	-2.61430	3.33101
H	3.84506	-2.40936	1.64651
H	4.73192	-1.60936	2.95573
H	2.14534	-0.68351	4.54712
H	1.95960	0.89341	3.75881
H	3.55912	0.34197	4.28656

Anthracenyl Nitroester Complex 1
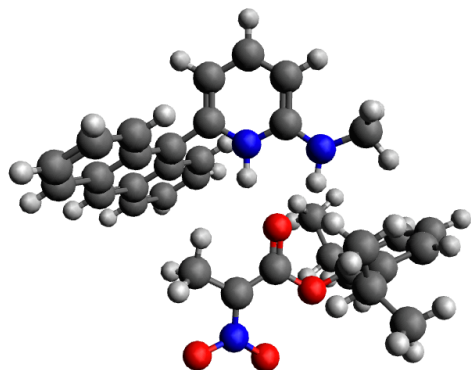
#T B3LYP/6-31G* opt freq=noraman scrf=(iefpcm,solvent=toluene,smd) temperature=253

Zero-point correction=   0.654873 (Hartree/Particle)
Thermal correction to Energy=   0.684399
Thermal correction to Enthalpy=   0.685200
Thermal correction to Gibbs Free Energy=   0.596055
Sum of electronic and zero-point Energies=   -1820.486380
Sum of electronic and thermal Energies=   -1820.456854
Sum of electronic and thermal Enthalpies=   -1820.456053
Sum of electronic and thermal Free Energies=   -1820.545198

Charge = 0 Multiplicity = 1

C	0.65589	4.21755	0.38371
C	2.01131	4.36498	0.57171
C	2.87683	3.25275	0.54546
C	2.35114	1.99833	0.32120
N	1.00207	1.87063	0.12771
C	0.12258	2.92217	0.15391
C	3.18403	0.76199	0.29094
C	3.95328	0.47122	-0.86038
C	4.79267	-0.70592	-0.86157
C	4.82376	-1.53013	0.26796
C	4.06754	-1.24772	1.41023
C	3.22245	-0.07546	1.43062
C	3.93453	1.28006	-2.04223
C	4.69165	0.95153	-3.13719
C	5.52124	-0.20606	-3.13251
C	5.56552	-1.01068	-2.02574
C	4.11280	-2.09572	2.56096
C	3.37786	-1.80608	3.67918
C	2.55499	-0.64390	3.70833
C	2.48100	0.19442	2.62577
N	-1.17361	2.66250	-0.03768

C	-2.20703	3.68601	-0.03724
H	-0.01118	5.06915	0.40564
H	2.41958	5.35586	0.74856
H	3.94239	3.36351	0.70270
H	0.59063	0.93764	-0.07006
H	5.45449	-2.41608	0.25805
H	3.30580	2.16384	-2.07154
H	4.65705	1.57887	-4.02364
H	6.11044	-0.44805	-4.01236
H	6.18740	-1.90193	-2.01006
H	4.74800	-2.97711	2.52470
H	3.41781	-2.45726	4.54760
H	1.98099	-0.41935	4.60310
H	1.85176	1.07724	2.67609
H	-1.43499	1.68033	-0.19226
H	-2.22989	4.23290	0.91283
H	-2.06483	4.40233	-0.85554
H	-3.16742	3.18834	-0.17115
O	-2.11909	-3.95720	-0.91246
N	-0.98072	-3.59644	-1.28038
O	-0.16509	-4.41892	-1.77202
C	-0.53551	-2.26826	-1.15823
C	0.86900	-2.01660	-1.62403
C	-3.48628	-0.47914	0.05349
C	-3.69523	-0.29309	1.43232
C	-4.64383	0.66212	1.82069
C	-5.36809	1.38519	0.87371
C	-5.15733	1.15858	-0.48646
C	-4.21756	0.21635	-0.92764
C	-2.91167	-1.09899	2.46309
C	-1.82044	-0.23468	3.12318
C	-3.82176	-1.74443	3.52223
C	-4.00187	-0.04824	-2.41437
C	-5.31763	-0.36978	-3.14536
C	-3.26430	1.12181	-3.09413
O	-2.63223	-1.49617	-0.35618
C	-1.31728	-1.22012	-0.64484
O	-0.88662	-0.04436	-0.45626
H	1.07833	-0.94528	-1.61315
H	1.61610	-2.52442	-0.99994
H	1.01762	-2.38566	-2.64527
H	-4.82675	0.83369	2.87813
H	-6.10712	2.11480	1.19546
H	-5.74215	1.71074	-1.21759

H	-2.41203	-1.91101	1.92644
H	-2.25853	0.59702	3.69013
H	-1.21782	-0.83389	3.81714
H	-1.14854	0.18438	2.36688
H	-3.22966	-2.38178	4.19008
H	-4.59193	-2.37068	3.05802
H	-4.32580	-0.99603	4.14574
H	-3.36313	-0.93205	-2.49777
H	-5.11285	-0.64452	-4.18714
H	-5.84041	-1.20920	-2.67336
H	-6.00166	0.48773	-3.16020
H	-3.85559	2.04595	-3.05610
H	-3.07316	0.89329	-4.15000
H	-2.29865	1.31295	-2.61327

Anthracenyl Nitroester Complex 2
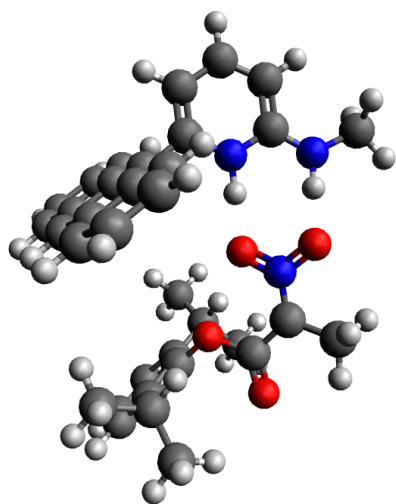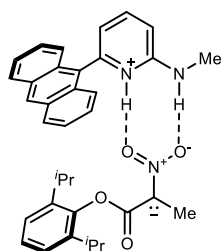
#T B3LYP/6-31G* opt freq=noraman scrf=(iefpcm,solvent=toluene,smd) temperature=253

Zero-point correction=	0.654352 (Hartree/Particle)
Thermal correction to Energy=	0.683716
Thermal correction to Enthalpy=	0.684517
Thermal correction to Gibbs Free Energy=	0.596798
Sum of electronic and zero-point Energies=	-1820.505623
Sum of electronic and thermal Energies=	-1820.476258

Sum of electronic and thermal Enthalpies=   -1820.475457

Sum of electronic and thermal Free Energies=   -1820.563177

Charge = 0 Multiplicity = 1

C	-5.33918	1.39811	-0.93059
C	-5.66547	0.06514	-1.04868
C	-4.73846	-0.94547	-0.72393
C	-3.47793	-0.58261	-0.29359
N	-3.16822	0.74246	-0.18506
C	-4.04322	1.75513	-0.47335
C	-2.41823	-1.56571	0.07228
C	-2.07701	-1.74495	1.43458
C	-1.06169	-2.71271	1.78191
C	-0.44105	-3.45175	0.77011
C	-0.77377	-3.28322	-0.57729
C	-1.78462	-2.31763	-0.94567
C	-2.71054	-1.03022	2.50199
C	-2.35187	-1.24250	3.80813
C	-1.33976	-2.18592	4.14471
C	-0.71656	-2.90060	3.15728
C	-0.12738	-4.04467	-1.60084
C	-0.44881	-3.87004	-2.92003
C	-1.43635	-2.91233	-3.28918
C	-2.07887	-2.16095	-2.33889
N	-3.60713	3.00659	-0.31128
C	-4.41273	4.18383	-0.58238
H	-6.05255	2.17613	-1.17045
H	-6.65915	-0.21173	-1.38952
H	-4.99648	-1.99414	-0.80286
H	-2.17260	1.02352	0.04319
H	0.32129	-4.17969	1.03862
H	-3.48650	-0.30731	2.27410
H	-2.84598	-0.68505	4.59906
H	-1.06923	-2.33487	5.18620
H	0.05435	-3.62814	3.39853
H	0.63057	-4.76492	-1.30344
H	0.04927	-4.45284	-3.68961
H	-1.67830	-2.77316	-4.33935
H	-2.82039	-1.43169	-2.64642
H	-2.69386	3.13506	0.16948
H	-4.74080	4.21344	-1.62803
H	-5.29703	4.23859	0.06606
H	-3.79152	5.06091	-0.39215

O	-0.58070	1.52909	0.00335
N	-0.31736	2.56144	0.72159
O	-1.30032	3.25168	1.18782
C	0.93419	2.98395	0.98838
C	1.06604	4.29094	1.71537
C	3.10107	0.32550	-0.34533
C	3.29235	0.33370	-1.73765
C	4.38059	-0.38907	-2.24295
C	5.22979	-1.09807	-1.39507
C	4.99724	-1.10313	-0.02122
C	3.92402	-0.39460	0.53543
C	2.36608	1.12255	-2.65780
C	3.04399	2.42278	-3.13286
C	1.87282	0.28994	-3.85370
C	3.68041	-0.39494	2.04067
C	3.59736	-1.81956	2.61686
C	4.74855	0.43822	2.77464
O	1.98099	0.99268	0.16323
C	2.14721	2.29111	0.57608
O	3.25458	2.81126	0.62777
H	2.12281	4.54778	1.80160
H	0.54625	5.09955	1.18588
H	0.62926	4.24235	2.72076
H	4.56571	-0.39614	-3.31369
H	6.07070	-1.65103	-1.80620
H	5.66141	-1.66335	0.63165
H	1.48481	1.39937	-2.07129
H	3.93118	2.20759	-3.74226
H	2.35374	3.01767	-3.74465
H	3.36181	3.03636	-2.28310
H	1.14992	0.86812	-4.44258
H	1.37756	-0.63028	-3.52347
H	2.69118	0.00961	-4.52801
H	2.71100	0.08157	2.21687
H	3.34750	-1.78248	3.68446
H	2.82530	-2.41016	2.11033
H	4.54849	-2.35698	2.52135
H	5.74888	0.00594	2.64502
H	4.53687	0.47352	3.85094
H	4.76800	1.46419	2.39439

Anthracenyl Nitroester Complex 3
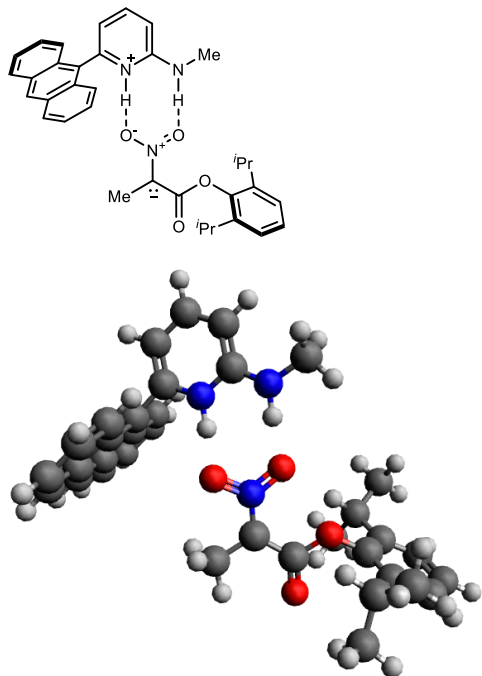
#T B3LYP/6-31G* opt freq=noraman scrf=(iefpcm,solvent=toluene,smd) temperature=253

Zero-point correction=   0.654001 (Hartree/Particle)
 Thermal correction to Energy=   0.683538
 Thermal correction to Enthalpy=   0.684339
 Thermal correction to Gibbs Free Energy=   0.594663
 Sum of electronic and zero-point Energies=   -1820.505568
 Sum of electronic and thermal Energies=   -1820.476031
 Sum of electronic and thermal Enthalpies=   -1820.475229
 Sum of electronic and thermal Free Energies=   -1820.564906

Charge = 0 Multiplicity = 1

C	-2.78131	-2.82598	-3.09405
C	-4.09662	-2.85762	-2.68671
C	-4.56692	-2.00251	-1.66938
C	-3.68557	-1.11812	-1.08193
N	-2.38399	-1.10326	-1.49060
C	-1.88417	-1.92022	-2.46813
C	-4.09046	-0.13426	-0.03470
C	-4.31961	1.21098	-0.40789
C	-4.75910	2.15283	0.59597
C	-4.94877	1.71674	1.91092
C	-4.72123	0.38964	2.28836

C	-4.27831	-0.56609	1.29809
C	-4.15495	1.68939	-1.74747
C	-4.39497	3.00099	-2.06578
C	-4.82019	3.92818	-1.07179
C	-4.99751	3.51219	0.22037
C	-4.91550	-0.04340	3.63757
C	-4.68231	-1.34218	4.00254
C	-4.23534	-2.28435	3.03214
C	-4.03920	-1.91142	1.72744
N	-0.58875	-1.79579	-2.76839
C	0.09033	-2.61322	-3.75883
H	-2.41730	-3.48281	-3.87365
H	-4.78442	-3.55237	-3.16053
H	-5.60288	-2.01615	-1.35416
H	-1.71350	-0.40571	-1.05236
H	-5.28192	2.43001	2.66155
H	-3.83228	1.00261	-2.52280
H	-4.25958	3.34014	-3.08914
H	-5.00271	4.96333	-1.34623
H	-5.32414	4.20769	0.98938
H	-5.25082	0.68851	4.36814
H	-4.83084	-1.65938	5.03091
H	-4.04405	-3.31069	3.33350
H	-3.69260	-2.64464	1.00670
H	-0.00321	-1.22800	-2.12369
H	0.06579	-3.68054	-3.50287
H	-0.34636	-2.47962	-4.75545
H	1.13258	-2.29135	-3.79464
O	0.96204	-0.58167	-0.84191
N	0.50633	0.49230	-0.31654
O	-0.72862	0.81210	-0.53259
C	1.22881	1.30362	0.48111
C	0.50116	2.44049	1.13844
C	4.64776	-0.03332	0.21381
C	5.66289	0.78587	-0.30492
C	6.98805	0.40102	-0.05969
C	7.28165	-0.75294	0.66358
C	6.24861	-1.55273	1.15034
C	4.90737	-1.21364	0.93232
C	5.34797	2.05584	-1.08780
C	5.70597	3.31249	-0.27174
C	6.03245	2.07547	-2.46643
C	3.76614	-2.06758	1.47599
C	3.97802	-3.57220	1.23797

C	3.53211	-1.77482	2.97199
O	3.31287	0.26902	-0.07580
C	2.64521	1.12051	0.76830
O	3.22126	1.71503	1.67032
H	1.18450	2.96078	1.81136
H	0.11545	3.15622	0.40142
H	-0.36321	2.08637	1.71361
H	7.79973	1.01601	-0.43957
H	8.31647	-1.03287	0.84406
H	6.48802	-2.45374	1.70817
H	4.26808	2.07494	-1.26373
H	6.78320	3.36294	-0.06919
H	5.42622	4.22046	-0.82112
H	5.17698	3.31471	0.68632
H	5.73142	2.96957	-3.02642
H	5.75863	1.19718	-3.06283
H	7.12570	2.09473	-2.38093
H	2.86027	-1.77773	0.93427
H	3.08762	-4.13071	1.55201
H	4.15461	-3.79011	0.17808
H	4.82674	-3.96793	1.80872
H	4.40698	-2.05781	3.57143
H	2.66968	-2.34063	3.34694
H	3.34101	-0.70985	3.14141

Complex 182
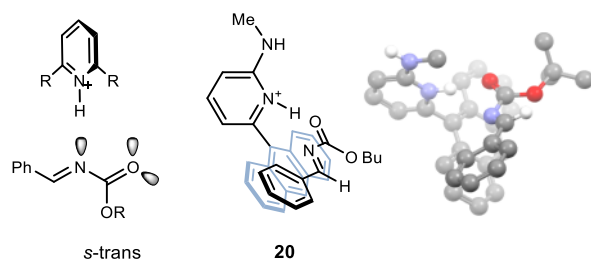
#T B3LYP/6-31G* opt freq=noraman scrf=(iefpcm,solvent=toluene,smd) temperature=253

Zero-point correction=	0.573580 (Hartree/Particle)
Thermal correction to Energy=	0.598832
Thermal correction to Enthalpy=	0.599633
Thermal correction to Gibbs Free Energy=	0.520071
Sum of electronic and zero-point Energies=	-1552.738392
Sum of electronic and thermal Energies=	-1552.713141
Sum of electronic and thermal Enthalpies=	-1552.712339
Sum of electronic and thermal Free Energies=	-1552.791901

Charge = 1 Multiplicity = 1

C	-0.65619	-2.61273	-2.50019
C	-1.31356	-3.87015	-2.54262
C	-2.18710	-4.21448	-1.54136
C	-2.43715	-3.33001	-0.46965
C	-1.80547	-2.10981	-0.44060
N	-0.93568	-1.77876	-1.45860
N	0.21911	-2.25683	-3.45245
C	1.02975	-1.04686	-3.49224
H	-0.51714	-0.82863	-1.42506
C	-2.00837	-1.11739	0.65472
C	-3.11388	-0.23798	0.59735
C	-3.32450	0.69127	1.68430
C	-2.43816	0.69646	2.76647
C	-1.34811	-0.17734	2.83330
C	-1.12504	-1.11757	1.75883
C	-4.03551	-0.20871	-0.49815
C	-5.09180	0.66563	-0.51048
C	-5.29993	1.57611	0.56509
C	-4.43963	1.58558	1.63035
C	-0.45870	-0.17478	3.95351
C	0.59092	-1.05089	4.02323
C	0.80769	-1.98597	2.97089
C	-0.01603	-2.01606	1.87466
H	0.34912	-2.93023	-4.19555
H	-1.10094	-4.53865	-3.36983
H	-2.68527	-5.17876	-1.57097
H	-3.11713	-3.59578	0.33003
H	0.41470	-0.15621	-3.65335
H	1.59519	-0.92467	-2.56286
H	1.73175	-1.14732	-4.32106
H	-2.60440	1.39690	3.58181
H	-3.89633	-0.89313	-1.32905
H	-5.78052	0.66706	-1.35083
H	-6.14389	2.25907	0.53375
H	-4.58702	2.27472	2.45800
H	-0.64081	0.53894	4.75283
H	1.25799	-1.04310	4.88030
H	1.63619	-2.68515	3.04234
H	0.16554	-2.74216	1.08864
N	1.83393	0.61006	-0.39367
C	3.03508	1.07704	-0.30385
H	3.26111	2.11310	-0.57512

C	0.80955	1.45813	-0.83918
O	1.01515	2.74904	-0.59843
O	-0.19196	0.98854	-1.37888
C	0.10991	3.83491	-1.08514
C	-1.28295	3.66945	-0.47946
C	0.79775	5.08946	-0.54832
C	0.09486	3.82285	-2.61352
C	4.16673	0.27271	0.13656
C	5.44314	0.86338	0.15779
C	6.55308	0.12660	0.56441
C	6.39604	-1.20556	0.95400
C	5.12818	-1.80209	0.93847
C	4.01870	-1.07100	0.53263
H	-1.87560	4.56435	-0.69911
H	-1.80255	2.80318	-0.89075
H	-1.22191	3.56449	0.60895
H	0.23765	5.97864	-0.85506
H	1.81771	5.17600	-0.93758
H	0.84351	5.07276	0.54550
H	1.11235	3.89597	-3.01344
H	-0.37796	2.91850	-3.00339
H	-0.47210	4.68729	-2.97578
H	5.55706	1.90121	-0.14536
H	7.53613	0.58773	0.57847
H	7.26059	-1.78224	1.27087
H	5.01369	-2.83811	1.24441
H	3.03040	-1.51872	0.51890

Complex 183

s-cis   **21**

#T B3LYP/6-31G* opt freq=noraman scrf=(iefpcm,solvent=toluene,smd) temperature=253

Zero-point correction=   0.573880 (Hartree/Particle)
  Thermal correction to Energy=   0.598986
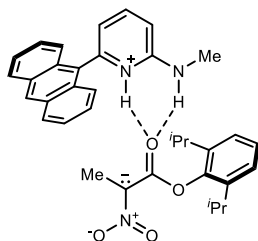 Thermal correction to Enthalpy=   0.599787

Thermal correction to Gibbs Free Energy=   0.521033
Sum of electronic and zero-point Energies=   -1552.731752
Sum of electronic and thermal Energies=   -1552.706645
Sum of electronic and thermal Enthalpies=   -1552.705844
Sum of electronic and thermal Free Energies=   -1552.784598

Charge = 1 Multiplicity = 1

C	0.27248	-1.28358	3.03242
C	0.45700	-0.68710	4.30811
C	0.42274	0.67879	4.43336
C	0.19276	1.49799	3.30633
C	0.02517	0.91899	2.07198
N	0.08766	-0.45772	1.96079
N	0.28513	-2.61818	2.89204
C	0.03590	-3.40199	1.68746
H	0.05415	-0.85473	1.00322
C	-0.25966	1.71094	0.83999
C	-1.60722	1.96230	0.48986
C	-1.88801	2.75188	-0.68772
C	-0.82715	3.24650	-1.45307
C	0.50705	3.03134	-1.09257
C	0.80775	2.25610	0.08993
C	-2.71816	1.50042	1.26705
C	-4.00744	1.80170	0.90777
C	-4.28098	2.57122	-0.25992
C	-3.24822	3.02659	-1.03547
C	1.58285	3.57713	-1.86095
C	2.88534	3.38950	-1.48247
C	3.18460	2.63993	-0.30917
C	2.18345	2.08811	0.44834
H	0.47403	-3.13421	3.74150
H	0.61481	-1.33477	5.16372
H	0.56112	1.13286	5.40985
H	0.13898	2.57567	3.39818
H	-0.79477	-2.98527	1.11419
H	0.92077	-3.45131	1.04478
H	-0.22789	-4.41349	2.00188
H	-1.04601	3.83308	-2.34234
H	-2.53617	0.91834	2.16491
H	-4.83328	1.45404	1.52240
H	-5.30953	2.79647	-0.52611
H	-3.44192	3.61899	-1.92592
H	1.33963	4.15335	-2.74995

H	3.69491	3.81385	-2.06911
H	4.22112	2.50195	-0.01457
H	2.43383	1.52147	1.33912
N	0.36412	-1.44101	-0.96438
C	1.40603	-1.45295	-1.73147
H	1.26314	-1.54113	-2.81300
C	-0.86629	-1.61116	-1.67923
O	-1.83240	-1.88270	-0.79394
O	-0.99770	-1.53210	-2.88437
C	-3.19723	-2.29191	-1.24316
C	-3.09081	-3.59557	-2.03635
C	-3.92792	-2.51453	0.08067
C	-3.85442	-1.16999	-2.04836
C	2.79022	-1.37272	-1.28535
C	3.78668	-1.25441	-2.27269
C	5.13082	-1.17427	-1.91642
C	5.49629	-1.22803	-0.56965
C	4.51559	-1.36056	0.42148
C	3.17279	-1.42826	0.06901
H	-4.09731	-3.96303	-2.26395
H	-2.55909	-3.45102	-2.97901
H	-2.57531	-4.36581	-1.45164
H	-4.96344	-2.81113	-0.11428
H	-3.94114	-1.59768	0.67878
H	-3.45183	-3.30876	0.66586
H	-3.86258	-0.23419	-1.48071
H	-3.34423	-1.00430	-2.99806
H	-4.89427	-1.44532	-2.25737
H	3.49758	-1.22069	-3.31991
H	5.89131	-1.07754	-2.68545
H	6.54466	-1.17468	-0.28959
H	4.80534	-1.41279	1.46714
H	2.41376	-1.53603	0.83451

Full catalyst calculations with unsymmetric catalyst 2

transition state	opt WB97X-D/ 6-31g*	SP WB97X-D/ 6-311+g**	SP M062x/ 6-311+g**
syn-(S,R)	0	0	0
anti-(R,R)	0.87	3.9	2.9

Starting Materials	opt WB97X-D/ 6-31g*	SP WB97X-D/ 6-311+g**	SP M062x/ 6-311+g**
syn-(S,R)	0	0	0
anti-(R,R)	-3.8	1.2	0.9

products	opt WB97X-D/ 6-31g*	SP WB97X-D/ 6-311+g**	SP M062x/ 6-311+g**
syn-(S,R)	0	0	0
anti-(R,R)	4.7	1.1	-1.5

opt = energies from optimization and frequency calculation
SP = energies from a single point energy calculation with thermal correction from optimization of WB97X-D/631g* frequency calculation

representation of *syn*-(S,R) binding of starting materials and in transition state

representation of *anti*-(R,R) binding of starting materials

representation of *anti*-(R,R) binding in transition state

large ester forces monodentate binding because of steric clash with backbone
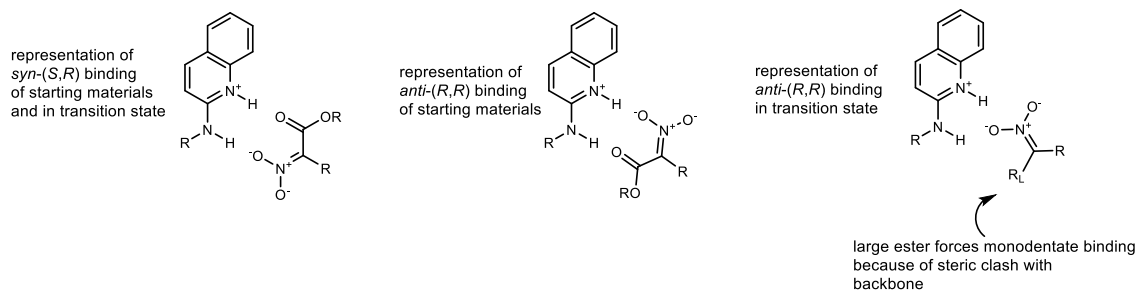
Starting Materials

Major (*syn*, *S,R*)
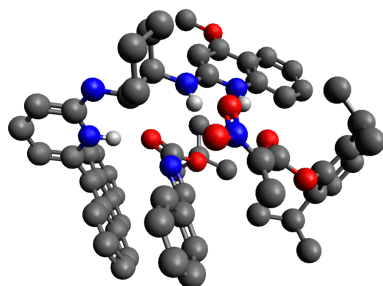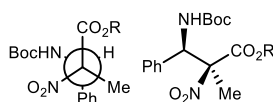
opt freq=noraman wB97XD/6-31G(d) scrf=(iefpcm,solvent=toluene,smd) maxdisk=16GB temperature=253

Zero-point correction=   1.228235 (Hartree/Particle)
Thermal correction to Energy=   1.279072

Thermal correction to Enthalpy=   1.279873

Thermal correction to Gibbs Free Energy=   1.147850

Sum of electronic and zero-point Energies=   -3256.969512

Sum of electronic and thermal Energies=   -3256.918675

Sum of electronic and thermal Enthalpies=   -3256.917874

Sum of electronic and thermal Free Energies=   -3257.049897

Quasiharmonic correction = 0.015043

SCF (wb97xd/6-311+g(d,p)) = -3258.989892

SCF (m062x/6-311+g(d,p)) = -3258.991236

Charge = 1 Multiplicity = 1

C	-0.09581	2.25103	4.89584
C	-0.93507	1.04171	5.30966
C	-1.23084	0.15828	4.09562
C	-1.86313	0.92205	2.92314
C	-1.09946	2.21652	2.55823
C	-0.81117	3.06036	3.81204
N	0.11661	1.83993	1.84913
N	-3.25418	1.25315	3.23519
C	-4.33909	0.94279	2.51429
C	0.84479	2.67282	1.10154
N	1.95977	2.18565	0.52323
C	2.77908	2.94646	-0.29215
C	2.47187	4.29892	-0.52222
C	1.27338	4.82364	0.08346
C	0.47707	4.02611	0.86422
C	3.89982	2.36453	-0.90949
C	4.70165	3.14175	-1.71886
C	4.41646	4.50000	-1.93758
C	3.30945	5.07143	-1.34952
C	-5.64398	1.05476	3.05413
C	-6.72284	0.69112	2.29337
C	-6.55064	0.18761	0.98784
C	-5.28488	0.09952	0.47612
N	-4.22094	0.50407	1.23875
C	-4.97587	-0.47163	-0.86097
C	-5.23549	0.27778	-2.02257
C	-5.00171	-0.32404	-3.30349
C	-4.50720	-1.62624	-3.37105
C	-4.22546	-2.36385	-2.22178
C	-4.46813	-1.78317	-0.93218

C	-5.69260	1.63437	-1.98816
C	-5.90944	2.32927	-3.14189
C	-5.69192	1.72380	-4.41282
C	-5.25280	0.43631	-4.48877
C	-3.71244	-3.69776	-2.30258
C	-3.46842	-4.42164	-1.17513
C	-3.71950	-3.85255	0.10652
C	-4.19773	-2.58160	0.22730
H	0.87150	1.90044	4.51347
H	0.11076	2.89153	5.75952
H	-1.86516	1.38533	5.78751
H	-0.40587	0.44674	6.06055
H	-1.89397	-0.67294	4.36191
H	-0.28905	-0.28892	3.75773
H	-1.85399	0.25941	2.05541
H	-1.73333	2.77744	1.86365
H	-1.76765	3.43818	4.19979
H	-0.21872	3.93906	3.53667
H	0.55548	0.93735	2.07898
H	-3.44355	1.56044	4.18032
H	-0.42473	4.40800	1.31696
H	4.10602	1.31167	-0.75309
H	5.56505	2.68499	-2.19283
H	5.06195	5.09562	-2.57451
H	3.06856	6.11489	-1.51719
H	-5.75913	1.41481	4.07015
H	-7.72115	0.77082	2.71109
H	-7.39346	-0.13857	0.39205
H	-4.33199	-2.07667	-4.34533
H	-5.85882	2.11590	-1.02976
H	-6.25097	3.35893	-3.09501
H	-5.87651	2.29513	-5.31709
H	-5.07744	-0.03649	-5.45117
H	-3.53251	-4.12218	-3.28658
H	-3.08059	-5.43297	-1.24278
H	-3.50980	-4.43717	0.99691
H	-4.37472	-2.17142	1.21604
H	0.68822	2.67014	-1.87263
H	-1.07583	2.85374	-1.68084
H	-0.29959	3.19680	-3.23929
C	-0.28045	2.54408	-2.36042
O	-2.08938	0.98888	-0.47448
H	1.65764	0.78611	-3.17936
C	-1.20084	0.16443	-0.66341

N	-1.02637	-0.88957	0.23552
H	-1.03481	-2.21205	2.45375
C	-0.65383	-2.02938	-0.22495
C	-0.80104	-3.16333	1.99025
H	-0.97006	-4.28548	3.80947
C	-0.52830	-3.21148	0.61821
C	-0.76977	-4.32764	2.74393
O	-0.33345	0.18845	-1.65505
C	-0.45713	1.10121	-2.81047
C	-0.20793	-4.43447	0.01530
C	-0.46747	-5.54576	2.13471
H	0.00306	-4.46805	-1.05004
H	-0.44752	-6.45619	2.72640
C	-0.17776	-5.59924	0.77164
H	0.06592	-6.54658	0.30140
C	0.70151	0.66530	-3.69837
H	0.72075	1.27890	-4.60450
H	-2.62879	1.20846	-2.87060
C	-1.79889	0.86525	-3.49121
H	-1.82612	1.41543	-4.43697
H	0.59300	-0.38286	-3.99405
H	-1.93590	-0.19841	-3.71056
H	6.97198	-2.69802	1.14764
H	4.92875	-4.28249	-3.14966
H	3.40809	-3.62627	3.09247
H	7.19105	-1.68880	2.58749
H	4.15753	-4.35022	-1.55401
H	2.01634	-4.05903	2.10356
C	6.56242	-1.84842	1.70418
H	3.24076	-4.80898	-3.00152
C	3.99125	-4.11171	-2.61006
H	3.62377	-3.94939	1.36148
C	2.95886	-3.50060	2.10035
H	5.56427	-2.12236	2.05429
H	7.60096	-0.26183	0.75456
C	6.55249	-0.56878	0.85692
O	4.22406	-2.16366	0.00686
C	6.06428	-0.73816	-0.58049
C	4.96269	-1.50971	-0.97385
H	7.62910	0.52958	-1.31868
C	6.77061	-0.07914	-1.59261
C	3.51303	-2.66076	-2.76719
C	4.59850	-1.69385	-2.31309
H	3.38524	-2.47354	-3.84048

C	6.40794	-0.19664	-2.92798
C	5.33900	-1.01171	-3.28083
H	6.97310	0.32511	-3.69483
H	5.07706	-1.13467	-4.32873
C	2.73359	-2.05512	1.78092
H	6.30895	0.72404	2.57864
C	3.26942	-1.40223	0.63145
O	1.45803	-1.92640	3.63163
C	5.84206	0.57533	1.59797
H	2.09526	-2.94070	-1.12722
C	2.13452	-2.47942	-2.11848
H	1.37702	-2.97359	-2.73967
N	1.98349	-1.33842	2.66374
H	4.78019	0.37065	1.76206
H	5.92219	1.51600	1.04236
O	2.97841	-0.30724	0.15638
H	1.86152	-1.42672	-2.01288
O	1.85751	-0.07620	2.55890
H	-3.30929	0.55102	0.74600
H	2.21553	1.18934	0.65923
O	1.02174	6.10048	-0.18608
C	-0.14468	6.70537	0.36131
H	-1.04892	6.20282	0.00203
H	-0.13420	7.73592	0.00778
H	-0.11383	6.69235	1.45590
H	-0.46485	-2.17132	-1.29288

Minor (*anti, R,R*)
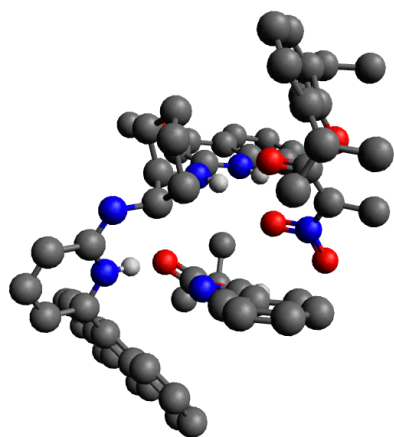
opt freq=noraman wB97XD/6-31G(d) scrf=(iefpcm,solvent=toluene,smd) maxdisk=16GB temperature=253
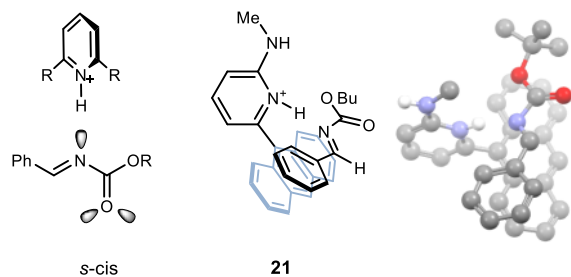
Zero-point correction=   1.226922 (Hartree/Particle)
 Thermal correction to Energy=   1.278327

Thermal correction to Enthalpy=   1.279128

Thermal correction to Gibbs Free Energy=   1.144541

Sum of electronic and zero-point Energies=   -3256.973674

Sum of electronic and thermal Energies=   -3256.922269

Sum of electronic and thermal Enthalpies=   -3256.921468

Sum of electronic and thermal Free Energies=   -3257.056055

Quasiharmonic correction = 0.016776

SCF (wb97xd/6-311+g(d,p)) = -3258.991236

SCF (m062x/6-311+g(d,p)) = -3258.68324

Charge = 1 Multiplicity = 1

C	2.43222	-0.17321	3.42746
C	1.99131	-1.63417	3.31985
C	0.99877	-1.82142	2.16886
C	-0.19607	-0.86123	2.23181
C	0.23573	0.61001	2.41380
C	1.22373	0.75452	3.58389
N	0.80581	1.06831	1.15516
N	-1.08640	-1.24830	3.32472
C	-2.41155	-1.43428	3.26571
C	0.98334	2.34712	0.82260
N	1.61530	2.58113	-0.34169
C	1.83796	3.84073	-0.84579
C	1.42826	4.96419	-0.11027
C	0.75878	4.72761	1.14716
C	0.54010	3.45015	1.60094
C	2.46315	3.99228	-2.09299
C	2.68248	5.26221	-2.58420
C	2.28879	6.39624	-1.85241
C	1.66722	6.25002	-0.63075
C	-3.11473	-2.05802	4.32517
C	-4.46353	-2.26407	4.21198
C	-5.15674	-1.87845	3.04735
C	-4.46530	-1.26263	2.04030
N	-3.12277	-1.03098	2.18666
C	-5.08939	-0.86082	0.75222
C	-5.75837	0.37097	0.65384
C	-6.42019	0.70303	-0.57388
C	-6.35797	-0.18310	-1.64935
C	-5.66824	-1.39201	-1.56507
C	-5.02801	-1.75320	-0.33339

C	-5.79728	1.32226	1.72311
C	-6.44646	2.51269	1.57593
C	-7.11162	2.83706	0.35804
C	-7.09909	1.95737	-0.68214
C	-5.58763	-2.28544	-2.67995
C	-4.92265	-3.46993	-2.57937
C	-4.30286	-3.83981	-1.35068
C	-4.35437	-3.01511	-0.26654
H	2.99223	0.09410	2.52310
H	3.11280	-0.04225	4.27495
H	1.54929	-1.95914	4.27401
H	2.86123	-2.27729	3.15024
H	0.61796	-2.84788	2.12867
H	1.52220	-1.64490	1.22409
H	-0.74787	-0.95249	1.29399
H	-0.67247	1.19123	2.60406
H	0.68954	0.52131	4.51542
H	1.54700	1.79785	3.66462
H	1.31950	0.39760	0.57498
H	-0.64542	-1.59066	4.16815
H	0.03935	3.26200	2.53873
H	2.76456	3.11072	-2.65062
H	3.16667	5.38475	-3.54775
H	2.47090	7.38747	-2.25365
H	1.35472	7.11803	-0.06140
H	-2.56174	-2.37328	5.20278
H	-4.99943	-2.74791	5.02206
H	-6.21629	-2.06594	2.92919
H	-6.85270	0.07988	-2.58152
H	-5.29624	1.09346	2.65879
H	-6.46047	3.22635	2.39422
H	-7.62330	3.78983	0.26549
H	-7.59723	2.19446	-1.61826
H	-6.07160	-1.99594	-3.60858
H	-4.86510	-4.14203	-3.42975
H	-3.77995	-4.78880	-1.28297
H	-3.87513	-3.31490	0.65980
H	-0.33857	2.36576	-2.15336
H	-1.35990	2.91108	-0.79601
H	-1.32668	3.83851	-2.30854
C	-1.29042	2.83021	-1.88378
O	-2.34715	0.79864	0.15544
H	-1.38119	1.58190	-4.30061
C	-2.10329	0.15813	-0.86350

N	-1.69204	-1.17415	-0.74649
H	-1.40866	-3.50229	0.25392
C	-0.94456	-1.65890	-1.67359
C	-0.74323	-3.86576	-0.52260
H	-0.49350	-5.81533	0.34306
C	-0.40939	-3.01514	-1.58642
C	-0.23133	-5.15381	-0.47709
O	-2.23296	0.58706	-2.09855
C	-2.43319	2.00242	-2.45616
C	0.45505	-3.46472	-2.59174
C	0.61957	-5.60170	-1.49059
H	0.73249	-2.78914	-3.39777
H	1.01957	-6.61070	-1.45253
C	0.96795	-4.75710	-2.54149
H	1.64145	-5.10337	-3.31911
C	-2.35666	1.95826	-3.97723
H	-2.49857	2.96287	-4.38735
H	-3.87930	2.45051	-0.89406
C	-3.80148	2.47155	-1.98317
H	-3.96479	3.49901	-2.32496
H	-3.13492	1.30473	-4.38403
H	-4.58767	1.84099	-2.40683
H	6.67216	-3.95356	-0.77146
H	8.08136	0.49767	-0.80127
H	3.44179	-2.37650	-3.69843
H	5.34045	-5.02163	-1.24798
H	6.64475	0.38795	-1.83487
H	3.75081	-0.79660	-4.41295
C	5.58840	-4.00529	-0.92100
H	7.42950	1.95478	-1.57122
C	7.15693	1.00739	-1.09227
H	4.88610	-1.46501	-3.22543
C	3.83140	-1.37211	-3.48606
H	5.32240	-3.31614	-1.72647
H	5.09055	-4.46431	1.09361
C	4.83526	-3.67568	0.37483
O	4.83638	-1.07043	-0.92659
C	5.31847	-2.38127	1.01925
C	5.36648	-1.14704	0.35977
H	5.78957	-3.37148	2.86332
C	5.81688	-2.42754	2.32470
C	6.25845	1.26971	0.12525
C	5.98640	-0.01419	0.90316
H	6.83181	1.90354	0.81269

C	6.36217	-1.30292	2.93043
C	6.46647	-0.11853	2.21164
H	6.74299	-1.36041	3.94583
H	6.94497	0.74544	2.66557
C	3.07606	-0.70173	-2.37892
H	3.05226	-4.76191	-0.18122
C	3.54039	-0.64100	-1.02418
O	1.34295	-0.48949	-3.80842
C	3.31900	-3.75970	0.17062
H	4.50583	1.64379	-1.13668
C	5.02205	2.08401	-0.27871
H	5.33277	3.09366	-0.57112
N	1.82709	-0.25350	-2.67891
H	2.95411	-3.04677	-0.57439
H	2.78491	-3.58288	1.10868
O	2.94029	-0.28846	-0.01265
H	4.30757	2.17016	0.54408
O	1.13027	0.41365	-1.84498
H	-2.67555	-0.47218	1.43724
H	1.77205	1.75904	-0.95084
H	-0.65642	-1.06791	-2.54570
O	0.39101	5.82648	1.79642
C	-0.25124	5.69957	3.06119
H	-1.20475	5.17073	2.96148
H	-0.43229	6.71833	3.40201
H	0.39785	5.18285	3.77581

Transition States

Major (*syn, S,R*)
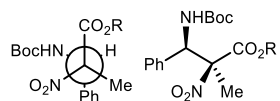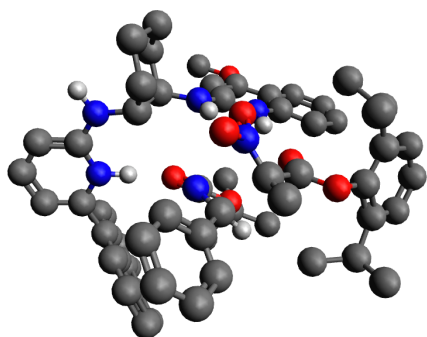
\# opt=(calcfc,ts,noeigen) freq=noraman wB97XD/6-31G(d) scrf=(iefpcm,solvent=toluene,smd) maxdisk=16000MB guess=read geom=allcheck temperatur e=253

Zero-point correction=   1.229872 (Hartree/Particle)
Thermal correction to Energy=   1.278804
Thermal correction to Enthalpy=   1.279605
Thermal correction to Gibbs Free Energy=   1.154597
Sum of electronic and zero-point Energies=   -3256.942599
Sum of electronic and thermal Energies=   -3256.893668
Sum of electronic and thermal Enthalpies=   -3256.892866
Sum of electronic and thermal Free Energies=   -3257.017874

Quasiharmonic correction = 0.011362

SCF (wb97xd/6-311+g(d,p)) = -3258.961737
SCF (m062x/6-311+g(d,p)) = -3258.659009

Charge = 1 Multiplicity = 1

C	-0.37104	2.86176	4.80858
C	-0.99225	1.57909	5.36202
C	-1.08261	0.50610	4.27425
C	-1.78820	0.98569	2.99811
C	-1.23191	2.33265	2.47013
C	-1.15706	3.37301	3.60000
N	0.06856	2.06223	1.86841
N	-3.21535	1.12411	3.26007
C	-4.23509	0.80941	2.45172
C	0.70040	2.84023	0.99188
N	1.80468	2.34462	0.39576
C	2.57860	3.07334	-0.48994
C	2.21768	4.39491	-0.80089
C	1.00386	4.91091	-0.21507

C	0.26341	4.14849	0.65156
C	3.70157	2.48745	-1.09646
C	4.46205	3.23611	-1.97087
C	4.12798	4.56800	-2.26616
C	3.01256	5.13919	-1.69261
C	-5.56895	0.88378	2.92267
C	-6.59962	0.53679	2.09303
C	-6.34164	0.09992	0.78081
C	-5.04645	0.04286	0.33701
N	-4.02373	0.41048	1.17333
C	-4.72606	-0.44924	-1.02875
C	-5.09519	0.33085	-2.14216
C	-4.95682	-0.22568	-3.45775
C	-4.45413	-1.51712	-3.60768
C	-4.05990	-2.28193	-2.51080
C	-4.19571	-1.74467	-1.18696
C	-5.58786	1.67144	-2.02856
C	-5.92284	2.39235	-3.13711
C	-5.79539	1.83215	-4.44066
C	-5.32618	0.56249	-4.59307
C	-3.52196	-3.59639	-2.68124
C	-3.16085	-4.34758	-1.60378
C	-3.32076	-3.82837	-0.28799
C	-3.81284	-2.57330	-0.08366
H	0.66722	2.66480	4.51101
H	-0.34015	3.63680	5.58148
H	-1.98601	1.80543	5.77699
H	-0.39758	1.19373	6.19636
H	-1.60327	-0.38591	4.63995
H	-0.07285	0.18146	4.00568
H	-1.64639	0.21847	2.23078
H	-1.90507	2.67946	1.67732
H	-2.18554	3.61592	3.89996
H	-0.71501	4.30300	3.22955
H	0.46879	1.13671	2.02444
H	-3.48226	1.40892	4.19265
H	-0.64780	4.52243	1.09187
H	3.94902	1.45456	-0.88129
H	5.33117	2.77890	-2.43366
H	4.74184	5.14354	-2.95086
H	2.73319	6.16125	-1.92128
H	-5.74202	1.20593	3.94338
H	-7.62145	0.58714	2.45472
H	-7.14279	-0.19762	0.11640

H	-4.35503	-1.93542	-4.60660
H	-5.68504	2.12176	-1.04598
H	-6.28973	3.40863	-3.02851
H	-6.07071	2.42451	-5.30770
H	-5.21767	0.12291	-5.58082
H	-3.41259	-3.98127	-3.69158
H	-2.75178	-5.34410	-1.73730
H	-3.03698	-4.44022	0.56186
H	-3.91074	-2.20115	0.93062
H	0.66651	2.42031	-2.01498
H	-1.08494	2.30746	-1.70426
H	-0.47096	2.49911	-3.36094
C	-0.28304	2.03169	-2.38835
O	-1.66996	0.66163	-0.19876
H	1.92703	0.45101	-2.97554
C	-0.72939	-0.15188	-0.26705
N	-0.51612	-1.05381	0.72092
H	-1.16994	-2.45627	2.79541
C	0.22236	-2.15413	0.48176
C	-0.97668	-3.40282	2.30367
H	-1.97798	-4.58003	3.79451
C	-0.26055	-3.41287	1.10258
C	-1.43351	-4.59381	2.85490
O	0.09937	-0.17319	-1.32089
C	-0.20298	0.51957	-2.57610
C	-0.03268	-4.62811	0.45253
C	-1.19804	-5.80536	2.20369
H	0.51038	-4.63737	-0.48933
H	-1.56134	-6.73379	2.63420
C	-0.50287	-5.81950	0.99660
H	-0.32580	-6.75808	0.47995
C	0.98751	0.17221	-3.46361
H	0.91289	0.71634	-4.41065
H	-2.34368	0.21616	-2.52162
C	-1.49307	-0.04552	-3.15231
H	-1.66430	0.36306	-4.15364
H	1.01168	-0.89789	-3.68882
H	-1.42879	-1.13525	-3.23047
H	6.30708	-2.28260	1.85959
H	5.77956	-4.16382	-2.90075
H	3.54823	-3.42536	2.32370
H	6.37713	-1.12163	3.19504
H	4.85981	-4.39005	-1.40140
H	1.86218	-3.94819	2.45673

C	5.87889	-1.35279	2.24729
H	4.21119	-4.99285	-2.93919
C	4.77184	-4.17454	-2.47262
H	2.70921	-4.07149	0.90756
C	2.58420	-3.46131	1.80409
H	4.82428	-1.53013	2.47478
H	7.13504	0.10071	1.35494
C	6.07747	-0.18004	1.27816
O	4.05907	-2.03227	0.11136
C	5.88292	-0.48869	-0.20687
C	4.95255	-1.38317	-0.75030
H	7.45505	0.87411	-0.72525
C	6.72441	0.16785	-1.11196
C	4.05507	-2.83413	-2.69684
C	4.89490	-1.70526	-2.11140
H	4.03289	-2.64997	-3.77745
C	6.65238	-0.06989	-2.47765
C	5.75738	-1.01418	-2.96496
H	7.31461	0.45671	-3.15841
H	5.73105	-1.23557	-4.02877
C	2.11867	-2.07536	1.42911
H	5.54778	1.29926	2.77032
C	2.96049	-1.33044	0.46424
O	1.36974	-1.86736	3.57426
C	5.27221	1.04374	1.74059
H	2.52038	-3.45467	-1.27520
C	2.59777	-2.92855	-2.23060
H	2.01258	-3.49757	-2.96170
N	1.73993	-1.29346	2.55169
H	4.19593	0.84864	1.72606
H	5.47457	1.91615	1.11060
O	2.72799	-0.23700	-0.00949
H	2.13698	-1.94385	-2.12231
O	1.73396	-0.04903	2.47229
H	-3.05836	0.41810	0.75888
H	2.04079	1.35113	0.51945
H	0.65614	-2.28692	-0.50964
O	0.68566	6.14504	-0.58709
C	-0.49911	6.74137	-0.06856
H	-1.38382	6.16534	-0.35944
H	-0.54727	7.73391	-0.51517
H	-0.44420	6.83097	1.02141

Minor (*anti, R,R*)
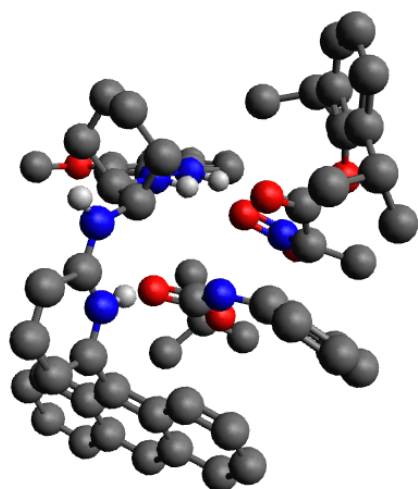
opt=(calcfc,ts,noeigen) freq=noraman wB97XD/6-31G(d) scrf=(iefpcm,solvent=toluene,smd) maxdisk=8000MB temperature=253

Zero-point correction=   1.228644 (Hartree/Particle)
Thermal correction to Energy=   1.278124
Thermal correction to Enthalpy=   1.278925
Thermal correction to Gibbs Free Energy=   1.152259
Sum of electronic and zero-point Energies=   -3256.940100
Sum of electronic and thermal Energies=   -3256.890621
Sum of electronic and thermal Enthalpies=   -3256.889819
Sum of electronic and thermal Free Energies=   -3257.016486

Quasiharmonic correction = 0.011943

SCF (wb97xd/6-311+g(d,p)) = -3258.95779
SCF (m062x/6-311+g(d,p)) = -3258.656721

Charge = 1 Multiplicity = 1

C	1.48998	2.41798	4.19016
C	1.99111	0.98096	4.32960
C	1.67595	0.17371	3.06891
C	0.19354	0.21537	2.66771
C	-0.33994	1.66755	2.57624
C	-0.00287	2.44490	3.85991
N	0.26342	2.25267	1.38074
N	-0.57783	-0.53155	3.65524
C	-1.64682	-1.31958	3.47102
C	-0.11385	3.39120	0.78875

N	0.46636	3.69134	-0.38978
C	0.17241	4.82278	-1.11822
C	-0.75443	5.74824	-0.61593
C	-1.39432	5.43315	0.63831
C	-1.08148	4.28133	1.31999
C	0.79057	5.03039	-2.36008
C	0.48849	6.16992	-3.07615
C	-0.42499	7.11483	-2.57700
C	-1.04273	6.90604	-1.36271
C	-2.13390	-2.11176	4.53957
C	-3.21887	-2.92155	4.34339
C	-3.84374	-2.98024	3.08422
C	-3.35967	-2.20609	2.06349
N	-2.28716	-1.38192	2.28026
C	-3.95980	-2.26495	0.70270
C	-5.07866	-1.47056	0.40053
C	-5.74650	-1.66125	-0.85349
C	-5.26185	-2.61094	-1.75352
C	-4.13211	-3.37766	-1.47091
C	-3.46727	-3.21412	-0.21011
C	-5.57786	-0.46489	1.28877
C	-6.65520	0.29847	0.94584
C	-7.31734	0.10805	-0.30136
C	-6.87722	-0.84508	-1.17027
C	-3.62704	-4.33754	-2.40464
C	-2.53976	-5.10025	-2.10109
C	-1.88909	-4.95053	-0.84284
C	-2.33188	-4.03965	0.06887
H	2.04879	2.92347	3.39193
H	1.67213	2.97923	5.11273
H	1.53611	0.52250	5.22049
H	3.07207	0.96455	4.50278
H	1.97480	-0.87327	3.17792
H	2.26712	0.56133	2.23614
H	0.08313	-0.27706	1.69360
H	-1.42636	1.62618	2.43206
H	-0.57258	1.98464	4.67791
H	-0.35164	3.47875	3.79073
H	0.79893	1.61264	0.79854
H	-0.18798	-0.57176	4.58695
H	-1.58261	4.01891	2.23821
H	1.48876	4.29043	-2.74003
H	0.96419	6.33609	-4.03739
H	-0.64703	8.00765	-3.15175

H	-1.75635	7.62298	-0.97316
H	-1.62646	-2.06207	5.49633
H	-3.59036	-3.53106	5.16074
H	-4.68976	-3.63043	2.90205
H	-5.77044	-2.74726	-2.70517
H	-5.08366	-0.30431	2.24209
H	-7.01671	1.06131	1.62898
H	-8.17325	0.72674	-0.55276
H	-7.37173	-0.99736	-2.12580
H	-4.13413	-4.44485	-3.35967
H	-2.16073	-5.82612	-2.81385
H	-1.01734	-5.55713	-0.61821
H	-1.80656	-3.92600	1.01137
H	-0.81649	2.44755	-2.40087
H	-2.01200	2.45143	-1.07384
H	-2.44198	3.11607	-2.66360
C	-1.87326	2.33319	-2.15076
O	-1.93093	0.25808	0.11575
H	-1.09981	0.95922	-4.37674
C	-1.26828	-0.29818	-0.77833
N	-0.33497	-1.24070	-0.47478
H	0.97325	-2.90487	0.93841
C	0.34367	-1.82371	-1.46399
C	1.17418	-3.58734	0.12075
H	1.81290	-5.20164	1.38214
C	0.94146	-3.15544	-1.18787
C	1.63791	-4.87468	0.36143
O	-1.46830	-0.06962	-2.07723
C	-2.34965	0.96355	-2.61284
C	1.18220	-4.03400	-2.24778
C	1.88374	-5.74483	-0.70100
H	0.97780	-3.71400	-3.26584
H	2.24846	-6.74977	-0.50978
C	1.65599	-5.32077	-2.00796
H	1.83656	-5.99481	-2.83991
C	-2.15215	0.81109	-4.11773
H	-2.75675	1.54960	-4.65390
H	-3.94690	0.77192	-1.15068
C	-3.79565	0.68634	-2.22803
H	-4.45163	1.40277	-2.73442
H	-2.45607	-0.18818	-4.44684
H	-4.08038	-0.31958	-2.54625
H	5.36064	-3.07346	-1.93209
H	5.63277	1.62063	-2.59770

H	1.84568	-1.38595	-3.96688
H	4.89248	-4.59429	-1.15490
H	3.90316	1.46276	-2.28024
H	3.39265	-0.58133	-3.67244
C	4.84676	-3.50354	-1.06700
H	4.63097	3.06456	-2.38431
C	4.79525	2.03995	-2.03112
H	3.12304	-2.22413	-3.06487
C	2.64824	-1.25656	-3.23581
H	3.79118	-3.22523	-1.11475
H	6.43551	-3.64644	0.32978
C	5.49637	-3.08420	0.25487
O	4.28336	-0.68930	-1.12563
C	5.90503	-1.62299	0.41411
C	5.29326	-0.50980	-0.17204
H	7.46507	-2.22804	1.75157
C	6.97357	-1.37772	1.28506
C	5.09457	2.06662	-0.52695
C	5.72458	0.80707	0.06248
H	5.85068	2.84843	-0.38673
C	7.41515	-0.09377	1.55765
C	6.79135	0.98492	0.94524
H	8.24956	0.06710	2.23352
H	7.14197	1.99436	1.14449
C	2.09841	-0.71650	-1.94424
H	4.38649	-4.57077	1.38905
C	2.99010	-0.75923	-0.73313
O	1.22839	0.98787	-3.19532
C	4.62746	-3.50377	1.45005
H	3.07361	1.74744	0.23340
C	3.86630	2.49635	0.29069
H	3.46607	3.44508	-0.08871
N	1.49167	0.53080	-2.07839
H	3.69144	-2.93706	1.46064
H	5.14687	-3.32509	2.39794
O	2.65248	-0.81569	0.42174
H	4.12964	2.63654	1.34485
O	1.16214	1.14953	-1.03082
H	-2.00111	-0.76614	1.47696
H	0.98766	2.93699	-0.85335
H	0.01322	-1.68647	-2.49609
O	-2.28874	6.32327	1.04668
C	-2.95968	6.11375	2.28683
H	-3.56733	5.20383	2.25128

H	-3.60554	6.98065	2.42025
H	-2.23963	6.05980	3.10980

Products

Major (*syn, S,R*)
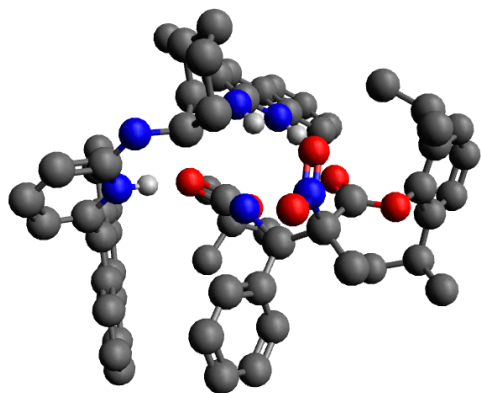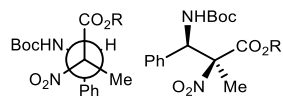
opt freq=noraman wB97XD/6-31G(d) scrf=(iefpcm,solvent=toluene,smd) maxdisk=16GB guess=read geom=allcheck temperature=253

Zero-point correction=   1.230061 (Hartree/Particle)
Thermal correction to Energy=   1.279704
Thermal correction to Enthalpy=   1.280506
Thermal correction to Gibbs Free Energy=   1.153083
Sum of electronic and zero-point Energies=   -3256.958822
Sum of electronic and thermal Energies=   -3256.909179
Sum of electronic and thermal Enthalpies=   -3256.908378
Sum of electronic and thermal Free Energies=   -3257.03580

Quasiharmonic correction = 0.012546

SCF (wb97xd/6-311+g(d,p)) = -3258.978562
SCF (m062x/6-311+g(d,p)) = -3258.672881

Charge = 1 Multiplicity = 1

C	0.23985	2.84908	4.82889

C	-0.18508	1.55192	5.51680
C	-0.26723	0.40991	4.50049
C	-1.16406	0.72545	3.29619
C	-0.84217	2.09375	2.64970
C	-0.73066	3.20451	3.70289
N	0.38734	1.93680	1.86827
N	-2.55313	0.70369	3.73813
C	-3.63816	0.32226	3.04859
C	0.64111	2.65903	0.76851
N	1.58850	2.20944	-0.07226
C	1.97132	2.87726	-1.21797
C	1.32947	4.07665	-1.56332
C	0.27681	4.54328	-0.69483
C	-0.04148	3.86090	0.45196
C	2.98757	2.35294	-2.03251
C	3.33946	3.02939	-3.18258
C	2.69991	4.22763	-3.54313
C	1.70644	4.74693	-2.74196
C	-4.86484	0.13189	3.73077
C	-5.97854	-0.24678	3.03408
C	-5.90821	-0.43366	1.64336
C	-4.71417	-0.23666	0.99888
N	-3.59786	0.12531	1.70702
C	-4.65216	-0.36494	-0.48170
C	-4.65341	0.79768	-1.27460
C	-4.82164	0.67084	-2.69341
C	-4.99166	-0.59410	-3.25565
C	-4.95888	-1.75124	-2.47830
C	-4.77780	-1.64258	-1.05901
C	-4.51466	2.11371	-0.72755
C	-4.51971	3.21262	-1.53540
C	-4.66951	3.08358	-2.94614
C	-4.82102	1.85018	-3.50408
C	-5.07567	-3.04874	-3.06859
C	-5.00277	-4.17397	-2.30379
C	-4.80908	-4.06913	-0.89652
C	-4.70582	-2.85075	-0.29336
H	1.24941	2.72900	4.41427
H	0.28446	3.67071	5.55140
H	-1.15172	1.70820	6.01865
H	0.52653	1.28054	6.30323
H	-0.62392	-0.51569	4.96485
H	0.73777	0.19653	4.12945
H	-1.02176	-0.05288	2.53587

H	-1.65161	2.31969	1.94686
H	-1.73390	3.36880	4.11855
H	-0.43027	4.14409	3.22852
H	0.78911	0.99992	1.87174
H	-2.70723	0.81566	4.73090
H	-0.82124	4.20743	1.11146
H	3.47737	1.42788	-1.74924
H	4.12454	2.62657	-3.81472
H	2.98961	4.74405	-4.45202
H	1.20534	5.67070	-3.00717
H	-4.89103	0.28673	4.80356
H	-6.91826	-0.39759	3.55524
H	-6.77994	-0.71619	1.06692
H	-5.13295	-0.68259	-4.33027
H	-4.39808	2.23891	0.34361
H	-4.41618	4.20211	-1.09987
H	-4.66862	3.97274	-3.56890
H	-4.94480	1.73634	-4.57752
H	-5.21449	-3.11585	-4.14416
H	-5.08474	-5.15480	-2.76140
H	-4.73281	-4.97366	-0.30134
H	-4.54055	-2.79229	0.77739
H	-0.41843	2.21127	-2.73550
H	-1.94919	1.64651	-2.03112
H	-1.67680	1.54951	-3.79085
C	-1.20674	1.45358	-2.80604
O	-1.55178	0.59815	0.02806
H	1.28330	0.58712	-3.57288
C	-0.56333	-0.15944	-0.18659
N	-0.03373	-0.94989	0.72132
H	-1.14556	-2.81385	2.08834
C	0.74909	-2.06785	0.25696
C	-1.02146	-3.56350	1.31472
H	-2.51811	-4.88028	2.11581
C	-0.08297	-3.34404	0.30334
C	-1.79424	-4.71983	1.32139
O	0.08405	-0.09042	-1.39139
C	-0.60786	0.05706	-2.65190
C	0.05037	-4.29547	-0.70939
C	-1.64973	-5.66851	0.30960
H	0.76689	-4.12662	-1.51089
H	-2.25691	-6.56920	0.31374
C	-0.72757	-5.45158	-0.70970
H	-0.61563	-6.17947	-1.50801

C	0.49238	-0.16184	-3.68659
H	0.08164	-0.07789	-4.69830
H	-2.41615	-0.91088	-1.97913
C	-1.66142	-1.03722	-2.75663
H	-2.15788	-1.00286	-3.73077
H	0.93514	-1.15750	-3.57369
H	-1.20218	-2.02501	-2.63657
H	6.44699	-1.43063	2.70055
H	6.45137	-4.15447	-1.50234
H	3.55621	-3.64137	1.78675
H	5.79103	-0.21968	3.81329
H	4.96624	-4.02630	-0.54858
H	1.87022	-4.21194	1.77028
C	5.68514	-0.65182	2.81224
H	4.94531	-4.86455	-2.10946
C	5.36753	-4.01175	-1.56587
H	2.77116	-4.07796	0.25587
C	2.61358	-3.62161	1.23553
H	4.70381	-1.12581	2.76574
H	6.80362	0.95495	2.01490
C	5.86142	0.45297	1.76435
O	4.38505	-1.78083	0.39719
C	6.06355	-0.02656	0.32978
C	5.38208	-1.06750	-0.30863
H	7.57214	1.46536	0.03259
C	7.02822	0.64590	-0.42976
C	5.02749	-2.70207	-2.28969
C	5.66609	-1.49486	-1.61328
H	5.49975	-2.75642	-3.27746
C	7.30649	0.29104	-1.74015
C	6.63962	-0.78210	-2.31611
H	8.05961	0.83272	-2.30413
H	6.87955	-1.08502	-3.33159
C	2.11227	-2.19530	1.05703
H	4.77642	1.97683	2.86389
C	3.15015	-1.28087	0.37344
O	1.28296	-2.30372	3.24266
C	4.76562	1.52595	1.86507
H	2.93189	-2.77827	-1.64714
C	3.51962	-2.57077	-2.54446
H	3.20757	-3.30080	-3.29929
N	1.86615	-1.61575	2.43430
H	3.77234	1.10531	1.70189
H	4.92787	2.32215	1.13003

O	2.87411	-0.24501	-0.18352
H	3.25507	-1.57238	-2.90563
O	2.25196	-0.47128	2.65331
H	-2.70164	0.26289	1.14010
H	1.96050	1.26292	0.05186
H	1.07091	-1.93970	-0.78222
O	-0.32897	5.65332	-1.09901
C	-1.42152	6.16035	-0.33871
H	-2.22339	5.41755	-0.27624
H	-1.77331	7.03792	-0.88000
H	-1.09601	6.45490	0.66436

Minor (*anti, R,R*)
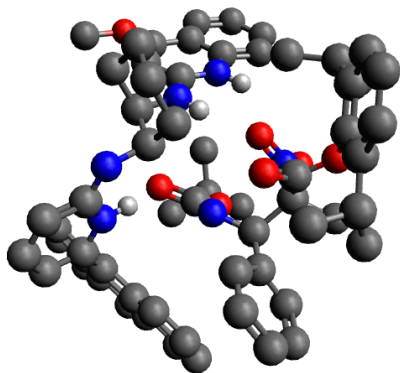
opt freq=noraman wB97XD/6-31G(d) scrf=(iefpcm,solvent=toluene,smd) maxdisk=16GB temperature=253

Zero-point correction=	1.231410 (Hartree/Particle)
Thermal correction to Energy=	1.280450
Thermal correction to Enthalpy=	1.281251
Thermal correction to Gibbs Free Energy=	1.155673
Sum of electronic and zero-point Energies=	-3256.952534
Sum of electronic and thermal Energies=	-3256.903495
Sum of electronic and thermal Enthalpies=	-3256.902694
Sum of electronic and thermal Free Energies=	-3257.028272

Quasiharmonic correction = 0.011822

SCF (wb97xd/6-311+g(d,p)) = -3258.974289
SCF (m062x/6-311+g(d,p)) = -3258.67269

Charge = 1 Multiplicity = 1

C	1.39780	2.38649	4.18952
C	1.91786	0.95856	4.35170
C	1.64840	0.13857	3.08825
C	0.17941	0.15570	2.64217
C	-0.37594	1.59757	2.53157
C	-0.08577	2.38985	3.81729
N	0.24072	2.20138	1.35020
N	-0.61200	-0.59611	3.60677
C	-1.73924	-1.29772	3.41094
C	-0.15926	3.33425	0.76548
N	0.47043	3.70852	-0.36654
C	0.15752	4.84764	-1.07791
C	-0.85198	5.69971	-0.60831
C	-1.55000	5.30315	0.59124
C	-1.20669	4.15286	1.26021
C	0.83999	5.13304	-2.26865
C	0.51768	6.27770	-2.96798
C	-0.47983	7.15043	-2.50055
C	-1.16048	6.86403	-1.33644
C	-2.31805	-2.00619	4.49281
C	-3.46225	-2.72944	4.29504
C	-4.05450	-2.78142	3.02157
C	-3.47920	-2.08385	1.99070
N	-2.34937	-1.34231	2.20351
C	-4.05917	-2.15684	0.62093
C	-5.20635	-1.40496	0.31495
C	-5.87484	-1.63043	-0.93355
C	-5.37193	-2.58344	-1.81963
C	-4.21734	-3.31141	-1.53275
C	-3.54217	-3.10065	-0.28397
C	-5.73072	-0.40262	1.19251
C	-6.83412	0.32188	0.84850
C	-7.49844	0.09456	-0.39123
C	-7.03240	-0.85333	-1.25253
C	-3.69584	-4.27689	-2.45151
C	-2.58512	-5.00364	-2.14400
C	-1.92524	-4.80867	-0.89691
C	-2.38110	-3.88835	-0.00107
H	1.97166	2.89633	3.40459
H	1.54583	2.95585	5.11329
H	1.44582	0.49787	5.23235
H	2.99389	0.96158	4.55477
H	1.96134	-0.90254	3.21238

H	2.25743	0.53316	2.27053
H	0.10898	-0.34210	1.66552
H	-1.45573	1.53180	2.35624
H	-0.67119	1.92754	4.62289
H	-0.44718	3.41849	3.73010
H	0.80859	1.57958	0.78199
H	-0.25693	-0.63045	4.55215
H	-1.74990	3.83060	2.13453
H	1.60374	4.44832	-2.62534
H	1.04183	6.50324	-3.89111
H	-0.71751	8.04848	-3.06064
H	-1.93827	7.52554	-0.97275
H	-1.83338	-1.96218	5.46173
H	-3.90733	-3.27164	5.12303
H	-4.94840	-3.36317	2.83609
H	-5.88461	-2.75304	-2.76367
H	-5.23252	-0.21308	2.13817
H	-7.21380	1.08228	1.52452
H	-8.37620	0.68156	-0.64357
H	-7.52829	-1.03287	-2.20267
H	-4.21013	-4.41830	-3.39829
H	-2.19495	-5.73520	-2.84501
H	-1.03857	-5.39001	-0.66536
H	-1.84700	-3.74300	0.93188
H	-0.80755	2.50926	-2.42897
H	-1.99067	2.37643	-1.09697
H	-2.49529	2.99310	-2.68586
C	-1.84574	2.27423	-2.17500
O	-1.85154	0.18281	0.10780
H	-0.90364	0.94743	-4.38211
C	-1.05714	-0.33383	-0.73448
N	-0.07335	-1.13547	-0.39823
H	1.09047	-2.85718	1.00976
C	0.71085	-1.72393	-1.44029
C	1.23790	-3.58098	0.21796
H	1.70218	-5.20214	1.54730
C	1.07895	-3.16578	-1.10531
C	1.57499	-4.89858	0.51187
O	-1.19807	-0.06346	-2.06282
C	-2.16886	0.85320	-2.62258
C	1.22996	-4.10942	-2.12435
C	1.75591	-5.82584	-0.51344
H	1.06492	-3.81568	-3.15764
H	2.02255	-6.85318	-0.28302

C	1.57506	-5.42767	-1.83546
H	1.68978	-6.14550	-2.64251
C	-1.93962	0.70545	-4.12553
H	-2.60352	1.37566	-4.68130
H	-3.78752	0.57514	-1.20244
C	-3.59335	0.44719	-2.26726
H	-4.30471	1.05454	-2.83818
H	-2.14224	-0.32295	-4.44291
H	-3.75518	-0.60168	-2.52930
H	5.30147	-2.94348	-1.95416
H	5.68028	1.90831	-2.52766
H	1.94606	-1.52035	-3.87780
H	4.99728	-4.51067	-1.19135
H	3.98132	1.55864	-2.21565
H	3.50079	-0.79204	-3.42507
C	4.88589	-3.42860	-1.06596
H	4.54415	3.23201	-2.22870
C	4.80954	2.20959	-1.93595
H	3.11435	-2.43759	-2.91404
C	2.69598	-1.44745	-3.08828
H	3.81211	-3.23330	-1.01796
H	6.55724	-3.53513	0.22932
C	5.59826	-3.00315	0.21992
O	4.28787	-0.55449	-1.07511
C	5.98235	-1.53181	0.38029
C	5.34947	-0.40465	-0.16068
H	7.59888	-2.15455	1.63771
C	7.08974	-1.29671	1.20576
C	5.12763	2.17636	-0.43705
C	5.79495	0.90641	0.07898
H	5.86735	2.96966	-0.27672
C	7.55142	-0.02024	1.47587
C	6.90487	1.06883	0.90933
H	8.41822	0.12637	2.11285
H	7.26581	2.07441	1.10792
C	2.05674	-0.92397	-1.80761
H	4.59803	-4.55173	1.36925
C	3.05529	-0.84663	-0.62589
O	1.46310	0.89037	-3.19910
C	4.81125	-3.47991	1.45131
H	3.17026	1.73330	0.42457
C	3.91520	2.53161	0.43778
H	3.44045	3.45529	0.08413
N	1.64492	0.50538	-2.06631

H	3.86094	-2.94489	1.53231
H	5.37802	-3.31435	2.37388
O	2.78552	-1.01331	0.53156
H	4.22393	2.68535	1.47746
O	1.50408	1.22523	-1.07641
H	-2.01156	-0.74688	1.37018
H	1.10431	3.03878	-0.80328
H	0.18293	-1.73648	-2.40182
O	-2.52862	6.11754	0.95942
C	-3.30405	5.79954	2.11286
H	-3.81096	4.83774	1.98511
H	-4.04379	6.59501	2.19445
H	-2.67767	5.78512	3.01092